Typha capensis—An Electron Rich Resource For The Synthesis of Phytochemical-Encapsulated Gold Nanoparticles Through Green Nanotechnology

Keenau Mark Pearce

A thesis submitted in conformity with the requirements for the degree of Philosophiae Doctor (PhD) in the Department of Medical Biosciences, University of the Western Cape

Supervisor: Prof. R. Henkel
Co-supervisor: Prof. K. Katti

February 2020

Declaration

I declare that *Typha capensis—An Electron Rich Resource For The Synthesis of Phytochemical-Encapsulated Gold Nanoparticles Through Green Nanotechnology* is my own work, that has not been submitted before for any degree or examination in any other university, and that all sources I have used or quoted have been indicated and acknowledged as complete references.

Keenau Mark Pearce February 2020

Signed:……

Dedications

This thesis is dedicated to my parents. My father and mother have been examples of what hard work, dedication and passion can achieve, and have taught me to always reach for my goals. They have taught me to be hardworking, understanding, patient, and to never quit on my dreams and aspirations. I would also like to dedicate this thesis to my brother, who has been an unmatched source of inspiration and motivation in persusing my academic goals.

Acknowledgements

I wish to express my admiration and gratitude to my supervisor, Prof. R Henkel and co-supervisor, Prof. K.V Katti, along with Mrs. K. Katti, for their endless patience, guidance and continual support, as well as for the use of laboratory materials and equipment. Without your support and guidance I would not be able to have achieved my goals. I wish to extend a sincere thank you to the National Research Foundation for providing me with a bursary and travel grant, along with Prof. R. Henkel and Prof. K. Katti for providing research funding, without which my PhD project would not have been possible.

To my family, I would to extend my undying gratitude for providing me with the encouragement I needed and for having patience with me, especially when I needed it most.

To my colleagues and friends; Nicole Haines-Arries, Eurinah Harris, Maryam Kisten, Lutho Menyane, Lyle Solomons, Velaphi Thipe, Alice Karikachery, Menka Khoobchandan, and Abdulkarem Ilfergane, thank you for the endless kindness, help, assistance and support you have provided me with. To the staff at the Department of Medical Biosciences, thank you for all your assistance, suggestions and technical support. A special thank you to Mr. Franz Weitz from the Department of Biodiversity and Conservation Biology for their support and assistance with sample collection.

I would like to acknowledge the staff at the Electron Microscopy Core, at the University of Missouri, and the following grant which was pivotal for the characterisation and cell internalisation studies conducted in the this study: Excellence in Electron Microscopy Award (June 2018), Electron Microscopy Core (EMC) and Office of Research, University of Missouri, Columbia, MO.

Table of Contents

Chapter 1 1

1. Introduction 1

1.1 Nanotechnology 1

1.2 Nanoparticles 1

1.3 Gold nanoparticles 1

1.3.1 Historical overview of gold nanoparticles 2

1.3.2 Unique optical properties of gold nanoparticles 4

1.3.3 Gold nanoparticle synthesis 5

1.3.3.1 Conventional synthesis 5

1.3.3.2 Green Synthesis 6

1.3.4 Gold nanoparticles in nano-medicine 8

1.3.5 Gold nanoparticles in cancer therapy 9

1.3.5.1 Tumour imaging 9

1.3.5.2 Photo-thermal therapy 10

1.3.5.3 Tumour radio sensitization 11

1.3.5.4 Drug delivery agents 13

1.4 Overview of the male reproductive system 14

1.4.1 The testes 15

1.4.2 Cell types of the testes 15

1.4.2.1 Sertoli cells 16

1.4.2.2 Leydig cells 17
1.4.3 The prostate gland 19
1.4.3.1 Histology of the prostate 22
1.4.3.2 Age related changes in the prostate 23
1.4.3.3 Prostatitis 23
1.4.3.4 Benign prostatic hyperplasia 24
1.4.3.5 Prostate cancer 26
1.4.3.6 Treatment of prostate cancer 29
1.5 Traditional medicine 31
1.5.1 Traditional medicine in Southern Africa 32
1.6 *Typha capensis* 33
1.7. Aims of the study: 38
Chapter 2 39
2.1 Chemical Supply 39
2.2 Equipment and supply 43
2.3 Study design. 44
2.3.1 Part A: Gold nanoparticle Synthesis and Characterisation 44
2.3.2 Part B: *In vitro* studies 44
2.3.3 Part C: *In vivo* study 45
2.4 Plant extract 45
2.4.1 Rhizome collection 45
2.4.2 Extract preparation 45

2.5 Gold nanoparticle synthesis 46
2.5.1 *T. capensis* extract-Sample 1 gold nanoparticles (S1-AuNP's and S1x2-AuNP's). 46
2.5.2 *T. capensis extract*-Sample 2 gold nanoparticles (S2-AuNP's and S2x2-AuNP's). 46
2.5.3 Naringenin gold nanoparticles (Ng-AuNP's pH7 and Ng-AuNP's pH8). 47
2.6 Gold nanoparticle characterization 47
2.6.1 Spectrophotometry 47
2.6.2 Dynamic light scattering 48
2.6.3 Zeta potential 48
2.6.4 Transmission Electron Microscopy (TEM) and size distribution. 49
2.6.5 Total polyphenolic quantification 49
2.6.5.1 Gallic acid standard curve 50
2.6.6 LC-MRM analysis of extracts and nanoparticles 51
2.6.6.1 Sample preparation and standard curve 51
2.6.6.2 Analytical method 52
2.6.6.3 Quantification of quercetin and naringenin 52
2.6.7 Gold content analysis 53
2.7 Gold nanoparticle stability in challenging media 53
2.8 *In vitro* studies 54
2.8.1 Cell culture 54
2.8.1.1 LNCaP prostate cancer cell line 55
2.8.1.2 PC-3 prostate cancer cell line 55
2.8.1.3 PANC 1 pancreatic cancer cell line 55

2.8.1.4 HAEC human aortic endothelial cell line 56
2.8.2 Culture of LNCaP cells 56
2.8.3 Culture of PC-3 cells 56
2.8.4 Culture of PANC 1 cells 57
2.8.5 Culture of HAEC cells 58
2.8.6 Cell counting and seeding 58
2.8.7 Cell freezing 59
2.8.7.1 LNCaP cells 59
2.8.7.2 PC-3 cells 59
2.8.7.3 PANC 1 cells 60
2.8.7.4 HAEC cells 60
2.8.8 Cell thawing 61
2.8.8.1 LNCaP cells 61
2.8.8.2 PC-3 cells 61
2.8.8.3 PANC 1 cells 61
2.8.8.4 HAEC cells 62
2.8.9 Test parameters 62
2.8.9.1 Determination of cell viability 62
2.8.9.2 LNCaP cell viability 63
2.8.9.3 PC-3 cell viability 64
2.8.9.4 PANC 1 cell viability 64
2.8.9.5 HAEC cell viability 64

2.8.10 Cell internalisation of nanoparticles by hyperspectral dark field microscopy 65
2.8.10.1 LNCaP cell internalisation by Dark-field microscopy 66
2.8.10.2 PC-3 cell internalisation by Dark-field microscopy 67
2.8.11 Cell internalisation of nanoparticles by transmission electron microscopy (TEM) .. 67
2.9 *In vivo* experiments 68
2.9.1 Prostate cancer tumour xenograft studies 68
2.10 Statistical Analysis 70
Chapter 3 71
3. Results 71
3.1 Gold nanoparticle characterisation 71
3.1.1 Gold nanoparticle synthesis 71
3.1.2 Ultraviolet spectroscopy 72
3.1.3 Dynamic light scattering (DLS) 73
3.1.3.1 S1-nanoparticles 73
3.1.3.2 S2-nanoparticles 74
3.1.3.3 Naringenin-nanoparticles 75
3.1.3.4 DLS and PDI summary 76
3.1.4 Zeta potential 77
3.1.4.1 S1-nanoparticles 77
3.1.4.2 S2-nanoparticles 78
3.1.4.3 Naringenin nanoparticles 79
3.1.4.4 Zeta potential summary 80

3.1.5 Transmission electron microscopy 80
3.1.6 Size distribution histograms 82
3.1.6.1 S1-nanoparticles 82
3.1.6.2 S2-nanoparticles 83
3.1.6.3 Naringenin-nanoparticles 84
3.1.7 Total polyphenolic quantification 85
3.1.8 LC-MRM analysis 86
3.1.9 Gold content analysis 87
3.1.10 Gold nanoparticle stability in challenging media 87
3.1.10.1 S1-AuNP's and S1x2-AuNP's 87
3.1.10.2 S2-AuNP's and S2x2-AuNP's 90
3.1.10.3 Ng-AuNPs pH 7 and Ng-AuNP's pH 8 93
3.2 Cell Viability 96
3.2.1 PC-3 cell viability 96
3.2.1.1 S1-AuNP's and S1 extract 96
3.2.1.2 S1x2-AuNP's and S1 extract 102
3.2.1.3 S2-AuNP's and S2 extract 108
3.2.1.4 S2x2-AuNP's and S2 extract 114
3.2.1.5 Ng-AuNP's pH 7 and naringenin 120
3.2.1.6 Ng-AuNP's pH 8 and naringenin 126
3.2.2 LNCaP cell viability 132
3.2.2.1 S1-AuNP's and Extract 132

3.2.2.2 S1x2-AuNP's and Extract 138
3.2.2.3 S2-AuNP's and S2 Extract 144
3.2.2.4 S2x2-AuNP's and S2 Extract 150
3.2.2.5 Ng-AuNP's pH 7 and naringenin 156
3.2.2.6 Ng-AuNP's pH 8 and naringenin 162
3.2.3 Panc1 cell viability 168
3.2.3.1 S1-AuNP's and Extracts 168
3.2.3.2 S1x2-AuNP's and Extracts 174
3.2.3.3 S2-AuNP's and S2 extract 180
3.2.3.4 S2x2-AuNP's and S2 extract 186
3.2.3.5 Ng-AuNP's pH 7 and naringenin 192
3.2.3.6 Ng-AuNP's pH 8 and naringenin 198
3.2.4 HAEC cell viability 204
3.2.4.1 S1-AuNP's and extract 204
3.2.4.2 S1x2-AuNP's and extract 210
3.2.4.3 S2-AuNP's and S2 extract 216
3.2.4.4 S2x2-AuNP's and S2 extract 222
3.2.4.5 Ng-AuNP's pH 7 and naringenin 228
3.2.4.6 Ng-AuNP's pH 8 and naringenin 234
3.3 AuNP-cell internalisation by Dark-field microscopy (Cytoviva) 240
3.3.1 PC-3 Cells 240
3.3.1.1 S1-AuNP's 240

3.3.1.2 S2-AuNP's 242

3.3.1.3 Ng-AuNP's pH 8 244

3.3.2 LNCaP Cells 246

3.3.2.1 S1-AuNP's 246

3.3.2.2 S2-AuNP's 248

3.3.2.3 Ng-AuNP's pH 8 250

3.4 PC-3 cell AuNP internalisation by transmission electron microscopy (TEM) 252

3.4.1 S1-AuNP's 50 µg/ml 252

3.4.2 S1-AuNP's 100 µg/ml 253

3.4.3 Ng-AuNP's pH 8 50 µg/ml 254

3.4.4 Ng-AuNP's pH 8 100 µg/ml 255

3.5 *In vivo* studies 256

3.5.1 Change in Tumour Volume 256

3.5.2 Change in bodyweight 262

3.5.3 Blood analysis 265

3.5.4 Neutrophil-Lymphocyte ratio 268

Chapter 4 270

4. Discussion 270

4.1 Gold nanoparticle synthesis and characterisation 270

4.1.1 Introduction: 270

4.1.2 Gold nanoparticle synthesis 270

4.1.3 Characterisation of gold nanoparticles 275

4.1.3.1 Presence of gold nanoparticles 276

4.1.3.2 Size and size distribution 277

4.1.3.3 DLS measurements 277

4.1.3.4 TEM imaging and size distribution analysis 279

4.1.3.5 Zeta potential 281

4.1.4 Phenolic quantification 284

4.1.5 Stability studies 285

4.2. *In vitro* studies 288

4.2.1 LNCaP and PC-3 cell viability and gold nanoparticle uptake 288

4.2.1.1 Extracts, S1-AuNPs, S1x2-AuNP's, S2-AuNP's, and S2x2-AuNP's. 288

4.2.1.2 Naringenin, Ng-AuNP's pH 7, and Ng-AuNP's pH 8 293

4.2.2 Panc1 cell viability 297

4.2.3 HAEC cell viability 301

4.3 *In vivo* studies 308

4.3.1 Change in tumour volume 309

4.3.2 Change in bodyweight 315

4.3.3 Blood analysis 318

4. Conclusion 323

Chapter 5 325

5. References 325

Key words

Typha capensis (*T. capensis*)

Cytotoxicity

Viability

Quercetin

Naringenin

AuNP's (Gold nanoparticles)

LNCaP (Prostate cancer cells)

PC-3 (Prostate cancer cells)

Panc1 (Pancreatic cancer cells)

HAEC (Human aortic endothelial cells)

Abstract

Introduction

Typha capensis (*T. capensis*), commonly known as bulrush, is a medicinal plant found growing in the wetland areas of South Africa. In traditional medicine, rhizome decoctions of *T. capensis* are used to treat a wide variety of ailments, including venereal disease, dysentery, diarrhoea and low libido in men. Previously, *T. capensis* rhizomes were shown to be a rich source of antioxidants, such as catechin and epicatechin, inhibiting both reactive oxygen species and reactive nitrogen species. The antioxidant capacity of such plant species serves as a reservoir of electrons to transport them into gold salt for the production of gold nanoparticles through green nanotechnology. Therefore, this study aimed to investigate the application of *T. capensis* in green nanotechnology and nano-medicine.

Material and methods

This study investigated the synthesis of gold nanoparticles (AuNP's) from two aqueous *T. capensis* extracts, the S1 and S2 extracts, along with the bioactive compound naringenin. The following parameters were used for AuNP characterisation: spectrophotometry, dynamic light scattering, zeta potential, transmission electron microscopy (TEM), Folin-ciocalteu phenol assay, inductively coupled plasma mass spectrometry (ICP-MS). Hereafter, the effects of these AuNP's were investigated toward the LNCaP and PC-3 prostate cancer, Panc1 pancreatic cancer, and HAEC human aortic endothelial cell lines over 24, 48 and 72 hours. Additionally, possible AuNP cell internalisation was investigated in the LNCaP and PC-3 cells by dark field hyperspectral microscopy, and definitive AuNP-cell internalisation in PC-3 cells by TEM imaging. Finally, selected AuNP's, along with the S1 extract and naringenin, were investigated *in vivo* using SCID-mice bearing PC-3 prostate cancer tumour xenografts.

Results

Aqueous *T. capensis* rhizome extracts produced AuNP's in a single step reaction, yielding the S1-AuNP's, S1x2-AuNP's, S2-AuNP's and S2x2-AuNP's. Similarly, the isolated bioactive compound naringenin also produced AuNP's when the reaction was controlled at pH 7 and pH 8, yielding the Ng-AuNPs pH 7 and Ng-AuNP's pH 8. These particles proved to be highly stable, showing no agglomeration over time. The extracts, naringenin, and their subsequent AuNPs yielded comparable levels of toxicity toward the LNCaP cells at each time point. Compared to the S1 extract, the S1-AuNP's yielded significantly ($P=0.0001$, $P=0.0004$, $P<0.0001$) greater reduction in PC-3 cell viability at the highest concentration used, over each time point. Similarly, the highest concentration of the S2-AuNP's produced significantly ($P=0.0319$, $P=0.0006$, $P=0.0003$) greater reductions in PC-3 cell viability at each time point in comparison to the S2 extract. The highest concentration of the Ng-AuNP's pH 8 were also found to yield significantly ($P=0.0009$, $P=0.0002$, $P=0.0125$) greater reductions in PC-3 cell viability over each time point. The S1-AuNP's, S1x2-AuNP's, S2-AuNP's, S2x2-AuNP's, Ng-AuNP's pH 7 and Ng-AuNP's pH 8 yielded improved toxicity toward Panc1 cells in both a dose- and time-dependent manner. However, each AuNP formulation, along with their extract or bioactive compound counterpart, produced a degree of dose and time-dependent toxicity toward the non-cancerous HAEC cell line.

Under *in vivo* conditions, the S1 extract and S1-AuNP's were well tolerated by SCID-mice bearing PC-3 prostate cancer tumour xenografts, with 1.5 mg/kg of the S1-AuNPs significantly ($P=0.0027$) inhibiting tumour growth by the end of the study. Additionally, 1.5 mg/kg of the S1-AuNP's yielded a significantly ($P=0.0339$) lowered neutrophil to lymphocyte ratio by the end of the study. Similarly, naringenin at a dose of 0.5 mg/kg, and the Ng-AuNPs pH 8 at 0.5 and 1.5 mg/kg significantly ($P=0.0038$, $P=0.0038$, $P=0.006$) inhibited tumour growth, and greatly improved bodyweight by the end of the study.

Conclusion

In summary, the collected data showthat highly stable gold nanoparticles, encapsulated with a plethora of phytochemicals from both *Typha capensis* and the bioactive compound naringenin, have been synthesized through a single step process. These nanoparticles exhibited robust stability under *in vitro* conditions and clear signs of cell internalisation, observed using dark-field microscopy and TEM. When compared to the effects of the extracts, similar levels of toxicity were observed in the case of the LNCaP and PC-3 cells. However, these nanoparticles were found to yield improved toxicity toward Panc1 cells in both a dose- and time-dependent manner. Furthermore, the present study demonstrated for the first time the positive therapeutic effects of *T. capensis* extract toward prostate cancer under *in vivo* conditions, adding a degree of validity to its clinical usage suggested by Ilfergane (2016). However, these positive effects were not found to be improved, nor maintained, by nano-encapsulation of the extract. The Ng-AuNP's, however, were able to maintain the anti-cancer effects of free naringenin under *in vivo* conditions, having favourable outcomes toward tumour growth, body weight and blood parameters in tumour-bearing SCID-mice

.

Chapter 1

Introduction

1.1 Nanotechnology

Nanotechnology refers to the branch of science dedicated to studying and controlling molecules at the nano-meter scale (10^{-9}) in one or more dimensions, with the ultimate goal of gaining control of structures and devices at the atomic, molecular and supramolecular level (Mansoori and Soelaiman 2005; Wong et al. 2013; Krishna et al. 2018). Being a rapidly developing field, nanotechnology has been applied to various different areas including contaminant and heavy metal removal, imaging, antimicrobial research, bio-sensors and the realm of cancer therapeutics (Mody et al. 2010; Babu et al. 2013; Lee et al. 2014; Krishna et al. 2018).

1.2 Nanoparticles

A common definition of nanoparticles are structures ranging between 1-100 nano-meters (nm), which often possess properties significantly different from the bulk material used to create them (Hasan 2015). Many different types of nanoparticles exist, ranging from those synthesised from metals such as gold and silver nanoparticles (Mody et al. 2010; Hasan 2015), nanoparticles synthesised from organic or synthetic lipids, such as liposomes (Shapley and Mello 2011; Bhatia 2016), and polymeric nanoparticles synthesised from biodegradable or biocompatible polymers (Shapley and Mello 2011; Bhatia 2016).

1.3 Gold nanoparticles

Gold nanoparticles, otherwise known as colloidal gold, occur as a suspension of nano-meter-sized particles of gold that can occur in different shapes, such as spheres, stars, cubes and rods, have different sizes and possess varying degrees of surface charges, known as zeta-potential (Mody et al. 2010)

1.3.1 Historical overview of gold nanoparticles

Gold has been revered by many civilisations who held it in high regard, considering it a highly valuable substance, having significant decorative and medicinal applications. As far back as the 5th century BC, colloidal gold was considered to have medicinal properties and was highly sought after by Chinese, Arabian and Indian civilisations (Sharma et al. 2009; Sajanlal and Pradeep 2012). An example of this would be the medicinal tonic preparations known as saraswatharishtan and makarandwajan used in the Indian system of medicine known as Ayurveda (Sharma et al. 2009; Sajanlal and Pradeep 2012). Another example is the medicinal use of colloidal gold in Europe during the middle-ages as a treatment for many ailments including diarrhoea, epilepsy, syphilis, plague and leprosy (Daraee et al. 2016). Furthermore, colloidal gold was also highly revered for its decorative properties.

During the 4th century AD, gold colloids were produced by combining molten glass and gold salts to produce a ruby-red colour, variations of which were used for decorative staining of glassware, pottery and various ceramics (Sajanlal and Pradeep 2012). Notable examples of this include the Lycarus cup (Figure 1.1), which has the unique ability to appear either green or ruby-red depending on whether reflected light or transmitted light falls upon it (Sajanlal and Pradeep 2012; Amendola et al. 2017). The "purple of Cassius" used to colour glassware red-ruby during the middle ages, and lustre plates produced during the 15-16th century (Amendola et al. 2017). Subsequently, the fascinating features of the Lycarus cup and many other glassware and pottery decoratively stained using colloidal gold, ultimately sparked a more in-depth understanding of gold colloids, beginning with the work of Michael Faraday (Sharma et al. 2009; Sajanlal and Pradeep 2012; Amendola et al. 2017) .

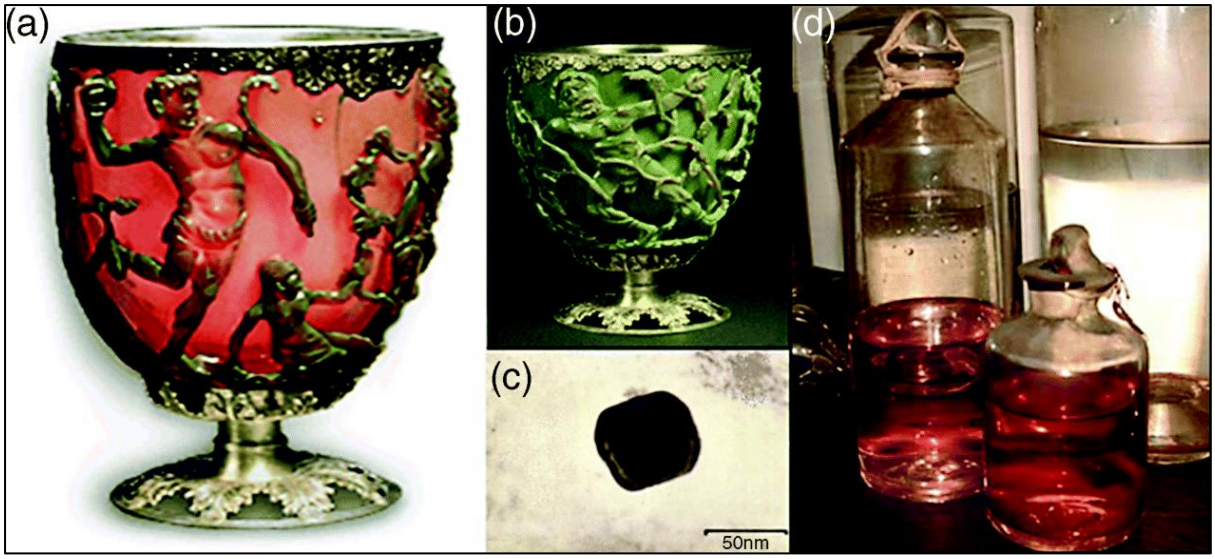

Figure 1.1: Photographical representation of the Lycarus cup appearing red under transmitted light (A), green under reflected light (B), transmission electron microscopy of nanoparticles found within the glass of the Lycarus cup (C), and preserved samples of Faraday's gold (D). Image generated by and excerpted from (Sajanlal and Pradeep 2012)

During the 1850's, a more intimate understanding of colloidal gold began to develop when Michael Faraday, fascinated by gold-stained glassware, studied the relationship between light and gold particles (Thompson 2008; Sajanlal and Pradeep 2012). In his experiments, he observed that when a gold salt, such as sodium tetrachloroaurate, was chemically reduced with a mixture of phosphorous and carbon disulphide, an intense colour shift consistent with the presence of colloidal gold was produced, specifically a shift from bright yellow to deep ruby (Edwards and Thomas 2007; Thompson 2008; Sharma et al. 2009). Based on his observations, he concluded that "finely divided" particles of gold existed within the solution, whose presence was observable by a red-coloured opalescence upon being bombarded by a narrow beam of light. Furthermore, he was arguably the first to conclude that clear differences existed between the properties of bulk and colloidal gold (Edwards and Thomas 2007; Thompson 2008). Nearly a century late, after the advent of electron

microscopy, it was revealed that Faraday had indeed produced highly stable gold nanoparticles in the range of 6 nm (Thompson 2008).

These important first steps went on to inspire many other scientists, such as Richard Adolf Zsigmondy, who combined his own synthesis procedure with that of Faraday's in what is now known as the "seed-mediated" synthesis method. Further contributions to gold nanoparticle synthesis, along with size and shape mediated mobility, were provided by Theodor Svedberg, and the theoretical work delving into the unique optical properties of gold nanoparticles by Gustav Mie (Sharma et al. 2009; Amendola et al. 2017).

1.3.2 Unique optical properties of gold nanoparticles

Presently, the unique relationship between gold nanoparticles and light is more thoroughly understood. When the electromagnetic field of light interacts with metallic nanoparticles, free electrons across the particle surface begin to oscillate in relation to the metal lattice, which ultimately resonates at a specific wavelength of light, thereby creating what is known as the surface plasmon resonance (SPR) (Mody et al. 2010; Amendola et al. 2017; Elahi et al. 2018). In the case of gold nanoparticles solutions, it is common to observe a range of colours, such as orange, red, ruby and purple, often exhibiting absorption maximums in the in the 500 to 600 nm range (Homberger and Simon 2010; Mody et al. 2010; Elahi et al. 2018). An example would be the characteristic absorption maximum at 520 nm for spherically shaped gold nanoparticles, with an average core size of 10 nm (Mody et al. 2010).

Many factors can influence the intensity and specific wavelength of the SPR, such as the size, shape, structure and composition of nanoparticles (Mody et al. 2010; Elahi et al. 2018). Notable examples include a direct relationship between the size of gold nanoparticles and the intensity of the SPR, whereby an increase in gold nanoparticle core size results in a shift of the SPR wavelength, subsequently increasing the absorption maximum and altering the observed colour of the gold

nanoparticle solution (Homberger and Simon 2010; Mody et al. 2010b; Elahi et al. 2018). Specifically, the observed colour of the gold nanoparticle suspension may shift from shades of orange, to red, and eventually to purple with a stepwise increase of core size, along with shifting absorption maximums from 500-550 nm, respectively (Mody et al. 2010; Elahi et al. 2018). Unsurprisingly, the unique optical properties of gold nanoparticles has yielded extensive research and applications in biological imaging, biomedical sciences, material sciences and electronics (Mody et al. 2010; Daraee et al. 2016; Elahi et al. 2018).

1.3.3 Gold nanoparticle synthesis

1.3.3.1 Conventional synthesis

Many different methods to synthesise gold nanoparticles exist, however they all generally fall within one of two categories. Namely, methods for gold nanoparticle synthesis either follows what is known as a "top-down" approach or a "bottom-up" approach (Shah et al. 2014). Top-down methods of gold nanoparticle synthesis involve the removal of matter from bulk material in order to assemble the desired nanostructure. In comparison, bottom-up approaches to gold nanoparticle synthesis involved the assembly of atoms into the desired nanostructure, which is usually accomplished by the reduction of ions. Generally speaking, bottom-up approaches are more favourable and have been extensively utilised. Notable examples include the Turkevich method, Brust method, and biological (Green) methods of synthesis(Shah et al. 2014; Elahi et al. 2018).

In 1951, a procedure for the synthesis of spherically shaped gold nanoparticles, known as the Turkevich method, was developed and has been one of the most commonly used methods ever since (Turkevich et al. 1951). Briefly, the Turkevish method involves the reduction of gold ions to gold atoms in the presence of a reducing agent; the most common of which is sodium citrate. Gold nanoparticles synthesised using this method often range between 10-20 nm, and their size is generally controlled using various capping or stabilising agents (Turkevich et al. 1951; Shah et al.

2014). Continuous modifications and advancements to the original method described by Turkevich has allowed for a greater range of gold nanoparticles sizes, specifically between 16-145 nm, along with improved understanding regarding the role of sodium citrate, pH and temperature during synthesis (Kimling et al. 2006; Shah et al. 2014; Dobrowolska et al. 2015). Another popular method for gold nanoparticle synthesis, first described in 1994, is known as the Brust method (Brust et al. 1994). In short, this method and involves transferring a gold salt from an aqueous solution to an organic solvent by means of a phase transfer agent, after which the gold salt is reduced by sodium borohydride in the presence of alkanethiols, which are responsible for stabilising the gold nanoparticles (Brust et al. 1994; Shah et al. 2014).

1.3.3.2 Green Synthesis

The major drawback to conventional nanoparticle synthesis methods are the requirement for, or generation, of toxic by-products that may have long-lasting environmental impacts, especially during large-scale production (De la Guardia 2014; Shah et al. 2014; Parveen et al. 2016). Furthermore, the use of toxic chemicals may prove problematic and pose potential down-stream health risks when biomedical applications are concerned. Thus, strategies avoiding the use of toxic chemicals were highly sought after, leading to the emergence of green nanotechnology.

The field of green nanotechnology, pioneered by the director of the Institute of Green Nanotechnology at the University of Missouri; Prof. Kattesh Katti, embraces the ideals of "green" chemistry. This emphasises the use of non-toxic chemicals, using easily biodegradable reagents, severely limiting waste by-products and cost, earning him global recognition as "the father of green nanotechnology" (Shah et al. 2014; Parveen et al. 2016; Barabadi et al. 2017). In short, the process involves mixing gold salt, such as $NaAuCl_4$, with a plant extract or isolated plant-derived compound under specific reaction conditions such as pH, temperature and incubation time. This method utilises plant phytochemicals and bio-components found in extracts as reducing agents to drive the chemical

reaction, and capping agents to stabilise the gold nanoparticles during the synthesis (Kannan et al. 2006; Shukla et al. 2008; Katti et al. 2009; Elia et al. 2014b; Shah et al. 2014; Parveen et al. 2016; Barabadi et al. 2017)

To date, the research team led by Prof. Kattesh Katti has made a number of significant contributions to the field of green nanotechnology and the emergence of the field known as nano-medicine. For example, early work clearly outlined the role of phytochemicals in the synthesis of biocompatible gold nanoparticles by utilising phytochemicals derived from various plants, including cumin (Katti et al. 2009), soybeans (Shukla et al. 2008), tea (Nune et al. 2009a), and cinnamon (Chanda et al. 2011). Since then, a number of highly stable and biocompatible gold nanoparticles conforming to "green chemistry" have been developed under his supervision with an intended usage as nano-medicines. These include the gold nanoparticles synthesised using broccoli-derived phytochemicals, which displayed cytotoxicity toward breast cancer, prostate cancer PC-3 cells, myeloma U266 cells, along with breast cancer SkBr3, MDA-MB-231 and t47D cells (Khoobchandani et al. 2013). Another example are the epigallocatechin-3-gallate conjugated gold nanoparticles that were shown to have potential application as an alternative to drug-coated stents in the treatment of cardiovascular disease (Khoobchandani et al. 2016). Most recently, his team developed gold nanoparticles synthesised from resveratrol, a polyphenol commonly found in red wine, which were shown to have promising cytotoxic, and potential anti-angiogenic effects toward the prostate cancer PC-3, pancreatic cancer PANC-1, and breast cancer MDA-MB-231 cells (Thipe et al. 2019).

Based on the continual pioneering work by Prof. Kattesh Katti and his research team, a number of gold nanoparticles synthesised from plants and their extracts have been investigated for application in the emerging field known as nano-medicine (Ramezani et al. 2008; Elia et al. 2014a; Noruzi 2015; Elbagory et al. 2016; Barabadi et al. 2017).

1.3.4 Gold nanoparticles in nano-medicine

New technologies and devices are continuously being developed at the nano-scale with the goal of improving diagnostics and therapeutics in an emerging field known as nano-medicine (Xu et al. 2015; Mendes et al. 2017). This branch of nanotechnology allows for the control and manipulation of matter, such as shape and size, at nano-meter range, thereby allowing for the design, characterisation, production, and application of new structures, devices, and systems.

Nano-scale materials are vastly different to their bulk counterparts with lengths that range from 1 to 100 nm in two or three dimensions as described by the American Society for Testing and Materials (ASTM) (Conde 2015; Mendes et al. 2017).

To date, the primary focal point of nano-medicine has been improving conventional medicines by combining them with new biocompatible therapeutic agents, such as nanoparticles, thereby enabling new administration strategies and diagnostics platforms (Parveen et al. 2012; Mendes et al. 2017). The use of these structures carries a number of advantages, such as the large surface area to volume ratio exhibited by nanoparticles, which may be utilised for functionalisation with various biomolecules on the same platform, thereby enabling targeting capabilities in various forms of therapeutics (Pedrosa et al. 2015; Mendes et al. 2016; Mendes et al. 2017). In the realm of cancer therapeutics, a number of nanoparticles have been developed and utilised, including liposomes and dendrimers, along with silver, iron oxide and gold nanoparticles (Mendes et al. 2017).

Gold nanoparticles have multiple unique physical and chemical attributes, which allow for various types of biomedical applications, such as detection and diagnostics, drug delivery and biological sensing, to name a few (Babu et al. 2013; Das et al. 2014; Elahi et al. 2018). More specifically, the true value of gold nanoparticle in biomedical application lies within their excellent biocompatibility, low toxicity and large surface area to volume ratio (Mody et al. 2010; Elahi et al. 2018). Due to their unique optical properties, gold nanoparticles have been become favourable agents for use in photo-thermal therapy, a minimally invasive technique whereby localised heat is generated by

bombarding the nanoparticles with a laser, yielding tumour cell death (Mody et al. 2010b; Sumbayev et al. 2012; Elahi et al. 2018).

Similarly, these features have been utilised in photodynamic therapy, whereby gold nanoparticles conjugated with photodynamic dyes that have been internalised by target cells are bombarded with light of a specific wavelength, generating singlet oxygen and highly active free radicals which ultimately induce necrosis and apoptosis in tumour cells (Sumbayev et al. 2012; Elahi et al. 2018). Furthermore, the unique features of gold nanoparticle have also been employed in the production various types of biosensors for the detection of metal ions, proteins and toxins, to name a few (Sumbayev et al. 2012; Yeo et al. 2017; Elahi et al. 2018). These sensors may be based on observed colour changes due to aggregation of the nanoparticles, quenching of fluorescence, electrical conductivity and catalytic properties of gold nanoparticles (Yeo et al. 2017; Elahi et al. 2018).

1.3.5 Gold nanoparticles in cancer therapy

1.3.5.1 Tumour imaging

With regard to tumour-related surgery, one of the biggest challenges faced by surgeons is having a clearly defined idea of where tumorous tissue ends and healthy tissue begins (Menon et al. 2013; Singh et al. 2018). For example, if the extent of the tumour is overestimated, healthy tissue may be removed, but if underestimated and too little is removed, tumours may recur over time. As a result, correctly deciding the extent of tumorous tissue to be removed is of utmost importance, and currently poses a great challenge to surgeons (Menon et al. 2013; Singh et al. 2018).

To achieve this, magnetic resonance imaging and computed tomography scans have been used. However, these techniques are expensive and are limited in their ability to detect tumours smaller than a threshold of approximately 10 million cells. For this reason, photo-imaging as a novel technique for cancer imaging has emerged. This technique makes use of gold nanoparticles, which have been functionalised to be site specific, being injected into the tumour site (Menon et al. 2013;

Singh et al. 2018). Once injected, these gold nanoparticles will bind to cancer cells only and their optical properties can be exploited to scatter light, thereby giving surgeons a clear image of where the tumour begins and ends. For this purpose, the most utilised gold nanoparticles are nano-rods, nano-cages and nano-shells, as these tend exert the greatest temporal and special resolution for imaging, while also exhibited a great deal of non-reactivity under biological conditions (Menon et al. 2013; Singh et al. 2018). Furthermore, gold nanoparticles have also been utilised as high quality computed tomography (CT) imaging agents due to better X-ray attenuation properties than that of iodinated CT contrast agents, along with improved pharmacokinetics in comparison to iodinated contrast agents, allowing for better imaging (Jokerst et al. 2011).

1.3.5.2 Photo-thermal therapy

Therapies aimed at utilising temperature as a modality to reduce tumour growth initially emerged based on observations made for patients shuddering from erysipelas, who presented with high fevers, and also exhibited reduced tumour growth or tumour regression (Moyer and Delman 2008). Subsequently, researchers have investigated maintained hyper-thermic conditions, usually in the vicinity of 42ºC, at the tumour site to impede tumour growth (Vines et al. 2019). However, it is critical that the areas exposed to the hyper-thermic temperatures be contained to the tumour alone, and not to healthy tissue to prevent unwanted tissue destruction (Vines et al. 2019). Thus, nanotechnology has been investigated as a potential avenue.

Nanoparticle-based photo-thermal therapy is a technique which exploits both the excellent biocompatibility and unique optical properties of metallic nanoparticles, which allows for cancer cell to take up nanoparticles, followed by photon mediated heat induction (Mody et al. 2010b; Sumbayev et al. 2012; Elahi et al. 2018; Vines et al. 2019). In essence, this techniques allows for nanoparticles internalised by cancer cells to convert either visible or near infra-red light to heat,

thereby stimulating a hyper-thermic response at the tumour site (Mody et al. 2010b; Sumbayev et al. 2012; Elahi et al. 2018; Vines et al. 2019).

Furthermore, recent developments in the multi-functional design of gold nanoparticles allow for the generation of localised heat in the proximity of cancerous tissues and additionally allow for the delivery of multiple desired drugs in a controlled and targeted manner. Gold nanoparticles have many benefits that make them well suited to photo-thermal, including high cell-specificity, near infrared activation, easily passing through vasculature into deeper lying biological tissues, and can be modified to yield complex cancer photo-thermal and drug delivery systems (Vines et al. 2019).

1.3.5.3 Tumour radio sensitization

Radio therapy is a widely used technique in the treatment of multiple forms of cancer, including breast cancer, prostate and pancreatic cancer, and utilises X-rays, γ-rays and high energy particles to induce cancer cell death (Rosa et al. 2017; Peng and Liang 2019). However, while radio therapy is an effective form of therapy, it does not possess the ability to distinguish between cancerous and non-cancerous cells, thus leading to a great deal of systemic damage (Rosa et al. 2017; Peng and Liang 2019). Additionally, the associated toxicity toward healthy surrounding tissues severely limits the doses, which may be administered to patients (Rosa et al. 2017; Peng and Liang 2019). Consequently, developing ways of sensitising tumours to radiation, while minimising the associated toxicity, has been the focal point of a growing body of research.

It has been well established that ionizing radiation may induce both direct and indirect DNA damage. Once this occurs, repair mechanisms may no longer be sufficient to repair damaged DNA, leading to the cessation of cell division, cell death, or cellular mutations, which in turn may lead to malignant transformations (Begg et al. 2011; Kavanagh et al. 2013; Rosa et al. 2017). Thus, it is clear that the effects of radiotherapy should be limited to tumour tissue only to avoid the occurrence of these adverse effects.. Consequently, agents such as metallic nanoparticle, such as gold

nanoparticles, have been investigated to overcome these challenges, and have been found to improve the contrast between tumorous and healthy tissues, thereby opening the possibility of radio sensitisation (Regulla et al. 2002; Rosa et al. 2017). Furthermore, these properties of metallic nanoparticles may be utilised to improve tumour control, while minimising the associated side effects.

Gold nanoparticles are believed to improve radio sensitisation through biological processes. Biologically speaking, gold nanoparticles have been shown to favourably augment radio sensitisation via the induction of reactive oxygen species (ROS), subsequently leading to oxidative DNA damage (Mikami et al. 2013; Rosa et al. 2017). Another mechanism by which gold nanoparticles may improve radio sensitization is by disrupting the cell cycle, along with the induction of apoptosis. With regard to the cell cycle, different phases exhibit varying radiation sensitivity, with the S-phase cell possessing the greatest radio-resistance, while the late-G2 phase and mitosis exhibiting the greatest radio-sensitivity (Pawlik and Keyomarsi 2004; Rosa et al. 2017). When radiation is applied to cells, they respond by activating cell cycle checkpoints in the G1, S and G2 phases in an attempt to repair genomic defects, or to activate cell death mechanisms (Kastan and Bartek 2004; Rosa et al. 2017). Similarly, it has previously been shown that metallic nanoparticles, such as gold nanoparticles, also yielded cell cycle arrest in the G2 and mitotic phases in number of cells (Rosa et al. 2017), including prostate cancer DU-145 (Ganesh Kumar et al. 2015), ovarian cancer SK-OV-3 cells (Geng et al. 2011), and human oral squamous carcinoma HSC-3 cells (Mackey and El-Sayed 2014), to name a few. Thus, metallic nanoparticles have application as agents, which sensitise cells to the effects of radiation.

Additionally, DNA damage is another mechanism by which gold nanoparticles may induce radio-sensitisation (Rosa et al. 2017). Particularly, radiation has been found to induce double stranded DNA breaks, the repair of which is essential for cell survival. Considering the absolute importance of maintaining DNA integrity, particularly with regard to cellular propagation, it is an attractive

target for agents aimed at halting cancer cell division. For this reason, known cytotoxic agents targeting the DNA, such as cisplatin, have been investigated and used as radio- sensitizers (Choudhury et al. 2006; Rosa et al. 2017). Similarly, gold nanoparticles have also been reported to induce double-stranded DNA breaks, and have also shown application in radio-sensitisation, having a dose-lowering effect toward radiotherapy (Chithrani et al. 2010; McQuaid et al. 2016; Rosa et al. 2017).

1.3.5.4 Drug delivery agents

Conventionally, chemotherapeutic drugs utilise oral administration or intravenous administration as a delivery system, which leads to wide spread systemic drug accumulation with only a fraction actually reaching the target site (Bahrami et al. 2017; Singh et al. 2018). Unsurprisingly, this leads to unfavourable side effects toward otherwise heathy tissue and organs. Thus, it became of the utmost importance to achieve more targeted drug delivery systems to improve tumour site drug accumulations, along with minimising unwanted side effects (Bahrami et al. 2017; Singh et al. 2018). Subsequently, the continual strides achieved in nanotechnology has created new avenues for targeted drug delivery.

Due to their small size, nanoparticles have the ability to easily pass through capillaries and more effectively reach the tumour sites (Babu et al. 2013; Lee et al. 2014; Bahrami et al. 2017; Kong et al. 2017; Singh et al. 2018; Peng and Liang 2019). Furthermore, chemotherapeutic drugs can be loaded to nanoparticles, which may then be targeted actively or passively to the tumour site, thereby improving drug pharmacokinetics and yielding superior delivery to targeted sites, minimising non-specific side effects (Peng and Liang 2019). For example, a study conducted by Wang et al. (2011) demonstrated that intracellular doxorubicin (DOX) concentration was effectively increased in drug-resistant tumour cells by attaching DOX to gold nanoparticles via a pH-sensitive linker (Wang et al. 2011). Similarly, a study investigating the use of the anti-cancer drugs DOX and bleomycin

demonstrated improved cytotoxicity toward cervical cancer (Hela) cells upon simultaneously loading the drugs onto gold nanoparticles, in comparison to unbound drug (Farooq et al. 2018).

Gold nanoparticles in particular have been extensively investigated as drug carries due to their unique properties, such as their surface plasmon resonance, along with their optical and tuneable properties. Furthermore, these nanoparticles may be prepared at a wide variety of core sizes, thereby allowing for significantly easier control over dispersion (Bahrami et al. 2017; Kong et al. 2017; Singh et al. 2018) Additionally, the presence of a negative surface charge allow gold nanoparticles to be easily modified and functionalised with various biomolecules, including chemotherapeutic drugs, targeted ligands, and genes. Moreover, the excellent biocompatibility, high surface area to volume ration, lack of inflammatory effects, and the overall inert nature of gold nanoparticles make them ideal agents for drug delivery systems (Mody et al. 2010; Yeo et al. 2017; Elahi et al. 2018).

1.4 Overview of the male reproductive system

Characteristically, the male reproductive system is responsible for a number of functions, including the synthesis of androgen hormones, such as testosterone, along with the production, nourishment, and deposition of spermatozoa into the female genital tract.(Basu 2011; Assi et al. 2017). Testosterone is synthesised in the testes under influence of endocrine hormones, namely gonadotropin-releasing hormone (GnRH) and luteinizing hormone (LH), via the process of steroidogenesis. Moreover, testosterone is absolutely essential for male sexual differentiation, the development and maintenance of secondary male characteristics, cognitive function, emotional well-being, and fertility in men. (O'Donnell and McLachlan 2012; Wahjoepramono et al. 2016; Ali et al. 2018) To achieve this, the major reproductive organs, namely the testes, penis, ductus deference, ejaculatory ducts and epididymis, work closely together with the accessory sex glands, prostate, seminal vesicles and bulbourethral glands (Basu 2011; Assi et al. 2017).

1.4.1 The testes

Steroid synthesis and semen production are the main functions of the testes, which are suspended by the spermatic cord in the scrotum, and are considered the primary male sex glands (Basu 2011; Assi et al. 2017; Mohanty and Singh 2017). More specifically, the testes are responsible for synthesising androgens via steroidogenesis, as well as the generation of spermatozoa, the haploid male germ cells in the process called spermatogenesis (Assi et al. 2017; Mohanty and Singh 2017). Characteristically, testes are positioned obliquely in the scrotum with the upper end directed anteriorly, while the lower end is directed posteriorly and medially. Structurally, the testes consist of the convex anterior border and the flat posterior borders.

Different coverings are found in the testes, namely the tunica vaginalis, tunica albuginea and the tunica vasculosa (Basu 2011; Assi et al. 2017; Mohanty and Singh 2017). Described as a serous covering, the tunica vaginalis is derived from the sac of the peritoneum that precedes the descent of the testes. The tunica albuginea provides the dense fibrous covering of the testes, consisting of bundles of white fibrous septa which divides into proximately 200-300 lobules (Basu 2011; Assi et al. 2017). Each lobule contains tightly coiled seminiferous tubules, in which sperm are produced (Assi et al. 2017; Mohanty and Singh 2017). Finally, the tunica vasculosa consists of a plexus of blood vessels held together by areolar tissue; covering the inner surface of the tunica albuginea and the different septa in the interior of the gland (Basu 2011; Mohanty and Singh 2017).

1.4.2 Cell types of the testes

Histologically, the interstitial tissues and the seminiferous tubules are the major structures of the testes. Moreover, Sertoli cells constitute the seminiferous epithelium, while Leydig cells are located in the interstitial tissue, which occupies approximately one-fourth of the total testicular volume (Basu 2011; Mohanty and Singh 2017).

1.4.2.1 Sertoli cells

Sertoli cells are considered to act in a nurse-like manner, thereby serving a unique function in the development of germ cells (Johnson et al. 2008). More specifically, these cells play an integral role in the regulation of male fertility (Basu 2011) by providing structural support and nutrition to developing germs cells (Johnson et al. 2008), phagocytosis of degenerating germ cells and residual bodies (Johnson et al. 2008), and the release of spermatids at spermiation. Furthermore, Sertoli cells produce a number of proteins, such as transport proteins, that regulate or respond to pituitary hormone release and influence mitotic activities of spermatogonia (Walker and Cheng 2005; Basu, 2011; Galardo et al., 2014).

Transport proteins, which are secreted by Sertoli cells under the influence of follicle stimulating hormone include transferrin, lactate, ceruloplasmin and Androgen Binding Protein (APB) (Johnson et al. 2008). These transport proteins supply the germinal cells with essential elements an molecules such as Fe^{3+}, Cu^{2+},testosterone and dihydrotestosterone (DHT) (Griswold 1988; Walker and Cheng 2005). Furthermore, this transport is a crucial step in fuelling spermatogenesis, and therefore crucial for fertility (Galardo et al. 2014).

Lactate secretion is essential to maintaining the acidic environment needed inside the seminiferous tubules and to meet the energy requirements of developing germ cells (Walker and Cheng 2005; Basu 2011). Furthermore, Sertoli cells have been shown to secrete a number of proteins possessing hormonal or growth-like activities, namely inhibin, mullerian-inhibiting substance (MIS), somatomedin C, transforming growth factors alpha and beta, and stem cell growth factor (Griswold 1988; Bardin et al. 1993). Proteins with enzymatic activities, such as plasminogen activator are also secreted by Sertoli cells (Ebisch et al. 2008). Another class of proteins secreted by Sertoli cells are those contributing to the basement membrane (Griswold 1988; Bardin et al. 1993) such as type IV collagen and laminin. Additionally, Sertoli cells form an essential structure known as the blood-testis barrier (Assi et al. 2017).

The blood-testis barrier is formed by tight junctions between adjacent Sertoli cells, creating a physical barrier which compartmentalises seminiferous epithelium into the basal and adluminal compartments (Bardin et al. 1993; Basu 2011; Assi et al. 2017). Functionally, this barrier limits the para-cellular movement of substances, such as water, electrolytes, ions, nutrients, hormones, paracrine factors, and biological molecules, across the into the adluminal compartment (Chen and Mruk 2012; Assi et al. 2017). Furthermore, this barrier regulates the movement of potentially harmful substances, such as drugs, environmental toxicants and chemicals, into the adluminal compartment (Chen and Mruk 2012), and in this manner creating a unique microenvironment for post-meiotic spermatid development (Basu 2011; Chen and Mruk 2012; Assi et al. 2017).

Specifically, the key feature of this unique environment is the creation of an physiological and immunologic barrier (Bardin et al. 1993), thereby isolating spermatocytes and spermatids from the immune system (Basu 2011; Assi et al. 2017; Mohanty and Singh 2017). Without this absolute isolation, the production of anti-sperm antibodies becomes a likely scenario, in turn leading to an autoimmune response and sperm cell destruction (Bardin et al. 1993; Basu 2011; Assi et al. 2017). An autoimmune response of this nature can lead to male infertility (Bardin et al. 1993; Basu 2011; Assi et al. 2017; Mohanty and Singh 2017). In addition to this barrier, Sertoli cells have been shown to secrete immunosuppressive molecules to block immune responses, to transiently expressed auto-antigens in developing germ cells, thereby working to maintain the immune-privileged nature of the testis (Chen and Mruk 2012; Mohanty and Singh 2017).

1.4.2.2 Leydig cells

Leydig cells are the primary cells of the interstitium, located adjacent to the seminiferous tubules. These cells are characteristically rich in smooth endoplasmic reticulum and mitochondria (Weinbauer et al. 2010; Assi et al. 2017) and a number of important cytoplasmic components, namely lipofuscin granules and lipid droplets, which are the final product of endocytosis and

lysosomal degradation and contain intermediate products of the testosterone synthesis, respectively (Weinbauer et al. 2010; Assi et al. 2017; Mohanty and Singh 2017). Moreover, Leydig cells often contain Reinke's crystals, which are special formations thought to be subunits of globular proteins (Weinbauer et al. 2010; Assi et al. 2017; Mohanty and Singh 2017).

Leydig cells have a characteristically low rate of proliferation, which occurs under the influence of luteinizing hormone (LH) (Weinbauer et al. 2010; Basu 2011; Assi et al. 2017; Mohanty and Singh 2017). Additionally, when Leydig cells are under the influence of LH, they act as the central site of testosterone production via the hypothalamic-pituitary-gonadal (HPG) axis (Ge et al. 2008; Weinbauer et al. 2010; Basu 2011; Assi et al. 2017). More specifically, secretions from the hypothalamus, namely gonadotropin-releasing hormone (GnRH), cause the anterior pituitary to produce LH and follicle stimulating hormone (FSH) (Weinbauer et al. 2010; Assi et al. 2017; Mohanty and Singh 2017). LH stimulates Leydig cells to synthesise testosterone, which in turn creates a negative feedback loop in which testosterone inhibits the frequency and amplitude of hypothalamic and anterior pituitary secretions (Weinbauer et al. 2010; Assi et al. 2017; Mohanty and Singh 2017).

Testosterone is an androgen pivotal to maintaining fertility in men, as it is the primary driver of spermatogenesis, and to maintain secondary male characteristics (Ge et al. 2008; Basu 2011). Testosterone deficiency is commonly associated with men over the age of 40 (Feldman et al. 2002; Wu et al. 2010; Davidiuk and Broderick 2016; Dudek et al. 2017). Termed late-onset hypogonadism, sometimes androgen-deficiency syndrome, (Wu et al. 2010; Davidiuk and Broderick 2016; Dudek et al. 2017), is the age-associated decrease in testosterone is considered an indicator of natural male ageing, accounting for a decrease of the serum testosterone concentration of about 1% each year (Feldman et al. 2002; Davidiuk and Broderick 2016). Late-onset hypogonadism can occur as the result of primary or secondary causes, or as a combination of the two, particularly in men with long-term systemic diseases such as cirrhosis or chronic kidney

disease (Wu et al. 2010; Dudek et al. 2017) and is associated with deleterious consequences. These include; a decrease in lean muscle mass, a sharp increase in total body fat mass, and a decrease in muscle strength (Taher 2005; Snyder 2009; Davidiuk and Broderick 2016; Dudek et al. 2017). However, testosterone therapy has been shown to be effective in treating those suffering from late-onset hypogonadism (Hohl et al. 2009; Snyder 2009; Morgentaler et al. 2011; Davidiuk and Broderick 2016). This therapy is aimed at raising testosterone concentrations to approximate natural levels with the ultimate goal of improving quality of life (Bassil et al. 2009; Ullah et al. 2014; Corona et al. 2017; Elliott et al. 2017; Tsametis and Isidori 2018). Conventionally, several types of testosterone replacement therapy exist, namely tablets, injections, transdermal systems, pellets, and buccal preparations of testosterone (Bassil et al. 2009; Ullah et al. 2014; Elliott et al. 2017). Unfortunately, the high cost and large number of adverse effects attributed to conventional testosterone replacement therapy, including an increased risk of prostate cancer, worsening of symptoms of benign prostatic hyperplasia, liver toxicity, sleep apnoea, congestive heart failure, gynecomastia and skin disease, highlight the necessity for cheaper, more accessible, and safer methods of testosterone replacement therapy (Bassil et al. 2009; Ullah et al. 2014; Corona et al. 2017; Tsametis and Isidori 2018).

1.4.3 The prostate gland

Typically, the prostate gland develops during the third month of gestation from epithelial invaginations derived from the posterior urogenital sinus, and under the influence of the underlying mesenchyme and the hormone dihydrotestosterone (DHT) (Hammerich et al. 2008). DHT is synthesised from foetal testosterone by the action of the 5α-reductase localised in the urogenital sinus and external genitalia, and without which abnormal genital and prostatic development would occur (Hammerich et al. 2008). Following foetal development, the prostate remains relatively

unchanged until puberty, during which time certain morphological changes occur yielding the adult phenotype (Hammerich et al. 2008).

Being triangular in shape, the adult prostate is often described as having a walnut-like appearance, with an approximate weight of 20 grams in healthy males between 25-30 years of age (Hammerich et al. 2008; Aaron et al. 2016). It is located in the abdominal cavity around the neck of the urinary bladder and consists of four regions; namely the peripheral zone, central zone, transitional zone, and the anterior fibromuscular stroma (Figure1.2) (Burden et al. 2006; Hammerich et al. 2008; Aaron et al. 2016).

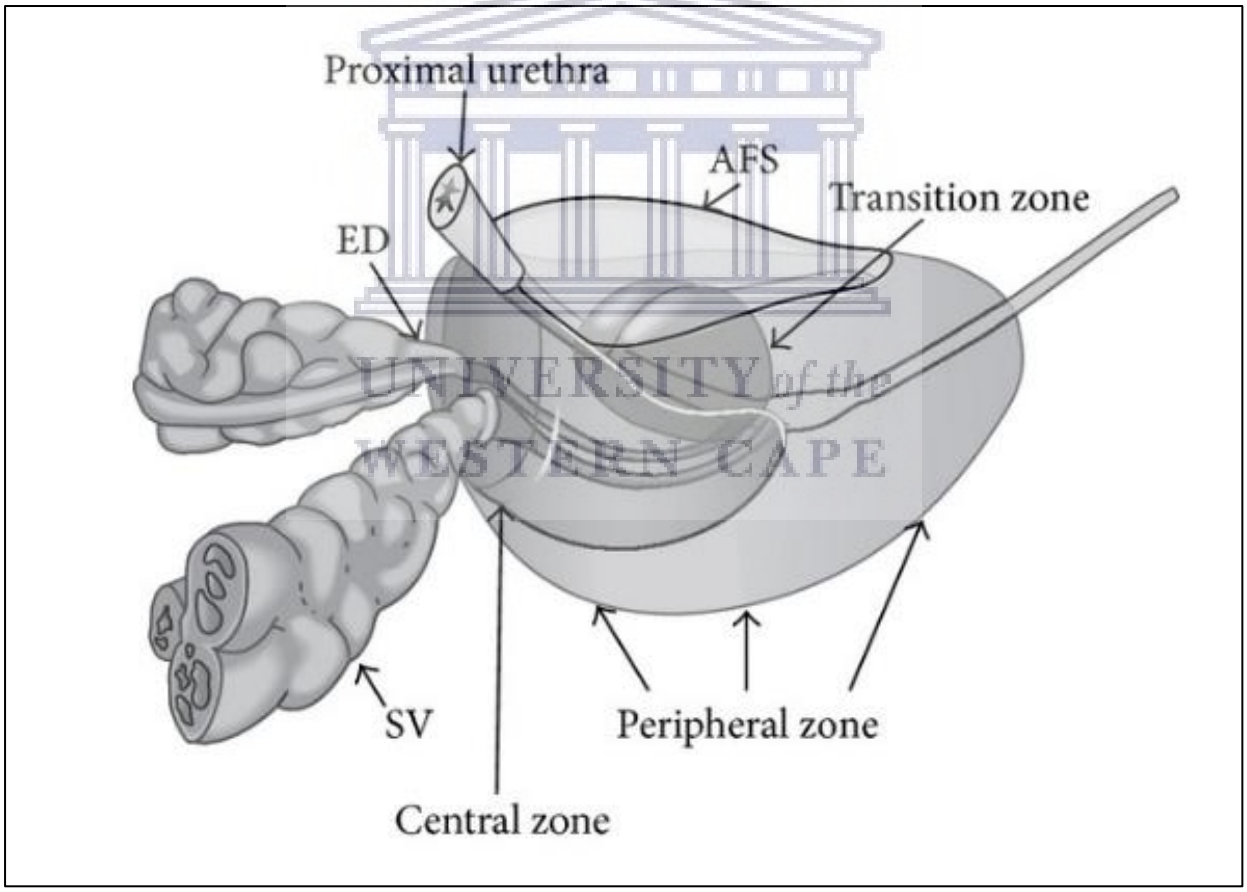

Figure 1.2: Zonal anatomy of the prostate gland showing the ejaculatory ducts (ED), seminal vesicles (SV), anterior fibromuscular stroma (AFS), peripheral zone, central zone and transitional zone. Image generated by and excerpted from (Bhavsar and Verma 2014)

The base of the prostate is located at the neck of the bladder, and the apex at the urogenital diaphragm (Burden et al. 2006), thus the urethra passes through the prostate prior to entering the penis. Moreover, a thin layer of tissue, known as Denovilliers fascia, separates the prostate and attached seminal vesicles from the rectum (Martínez-Piñeiro 2007).

Functionally, the prostate plays a role in controlling urine output from the bladder and seminal fluid during the process of ejaculation, in addition to contributing to seminal secretions (Burden et al. 2006). Secretions from the prostate are a highly complex, heterogeneous mixture of organic and inorganic compounds, accounting for approximately 20-30% of the seminal volume (Grayhack et al. 2002; Aaron et al. 2016). Prostatic fluid has previously been described as clear in appearance and slightly acidic in nature. It is the primary source of various seminal fluid components, such as zinc, magnesium, calcium and citrate, in addition to prostatic phosphatase and prostate specific antigen (Grayhack et al. 2002). In the healthy prostate, zinc tends to exist in particularly high amounts with concentrations ranging from 140-1000 mg/ml (Grayhack et al. 2002).

Functionally, prostatic zinc is important for a number of fertility parameters, including sperm motility, acrosome reaction, capacitation, and stabilizing cell membrane and nuclear chromatin of spermatozoa (Ali et al. 2007), along with preventing degeneration in the testis and acting as an antimicrobial agent (Ali et al. 2007; Kelleher et al. 2011).Various other compounds found in prostatic fluid include the polyamines, spermine and spermidine (Grayhack et al. 2002), whose enzymatic degradation produces reactive aldehydes, resulting in the characteristic odour associated with semen (Grayhack et al. 2002). Furthermore, these polyamines have also been shown to serve as antimicrobial agents (Grayhack et al. 2002). Additionally, phospholipids and cholesterol are also found in prostatic secretions with concentrations of about 180 mg/dl and 80 mg/ml, respectively (Grayhack et al. 2002). Another component of prostatic fluid are the glycoproteins prostatic acid phosphatase and prostate specific antigen, which secreted by epithelial cells, and are commonly

used as biomarkers in the characterisation of prostate-related diseases (Grayhack et al. 2002; White et al. 2009).

As previously mentioned, the prostate is an androgen-dependent organ, with androgens regulate the normal growth, maintenance, and secretory function of the prostate (Burden et al. 2006; Walters et al. 2010; Steers 2011). Cessation of androgen secretion, particularly via castration, has previously been shown to reduce prostatic size, prostatic secretion volume, muscarinic receptor expression, and noradrenergic innervation of the prostate (Steers 2011).

The primary hormone governing the regulation of normal prostate function and growth is dihydrotestosterone (Burden et al. 2006; Walters et al. 2010; Steers 2011). Within the prostate, the dihydrotestosterone concentration is up to 5 times higher than that of testosterone. This hormone is synthesized from testosterone mainly by the action of type-II 5α-reductase (Steers 2011). In addition to dihydrotestosterone, estrogens and adrenal steroids also influence prostate function and growth. More specifically, testosterone can be converted to estradiol and estrone by the aromatase enzyme (Steers 2011). Additionally, zinc metabolism, citrate and fructose production, and androgen uptake and metabolism, can be regulated by prolactin (Steers 2011). Estrogens combined with the effect of prolactin are thought to play a role in the development of benign prostatic hyperplasia (Steers 2011).

1.4.3.1 Histology of the prostate

The prostate is highly structured with large peripheral ducts in the glandular portion of the gland, possessing bi-layered epithelial acini and fibro-muscular stroma, separated from each other by a basement membrane (Burden et al. 2006). This epithelial bi-layer yields three distinct cell types, namely basal cells, luminal cells and neuro-endocrine cells (Burden et al. 2006). Characteristically, basal cells are classified as flattened, cuboidal cells found at the periphery of the gland (Burden et al. 2006; Walters et al. 2010). Furthermore, these cells are contractile, generate many growth factors

needed for regulation of the gland and are regarded to act as stem cells that replenish the secretory cell layer (Burden et al. 2006; Walters et al. 2010).

Above the basal cell layer exist neuro-endocrine cells (Burden et al. 2006; Walters et al. 2010). Although these cells are not particularly common, they have been found to exist among a vast number of secretory epithelial cells (Burden et al. 2006; Walters et al. 2010). While the specific function of these cells remains unclear, they are suggested to play a role in the regulation of growth and development in an endocrine-paracrine fashion, similar to that of neuro-endocrine cells in other organs (Burden et al. 2006; Walters et al. 2010). Production of prostatic secretions, as well expression of androgen receptors, is present with the luminal cells. These cells, however, have no proliferative potential (Burden et al. 2006; Walters et al. 2010).

1.4.3.2 Age related changes in the prostate

Previously, the prostate gland has been shown to undergo two growth spurts (Xia et al. 2002); particularly a rapid growth phase between the ages of 10-30, followed by a slow growth phase between ages between 30-90 (Xia et al. 2002). Along with this, the rate at which testosterone is converted to dihydrotestosterone in the prostate also increases; leading to a greater build of dihydrotestosterone and thereby an increase in cell growth (Grayhack et al. 2002). Subsequently, men begin to experience a few characteristic symptoms as the prostate enlarges, including difficulty emptying the bladder, increased frequency of night time urination, incontinence, and impotence (Grayhack et al. 2002; Schenk et al. 2009; Lim 2017). Additionally, a few diseases are associated with the increased growth of the prostate that occurs as men age; namely prostatitis, benign prostatic hyperplasia and prostate cancer (Grayhack et al. 2002; Schenk et al. 2009; Lim 2017).

1.4.3.3 Prostatitis

Prostatitis, classified as an inflammatory prostate disease, is a common urological occurrence in men under the age of 50. Although not always serious, it is a challenge that greatly diminishes

quality of life; characterised by the occurrence of voiding frequency, reduced urinary flow, perineal pain, and often severe pelvic discomfort and pain (Prezioso et al. 2006; Macaluso 2007; Khan et al. 2017). Moreover, it is the third most commonly occurring prostatic disease after benign prostatic hyperplasia and prostate cancer, and reportedly accounts for approximately 25% of all urological clinic visits on global scale. Unlike prostate cancer and benign prostatic hyperplasia, prostatitis has been found to affect men of all ages, rather than elderly men specifically(Khan et al. 2017). Present treatment options for prostatitis is usually guided by the category into which it falls, and often includes the use of antimicrobial therapy, urinary drainage, alpha blockers, anti-inflammatory medications and hormone therapy (Anothaisintawee et al. 2011; Khan et al. 2017). However, the efficacy of these treatments remains controversial, as clinical evaluation of these treatment options are limited (Anothaisintawee et al. 2011; Khan et al. 2017).

1.4.3.4 Benign prostatic hyperplasia

Benign prostatic hyperplasia is a condition characterized by the enlargement of the prostate, along with lower unitary tract symptoms (Schenk et al. 2009; Lim 2017). Arising in the peri-urethral and transitional zones, benign prostatic hyperplasia has been described as an inescapable phenomenon for aging males, with the prevalence increasing after age 40, affecting approximately 60% of men by the age of 90 (Schenk et al. 2009; Lim 2017).

Histologically, benign prostatic hyperplasia is characterised by hyper-proliferation of stromal and epithelial regions of the prostate, yielding a number of lower unitary tract symptoms which often prompt men to seek medical attention (Schenk et al. 2009). While the pathogenesis of benign prostatic hyperplasia remains poorly understood, it has been suggested that inflammation plays a role in its development and progression, as evidence of acute and chronic inflammation is found in prostate biopsies of benign prostatic hyperplasia patients (Schenk et al. 2009; Lim 2017).

It has previously been hypothesized that tissue damage due to infection, autoimmune response, along with obesity and increased abdominal fat may be attributed to the associated inflammation (Carson and Rittmaster 2003; Schenk et al. 2009; Lim 2017).Selective and non-selective α-blockers are generally involved in the treatment of benign prostatic hyperplasia, which often alleviate the associated symptoms by relaxing the smooth muscle in the prostate and bladder neck, resulting in urethral lumen widening, and thereby improving urinary flow (Carson and Rittmaster 2003; Briganti et al. 2009; Vasanwala et al. 2017; Jiwrajka et al. 2018). However, while effective at alleviating symptoms, α-blockers do not decrease the prostatic size, and pose a number of adverse effects such as ejaculatory dysfunction, retrograde ejaculation, erectile dysfunction hypotension and tachycardia (Carson and Rittmaster 2003; Briganti et al. 2009; Vasanwala et al. 2017; Jiwrajka et al. 2018).

Additionally, 5α-reductase inhibitors are also used in the treatment of benign prostatic hyperplasia, as these inhibitors inhibit the conversion of testosterone to dihydrotestosterone in the prostate, thereby halting the progression of the disease, alleviating the associated symptoms, and reducing the overall size of the prostate by approximately 20-30% (Carson and Rittmaster 2003; Briganti et al. 2009; Vasanwala et al. 2017; Jiwrajka et al. 2018). However, while this may be promising, side effects often including erectile dysfunction, decreased libido, ejaculation disorders and lowered semen count. Furthermore, these debilitating side effects associated with 5α-reductase inhibitors may be irreversible (Carson and Rittmaster 2003; Briganti et al. 2009; Vasanwala et al. 2017; Jiwrajka et al. 2018). Surgically intervention for benign prostatic hyperplasia often involves transurethral re-sectioning to remove obstructing portions of the prostate (Carson and Rittmaster 2003; Briganti et al. 2009; Vasanwala et al. 2017; Jiwrajka et al. 2018).

1.4.3.5 Prostate cancer

Prostate cancer is an adenocarcinoma and the most commonly reported cancer among ageing men. It is the second leading cause of cancer-related deaths in men. In 2008, a prevalence of 14% of the total new cases and 6% of the total cancer deaths in men was reported (Jemal et al. 2011). In 2018, prostate cancer was reported to account for an estimated 1.3 million new cancer cases, and approximately 359 000 associated deaths on a global scale. Furthermore, worldwide incidence rates were found to be variable, with the highest rates found in developed countries such as Australia, New Zealand, Northern and Western Europe, and Northern America (Figure 1.3) (Bray et al. 2018). Mortality rates, however, do not follow the same trend, and were reported to be higher in developing countries such as South Africa, Zambia, Zimbabwe, Jamaica and Haiti (Bray et al. 2018).

Prostate cancer generally occurs in the peripheral zone of the prostate, arising when the normal prostatic cells undergo mutation into cancerous cells (Burden et al. 2006; Lee and Shen 2015). Once mutated and cancer of the prostate arises, metastasis frequently follows in lymph nodes, distant sites and in the surrounding bony structures. Prostate cancer is commonly accepted to be linked to any one or a combination of different factors including a poor diet, genetic susceptibility, inflammation, age or infectious agents (Nelson et al. 2003; Stangelberger et al. 2008; Peisch et al. 2017). Additionally, prostate cancer was one of the first cancers previously shown to be hormone-dependent, with particular regard to androgens. Hence, raising the concern of increased serum testosterone levels feeding the cancer itself (Snyder 2009; Nelles et al. 2011; Banerjee et al. 2018).

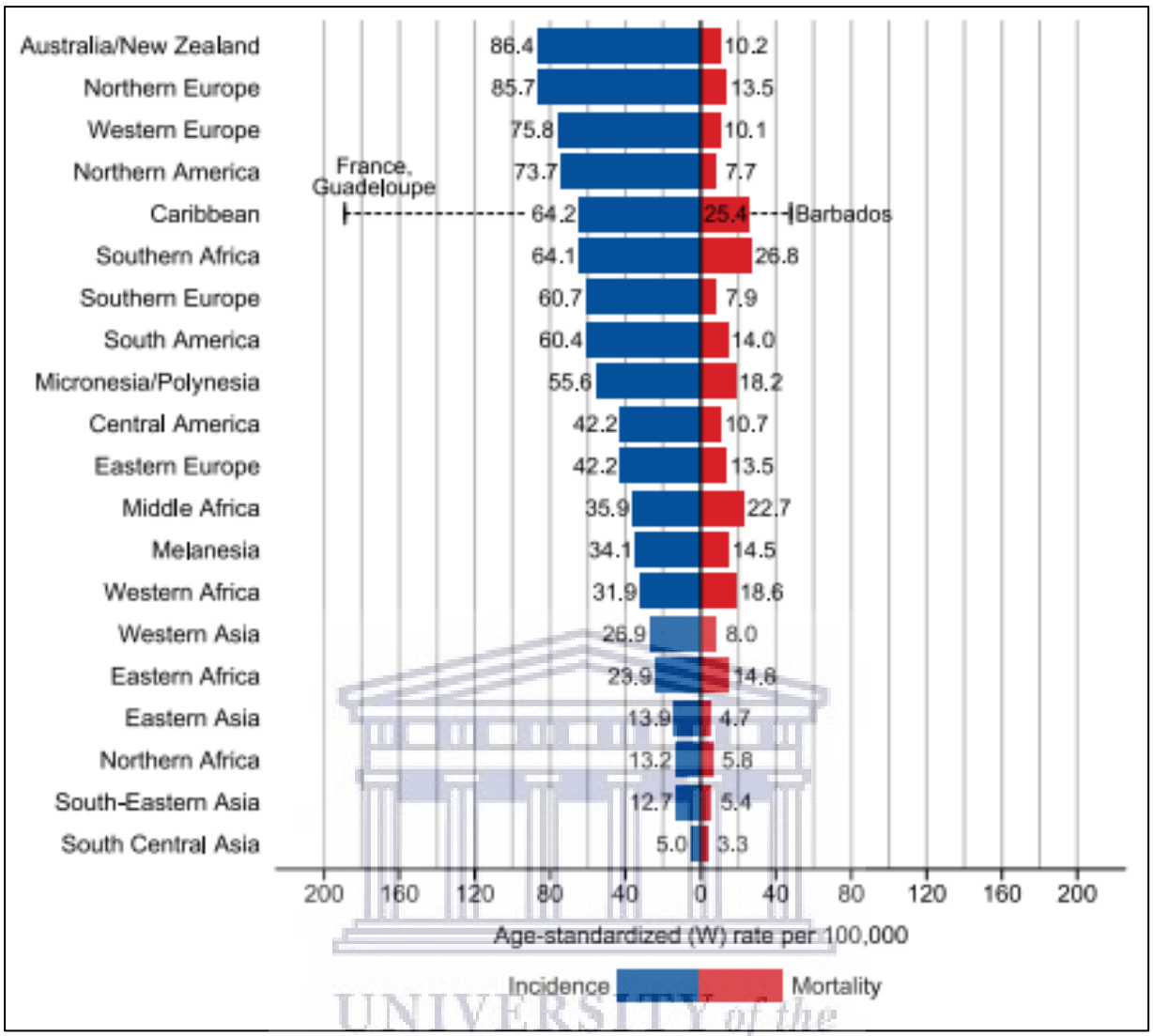

Figure 1.3: Region-specific incidence and mortality of prostate cancer in 2018. Image generated by and excerpted from(Bray et al. 2018).

The concern regarding testosterone levels and prostate cancer was based on the observed regression of prostate cancer in androgen-deprived males that was reflected by lowered PSA levels, followed by the subsequent increase in PSA levels when testosterone levels were normalised (Huggins et al., 1941; Hohl et al., 2009; Morgentaler, 2009; Morgentaler et al., 2011). However, the relationship between prostate cancer and increased testosterone levels has since been question, with a multitude of conflicting results being reported (Morgentaler 2006; Morgentaler 2009; Chuu et al. 2011). For example, Morgentaler (2006) clearly outlined contradictions in the available literature, stating that

administration of testosterone to men with, or suspected of having prostate cancer may not be contraindicated, as previously believed. An example used by Morgentaler was the rare occurrence of prostate cancer during the peak testosterone years of the early 20's, despite the common presence of microfocci in these young men (Morgentaler 2006). Subsequently, a review by Rhoden and Averbeck (2009) also clearly outlined that no compelling scientific evidence supported the belief that higher testosterone levels worsened the occurrence of prostate cancer. Nevertheless, higher testosterone levels, worsening the occurrence of prostate cancer, remains a concern. Therefore, testosterone replacement therapy for the treatment of ageing male symptoms is largely thought to be an absolute contraindication if prostate cancer is present (Bhasin et al. 2010; Bell et al. 2018).

Historically, patients with prostate cancer were categorized based on the stage of the cancer and whether or not they were candidates for surgery (Marciscano et al. 2012). Thus, the term "localized prostate cancer" refers to prostate cancer that is manageable with local therapy, such as surgery, radiotherapy or active surveillance (Marciscano et al. 2012; Schulman and Polascik 2017). Following local therapy however, patients often exhibit increasing PSA levels in a condition known as biochemical recurrence, which often precedes metastasis and eventual death (Rosenberg et al. 2010; Schulman and Polascik 2017).

The classic model of cancer metastasis, including prostate cancer, is guided by the "seed and soil" hypothesis first proposed by Stephen Paget in 1889. In this model, the "seeds" (tumour cells) metastasize only to "soil" (specific organ) well suited to tumour growth (Jin et al. 2011). Metastasis of the prostate specifically involves multiple steps, namely angiogenesis, local migration, invasion, extravasation, circulation and extravasation of tumour cells, followed by angiogenesis and colonization in new sites (Jin et al. 2011). Often, the bone is the common site of metastasis in prostate cancer and is the leading cause of death in advanced prostate cancer (Jin et al. 2011).

1.4.3.6 Treatment of prostate cancer

Increasing the rates of PSA screening has allowed prostate cancer to be detected much earlier than previously possible. Thus, allowing for earlier medical intervention and thereby greatly improving survival outcomes (Wallace et al. 2014). Three broad intervention categories exist, namely intervention with curative intent, intervention with palliative intent, and the monitoring of the disease and providing treatment when progression is evident (Hegarty et al. 2010; Wallace et al. 2014). Curative intent is comprised of a number of procedures, namely radical prostatectomy, radiotherapy, cryo-therapy, or high-intensity ultrasound therapy (Hegarty et al. 2010; Wallace et al. 2014; Teo et al. 2019). Radical prostatectomy involves the removal of the entire prostate gland and some surrounding tissue (Hegarty et al. 2010; Teo et al. 2019). While this procedure yields a number of benefits including a diminished risk of mortality, cancer progression or metastasis, the associated side effects affects up to 60% of men undergoing this procedure, and include sexual dysfunction and urinary incontinence, and drastically lowers quality of life in patients (Hegarty et al. 2010; Marzorati et al. 2019).

External-beam radiation therapy employs high-speed electrons to split water molecules, yielding hydroxyl radicals which damage tumour cell DNA (Torres-Roca 2006). This techniques carries two substantial advantages, such as the absence of pain during the procedure and a low rate of clinical failure (15% when measured after 2.5 years) (Torres-Roca 2006). Despite the advantages, the associated side effects vastly outweighs the positive aspects of this technique, such haemorrhoids and diarrhoea due to inflammation of the rectum, altered frequency in urination due to inflammation of the bladder, fatigue and sexual dysfunction (Mongra et al. 1999; Torres-Roca 2006; Gay and Michalski 2018). Additionally, the implantation of a radioactive sources directly into the tumour, known as interstitial brachytherapy is a common alternative (Koukourakis et al. 2009; Gay and Michalski 2018). Although shown to be an excellent treatment option for localized prostate cancer,

there are issues that remain to be further addressed, such as the ideal radiation dose and side effects such as disturbances in urinary function (Koukourakis et al. 2009; Gay and Michalski 2018).

Cryo-therapy involves the use of gasses and probes to rapidly freeze and thaw tumour tissue (Wilt et al. 2008). Currently, cryo-therapy is indicated in low-risk patients as an alternative to radical prostatectomy or radiotherapy. In higher-risk groups, cryo-therapy is used as primary therapy, and in patients who have not responded well to radiation therapy (Simoneau 2006; Gao et al. 2016). A number of complications have been associated with cryo-therapy, such as urethral sloughing, rectal fistula, incontinence, and erectile dysfunction (Simoneau 2006; Gao et al. 2016). High intensity ultrasound therapy is a non-invasive technique capable of inducing instantaneous, but irreversible, coagulative necrosis in tissue by thermal effects (Mearini and Porena 2010; Hsiao et al. 2016). It is an attractive approach for the treatment of localized prostate cancer in patients who have a life expectancy of less than 10 years, but who wish to avoid the potential risk associated with radical prostatectomy (Mearini and Porena 2010; Hsiao et al. 2016). Unfortunately, unwanted side effects such as prostate swelling and thereby urinary retention, dysuria due to sloughing of necrotic tissue, bladder neck or prostatic urethra constriction, impotence and rectal fistula often occur (Mearini and Porena 2010; Hsiao et al. 2016).

These serious side effects resulting from conventional forms medical intervention led to increased interest in alternative and complimentary medicine, with the hope of obtaining viable forms of treatments, that limit or eliminate serious side effects (Klempner and Bubley 2012). To this end, a number of herbs and their extract derivatives have been scientifically investigated (Klempner and Bubley 2012). These include the polyphenols found in green tea, epicatechin, epigallocatechin, epicatechin-3-gallate, and epigallocatechin-3-gallate (ECGC), the soy isoflavones, *Scutellaria baicalensis*, β-carotene and lycopene, to name a few (Klempner and Bubley 2012; Yin et al. 2013). Recently, investigators demonstrated that extracts from the plant *Ficus deltoidea*, along with isolated active compounds, were capable of inducing cell death via the activation of apoptosis in

both LNCaP and PC-3 cells, while exhibiting no toxicity toward non-cancerous HDFa human fibroblast cells.(Hanafi et al. 2017). Thus, plant extracts, and their associated active compounds, clearly have potential in the treatment of prostate cancer.

1.5 Traditional medicine

According to the World Health Organisation (WHO), traditional medicine (TM) is defined as "the knowledge, skills and practices based on the theories, beliefs and experiences indigenous to different cultures, used in the maintenance of health and in the prevention, the diagnosis, the improvement or also in the treatment of physical and mental illness (WHO 2005). A multitude of traditional medicine modalities exist, namely traditional Chinese medicine, Ayurveda, Unani, and Kampo. Each modality follows philosophies and practices based on the environment through which they originated (WHO 2005b; Yuan et al. 2016; Shaheen et al. 2017), and share an emphasis on health, rather than disease, in relation to the body and mind (Yuan et al. 2016). Particularly, a more holistic approach is taken to individual health, which is achieved through the use of herbs and natural products (Schmidt et al. 2008; Yuan et al. 2016; Shaheen et al. 2017).

With the industrial revolution and advances in medical science, the ability to chemically synthesize and mass produce drugs arose, which greatly improved the health care system (WHO 2005b). Typically, people living in rural communities have limited access to this type of medicine, but generally live in environments surrounded by cheap and easily accessible herbs (Thorsen and Pouliot 2016; Shaheen et al. 2017). Furthermore, the extreme poverty often present in developing countries leave people unable to afford conventional medicine as their primary form of healthcare (Pal and Shukla 2003; Thorsen and Pouliot 2016; Shaheen et al. 2017). While poverty in the developing world is a multifaceted topic, the lack of conventional healthcare is often due to the inability to cope with the rapidly growing urban population, and thereby being unable to provide the appropriate healthcare. Thus, traditional medicine is the primary method of healthcare in these

counties (Pal and Shukla 2003; Thorsen and Pouliot 2016; Shaheen et al. 2017). From a global perspective, it is reported that about 80% of the population has to rely on traditional remedies for their primary health care (Ekor 2014).

Studies have shown that when patients were asked for their reason for traditional medicine usage, 15% said that herbs were more effective than conventional medicine, while 6% associated it with fewer side effects (Pal and Shukla 2003). Particularly, 35% of patients in Peru using traditional medicine stated that they used it more frequently than Western medicine (Pal and Shukla 2003; Andel and Carvalheiro 2013). Similarly, up to 67% of the Nigerian population is estimated to use traditional medicine (Pal and Shukla 2003). Subsequently, this high prevalence of traditional medicine has been hypothesized to be the result of large rural-to-urban migration, cultural influence, social surroundings, and the growing belief that natural products pose no risks (Pal and Shukla 2003; Andel and Carvalheiro 2013; Thorsen and Pouliot 2016).

1.5.1 Traditional medicine in Southern Africa

In Southern Africa, approximately 70-80% of the population has been reported to use traditional medicine as a primary source of health care, or in conjunction with conventional medicine (Chitindingu et al. 2014; James et al. 2018). This is particularly linked to the close proximity of traditional healers to their communities, making traditional medicine more readily available, particularly in rural communities (Chitindingu et al. 2014; James et al. 2018).

Traditional medicine in South Africa is governed by the Traditional Healers Council, which has worked to integrate traditional medicine into the health legislative framework (Chitindingu et al. 2014; James et al. 2018). Moreover, the Traditional Practitioners Act of 2007 was passed to monitor and regulate traditional medicine, with an absolute focus on ensuring the efficacy, safety and control of traditional healthcare services (Chitindingu et al. 2014; James et al. 2018).

South Africa has an array of indigenous plants that have previously been investigated scientifically for their medicinal benefits. These include *Cussonia spicata, Typha capensis, Sutherlandia frutescens*, *Cussonia paniculata,* and *Bulbine natalensis* to name a few that have shown abilities ranging from strong antiviral effects (Mehrbod et al. 2018), affecting sperm function (Henkel et al. 2012), acting as an antioxidant (Katerere and Eloff 2005), boosting testosterone production (Yakubu and Afolayan 2008), treating Alzheimer's disease (Thakur et al. 2019), and having the potential as anti-cancer agents (Chinkwo 2005; Saeed et al. 2016). Furthermore, the growing interest in traditional medicinal plants, and subsequently their active compounds has led to the identification of novel plant-derived pharmaceuticals, accounting for an estimated 122 drugs from 94 plant species (Chitindingu et al. 2014).

However, despite ongoing scientific investigation, the vast majority of plants used in South African traditional medicine remain unevaluated for their reported medicinal benefit, or indeed their safety. Particularly, information regarding the potential geno-toxic effects following long-term use does not exist for most of these plants (Chitindingu et al. 2014). Potential for interaction between compounds found in these medicinal plants with pharmaceutical drugs also exists, which may diminish the effectiveness of conventional medicine, and carry the risks of toxicity, geno-toxicity and chromosomal damage (Fennell et al. 2004; Chitindingu et al. 2014).

1.6 *Typha capensis*

The Typhaceae family, commonly known as the cattail family, consists of 2 genera, namely *Typha* and *Sparganium*, and have approximately 30 different collective species which are global in their distribution (Sulman et al. 2013; Zhou et al. 2018). Members of the Typhaceae family are distinctively perennial, rhizomatous, monoecious plants, commonly found growing in ponds, ditches, marshes and wet-land areas (Marloth 1915; Simpson 2010). Two species of *Typha* are commonly found growing throughout South Africa, namely *Typha capensis* (T. capensis) which is

thought to be closely related to the European species *Typha latifolia*, along with *Typha australis* which is thought to be closely related to the European species *Typha angustifolia* (Marloth 1915; Simpson 2010).

Throughout South Africa, *T. capensis* (Figure 1.4) is commonly found in seasonally wet areas, and is known by many different names in different cultures such as bulrush (English), papkuil (Afrikaans) and ibuma (Zulu) (Masoko et al. 2008; Henkel et al. 2012a). Typically, *T. capensis* is described as having a reed-like appearance, growing up to 3 meters in height and having thick, spongy, horizontally growing rhizomes (Marloth 1915; Vlotman 2003; Simpson 2010). Moreover, stems protrude vertically from the rhizomes, exhibiting strappy, hairless leaves, along with sparse male flowers located towards the tip and the more densely packed, brown female flowers located below it (Marloth 1915; Vlotman 2003; Simpson 2010).

Figure 1.4: Images of Typha capensis depicting the characteristic spongy flowers (A) and the spongy rhizomes (B).

Traditionally, *T. capensis* has been used within indigenous cultures for various purposes, ranging from using the leaves for weaving and thatching for huts, baskets, mats and making brooms (Marloth 1915; Masoko et al. 2008), to using the rhizomes and pollen as a food source providing

starch and protein (Gott 2008; Masoko et al. 2008). More importantly, the rhizomes are commonly used for medicinal preparations (Masoko et al. 2008). In traditional medicine, the rhizomes are infused in water to prepare a decoction that is taken for up to a week, and is thought to have a variety of medicinal applications (Della Greca et al. 1990). More specifically, these decoctions have been used to ease delivery during pregnancy, as a treatment for infertility, dysmenorrhea, dysentery, diarrhoea, venereal disease, to improve circulation and most commonly to boost libido in men (Steenkamp 2003; Masoko et al. 2008; Abdillahi and Van Staden 2012;).

Previously scientific investigation demonstrated that *T. capensis* extracts indeed possessed medicinal value as it was reported to inhibit bacterial growth (Masoko et al. 2008), and act as a powerful antioxidant *in vitro*, scavenging away both reactive oxygen and reactive nitrogen species (Henkel et al. 2012). Furthermore, it was also proposed that *T. capensis* extracts may possess anti-cancer capabilities (Henkel et al. 2012). Subsequently, a more recent investigation subjected seasonally produced extracts to *in vitro* testing and HPLC analysis (Ilfergane 2016). Particularly, extracts produced from summer harvest were reported to be the most bioactive, having the ability to reduce cell viability, induce DNA fragmentation and apoptosis in the prostate cancer LNCaP cell line, while remaining virtually non-toxic toward the non-cancerous TM3 Leydig and PWR-1E benign prostatic hyperplasia cell lines (Ilfergane 2016). In addition to being non-toxic, it was further reported that these extracts boosted testosterone synthesis in TM3 Leydig cells. Consequently, two phenolic compounds, namely naringenin and quercetin, were isolated and were attributed with the reported effects (Figure 1.5). Finally, Ilfergane (2016) concluded that the summer rhizome extracts, and particularly the identified bioactive compounds quercetin and naringenin, have medicinal applications in improving male reproductive health and in the treatment of prostate cancer.

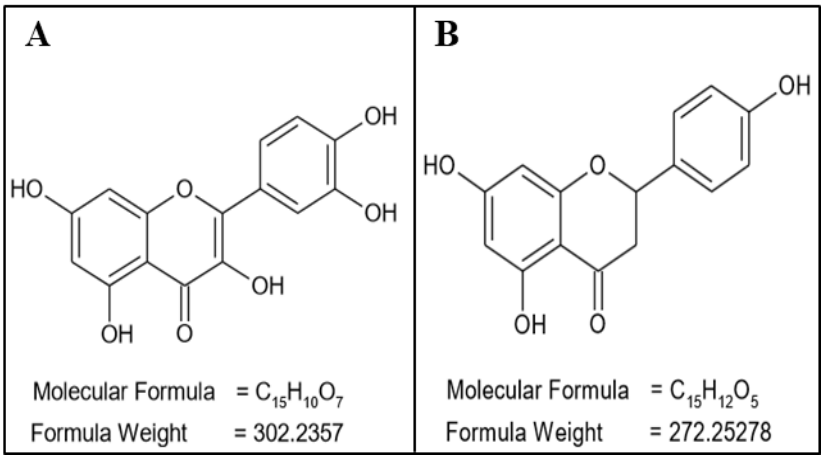

Figure 1.5: Chemical structure and molecular formula for quercetin (A) and naringenin (B). Images generated by and excerpted from Ilfergane (2016).

However, it must be mentioned that while quercetin and naringenin may have been reported to yield promising results *in vitro*, their usage in humans is limited. Both compounds have notoriously poor water solubility (Goncalves et al. 2015; Gera et al. 2017), variable oral bioavailability depending the method of delivery (Graefe et al. 2001; Shulman et al. 2011; Kaşıkcı and Bağdatlıoğlu 2016; Gera et al. 2017), along with rapid metabolism in the gut in the case of quercetin (Goncalves et al. 2015). Thus, to fully utilise these compounds medicinally, these inherent limitations must be overcome.

While the observations reported by the study conducted by Ilfergane (2016) were largely attributed to quercetin and naringenin, *T. capensis* extracts have also been shown to be a source of several other flavones, phenolic compounds, long chain hydrocarbons and various triperpenoids. Specifically, *T. capensis* extracts have been found to contain afzelechin, epiafzelechin, catechin, epicatachin, along with the two novel phenolic compounds known as typharin and typhaphthalide (Figure 1.6) (Shode et al. 2002).

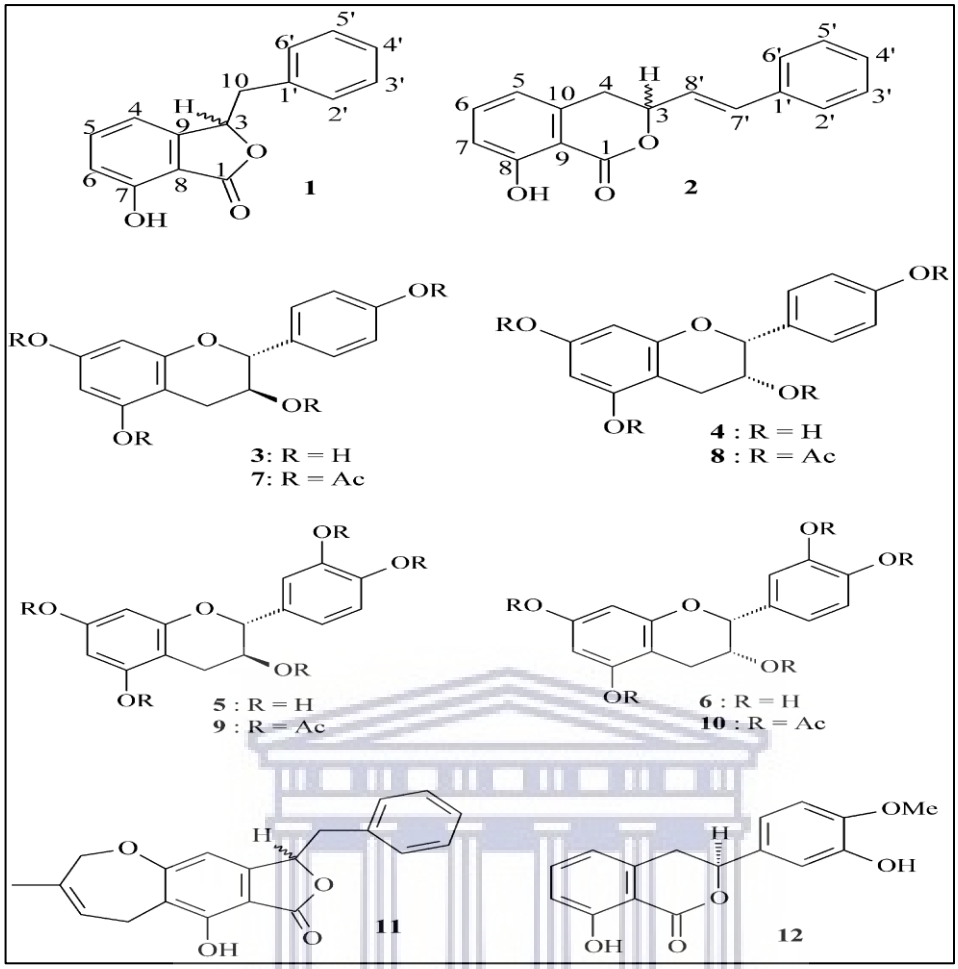

Figure 1.6: Chemical structures of compounds isolated from *Typha capensis*. Typhaphthalide (1), typharin (2), afzelechin (3), epiafzelechin (4), (+)-catechin (5), (-)-epicatechin (6), afzelechin tetraacetate (7), epiafzelechin tetraacetate (7), catechin pentaacetate (9), epicatechin pentaacetate (10). Hydroxyl-3-benzylphthalide (11) and 8E-hydroxy-3-[2-(phenyl)ethenyl]dihydro-isocoumarin (12) were used for spectral data comparison in the identification of Typhaphthalide and typharin. Image generated by and excerpted from (Shode et al. 2002).

Many phytochemicals with strong antioxidant capabilities, such as catechin and epicatachin, were previously shown to be particularly useful in studies investigating green nanoparticle synthesis using plant extracts, often playing dual roles as both reducing and stabilising agents during the synthesis procedure (Nune et al. 2009b; Choi et al. 2014; Biao et al. 2018). Considering that *T.*

capensis extracts have been shown to contain an array of compounds, including catechin and epicatechin (Shode et al. 2002), and possesses strong antioxidant capabilities (Henkel et al. 2012), it can be hypothesized that gold nanoparticles encapsulated with a cocktail of phytochemicals, including quercetin and naringenin, may be synthesised from *T. capensis* extracts. Furthermore, it may also be hypothesised that these nanoparticles could maintain, or potentially improve, the anti-cancer effects reported by Ilfergane (2016), while simultaneously overcoming the previously mentioned limitations associated with quercetin and naringenin. However, no scientifically documented information regarding the application of *T. capensis* toward these parameters exist. Thus, the present study aimed to investigate these possible effects.

1.7. Aims of the study:

T. capensis is a widely used plant in South African traditional medicine that has been shown to act as a potent antioxidant, possess an array of phytochemicals, and shown promising results in the treatment of prostate cancer and male reproductive health. However, no information regarding its application toward green nanotechnology exist.

Therefore, this study aims to investigate:

- The ability of *T. capensis* extracts to synthesise gold nanoparticles
- The synthesis of gold nanoparticles from previously identified bioactive compounds
- Characterisation of newly synthesised gold nanoparticles.
- The effect of newly synthesised gold nanoparticles toward prostate cancer LNCaP and PC-3 cell lines, along with pancreatic cancer PANC-1 cells and human aortic HAEC cells.
- The effect of newly synthesised gold nanoparticles toward SCID-mice bearing prostate tumour xenografts.

Chapter 2

Materials and Methods

2.1 Chemical Supply

The chemicals used in the current study were of the highest possible quality, and were purchased from the following companies:

Acros Organics, Geel, Belgium:

- Gum Arabic
- Histidine

American Type Cell Culture (ATCC), Manassas, USA:

- Prostate cancer cell line LNCaP
- Prostate cancer cell line PC-3
- Pancreatic cancer PANC-1
- Human aortic endothelial cells HAEC
- Benign prostatic hyperplasia cell line PWR-1E
- Leydig cell line TM3

Baxter, Columbia MO, USA:

- Injectable water

Bio-Rad, Hercules CA, USA:

- DC protein assay reagent A and reagent B

Corning incorporated, New York, USA:

- Tissue culture flasks (25 cm^2, 75 cm^2)
- Eppendorf vials
- Pipette Tips 1000 µl, 200 µl, 10 µl
- Serological pipettes (10ml)

Culligan International, Illinois, USA:

- Distilled water

Electron Microscopy Sciences, Hatfield PA, USA:

- Copper gilder grid

Eppingdust, Cape Town, South Africa:

Ethanol absolute (100%)

Gibco Invitrogen, Karlsruhe, Germany:

- Roswell Park Memorial Institute (RPMI 1640) Medium
- Kaighn's modification of Ham's F-12 medium (F-12K)
- Dulbecco's Modified Eagle Medium / Nutrient Mixture F12 Ham (DMEM/F12, 1:1 mixture)
- Keratinocyte serum free medium (K-SFM)
- Fetal Bovine Serum (FBS)
- Trypsin/Ethyl Diamine Tetra Acetic acid (EDTA) (0.25%)
- Formaldehyde (37%)

Greiner Bio-One, Frickenhausen, Germany:

- Tissue culture plates (6-, 24- and 96-well plates)
- Test tubes (15 ml and 50 ml)

Kimtech

- Kimwipes

Knittel Gläser, Braunschweig, Germany:

- Cover slips (22 x 22 mm)
- Microscope slides (76 x 26 mm)
- Superfrost slides

Lasec, Cape Town, South Africa:

- Syringes (5, 10 and 25 ml)

Malvern Panalytical, Worstershire, UK:

- 20 ml scintillation vials
- Folded-capillary cell

Merck, Wadeville Gauteng, South Africa:

- Sodium hydroxide (NaOH)

Promega, Madison, USA:

The DeadEnd™ Colorimetric TUNEL System kit

Oxoid, Basingstoke, Hampshire, RG24 SPW, England:

- Phosphate Buffered Saline (PBS) with $Ca^{2+/}Mg^{2+}$

Sigma-Aldrich, Steinheim, Germany:

- Dimethylsulphoxide (DMSO) for freezing medium
- Penicillin
- Streptomycin
- 3-(4, 5-dimethylthiazolyl-2)-2, 5-diphenyltetrazolium bromine (MTT)
- Naringenin natural 98%
- Quercetin ≥ 95%
- Trypan Blue (TB)
- Triton X-100
- Millex syringe filter units (0.22 μm, 0.45 μm)
- Bovine serum albumin (BSA)
- Human Serum Albumin (HSA)
- Semi-micro polystyrene cuvette
- Gallic acid
- Cystein
- Sodium tetrachloroaurate (III) dehydrate ($NaAuCl_4$)

Whatman, Maidstone, UK:

- Indicator paper pH 0-14

2.2 Equipment and supply

ELISA-reader

- GloMax Multi Detection System plate reader (Promega Corporation, Madison, USA)
- Labtech System LT 4000 microplate reader (Lasec, Cape Town, South Africa)
- Spectramax M2 (Molecular devices, San Jose CA, USA)

Laminar Flow

- LN Series (Nuve, Ankara, Turkey)

Incubator

- Series 2000 (Lasec, Cape Town, South Africa)

Scale

- WAS 160/X (Lasec, Cape Town, South Africa)

Plate shaker

- 96-well flat bottomed plate (Greiner Bio-One, Frickenhausen, Germany).

Centrifuge

- Hermle Z200a (Labortechnik, Wehingen, Germany)
- Accuspin Micro 17R (Thermofisher, Waltham MA, USA)

Microscope

- Inverted System Microscope (Lasec, Cape Town, South Africa)
- Joel 1400 Transmission Electron Miscroscope (Peabody MA, USA)

- CytoViva's hyperspectral dark field microscope (CytoViva Inc, Auburn AL, USA)

Magnetic stir stage

- Isotemp (Thermofisher, Waltham MA, USA)

Zeta-Sizer

- Nano-series (Malvern Panalytical, Worstershire, UK)

Spectrophotometer

- Cary 60 UV-Vis (Agilent Technologies, Santa Clara CA, USA)

2.3 Study design.

2.3.1 Part A: Gold nanoparticle Synthesis and Characterisation

First, aqueous extracts of *T. capensis* were produced from plants harvested during the beginning and the middle-end of summer, namely January and March months, respectively. Next, the ability of each extract to reduce gold salt to gold nanoparticles (AuNP's) was investigated. Hereafter, the known active compound naringenin found within *T. capensis* was investigated for AuNP synthesis. Following this, each AuNP formulation was characterised on both physical and chemical basis.

2.3.2 Part B: *In vitro* studies

Gold nanoparticle formulations were subjected to *in vitro* testing for toxicity toward four different cell lines, namely the LNCaP and PC-3 prostate cancer cell lines, the Panc1 pancreatic cancer cell lines, and the non-cancerous HAEC human aortic endothelial cell line. Hereafter, possible cell

internalisation was investigated using selected nanoparticle formulations in LNCaP and PC-3 cells by means of dark-field microscopy. Next, cell internalisation of select nanoparticle formulations was further investigated in PC-3 cells by means of TEM imaging.

2.3.3 Part C: *In vivo* study

The potential therapeutic effects of select gold nanoparticle formulations towards prostate cancer was investigated further using SCID-mice bearing PC-3 prostate cancer tumor xenografts by investigating the effects towards bodyweight and health scores, tumor volume, tumor weight and blood analysis.

2.4 Plant extract

2.4.1 Rhizome collection

Rhizomes of *T. capensis* were collected during the summer months, January and March, on the Cape Nature Reserve, located in the suburb of Belhar in the Western Cape province of South Africa. Once collected, the rhizomes were washed thoroughly, chopped into 1-2 cm pieces and allowed to dry at 25ºC in an air oven. Thereafter, the dried rhizomes were milled into a fine powder and stored in air-tight containers prior to the extraction process.

2.4.2 Extract preparation

To prepare an aqueous rhizome extracts of *T. capensis*, the powdered rhizomes were infused in distilled water that was heated to approximately 70-75ºC. The resulting mixture was allowed to stand at room temperature for 1 hour, after which it was filtered. The filtrate was then frozen at -80ºC and finally freeze-dried under the supervision of Mr. Andre Braaf, Department of Medical Bioscience, using a Zirbus freeze drier to yield the water-soluble extract. This procedure was

performed for samples collected in January and in March, yielding two distinct extracts, labelled *T. capensis* extract sample 1 and sample 2, respectively.

2.5 Gold nanoparticle synthesis

2.5.1 *T. capensis* extract-Sample 1 gold nanoparticles (S1-AuNP's and S1x2-AuNP's).

To prepare the reaction mixture, 3 mg of Gum Arabic was added to a glass scintillation vial and dissolved in 3 ml of distilled water. Next, the mixture placed on magnetic stage and stirred continuously for 30 minutes, at a temperature of 50˚C. Hereafter, the temperature was reduced to ambient temperature and 4 mg of the sample-1 extract was added to vial and allowed to dissolve for 10 minutes. Finally, 50 µl of a 0.1 M sodium tetrachloroaurate ($NaAuCl_4$) solution was to the vial in a drop-wise fashion, and the mixture was allowed to stir continuously for 24 hours. The resulting gold nanoparticles were labelled S1-AuNP's.

In an attempt to concentrate as many plant phytochemical onto the gold nanoparticle as possible, the same procedure was followed using double the amount of the sample-1 extract, whereby 8 mg of the extract was added to the glass vial containing 3 mg Gum Arabic and 3 ml distilled water. The resulting gold nanoparticles were labelled S1x2-AuNP's

2.5.2 *T. capensis extract*-Sample 2 gold nanoparticles (S2-AuNP's and S2x2-AuNP's).

To prepare the reaction mixture, 3 mg of Gum Arabic was added to a glass scintillation vial and mixed with 3 ml of distilled water. Next, the mixture placed on stage and stirred continuously for 30 minutes, at a temperature of 50˚C. Hereafter, the temperature was reduced to ambient temperature and 4 mg of the sample-2 extract was added to vial and allowed to dissolve for 10 minutes. Finally, 50 µl of a 0.1 M $NaAuCl_4$ solution was added to the vial in a drop-wise fashion, and the mixture allowed to stir continuously for 24 hours. The resulting gold nanoparticles were labelled S2-AuNP's.

In an attempt to concentrate as many plant phytochemical onto the gold nanoparticle as possible, the same procedure was followed using double the amount of the Sample-2 extract, whereby 8 mg of the extract was added to the glass vial containing 3 mg Gum Arabic and 3 ml distilled water. The resulting gold nanoparticles were labelled S2x2-AuNP's.

2.5.3 Naringenin gold nanoparticles (Ng-AuNP's pH7 and Ng-AuNP's pH8).

To prepare the reaction mixture, 3 mg of naringenin was added to a glass scintillation vial and combined with 3 ml of distilled water. Next, a stir bar was added, the mixture placed on magnetic stage and stirred continuously at ambient temperature. Finally, 50 µl of a 0.1 M $NaAuCl_4$ solution prepared at pH 7 was to the vial in a drop-wise fashion, and the mixture was allowed to stir continuously for 24 hours. The resulting gold nanoparticles were labelled Ng-AuNP's pH 7. This procedure was repeated using a 0.1 M $NaAuCl_4$ solution prepared at pH 8, yielding Ng-AuNP's pH 8.

2.6 Gold nanoparticle characterization

2.6.1 Spectrophotometry

Spectrophotometric analysis of each nanoparticle formulation was conducted to confirm the reduction of the $NaAuCl_4$ gold salt to gold nanoparticles, by observing the characteristic absorption maxima in the 500-600 nm range. To achieve this, 200 µl of each gold nanoparticle formulation was diluted in 800 µl of distilled water and transferred into a disposable cuvette. Next, spectral analysis was performed using a spectrophotometer (Cary 60 UV-Vis, Agilent Technologies, Santa Clara CA, USA) and absorption maxima measured.

2.6.2 Dynamic light scattering

Dynamic light scattering (DLS) is a widely accepted characterisation technique used to determine the size and dispersity of various forms of nanoparticles (Clayton et al. 2016; Stetefeld et al. 2016). In the present study, DLS was used to characterise the various gold nanoparticle formulations and was performed on a Zetasizer NanoZs (Malvern Panalytical, Worstershire, UK). In short, 200 µl of each respective nanoparticle formulation were diluted in 800 µl of distilled water, to a final volume of 1 ml, and samples were transferred into a disposable cuvette. Following this, samples were analysed using the Zetasizer NanoZs and the average of 3 measurements were taken.

2.6.3 Zeta potential

Zeta-potential provides a valuable insight regarding the interaction between colloidal particles in solution, and is a strong predictor of particle stability (Deryabin et al. 2015). When particles in suspension carry a sufficient positive or negative charge, typically around +30 mV or -30 mV, respectively, they will tend to repel one another, diminishes the possibility of particle aggregation, and thereby creating stability (Saeb et al. 2014). Without these repulsive forces, particles will form large aggregates and stability will have been lost.

The zeta-potential of the various gold nanoparticle formulations used in the present study was measured using the Zetasizer NanoZs. In short, 200 µl of each respective nanoparticle formulation was diluted in 800 µl of distilled water and transferred into a disposable folded-capillary cell. Samples were then placed into the instrument (Zetasizer) and zeta-potential measured, where average of 3 measurements were taken.

2.6.4 Transmission Electron Microscopy (TEM) and size distribution.

Transmission electron microscopy (TEM) is a widely used technique used to reveal valuable information regarding nanoparticle presence, size and shape (Costanzo et al. 2017). Thus, TEM was used to visualise each gold nanoparticle formulation reported in the present study.

In short, gold nanoparticle samples were synthesised according to the previously mentioned protocols and purified by centrifugation. Hereafter, 20 µl of each respective sample were placed onto a copper gilder grid (Electron Microscopy Sciences) and allowed to air-dry. Finally, grids were viewed at the Electron Microscopy Core Facility (EMC) and office of research, at the University of Missouri, Columbia MO, using a Joel 1400 transmission electron microscope.

Thereafter, images of gold nanoparticles were analysed using the java-based processing software ImageJ version 1.8.0 (National Institutes of Health, USA) to measure individual particle size. Subsequently, size distribution histograms were generated and the average particle size was calculated.

2.6.5 Total polyphenolic quantification

Polyphenolic quantification of the various gold nanoparticles formulations was achieved by means of the widely used Folin-ciocalteu phenol (FC) method. The FC method is based on the reduction of the Folin-ciocalteu reagent, which is a mixture of phosphomolybdate and phosphotungstate, by phenolic compounds and phenolic antioxidants to a highly coloured blue dye (Ahmad et al. 2015a; Abdelhady et al. 2016; Madhanraj et al. 2017).

To measure polyphenolic concentration of the gold nanoparticles produced in the current study, 1 ml of each respective sample was transferred to a 2 ml Eppendorf tube and centrifuged at 15xg for 15 minutes to yield a pellet. Once pelleted, the supernatants were removed from each tube and 500 µl of the Folin-ciocalteu phenol reagent, diluted 1:10 in distilled water, was added to each pellet, followed by 1 ml of a 7.5 % (w/v) sodium carbonate solution, yielding a final volume of 1.5 ml.

Hereafter, samples were briefly mixed and incubated at 30°C for 30 minutes. After incubation, 200 µl of each sample were transferred to a 96-well plate and absorbance was determined at 760 nm using an ELISA plate reader (GloMax Multi Detection System). Finally, the absorbance was compared to a standard curve established using Gallic acid under the same conditions, and the total polyphenolic concentration was expressed as µg/ml, equivalent to Gallic acid.

2.6.5.1 Gallic acid standard curve

A stock solution of 1000 µg/ml of Gallic acid was prepared by dissolving it in 1 ml of distilled water and further serial diluted into concentrations of 500, 250, 125, 62.5, 31.25, 15.62, 7.18, 3.9 and 1.95 µg/ml. The blank was distilled water. Thereafter, the Folin-cicalteu phenol method was performed, a standard curve (Figure 2.1) was calculated and the results used to determine the total polyphenolic concentration of the various gold nanoparticle samples.

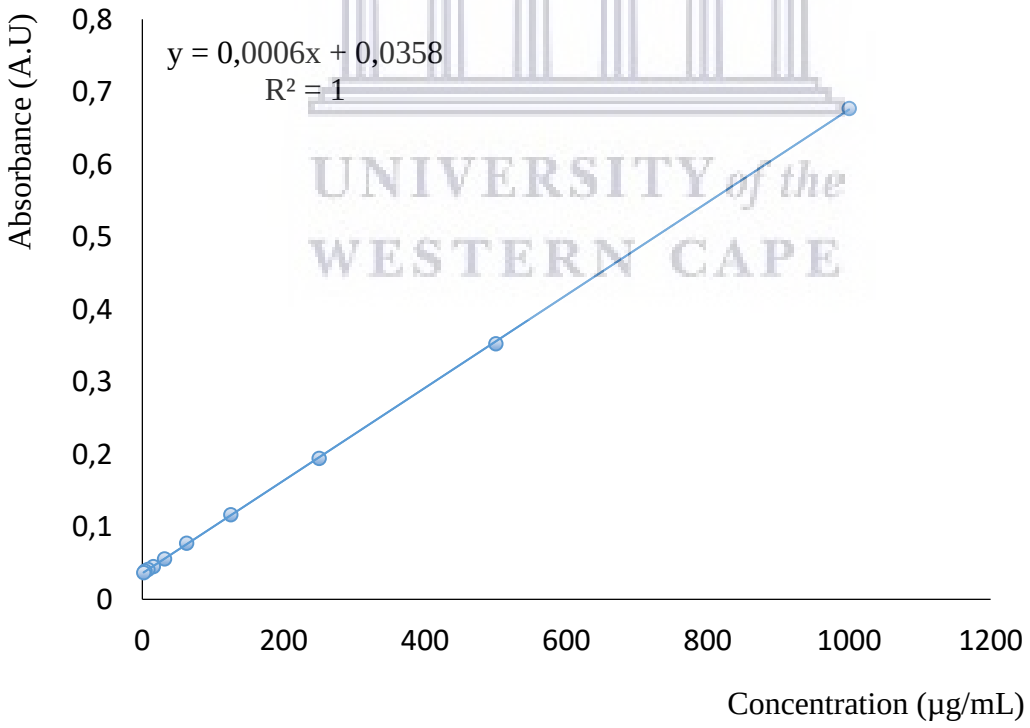

Figure 2.1: Gallic acid standard curve for total polyphenolic concentration determination.

2.6.6 LC-MRM analysis of extracts and nanoparticles

2.6.6.1 Sample preparation and standard curve

Samples were dissolved with 1ml of a solution consisting of 50% methanol, 50% water, 0.01% formic acid and containing 25ng/ml chloramphenicol. Once dissolved, samples were vortexed for 5 minutes, then centrifuged 16000 x g, and finally 200 µl transferred into autosampler vials. Supernatants were diluted 1:10, 1:1000 and 1:1000 with chloramphenicol. Next, standards were diluted in methanol to yield a 500 µg/ml working solution. Following this, standards were serial diluted 1:1 to concentrations ranging from 200 µg/ml to 1.5625 µg/ml. Finally, standard curves were generated for naringenin (Figure 2.2 A), and quercetin (Figure 2.2 B).

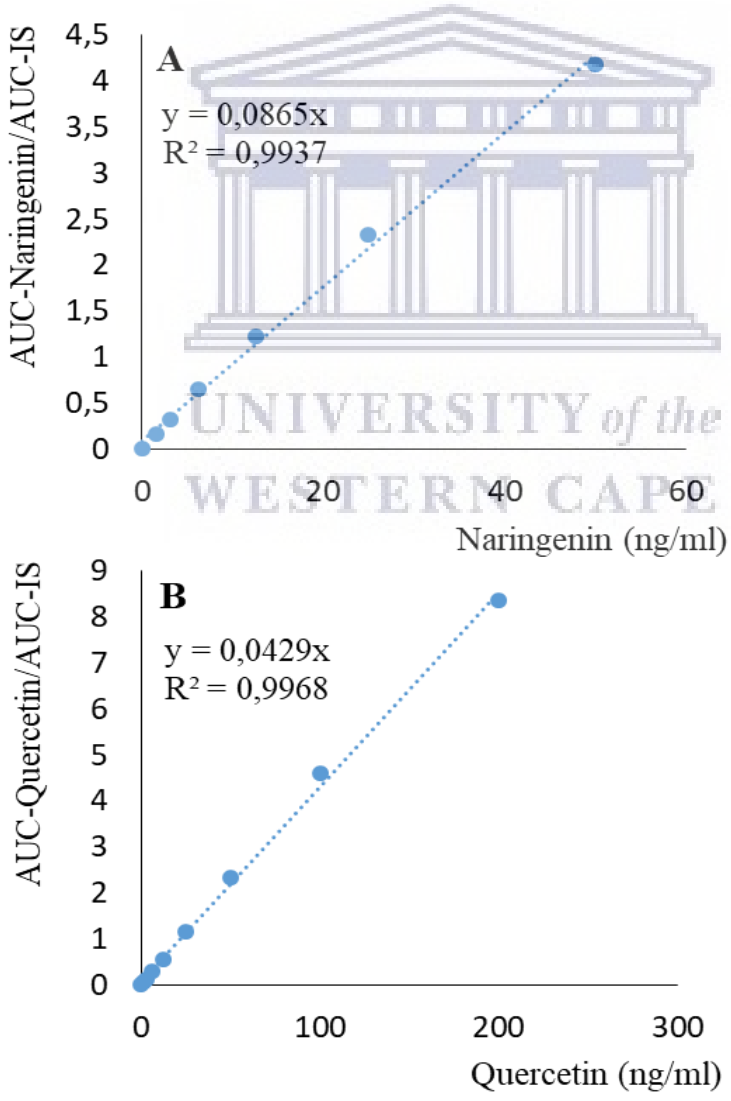

Figure 2.2: Standard curves for the determination of naringenin (A) and quercetin (B).

2.6.6.2 Analytical method

The S1 and S2 extracts, S1-AuNPs, S2-AuNP's and Ng-AuNP's pH8 were analysed using a Xevo TQS mass spectrometer (Waters, Milford MA, USA) with chloramphenicol as internal standard. Quercetin and naringenin were used as standards.

The Xevo TQS was operated in negative-ion mode and a client specific tune file saved for future analyses. Two transitions were used for each molecule, based on optimized cone and collision generated by the Xevo instrument: transitions (0.025 s dwell time) were 301.1>150.9 (quantifying Quercetin, cone=54V, CE=18), 301.1>179.0 (Quercetin, cone=54V, CE=16); 271.0>150.9 (quantifying Naringenin, cone=50V, CE=16), 271.0>119.1 (Naringenin, cone=50V, CE=18); and 321.0>257.3 (quantifying Chloramphenicol, internal standard, cone=30V, CE=10), 321.0>152.6 (Chloramphenicol, cone=30V, CE=20).

Separation was carried out using an Acquity H-class UPLC (Waters) on a Waters BEH C18 column (2.7 µm, 5 cm x 2.1 mm) by gradient delivery (0.4 mL/min) of solvent. Solvent A: 0.01% formic acid in water. Solvent B: 0.01% FA in acetonitrile. Initial conditions were 2%B followed by a 0.25min ramp to 30%B, 1min gradient to 60%B, 0.25min ramp to 98%B, hold at 98%B for 1.25min, 0.2min ramp to 2%B, and hold at 2%B for 1.3min. Total run time was 4min. The column was heated to 45 °C and the samples cooled to 20 °C in the autosampler.

2.6.6.3 Quantification of quercetin and naringenin

TargetLynx version 4.1 (Waters, Milford MA, USA) was used to calculate the area under the curve (AUC) and reported as both a response (AUC-compound/AUC-internal standard) and as ng/ml. To quantify Quercetin and Naringenin, the linear response function was calculated and the line equation was used to calculate ng/mL from the peak integration data exported from TargetLynx.

2.6.7 Gold content analysis

Inductively coupled plasma mass spectrometry (ICP-MS) is a widely used technique for the determination of major, minor and trace elemental constituents in metals and related materials (Boss and Fredeen 2004), making it a well suited technique for gold nanoparticle characterisation by determining gold (Au) content (Yu 2012; Gadogbe et al. 2013). Thus, ICP-OES was used to investigate the Au content of selected gold nanoparticle formulations, namely the S1-AuNP's, S2-AuNP's and Ng-AuNP's pH 8.

Gold nanoparticles were prepared according to the previously mentioned protocols and purified by centrifugation. Hereafter, 1 ml of each sample was submitted to the Experimental Station Chemical Laboratories, at the University of Missouri, Columbia MO, for ICP-OES analysis under the supervision of Dr. James K. Waters.

2.7 Gold nanoparticle stability in challenging media

Nanoparticle stability was investigated by combining 200 µl of each nanoparticle formulation and 800 µl of each challenging medium, specifically 1% Sodium chloride, 0.2% Histidine, 0.5% Human Serum Albumin, 0.5% Bovine Serum Albumin, 0.5% Cysteine and Phosphate Buffered Saline solution, to a final volume of 1 ml, respectively. Controls were combined with distilled water. Each mixture was then incubated for 0, 1 and 48-hour periods. Additionally, nanoparticles were also incubated in each challenging medium for 7 day. Once incubated for each of the respective time intervals, nanoparticles were screened visually for agglomeration, transferred to a disposable cuvette and absorption maxima's were measured using a spectrophotometer (Cary 60 UV-Vis).

2.8 *In vitro* studies

2.8.1 Cell culture

The LNCaP and PC-3 prostate cancer, PANC 1 pancreatic cancer, and HAEC primary human aortic endothelial cell lines were used for the purpose of the study. They were cultivated at 37°C in 95% air and 5% CO_2, following standard aseptic work procedures. LNCaP and PC-3 cells were cultured in complete RPMI 1640 growth medium, supplemented with 10% fetal bovine serum, 1% penicillin (100 IU/ml) and streptomycin (100 µg/ml), in 75 cm^2 culture flasks. PANC 1 cells were cultured in 75 cm^2 culture flasks, using complete DMEM supplemented with 10% fetal bovine serum, 1% penicillin (100 IU/ml) and streptomycin (100 µg/ml). HAEC cells were cultured in complete Vascular Cell Basal Medium supplemented with the Endothelial Cell Growth Kit-VEGF (ATCC), according to table 2.1, along with 1% penicillin (100 IU/ml) and streptomycin (100 µg/ml) in 75 cm^2 culture flasks.

Table 2.1: Supplementation of Basal Cell Vascular Medium using the Endothelial Cell Growth kit-VEGF (ATCC).

Component	Volume	Final concentration
rh VEGF	0.5 ml	5 ng/ml
rh EGF	0.5 ml	5 ng/ml
rh FGF basic	0.5 ml	5 ng/ml
rh IGF-1	0.5 ml	15 ng/ml
L-glutamine	25 ml	10 nM
Heparin sulfate	0.5ml	0.75 Units/ml
Hydrocortisone hemi succinate	0.5ml	1 µg/ml
Fetal bovine serum	10 ml	2%
Ascorbic acid	0.5 ml	50 µg/ml

2.8.1.1 LNCaP prostate cancer cell line

LNCaP is a human prostate cancer cell line derived from a needle aspirate biopsy in 1977 from a 50-year old male, diagnosed with stage D prostate cancer (Horoszewicz et al. 1980). These cells express a mutated form of the androgen receptor, resulting in some differences in androgenic response (Horoszewicz et al. 1983). Most prostate cancer cell lines express little to no androgen receptor, making LNCaP the ideal model for investigating early prostate cancer (Horoszewicz et al. 1983).

2.8.1.2 PC-3 prostate cancer cell line

PC-3 is a human prostate cancer cell line established from bone metastasis in a 62-year old male (Kaighn et al. 1979). PC-3 cells do not express prostate specific antigen (PSA), and do not express prostate specific membrane antigen (PSMA) (Kaighn et al. 1979). Additionally, these cells are not androgen responsive, making them ideal models for investigating androgen independent prostate cancer (Kaighn et al. 1979).

2.8.1.3 PANC 1 pancreatic cancer cell line

PANC 1 is human pancreatic cell line derived from a ductal-origin pancreatic carcinoma isolated from a 56-year old male (Lieber et al. 1975). These cells were found to possess the type B phenotype for G6PD, and serve as a representation of genetic instability in cancer cells by absence of the Y chromosome (Lieber et al. 1975). Additionally, these cells possess SSTR2 receptors and exhibit neuroendocrine differentiation, making them ideal models for studying pancreatic cancer neuroendocrine chemotherapy, along with peptide receptor radionuclide therapy (Gradiz et al. 2016).

2.8.1.4 HAEC human aortic endothelial cell line

HAEC is a primary human aortic endothelial cell line derived from an aorta on a batch-specific basis. These cells present with a characteristic cobblestone appearance with large dark nuclei, and are commonly used for as a model for cardiovascular-based research, including arteriolosclerosis, hypertension and arterial disease (http://www.lgcstandards-atcc.org/Products/All/PCS-100-011.aspx?geo_country=za#generalinformation).

2.8.2 Culture of LNCaP cells

Cells were cultured in 75 cm^2 flasks, allowed to grow to 80% confluency and finally passaged once this was reached. To remove compounds that may interfere with the actions of trypsin, the growth medium was discarded and the cells rinsed with 5 ml sterile PBS. Subsequently, 1-2 ml of 0.25% trypsin were added, allowed to cover the surface of the flask, and incubated at 37ºC until cells began to detach. This took approximately 5 minutes and was performed under intermittent visual control. Once cells detached, 2 ml of complete growth medium was added to neutralize the action of the trypsin. Cells were then carefully re-suspended by repeated aspiration and then finally transferred to a 15 ml conical tube to be centrifuged at 125 x g for 5-10 minutes. Following this, the supernatant was removed and the cell pellet re-suspended in 5 ml complete growth medium. Thereafter, 1 ml of the resulting suspension was transferred into a new 75 cm^2 flask, containing complete growth medium, and the passage was recorded to track the age and physiology of the cells. Additionally, cell morphology was observed and compared with cell viability.

2.8.3 Culture of PC-3 cells

Cells were cultured in 75 cm^2 flasks, allowed to grow to 80% confluency and finally passaged once this was reached. To remove compounds that may interfere with the actions of trypsin, the growth medium was discarded and the cells rinsed with 5 ml sterile PBS. Subsequently, 1-2 ml of 0.25%

trypsin were added, allowed to cover the surface of the flask, and incubated at 37ºC until cells began to detach. This took approximately 5-10 minutes and was performed under intermittent visual control.

Once cells detached, 2-5 ml of complete growth medium was added to neutralize the action of the trypsin. Cells were then carefully re-suspended by repeated aspiration and then finally transferred to a 15 ml conical tube to be centrifuged at 125 x g for 5-10 minutes. Following this, the supernatant was removed and the cell pellet re-suspended in 5 ml complete growth medium. Thereafter, 1 ml of the resulting suspension was transferred into new 75 cm^2 flasks, containing complete growth medium, and the passage was recorded to track the age and physiology of the cells. Additionally, cell morphology was observed and compared with cell viability.

2.8.4 Culture of PANC 1 cells

Cells were cultured in 75 cm^2 flasks, allowed to grow to 80% confluency and finally passaged once this was reached. To remove compounds that may interfere with the actions of trypsin, the growth medium was discarded and the cells rinsed with 5 ml sterile PBS. Subsequently, 1-2 ml of 0.25% trypsin were added, allowed to cover the surface of the flask, and incubated at 37ºC until cells began to detach. This took approximately 5-10 minutes and was performed under intermittent visual control. Hereafter, 2-5 ml of complete growth medium was added to neutralize the action of the trypsin. Cells were then carefully transferred to a 15 ml conical tube to be centrifuged at 125 x g for 10 minutes. Following this, the supernatant was removed and the cell pellet re-suspended in 5 ml complete growth medium. Thereafter, 1 ml of the resulting suspension was transferred into new 75 cm^2 flasks, containing complete growth medium, and the passage was recorded to track the age and physiology of the cells. Additionally, cell morphology was observed and compared with cell viability.

2.8.5 Culture of HAEC cells

Cells were cultured in 75 cm^2 flasks, allowed to reach 80% confluency and finally passaged once this was reached. To remove compounds that may interfere with the actions of trypsin, the growth medium was discarded and cells washed with 5 ml sterile PBS. Following this, 1-2 ml of 0.25% trypsin was added, allowed to cover the surface of the flash and incubated at 37ºC until cells detached. This took approximately 10 minutes and was performed with intermittent visual control. To neutralize the trypsin, 2 ml of complete growth medium was added, the cells re-suspended and finally transferred to a 15 ml conical tube to be centrifuged at 125 x g for 5 minutes. Thereafter, the supernatant was removed, the cell pellet re-suspended in 5 ml complete growth medium and 1 ml of the resulting suspension was transferred into a new 75 cm^2 flask, containing complete growth medium. Passage numbers were recorded to track the age and physiology of the cells. Additionally, cell morphology was observed and compared with cell viability.

2.8.6 Cell counting and seeding

Following the detachment of the cells with trypsin and re-suspension in fresh growth medium, cell counts were performed using a hemocytometer so that a specific cell concentration could be reached in 6-well plates or 96-well plates. This was achieved by combining 50 µl of cell suspension with an equal volume of 2% trypan blue and transferring 10 µl of this mixture to a hemocytometer counting chamber. The chamber was viewed under a microscope and the total cell count for each experiment was calculated according to equation 1. Following this, a dilution of cells was made according to the final cell number needed for each experiment as needed.

Equation 1: Volume of cells required (µl) = $\frac{\text{Number of cells needed x100}}{\text{Total number of cells counted}}$

2.8.7 Cell freezing

2.8.7.1 LNCaP cells

Cells were grown to 80% confluency prior to cell freezing. To remove compounds that may interfere with the actions of trypsin, the growth medium was discarded and cells rinsed with 5 ml sterile PBS. Subsequently, 1-2 ml of 0.25% trypsin were added, allowed to cover the surface of the flask, and incubated at 37ºC until cells began to detach. This took approximately 5 minutes and was performed under intermittent visual control.

Once cells detached, 2 ml of complete growth medium was added to neutralize the action of the trypsin. Cells were then carefully re-suspended by repeated aspiration, counted and then finally transferred to a 15 ml conical tube to be centrifuged at 125 x g for 5-10 minutes. Following this, the supernatant was removed, the cell pellet re-suspended in 5 ml freezing medium (85% RPMI 1640, 10% FBS and 5% DMSO), dispensed into cryogenic vials and immediately frozen at -80ºC for 24 hours. Thereafter, the vials were transferred to liquid nitrogen for long-term storage.

2.8.7.2 PC-3 cells

Cells were grown to 80% confluency prior to cell freezing. To remove compounds that may interfere with the actions of trypsin, the growth medium was discarded and cells rinsed with 5 ml sterile PBS. Subsequently, 1-2 ml of 0.25% trypsin were added, allowed to cover the surface of the flask, and incubated at 37ºC until cells began to detach. This took approximately 5 minutes and was performed under intermittent visual control.

Once cells detached, 2 ml of complete growth medium was added to neutralize the action of the trypsin. Cells were then carefully re-suspended by repeated aspiration, counted and then finally transferred to a 15 ml conical tube to be centrifuged at 125 x g for 5-10 minutes. Following this, the supernatant was removed, the cell pellet re-suspended in 5 ml freezing medium (85% RPMI 1640,

10% FBS and 5% DMSO), dispensed into cryogenic vials and immediately frozen at -80ºC for 24 hours. Thereafter, the vials were transferred to liquid nitrogen for long-term storage.

2.8.7.3 PANC 1 cells

Cells were grown to 80% confluency prior to cell freezing. To remove compounds that may interfere with the actions of trypsin, the growth medium was discarded and cells rinsed with 5 ml sterile PBS. Subsequently, 1-2 ml of 0.25% trypsin were added, allowed to cover the surface of the flask, and incubated at 37ºC until cells began to detach. This took approximately 5 minutes and was performed under intermittent visual control.

Once cells detached, 2 ml of complete growth medium were added to neutralize the action of the trypsin. Cells were then carefully re-suspended by repeated aspiration, counted and then finally transferred to a 15 ml conical tube to be centrifuged at 125 x g for 5-10 minutes. Following this, the supernatant was removed, the cell pellet re-suspended in 5 ml freezing medium (85% DMEM, 10% FBS and 5% DMSO), dispensed into cryogenic vials and immediately frozen at -80ºC for 24 hours. Thereafter, the vials were transferred to liquid nitrogen for long-term storage.

2.8.7.4 HAEC cells

Cells were grown to 80% confluency prior to cell freezing. To remove compounds that may interfere with the actions of trypsin, the growth medium was discarded and the cells rinsed with 5 ml sterile PBS. Subsequently, 1-2 ml of 0.25% trypsin were added, allowed to cover the surface of the flask, and incubated at 37ºC until cells began to detach. This took approximately 5 minutes and was performed under intermittent visual control.

Once cells detached, 2 ml of complete growth medium was added to neutralize the action of the trypsin. Cells were then carefully re-suspended by repeated aspiration, counted and then finally transferred to a 15 ml conical tube to be centrifuged at 125 x g for 5-10 minutes.

Hereafter, the supernatant was removed and the cell pellet was re-suspended in 10 ml freezing medium (95% Vascular Cell Basal Medium and 5% DMSO), aliquoted into cryogenic vials and immediately frozen at -80ºC for 24. Thereafter, the vials were transferred to liquid nitrogen for long-term storage.

2.8.8 Cell thawing

2.8.8.1 LNCaP cells

To propagate the cells, the vial containing the frozen LNCaP cells was placed into a water bath heated to 37ºC to thaw the cells rapidly. Once thawed, the cells were transferred to a 15 ml conical tube containing 10 ml RPMI 1640 medium supplemented with penicillin, streptomycin, and FBS. The suspension was then centrifuged at 125 x g for 5 minutes, after which the supernatant was aseptically removed, the pellet re-suspended in 10 ml fresh RPMI 1640 and finally transferred to a 75 cm^2 culture flask and placed into the incubator.

2.8.8.2 PC-3 cells

To propagate the cells, the vial containing the frozen PC-3 cells was placed into a water bath heated to 37ºC to thaw the cells rapidly. Once thawed, the cells were transferred to a 15 ml conical tube containing 10 ml RMPI 1640 medium supplemented with penicillin, streptomycin, and FBS. The suspension was then centrifuged at 125 x g for 5 minutes, after which the supernatant was aseptically removed, the pellet re-suspended in 10 ml fresh RPMI 1640 and finally transferred to a 75 cm^2 culture flask and placed into the incubator.

2.8.8.3 PANC 1 cells

To propagate the cells, the vial containing the frozen PANC 1 cells was placed into a water bath heated to 37ºC to thaw the cells rapidly. Once thawed, the cells were transferred to a 15 ml conical

tube containing 10 ml DMEM medium supplemented with penicillin, streptomycin, and FBS. The suspension was then centrifuged at 125 x g for 5 minutes, after which the supernatant was aseptically removed, the pellet re-suspended in 10 ml fresh DMEM and finally transferred to a 75 cm^2 culture flask and placed into the incubator.

2.8.8.4 HAEC cells

To propagate the cells, the vials containing the frozen HAEC cells were placed into a water bath heated to 37°C to thaw the cells rapidly. Once thawed, the cells were transferred to a 15 ml conical tube containing 10 ml Vascular Cell Basal Medium supplemented with the Endothelial Cell Growth kit-VEGF (ATCC), along with penicillin and streptomycin. The suspension was then centrifuged at 125 x g for 5 minutes, after which the supernatant was aseptically removed and the pellet was re-suspended in 10 ml fresh Vascular Cell Basal Medium. The cells were then transferred to a 75 cm^2 flask and left undisturbed in the incubator for 48 hours.

2.8.9 Test parameters

2.8.9.1 Determination of cell viability

Cell viability was determined using the 3-(4, 5-dimethylthiazolyl-2)-2, 5-diphenyltetrazolium bromine (MTT) assay. This is a colorimetric assay, which allows for the detection of viable and dead cells. The detection of viable and dead cells is achieved by measuring cellular metabolic activities, such as the reduction of the yellow MTT salt to a highly coloured purple formazan dye (van Meerloo et al. 2011). The reduction of tetrazolium salts to the formazan dye occurs due to the action of mitochondrial reductases. These enzymes are only present in viable cells as they become deactivated shortly after cell death (Roehm et al. 1991; van Meerloo et al. 2011). Therefore, the degree in the colour change, and consequently the amount of formazan dye being produced, is proportional to the number of viable cells in the sample.

In short, cultures were removed from the incubator at the appropriate times and the MTT working solution was prepared by dissolving the MTT salt in PBS at a concentration of 5 mg/ml. If sediment appeared, the solution was heated to 37°C and swirled until no longer opaque. Then, 10 µl of this solution were added to each well and placed into the incubator for 4 hours. Next, the growth medium and MTT was removed and DMSO was added to each well in order to solubilise the remaining crystals. Finally, the absorbance was read at 570 nm Glomax Multi Detection System plate-reader (Promega Corperation, Madison, U.S.A) and results were expressed as percentage viability. This was calculated according to the absorbance of treated cells versus the absorbance of the controls, according to equation 3.

Equation 2: Percentage viability = $\frac{\text{ABSORBANCE sample X 100}}{\text{ABSORBANCE control}}$

2.8.9.2 LNCaP cell viability

LNCaP cells were grown to 80% confluency and were then trypsinated with 1-2 ml 0.25% trypsin. Thereafter, the trypsin was inactivated by adding 2 ml of complete growth medium and a cell count was performed. Following this, cells were seeded into sterile 96-well plates at 5×10^3 cells/well in 100 µl of complete growth medium. After exposing cells to various concentrations of the aqueous *T. capensis* rhizome extracts and various gold nanoparticles for 24 hours, 48 hours and 72 hours, respectively, 10 µl of MTT were added to each well. The plates were incubated at 37ºC for an additional 4 hours. Subsequently, the growth medium and MTT was removed from each well and the remaining crystals solubilised with 200 µl of DMSO. Finally, the absorbance of the samples was measured at 570 nm with an ELISA reader (GloMax Multi Detection System).

2.8.9.3 PC-3 cell viability

PC-3 cells were grown to 80% confluency and were then trypsinated with 1-2 ml 0.25% trypsin. Thereafter, the trypsin was inactivated by adding 2 ml of complete growth medium and a cell count was performed. Following this, cells were seeded into sterile 96-well plates at 5×10^3 cells/well in 100 µl of complete growth medium. After exposing cells to various concentrations of the aqueous *T. capensis* rhizome extracts and various gold nanoparticles for 24 hours, 48 hours and 72 hours, respectively, 10 µl of MTT were added to each well. The plates were incubated at 37ºC for an additional 4 hours. Subsequently, the growth medium and MTT was removed from each well and the remaining crystals solubilised with 200 µl of DMSO. Finally, the absorbance of the samples was measured at 570 nm with an ELISA reader (GloMax Multi Detection System).

2.8.9.4 PANC 1 cell viability

PANC 1 cells were grown to 80% confluency and were then trypsinated with 1-2 ml 0.25% trypsin. Thereafter, the trypsin was inactivated by adding 2 ml of complete growth medium and a cell count was performed. Following this, cells were seeded into sterile 96-well plates at 3×10^3 cells/well in 100 µl of complete growth medium. After exposing cells to various concentrations of the aqueous *T. capensis* rhizome extracts and various gold nanoparticles for 24 hours, 48 hours and 72 hours, respectively, 10 µl of MTT were added to each well. The plates were incubated at 37ºC for an additional 4 hours. Subsequently, the growth medium and MTT was removed from each well and the remaining crystals solubilised with 200 µl of DMSO. Finally, the absorbance of the samples was measured at 570 nm with an ELISA reader (GloMax Multi Detection System).

2.8.9.5 HAEC cell viability

HAEC cells were grown to 80% confluency and were then trypsinated with 1-2 ml 0.25% trypsin. Thereafter, the trypsin was inactivated by adding 2 ml of complete growth medium and a cell count

was performed. Following this, cells were seeded into sterile 96-well plates at 3×10^3 cells/well in 100 µl of complete growth medium. After exposing cells to various concentrations of the aqueous *T. capensis* rhizome extracts and various gold nanoparticles for 24 hours, 48 hours and 72 hours, respectively, 10 µl of MTT were added to each well. The plates were incubated at 37ºC for an additional 4 hours. Subsequently, the growth medium and MTT was removed from each well and the remaining crystals solubilised with 200 µl of DMSO. Finally, the absorbance of the samples was measured at 570 nm with an ELISA reader (GloMax Multi Detection System).

2.8.10 Cell internalisation of nanoparticles by hyperspectral dark field microscopy

CytoViva's patented darkfield-based microscope utilises hyperspectral imaging technology specifically designed for the quantitative spectral analysis of various forms of nano-scale materials, including nanoparticles, bacteria, viruses and liposomes. An array of valuable information can be gathered using this technology, such as mapping the presence and location of nanomaterials in a variety of environments, along with characterising surface chemistry and functional groups (https://schaefer-tec.com/en/products/nanoparticles-cytoviva/). This technology was used to investigate the possible cell internalisation of gold nanoparticles generated in the present study.

In short, cultures were removed from the incubator at the appropriate times, washed with PBS and fixed in 4% paraformaldehyde. Once fixed, cells were washed and mounted in DAPI (stain nuclear) on glass slides. Finally, slides were viewed using CytoViva's patented dark field hyperspectral microscope (CytoViva Inc, Auburn AL, USA), where the presence of gold nanoparticles was observed as yellow-gold coloured particulates or agglomerates found covering or surrounding the blue stained cells (Figure 2.3).

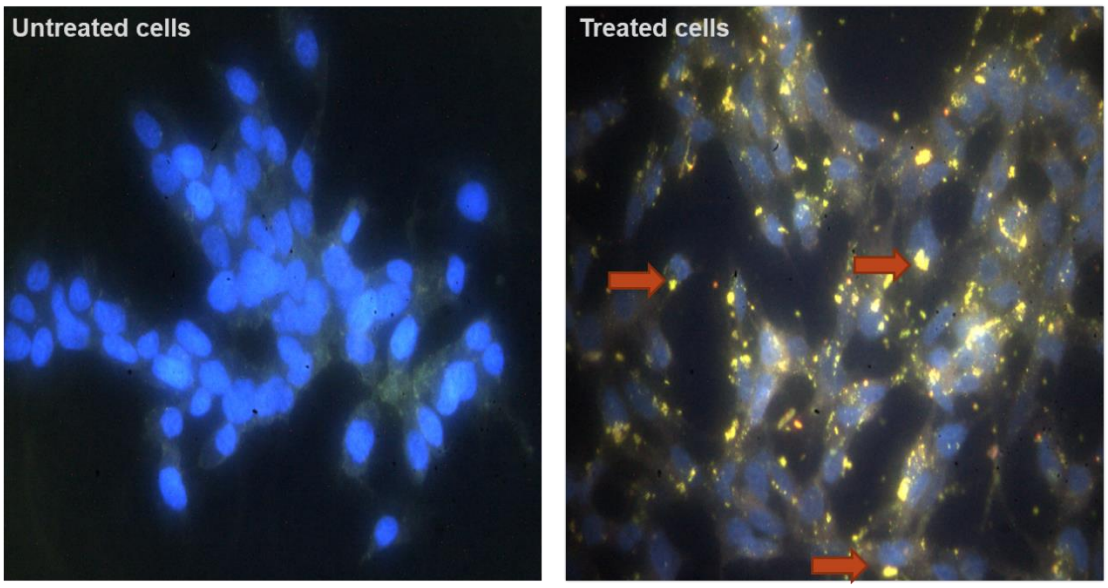

Figure 2.3: Determination of possible gold nanoparticle cell internalisation by hyperspectral dark field microscopy. Cells considered negative for possible internalisation are shown in untreated cells. Cells considered positive for internalisation are shown in treated cells, where red arrows show the presence of gold nanoparticles.

2.8.10.1 LNCaP cell internalisation by Dark-field microscopy

LNCaP cells were grown to 80% confluency and were then trypsinated with 1-2 ml 0.25% trypsin. Thereafter, the trypsin was inactivated by adding 2 ml of complete growth medium and a cell count was performed. Following this, cells were seeded over cover slips in sterile 6-well plates at 5×10^5 cells/well in 2 ml of complete growth medium. Cells were exposed to 50 and 100 µg/ml concentrations of the S1-AuNP's, S2-AuNP's and the Ng-AuNP's pH8, over 4, 6 and 24-hour periods, respectively. Hereafter, cells were washed 10 times with PBS and fixed 4% paraformaldehyde for 15 minutes at room temperature. The fixative was then removed and cells washed 3 times with PBS. To prepare the slides, cover slips were removed from the 6-well plates, inverted, mounted with DAPI (stain nuclear) on glass slides and allowed to incubate at room temperature for 10 minutes. Finally, staining was observed using a dark field microscope capable of hyperspectral imaging technology (CytoViva).

2.8.10.2 PC-3 cell internalisation by Dark-field microscopy

PC-3 cells were grown to 80% confluency and were then trypsinated with 1-2 ml 0.25% trypsin. Thereafter, the trypsin was inactivated by adding 2 ml of complete growth medium and a cell count was performed. Following this, cells were seeded over cover slips in sterile 6-well plates at 5×10^5 cells/well in 2 ml of complete growth medium. Cells were exposed cells to 50 and 100 µg/ml concentrations of the S1-AuNP's, S2-AuNP's and the Ng-AuNP's pH8, over 4, 6 and 24-hour periods, respectively. Hereafter, cells were washed 10 times with PBS and fixed 4% paraformaldehyde for 15 minutes at room temperature. The fixative was then removed and cells washed 3 times with PBS. To prepare the slides, cover slips were removed from the 6-well plates, inverted, mounted with DAPI (stain nuclear) on glass slides and allowed to incubate at room temperature for 10 minutes. Finally, staining was observed using a dark field microscope capable of hyperspectral imaging technology (CytoViva).

2.8.11 Cell internalisation of nanoparticles by transmission electron microscopy (TEM)

Transmission electron microscopy was used to further investigate the cell internalisation of gold nanoparticles generated in the present study in PC-3 prostate cancer cells.

PC-3 cells were grown to 80% confluency and were then trypsinated with 1-2 ml 0.25% trypsin. Thereafter, the trypsin was inactivated by adding 2 ml of complete growth medium and a cell count was performed. Following this, cells were seeded over cover slips in sterile 6-well plates at 5×10^5 cells/well in 2 ml of complete growth medium. Cells were exposed to 50 and 100 µg/ml concentrations of the S1-AuNP's, S2-AuNP's and the Ng-AuNP's pH8, over 6 and 24-hour periods, respectively. Hereafter, cells were washed 10-12 times with PBS and dislodged with 300 µl of 0.25% trypsin. The trypsin was inactivated by adding 500 µl of complete growth medium, cells transferred to 2 ml Eppendorf tubes and centrifuged at 125 x g to form a pellet. Next, supernatants were removed, cell pellets were washed with PBS and centrifuged once more at 125 x g.

Subsequently, the PBS was removed and carefully replaced with TEM fixative (100mM sodium cacodylate, 2% glutaraldehyde and 2% paraformaldehyde), without disturbing the cell pellet and stored at 4ºC. Finally, the fixed cell pellets were submitted to the Electron Microscopy Core Facility (EMC) at the University of Missouri, Columbia MO for grid preparation and viewed using a transmission electron microscope (Joel 1400).

2.9 *In vivo* experiments

2.9.1 Prostate cancer tumour xenograft studies

Preclinical prostate cancer mouse models provide an essential tool to improve our understanding of prostate cancer progression and development. These include xenografts mouse models, allografts mouse models, genetically engineered mouse models and knockout models. For the purpose of this study, the xenograft mouse model was used (Rea et al. 2016).

Clearance to perform the present animal study was obtained from the Institutional Animal Care and Use Committees (IACUC) of the Harry S. Truman Memorial Veterans Hospital and the University of Missouri, and was performed according to the Guide for the Care and Use of Laboratory Animals. For tumour studies, 49 male imprinting control region-severe combined immunodeficiency (SCID) mice (Taconic Farms, Hudson, New York) were inoculated on the right flank with PC-3 prostate cancer cells at a concentration of $10x10^6$ cells/ mouse, and tumours were allowed to develop for 4 weeks prior to first treatment. Hereafter, the mice were divided into 7 groups and randomised to achieve a comparable body weight (Table 2.2). Once randomised, the mice were treated twice weekly with the various samples at a concentration of 0.5 mg or 1.5 mg of gold/extract per kg of body weight by intra peritoneal (IP) injection, according to table#. Prior to each treatment, mice were weighed and bodyweight was recorded, tumours were measured using digital callipers for tumour volume calculations, and body condition scores were determined. Individual mice were removed from the study when body condition scores and body weight fell too low. The study was

continued until a sample size of 6 animals per group could no longer be maintained. Once the study had concluded, the mice were sacrificed by cervical-dislocation, blood samples were collected and tumours were excised and weighed. White blood cell counts, red blood cell and platelet parameters were measured using a haematological analyser (Hemavet 950FS)

Table 2.2: Dose design for *in vivo* study. Dosages ranged from 0.5 mg to 1.5 mg of extract or gold nanoparticle per kilogram bodyweight (0.5-1.5 mg/kg bw). Doses for gold nanoparticles was calculated based on total gold content, as determined by ICP-MS analysis.

Group	**Animals per group**	**Sample**	**Dose (mg/kg bw)**	**Dose per treatment**	**Treatments per week**	**Mode of Administration**
Group 1	7	Injectable water	Tumour only	1	2	IP
Group 2-7: tumour+ treatment						
Group 2	7	S1-AuNP	0.5	1	2	IP
Group 3	7	S1-AuNP	1.5	1	2	IP
Group 4	7	Ng-AuNP pH 8	0.5	1	2	IP
Group 5	7	Ng-AuNP	1.5	1	2	IP
Group 6	7	Naringenin	0.5	1	2	IP
Group 7	7	S1	0.5	1	2	IP

2.10 Statistical Analysis

Data generated in the present study were recorded and analysed statistically using MedCalc for Windows, version 19 (MedCalc Software, Mariakerke, Belgium). Experiments were run in triplicate and sample sizes were kept to 10. After calculating the summary stats, including the Kolmogorov-Smirnov test for normal distribution, data were analysed by means of the independent t-test if normally distributed. If the samples were not normally distributed, the Mann-Whitney test was used. To test for a trend between parameters, the repeated measures and one-way ANOVA was performed. A P-value of less than 0.05 was considered significant

Chapter 3

Results

3.1 Gold nanoparticle characterisation

3.1.1 Gold nanoparticle synthesis

Upon completion of each respective gold nanoparticle synthesis, images were taken to record their characteristic colours (Figure 3.1). Each of the extract-derived gold nanoparticles, namely the S1-AuNP's, S1x2-AuN's, S2-AuNP's and S2x2-AuNPs (A-D), were found to have a very deep-ruby colour. Conversely, the naringenin-derived gold nanoparticles (E-F) were found to have slightly varying colours, where the Ng-AuNP's pH 7 (E) were ruby-red in colour, and the Ng-AuNP's pH 8 (F) were found to be wine-red in colour.

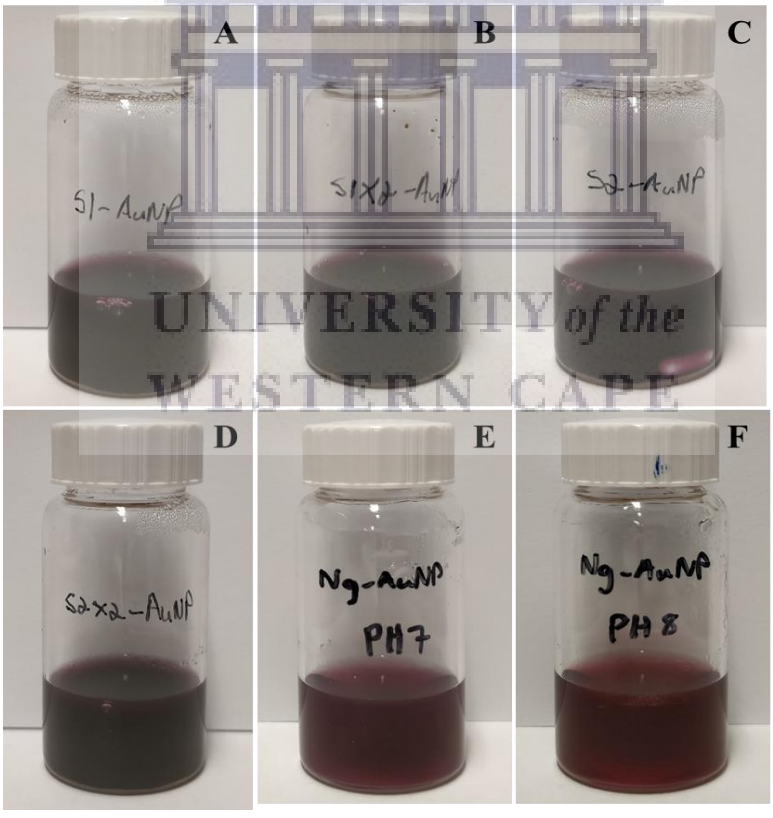

Figure 3.1: Characteristic colours of the S1-AuNP's (A), S1x2-AuNP's (B), S2-AuNP's (C), S2x2-AuNP's (D), Ng-AuNP's pH 7 (E) and Ng-AuNP's pH 8 (F). Extract-derived gold nanoparticles were deep-ruby in colour (A-D), while the Ng-AuNP's pH 7 were ruby-red in colour (E), and the Ng-AuNP's pH 8 were wine-red colour (F).

3.1.2 Ultraviolet spectroscopy

Spectrophotometric analysis was performed for each formulation (A-F) as the first step to confirm the presence of gold nanoparticles (Figure 3.2). UV-vis spectrometry yielded an absorption maximum consistent with the presence of gold nanoparticle for each formulation, specifically observed at 540 nm for the S1-AuNPs (A), 535 nm for the S1x2-AuNPs (B), 534 nm for the S2-AuNPs (C), 540 for the S2x2-AuNPs (D), 535 nm for the Ng-AuNPs pH 7 (E), and finally at 540 nm for the Ng-AuNPs pH 8 (F), respectively.

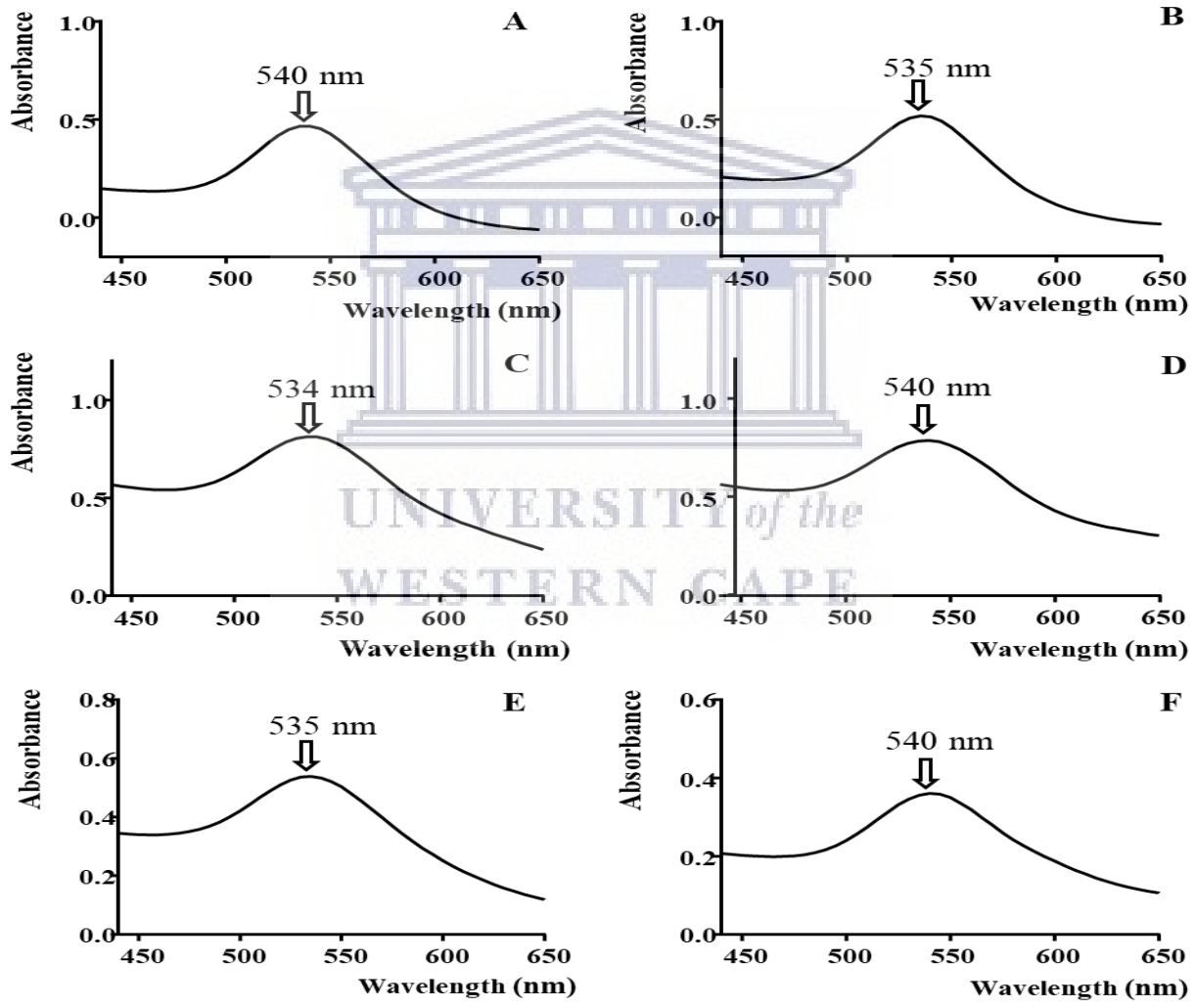

Figure 3.2: Spectrophotometric analysis of gold nanoparticles displaying the absorption maximums for S1-AuNP's (A), S1x2-AuNP's (B), S2-AuNP's (C), S2x2-AuNP's (D), Ng-AuNP's pH 7 (E) and Ng-AuNP's pH 8 (F).

3.1.3 Dynamic light scattering (DLS)

3.1.3.1 S1-nanoparticles

DLS was used to determine the hydrodynamic size and polydispersity index (PDI) for the S1-AuNPs and S1x2-AuNPs (Figure 3.3). Measurements of the S1-AuNPs (A) yielded an average hydrodynamic size of 88.36 nm with a PDI of 0.284, indicating a more monodispersed solution (Table 3.1). Measurements of S1x2-AuNPs (B) yielded an average hydrodynamic size of 160.86 nm, along with a PDI of 0.265 (Table 3.1).

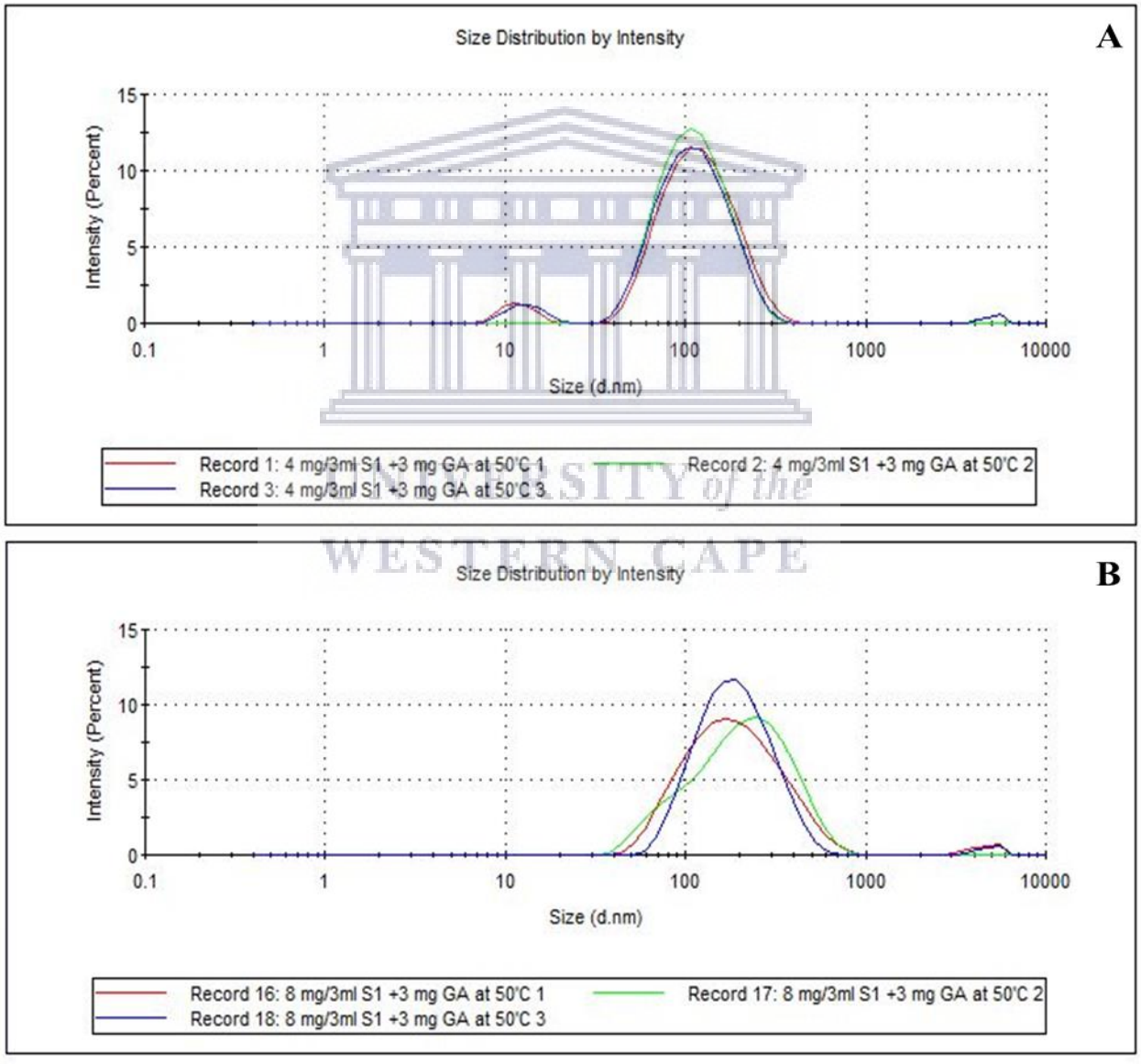

Figure 3.3: Hydrodynamic size measurements for the S1-AuNPs (A) with an average size of 88.36 nm, and S1x2-AuNPs (B) with an average size of 160.86 nm.

3.1.3.2 S2-nanoparticles

DLS was used to measure the hydrodynamic size and polydispersity index (PDI) for the S2-AuNPs and S2x2-AuNPs (Figure 3.4). Measurements of the S1-AuNPs (A) yielded an average hydrodynamic size of 96.73 nm with a PDI of 0.393, indicating a more monodispersed solution. Measurements of S2x2-AuNPs (B) yielded an average hydrodynamic size of 200.3 nm, along with a PDI of 0.223, indicating a higher degree of monodispersity.

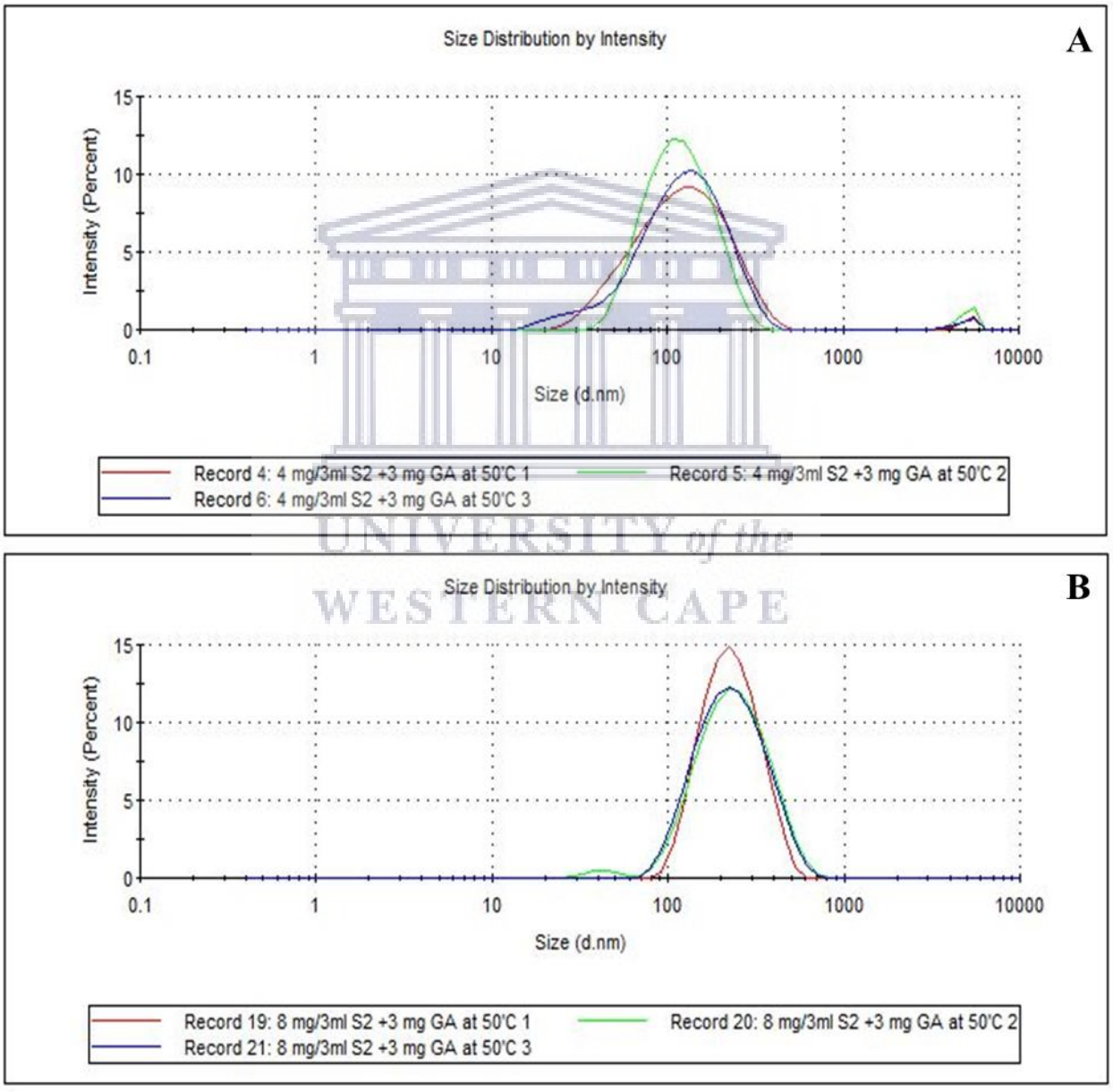

Figure 3.4: Hydrodynamic size measurements for the S2-AuNPs (A) with an average size of 96.73 nm, and S2x2-AuNPs (B) with an average size of 200.3 nm.

3.1.3.3 Naringenin-nanoparticles

DLS was measured to determine the hydrodynamic size and polydispersity index (PDI) for the NgAuNPs pH 7 and Ng-AuNPs pH 8 (Figure 3.5). Measurements of the Ng-AuNPs pH 7 (A) yielded an average hydrodynamic size of 27.1 nm with a PDI of 0.268, indicating a more monodispersed solution. Measurements of Ng-AuNPs pH 8 (B) yielded an average hydrodynamic size of 29.28 nm, along with a PDI of 0.685, indicating a more polydispersed solution.

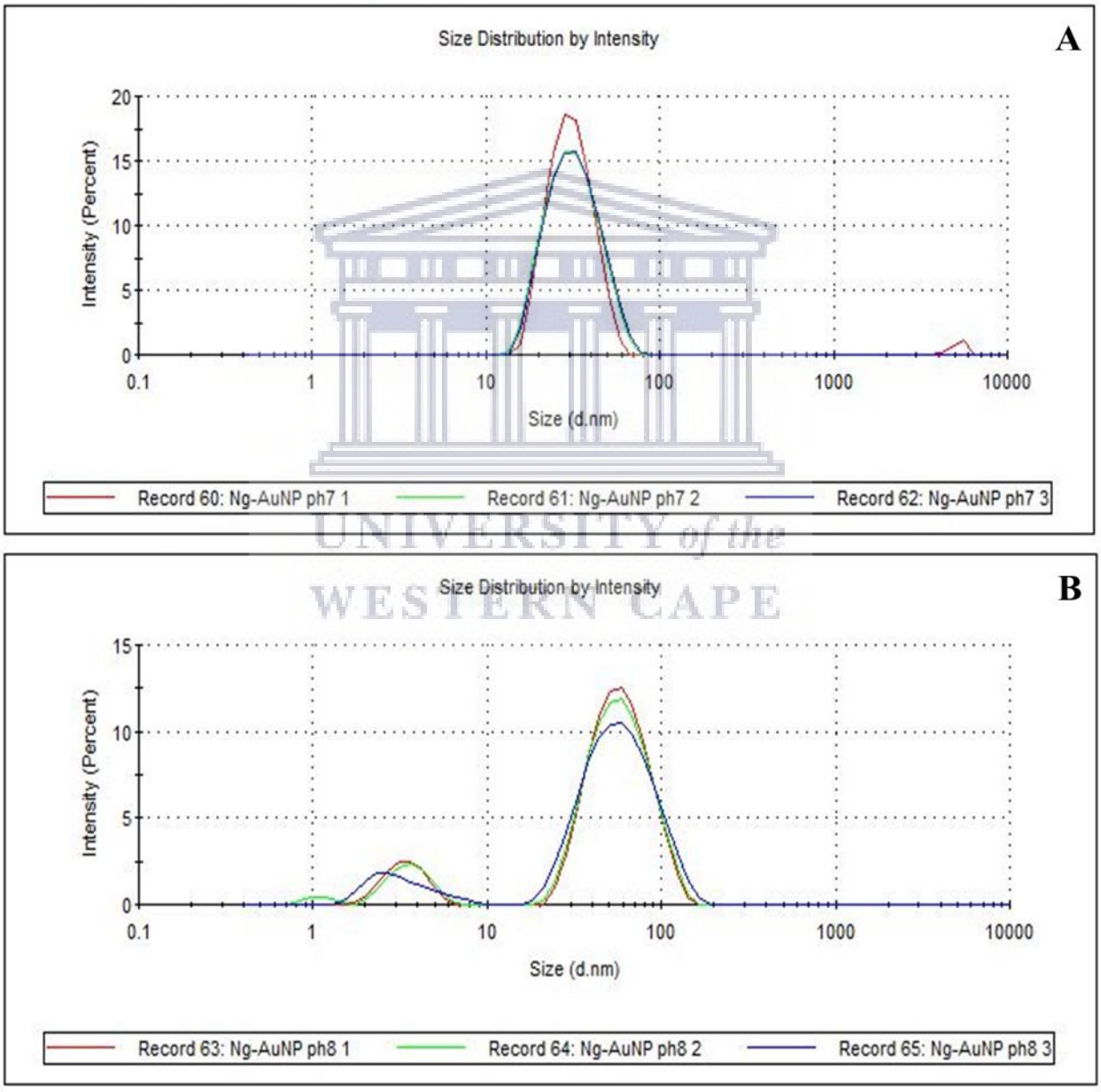

Figure 3.5: Hydrodynamic size measurements for the Ng-AuNPs pH 7 (A) with an average size of 27.1 nm, and Ng-AuNPs pH 8 (B) with an average size of 29.28 nm**.**

3.1.3.4 DLS and PDI summary

Table 3.1: Hydrodynamic size measurements and polydispersity index (PDI) measured for the S1-AuNP's, S1x2-AuNP's, S2-AuNP's, S2x2-AuNP's, Ng-AuNP's pH 7, and Ng-AuNP's pH 8.

Sample	DLS (nm)	Std Dev	PDI
S1-AuNP	88.36	1.410	0.284
S1x2-AuNP	160.9	1.716	0.265
S2-AuNP	95.73	1.935	0.393
S2x2AuNP	200.3	1.308	0.223
Ng-AuNP pH 7	27.1	0.680	0.264
Ng-AuNP pH 8	29.28	0.096	0.685

3.1.4 Zeta potential

3.1.4.1 S1-nanoparticles

Zeta potential was measured to determine the surface forces, and thereby stability, of the S1-AuNPs and S1x2-AuNPs (Figure 3.6). Measurements of the S1-AuNPs (A) yielded an average zeta potential of -21.1 mV, and the S1x2-AuNPs (B) yielded an average zeta potential of -26.2 mV, conferring acceptable colloidal stability for both formulations.

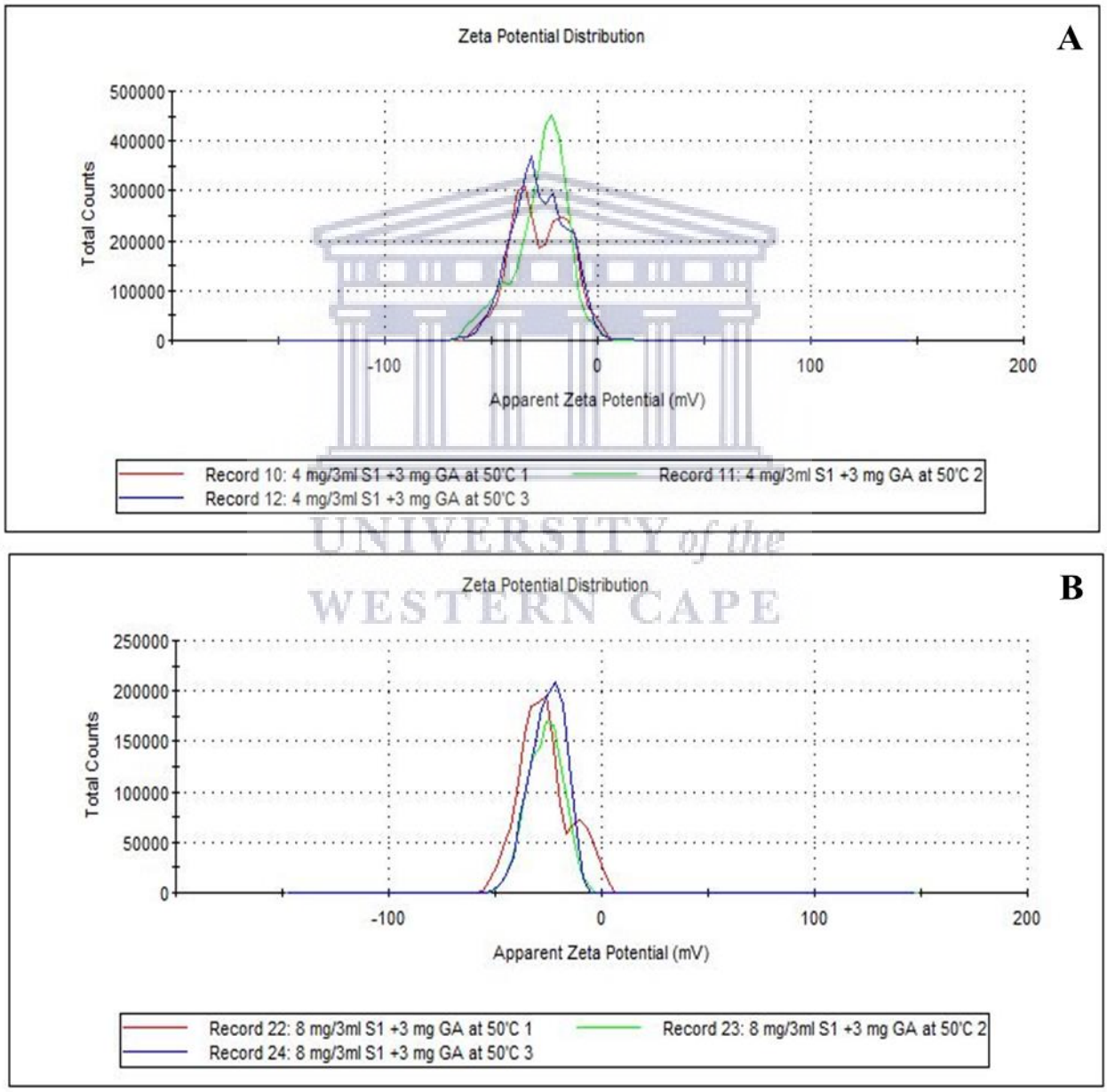

Figure 3.6: Zeta-potential measurements for the S1-AuNPs (A) with an average charge of -21.1 mV, and S1x2-AuNPs (B) with an average charge of -26.2 mV.

3.1.4.2 S2-nanoparticles

Zeta potential was measured to determine the surface forces, and thereby stability, of the S2-AuNPs and S2x2-AuNPs (Figure 3.7). Measurements of the S1-AuNPs (A) yielded an average zeta potential of -29.3 mV, and the S1x2-AuNPs (B) yielded an average zeta potential of -26.7 mv, conferring a high degree of stability for both formulations.

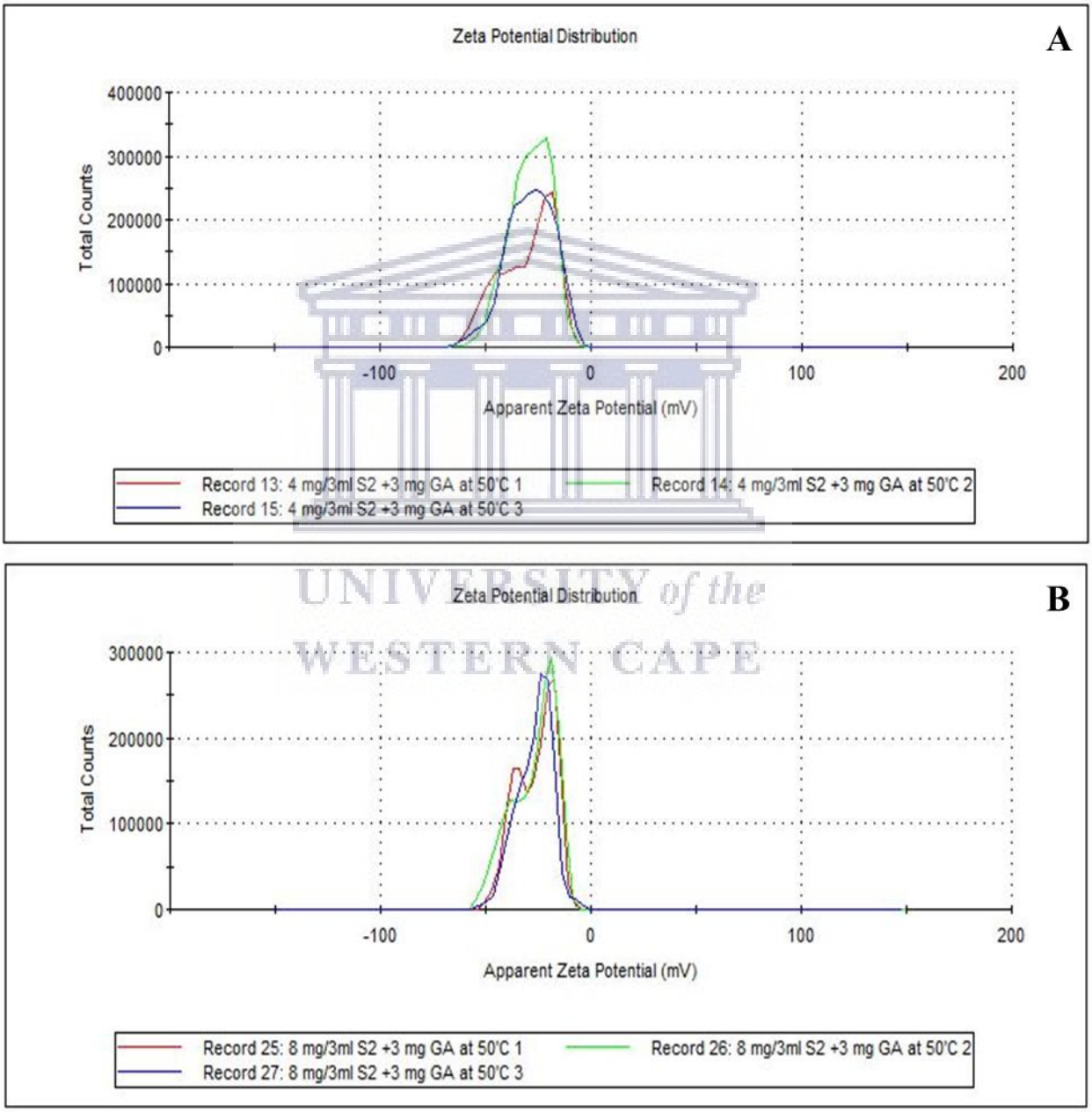

Figure 3.7: Zeta-potential measurements for the S2-AuNPs (A) with an average charge of -29.3 mV, and S2x2-AuNPs (B) with an average charge of -26.7 mV.

3.1.4.3 Naringenin nanoparticles

Zeta potential was measured to determine the surface forces, and thereby stability, of the Ng-AuNPs pH 7 and Ng-AuNPs pH 8 (Figure 3.8). Measurements of the Ng-AuNPs pH 7 (A) yielded an average zeta potential of -41.0 mV, and the Ng-AuNPs pH 8 (B) yielded an average zeta potential of -33.3 mV, conferring a high degree of stability for both formulations.

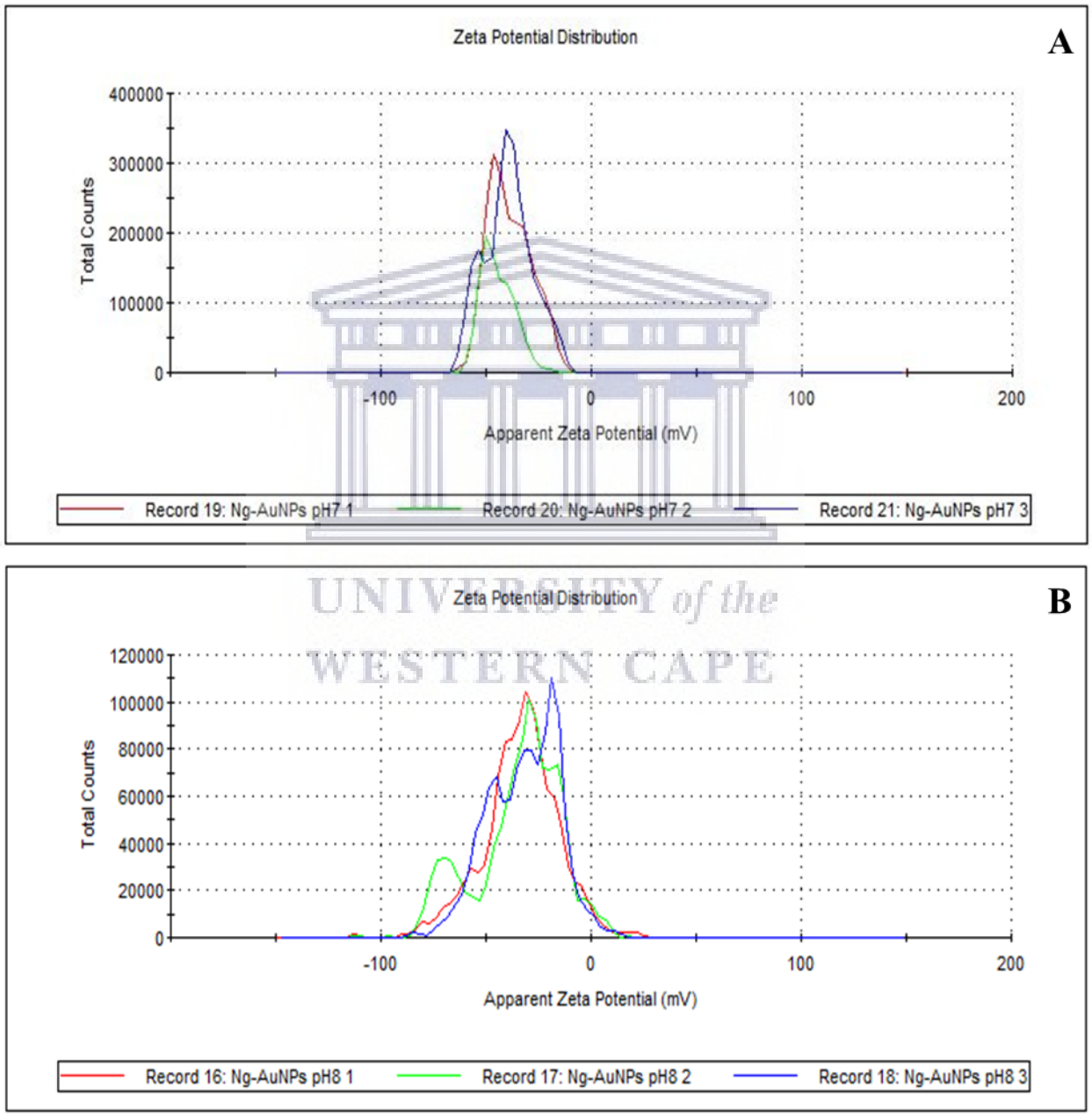

Figure 3.8: Zeta-potential measurements for the Ng-AuNPs pH 7 (A) with an average charge of -41.0 mV, and Ng-AuNPs pH 8 (B) with an average charge of --33.3 mV.

3.1.4.4 Zeta potential summary

Table 3.2 Zeta-potential measurements for the S1-AuNP's, S1x2-AuNP's, S2-AuNP's, S2x2-AuNP's, Ng-AuNP's pH 7, and Ng-AuNP's pH 8.

Sample	Zeta potential (mV)	Std Dev
S1-AuNP	-27.1	0.200
S1x1-AuNP	-26.2	0.781
S2-AuNP	-29.3	0.808
S2x2-AuNP	-26.7	0.256
Ng-AuNP pH 7	-41.0	3.17
Ng-AuNP pH 8	-33.3	1.31

3.1.5 Transmission electron microscopy

Transmission electron microscopy (TEM) imaging was used to visualise and definitively confirm the presence of gold nanoparticles in each formulation (A-F) (Figure 3.9).

Observably, S1-AuNPs (A) consisted of a majority spherically shaped nanoparticles, along with a small proportion of triangle shaped nanoparticles, of variable size. S1x2-AuNPs (B) presented with a uniformly spherical shape, along with low observable particle size variation. S2-AuNPs (C) a majority spherically shaped nanoparticles, along with a small proportion of triangle shaped nanoparticles, with moderate observable particle size variation. S2x2-AuNPs (D) consisted of spherically shaped nanoparticles of a consistent observable size. Similarly, both Ng-AuNPs pH 7 (E) and Ng-AuNPs pH 8 (F) were spherically shaped with a consistent observable size.

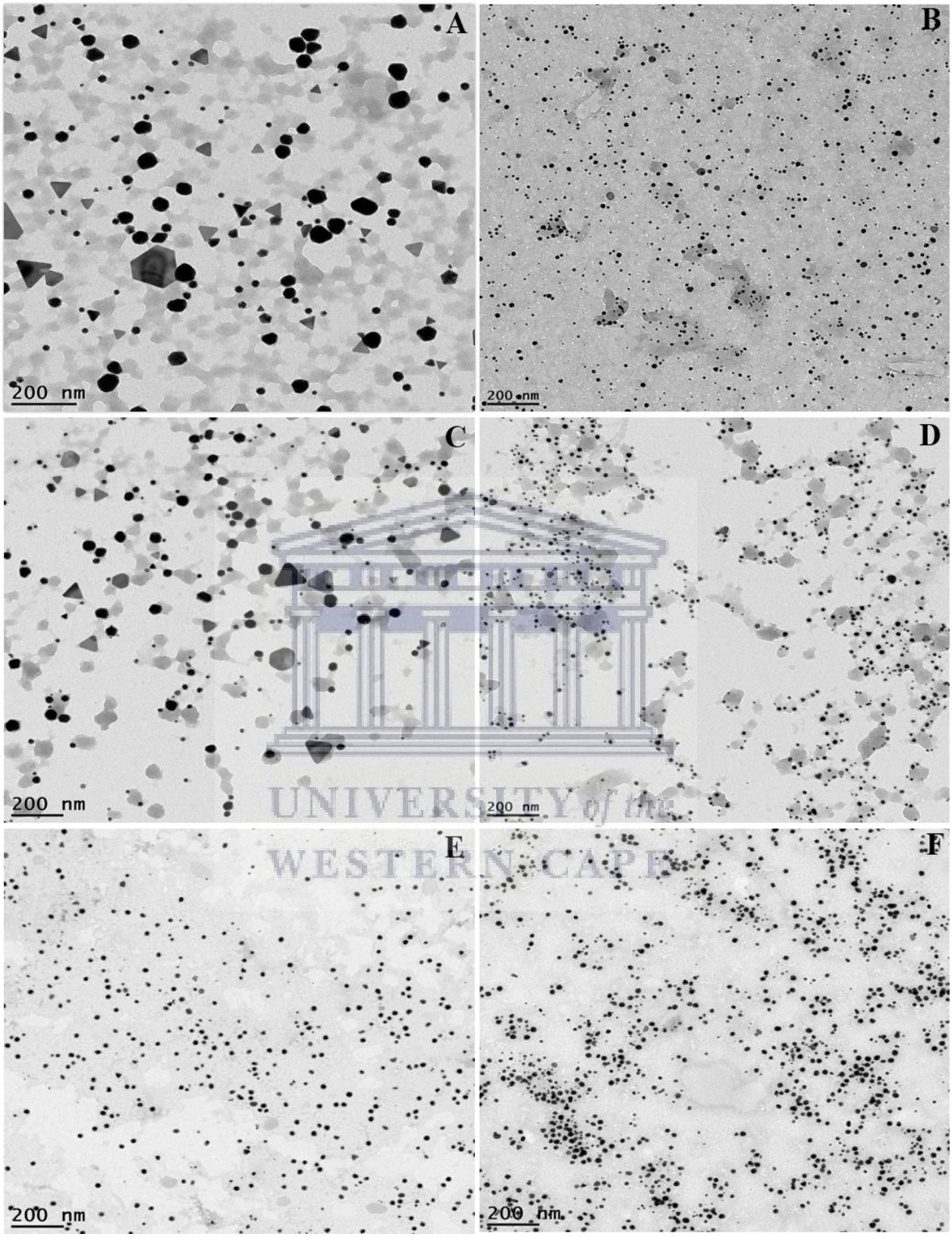

Figure: 3.9: Transmission electron microscopy (TEM) imaging depicting the S1-AuNP's (A), S1x2-AuNP's (B), S2-AuNP's (C), S2x2-AuNP's (D), Ng-AuNP's pH 7 (E), and Ng-AuNP's pH 8 (F).

3.1.6 Size distribution histograms

3.1.6.1 S1-nanoparticles

Size distribution histograms yielded a particle size range between 6 nm and 60 nm for S1-AuNPs (A) with a calculated average particle size of 28.29 nm, along with particle sizes ranging between 6 nm to24 nm for S1x2-AuNPs (B), with a calculated average size of 13.05 nm (Figure 3.10).

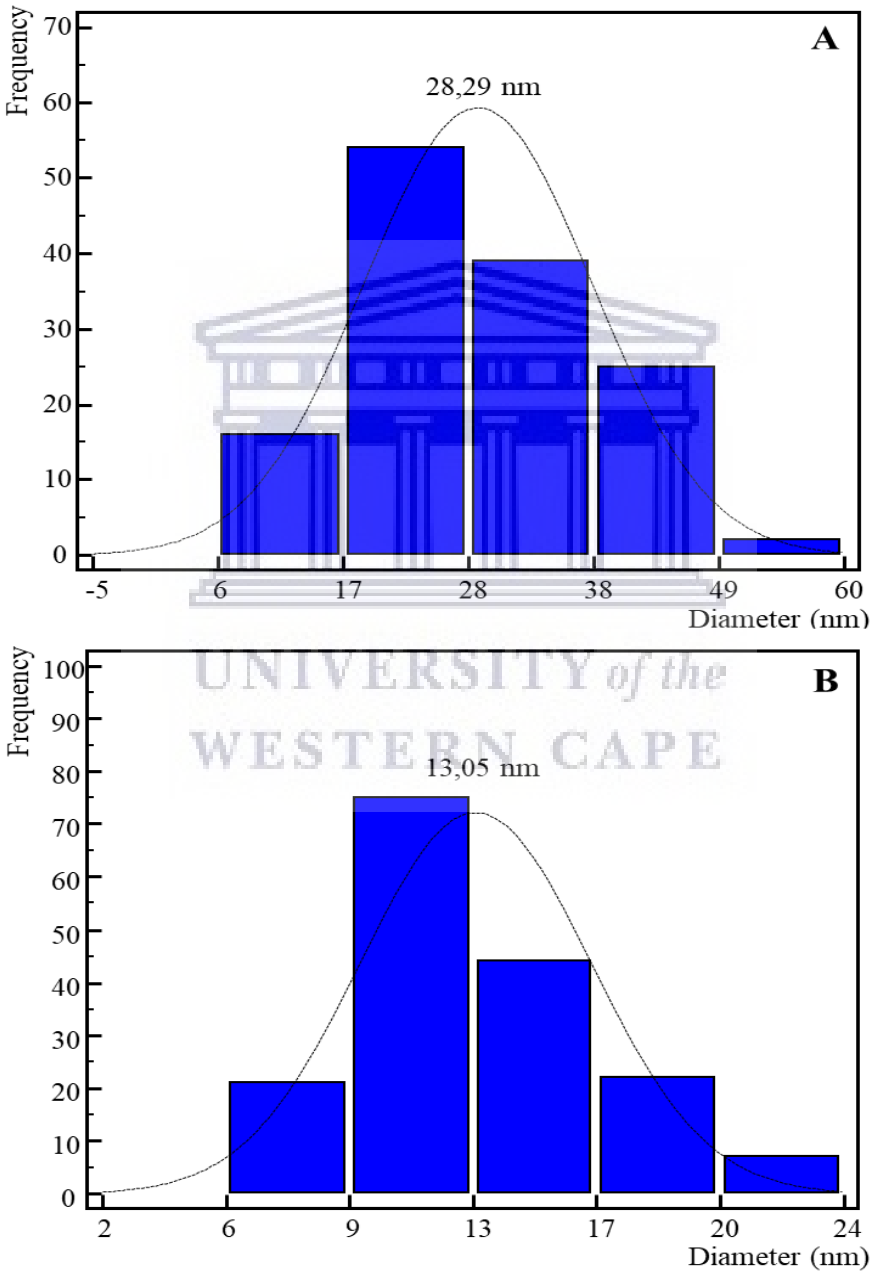

Figure 3.10: Size distribution histograms for the S1-AuNP's (A) with an average particles size of 28.29 nm, and the S1x2-AuNP's (B) with and average particles size of 13.05 nm.

3.1.6.2 S2-nanoparticles

Particle sizes ranging between 7 nm and 35 nm was observed for S2-AuNPs (A) with a calculated average particle size of 18.99 nm. Furthermore, particle sizes ranging between 3 nm to 35 nm was observed for S2x2-AuNPs (B), with a calculated average size of 13.02 nm (Figure 3.11).

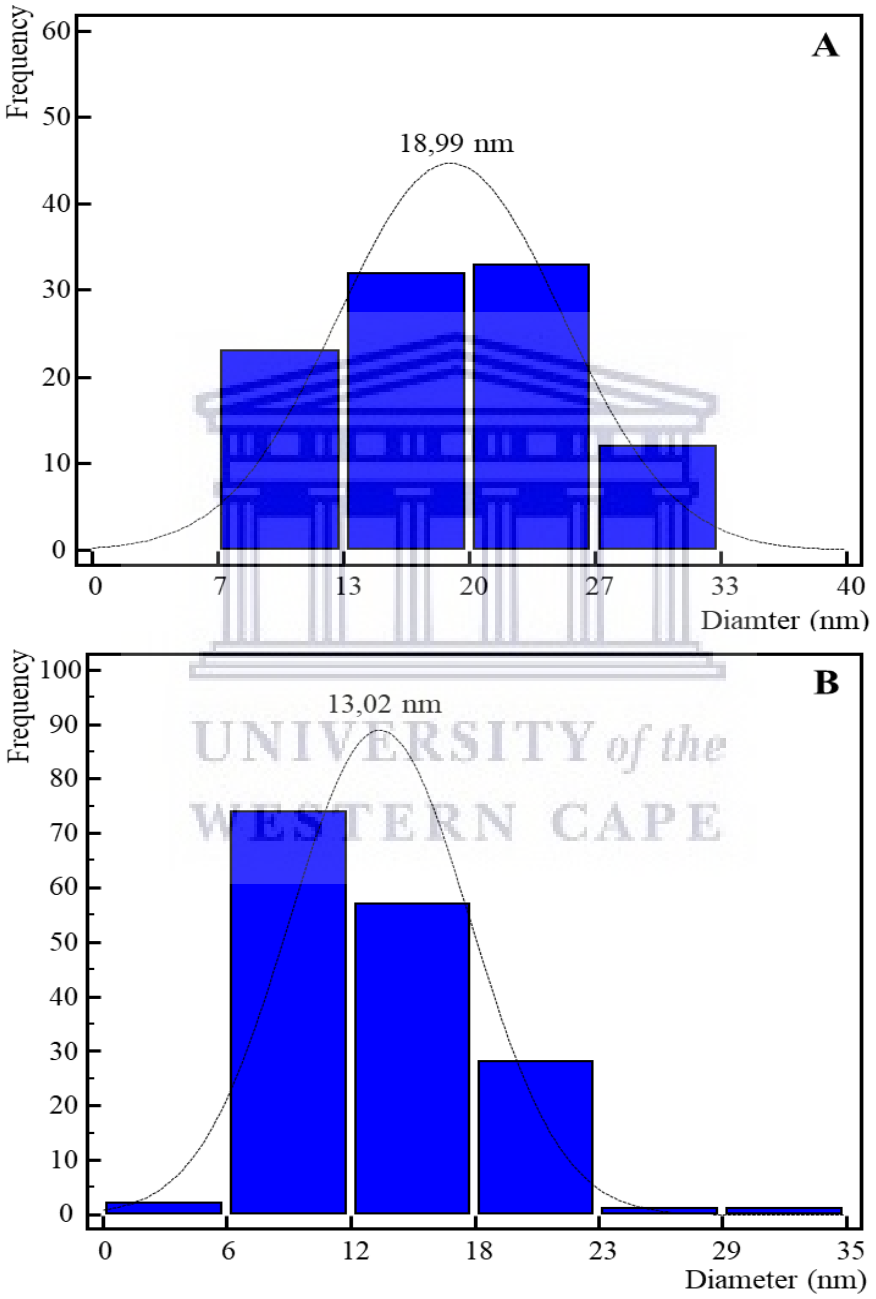

Figure 3.11: Size distribution histograms for the S2-AuNP's (A) with an average particles size of 18.99 nm, and the S2x2-AuNP's (B) with and average particles size of 13.02 nm.

3.1.6.3 Naringenin-nanoparticles

Size distribution histograms yielded a particle size range between 2 nm and 26 nm for Ng-AuNPs pH 7 (A) with a calculated average particle size of 15.71 nm, along with particle sizes ranging between 2 nm to 30 nm for Ng-AuNPs pH 8 (B), with a calculated average size of 12.53 nm (Figure 3.12).

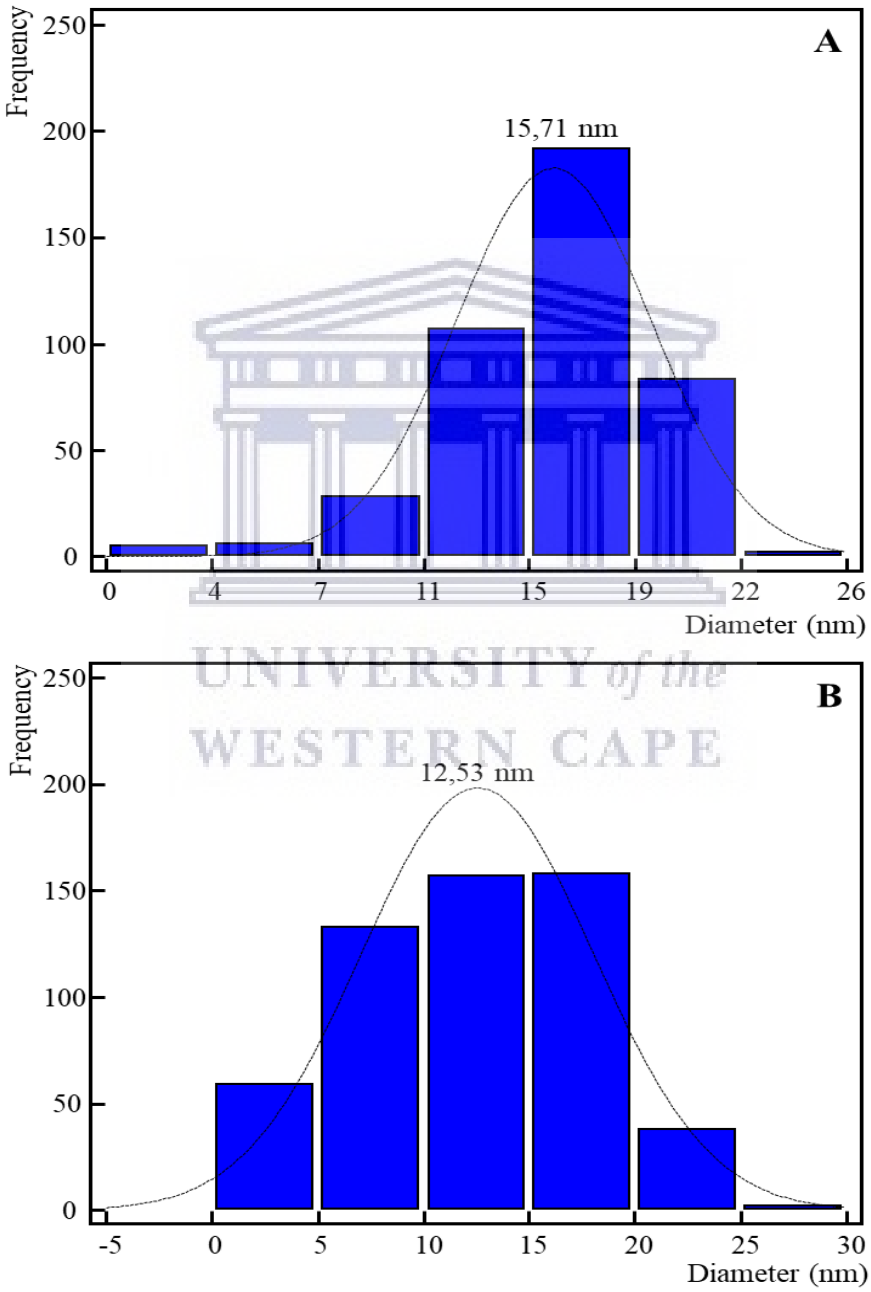

Figure 3.12: Size distribution histograms for the Ng-AuNP's pH 7 (A) with an average particles size of 15.71 nm, and the Ng-AuNP's pH 8 (B) with and average particles size of 12.53 nm.

3.1.7 Total polyphenolic quantification

As determined by the Folin-ciocalteu phenol (FC) method, the calculated total polyphenolic concentration, equivalent to Gallic acid, was 447 µg/ml for S1-AuNPs, 694 µg/ml for S1x2-AuNPs, 487 µg/ml for S2-AuNPs, 738 µg/ml for S2x2-AuNPs, 423 µg/ml for Ng-AuNPs pH 7, and 288 µg/ml for Ng-AuNPs pH 8, respectively (Table 3.3).

Table 3.3: Total polyphenol calculations for the S1-AuNP's, S1x2-AuNP's, S2-AuNP's, S2x2-AuNP's, Ng-AuNP's pH 7, and Ng-AuNP's pH 8, as measured by the FC pholin method.

Sample	**Absorbance at 760 nm**	**Calculated concentration (µg/ml) Gallic acid eq.**
S1-AuNP	0.3038	447
S1x2-AuNP	0.4523	694
S2-AuNP	0.3278	487
S2x2-AuNP	0.4786	738
Ng-AuNP pH 7	0.2503	423
Ng-AuNP pH 8	0.1817	288

3.1.8 LC-MRM analysis

Levels of naringenin were quantified in each *T. capensis* extract using LC-MRM analysis (Figure 3.13). Naringenin was found to be higher in the S1 extract and lower in the S2 extract (A), while quercetin was found to be lower in the S1 extract and higher in the S2 extract (B).

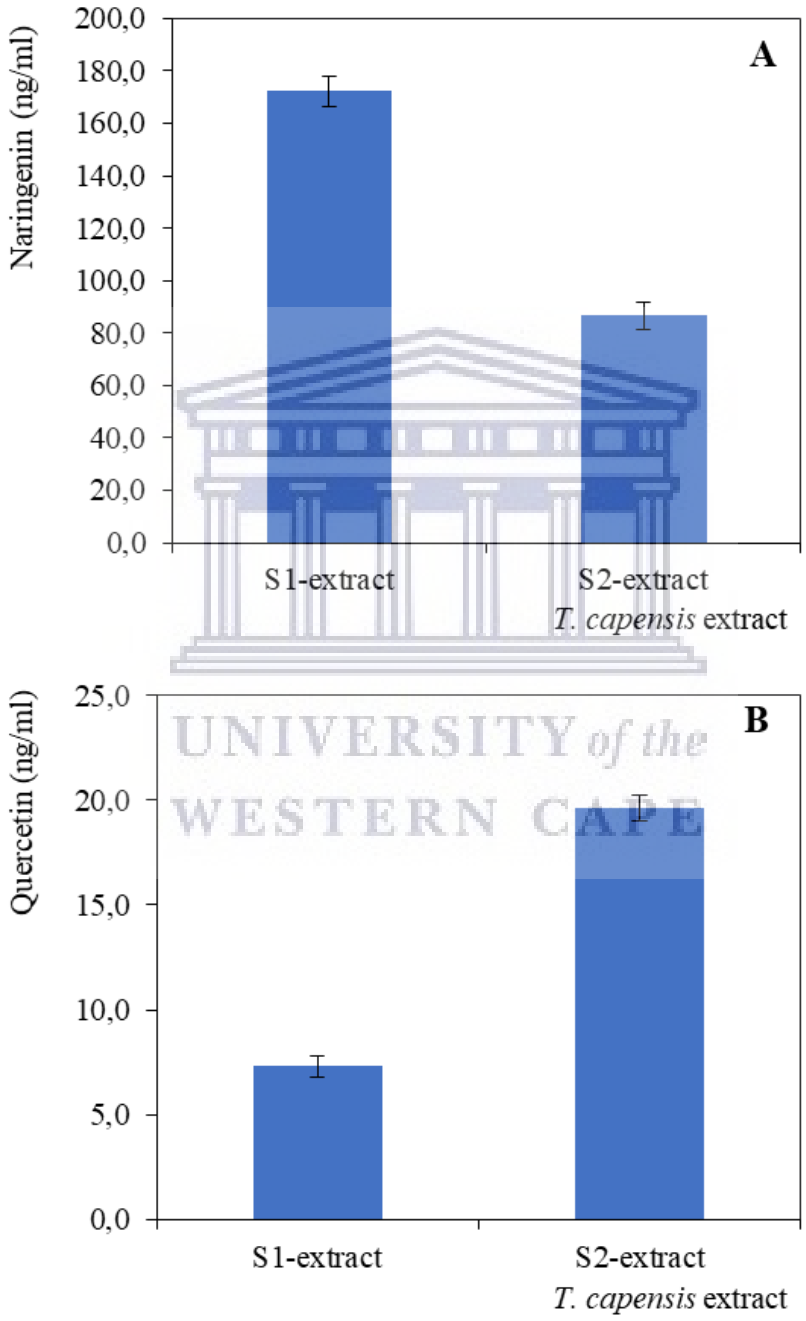

Figure 3.13: Naringenin and quercetin content of the S1 and S2 extract analysed by LC-MRM.

3.1.9 Gold content analysis

Gold content of samples considered to be candidates for *in vitro* study was analysed by ICP-MS (Table 3.4), and was later used to calculate the appropriate dosages. A gold content of 336 ppm was observed for S1-AuNPs, 318 ppm observed for S2-AuNPs, and finally 185 ppm observed for Ng-AuNPs pH 8.

Table 3.4: Gold content analysis for gold nanoparticle formulation by ICP-MS.

Sample	Gold content (ppm)
S1-AuNP	336
S2-AuNP	318
Ng-AuNP pH 8	185

3.1.10 Gold nanoparticle stability in challenging media

3.1.10.1 S1-AuNP's and S1x2-AuNP's

The S1-AuNP's (Figure 3.14) and S1x2-AuNP's (Figure 3.15) were incubated with various blood mimicking components, namely sodium chloride (NaCl), cysteine, histidine, human serum albumin (HSA), bovine serum albumin (BSA), and phosphate buffered saline (PBS), over 0 (A), 1 (B), 24 (C) and 48 (D) hour periods, as well as over a 7 day period (E).

The S1-AuNP's exhibited slight increases in absorption maxima was observed at each time point (A-E) following incubation with each medium, without the occurrence of peak widening between 0 and 48 hour incubation periods. Following 7 days of incubation (E), slight peak widening was observed for nanoparticles incubated with BSA, along with a slight decrease in absorption maxima for nanoparticle incubated with PBS. The S1x2-AuNP's exhibited no notable changes toward absorption maxima or peak width were observed for each medium used between 0 and 24 incubation

periods (A-C), followed by a slight decrease in absorption maxima for nanoparticles treated with PBS over 48 hour (D) and 7 day incubation periods (E).

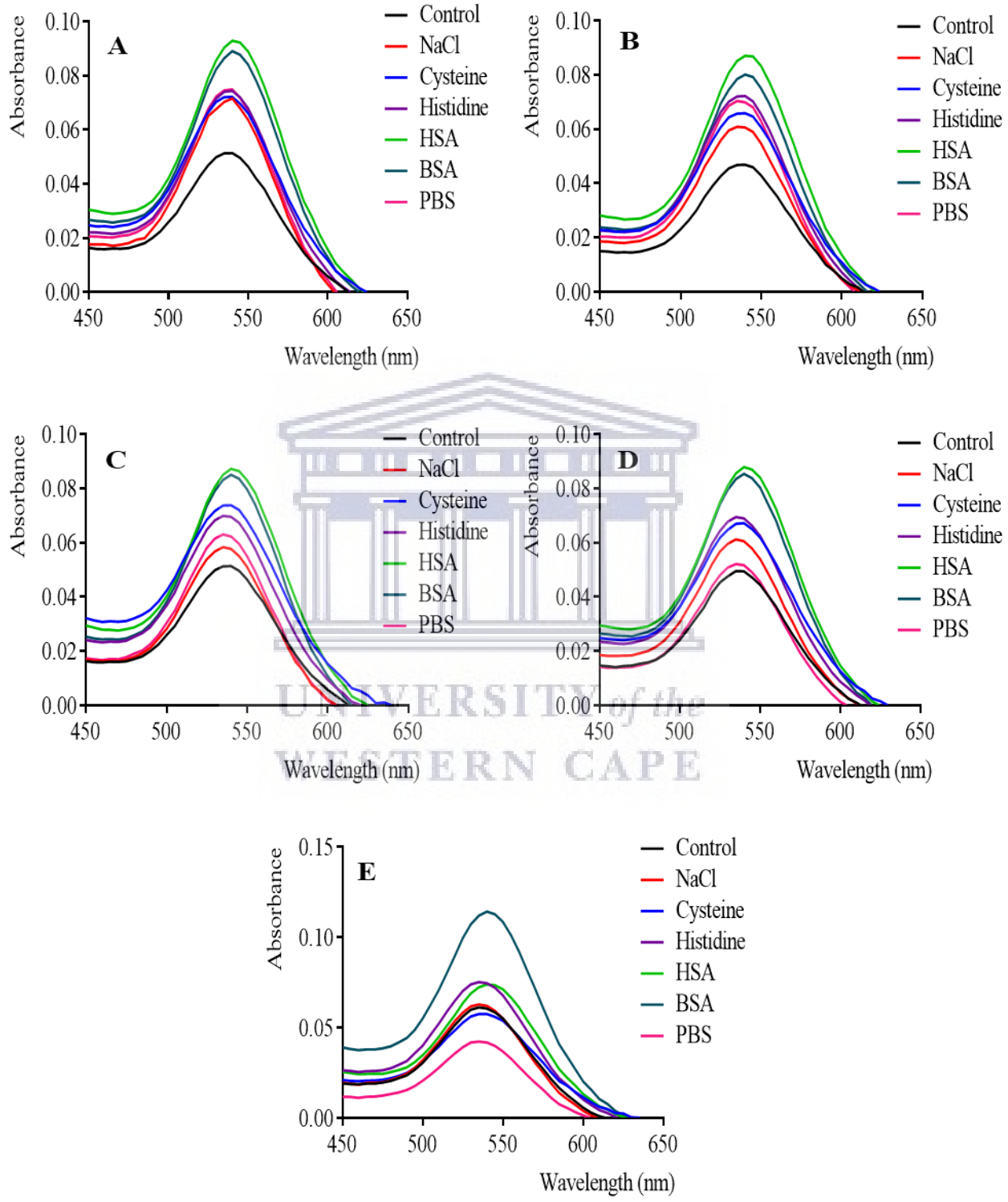

Figure 3.14: Stability of the S1-AuNP's in various blood mimicking components, over a 0 hour (A), 1 hour (B), 24 hour (C), 48 hour (D), and 7 day (E) incubation period.

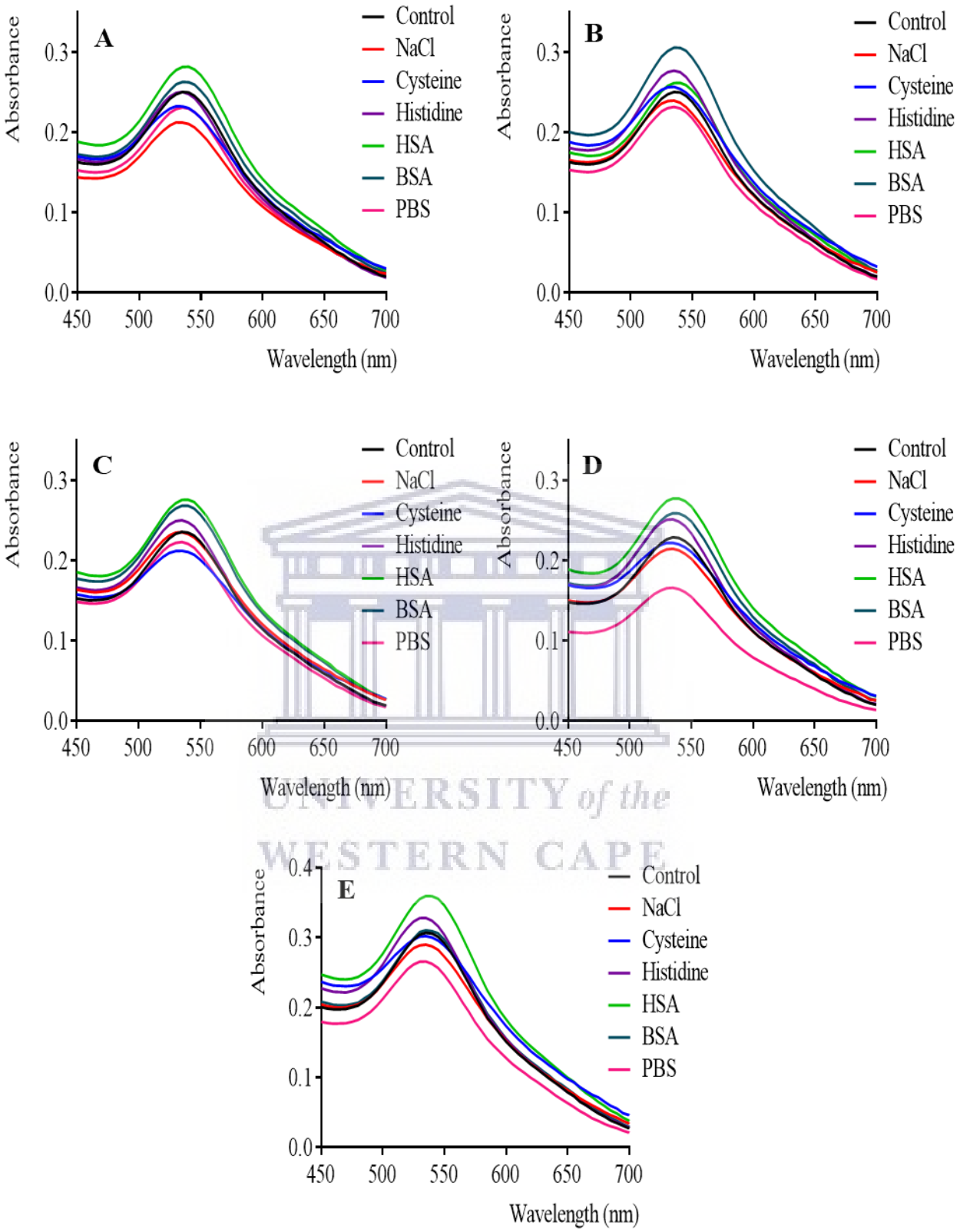

Figure 3.15: Stability of the S1x2-AuNP's in various blood mimicking components, over a 0 hour (A), 1 hour (B), 24 hour (C), 48 hour (D), and 7 day (E) incubation period.

3.1.10.2 S2-AuNP's and S2x2-AuNP's

The S2-AuNP's (Figure 3.16) and S2x2-AuNP's (Figure 3.17) were incubated with various blood mimicking components, namely sodium chloride (NaCl), cysteine, histidine, human serum albumin (HSA), bovine serum albumin (BSA), and phosphate buffered saline (PBS), over 0 (A), 1 (B), 24 (C) and 48 (D) hour periods, and over a 7 day period (E). Only S2-AuNP's treated with BSA exhibited slight increases in absorption maxima between 0 and 24 hour incubation periods (A-C), followed by histidine, cysteine and NaCl over 48 hour (D) and 7 day incubation periods (E). No notable peak widening was noted at each time point. The S2x2-AuNP's exhibited absorption maxima and peak widths relatively similar to control following incubation with each medium between 0 and 48 hour periods (A-D). Hereafter (E), slight increases in absorption maxima were exhibited by nanoparticles treated with NaCl, histidine, BSA and HAS, along with slight decreases exhibited by PBS and cysteine.

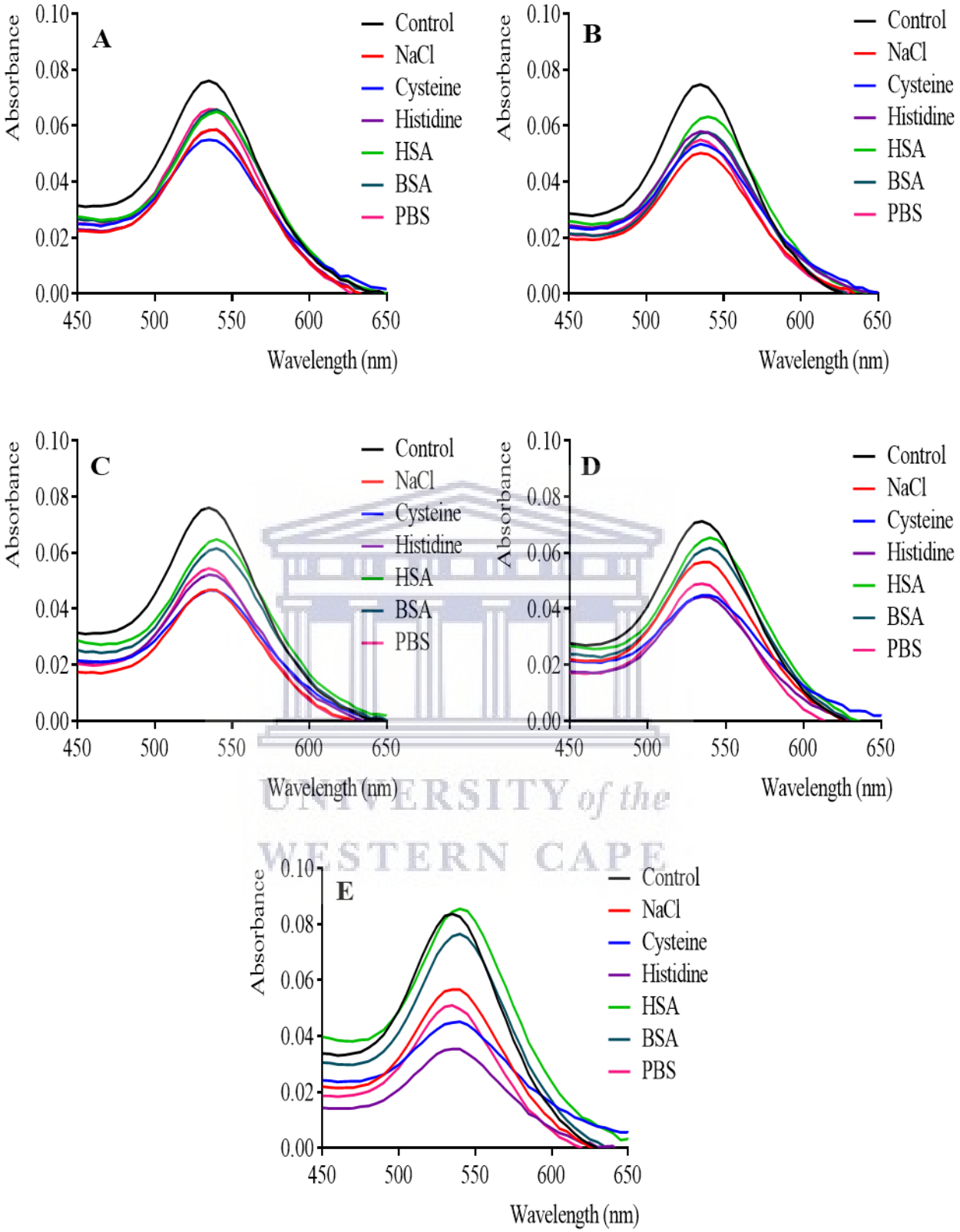

Figure 3.16: Stability of the S2-AuNP's in various blood mimicking components, over a 0 hour (A), 1 hour (B), 24 hour (C), 48 hour (D), and 7 day (E) incubation period.

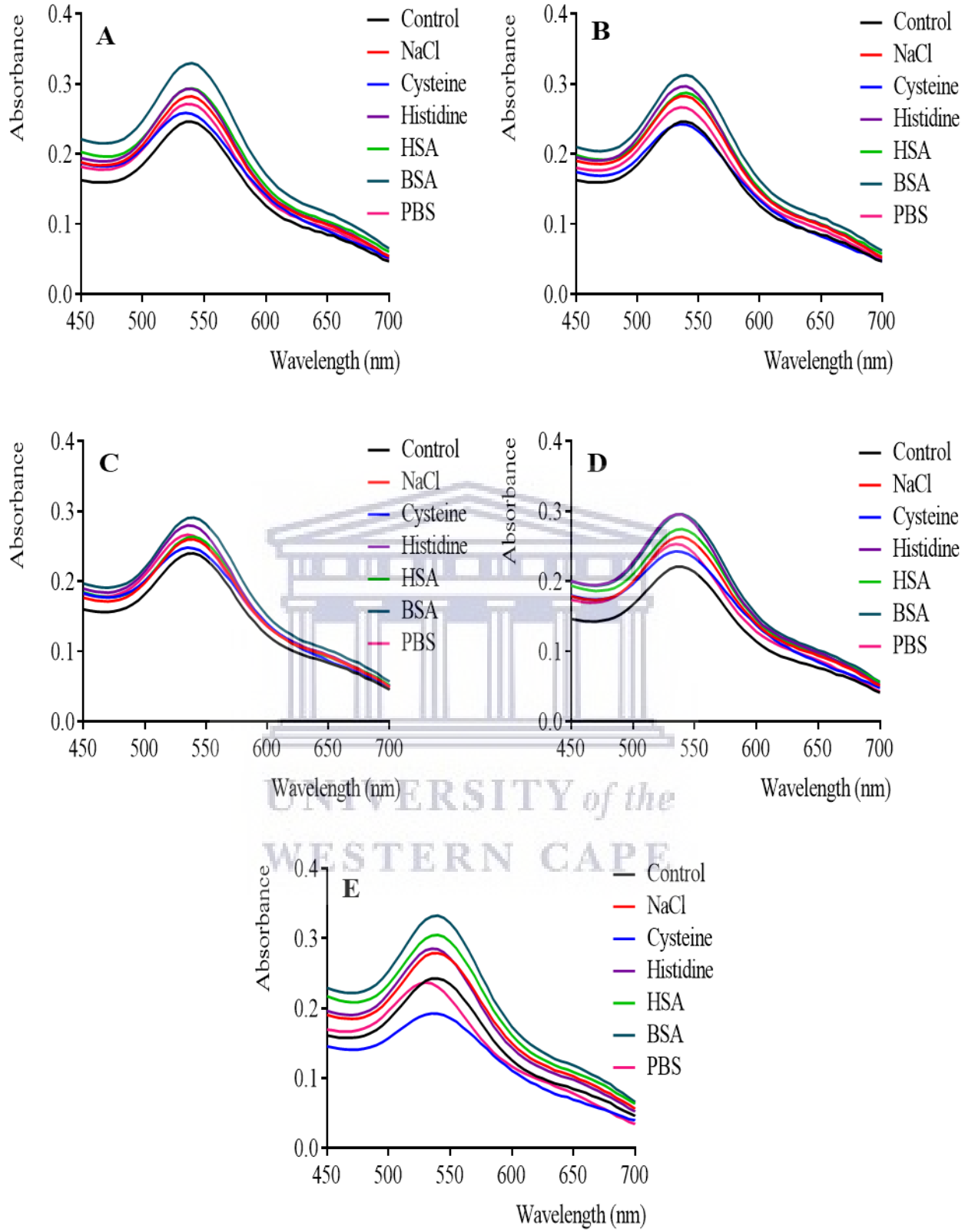

Figure 3.17: Stability of the S2x2-AuNP's in various blood mimicking components, over a 0 hour (A), 1 hour (B), 24 hour (C), 48 hour (D), and 7 day (E) incubation period.

3.1.10.3 Ng-AuNPs pH 7 and Ng-AuNP's pH 8

The Ng-AuNP's pH 7 (Figure 3.18) and Ng-AuNP's pH 8 (Figure 3.19) were incubated with various blood mimicking components, namely sodium chloride (NaCl), cysteine, histidine, human serum albumin (HSA), bovine serum albumin (BSA), and phosphate buffered saline (PBS), over 0 (A), 1 (B), 24 (C) and 48 (D) hour periods, and over a 7 day period (E). Slight, but progressive decreases in absorption maxima was observed for between 0 hours and 7 days of incubation (A-E), for nanoparticles treated with NaCl, histidine, PBS, cysteine and HAS. Despite the slightly decreasing absorption maxima, peak widths remained comparable to control between 0 hours and 7 days of incubation (A-E). Upon analysis of the Ng-AuNP's pH 8, each medium yielded absorption maxima and peak widths comparable to control between 0 and 24 hours of incubation (A-B), followed by decreased absorption maxima and increased peak width for nanoparticles treated with NaCl between 24 hours and 7 days of incubation (C-E). Additionally, PBS yielded decreased absorption maxima following 7 days of incubation (E).

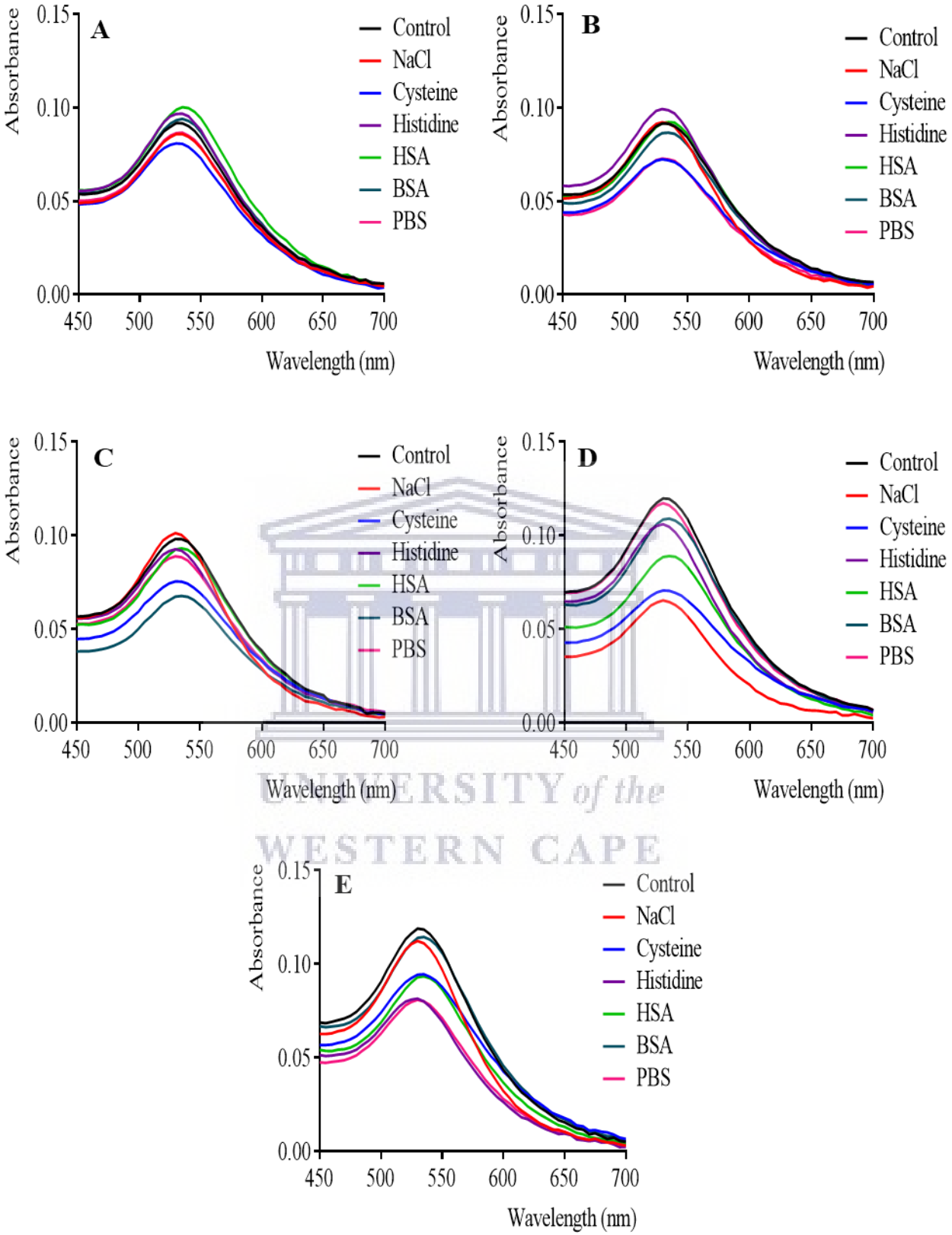

Figure 3.18: Stability of the Ng-AuNP's pH 7 in various blood mimicking components, over a 0 hour (A), 1 hour (B), 24 hour (C), 48 hour (D), and 7 day (E) incubation period.

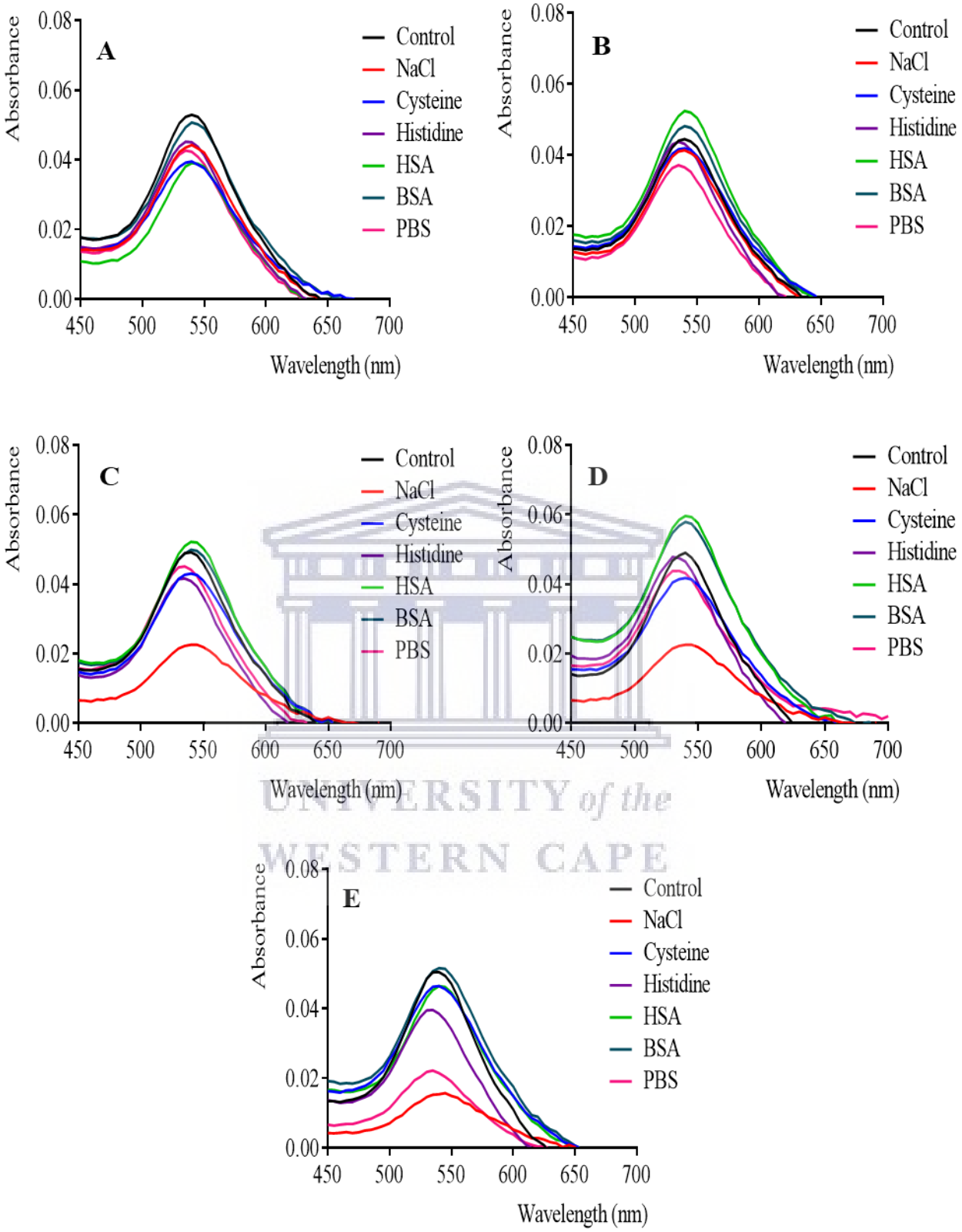

Figure 3.19: Stability of the Ng-AuNP's pH 8 in various blood mimicking components, over a 0 hour (A), 1 hour (B), 24 hour (C), 48 hour (D), and 7 day (E) incubation period.

3.2 Cell Viability

3.2.1 PC-3 cell viability

3.2.1.1 S1-AuNP's and S1 extract

After being exposed to increasing concentrations of the S1 extract (A-F) and S1-AuNP's (G-L) over 24 hours, cell morphology was observed and recorded (Figure 3.20). No observable change in the flat, polygonal morphology had occurred between the control and 200 µg/ml of the extract (A-F). At the highest concentration (F), cells became more sparely spaced. Similarly, no observable change in morphology was observed between the control and 12.5 µg/ml of the AuNP's (G-H). At higher concentrations (I-J) cells became more sparely spaced, atypically rounded, along with showing signs of cell stress (K) and cell death (L).

Following 48 hours of exposure to increasing concentrations of the S1 extract (A-F) and S1-AuNP's (G-L) over 48 hours, cell morphology was observed and recorded (Figure 3.21). The flat and polygonal morphology remained unchanged between the control and 50 µg/ml of the extract (A-E), while showing signs of cell rounding at the highest concentration (F). Similarly, no observable change in morphology was observed between the control and 25 µg/ml of the AuNP's (G-I). At higher concentrations (I-L), cells became progressively sparely spaced, atypically rounded, and displayed signs of cell stress (K) and cell death (L).

Post 72-hour exposure to increasing concentrations of the S1 extract (A-F) and S1-AuNP's (G-L), cell morphology was observed and recorded (Figure 3.22). Cell morphology remained relatively unchanged between the control and 200 µg/ml of the extract (A-F). Slightly fewer cells were observed at the highest concentration (F). Similarly, cell morphology remained unchanged between the control and lower concentrations of the AuNP's (G-J). Between 25-200 µg/ml, cells became progressively sparsely spaced, in addition to displaying atypical cell rounding at 100 µg/ml and signs of cell death at 200 µg/ml.

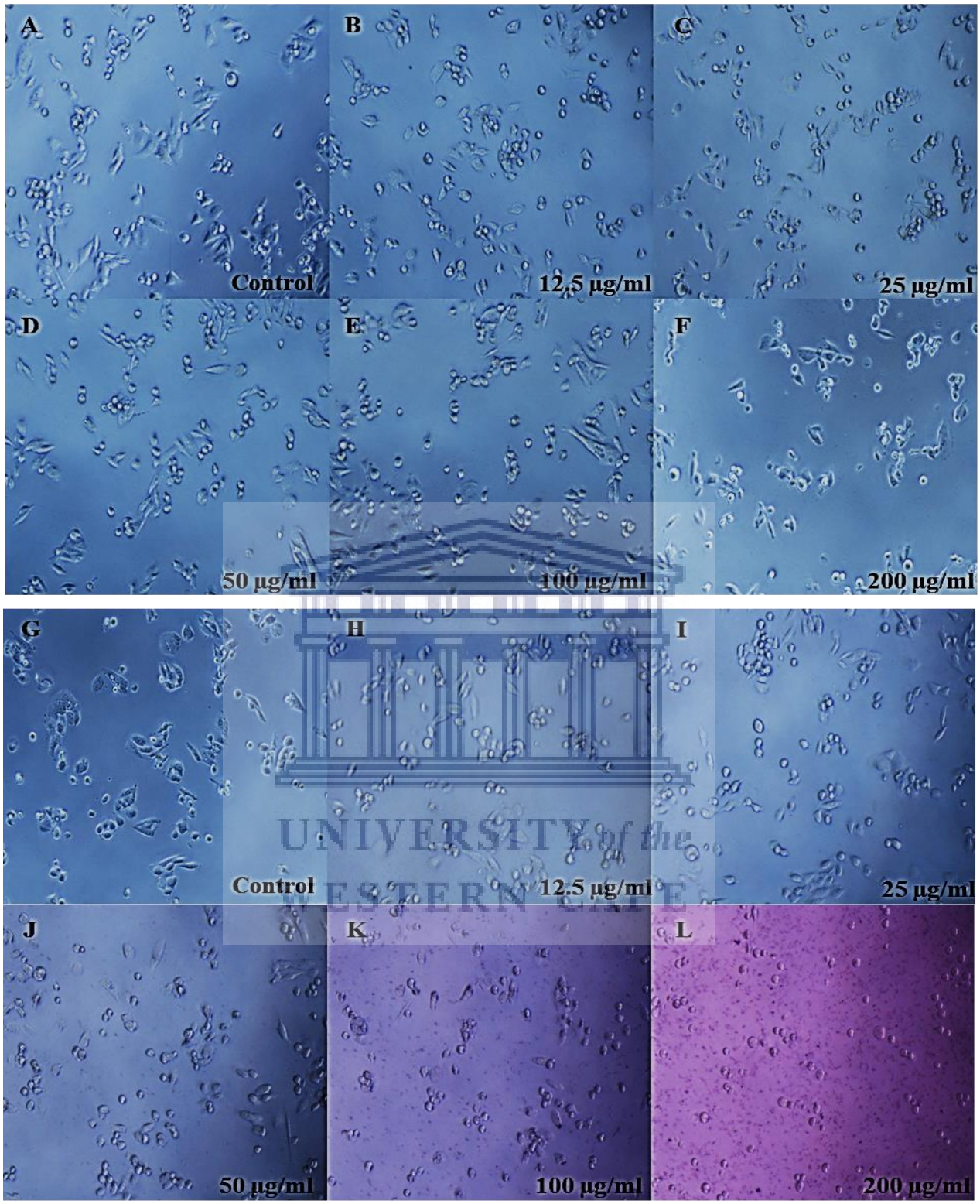

Figure 3.20: PC-3 cell morphology after being exposed to increasing concentrations of the S1 Extract and S1-AuNPs over a 24-hour period. The extract yielded no change in morphology, with slightly less observable cells at 200 µg/ml (F), whereas the AuNP's yielded cell rounding (K) and signs of cell death (L), at higher concentrations.

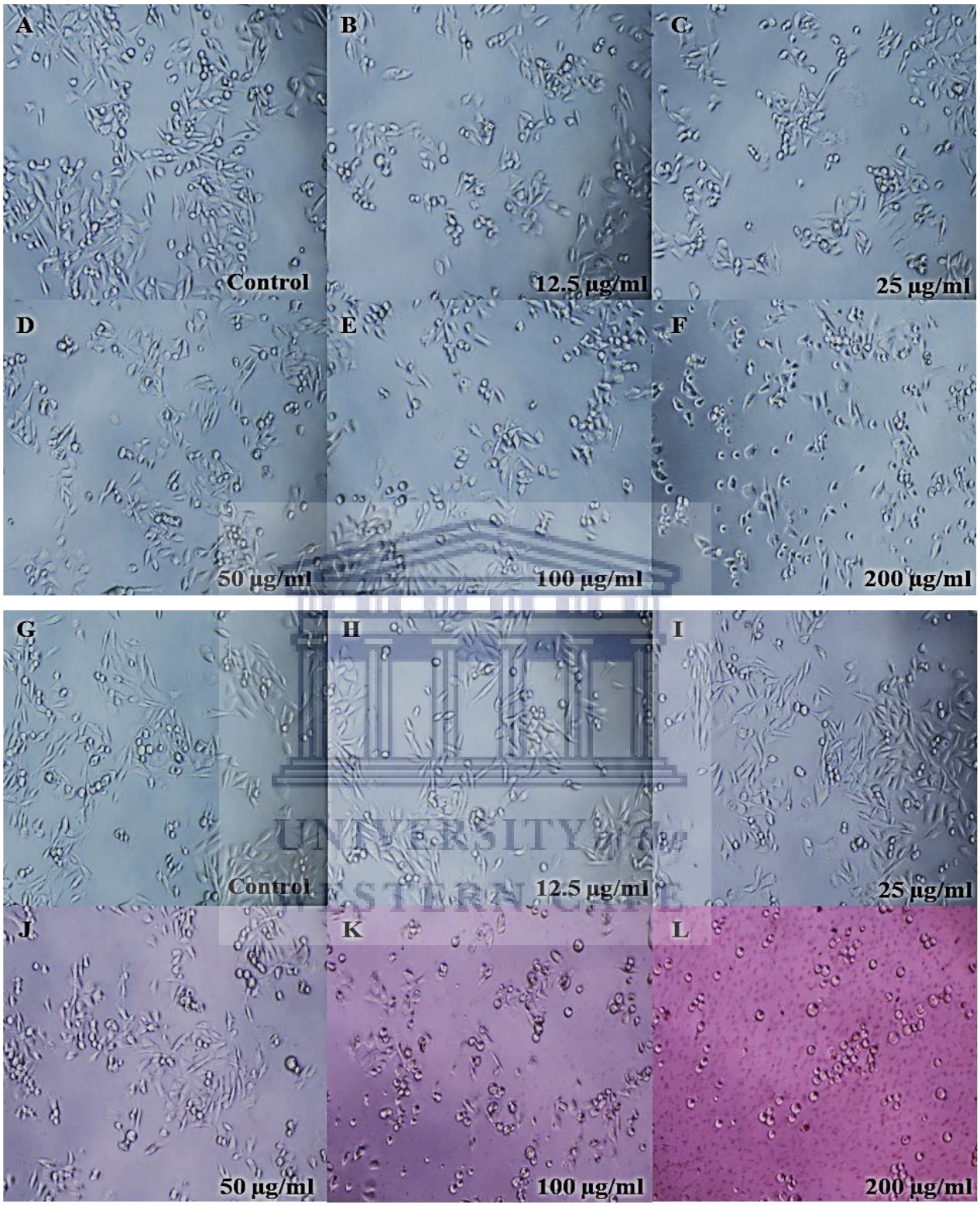

Figure 3.21: PC-3 cell morphology after being exposed to increasing concentrations of the S1 Extract and S1-AuNPs over a 48-hour period. The extract yielded no change in morphology at lower concentrations (A-E), with slight rounding at the highest concentration (F). The AuNP's yielded cell rounding and signs of death at higher concentrations (K-L).

Figure 3.22: PC-3 cell morphology after being exposed to increasing concentrations of the S1 Extract and S1-AuNPs over a 72-hour period. The extract yielded no change in morphology between the control and highest concentrations (A-F), with slight fewer observed cells at 200 µg/ml. The AuNP's yielded cell rounding at 1000 µg/ml and signs of death at 200 µg/ml.

After 24-hours of exposure to both the extract and AuNP's (Figure 3.23 A), the MTT assay revealed dose-depended decreases in cell viability between the control and 200 µg/ml with the AuNP's yielding sharper decreases between 50 µg/ml and 200 µg/ml. Significant (P=0.03, P=0.0001, P=0.0001) differences in the reduction of cell viability were observed between the extract and AuNP's at 50 µg/ml, 100 µg/ml and 200 µg/ml. The repeated measures ANOVA yielded a significant (P<0.0001, P<0.0001) trend for both the extract and AuNP's, respectively, between the control and 200 µg/ml. Similarly, one-way ANOVA revealed a significant (P<0.001, P<0.001) trend between the control and 200 µg/ml, for both the extract and AuNP's.

Similarly, 48-hours of exposure (Figure 3.23 B) yielded dose-depended decreases in cell viability between the control and 200 µg/ml, with the AuNP's yielding a greater reduction in cell viability at each concentration. Significant (P=0.0408, P=0.0012, P=0.0045, P<0.0001, P=0.0004) differences in the reduction of cell viability were observed between the extract and AuNP's at 12.5 µg/ml, 25 µg/ml, 50 µg/ml, 100 µg/ml and 200 µg/ml. The repeated measures ANOVA yielded a significant (P=0.0001, P<0.0001) trend for the extract and AuNP's between the control and 200 µg/ml. Similarly, one-way ANOVA revealed a significant (P<0.001 and P<0.001) trend between the control and 200 µg/ml, for the extract and AuNP's.

Equally, 72-hours of exposure yielded dose-depended decreases in cell viability between the control and 200 µg/ml, with the AuNP's yielding a notably greater reduction in cell viability at each concentration (Figure 3.23 C). Significant (P<0.0001, P=0.0001, P<0.001, P<0.0001, P<0.0001) differences in the reduction of cell viability were observed between the extract and AuNP's at 12.5 µg/ml, 25 µg/ml, 50 µg/ml, 100 µg/ml and 200 µg/ml, along with repeated measures ANOVA yielding a significant (P<0.0001, P<0.0001) trend for the extract and AuNP's between the control and 200 µg/ml. Similarly, one-way ANOVA revealed a significant (P<0.001 and P<0.001) trend between the control and 200 µg/ml, for the extract and AuNP's, respectively.

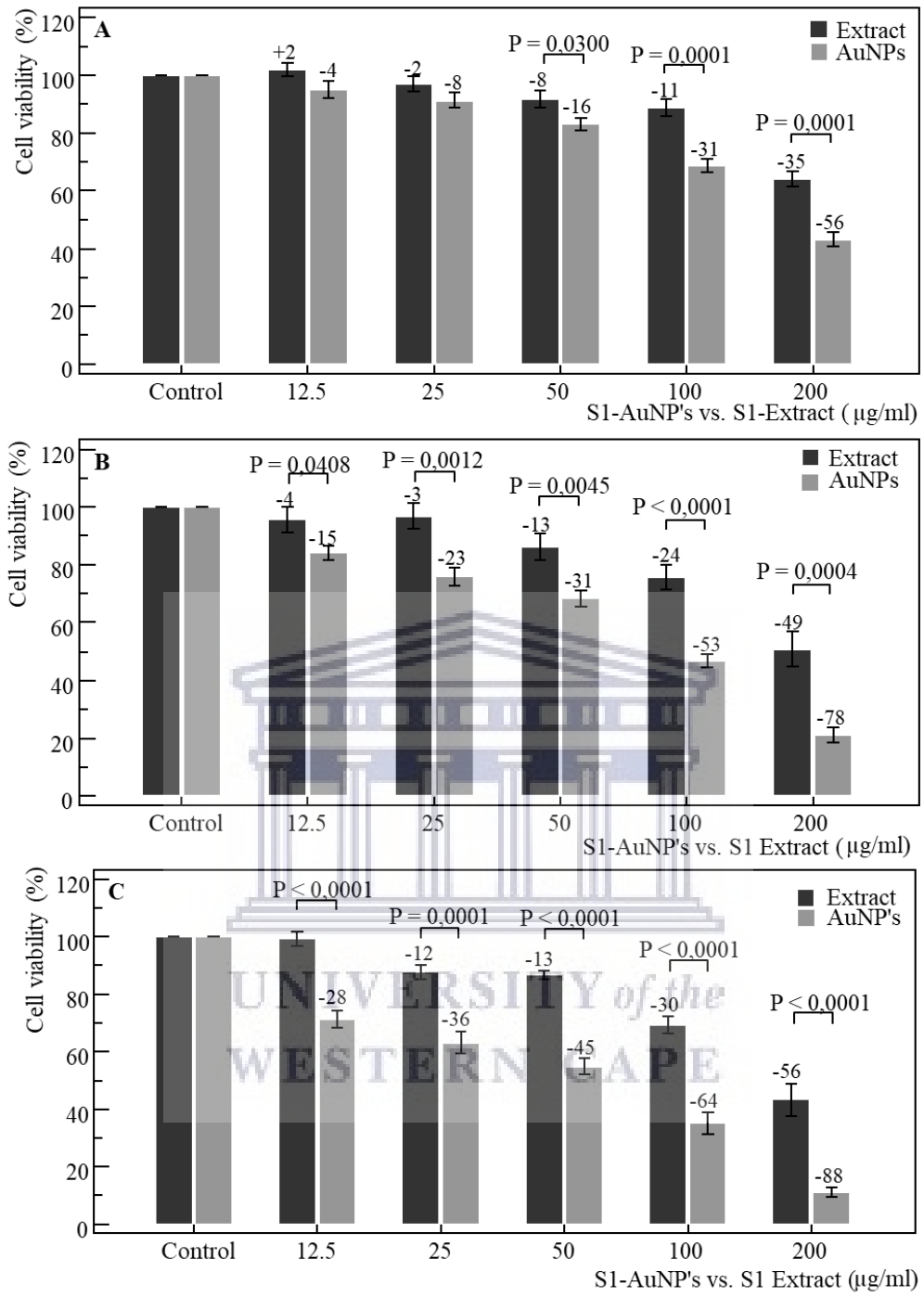

Figure 3.23: PC-3 cell viability as determined by the MTT assay over 24 (A), 48 (B) and 72 (C) hour exposure to the S1 Extract and S1-AuNP's, respectively. Significant (P=0.03, P=0.0001, P=0.0001) differences between the extract and AuNP's were observed between 50-200 µg/ml over 24 hours, significant (P=0.0408, P=0.0012, P=0.0045, P<0.0001, P=0.0004) differences between 12.5-200 µg/ml after 48 hours, and finally significant (P<0.0001, P=0.0001, P<0.001, P<0.0001, P<0.0001) differences between 12.5-200 µg/ml after 72 hours of exposure.

3.2.1.2 S1x2-AuNP's and S1 extract

After being exposed to increasing concentrations of the S1 extract (A-F) and S1x2-AuNP's (G-L) over 24 hours, cell morphology were observed and recorded (Figure 3.24). No observable change in the flat, polygonal morphology had occurred between the control and 200 µg/ml of the extract (A-F). At the highest concentration (F), cells became more sparely spaced. Similarly, no observable change in morphology were observed between the control and 50 µg/ml of the AuNP's (G-J). At higher concentrations (K-L) cells appeared slightly rounded, and slightly more sparely spaced.

Following 48 hours of exposure to increasing concentrations of the S1 extract (A-F) and S1-AuNP's (G-L) over 48 hours, cell morphology were observed and recorded (Figure 3.25). The flat and polygonal morphology remained unchanged between the control and 50 µg/ml of the extract (A-E), while showing signs of cell rounding at the highest concentration (F). A slight reduction in overall cell number was observed between the control and 100 µg/ml of the AuNP's (G-K), while the cell morphology remained observably unchanged. At the highest concentration (K), cells became more sparely spaced and displayed signs of slight rounding.

Post 72-hour exposure to increasing concentrations of the S1 extract (A-F) and S1-AuNP's (G-L), cell morphology were observed and recorded (Figure 3.26). Cell morphology remained relatively unchanged between the control and 200 µg/ml of the extract (A-F). Slightly fewer cells were observed at the highest concentration (F). Cells became observably fewer between the control and 100 µg/ml of the AuNP's (G-K), while cell morphology remained unchanged. Between 100 µg/ml and 200 µg/ml, cells became more notably sparsely spaced, in addition to displaying a slightly rounded appearance at 200 µg/ml.

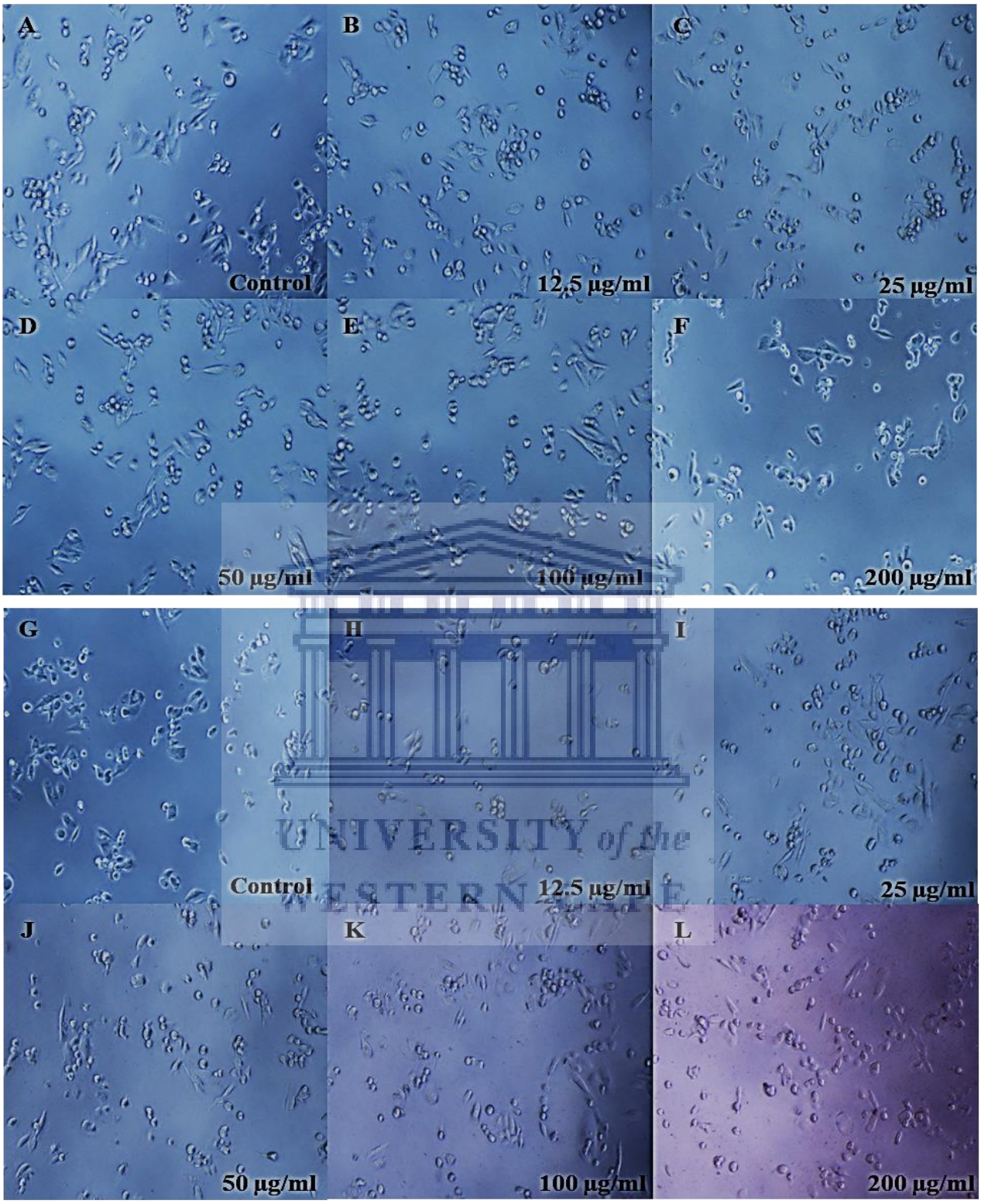

Figure 3.24: PC-3 cell morphology after being exposed to increasing concentrations of the S1 Extract and S1x2-AuNPs over a 24-hour period. The extract yielded no change in morphology, with slightly less observable cells at 200 µg/ml (F), whereas the AuNP's yielded slight cell rounding at higher concentrations (K-L).

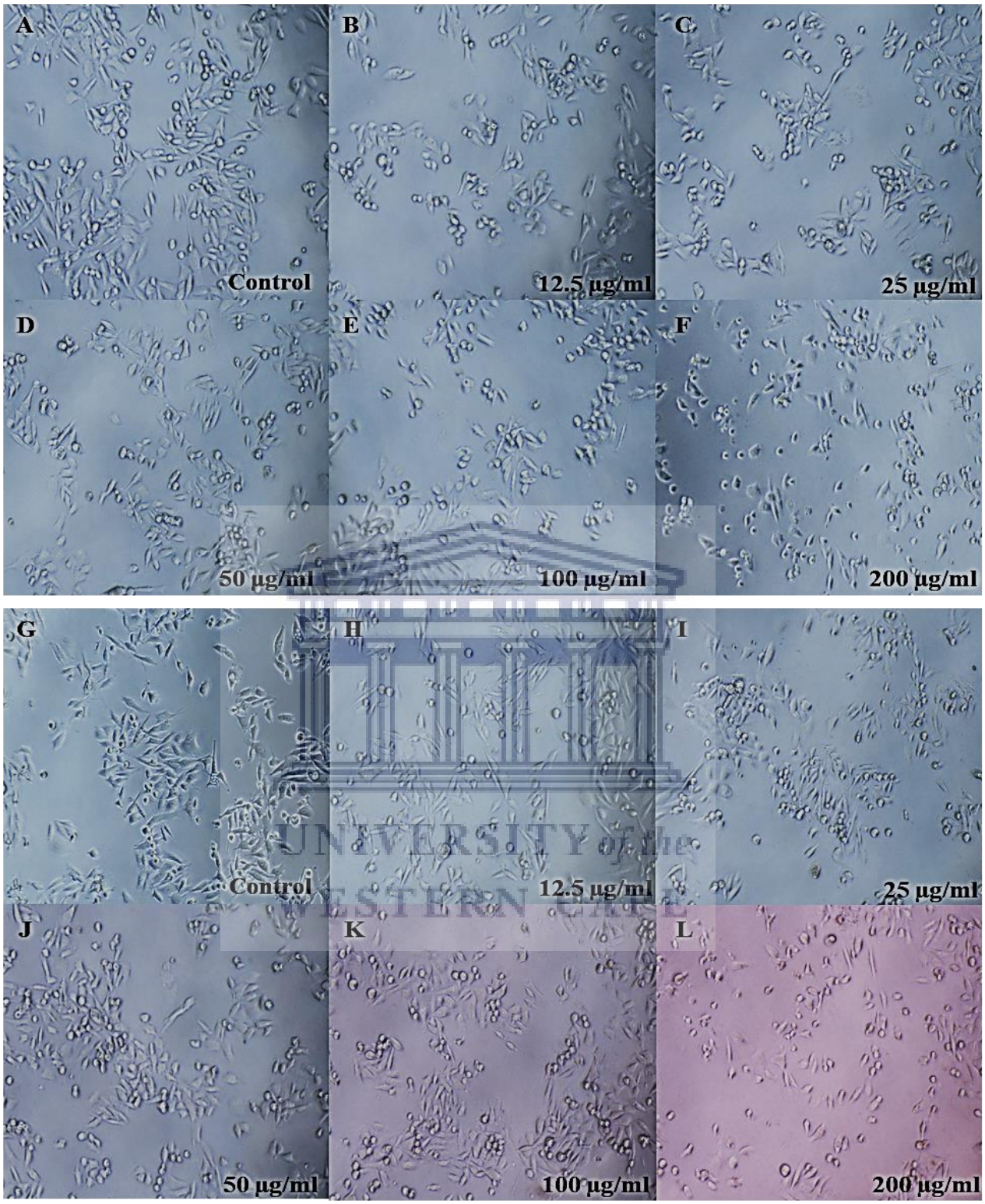

Figure 3.25: PC-3 cell morphology after being exposed to increasing concentrations of the S1 Extract and S1-AuNPs over a 48-hour period. The extract yielded no change in morphology at lower concentrations (A-E), with slight rounding at the highest concentration (F). The AuNP's, yielded slight cell rounding at the highest concentration (L).

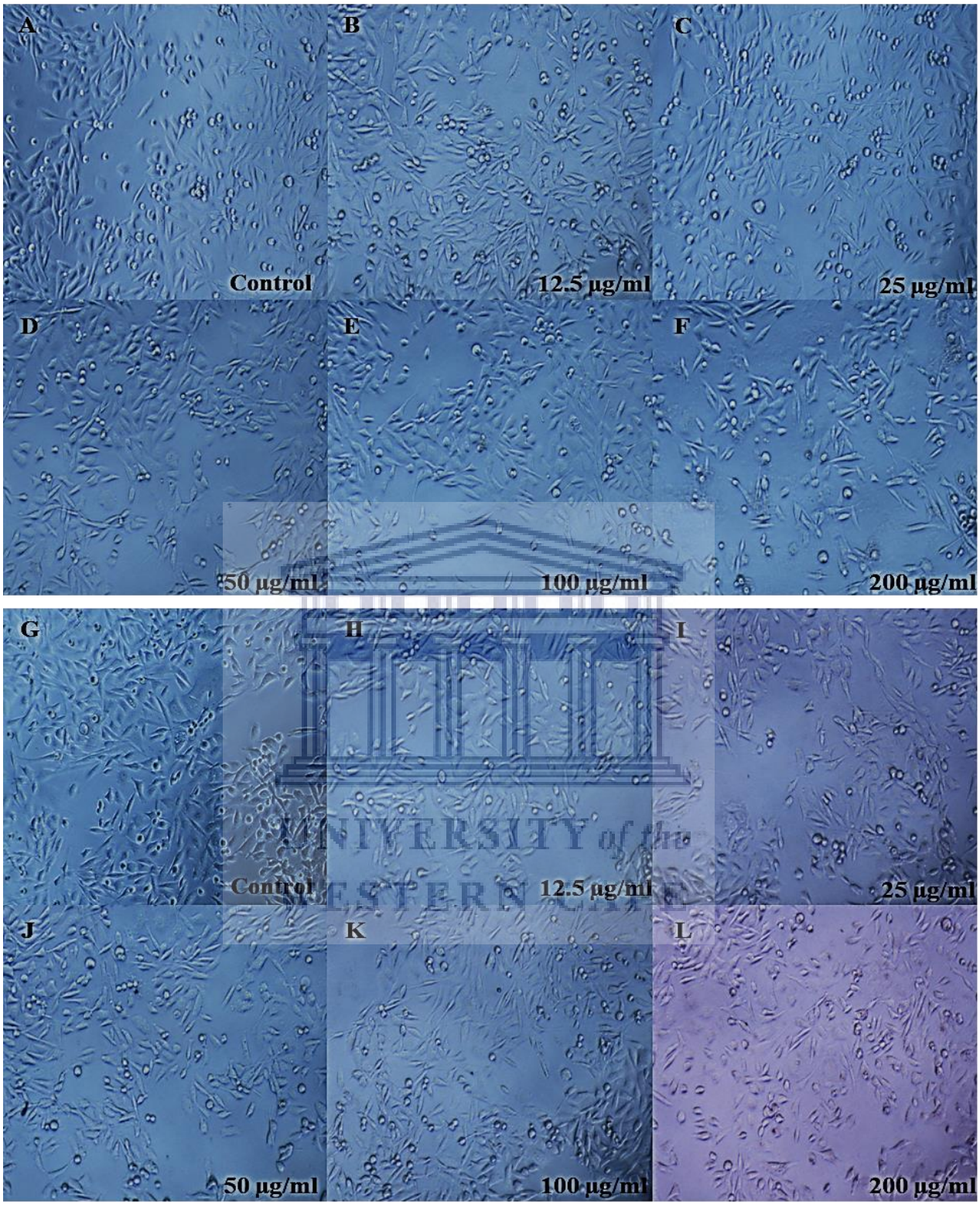

Figure 3.26: PC-3 cell morphology after being exposed to increasing concentrations of the S1 Extract and S1-AuNPs over a 72-hour period. The extract yielded no change in morphology between the control and highest concentrations (A-F), with slight fewer observed cells at 200 µg/ml. The AuNP's yielded fewer cells between control and at 100 µg/ml and cell rounding at 200 µg/ml.

After 24-hours of exposure to both the extract and AuNP's (Figure 3.27 A), the MTT assay revealed a dose-depended decreases in cell viability between the control and 200 µg/ml, with the AuNP's exhibiting greater decreases between 12.5 µg/ml and 100 µg/ml. Significant (P=0.0002, P=0.0005, P=0.0433, P=0.0031) differences in the reduction of cell viability were observed between the extract and AuNP's at 12.5 µg/ml, 25 µg/ml, 100 µg/ml and 200 µg/ml. The repeated measures ANOVA yielded a significant (P<0.0001, P=0.001) trend for the extract and AuNP's, respectively, between the control and 200 µg/ml. One-way ANOVA revealed significant (P<0.001, P<0.001) trends between the control and 200 µg/ml, for the extract and AuNP's.

Similarly, 48-hours of exposure (Figure 3.27 B) yielded dose-depended decreases in cell viability between the control and 200 µg/ml, with the AuNP's yielding a notable reduction in cell viability between 12.5 µg/ml and 100 µg/ml. Significant (P=0.0034, P=0.0003, P=0.0102) differences in the reduction of cell viability were observed between the extract and AuNP's at 12.5 µg/ml, 25 µg/ml and 50 µg/ml. The repeated measures ANOVA yielded significant (P=0.0001, P<0.0001) trends for the extract and AuNP's between the control and 200 µg/ml. One-way ANOVA revealed a significant (P<0.001, P<0.001) trend between the control and 200 µg/ml, for the extract and AuNP's.

Equally, 72-hours of exposure yielded dose-depended decreases in cell viability between the control and 200 µg/ml, with the AuNP's yielding considerably greater reductions in cell viability between 12.5 µg/ml and 100 µg/ml (Figure 3.27 C). Significant (P<0.0001, P<0.0001, P<0.001, P=0.018) differences in the reduction of cell viability were observed between the extract and AuNP's at 12.5 µg/ml, 25 µg/ml, 50 µg/ml and 100 µg/ml, respectively, along with the repeated measures ANOVA yielding a significant (P<0.0001, P<0.0001) trend for the extract and AuNP's between control and 200 µg/ml. One-way ANOVA revealed significant (P<0.001, P<0.001) trends between the control and 200 µg/ml, for the extract and AuNP's.

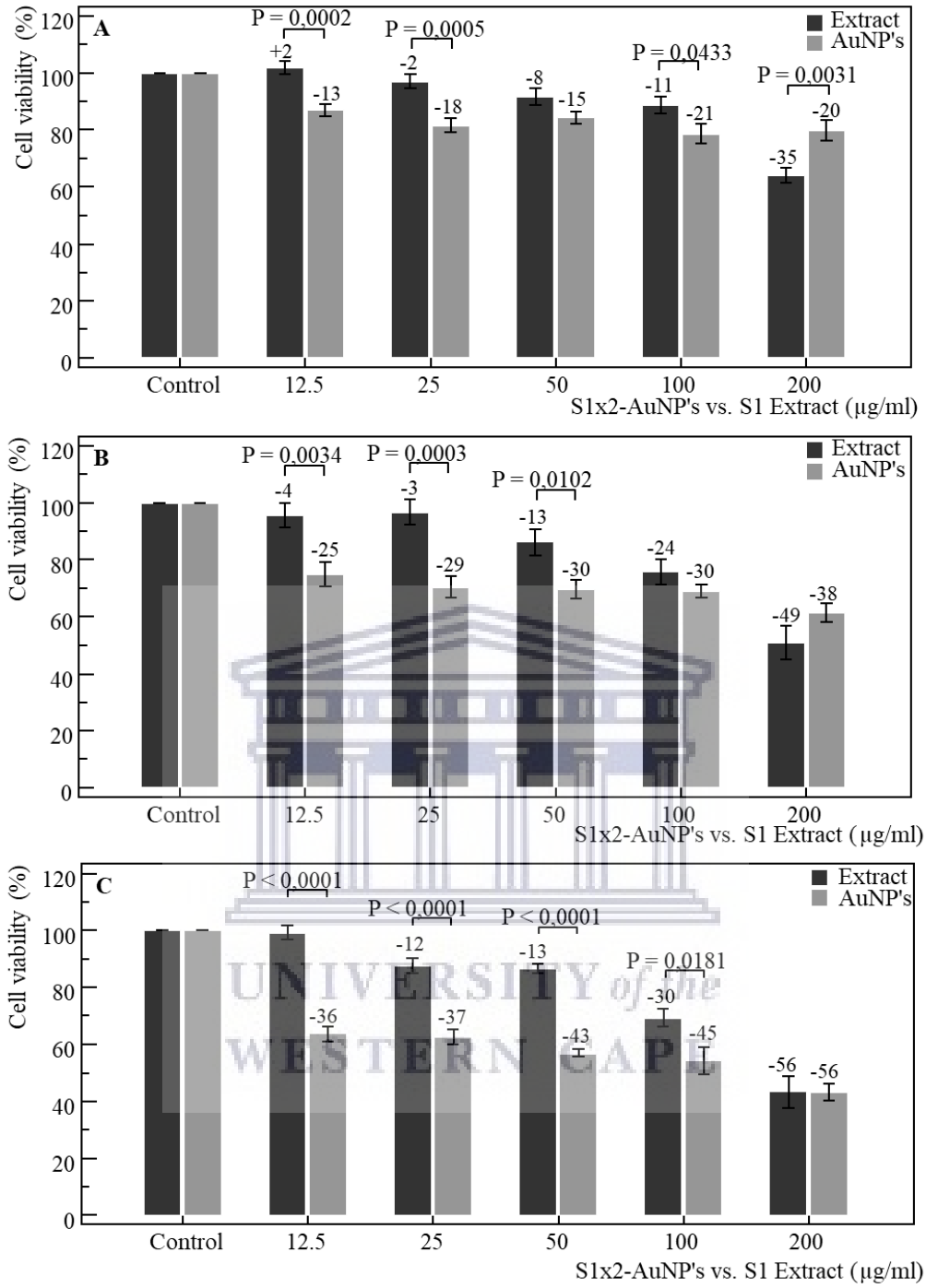

Figure 3.27: PC-3 cell viability as determined by the MTT assay over 24 (A), 48 (B) and 72 (C) hour exposure to the S1 Extract and S1-AuNP's, respectively. Significant (P=0.0002, P=0.0005, P=0.0433, P=0.0031) differences were observed between the extract and AuNP's between 12.5-200 µg/ml over 24 hours, along with significant (P=0.0034, P=0.0003, P=0.0102) differences observed between 12.5-50 µg/ml, after 48 hours, and finally significant (P<0.0001, P<0.0001, P<0.001, P=0.018) from 12.5 -00 µg/ml after 72 hours of exposure.

3.2.1.3 S2-AuNP's and S2 extract

After being exposed to increasing concentrations of the S2 extract (A-F) and S2-AuNP's (G-L) over 24 hours, cell morphology was observed and recorded (Figure 3.28). No observable change in the flat, polygonal morphology had occurred between the control and 50 µg/ml of the extract (A-D). At higher concentrations (E-F), cells became marginally more sparely spaced and appeared progressively rounded. Similarly, no observable change in morphology was observed between the control and 100 µg/ml of the AuNP's (G-K). At highest concentration (L) cells appeared slightly rounded, and slightly more sparely spaced.

Following 48 hours of exposure to increasing concentrations of the S2 extract (A-F) and S2-AuNP's (G-L) over 48 hours, cell morphology was observed and recorded (Figure 3.29). Cells appeared slightly more sparely spaced between the control and 100 µg/ml of the extract (A-E), however the typical flat and polygonal morphology remained unchanged. At 200 µg/ml (F), cells became visibly rounded and notably fewer. Similarly, a progressive reduction in observable cell number was noted between the control and 200 µg/ml of the AuNP's (G-L), without the presence of morphological changes up until 50 µg/ml (J). At higher concentrations (K-L), cells became more sparely spaced and progressively rounded.

Post 72-hour exposure to increasing concentrations of the S2 extract (A-F) and S2-AuNP's (G-L), cell morphology was observed and recorded (Figure 3.30). Cell morphology remained unchanged between the control and 200 µg/ml of the extract (A-F), with slightly fewer observable cells at 200 µg/ml (F). Similarly, no morphological changes were observed between the control and 50 µg/ml of the AuNP's (G-K), with cells becoming progressively fewer between 50 µg/ml and 200 µg/ml (J-L).At higher concentrations (K-L), cells appeared progressively rounded and displayed signs consistent with cell stress at (L).

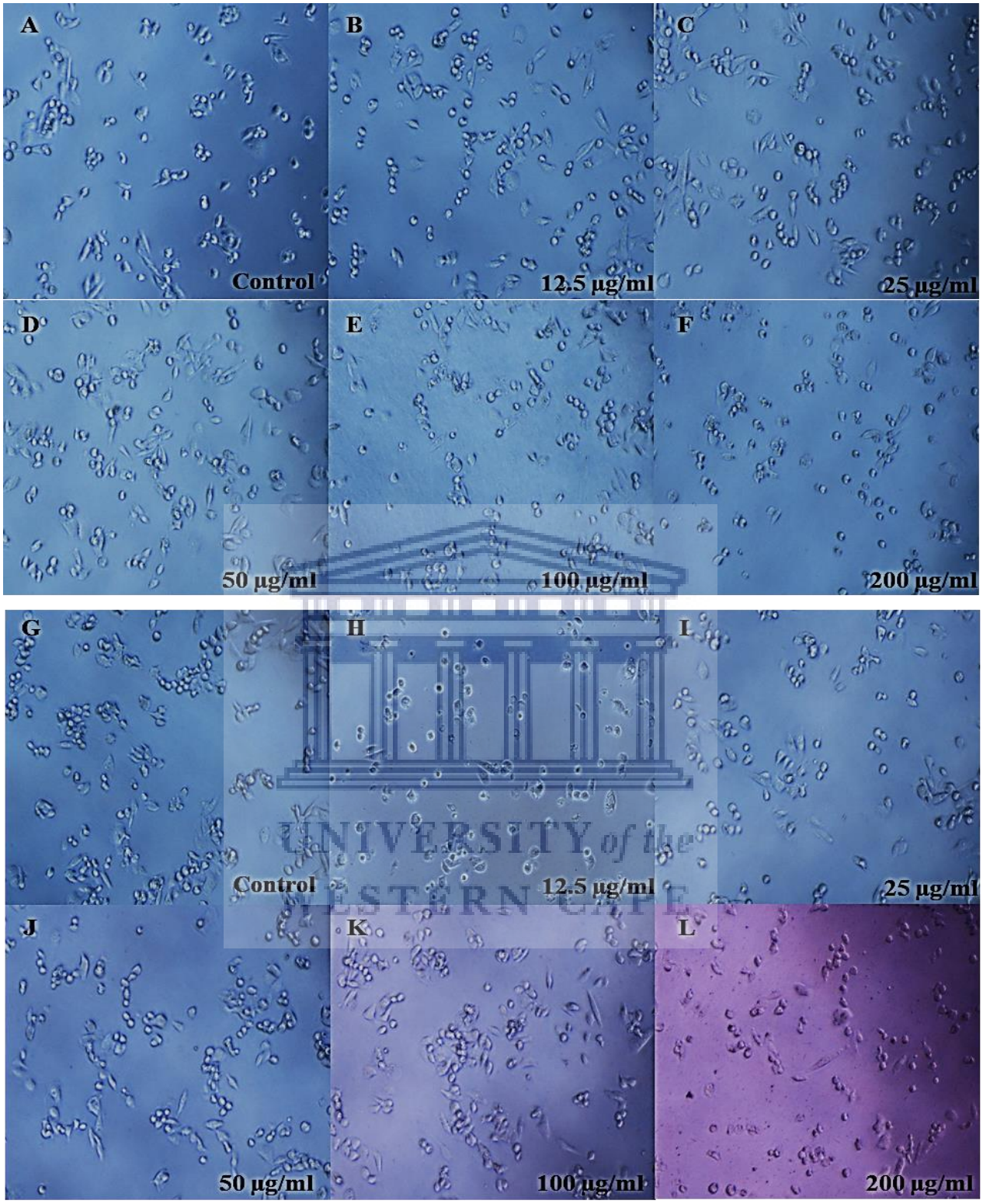

Figure 3.28: PC-3 cell morphology after being exposed to increasing concentrations of the S2 Extract and S2-AuNPs over a 24-hour period. The extract yielded no change in morphology at lower concentrations (A-D), with slight rounding at the higher concentrations (E-F). The AuNP's, yielded slight cell rounding at the highest concentration (L).

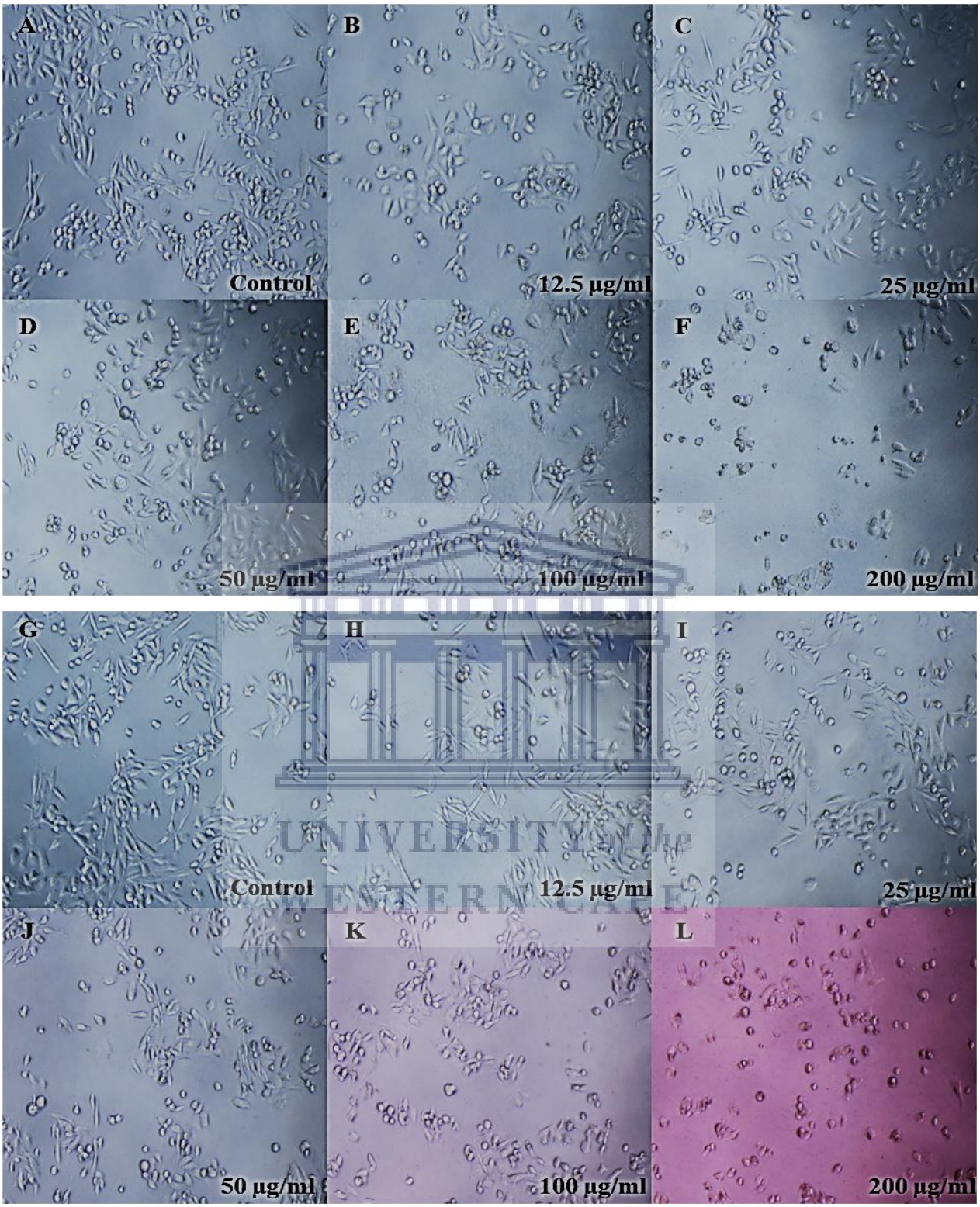

Figure 3.29: PC-3 cell morphology after being exposed to increasing concentrations of the S2 Extract and S2-AuNPs over a 48-hour period. The extract yielded no change in morphology at lower concentrations (A-E), with visible rounding at the highest concentration (F). Similarly, the AuNP's, yielded notable cell rounding at the highest concentration (L).

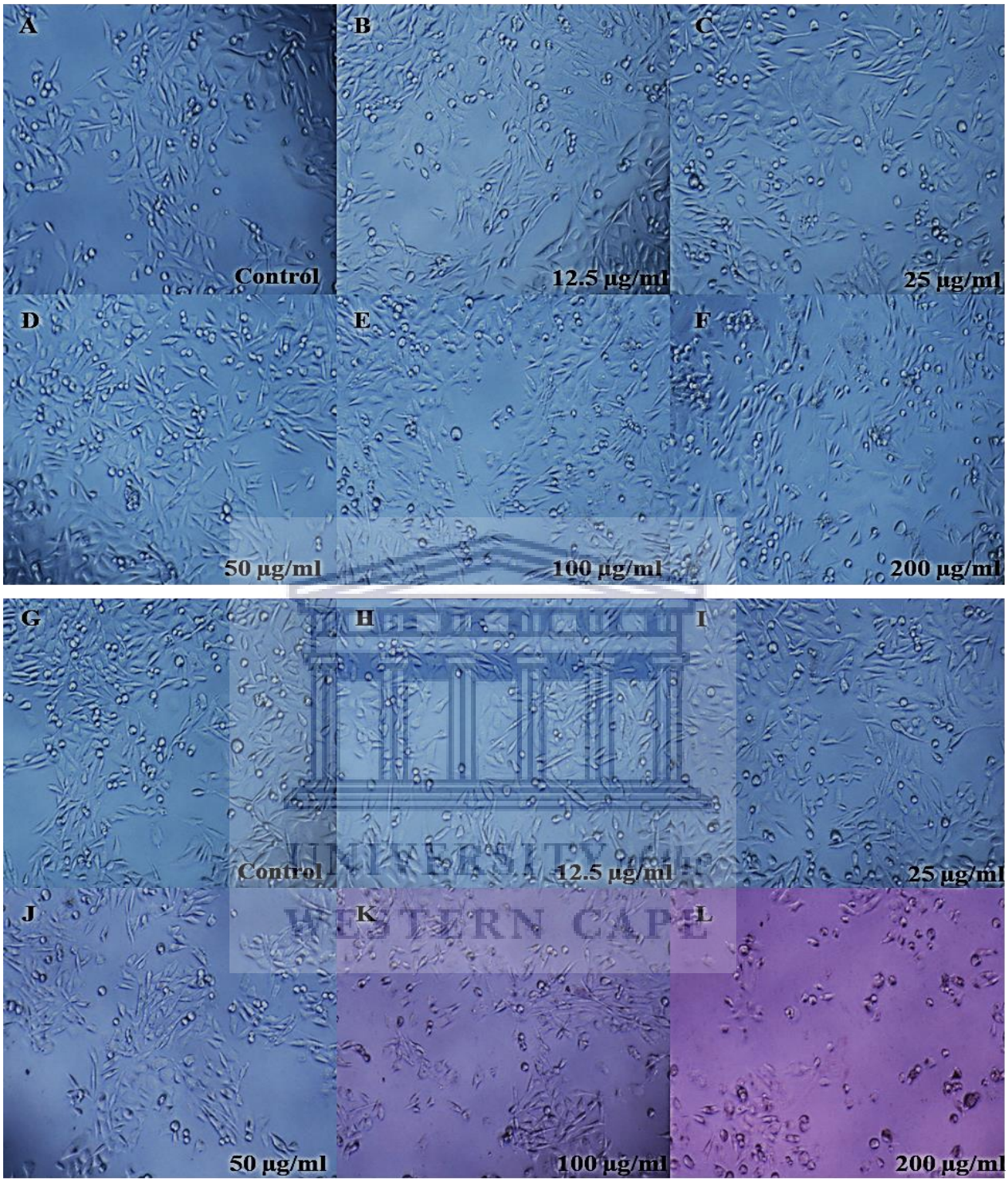

Figure 3.30: PC-3 cell morphology after being exposed to increasing concentrations of the S2 Extract and S2-AuNPs over a 72-hour period. The extract yielded no change in morphology between the control and highest concentrations (A-F), with slight fewer observed cells at 200 µg/ml (F). The AuNP's yielded progressive cell rounding between 100 µg/ml and 200 µg/ml, with signs of cell stress.

Following 24, 48 and 72 -hours of exposure the MTT assay was performed (Figure 3.31). The extract yielded a dose-depended increase in cell viability between the control and 100 µg/ml, followed by a sharp decrease at 100 µg/ml, whereas the AuNP's exhibiting a dose-dependent reduction between the control and 200 µg/ml (Figure 3.31 A). Significant (P=0.0006, P=0.0319) differences in the reduction of cell viability were observed between the extract and AuNP's at 100 µg/ml and 200 µg/ml, receptively. The repeated measures ANOVA yielded a significant (P<0.0103, P<0.0001) trend for the extract and AuNP's, respectively, between the control and 200 µg/ml. One-way ANOVA revealed significant (P=0.001, P<0.001) trends between the control and 200 µg/ml, for the extract and AuNP's.

Over 48-hours of exposure (Figure 3.31 B) dose-depended decreases in cell viability were observed between the control and 200 µg/ml for extract and AuNP's, with AuNP's yielding a greater reduction in cell viability at each concentration. Significant (P=0.0029, P=0.0035, P<0.0001, P=0.0001, P=0.0006) differences in the reduction of cell viability were observed between the extract and AuNP's at 12.5 µg/ml, 25 µg/ml and 50 µg/ml, 100 µg/ml and 200 µg/ml. The repeated measures ANOVA yielded significant (P<0.0001, P<0.0001) trends for the extract and AuNP's, respectively, between the control and 200 µg/ml, along with one-way ANOVA revealing significant (P<0.001, P<0.001) trends between the control and 200 µg/ml.

Equally, 72-hours of exposure (Figure 3.31 C) exhibited dose-depended decreases in cell viability between the control and 200 µg/ml for both extract and AuNP's, with AuNP's yielding a greater reduction in cell viability at each concentration. Significant (P=0.0021, P=0.0001, P=0.0004, P<0.0001, P=0.0003) differences in the reduction of cell viability were observed between the extract and AuNP's at 12.5 µg/ml, 25 µg/ml, 50 µg/ml, 100 µg/ml and 200 µg/ml, respectively. The repeated measures ANOVA yielded significant (P<0.0001, P<0.0001) trends for the extract and AuNP's between control and 200 µg/ml, along with one-way ANOVA revealing significant (P<0.001, P<0.001) trends between the control and 200 µg/ml.

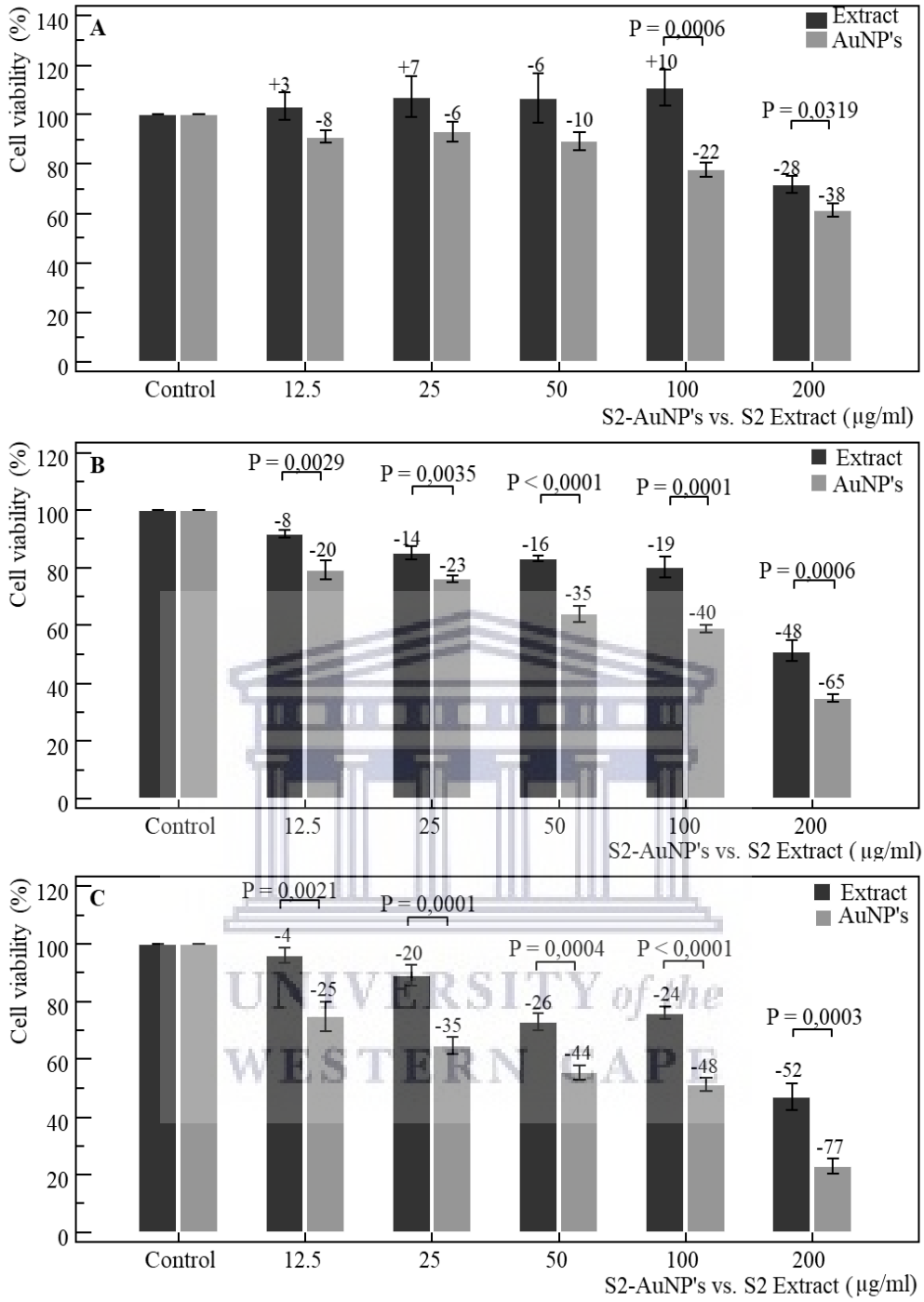

Figure 3.31: PC-3 cell viability as determined by the MTT assay over 24 (A), 48 (B) and 72 (C) hour exposure to the S2 Extract and S2-AuNP's, respectively. Significant (P=0.0006, P=0.0319) differences were observed between the extract and AuNP's from 100-200 µg/ml over 24 hours, along with significant (P=0.0029, P=0.0035, P<0.0001, P=0.0001, P=0.0006) differences from 12.5-200 µg/ml after 48 hours, and finally significant (P=0.0021, P=0.0001, P=0.0004, P<0.0001, P=0.0003) differences from 12.5-200 µg/ml after 72 hours of exposure.

3.2.1.4 S2x2-AuNP's and S2 extract

After being exposed to increasing concentrations of the S2 extract (A-F) and S2x2-AuNP's (G-L) over 24 hours, cell morphology was observed and recorded (Figure 3.32). No observable change in the flat, polygonal morphology had occurred between the control and 50 µg/ml of the extract (A-D). At higher concentrations (E-F), cells became marginally more sparely spaced and appeared progressively rounded. Similarly, no observable change in morphology or observable cell number was noted between the control and 200 µg/ml of the AuNP's (G-L).

Following 48 hours of exposure to increasing concentrations of the S2 extract (A-F) and S2x2-AuNP's (G-L) over 48 hours, cell morphology was observed and recorded (Figure 3.33). Cells appeared slightly more sparely spaced between the control and 100 µg/ml of the extract (A-E), however the typical morphology remained unchanged. At 200 µg/ml (F), cells became visibly rounded and markedly fewer. A marginal reduction in cell number was noted between the control and 200 µg/ml of the AuNP's (G-L), without notable morphological changes.

Post 72-hour exposure to the S2 extract (A-F) and S2x2-AuNP's (G-L), cell morphology was observed and recorded (Figure 3.34). Cell morphology remained unchanged between the control and 200 µg/ml of the extract (A-F), with slightly fewer observable cells at 200 µg/ml (F). Similarly, no morphological changes were observed between the control and 50 µg/ml of the AuNP's (G-K), with cells becoming slightly, but progressively fewer between 50 µg/ml and 200 µg/ml (J-L). At higher concentrations (K-L), cells exhibited signs consistent with stress, and appeared slightly rounded at 200 µg/ml (L).

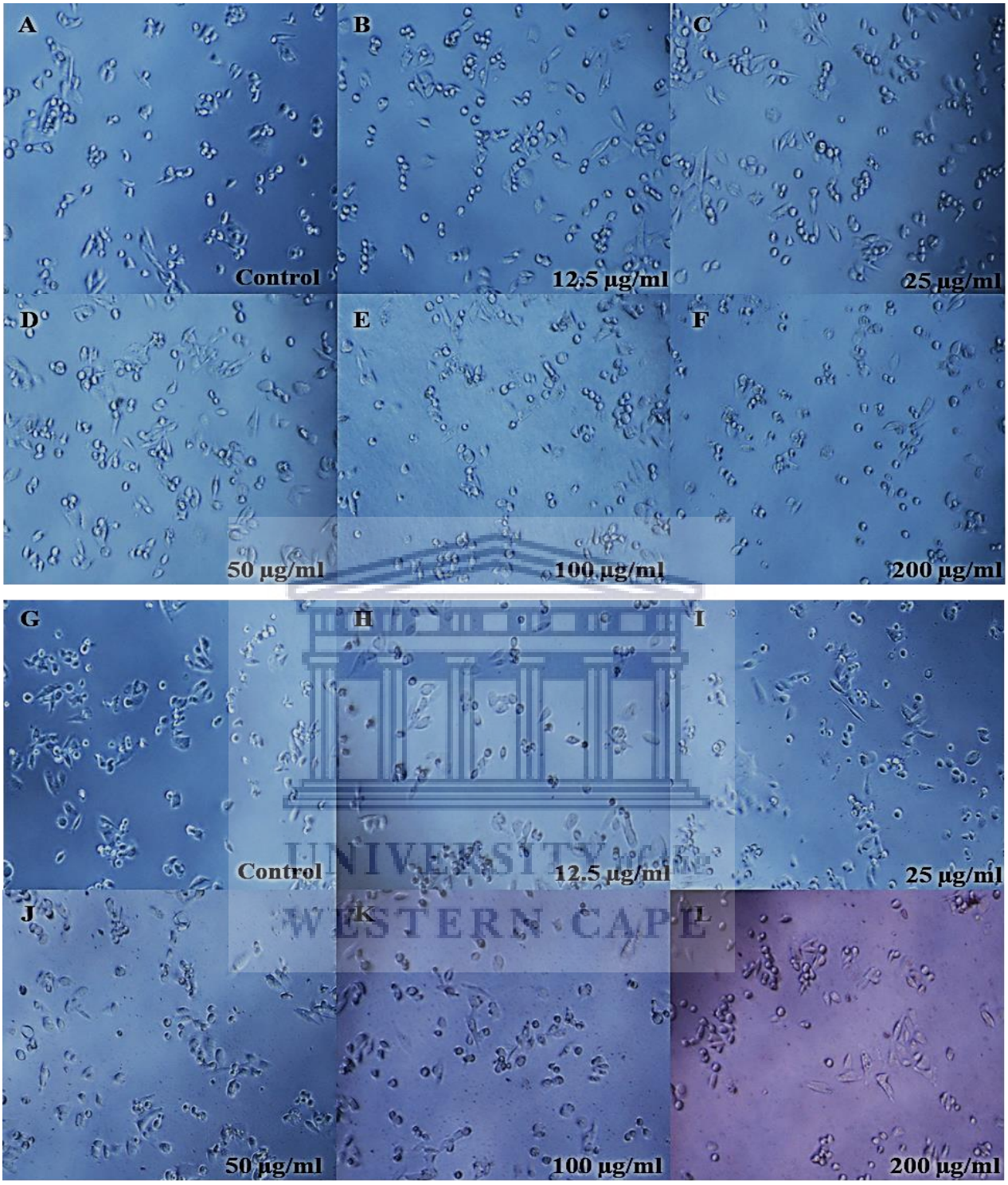

Figure 3.32: PC-3 cell morphology after being exposed to increasing concentrations of the S2 Extract and S2x2-AuNPs over a 24-hour period. The extract yielded no change in morphology at lower concentrations (A-D), with slight rounding at the higher concentrations (E-F).Similarly, the AuNP's, yielded no morphological changes, reduction in observable cell number, between the control and highest concentration (G-L).

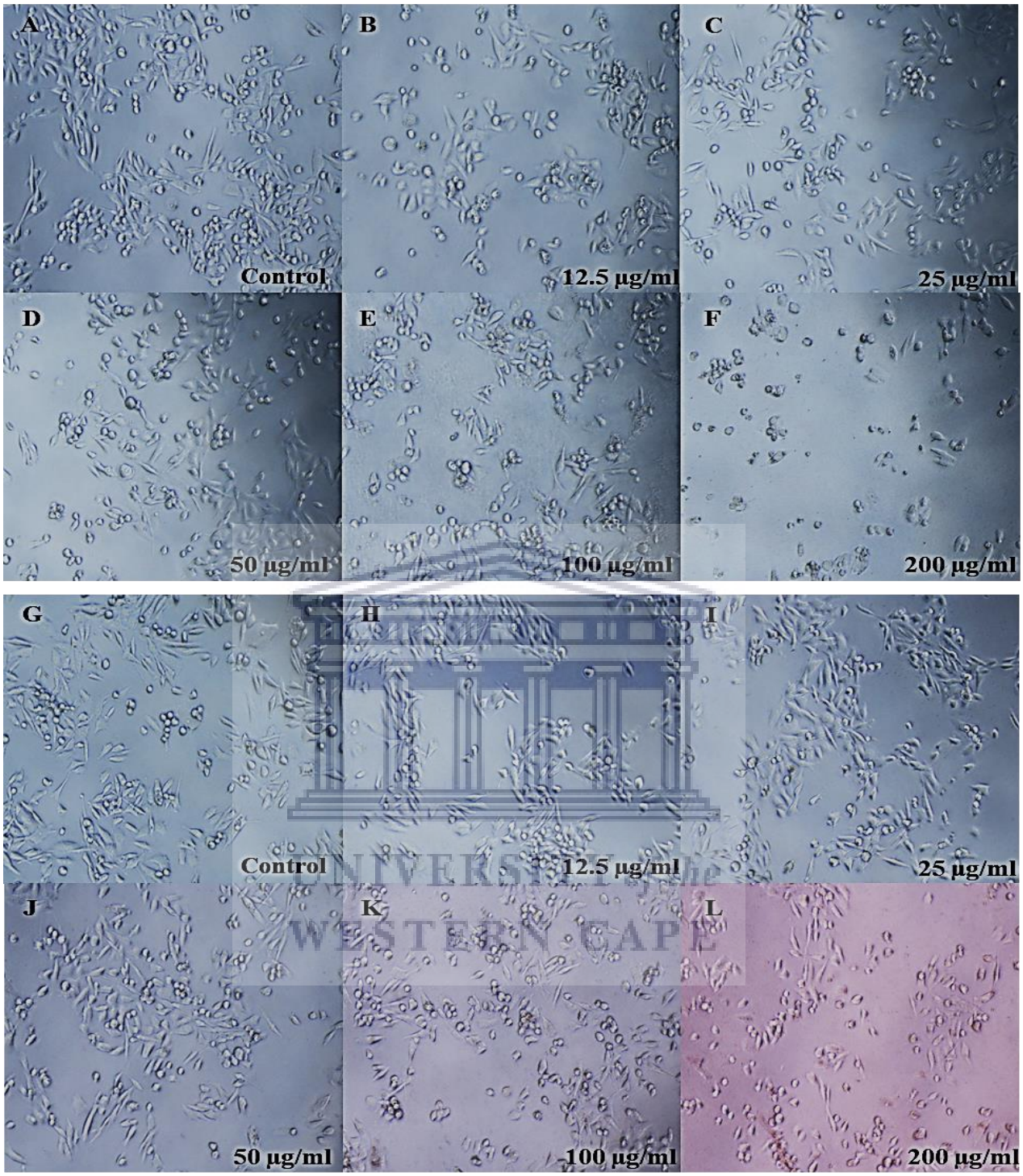

Figure 3.33: PC-3 cell morphology after being exposed to increasing concentrations of the S2 Extract and S2x2-AuNPs over a 48-hour period. The extract yielded no change in morphology at lower concentrations (A-E), with visible rounding at the highest concentration (F). Similarly, the AuNP's, exhibited no morphological changes between the control and highest concentration (G-L), along with marginal decreases the observed cell number.

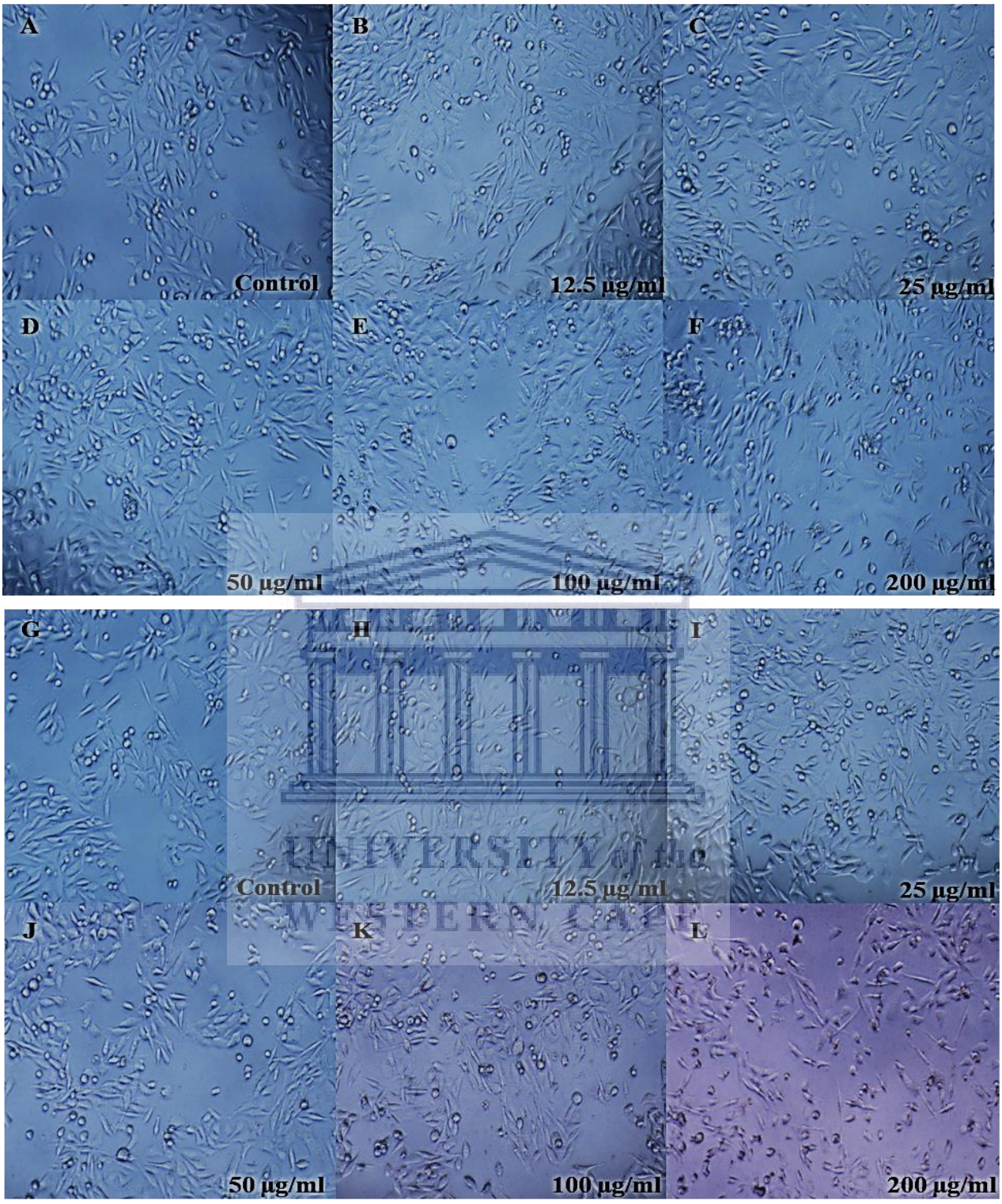

Figure 3.34: PC-3 cell morphology after being exposed to increasing concentrations of the S2 Extract and S2x2-AuNPs over a 72-hour period. The extract yielded no change in morphology between the control and highest concentrations (A-F), with slight fewer observed cells at 200 µg/ml (F). The AuNP's yielded cell stress and rounding at higher concentrations (K-L).

Following 24, 48 and 72 -hours of exposure the MTT assay was performed (Figure 3.35). The extract yielded a dose-depended increase in cell viability between the control and 100 µg/ml, followed by a decrease at 100 µg/ml, whereas the AuNP's exhibited a uniform reduction between the control and 200 µg/ml (Figure 3.35 A). Significant (P=0.0181, P=0.0147, P=0.0335, P=0.0011) differences in the reduction of cell viability were observed between the extract and AuNP's at 12.5 µg/ml, 25 µg/ml, 50 µg/ml and 100 µg/ml, respectively. The repeated measures ANOVA yielded a significant (P<0.0103, P=0.0081) trend for the extract and AuNP's, respectively, between the control and 200 µg/ml. One-way ANOVA revealed significant (P=0.001, P=0.004) trends between the control and 200 µg/ml, for the extract and AuNP's.

Over 48-hours of exposure (Figure 3.35 B) dose-depended decreases in cell viability were observed between the control and 200 µg/ml for extract and AuNP's, with AuNP's yielding a greater reduction in cell viability between control and 100 µg/ml. Significant (P<0.0001, P=0.0027, P=0.0002, P=0.002) differences in the reduction of cell viability were observed between the extract and AuNP's at 12.5 µg/ml, 25 µg/ml and 50 µg/ml and 100 µg/ml. The repeated measures ANOVA yielded significant (P<0.0001, P<0.0001) trends for the extract and AuNP's, respectively, between the control and 200 µg/ml, along with one-way ANOVA revealing significant (P<0.001, P<0.001) trends between the control and 200 µg/ml.

Equally, 72-hours of exposure (Figure 3.35 C) exhibited dose-depended decreases in cell viability between the control and 200 µg/ml for both extract and AuNP's, with AuNP's yielding a greater reduction in cell viability between the control and 100 µg/ml. Significant (P<0.0001, P<0.0001, P=0.0006, P<0.0001) differences in the reduction of cell viability was observed between the extract and AuNP's at 12.5 µg/ml, 25 µg/ml, 50 µg/ml and 100 µg/ml, respectively. The repeated measures ANOVA yielded significant (P<0.0001, P<0.0001) trends for the extract and AuNP's between control and 200 µg/ml, along with one-way ANOVA revealing significant (P<0.001, P<0.001) trends between the control and 200 µg/ml.

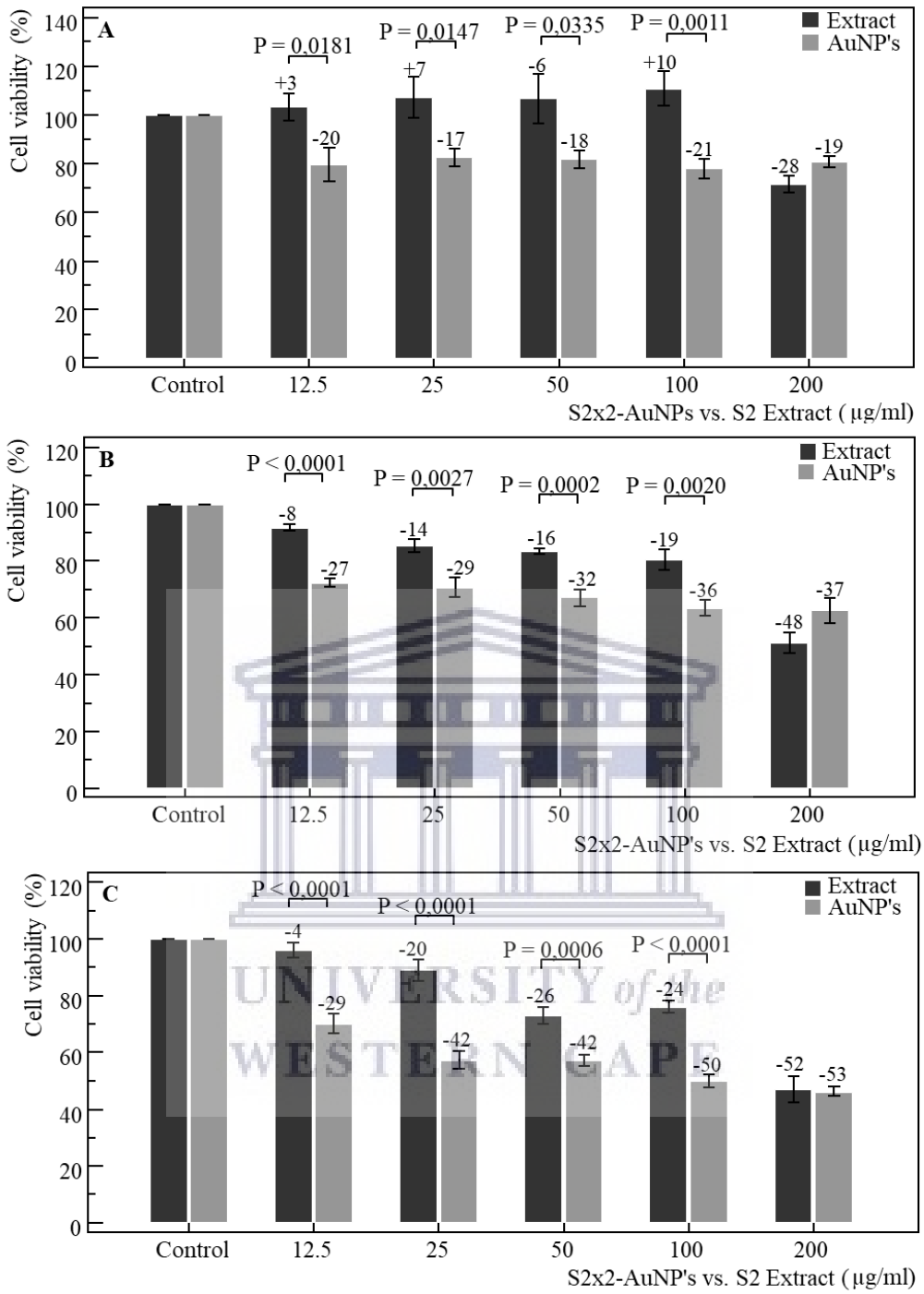

Figure 3.35: PC-3 cell viability as determined by the MTT assay over 24 (A), 48 (B) and 72 (C) hour exposure to the S2 Extract and S2x2-AuNP's, respectively. Significant (P=0.0181, P=0.0147, P=0.0335, P=0.0011) differences were observed between the extract and AuNP's from 12.5-100 µg/ml over 24 hours, along with significant (P<0.0001, P=0.0027, P=0.0002, P=0.002) differences from 12.5-100 µg/ml after 48 hours, and finally significant (P<0.0001, P<0.0001, P=0.0006, P<0.0001) differences from 12.5-100 µg/ml after 72 hours of exposure.

3.2.1.5 Ng-AuNP's pH 7 and naringenin

After being exposed to increasing concentrations of the naringenin (A-F) and Ng-AuNP's pH 7 (G-L) over 24 hours, cell morphology was observed and recorded (Figure 3.36). Morphology was unchanged between the control and 25 µg/ml of naringenin (A-C). At higher concentrations (D-F), cells were more sparely spaced, rounded and exhibited signs of cell stress at (F). Similarly, morphology remained unchanged between the control and 200 µg/ml of the AuNP's (G-L), along with a reduction in observable cells between 50 µg/ml and 200 µg/ml (J-L).

Following 48 hours of exposure to increasing concentrations of naringenin (A-F) and Ng-AuNP's pH 7 (G-L) over 48 hours, cell morphology was observed and recorded (Figure 3.37). Cells appeared progressively rounded and sparely spaced between the control and 200 µg/ml of naringenin (A-E), and exhibited signs consistent with cell stress (E) and death (F) at higher concentrations. A progressive reduction in cell number was noted between the control and 200 µg/ml of the AuNP's (G-L), without morphological changes up until 100 µg/ml (K). At a concentration of 200 µg/ml, cells appeared rounded and exhibited signs consistent with cell stress (L).

Post 72-hour exposure to naringenin (A-F) and Ng-AuNP's pH 7 (G-L), cell morphology was observed and recorded (Figure 3.38). Cell became notably fewer, and progressively rounded between the control and 200 µg/ml of naringenin (A-F), in addition to showing signs consistent with cell stress (E) and death (F), at higher concentrations. No morphological changes were observed between the control and 25 µg/ml of the AuNP's (G-I), with cells becoming progressively sparely spaced between 50 µg/ml and 100 µg/ml (J-K), and appearing rounded with signs consistent with cell stress at the highest concentration (L).

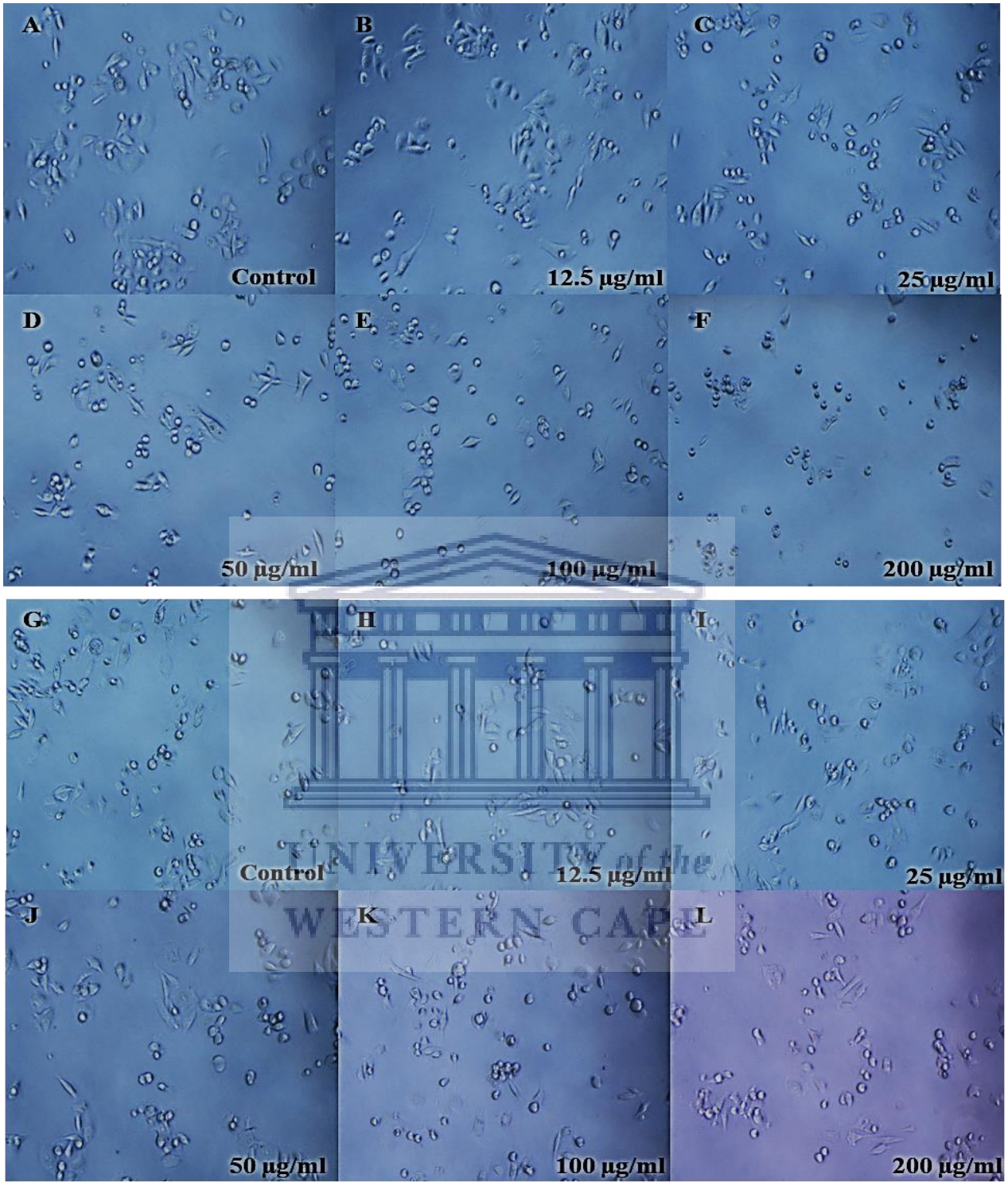

Figure 3.36: PC-3 cell morphology after being exposed to increasing concentrations of the naringenin and Ng-AuNP's pH 7 over a 24-hour period. Naringenin yielded no change in morphology at lower concentrations (A-C), with rounding and stress at the higher concentrations (E-F). The AuNP's yielded no morphological changes between the control and highest concentration (G-L), along with a reduction in cell number between 50 µg/ml and 200 µg/ml (J-L)

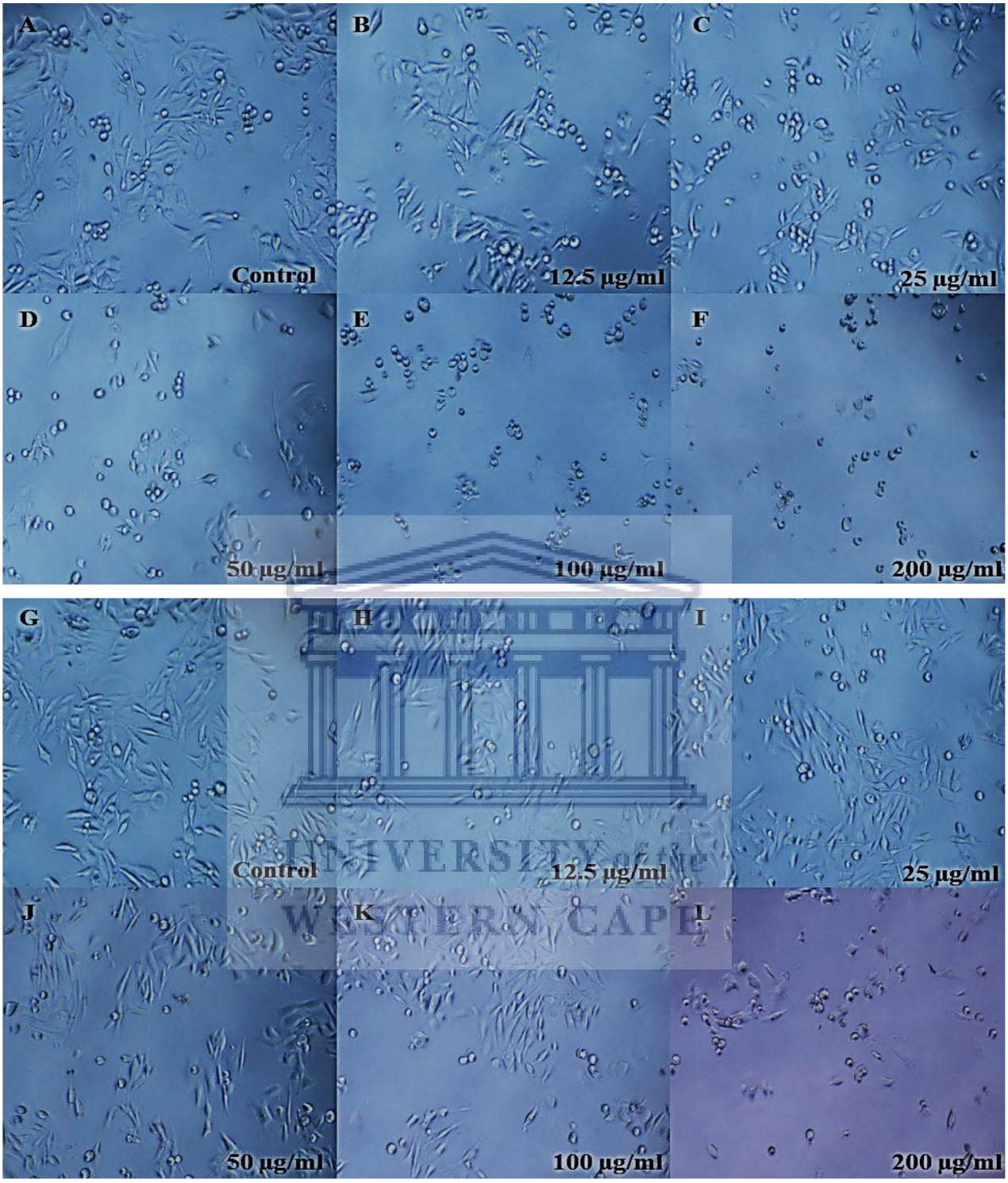

Figure 3.37: PC-3 cell morphology after being exposed to increasing concentrations of naringenin and Ng-AuNP's pH 7 over a 48-hour period. Naringenin yielded progressive cell rounding and sings of stress between the control and the highest concentration (A-F). The AuNP's, exhibited no morphological changes between the control and 100 µg/ml (G-K), along a consistent reduction in the observed cell number between the control and 200 µg/ml (G-L).

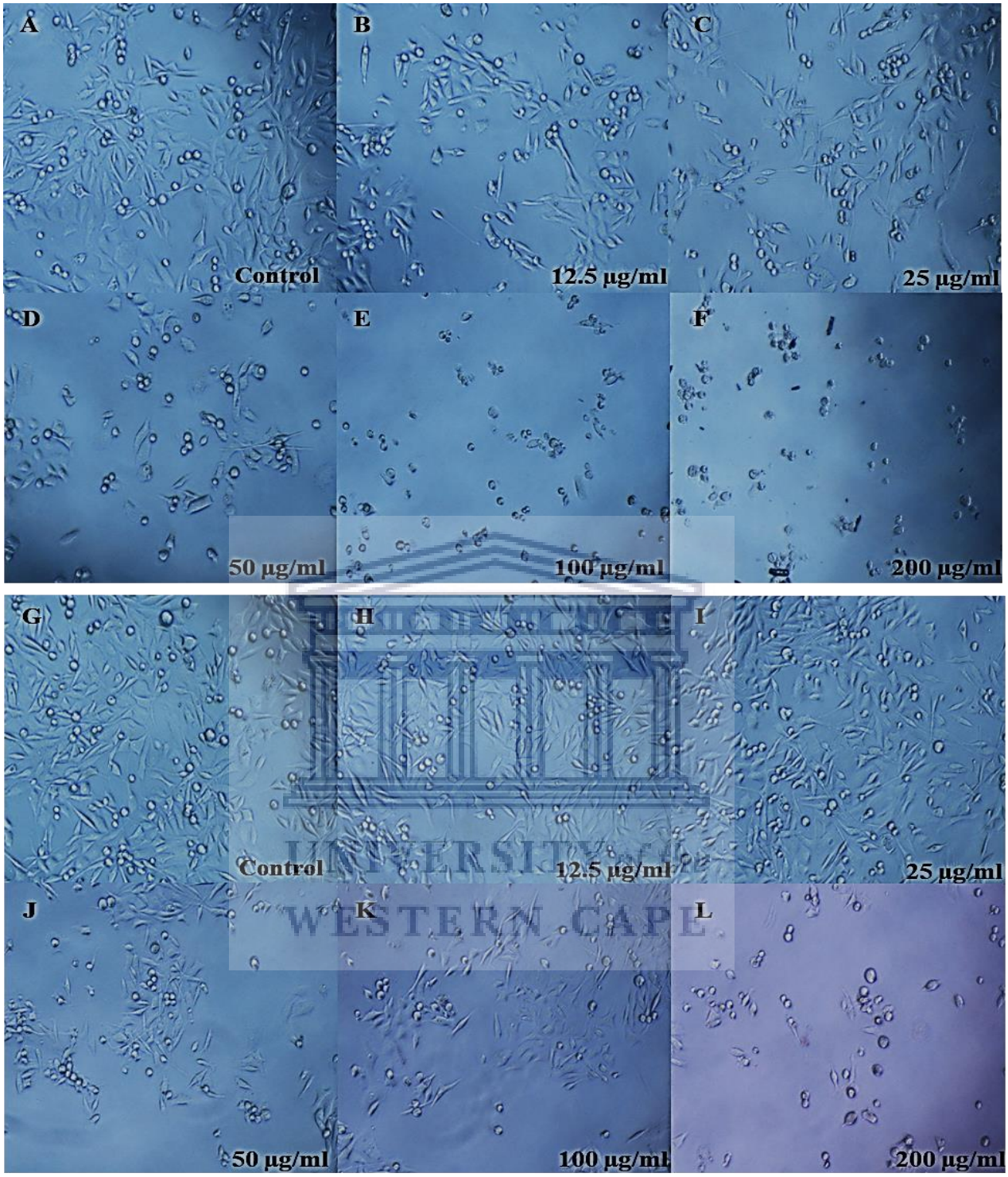

Figure 3.38: PC-3 cell morphology after being exposed to increasing concentrations of naringenin and Ng-AuNP's pH 7 over a 72-hour period. Naringenin yielded progressive rounding between the control and highest concentrations (A-F), with signs consistent with cell stress and death at higher concentrations (E-F). Similarly, the AuNP's yielded signs consistent with cell stress at the highest concentration (L).

Following 24, 48 and 72 -hours of exposure the MTT assay was performed (Figure 3.39). Both naringenin and the AuNP's yielded a dose-depended decrease in cell viability between the control and 200 µg/ml, where naringenin exhibited greater decreases between 25 µg/ml and 200 µg/ml (Figure 3.39 A). Significant (P<0.0001, P=0.0001, P=0.0207) differences in the reduction of cell viability was observed between naringenin and AuNP's at 50 µg/ml, 100 µg/ml and 200 µg/ml, respectively. The repeated measures ANOVA yielded a significant (P<0.0001, P<0.0001) trend for naringenin and AuNP's, respectively, between the control and 200 µg/ml. One-way ANOVA revealed significant (P<0.001, P<0.001) trends between the control and 200 µg/ml, for naringenin and AuNP's.

Over 48 hours of exposure (Figure 3.39 B), dose-depended decreases in cell viability were observed between the control and 200 µg/ml for both naringenin and the AuNP's. Naringenin yielded greater reductions in cell viability at each concentration, where a significant (P=0.0043) differences in the reduction of cell viability were observed between naringenin and AuNP's at 100 µg/ml. The repeated measures ANOVA yielded significant (P<0.0001, P<0.0001) trends for naringenin and AuNP's, respectively, between the control and 200 µg/ml, along with one-way ANOVA revealing significant (P<0.001, P<0.001) trends between the control and 200 µg/ml.

Equally, 72 hours of exposure (Figure 3.39 C) exhibited dose-depended decreases in cell viability between the control and 200 µg/ml for both naringenin and the AuNP's, whereby naringenin exhibited a greater reduction in cell viability at each concentration. Significant (P=0.0001, P<0.0001, P<0.0001) differences in the reduction of cell viability were observed between naringenin and the AuNP's at 25 µg/ml, 50 µg/ml and 100 µg/ml, respectively. The repeated measures ANOVA yielded significant (P<0.0001, P<0.0001) trends for naringenin and the AuNP's between control and 200 µg/ml, along with one-way ANOVA revealing significant (P<0.001, P<0.001) trends between the control and 200 µg/ml.

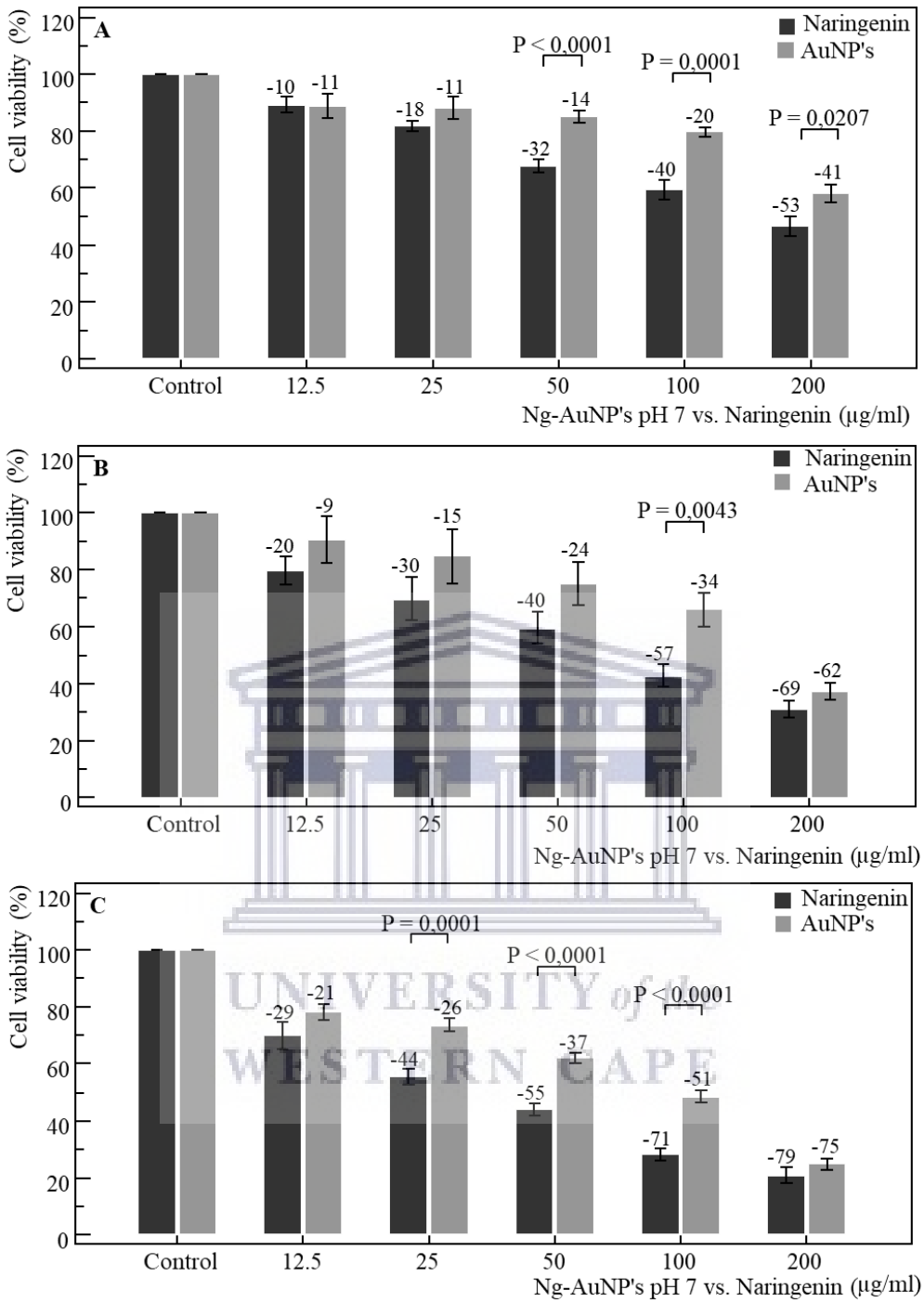

Figure 3.39: PC-3 cell viability as determined by the MTT assay over 24 (A), 48 (B) and 72 (C) hour exposure to naringenin and Ng-AuNP's pH 7, respectively. Significant (P<0.0001, P=0.0001, P=0.0207) differences were observed between naringenin and AuNP's at 50 µg/ml. 100 µg/ml and 200 µg/ml over 24 hours, along with a significant (P=0.0043) difference at 100 µg/ml after 48 hours, and finally significant (P=0.0001, P<0.0001, P<0.0001) differences at 25 µg/ml, 50 µg/ml and 100 µg/ml after 72 hours of exposure.

3.2.1.6 Ng-AuNP's pH 8 and naringenin

After being exposed to increasing concentrations of the naringenin (A-F) and Ng-AuNP's pH 8 (G-L) over 24 hours, cell morphology was observed and recorded (Figure 3.40). Morphology was unchanged between the control and 25 µg/ml of naringenin (A-C). Higher concentrations (D-F) yielded fewer and rounded cells, which exhibited signs of stress (F). Morphology remained unchanged between the control and 50 µg/ml of the AuNP's (G-L), and higher concentrations (E-F) yielded cell rounding and e signs of stress at 200 µg/ml (F). Additionally, cells were observably fewer between 50 µg/ml and 200 µg/ml (J-L).

Following 48 hours of exposure to increasing concentrations of naringenin (A-F) and Ng-AuNP's pH 8 (G-L) over 48 hours, cell morphology was observed and recorded (Figure 3.41). Cells appeared progressively rounded and sparely spaced between the control and 200 µg/ml of naringenin (A-E), exhibiting signs of with cell stress (E) and death (F) at higher concentrations. A progressive reduction in cell number was noted between the control and 200 µg/ml of the AuNP's (G-L), without morphological changes until 50 µg/ml (K). Between 100 µg/ml and 200 µg/ml, cells appeared rounded and exhibited signs of cell stress (L).

Post 72-hour exposure to naringenin (A-F) and Ng-AuNP's pH 8 (G-L), cell morphology was observed and recorded (Figure 3.42). Cell became notably fewer, and progressively rounded between the control and 200 µg/ml of naringenin (A-F), in addition to showing signs consistent with cell stress (E) and death (F), at higher concentrations. No morphological changes were observed between the control and 50 µg/ml of the AuNP's (G-I), with cells becoming increasingly sparely spaced between 50 µg/ml and 100 µg/ml (J-K), and appearing rounded with signs consistent with cell stress at the highest concentration (L).

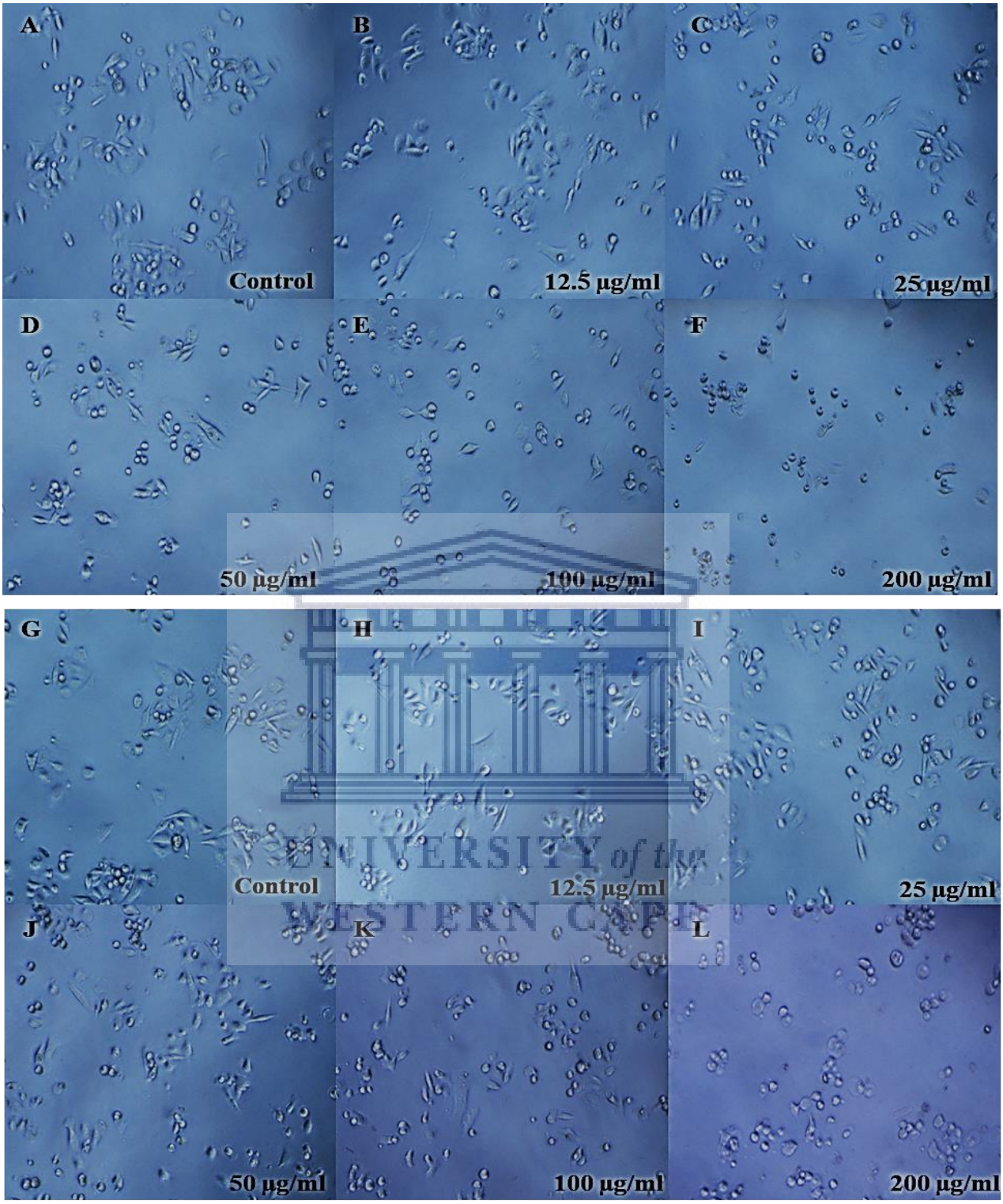

Figure 3.40: PC-3 cell morphology after being exposed to increasing concentrations of the naringenin and Ng-AuNP's pH 8 over a 24-hour period. Both, naringenin and the AuNP's exhibited no change in morphology at lower concentrations (A-C) and (G-L), respectively, along with cell rounding and stress at the higher concentrations (D-F) and (E-F), respectively.

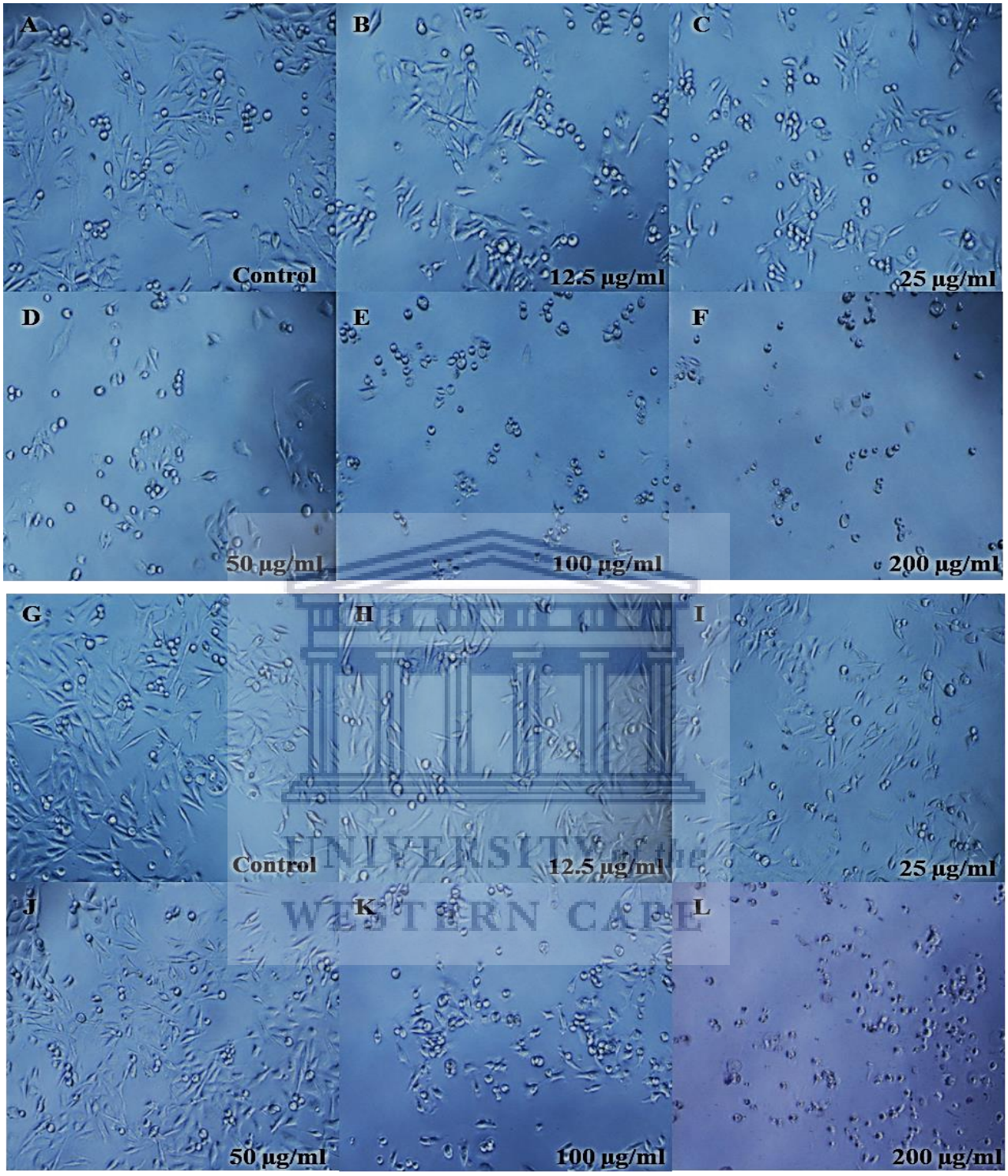

Figure 3.41: PC-3 cell morphology after being exposed to increasing concentrations of naringenin and Ng-AuNP's pH 8 over a 48-hour period. Naringenin yielded progressive cell rounding and sings of stress between the control and the highest concentration (A-F). The AuNP's, exhibited no morphological changes between the control and 50 µg/ml (G-K), along a consistent reduction in the observed cell number between the control and 200 µg/ml (G-L).

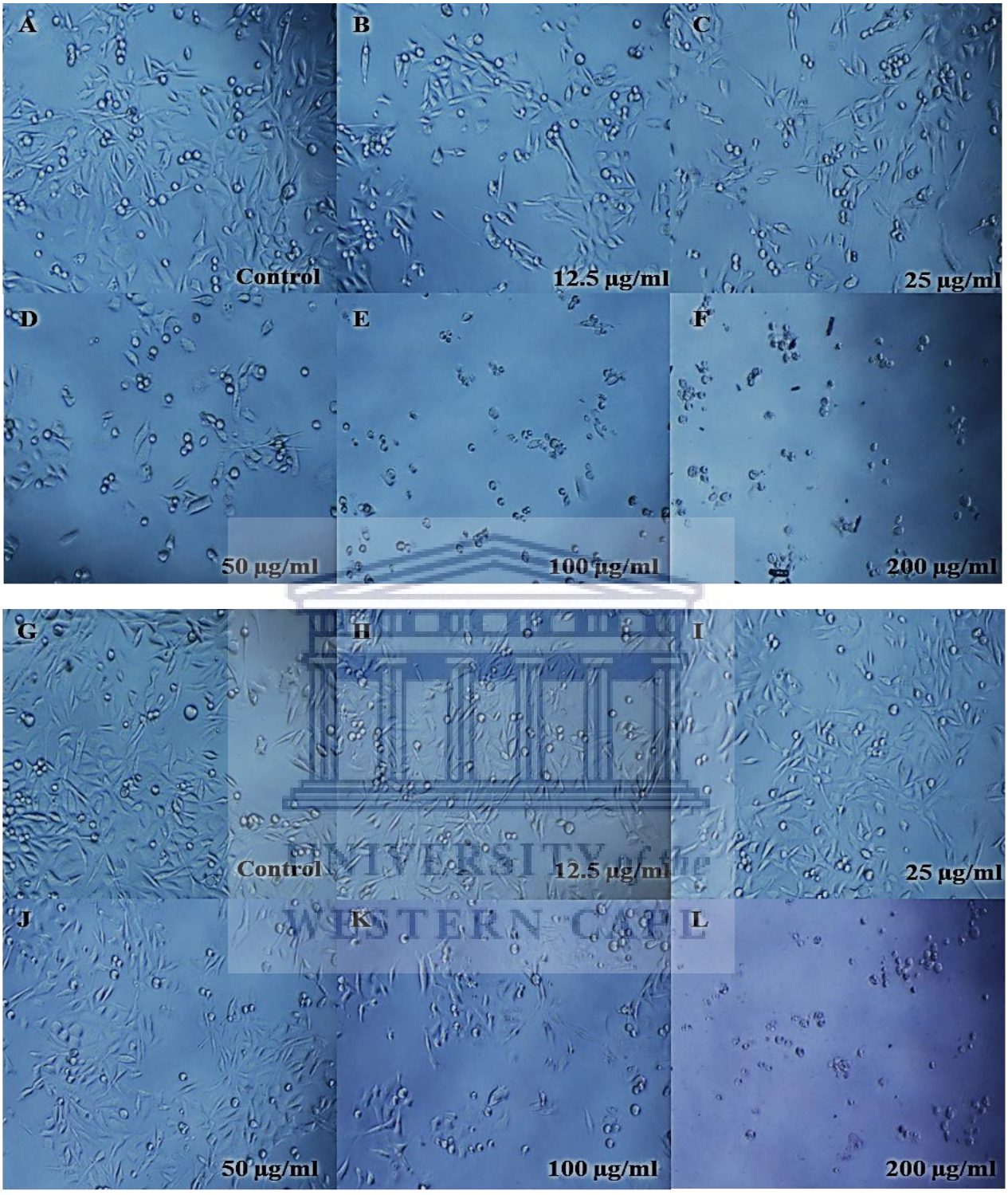

Figure 3.42: PC-3 cell morphology after being exposed to increasing concentrations of naringenin and Ng-AuNP's pH 8 over a 72-hour period. Naringenin yielded progressive rounding between the control and highest concentrations (A-F), with signs consistent with cell stress and death at higher concentrations (E-F). Similarly, the AuNP's yielded signs consistent with cell stress at the highest concentration (L).

Following 24, 48 and 72 -hours of exposure the MTT assay was performed (Figure 3.43). Naringenin and AuNP's yielded dose-depended decreases in cell viability between the control and 200 µg/ml (Figure 3.43 A), where naringenin exhibited greater decreases between 25 µg/ml and 200 µg/ml, and AuNP's exhibiting greater decreases at 200 µg/ml. Significant ($P=0.008$, $P<0.0001$, $P=0.0069$, $P=0.0009$) differences were observed between naringenin and AuNP's at 25 µg/ml, 50 µg/ml, 100 µg/ml and 200 µg/ml, respectively. The repeated measures ANOVA yielded a significant ($P<0.0001$, $P<0.0001$) trend for naringenin and AuNP's, respectively, between the control and 200 µg/ml. One-way ANOVA revealed significant ($P<0.001$, $P<0.001$) trends between the control and 200 µg/ml, for naringenin and AuNP's.

Over 48 hours of exposure (Figure 3.43 B), dose-depended decreases in cell viability were observed between the control and 200 µg/ml for both naringenin and the AuNP's. Naringenin yielded marginally greater reductions in cell viability between control and 100 µg/ml, followed by a notably greater decrease exhibited by the AuNP at 200 µg/ml that differed significantly ($P=0.0002$) from naringenin. The repeated measures ANOVA yielded significant ($P<0.0001$, $P<0.0001$) trends for naringenin and AuNP's, respectively, between the control and 200 µg/ml, along with one-way ANOVA revealing significant ($P<0.001$, $P<0.001$) trends between the control and 200 µg/ml.

Equally, 72 hours of exposure (Figure 3.43 C) exhibited comparable dose-depended decreases in cell viability between the control and 200 µg/ml for both naringenin and the AuNP's, whereby naringenin exhibited greater reductions in cell viability between control and 100 µg/ml, and AuNP's exhibiting greater reductions at 200 µg/ml. Significant ($P=0.0199$, $P<0.0125$) differences between naringenin and the AuNP's were observed at 100 µg/ml and 200 µg/ml, respectively. The repeated measures ANOVA yielded significant ($P<0.0001$, $P<0.0001$) trends for naringenin and the AuNP's between control and 200 µg/ml, along with one-way ANOVA revealing significant ($P<0.001$, $P<0.001$) trends between the control and 200 µg/ml.

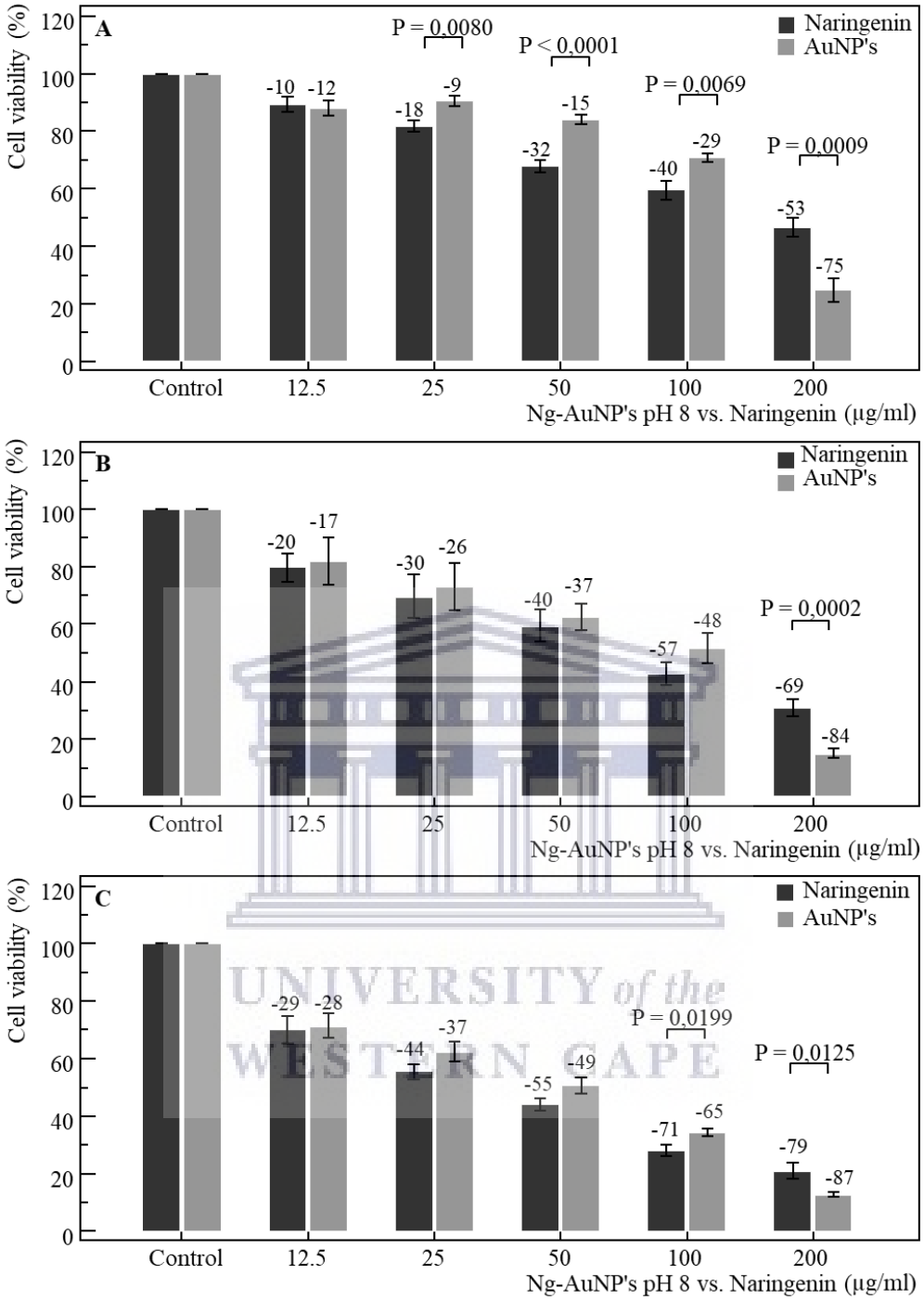

Figure 3.43: PC-3 cell viability as determined by the MTT assay over 24 (A), 48 (B) and 72 (C) hour exposure to naringenin and Ng-AuNP's pH 8, respectively. Significant (P=0.008, P<0.0001, P=0.0069, P=0.0009) differences were observed between naringenin and AuNP's at 25 µg/ml, 50 µg/ml, 100 µg/ml and 200 µg/ml over 24 hours, along with a significant (P=0.0002) difference observed at 200 µg/ml after 48 hours, and finally significant (P=0.0199, P<0.0125) differences at 100 µg/ml and 200 µg/ml after 72 hours of exposure.

3.2.2 LNCaP cell viability

3.2.2.1 S1-AuNP's and Extract

After being exposed to increasing concentrations of the S1 extract (A-F) and S1-AuNP's (G-L) over 24 hours, cell morphology were observed and recorded (Figure 3.44). Cells appeared increasingly sparely spaced and rounded between the control and 100 µg/ml of the extract, with signs indicative of cell stress (D) and death (E-F) at higher concentrations. Similarly, cells appeared progressively sparely spaced between the control and 200 µg/ml of the AuNP's (G-K), exhibiting rounding and cell stress at higher concentrations (J-L).

Following 48 hours of exposure to increasing concentrations of the S1 extract (A-F) and S1-AuNP's (G-L) over 48 hours, cell morphology was observed and recorded (Figure 3.45). Cells appeared increasingly sparely spaced and atypically rounded between the control and 200 µg/ml of the extract (A-E), showing signs consistent with stress(D-E) and death (F), at higher concentrations. Similarly, cells appeared increasingly sparely spaced between control and 200 µg/ml of the AuNP's, with signs indicative of stress and death increasingly appearing between 50 µg/ml and 200 µg/ml (J-L).

Post 72-hour exposure to S1 extract (A-F) and S1-AuNP's (G-L), cell morphology was observed and recorded (Figure 3.46). Cell became notably fewer and progressively rounded between the control and 200 µg/ml of the extract (A-F), in addition to showing signs consistent with cell stress (D-E) and death (F), at higher concentrations. A progressive decrease in observable cell number was apparent between the control and 200 µg/ml of the AuNP's (G-L), with morphology remaining comparable to the control until 50 µg/ml of the AuNP's (G-I). At higher concentrations (K-L), cells displayed signs consistent with cell stress (K) and death (L).

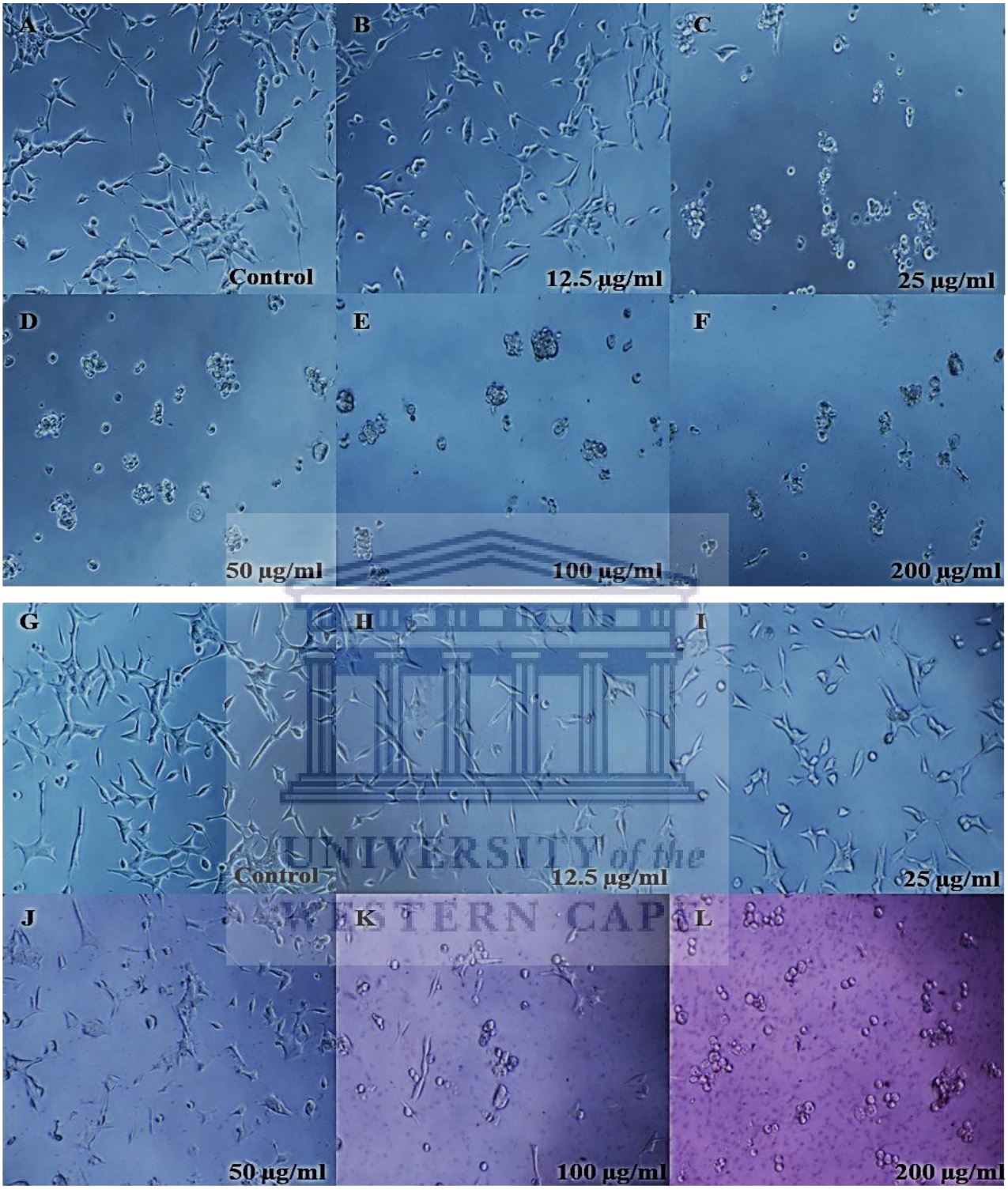

Figure 3.44: LNCaP cell morphology after being exposed to increasing concentrations of S1 extract and S1-AuNP's over a 24-hour period. The extract (A-F) and AuNP's (G-L) yielded progressive cell rounding, followed by stress at higher concentrations, respectively.

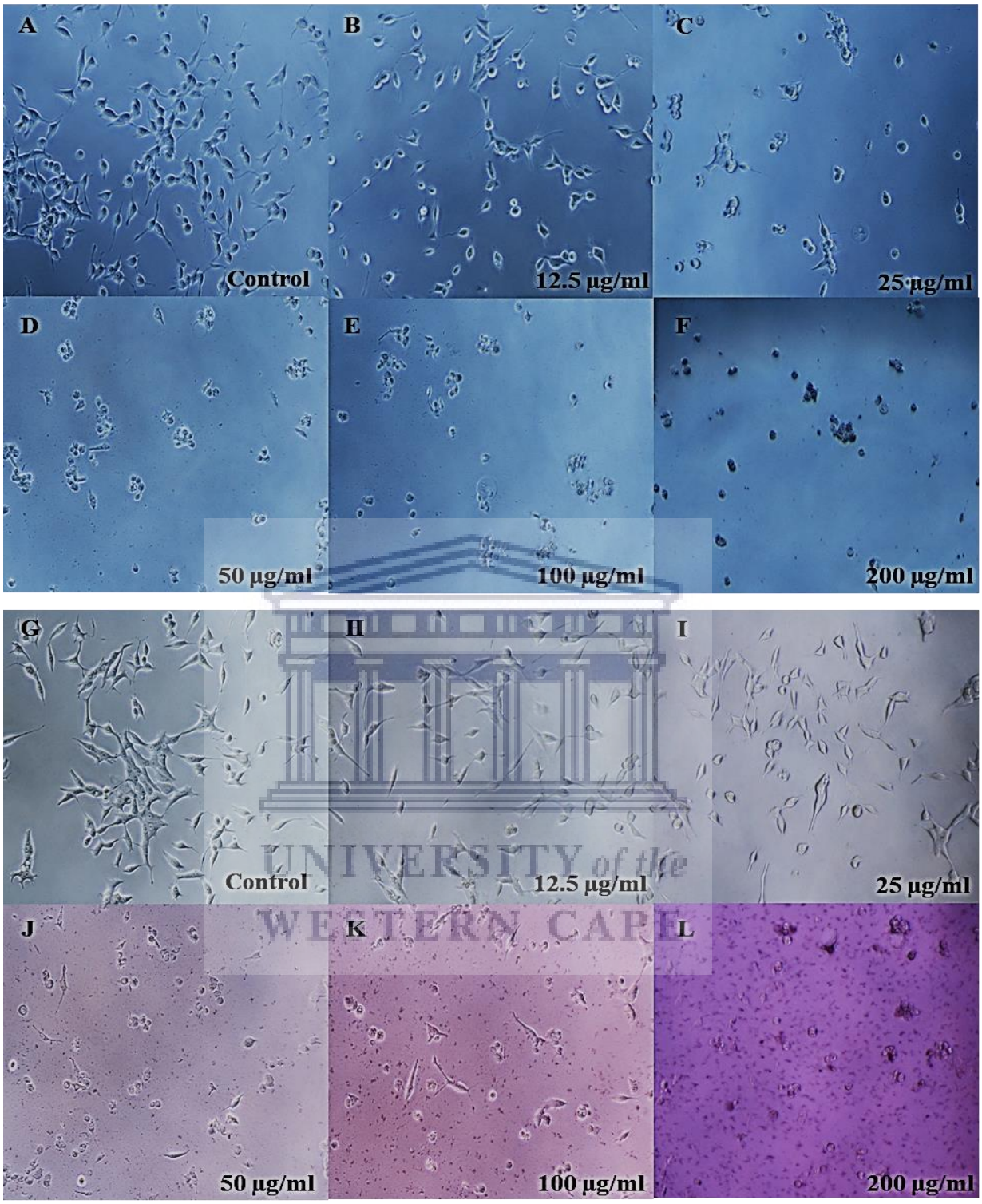

Figure 3.45: LNCaP cell morphology after being exposed to increasing concentrations of S1 extract and S1-AuNP's over a 48-hour period. The extract (A-F) and AuNP's (G-L) yielded progressive cell rounding at lower concentrations, followed by signs of stress and cell death at higher concentrations, respectively.

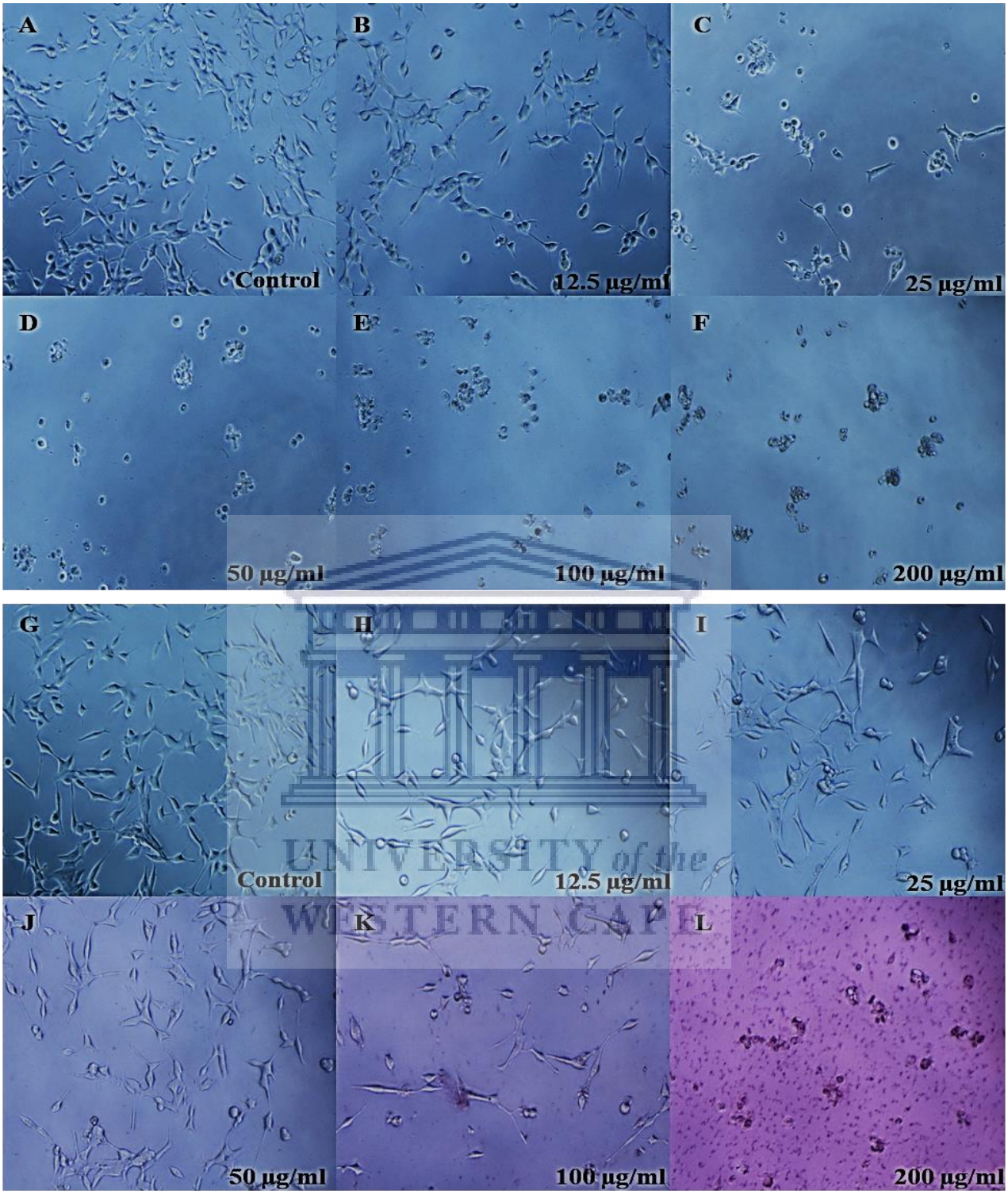

Figure 3.46: LNCaP cell morphology after being exposed to increasing concentrations of S1 extract and S1-AuNP's over a 72-hour period. Cells appeared progressively rounded between control and 200 µg/ml of the extract,

The MTT assay revealed dose-dependent effects at 24, 48 and 72-hours, respectively. After 24-hours (Figure 3.47 A), the extract exhibited increases in cell viability between the control and 12.5 µg/ml, followed by decreases between 12.5-200 µg/ml. AuNP's yielded decreases between the control and 200 µg/ml, differing significantly from the extract (P=0.0048, P=0.0056, P=0.0004, P=0.0123) at 12.5 and 50-200 µg/ml, respectively. For the extract, the repeated measures ANOVA yielded a significant (P=0.0352) positive trend between control and 12.5 µg/ml, followed by a significant (P<0.0001) negative trend between 12.5-200 µg/ml, and a significant (P<0.0001) trend between control and 200 µg/ml for the AuNP's. One-way ANOVA yielded significant (P<0.001) trends between control-200 µg/ml, for the extract and AuNP's.

Following 48 hours of exposure (Figure 3.47 B), the extract increased cell viability between the control and 12.5 µg/ml, followed by a steady decreases. AuNP's yielded decreases in cell viability, differing from the extract significantly (P=0.0115, P=0.005, P<0.0001) at 12.5-25 and 100 µg/ml, respectively. For the extract, the repeated measures ANOVA yielded a significant (P=0.0007) positive trend between control and 12.5 µg/ml, followed by a significant (P<0.0001) negative trend between 12.5-200 µg/ml, and a significant (P<0.0001) trend between control and 200 µg/ml for the AuNP's. One-way ANOVA yielded significant (P<0.001) trends between control and 200 µg/ml, for the extract and AuNP's, respectively.

After 72 hours of exposure (Figure 3.47 C), the extract increased cell viability between control and 12.5 µg/ml, followed by decreases hereafter, whereas the AuNP's progressively decreased cell viability, differing from the extract significantly (P=0.0001, P=0.0068, P=0.0001 P=0.0033) at 12.5-25 and 100-200 µg/ml, respectively. For the extract, the repeated measures ANOVA yielded a significant (P=0.0007) positive trend between control and 12.5 µg/ml, followed by a significant (P<0.0001) negative trend between 12.5-200 µg/ml, and a significant (P<0.0001) trend was observed between control and 200 µg/ml for the AuNP's. One-way ANOVA yielded significant (P<0.001) trends between the control and 200 µg/ml, for the extract and AuNP's.

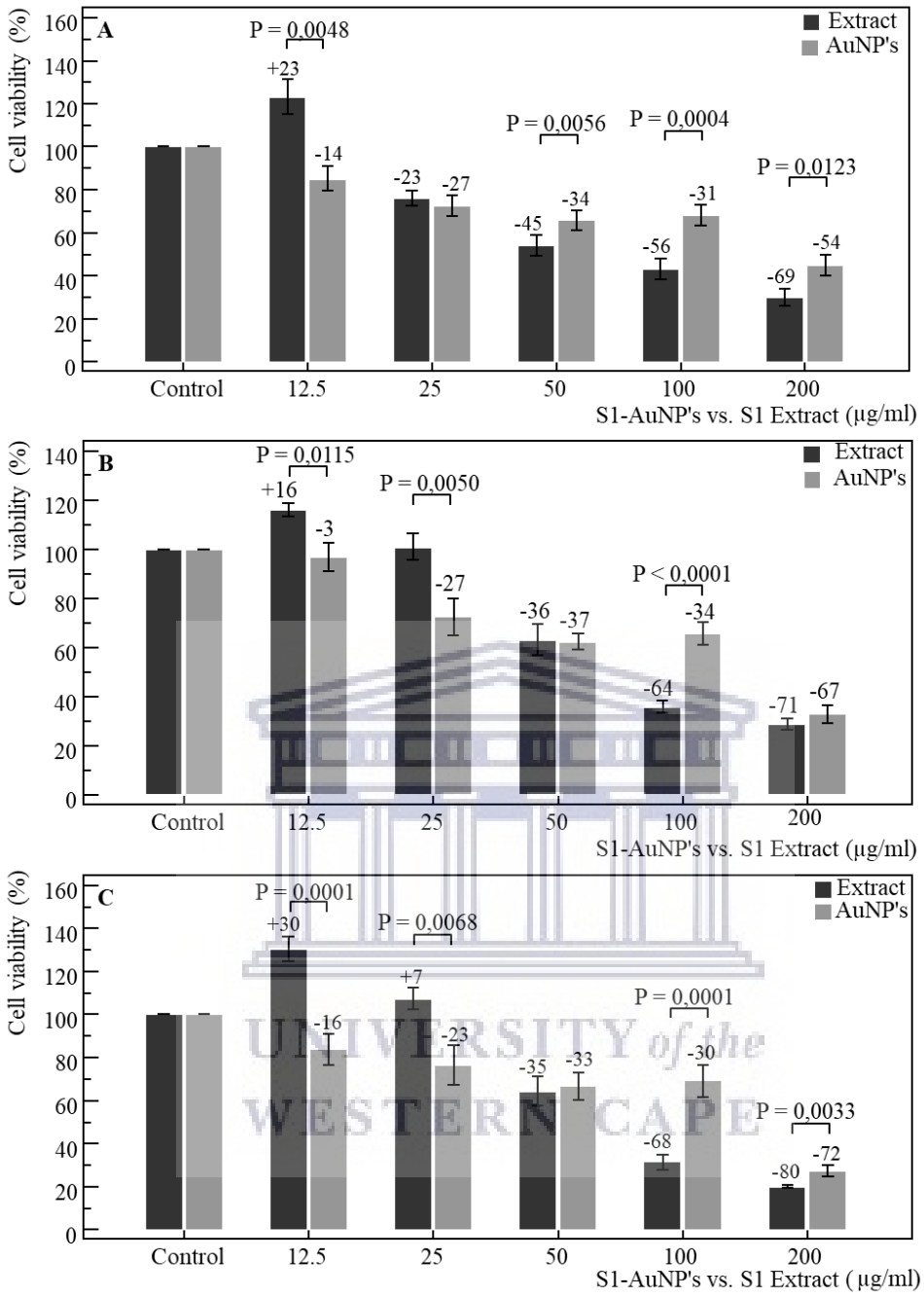

Figure 3.47: LNCaP cell viability as determined by the MTT assay over 24 (A), 48 (B) and 72 (C) hour exposure to the S1 extract and S1-AuNP's respectively. Significant (P=0.0048, P=0.0056, P=0.0004, P=0.0123) differences were observed between the extract and AuNP's at 12.5 µg/ml, 50 µg/ml, 100 µg/ml and 200 µg/ml over 24 hours, along with a significant (P=0.0115, P=0.005, P<0.0001) difference observed at 12.5 µg/ml, 25 µg/ml and 100 µg/ml after 48 hours, and finally significant (P=0.0001, P=0.0068, P=0.0001 P=0.0033) differences at 12.5 µg/ml, 25 µg/ml and 100 µg/ml after 72 hours of exposure.

3.2.2.2 S1x2-AuNP's and Extract

After being exposed to increasing concentrations of the S1 extract (A-F) and S1x2-AuNP's (G-L) over 24 hours, cell morphology was observed and recorded (Figure 3.48). Cells appeared increasingly sparely spaced and rounded between the control and 100 µg/ml of the extract, with signs indicative of cell stress (D) and death (E-F) at higher concentrations. Similarly, cells appeared marginally, but progressively, sparely spaced between the control and 200 µg/ml of the AuNP's (G-K), exhibiting rounding and signs consistent with cell stress at 200 µg/ml (L).

Following 48 hours of exposure to increasing concentrations of the S1 extract (A-F) and S1x2-AuNP's (G-L) over 48 hours, cell morphology was observed and recorded (Figure 3.49). Cells appeared increasingly sparely spaced and atypically rounded between the control and 200 µg/ml of the extract (A-E), showing signs consistent with stress(D-E) and death (F), at higher concentrations. Similarly, cells appeared slightly, yet increasingly rounded and sparely spaced between control and 200 µg/ml of the AuNP's, with signs indicative of stress increasingly appearing between 100 µg/ml and 200 µg/ml (K-L).

Post 72-hour exposure to S1 extract (A-F) and S1x2-AuNP's (G-L), cell morphology was observed and recorded (Figure 3.50). Cell became notably fewer and progressively rounded between the control and 200 µg/ml of the extract (A-F), in addition to showing signs consistent with cell stress (D-E) and death (F), at higher concentrations. A slight, yet fairly consistent decrease in observable cell number occurred between the control and 100 µg/ml of the AuNP's (G-K), without distinct morphological changes. At the highest concentration (L), cells appeared rounded and displayed signs consistent with cell stress (L)

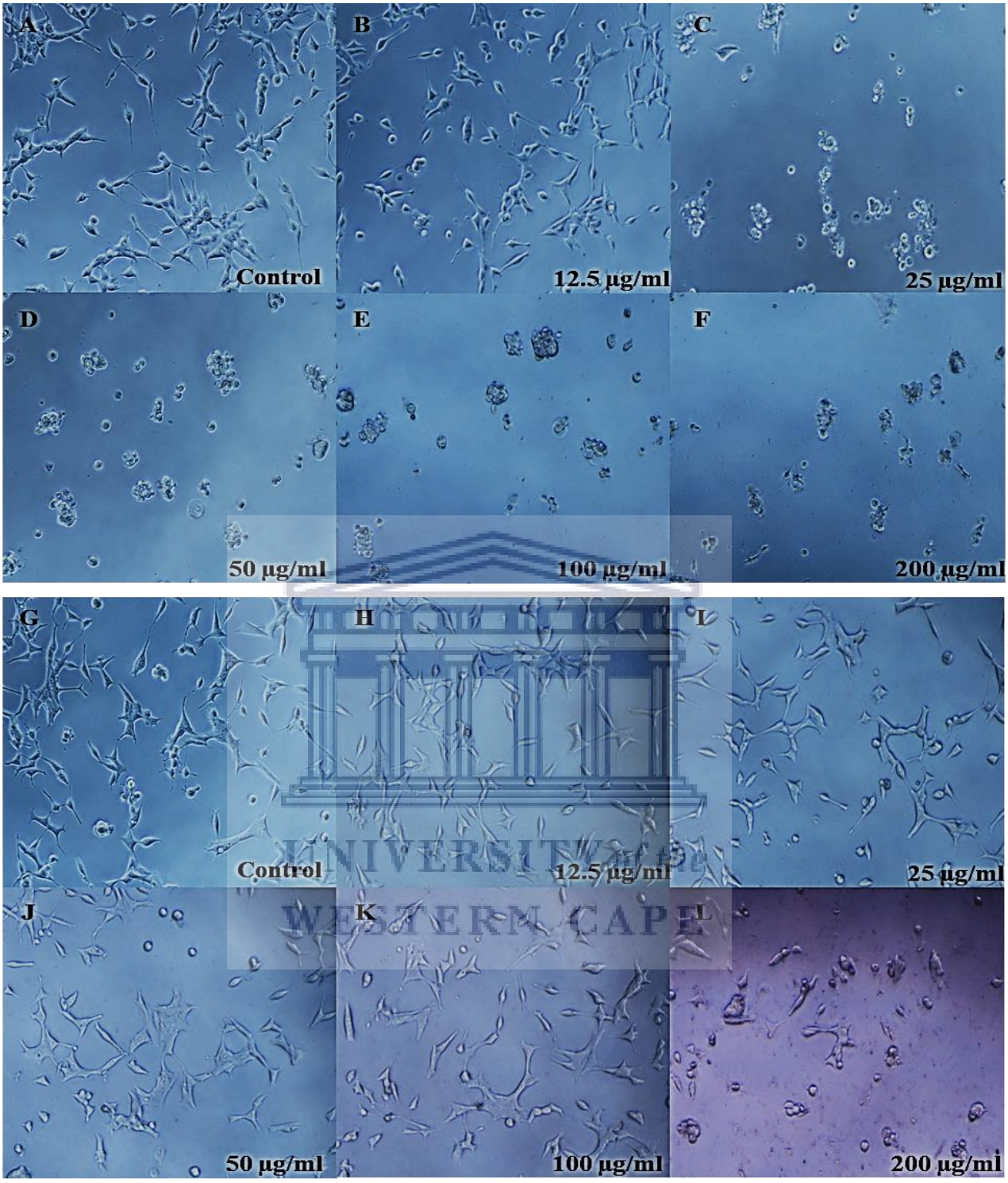

Figure 3.48: LNCaP cell morphology after being exposed to increasing concentrations of S1 extract and S1x2-AuNP's over a 24-hour period. The extract (A-F) yielded progressive cell rounding at lower concentrations, followed by stress at higher concentrations. AuNP's exhibited marginal decreased in the overall observed cell number (G-L), along with signs of rounding and cell stress at the highest concentration (L).

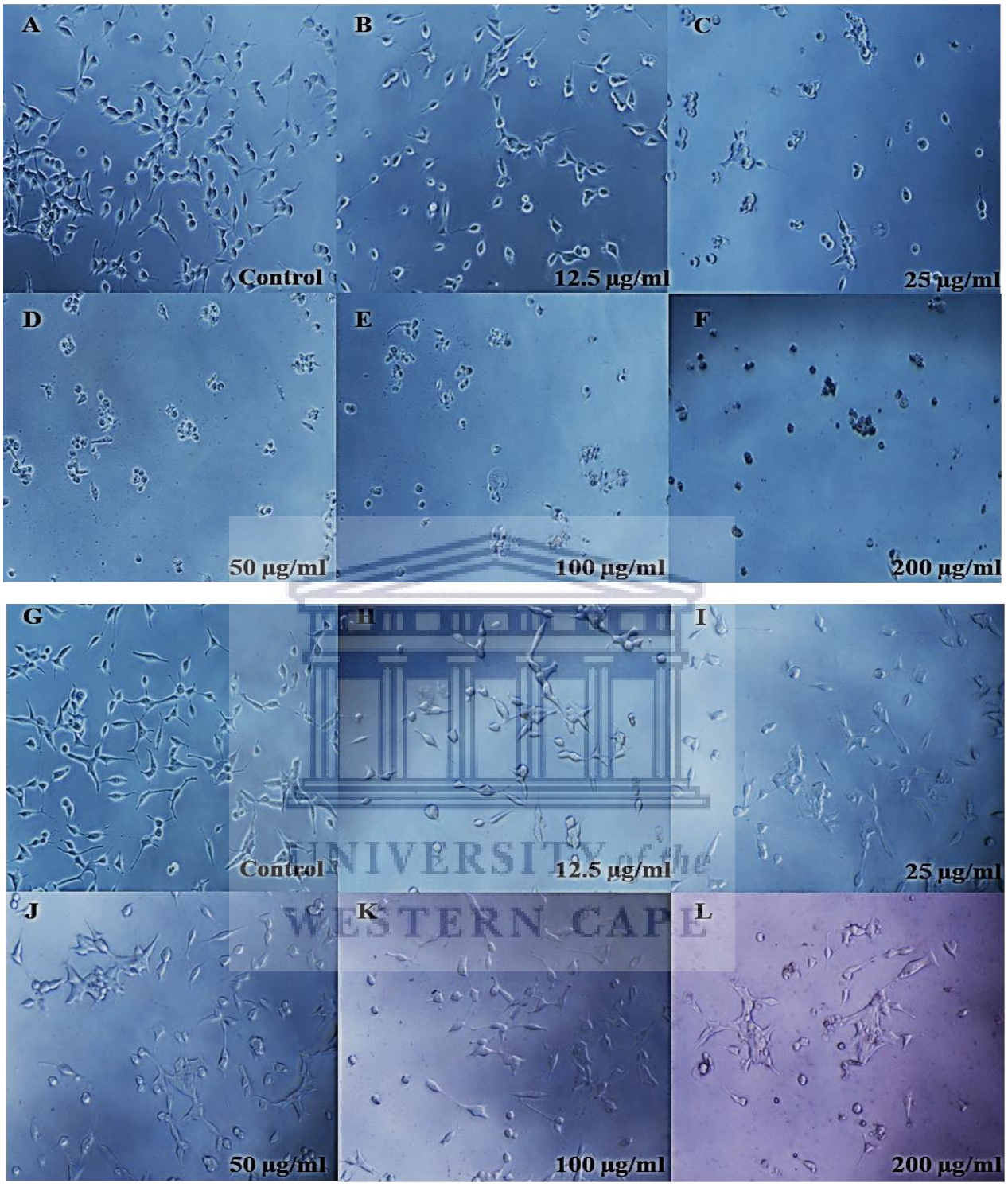

Figure 3.49: LNCaP cell morphology after being exposed to increasing concentrations of S1 extract and S1x2-AuNP's over a 48-hour period. The extract (A-F) progressive cell rounding at lower concentrations, followed by signs of stress and cell death at higher concentrations, respectively. The AuNP's exhibited marginal decreased in the overall observed cell number (G-L), along with signs of rounding and cell stress at the higher concentrations (K-L).

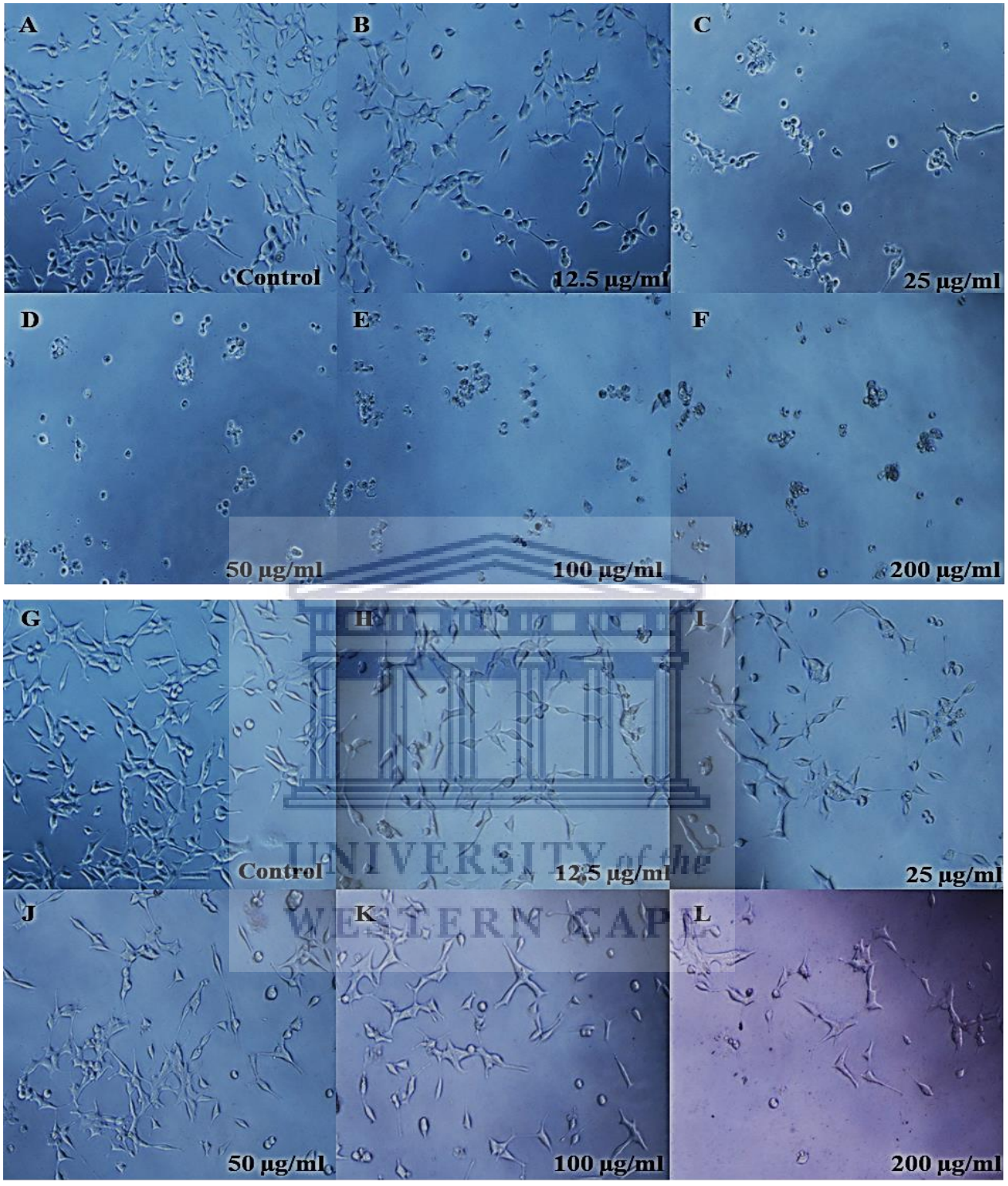

Figure 3.50: LNCaP cell morphology after being exposed to increasing concentrations of S1 extract and S1x2-AuNP's over a 72-hour period. Cells appeared progressively rounded between control and 200 µg/ml of the extract, displaying signs consistent with cell stress and death at higher concentrations (D-F). AuNP's exhibit slight reduction in overall observed cell number, with the presence of cell stress at the highest concentration (L).

The MTT assay revealed dose-dependent effects at 24, 48 and 72-hour exposure periods, respectively. After 24-hours (Figure 3.51 A), the extract exhibited increases in cell viability from control-12.5 µg/ml, followed by decreases between 12.5-200 µg/ml. The AuNP's yielded decreases in cell viability from control-200 µg/ml, differing significantly from the extract ($P=0.0325$, $P=0.0004$, $P=0.0001$) at 12.5 and 100-200 µg/ml, respectively. For the extract, the repeated measures ANOVA yielded a significant ($P=0.0352$) positive trend fromcontrol-12.5 µg/ml, followed by a significant ($P<0.0001$) negative trend between 12.5-200 µg/ml, along with a significant ($P=0.0002$) trend from control-200 µg/ml for the AuNP's. One-way ANOVA yielded significant ($P<0.001$, $P=0.004$) trends from control-200 µg/ml, for the extract and AuNP's.

Following 48-hours (Figure 3.51 B) the extract increased cell viability from control-12.5 µg/ml, followed by a steady decreases, while AuNP's yielded decreases in cell viability from control-200 µg/ml. AuNP's differed from the extract significantly ($P=0.0007$ and $P<0.0001$) at 12.5 µg/ml and 100-200 µg/ml. The repeated measures ANOVA yielded a significant ($P=0.0007$) positive trend from control-12.5 µg/ml, followed by a significant ($P<0.0001$) negative trend between 12.5-200 µg/ml for the extract, along with a significant ($P=0.0019$) trend from control-200 µg/ml for the AuNP's. One-way ANOVA yielded significant ($P<0.001$, $P=0.001$) trends from control-200 µg/ml, for the extract and AuNP's.

After 72-hours (Figure 3.51 C) the extract increased cell viability from control-12.5 µg/ml, followed by steady decreases hereafter. The AuNP's steadily decreased cell viability, differing from the extract significantly ($P<0.0001$, $P=0.0001$ and $P<0.0001$) at 12.5-25 and 100-200 µg/ml, respectively. The repeated measures ANOVA yielded a significant ($P=0.0007$) positive trend from control-12.5 µg/ml, followed by a significant ($P<0.0001$) negative trend between 12.5-200 µg/ml of the extract, along with a significant ($P<0.0001$) trend from control-200 µg/ml of the AuNP's. One-way ANOVA yielded significant ($P<0.001$) trends between the control and 200 µg/ml, for the extract and AuNP's, respectively

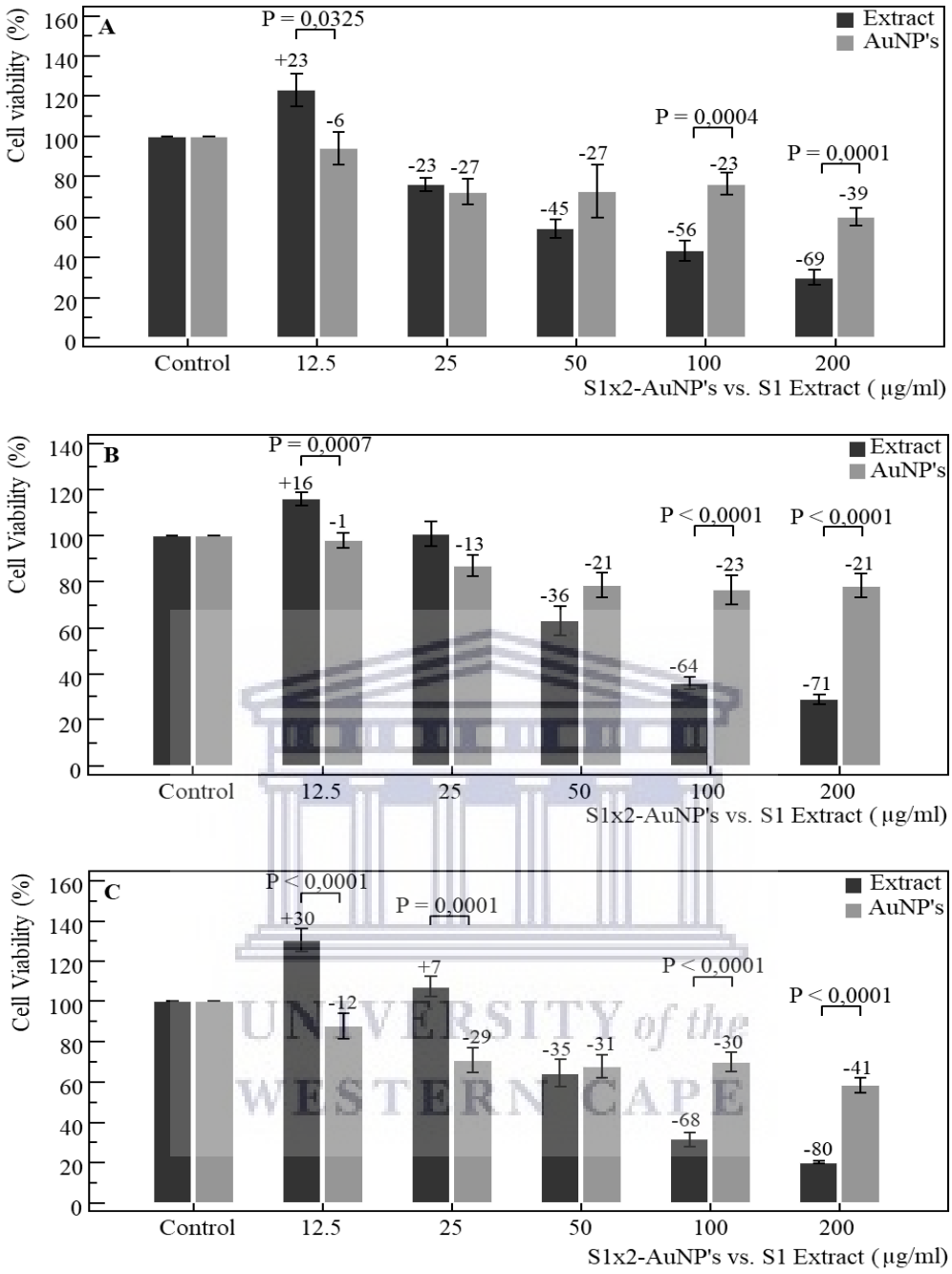

Figure 3.51: LNCaP cell viability as determined by the MTT assay over 24 (A), 48 (B) and 72 (C) hour exposure to the S1 extract and S1x2-AuNP's respectively. Significant (P=0.0325, P=0.0004, P=0.0001) differences were observed between the extract and AuNP's at 12.5 µg/ml,100 µg/ml and 200 µg/ml over 24 hours, along with a significant (P=0.0007, P<0.0001 and P<0.0001) difference observed at 12.5 µg/ml, 100 µg/ml and 200 µg/ml after 48 hours, and finally (P<0.0001, P=0.0001 and P<0.0001) differences at 12.5 µg/ml, 25 µg/ml, 100 µg/ml and 200 µg/ml after 72 hours of exposure.

3.2.2.3 S2-AuNP's and S2 Extract

After being exposed to increasing concentrations of the S2 extract (A-F) and S2-AuNP's (G-L) over 24 hours, cell morphology was observed and recorded (Figure 3.52).Between the control and 200 µg/ml (A-F), cells appeared progressively sparely spaced, rounded, and displayed signs indicative of cell stress (B-D) and cell death (E-F). Conversely, cells appeared marginally, but progressively sparely spaced between the control and 200 µg/ml of the AuNP's (G-K), without obvious morphological changes up until 50 µg/ml (J). At higher concentrations (K-L), cells became progressively rounded, exhibiting signs indicative of cell stress.

Following 48 hours of exposure to increasing concentrations of the S2 extract (A-F) and S2-AuNP's (G-L) over 48 hours, cell morphology was observed and recorded (Figure 3.53). Cells were notably fewer between the control and 200 µg/ml of the extract (A-E), exhibiting sings consistent with cell stress (B) and death (C-F) at the higher concentrations. Conversely, cells appeared slightly sparely spaced between control and 200 µg/ml of the AuNP's, with no signs of morphological changes until 100 µg/ml (K). At 200 µg/ml (L), cells appeared to be observably fewer than at lower concentrations (G-K), and had a slightly rounded appearance.

Post 72 hour exposure to S2 extract (A-F) and S2-AuNP's (G-L), cell morphology was observed and recorded (Figure 3.54). Cells were markedly fewer between the control and 200 µg/ml of the extract (A-E), exhibiting slight rounding (B), along with signs consistent with cell stress (C) and cell death (D-F) at the higher concentrations. Conversely, cells appeared marginally sparely spaced between control and 200 µg/ml of the AuNP's, with no obvious signs of morphological changes until 100 µg/ml (K). At 200 µg/ml (L), cells were observably fewer than lower concentrations (G-K), with signs consistent with cell stress.

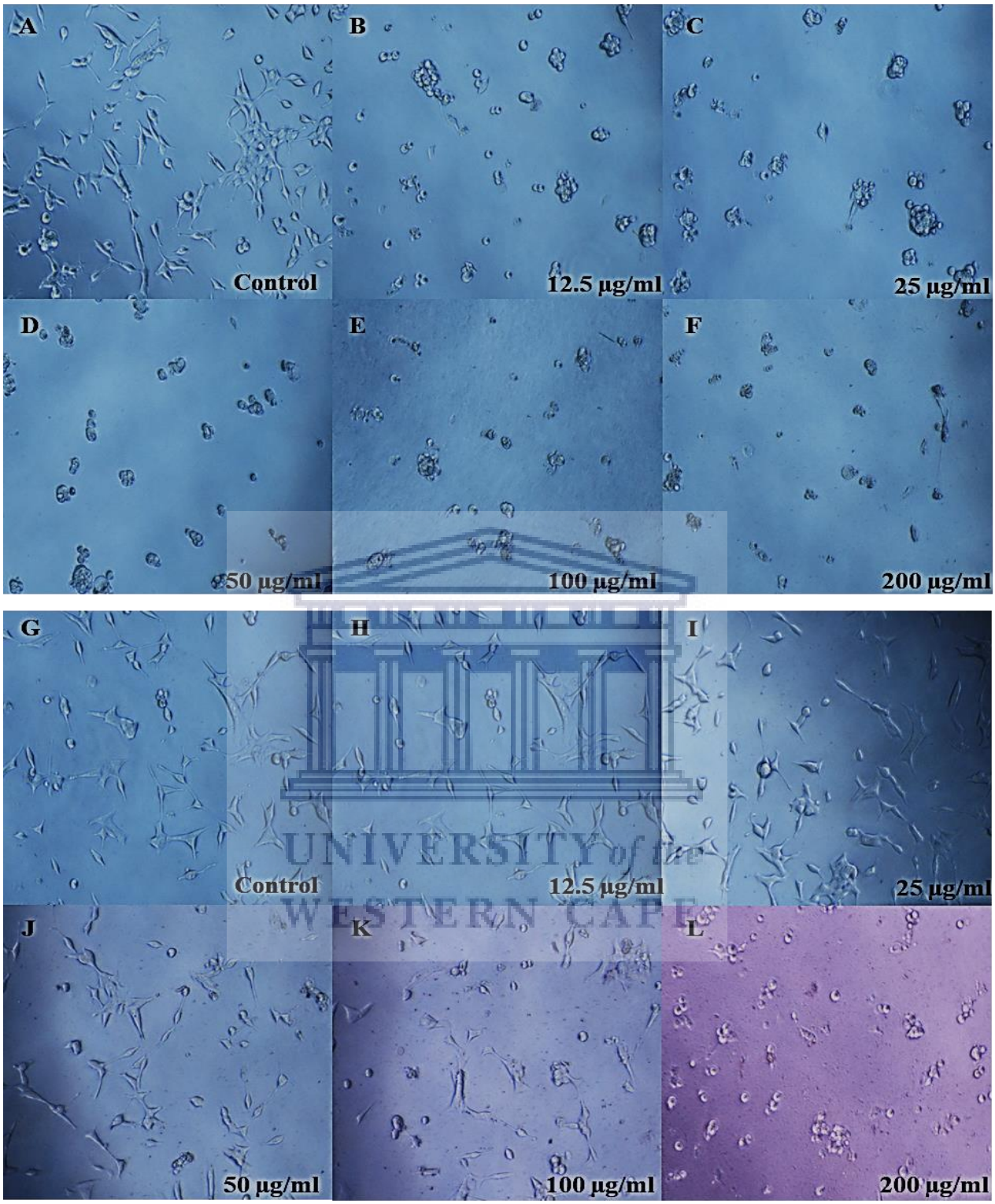

Figure 3.52: LNCaP cell morphology after being exposed to increasing concentrations of S2 extract and S2-AuNP's over a 24-hour period. The extract (A-F) yielded progressive cell rounding and signs of stress and death at higher concentrations, while AuNP's exhibited slight decreases in observed cell number (G-L), with signs of cell stress at the highest concentration (L).

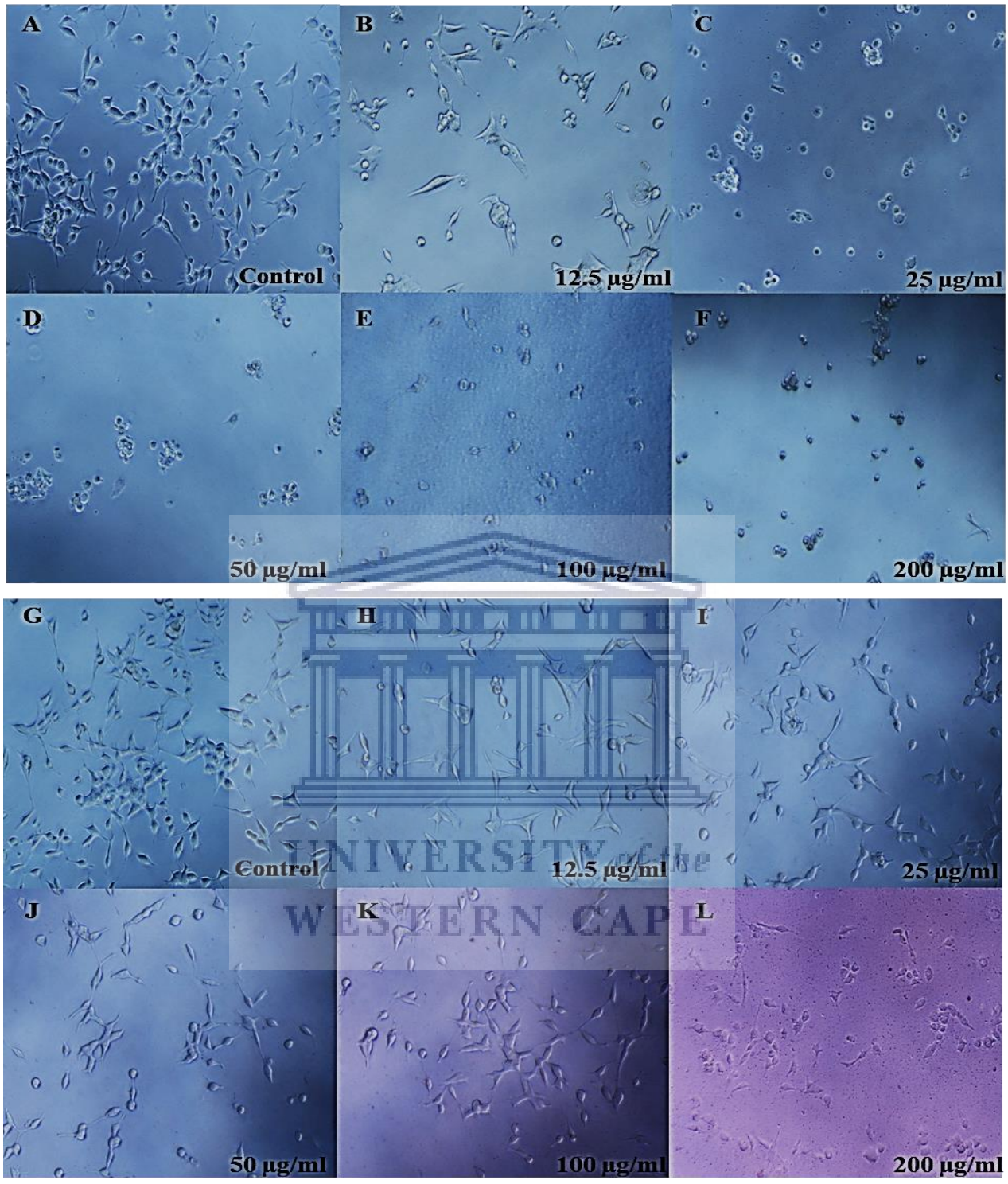

Figure 3.53: LNCaP cell morphology after being exposed to increasing concentrations of S2 extract and S2-AuNP's over a 48-hour period. The extract (A-F) exhibited notably fewer cells at each concentration, along with signs of stress and cell death at the higher concentrations. The AuNP's exhibited marginal decreased in the overall observed cell number (G-L), along with marginal signs of rounding at the highest concentration (L).

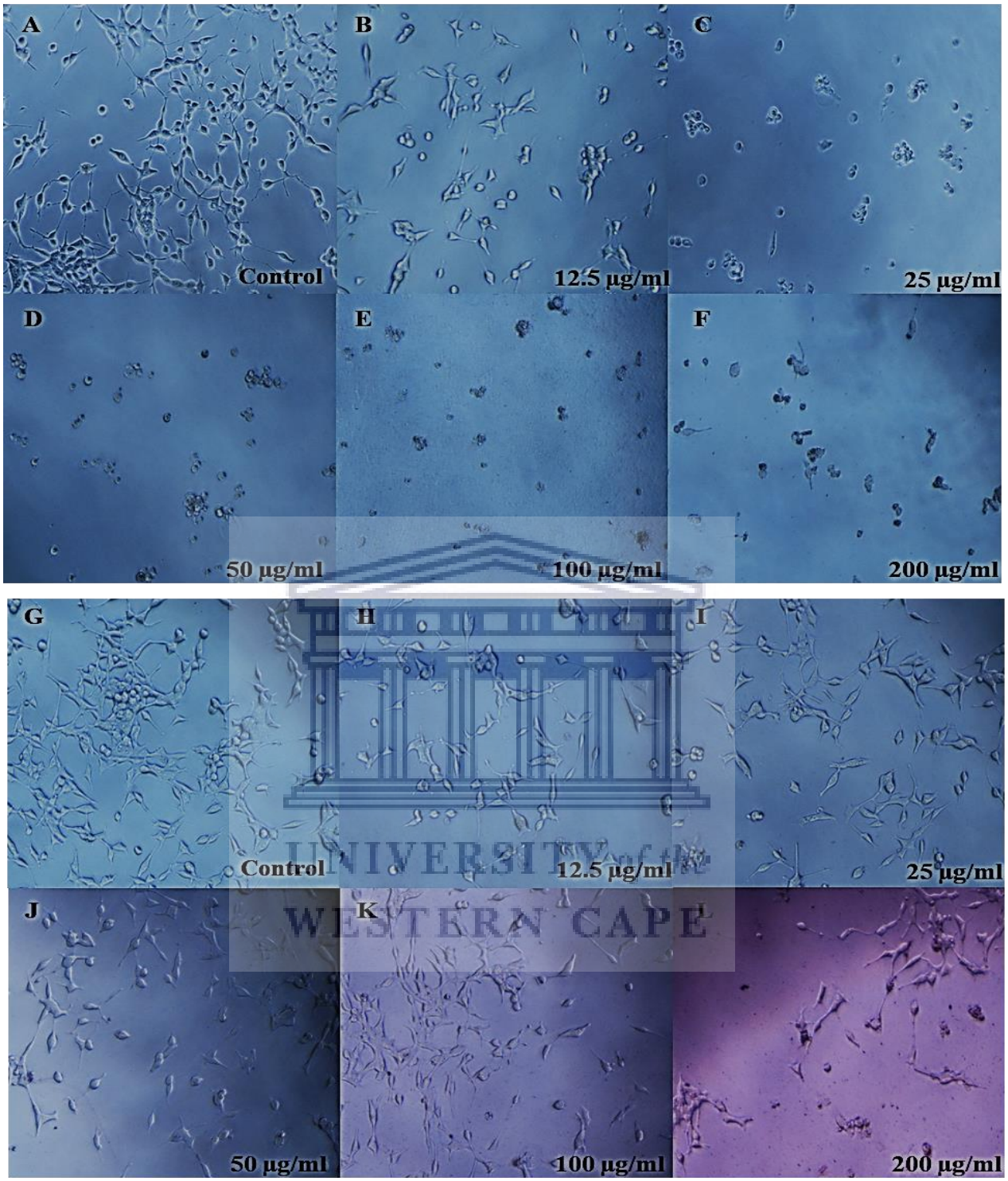

Figure 3.54: LNCaP cell morphology after being exposed to increasing concentrations of S2 extract and S2-AuNP's over a 72-hour period. Cells were observably fewer between control and 200 µg/ml of the extract, displaying signs consistent with cell stress and death at higher concentrations (D-F). AuNP's exhibit slight reduction in overall observed cell number, with the presence of cell stress at the highest concentration (L).

The MTT assay revealed dose-dependent effects at 24, 48 and 72-hour exposure periods, respectively. After 24-hours (Figure 3.55 A), both the extract and AuNP's exhibited steady decreases in cell viability between the control and 200 µg/ml. The extract yielded the greatest reduction in viability at each concentration, differing from the AuNP's significantly (P=0.0001 and P<0.0001) at 25 µg/ml and 50-200 µg/ml, respectively. For the extract, the repeated measures ANOVA revealed a significant (P<0.0001) negative trend from control-200 µg/ml, along with the AuNP's yielding a significant (P=0.0001) trend from control-200 µg/ml. One-way ANOVA yielded significant (P<0.001) trends from control-200 µg/ml, for both the extract and AuNP's, respectively.

Following 48-hours of exposure (Figure 3.55 B), both the extract and AuNP's yielded progressive decreases in cell viability between the control and 200 µg/ml. Notably, the extract yielded a greater reduction in cell viability at each concentration, differing from the AuNP's significantly (P=0.0012, P=0.0001 and P<0.0001) at 25 µg/ml, 50 µg/ml and 100-200 µg/ml, respectively. The repeated measures ANOVA revealed a significant (P<0.0001) negative trend from control-200 µg/ml when exposed to the extract, along with the AuNP's yielding a significant (P=0.0001) trend from control-200 µg/ml. One-way ANOVA revealed significant (P<0.001) trends from control-200 µg/ml, for both the extract and AuNP's, respectively.

After 72-hours (Figure 3.55 C) both the extract and AuNP's yielded consistent, and progressive, decreases in cell viability between the control and 200 µg/ml. The extract yielded markedly greater reductions in cell viability at each concentration, differing from the AuNP's significantly (P=0.0001 and P<0.0001) at 25 µg/ml and 50-200 µg/ml, respectively. The repeated measures ANOVA revealed a significant (P<0.0001) negative trend from control-200 µg/ml when cells were treated with the extract, along with the AuNP's yielding a significant (P=0.0001) trend from control-200 µg/ml. One-way ANOVA revealed significant (P<0.001) trends from control-200 µg/ml, for both the extract and AuNP's, respectively.

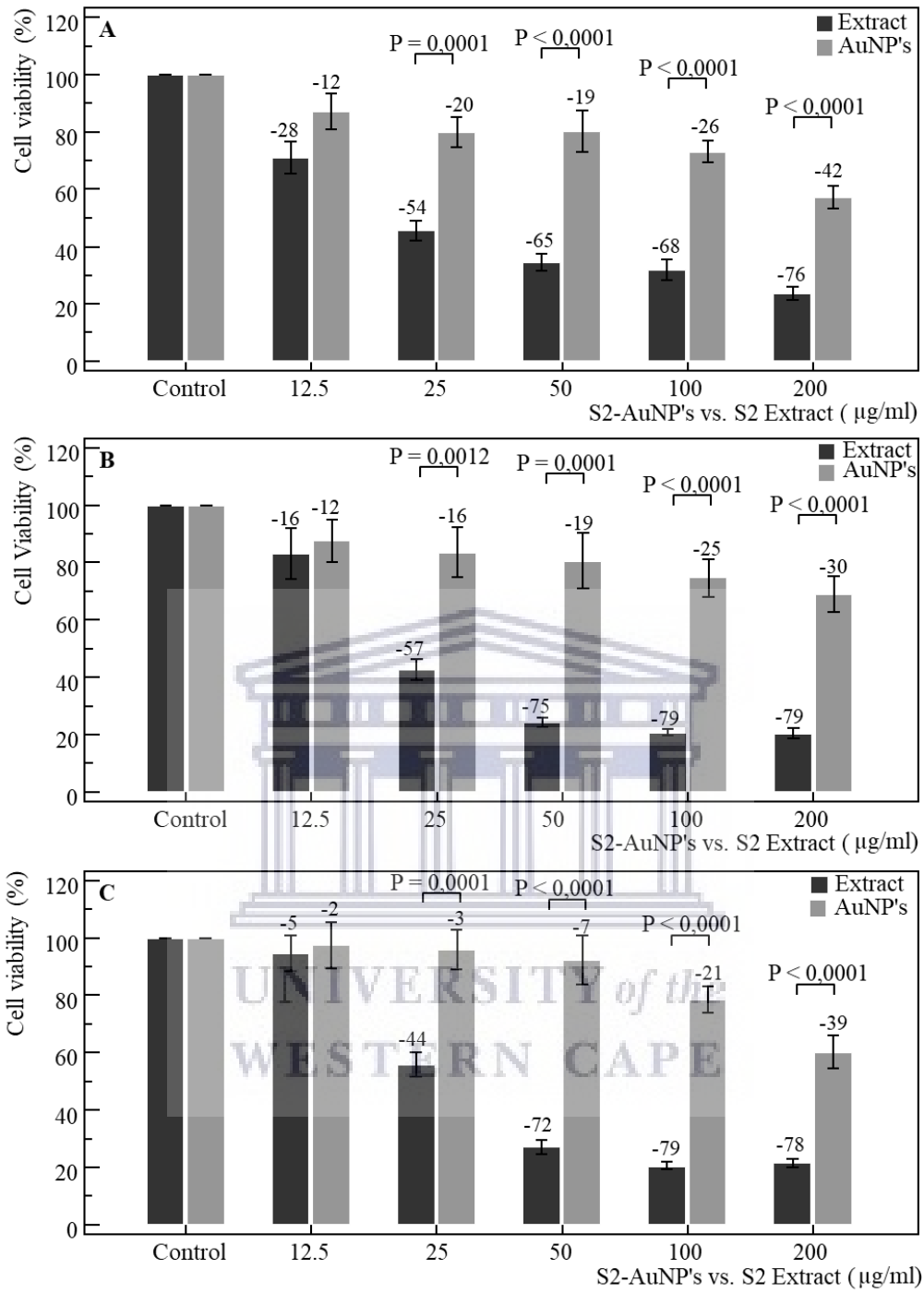

Figure 3.55: LNCaP cell viability as determined by the MTT assay over 24 (A), 48 (B) and 72 (C) hour exposure to the S2 extract and S2-AuNP's respectively. Significant (P=0.0001 and P<0.0001) differences were observed between the extract and AuNP's from 25-200 µg/ml, respectively, over 24 hours, along with a significant (P=0.0012, P=0.0001 and P<0.0001) difference from 25 µg/ml and 50-200 µg/ml after 48 hours, and finally significant (P=0.0001 and P<0.0001) differences at 25 µg/ml and 50 µg/ml, 100 µg/ml and 200 µg/ml after 72 hours of exposure

3.2.2.4 S2x2-AuNP's and S2 Extract

After being exposed to increasing concentrations of the S2 extract (A-F) and S2x2-AuNP's (G-L) over 24 hours, cell morphology was observed and recorded (Figure 3.56). Between the control and 200 µg/ml (A-F), cells appeared progressively sparely spaced, rounded, and displayed signs indicative of cell stress (B-D) and cell death (E-F). Conversely, cells appeared marginally sparely spaced between the control and 12.5 µg/ml of the AuNP's (G-H), while appearing more notably fewer in number between 25 µg/ml and 200 µg/ml (J-L). Cell morphology remained comparable to control at each concentration of the AuNP's.

Following 48 hours of exposure to increasing concentrations of the S2 extract (A-F) and S2x2-AuNP's (G-L) over 48 hours, cell morphology was observed and recorded (Figure 3.57). Cells were notably fewer between the control and 200 µg/ml of the extract (A-E), exhibiting sings consistent with cell stress (B) and death (C-F) at the higher concentrations. Conversely, cells appeared progressively sparely spaced between control and 200 µg/ml of the AuNP's, with no signs of morphological changes until 50 µg/ml (J). At higher concentrations (K-L) cells appeared progressively rounded, and exhibited signs indicative of cell stress (L)

Post 72-hour exposure to S2 extract (A-F) and S2x2-AuNP's (G-L), cell morphology was observed and recorded (Figure 3.58). Cells were markedly fewer between the control and 200 µg/ml of the extract (A-E), exhibiting slight rounding (B), along with signs consistent with cell stress (C) and cell death (D-F) at the higher concentrations. Conversely, cells appeared marginally, but progressively sparely spaced between control and 100 µg/ml of the AuNP's, along with no obvious signs of morphological changes. At 200 µg/ml (L) cells were observably fewer and appeared slightly rounded with signs consistent with cell stress.

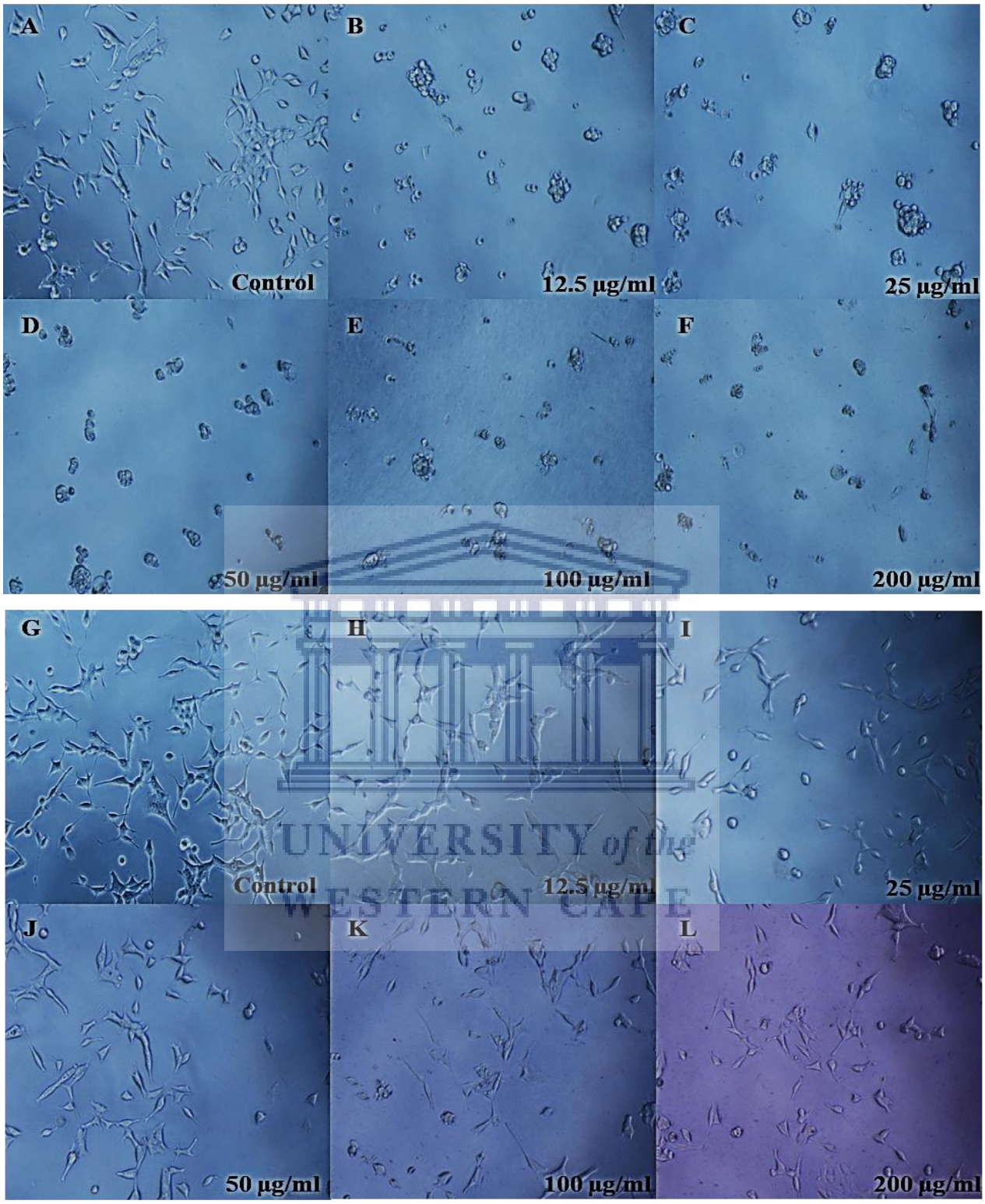

Figure 3.56: LNCaP Cell morphology after being exposed to increasing concentrations of S2 extract and S2-AuNP's over a 24-hour period. The extract (A-F) yielded progressive cell rounding and signs of stress and death at higher concentrations, while AuNP's exhibited slight decreases in cell number at low concentrations (G-H), and notable decreases at higher concentrations (I-L).

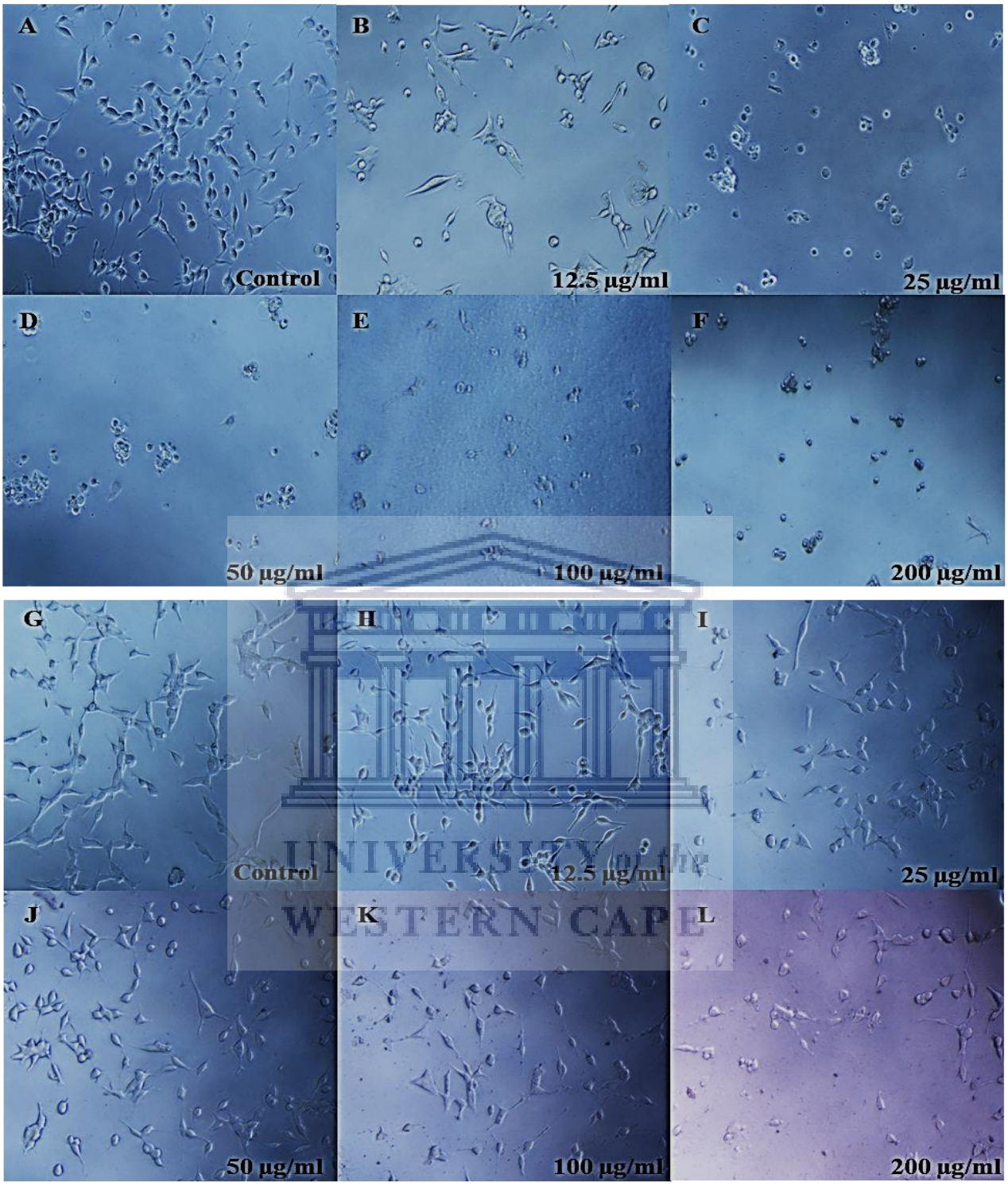

Figure 3.57: LNCaP cell morphology after being exposed to increasing concentrations of S2 extract and S2x2-AuNP's over a 48-hour period. The extract (A-F) exhibited notably fewer cells at each concentration, along with signs of stress and cell death at the higher concentrations. The AuNP's exhibited progressive decreases in the overall observed cell number (G-L), along with signs of rounding and stress at the higher concentration (K-L).

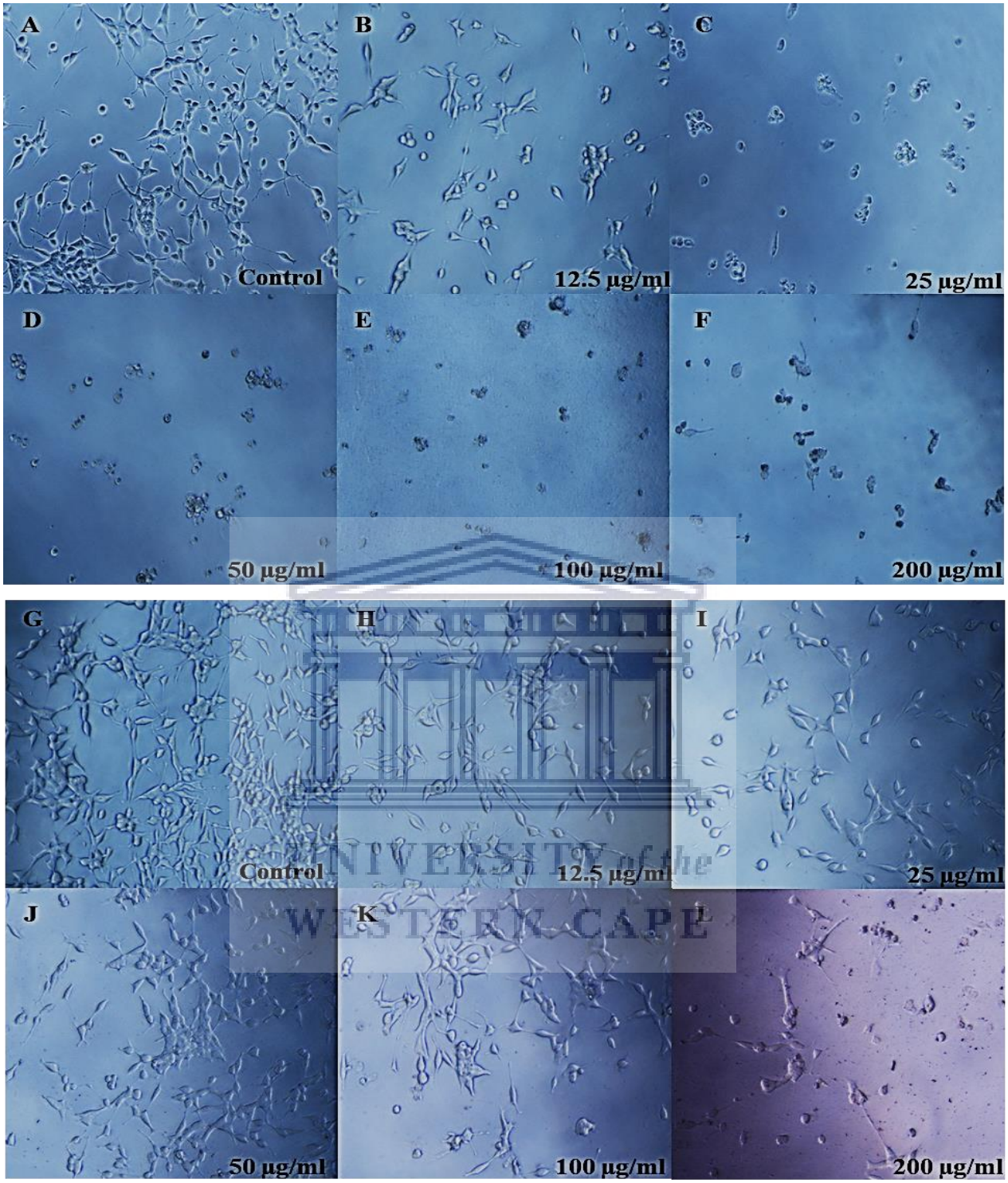

Figure 3.58: LNCaP cell morphology after being exposed to increasing concentrations of S2 extract and S2x2-AuNP's over a 72-hour period. Cells were observably fewer between control and 200 µg/ml of the extract, displaying signs consistent with cell stress and death at higher concentrations (D-F). AuNP's exhibit slight reduction in overall observed cell number, with the presence of cell stress at the highest concentration (L).

The MTT assay revealed dose-dependent effects at 24, 48 and 72-hour exposure periods, respectively. After 24-hours (Figure 3.59 A), both the extract and AuNP's exhibited progressive decreases in cell viability between the control and 200 µg/ml. The extract yielded greater reductions in cell viability, differing significantly (P=0.003 and P<0.0001) from the AuNP's at 25 µg/ml and 50-200 µg/ml, respectively. For the extract, the repeated measures ANOVA revealed a significant (P<0.0001) negative trend from control-200 µg/ml, along with the AuNP's yielding a significant (P<0.0001) negative trend from control-200 µg/ml. One-way ANOVA yielded significant (P<0.001) trends from control-200 µg/ml, for both the extract and AuNP's, respectively.

Following 48-hours of exposure (Figure 3.59 B), both the extract and AuNP's yielded progressive decreases in cell viability between the control and 200 µg/ml. Notably, the extract yielded a greater reduction in cell viability at each concentration used, differing from the AuNP's significantly (P<0.0001) at 25 µg/ml, 50 µg/ml, 100 µg/ml and 200 µg/ml, respectively. The repeated measures ANOVA revealed a significant (P<0.0001) negative trend from control-200 µg/ml when exposed to the extract, along with the AuNP's yielding a significant (P<0.0001) negative trend from control-200 µg/ml. One-way ANOVA revealed significant (P<0.001) trends from control-200 µg/ml, for both the extract and AuNP's, respectively.

After 72-hours (Figure 3.59 C) both the extract and AuNP's yielded consistent, and progressive, decreases in cell viability between the control and 200 µg/ml. The extract yielded markedly greater reductions in cell viability at each concentration, differing from the AuNP's significantly (P=0.0344, P=0.0002, P<0.0001 and P=0.0001) at 25-200 µg/ml, respectively. The repeated measures ANOVA revealed a significant (P<0.0001) negative trend from control-200 µg/ml when cells were treated with the extract, along with the AuNP's yielding a significant (P=0.0234) trend from control-200 µg/ml. One-way ANOVA revealed a significant (P<0.001) trends between the control and 200 µg/ml, for the extract

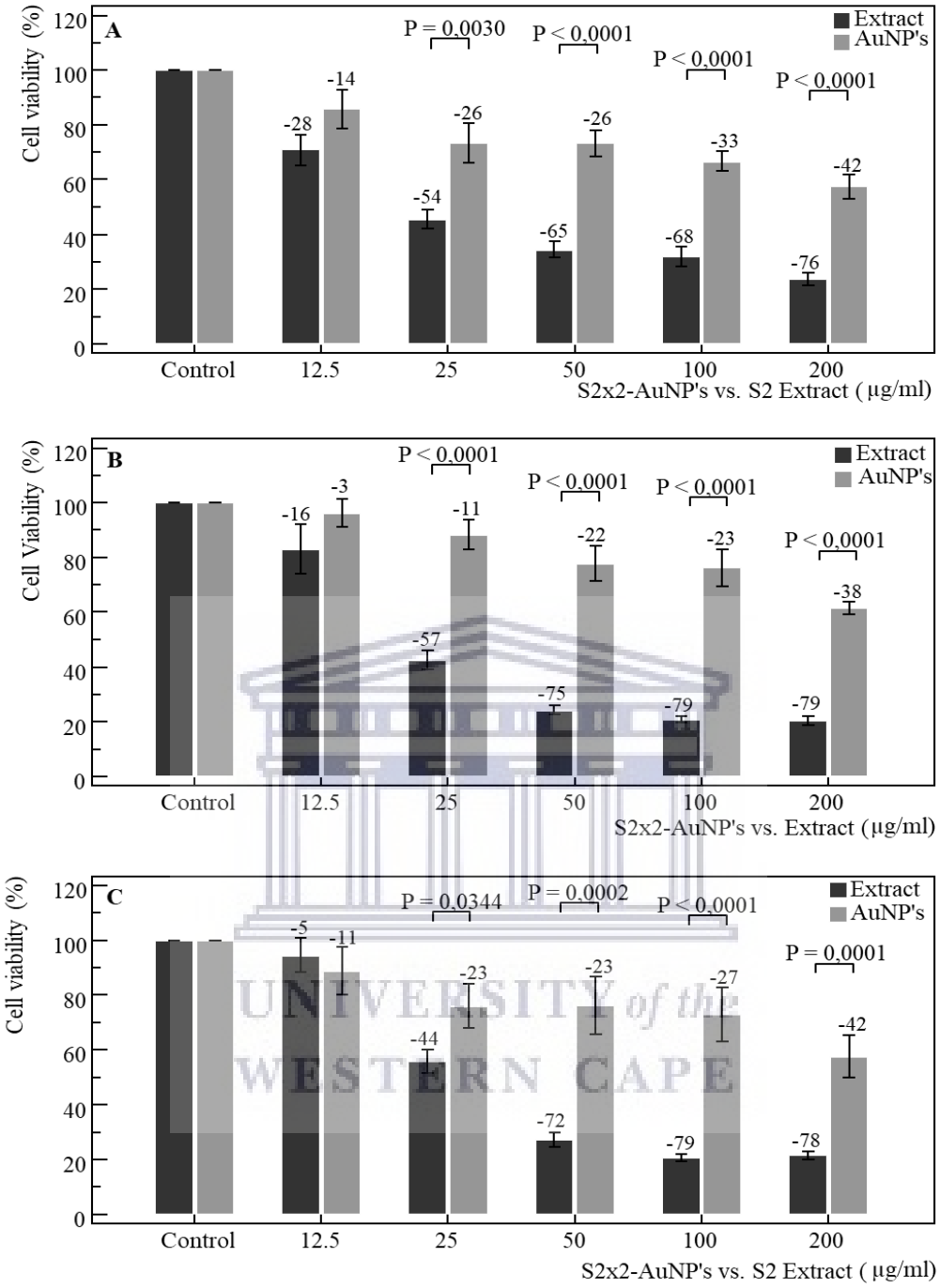

Figure 3.59: LNCaP cell viability as determined by the MTT assay over 24 (A), 48 (B) and 72 (C) hour exposure to the S2 extract and S2x2-AuNP's respectively. Significant (P=0.003 and P<0.0001) differences were observed between the extract and AuNP's from 25-200 µg/ml, respectively, over 24 hours, along with a significant (P<0.0001) difference from 25-200 µg/ml after 48 hours, and finally significant (P=0.0344, P=0.0002, P<0.0001 and P=0.0001) differences from 25-200 µg/ml, respectively, after 72 hours of exposure

3.2.2.5 Ng-AuNP's pH 7 and naringenin

After being exposed to increasing concentrations of naringenin (A-F) and Ng-AuNP's pH 7 (G-L) over 24 hours, cell morphology was observed and recorded (Figure 3.60). Between the control and 200 µg/ml (A-F), cells appeared progressively sparely spaced and rounded, displayed signs consistent with cell stress (C-D) and cell death (E-F). Similarly, cells appeared progressively sparely spaced between the control and 200 µg/ml of the AuNP's (G-L), while appearing more notably fewer in number, with signs consistent with cell stress, between 100 µg/ml and 200 µg/ml.

Following 48 hours of exposure to increasing concentrations of naringenin (A-F) and Ng-AuNP's pH 7 (G-L) over 48 hours, cell morphology was observed and recorded (Figure 3.61). Cells appeared progressively fewer between the control and 200 µg/ml of naringenin (A-E), exhibiting sings consistent with cell stress (C-E) and death (F). Similarly, cells appeared progressively sparely spaced between control and 200 µg/ml of the AuNP's, with morphology comparable to control up until 100 µg/ml (K). At the highest concentration (L) cells exhibited signs indicative of cell stress.

Post 72-hour exposure to naringenin (A-F) and Ng-AuNP's pH 7 (G-L), cell morphology was observed and recorded (Figure 3.62). Cells appeared progressively fewer between the control and 200 µg/ml of naringenin (A-F), exhibiting signs consistent with cell stress (D-E) and cell death (F) at the higher concentrations. Similarly, cells appeared progressively sparely spaced between control and 200 µg/ml of the AuNP's, however, without any distinct morphological changes up until 100 µg/ml (K). At the highest concentration (L) cells appeared rounded, and exhibited signs indicative of cell death.

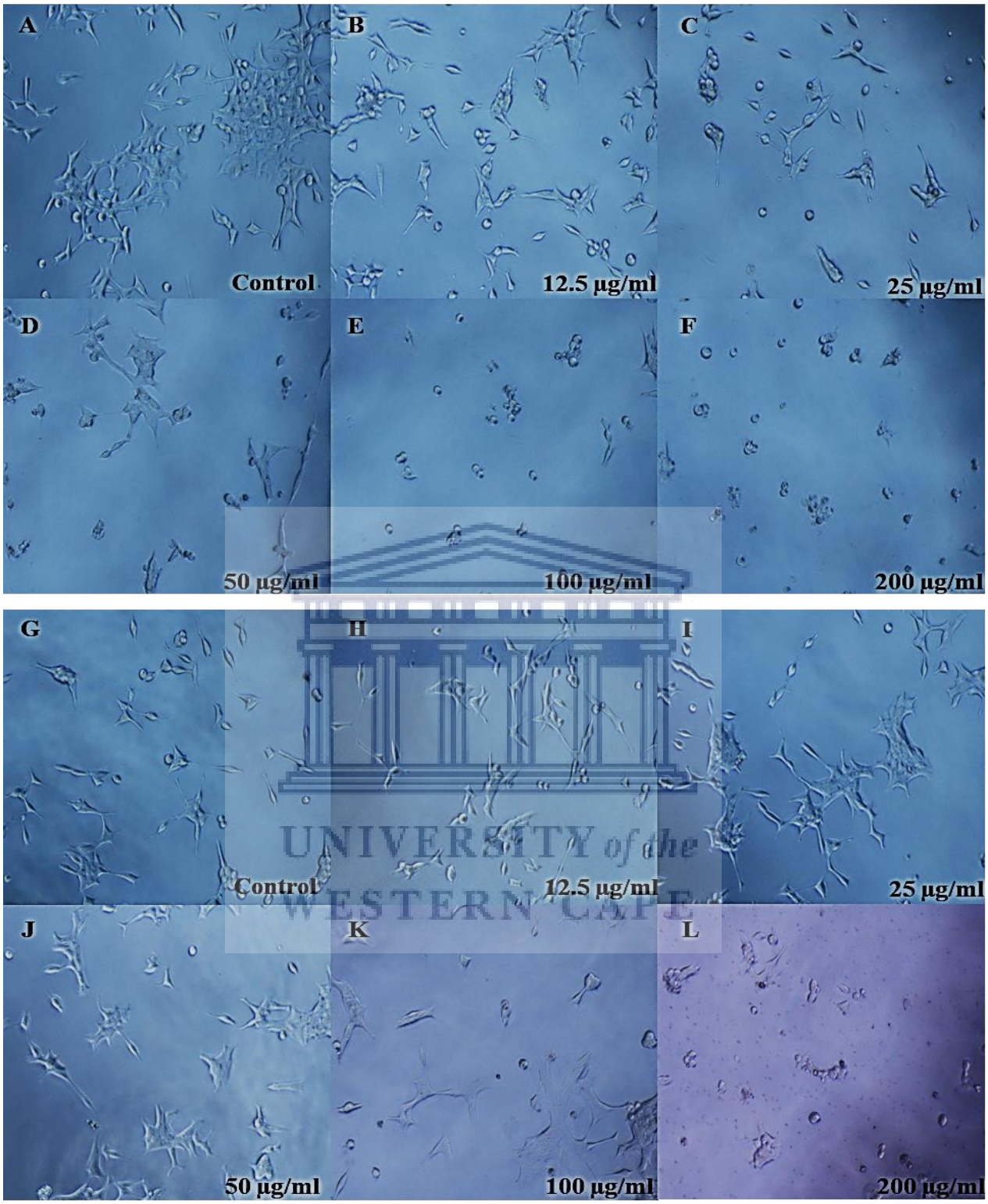

Figure 3.60: LNCaP Cell morphology after being exposed to increasing concentrations of naringenin and Ng-AuNP's pH 7 over a 24-hour period. Naringenin (A-F) yielded progressive cell rounding and signs of stress and death at higher concentrations, while the AuNP's exhibited notable decreases in cell number at higher concentrations (I-L), along with cell stress (L).

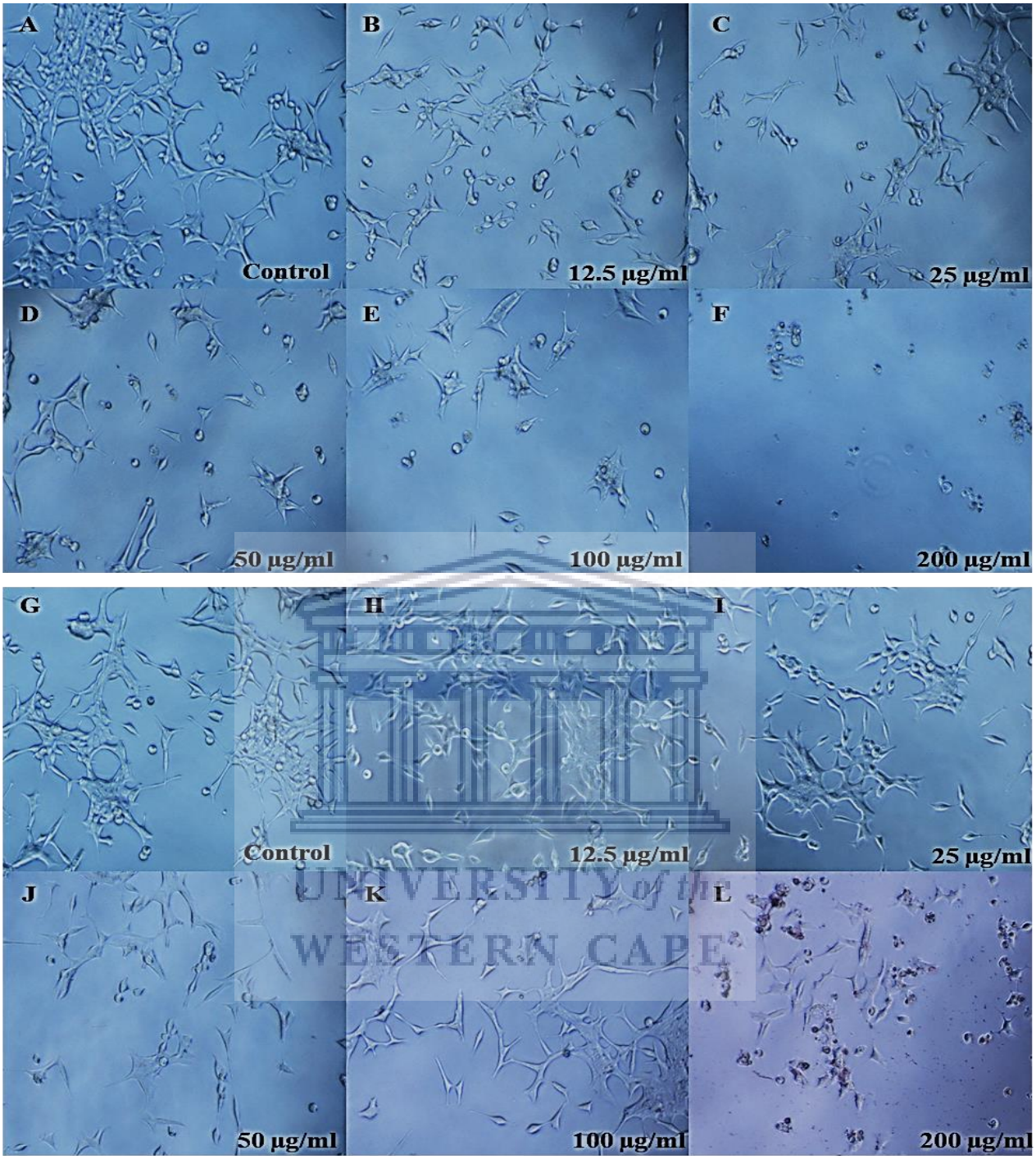

Figure 3.61: LNCaP cell morphology after being exposed to increasing concentrations of naringenin and Ng-AuNP's pH 7 over a 48-hour period. Naringenin (A-F) yielded progressively fewer cells at each concentration, along with signs of stress and cell death at the higher concentrations. The AuNP's (G-L) exhibited progressive decreases in the observed cell number between the control and 200 µg/ml, with signs consistent with cell stress at the highest concentration (L).

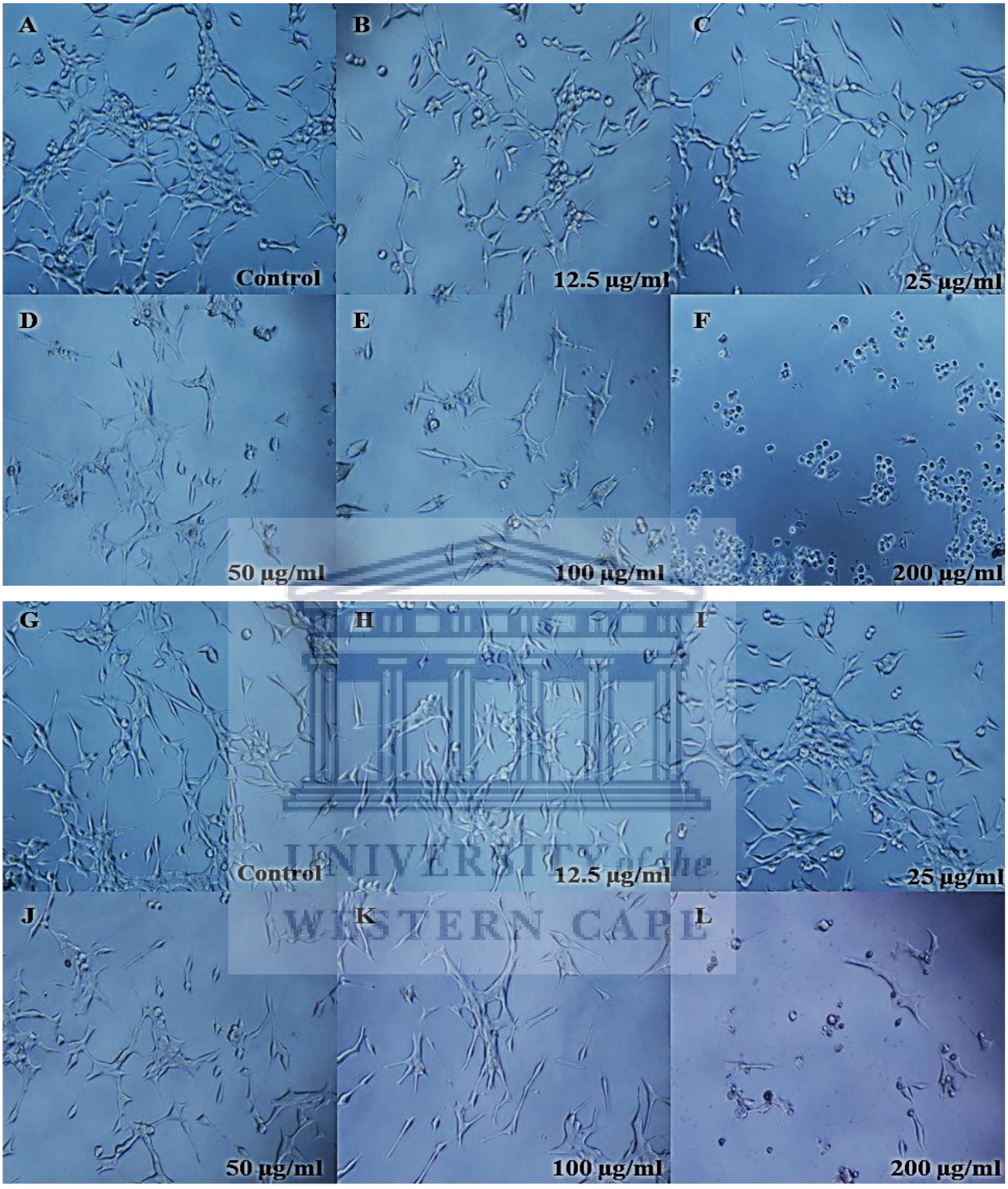

Figure 3.62: LNCaP cell morphology after being exposed to increasing concentrations of naringenin and Ng-AuNP's pH 7 over a 72-hour period. Cells were observably fewer between control and 200 µg/ml of the extract, displaying signs consistent with cell stress (D-E) and death (F) at higher concentrations. AuNP's exhibit slight reduction in overall observed cell number, with the presence of cell stress at the highest concentration (L).

The MTT assay revealed dose-dependent effects at 24, 48 and 72-hour exposure periods, respectively. After 24-hours (Figure 3.63 A), naringenin yielded an increase in cell viability from control-25 µg/ml, followed by decreases between 25-200 µg/ml. Similarly, the AuNP's yielded an increase in viability between control-12.5 µg/ml, followed by decrease between 12.5-200 µg/ml. Naringenin and the AuNP's differed significantly ($P=0.0103$, $P=0.0109$, $P=0.0289$) at 25 µg/ml and 50 µg/ml and 200 µg/ml, respectively. For naringenin, the repeated measures ANOVA revealed a significant ($P=0.0189$) positive trend from control-25 µg/ml, and a significant ($P<0.0001$) negative trend from 25-200 µg/ml. The AuNP's yielded an insignificant positive trend from control-12.5 µg/ml, and a significant ($P=0.0006$) negative trend from 12.5-200 µg/ml. One-way ANOVA yielded significant ($P<0.001$ and $P=0.013$) trends from control-200 µg/ml, for naringenin and the AuNP's, respectively.

Following 48-hours of exposure (Figure 3.63 B), both naringenin and the AuNP's yielded decreases in viability between the control and 200 µg/ml, differing significantly ($P=0.0001$, $P=0.0089$) at 25 µg/ml and 50 µg/ml, respectively. The repeated measures ANOVA revealed a significant ($P=0.008$) negative trend from control-200 µg/ml when exposed to naringenin, while the AuNP's yielded a significant ($P=0.001$) negative trend from control-200 µg/ml. One-way ANOVA revealed significant ($P<0.001$) trends from control-200 µg/ml, for both naringenin and AuNP's, respectively.

After 72-hours (Figure 3.63 C) both naringenin and the AuNP's yielded consistent decreases in cell viability between the control and 200 µg/ml. Naringenin differed from the AuNP's in its effect toward cell viability significantly ($P=0.0004$) at 200 µg/ml. The repeated measures ANOVA revealed a significant ($P<0.0001$) negative trend from control-200 µg/ml when cells were treated with naringenin, along with the AuNP's yielding a significant ($P=0.0001$) trend from control-200 µg/ml. One-way ANOVA revealed a significant ($P<0.001$) trends between the control and 200 µg/ml, for both naringenin and the AuNP's, respectively.

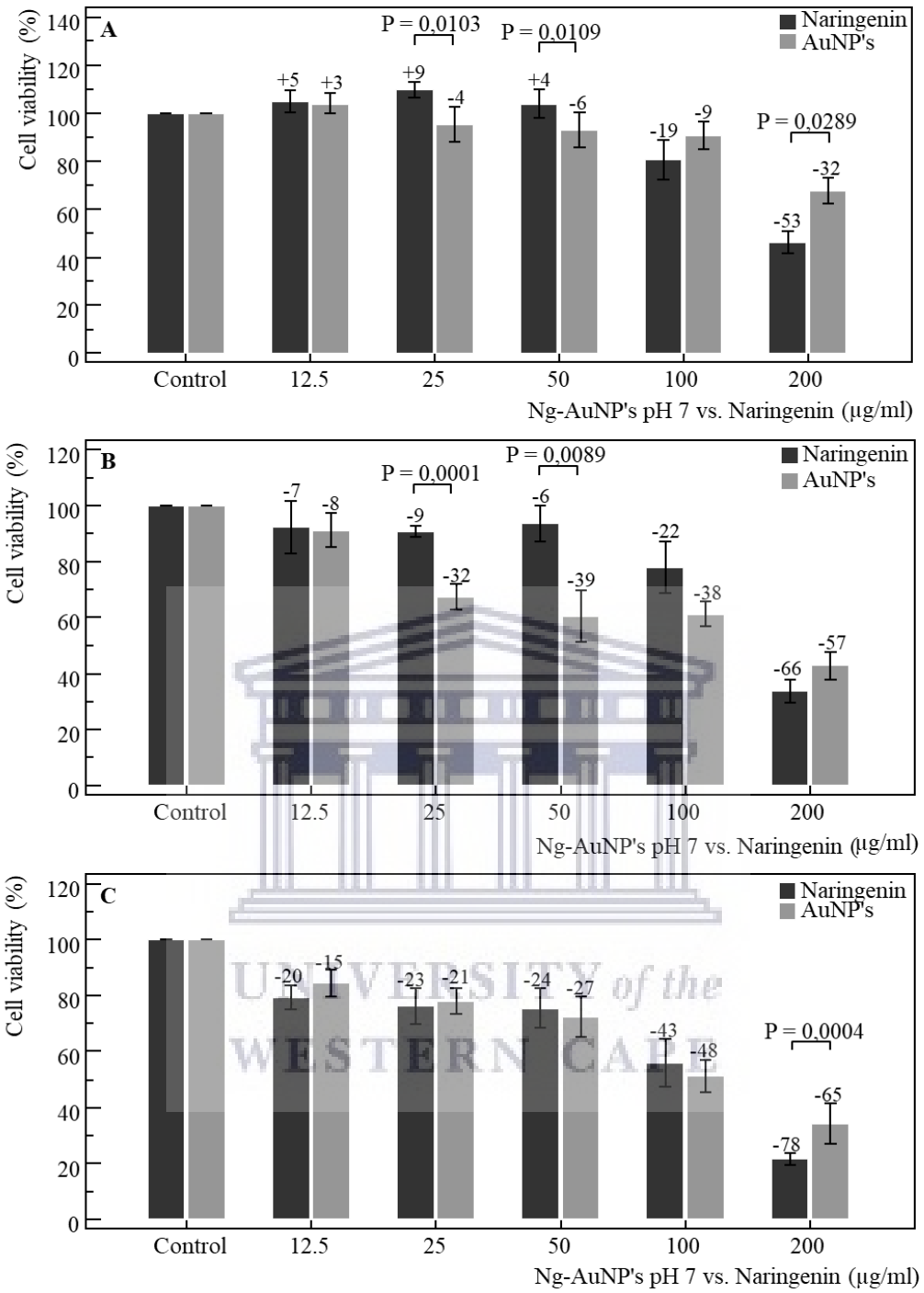

Figure 3.63: LNCaP cell viability as determined by the MTT assay over 24 (A), 48 (B) and 72 (C) hour exposure periods to naringenin and the Ng-AuNP's pH 7, respectively. Significant (P=0.0103, P=0.0109, P=0.0289) differences were observed between the extract and AuNP's at 25 µg/ml, and 50 µg/ml and 200 µg/ml, respectively, over 24 hours, along with a significant (P=0.0001, P=0.0089) difference observed at 25 µg/ml and 50 µg/ml after 48 hours, and finally a significant (P=0.0004) difference at 200 µg/ml, respectively, after 72 hours of exposure

3.2.2.6 Ng-AuNP's pH 8 and naringenin

After being exposed to increasing concentrations of naringenin (A-F) and Ng-AuNP's pH 8 (G-L) over 24 hours, cell morphology was observed and recorded (Figure 3.64). Between the control and 200 µg/ml (A-F), cells appeared progressively sparely spaced and rounded, displayed signs consistent with cell stress (C-D) and cell death (E-F). Similarly, cells appeared progressively sparely spaced between the control and 200 µg/ml of the AuNP's (G-L), while appearing more notably fewer in number, with cell rounding and signs consistent with cell stress between 50 µg/ml and 100 µg/ml (J-K), along with cell death at 200 µg/ml (L).

Following 48 hours of exposure to increasing concentrations of naringenin (A-F) and Ng-AuNP's pH 8 (G-L) over 48 hours, cell morphology was observed and recorded (Figure 3.65). Cells appeared progressively fewer between the control and 200 µg/ml of naringenin (A-E), exhibiting sings consistent with cell stress (C-E) and death (F). Similarly, cells appeared progressively sparely spaced between control and 200 µg/ml of the AuNP's, with morphology comparable to control up until 50 µg/ml (K). At higher concentrations (K-L) cells exhibited signs indicative of cell stress (K), along with signs consistent with cell death (L).

Post 72-hour exposure to naringenin (A-F) and Ng-AuNP's pH 8 (G-L), cell morphology was observed and recorded (Figure 3.66). Cells appeared progressively fewer between the control and 200 µg/ml of naringenin (A-F), exhibiting signs consistent with cell stress (D-E) and cell death (F) at the higher concentrations. Similarly, cells appeared progressively sparely spaced between control and 200 µg/ml of the AuNP's, however, without any distinct morphological changes up until 50 µg/ml (K). At higher concentrations (K-L) cells appeared rounded and stressed (K) and exhibited signs indicative of cell death (L).

Figure 3.64: LNCaP Cell morphology after being exposed to increasing concentrations of naringenin and Ng-AuNP's pH 8 over a 24-hour period. Naringenin (A-F) yielded progressive cell rounding and signs of stress and death at higher concentrations, while the AuNP's exhibited progressive decreases in observed cells (I-L), along with cell stress (K) and cell death (L).

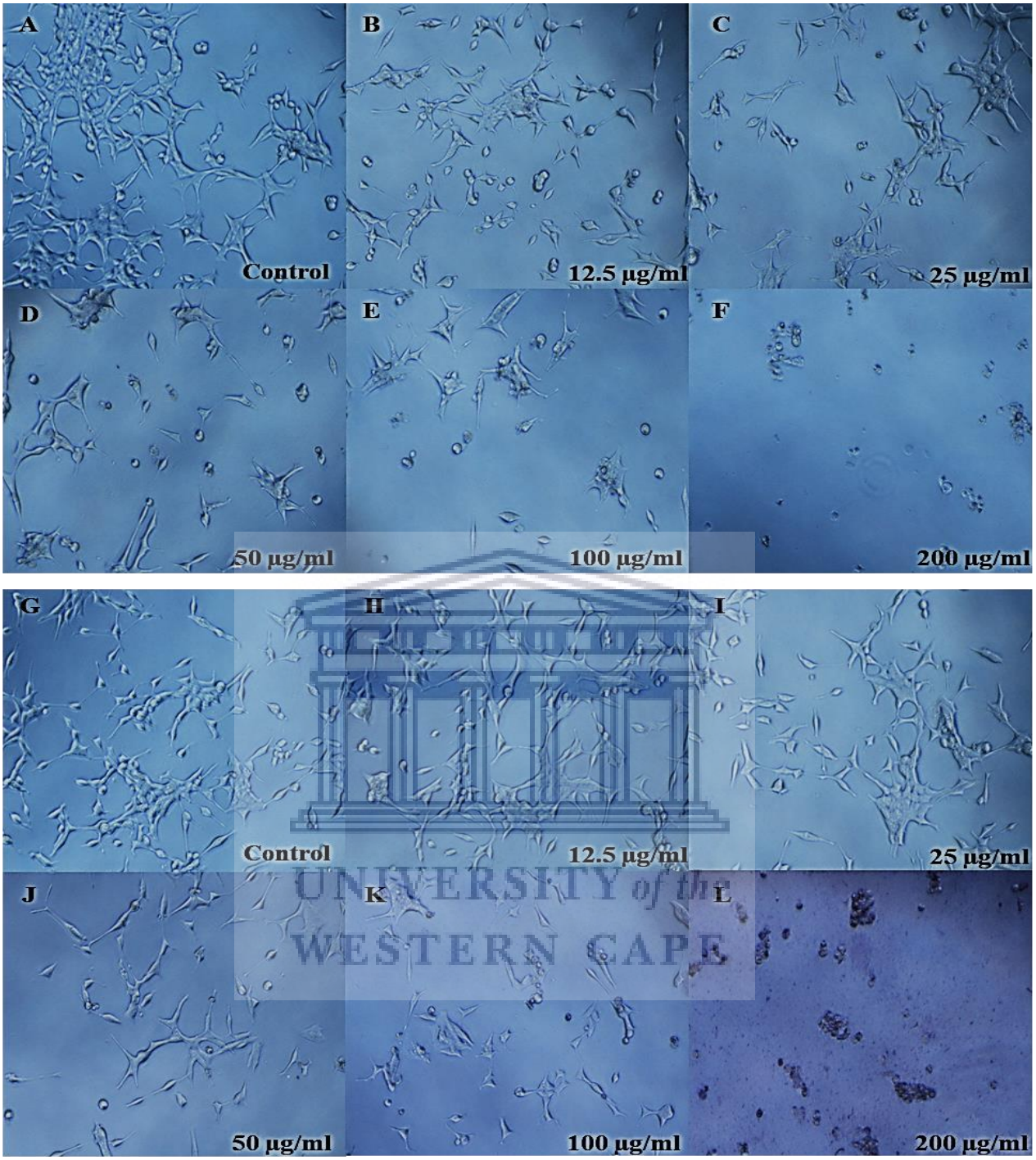

Figure 3.65: LNCaP cell morphology after being exposed to increasing concentrations of naringenin and Ng-AuNP's pH 8 over a 48-hour period. Naringenin (A-F) yielded progressively fewer cells at each concentration, along with signs of stress and cell death at the higher concentrations. The AuNP's (G-L) exhibited progressive decreases in the observed cell number between the control and 200 µg/ml, with signs of cell stress (K), and cell death (L) at higher concentrations.

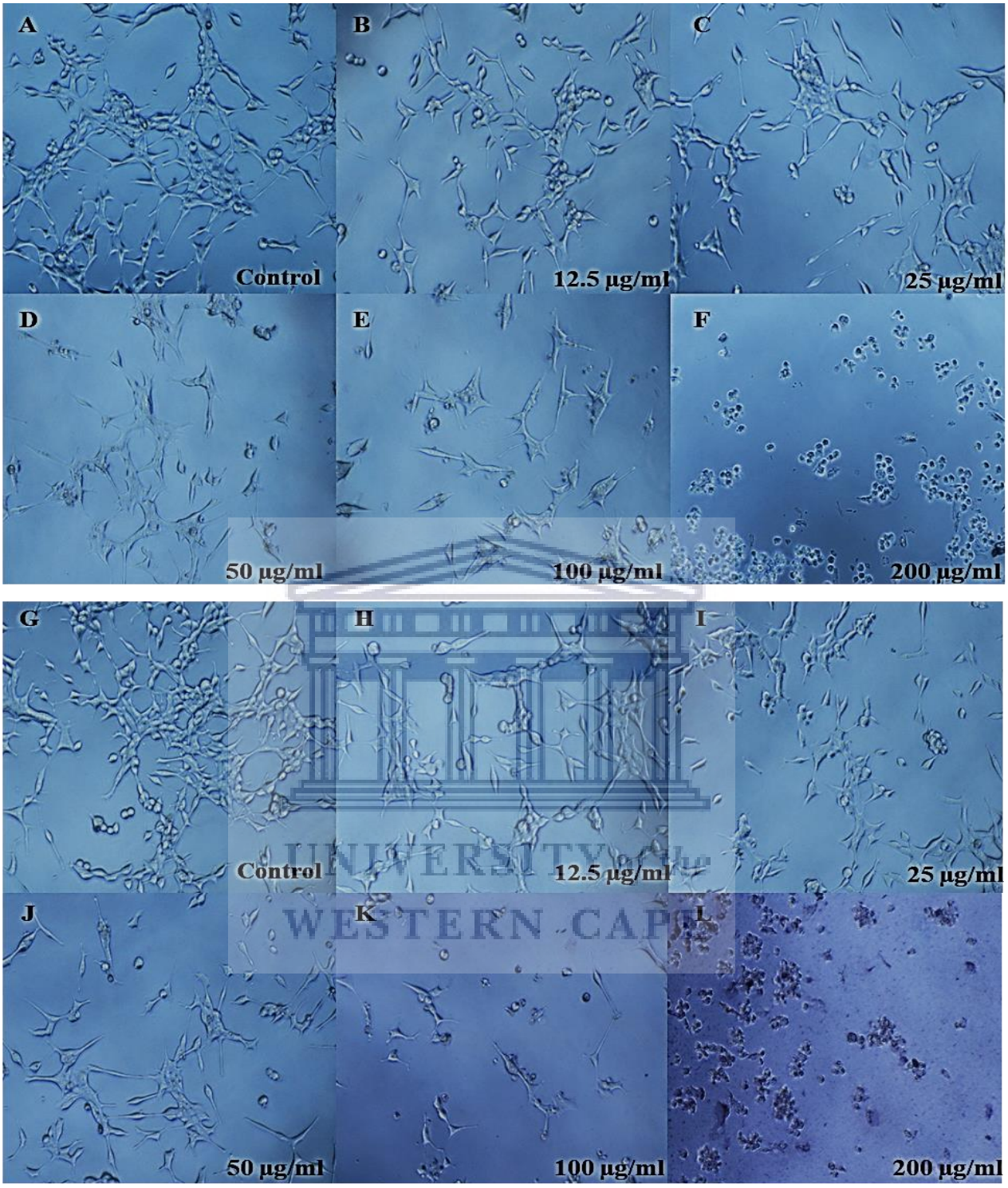

Figure 3.66: LNCaP cell morphology after being exposed to increasing concentrations of naringenin and Ng-AuNP's pH 8 over a 72-hour period. Cells were observably fewer between control and 200 µg/ml of the extract, displaying signs consistent with cell stress (D-E) and death (F) at higher concentrations. AuNP's exhibit slight reduction in overall observed cell number, with the presence of cell stress (K) and death (L) at higher concentrations.

The MTT assay revealed dose-dependent effects at 24, 48 and 72-hour exposure periods, respectively. After 24-hours (Figure 3.67 A), naringenin yielded an increase in cell viability from control-25 µg/ml, followed by decreases between 25-200 µg/ml. Similarly, the AuNP's yielded a slight increase in viability between control-12.5 µg/ml, followed by steady decreases between 12.5-200 µg/ml. Naringenin and the AuNP's differed significantly (P=0.0001, P=0.0003) at 25 µg/ml and 50 µg/ml, respectively. For naringenin, the repeated measures ANOVA revealed a significant (P=0.0189) positive trend from control-25 µg/ml, and a significant (P<0.0001) negative trend from 25-200 µg/ml. The AuNP's yielded an insignificant positive trend from control-12.5 µg/ml, followed by a significant (P<0.0001) negative trend from 12.5-200 µg/ml. One-way ANOVA yielded significant (P<0.001) trends from control-200 µg/ml, for both the extract and AuNP's, respectively.

Following 48-hours of exposure (Figure 3.67 B), both naringenin and the AuNP's yielded steady decreases in cell viability between the control and 200 µg/ml, differing significantly (P<0.0001, P=0.0001) at 25 µg/ml and 50 µg/ml, respectively. The repeated measures ANOVA revealed a significant (P=0.008) negative trend from control-200 µg/ml when exposed to naringenin, and the AuNP's yielded a significant (P<0.0001) negative trend from control-200 µg/ml. One-way ANOVA revealed significant (P<0.001) trends from control-200 µg/ml, for both naringenin and AuNP's, respectively.

After 72-hours (Figure 3.67 C) both naringenin and the AuNP's yielded steady, consistent decreases in cell viability between the control and 200 µg/ml. Naringenin and the AuNP's remained fairly comparable in their effects, only differing significantly (P=0.0245) at 12.5 µg/ml. The repeated measures ANOVA revealed significant (P<0.0001) negative trends from control-200 µg/ml when cells were treated with naringenin and the AuNP's, respectively. One-way ANOVA revealed a significant (P<0.001) trends between the control and 200 µg/ml, for both naringenin and the AuNP's.

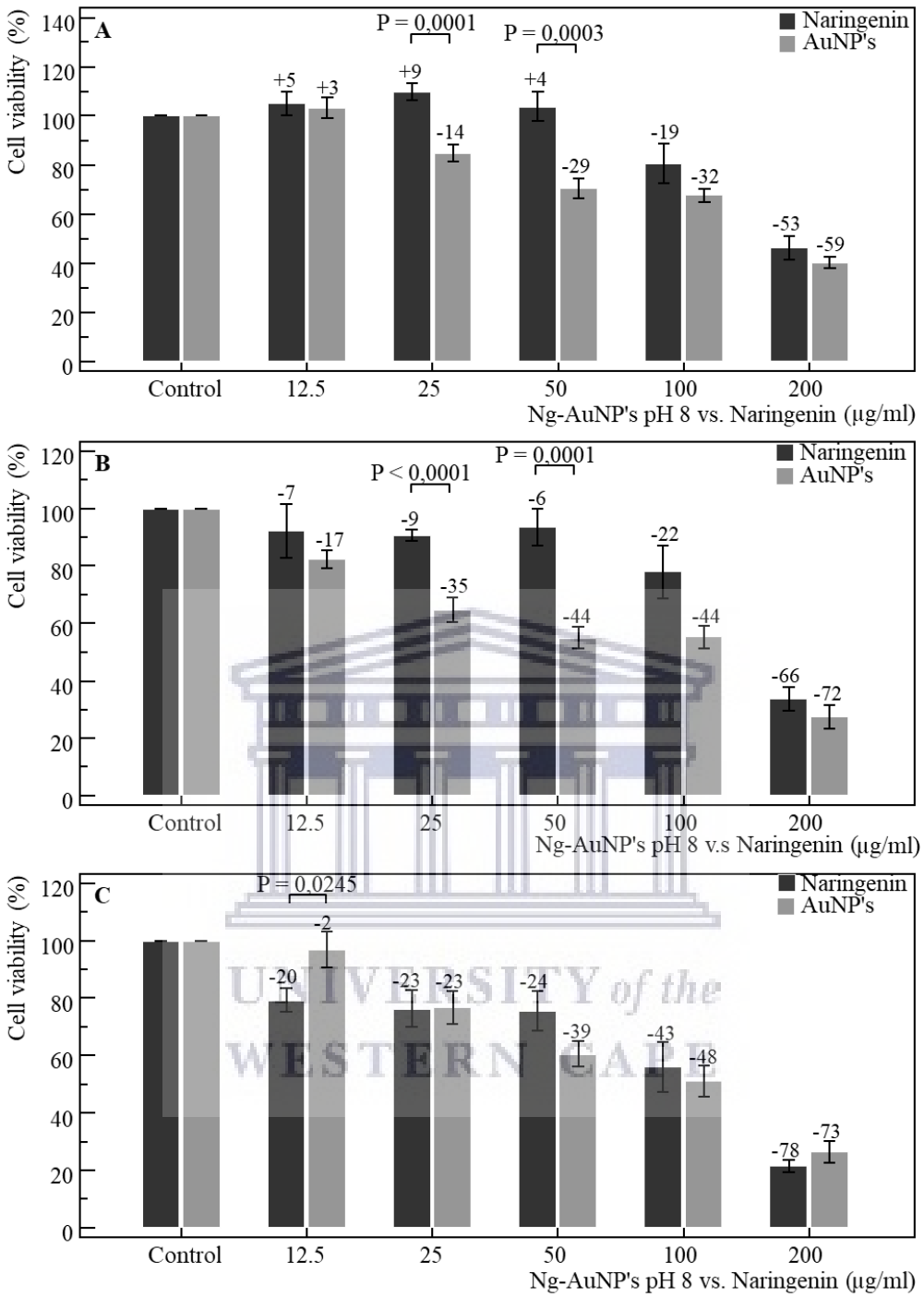

Figure 3.67: LNCaP cell viability as determined by the MTT assay over 24 (A), 48 (B) and 72 (C) hour exposure periods to naringenin and the Ng-AuNP's pH 8, respectively. Significant (P=0.0001, P=0.0003) differences were observed between the extract and AuNP's at 25 µg/ml, and 50 µg/ml and 200 µg/ml, respectively, over 24 hours, along with significant (P<0.0001, P=0.0001) differences observed at 25 µg/ml and 50 µg/ml after 48 hours, and finally a significant (P=0.0245) difference at 12.5 µg/ml, respectively, after 72 hours of exposure**.**

3.2.3 Panc1 cell viability

3.2.3.1 S1-AuNP's and Extracts

After being exposed to increasing concentrations of the S1 extract (A-F) and S1-AuNP's (G-L) over 24 hours, cell morphology was observed and recorded (Figure 3.68). When cells were treated with the extract, no change in cell number or typical morphology was observed between the control and 200 µg/ml (A-F). Conversely, cells appeared progressively sparely spaced between the control and 200 µg/ml of the AuNP's (G-L), appearing notably fewer, rounded and displaying signs indicative of cell stress between 100 µg/ml and 200 µg/ml (K-L).

Following 48 hours of exposure to increasing concentrations of the S1 extract (A-F) and S1-AuNP's (G-L) over 48 hours, cell morphology was observed and recorded (Figure 3.69). The extract yielded no observable change in cell number or typical morphology between the control and 200 µg/ml (A-F). Conversely, cells appeared increasingly sparely spaced and rounded between control and 200 µg/ml of the AuNP's (G-L), exhibiting signs consistent with cell stress between 50 µg/ml and 100 µg/ml (J-K) and cell death (L) at highest concentration.

Post 72-hour exposure to S1 extract (A-F) and S1-AuNP's (G-L), cell morphology was observed and recorded (Figure 3.70). The extract yielded no observable change in observable cell number or typical morphology between the control and 100 µg/ml (A-E), while exhibiting slight signs of cell stress at 200 µg/ml (F). Conversely, cells appeared progressively sparely spaced between control and 200 µg/ml of the AuNP's, along with notable increases in cell rounding and stress between 25 µg/ml and 100 µg/ml (I-K), and cell death at 200 µg/ml (L)

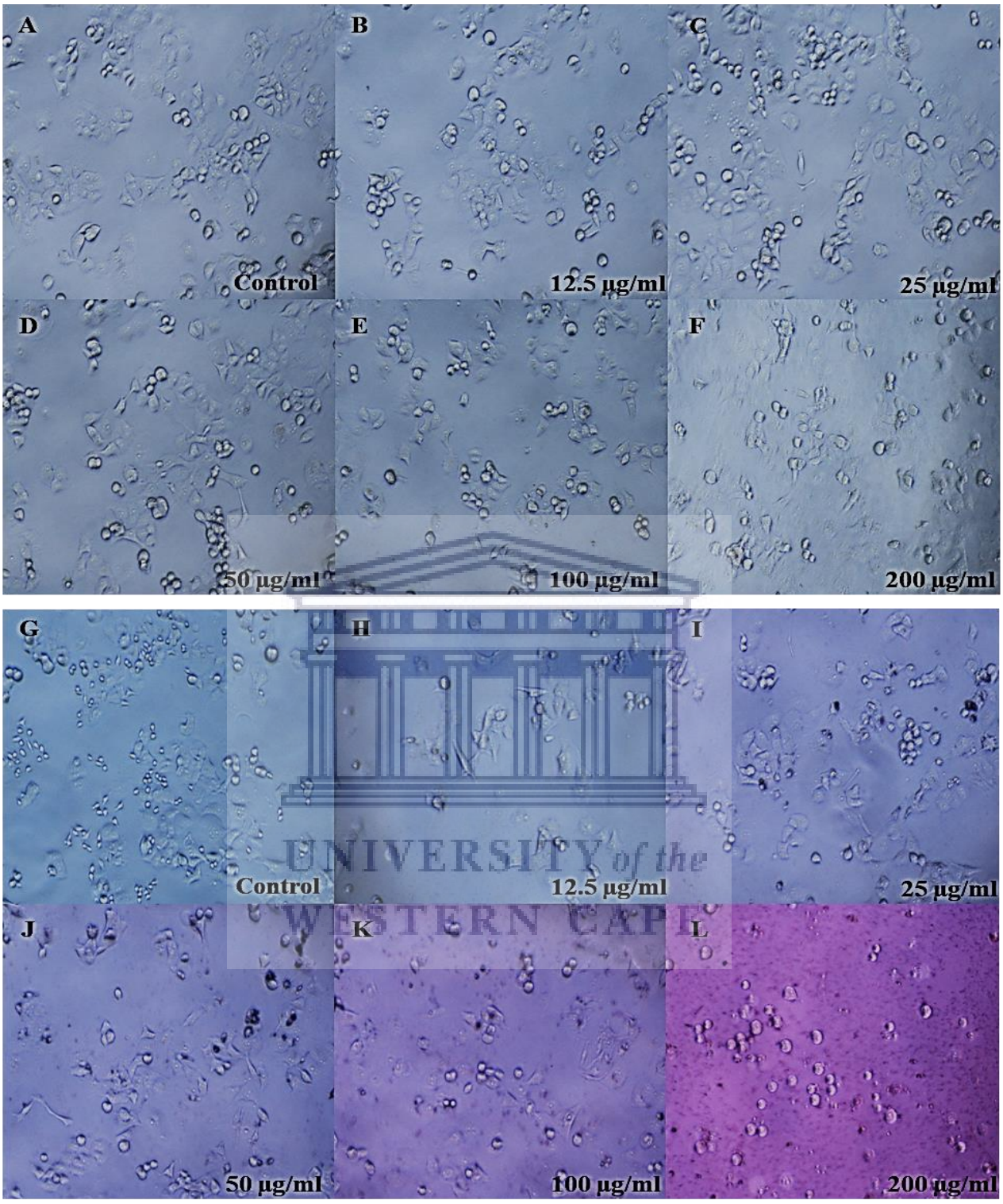

Figure 3.68: Panc1 Cell morphology after being exposed to increasing concentrations of S1 extract and S1-AuNP's over a 24-hour period. The extract (A-F) yielded no discernible change to cell morphology, while AuNP's exhibited decreases in cell number at low concentrations (G-H), notable decreases at higher concentrations (I-L), along with cell rounding and stress (K-L).

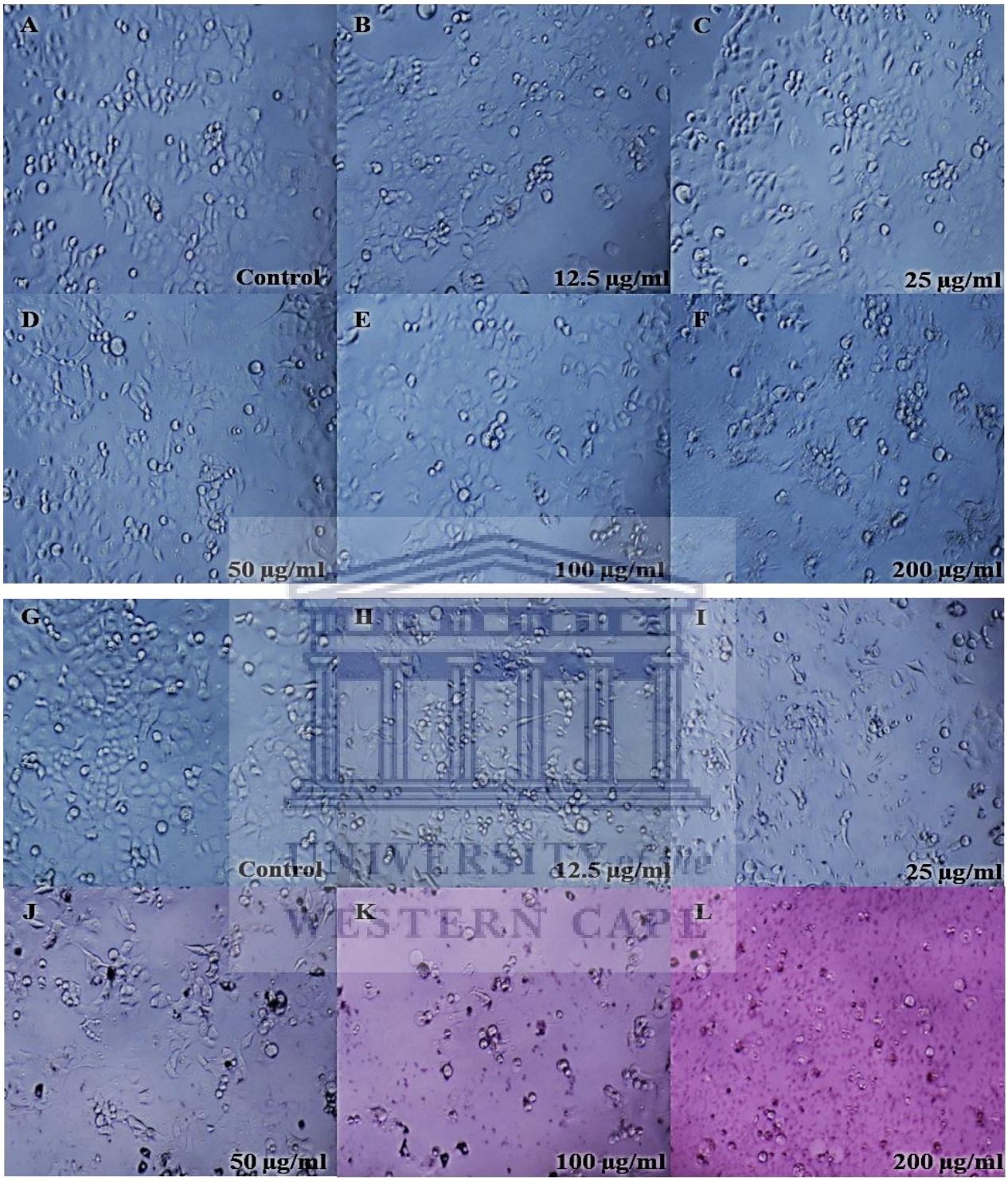

Figure 3.69: Panc1 cell morphology after being exposed to increasing concentrations of S1 extract and S1-AuNP's over a 48-hour period. The extract (A-F) exhibited no observable growth or morphological changes between control and the highest concentration, while the AuNP's exhibited progressive decreases in the overall observed cell number (G-L), along with signs of rounding and stress (J-K), and signs of death (L) at the highest concentration.

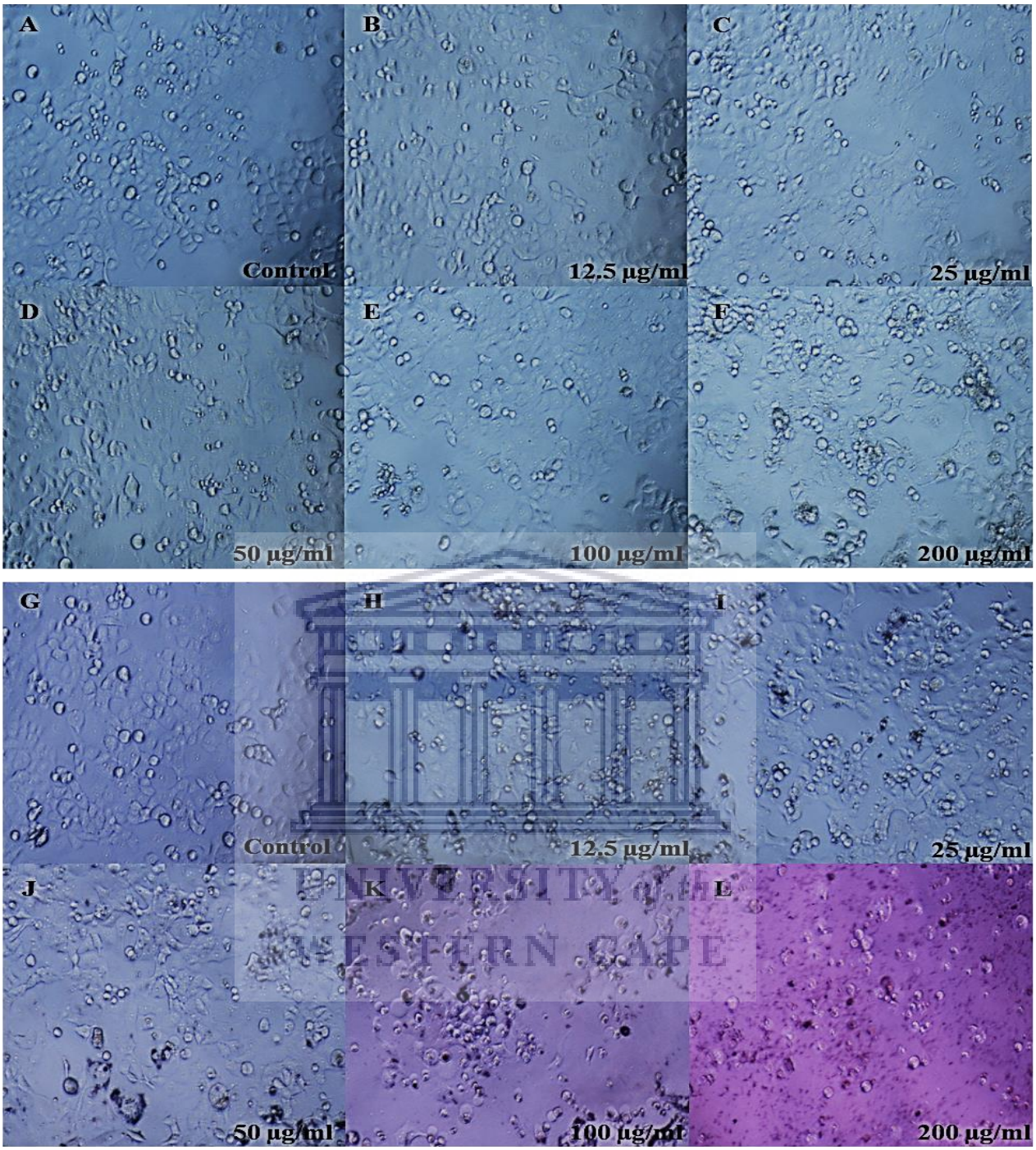

Figure 3.70: Panc1 cell morphology after being exposed to increasing concentrations of S1 extract and S1-AuNP's over a 72-hour period. The extract (A-F) exhibited no observable growth or morphological changes at lower concentrations (A-E), with slight cell stress at the highest concentration (F). The AuNP's exhibited progressive decreases in the overall observed cell number (G-L), along with signs of rounding and stress (I-K), and signs of death (L) at the highest concentration.

The MTT assay revealed dose-dependent effects at 24, 48 and 72-hour exposure periods, respectively. Following 24-hours of treatment (Figure 3.71 A) with the extract, cell viability was comparable to the control at each concentration, displaying only marginal increases at 25-100 µg/ml, along with slight decreases at 12 µg/ml and 200 µg/ml. Conversely, the AuNP's exhibited progressive reductions in cell viability between the control and 200 µg/ml, differing significantly (P=0.0104, P=0.0001 and P<0.0001) from the extract at 12.5 µg/ml, 25 µg/ml and 50-200 µg/ml, respectively. For the extract, the repeated measures ANOVA revealed an insignificant positive trend from control-200 µg/ml, along with the AuNP's yielding a significant (P<0.0001) negative trend from control-200 µg/ml. One-way ANOVA yielded a significant (P<0.001) trend from control-200 µg/ml following treatment with the AuNP's.

Following 48-hours of exposure (Figure 3.71 B), the extract yielded marginal increases in cell viability from control-200 µg/ml, followed by a slight reduction in cell viability at 200 µg/ml. Conversely, the AuNP's yielded steady decreases in cell viability from control-200 µg/ml, differing significantly (P=0.0001 and P<0.0001) from the extract at 12.5 µg/ml and 25-200 µg/ml, respectively. The repeated measures ANOVA revealed a significant (P<0.0001) negative trend from control-200 µg/ml when exposed to the AuNP's, in addition to one-way ANOVA revealing a significant (P<0.001) trend from control-200 µg/ml for both the AuNP's,

After 72-hours (Figure 3.71 C) the extract yielded very marginal increases in cell viability at 12.5 µg/ml and 50-200 µg/ml, along with a slight reduction in cell viability at 25 µg/ml. The AuNP's yielded progressive, dose-dependent decreases in cell viability from control-200 µg/ml, differing significantly (P=0.023, P=0.0066, P=0.0032, P<0.0001) from the extract at 25-200 µg/ml, respectively. The repeated measures ANOVA revealed an insignificant positive trend from control-200 µg/ml when cells were treated with the extract, while AuNP's yielded a significant (P<0.0001) negative trend from control-200 µg/ml. Additionally, one-way ANOVA revealed a significant (P<0.001) trend from control-200 µg/ml for the AuNP's

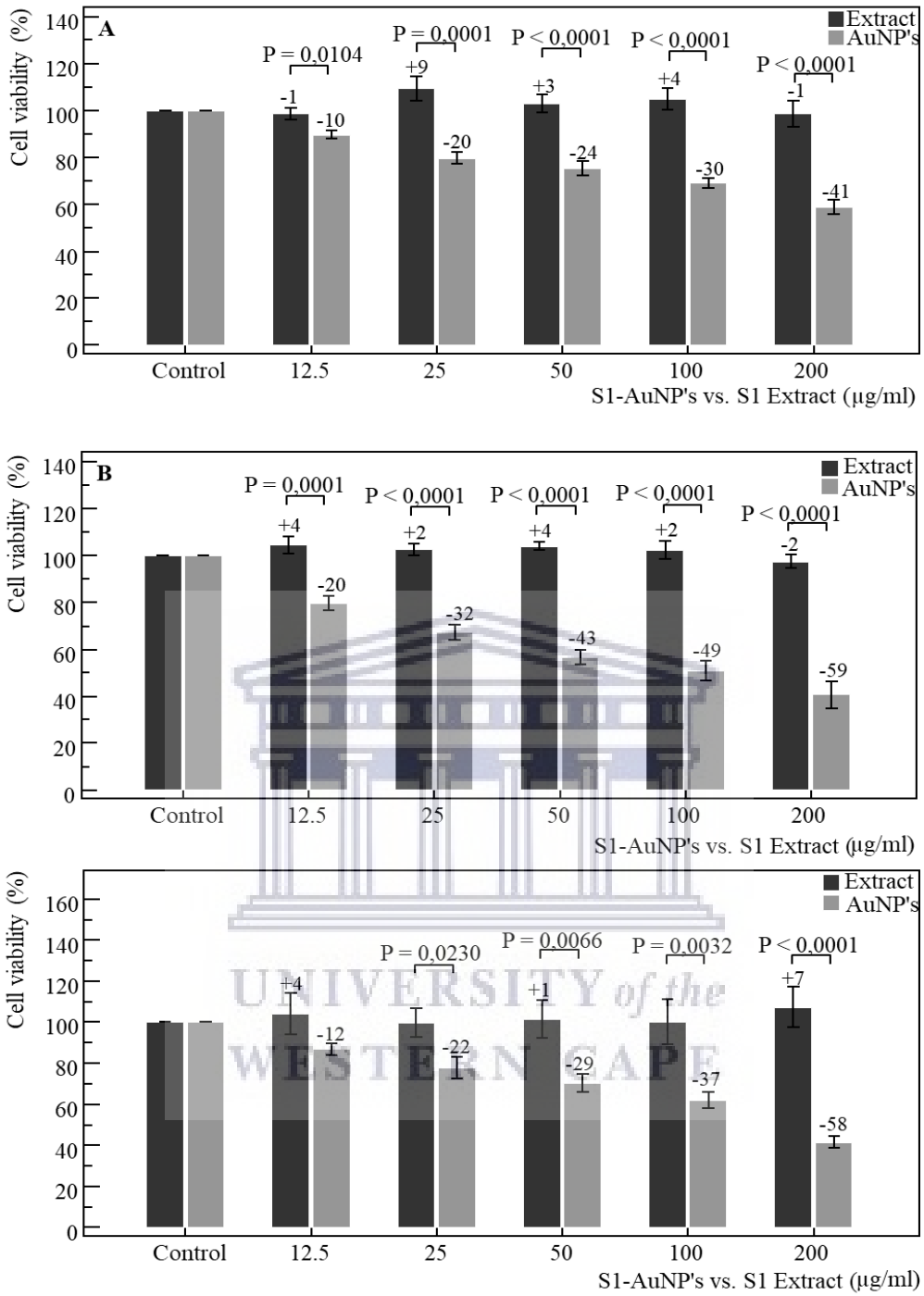

Figure 3.71: Panc1 cell viability as determined by the MTT assay over 24 (A), 48 (B) and 72 (C) hour exposure to the S1 extract and S1-AuNP's respectively. Significant (P=0.0104, P=0.0001 and P<0.0001) differences were observed between the extract and AuNP's at 12.5 µg/ml, 25 µg/ml and 50-200 µg/ml over 24 hours, along with significant (P=0.0001 and P<0.0001) differences observed at 12.5 µg/ml and 25-200 µg/ml after 48 hours, and finally significant (P=0.023, P=0.0066, P=0.0032, P<0.0001) differences at 25-200 µg/ml after 72 hours of exposure.

3.2.3.2 S1x2-AuNP's and Extracts

After being exposed to increasing concentrations of the S1 extract (A-F) and S1x2-AuNP's (G-L) over 24 hours, cell morphology was observed and recorded (Figure 3.72). When cells were treated with the extract, no change in cell number or typical morphology was observed between the control and 200 µg/ml (A-F). Conversely, cells appeared slightly, but progressively sparely spaced between the control and 200 µg/ml of the AuNP's (G-L), exhibiting slight cell rounding and signs indicative of cell stress between 100 µg/ml and 200 µg/ml (K-L).

After being exposed to increasing concentrations of the S1 extract (A-F) and S1x2-AuNP's (G-L) over 48 hours, cell morphology was observed and recorded (Figure 3.73). The extract yielded no observable cell growth or morphological changes between control and 200 µg/ml (A-F). Conversely, cells appeared progressively sparely spaced between the control and 200 µg/ml of the AuNP's (G-L), exhibiting cell rounding and signs consistent with cell stress between 50 µg/ml and 200 µg/ml (J-L).

Post 72-hour exposure to S1 extract (A-F) and S1x2-AuNP's (G-L), cell morphology was observed and recorded (Figure 3.74). The extract yielded no observable change in observable cell number or typical morphology between the control and 100 µg/ml (A-E), while exhibiting slight signs of cell stress at 200 µg/ml (F). Conversely, cells appeared progressively more sparely spaced between control and 200 µg/ml of the AuNP's, displaying increasingly notable cell rounding and signs consistent with cell stress between 25 µg/ml and 200 µg/ml (I-L).

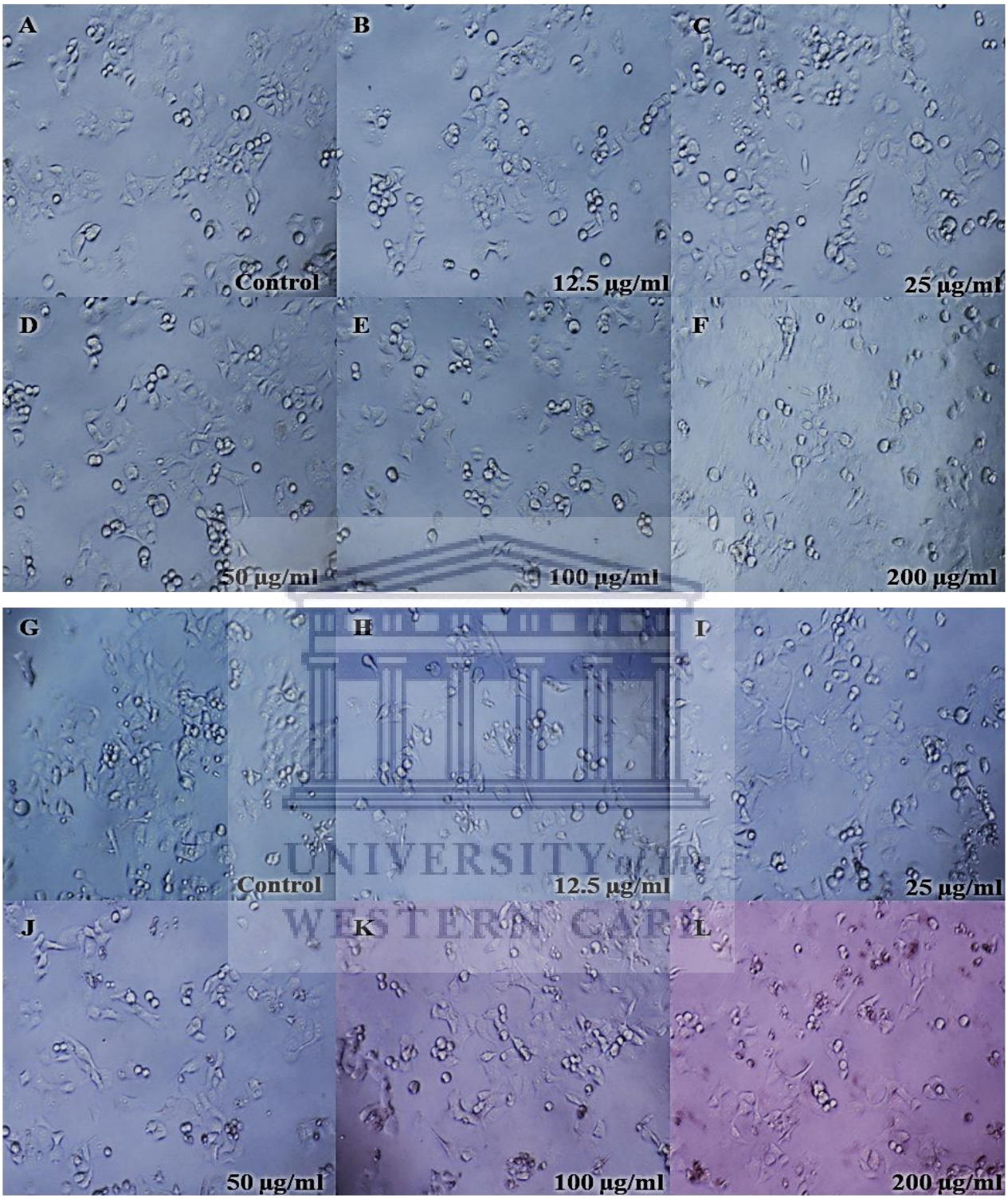

Figure 3.72: Panc1 Cell morphology after being exposed to increasing concentrations of S1 extract and S1x2-AuNP's over a 24-hour period. The extract (A-F) yielded no discernible change to cell morphology, while AuNP's exhibited slight decreases in cell number at low concentrations (G-H), along indications of cell rounding and stress at higher concentrations (K-L).

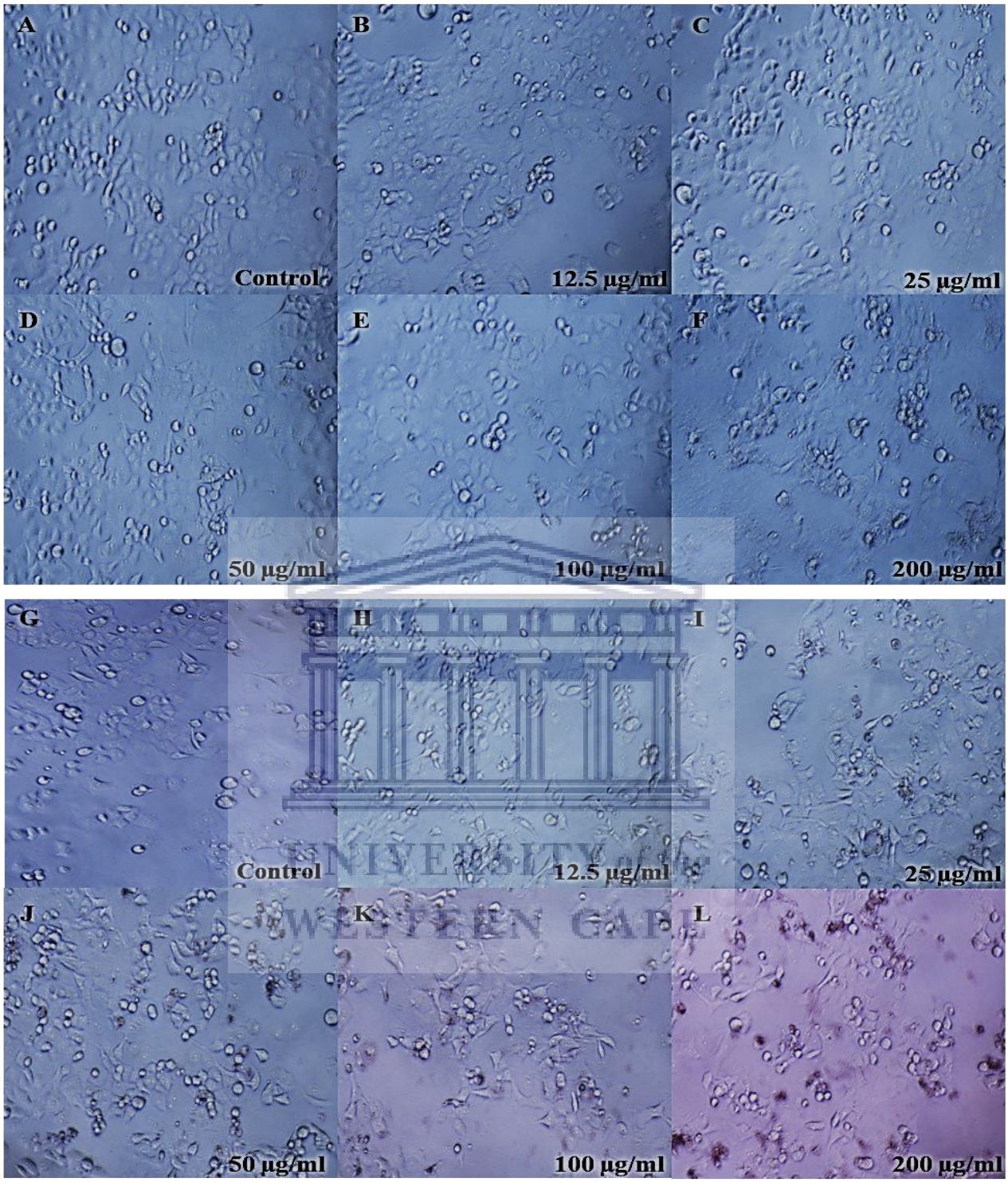

Figure 3.73: Panc1 cell morphology after being exposed to increasing concentrations of S1 extract and S1x2-AuNP's over a 48-hour period. The extract (A-F) exhibited no observable growth or morphological changes between control and the highest concentration, while the AuNP's exhibited progressive decreases in the overall observed cell number (G-L), along with signs indicative of cell rounding and cell stress at higher concentrations (J-L).

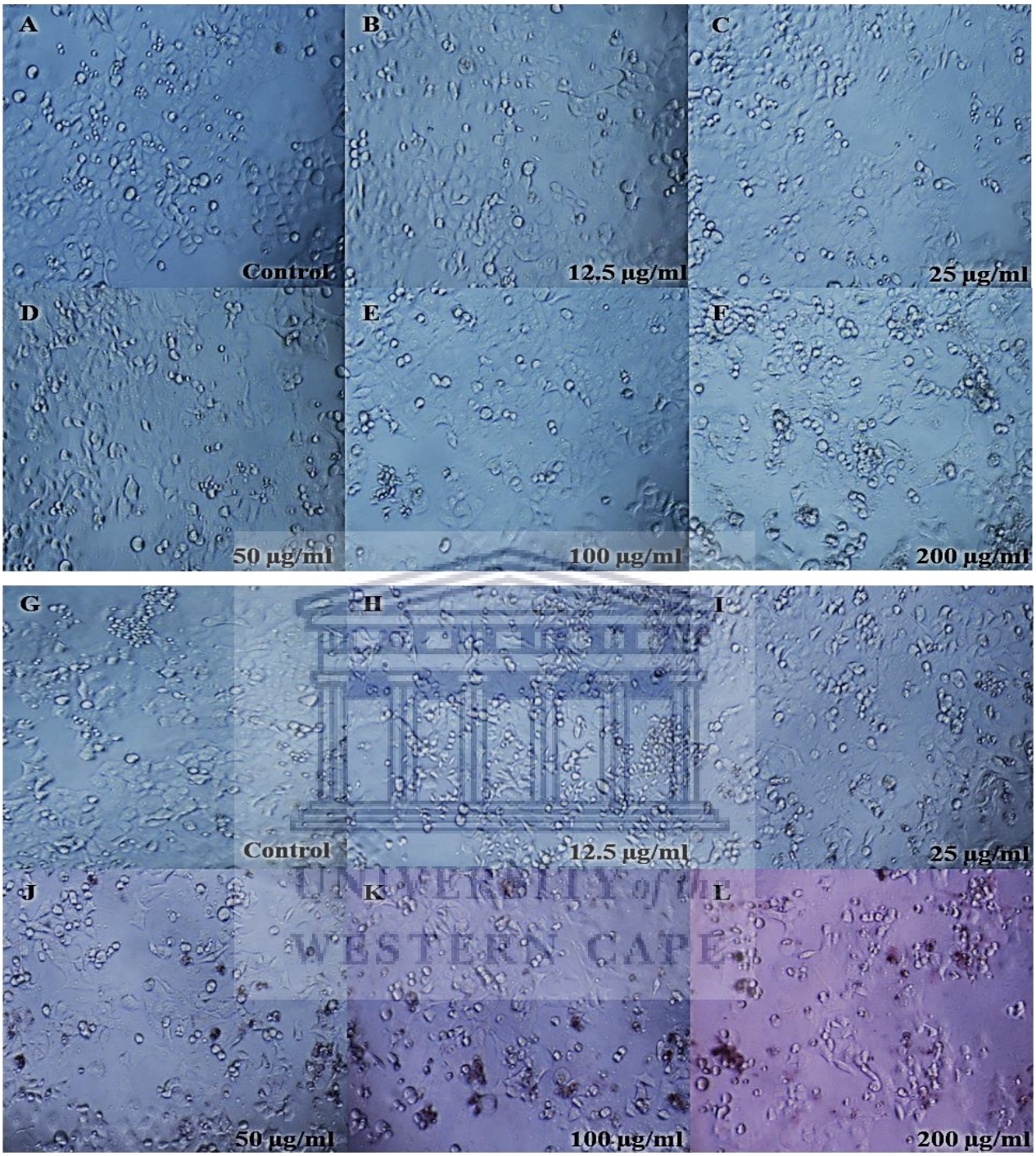

Figure 3.74: Panc1 cell morphology after being exposed to increasing concentrations of S1 extract and S1x2-AuNP's over a 72-hour period. The extract (A-F) exhibited no observable growth or morphological changes at lower concentrations (A-E), with slight cell stress at the highest concentration (F). The AuNP's exhibited progressive decreases in the overall observed cell number (G-L), along with increasing signs of rounding and stress at higher concentrations (I-L).

The MTT assay revealed dose-dependent effects at 24, 48 and 72-hour exposure periods, respectively. Following 24-hours of treatment (Figure 3.75 A) with the extract, cell viability was comparable to the control at each concentration, displaying only marginal increases at 25-100 µg/ml, along with slight decreases at 12 µg/ml and 200 µg/ml. Conversely, the AuNP's exhibited moderate, but progressive reductions in cell viability between the control and 200 µg/ml, differing significantly (P=0.003, P=0.0029, P=0.0005, P=0.0129) from the extract at 25 µg/ml, 50 µg/ml, 100 µg/ml and 200 µg/ml, respectively. For the extract, the repeated measures ANOVA revealed an insignificant positive trend from control-200 µg/ml, along with AuNP's yielding a significant (P=0.0071) negative trend from control-200 µg/ml. One-way ANOVA yielded a significant (P=0.008) trend from control-200 µg/ml following treatment with the AuNP's.

Following 48-hours of exposure (Figure 3.75 B), the extract yielded marginal increases in cell viability from control-200 µg/ml, followed by a slight reduction in cell viability at 200 µg/ml. Conversely, the AuNP's yielded steady, dose-dependent decreases in cell viability from control-200 µg/ml, differing significantly (P=0.0005 and P<0.0001) from the extract at 12.5 µg/ml and 25-200 µg/ml, respectively. The repeated measures ANOVA revealed a significant (P=0.0007) negative trend from control-200 µg/ml when exposed to the AuNP's, and one-way ANOVA revealing a significant (P<0.001) trend from control-200 µg/ml for both the AuNP's,

After 72-hours (Figure 3.75 C) the extract yielded very marginal increases in cell viability at 12.5 µg/ml and 50-200 µg/ml, along with a slight reduction in cell viability at 25 µg/ml. The AuNP's yielded progressive, dose-dependent decreases in cell viability from control-200 µg/ml, differing significantly (P=0.0423, P=0.0058, P=0.0078, P=0.0034) from the extract at 25 µg/ml, 50 µg/ml, 100 µg/ml and 200 µg/ml, respectively. For the extract, the repeated measures ANOVA revealed an insignificant positive trend from control-200 µg/ml, while AuNP's yielded a significant (P<0.0001) negative trend from control-200 µg/ml. One-way ANOVA revealed a significant (P<0.001) trend from control-200 µg/ml for the AuNP's

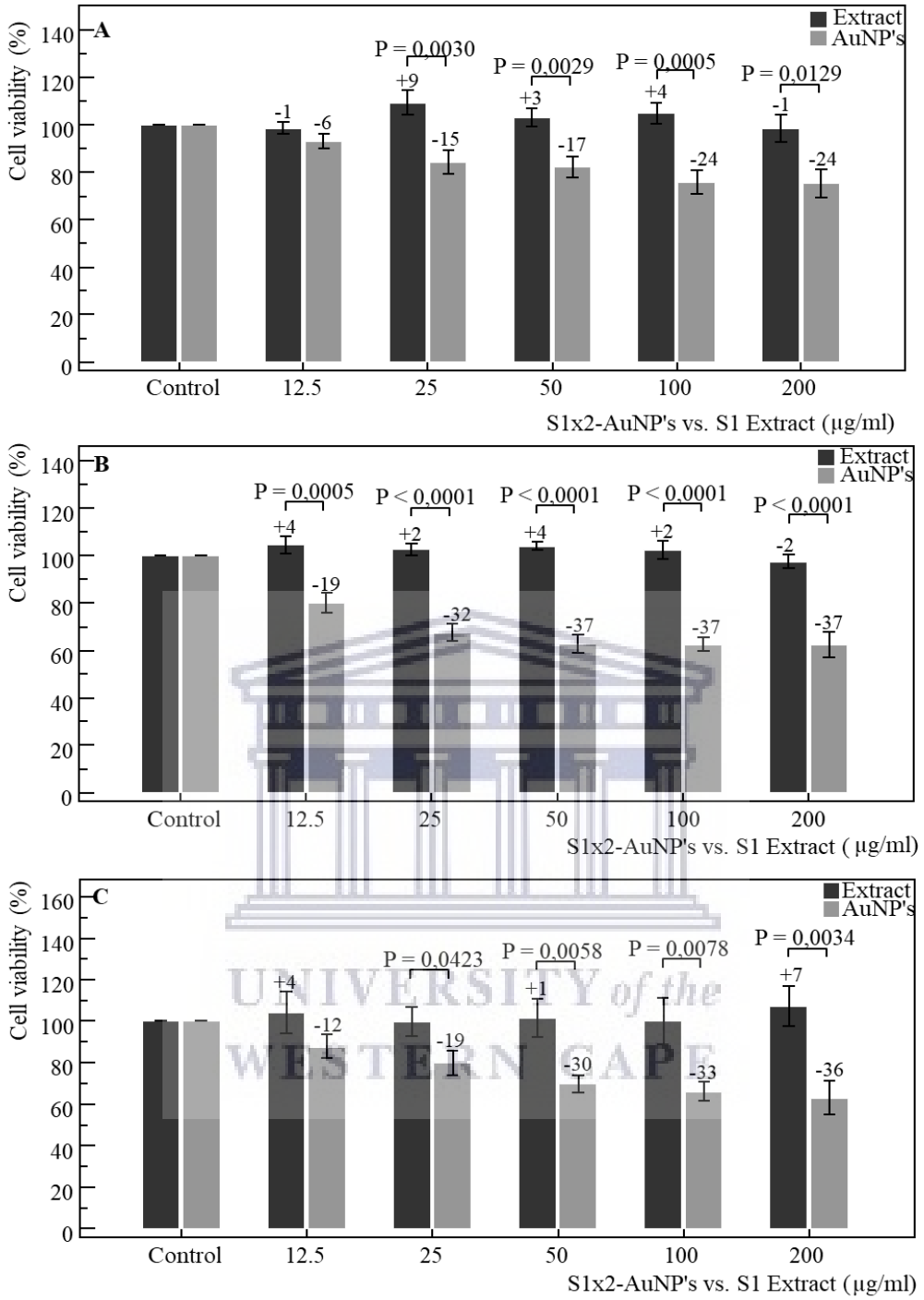

Figure 3.75: Panc1 cell viability as determined by the MTT assay over 24 (A), 48 (B) and 72 (C) hour exposure to the S1 extract and S1x2-AuNP's respectively. Significant (P=0.003, P=0.0029, P=0.0005, P=0.0129) differences were observed between the extract and AuNP's from 25-200 µg/ml over 24 hours, along with significant (P=0.0005 and P<0.0001) differences observed at 12.5 µg/ml and 25-200 µg/ml after 48 hours, and finally significant (P=0.0423, P=0.0058, P=0.0078, P=0.0034) differences from 25-200 µg/ml after 72 hours of exposure.

3.2.3.3 S2-AuNP's and S2 extract

After being exposed to increasing concentrations of the S2 extract (A-F) and S2-AuNP's (G-L) over 24 hours, cell morphology was observed and recorded (Figure 3.76). When cells were treated with the extract, no discernible change in typical cell morphology was observed between the control and 200 µg/ml (A-F). Conversely, cells appeared slightly, yet increasingly sparely spaced between the control and 200 µg/ml of the AuNP's (G-L), exhibiting marginal cell rounding and signs consistent with cell stress between 50 µg/ml and 200 µg/ml (J-L).

After being exposed to increasing concentrations of the S2 extract (A-F) and S2-AuNP's (G-L) over 48 hours, cell morphology was observed and recorded (Figure 3.77). The extract yielded no observable cell growth or morphological changes between control and 100 µg/ml (A-E), while exhibiting slight cell rounding and sings of stress at 200 µg/ml (F). Conversely, cells appeared progressively sparely spaced between the control and 200 µg/ml of the AuNP's (G-L), exhibiting cell rounding and signs indicative of cell stress between 25 µg/ml and 200 µg/ml (I-L).

Post 72-hour exposure to S2 extract (A-F) and S2-AuNP's (G-L), cell morphology was observed and recorded (Figure 3.78). When treated with the extract, no observable change in cell number or morphology was found between the control and 100 µg/ml (A-E), while exhibiting signs indicative of cell stress at 200 µg/ml (F). Conversely, cells appeared progressively more sparely spaced between control and 200 µg/ml of the AuNP's, displaying increasingly notable signs consistent with cell stress between 25 µg/ml and 200 µg/ml (I-L).

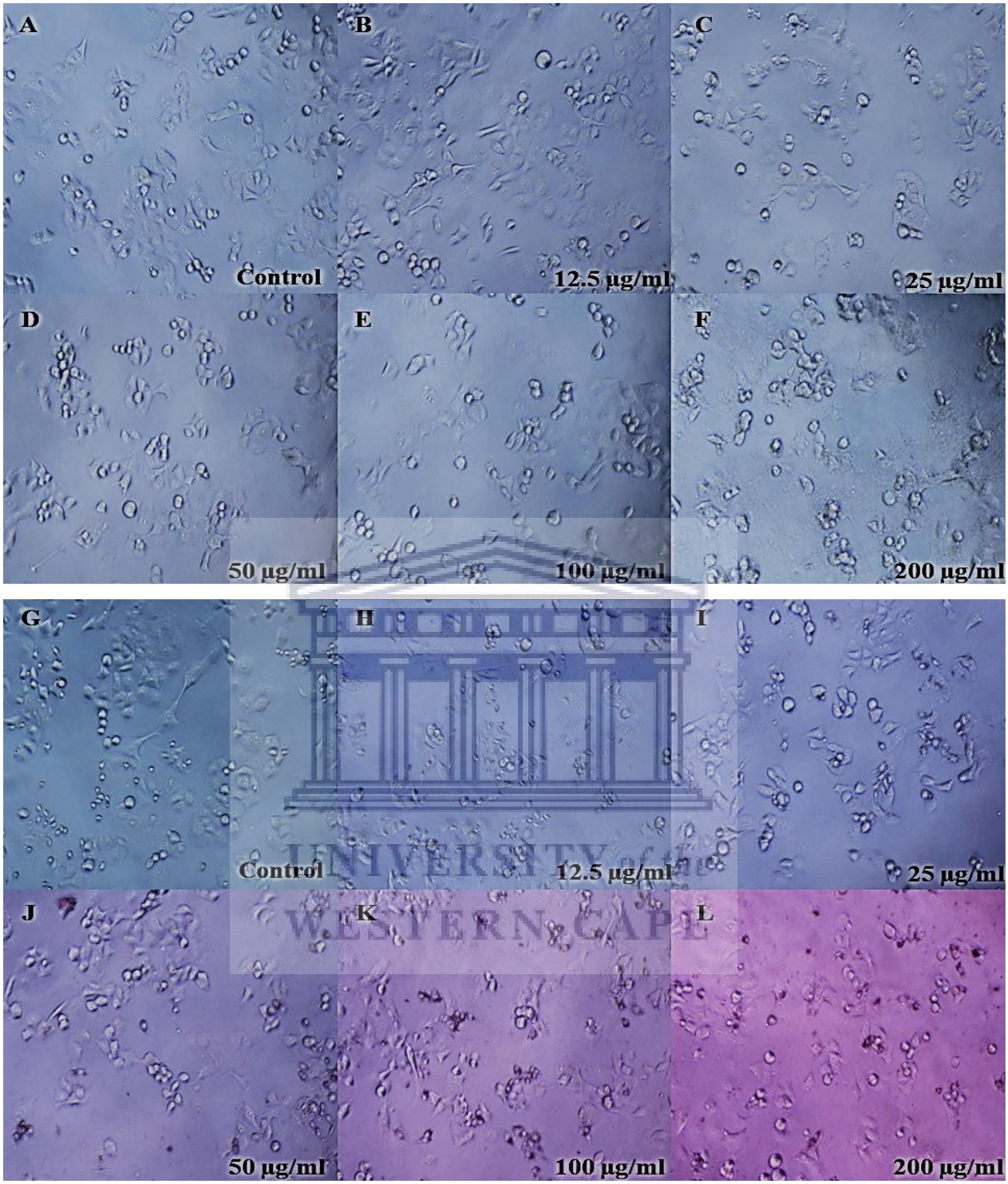

Figure 3.76: Panc1 Cell morphology after being exposed to increasing concentrations of S2 extract and S2-AuNP's over a 24-hour period. The extract (A-F) yielded no discernible change to cell morphology, while AuNP's exhibited slight decreases in cell number between the control and highest concentration (G-L), along indications of cell rounding and stress at higher concentrations (J-L).

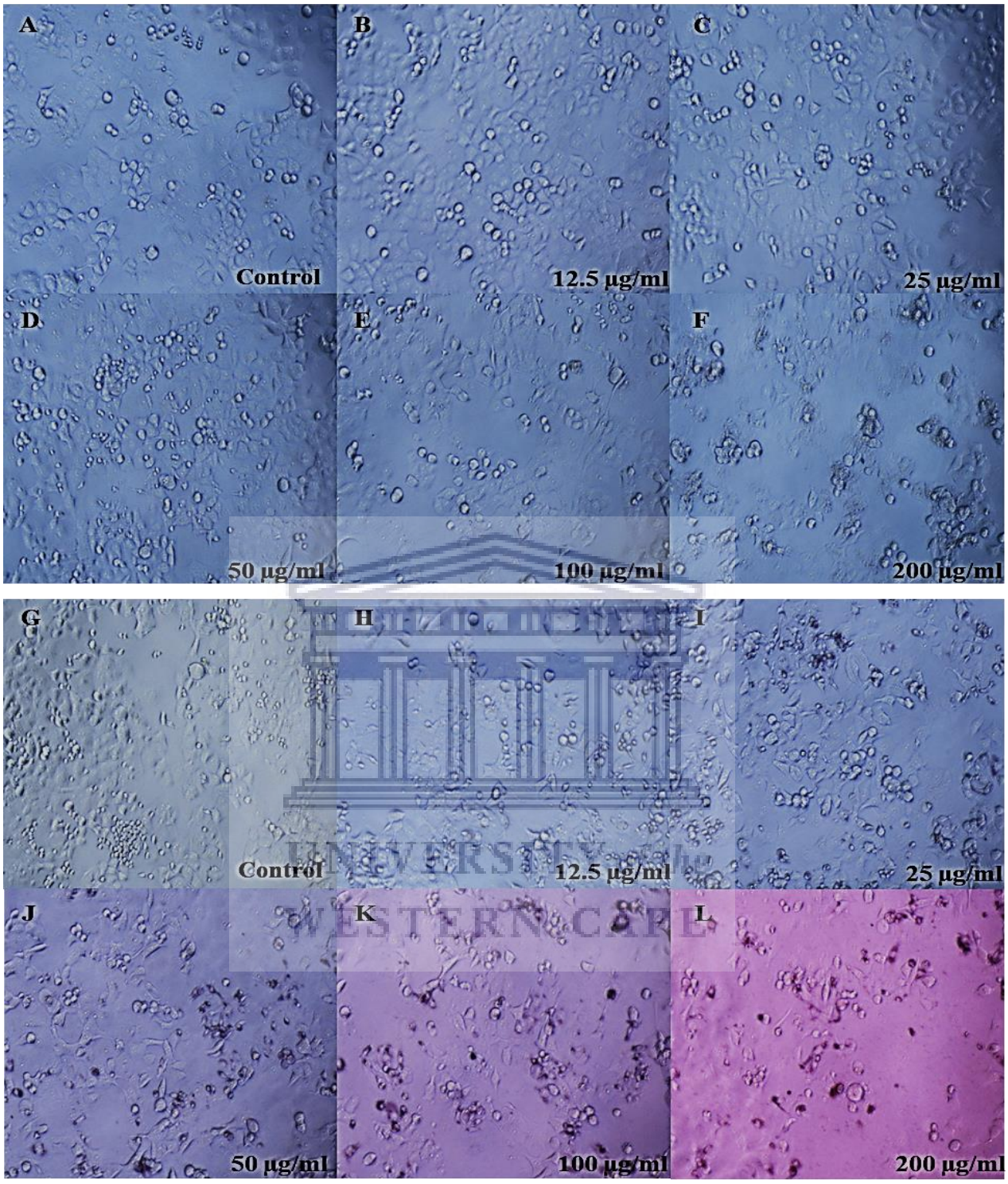

Figure 3.77: Panc1 cell morphology after being exposed to increasing concentrations of S2 extract and S2-AuNP's over a 48-hour period. The extract (A-F) exhibited no morphological changes between control and 100 µg/ml, while exhibiting signs of stress at the highest concentration (F). The AuNP's exhibited progressive decreases in the overall observed cell number (G-L), along with signs indicative of cell rounding and cell stress at higher concentrations (I-L).

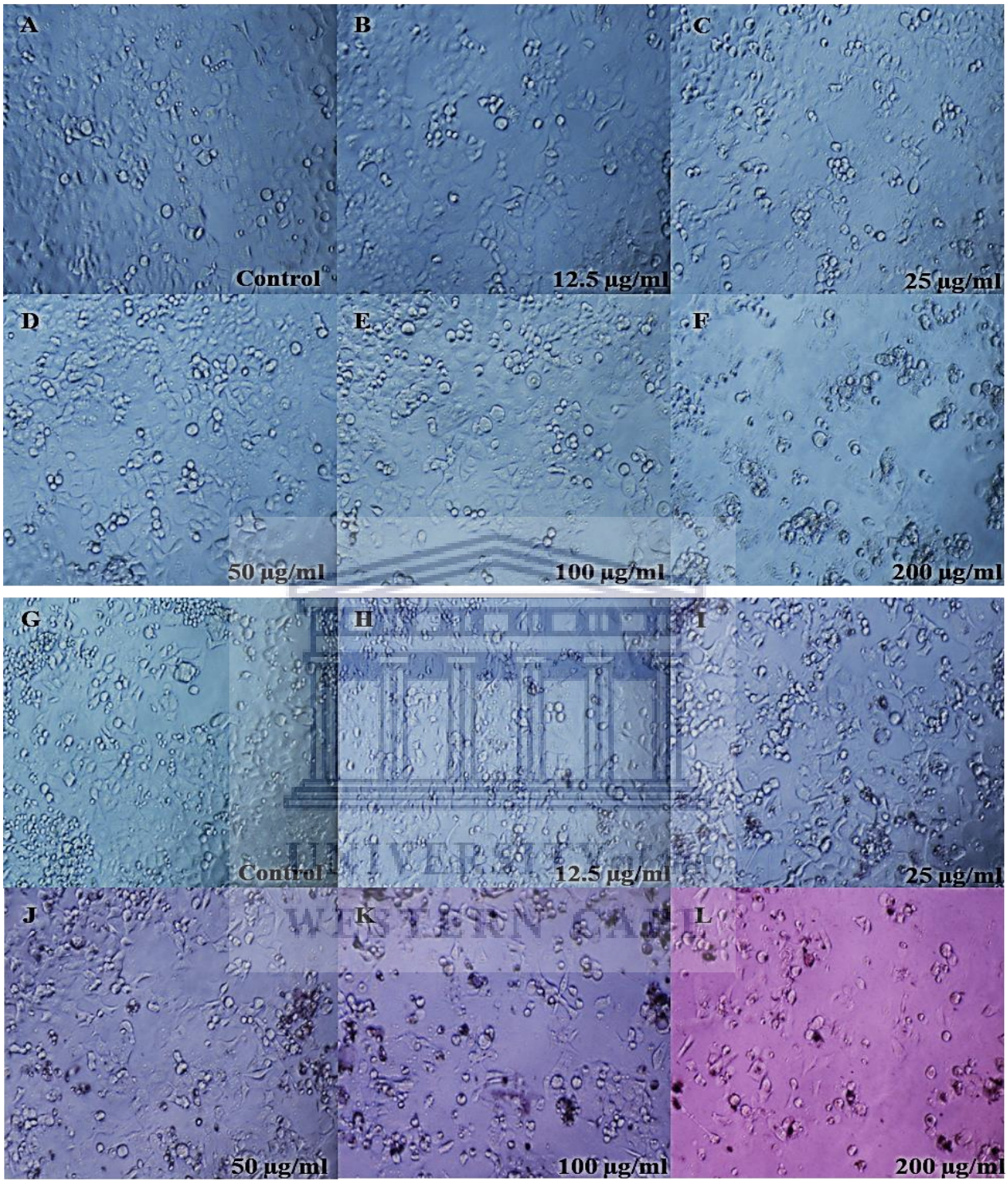

Figure 3.78: Panc1 cell morphology after being exposed to increasing concentrations of S2 extract and S2-AuNP's over a 72-hour period. The extract (A-F) exhibited no morphological changes at lower concentrations (A-E), with cell stress at the highest concentration (F). The AuNP's exhibited progressive decreases in observed cell number (G-L), with increasing signs of stress at higher concentrations (I-L).

The MTT assay revealed dose-dependent effects at 24, 48 and 72-hour exposure periods, respectively. Following 24-hours of treatment (Figure 3.79 A) with the extract, cell viability was slightly elevated above the control between 12 µg/ml and 200 µg/ml. Conversely, the AuNP's exhibited consistent reductions in cell viability between the control and 200 µg/ml, differing significantly ($P=0.0197$, $P<0.0001$ and $P=0.0002$) from the extract at 12.5 µg/ml, 25-100 µg/ml and 200 µg/ml, respectively. For the extract, the repeated measures ANOVA revealed an insignificant positive trend from control-200 µg/ml, along with AuNP's yielding a significant ($P=0.0007$) negative trend from control-200 µg/ml. One-way ANOVA yielded a significant ($P<0.001$) trend from control-200 µg/ml following treatment with the AuNP's.

Following 48-hours of exposure (Figure 3.79 B), the extract yielded marginal increases in cell viability at 25 µg/ml and 100 µg/ml, followed by a slight decreases in cell viability at 12.5 µg/ml, 50 µg/ml and 200 µg/ml. Conversely, the AuNP's yielded steady, dose-dependent decreases in cell viability from control-200 µg/ml, differing significantly ($P=0.001$, $P=0.0001$, $P<0.0001$ and $P=0.0016$) from the extract at 12.5 µg/ml, 25 µg/ml, 50-100 µg/ml and 200 µg/ml, respectively. The repeated measures ANOVA revealed a significant ($P=0.0004$) negative trend from control-200 µg/ml when exposed to the AuNP's, and one-way ANOVA revealing a significant ($P<0.001$) trend from control-200 µg/ml for both the AuNP's,

After 72-hours (Figure 3.79 C) the extract exhibited slight elevations in cell viability from control-100 µg/ml, followed by a sharp decrease from 100-200 µg/ml. The AuNP's yielded progressive, dose-dependent decreases in cell viability from control-200 µg/ml, differing significantly ($P=0.0106$, $P=0.0095$, $P=0.0194$) from the extract at 50 µg/ml, 100 µg/ml and 200 µg/ml, respectively. The repeated measures ANOVA revealed a significant ($P<0.0001$) negative trend from control-200 µg/ml when treated with the AuNP's, along with one-way ANOVA similarly revealing a significant ($P=0.001$) trend from control-200 µg/ml for the AuNP's

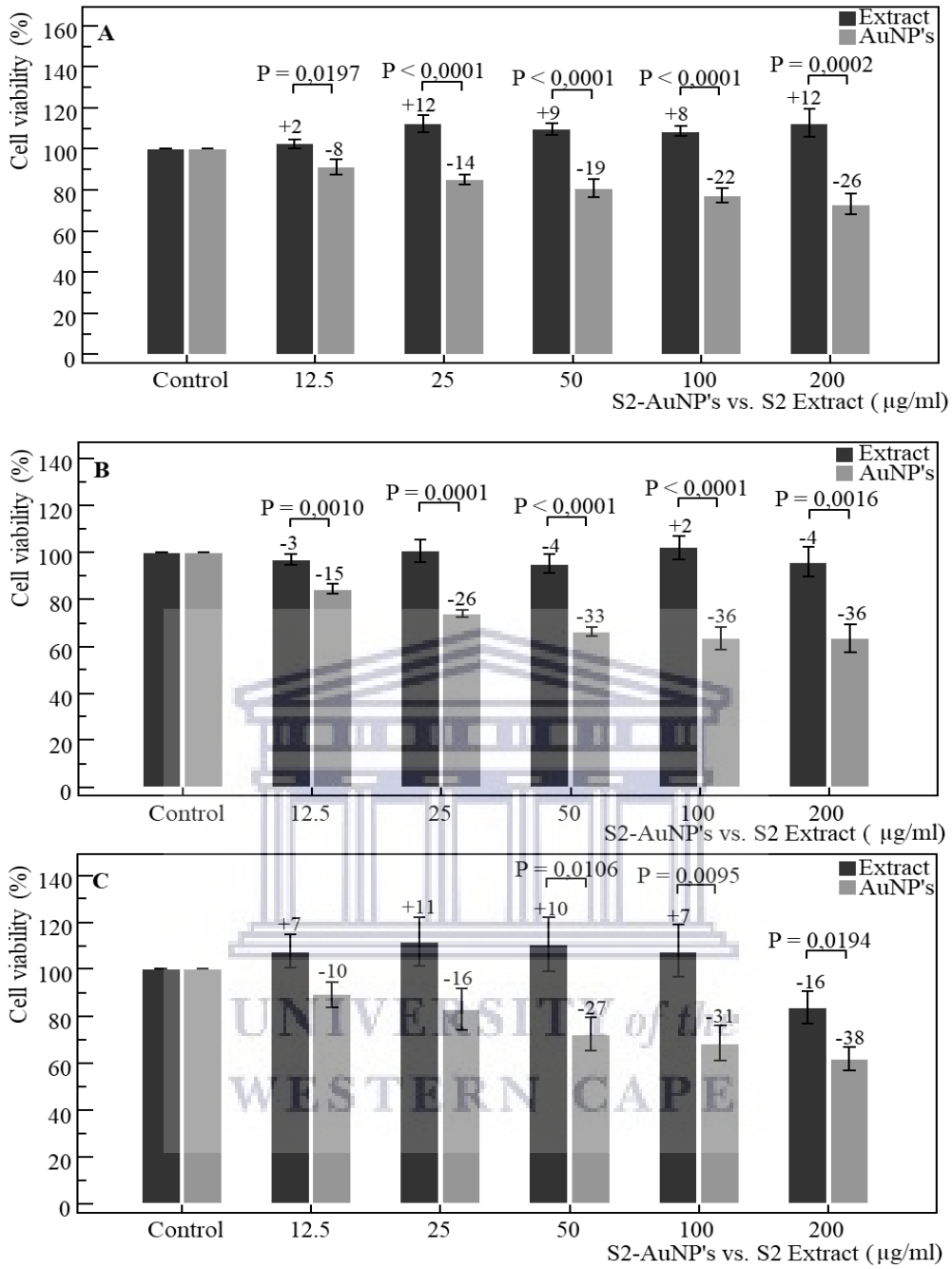

Figure 3.79: Panc1 cell viability as determined by the MTT assay over 24 (A), 48 (B) and 72 (C) hour exposure to the S2 extract and S2-AuNP's, respectively. Significant (P=0.0197, P<0.0001 and P=0.0002) differences were observed between the extract and AuNP's at 12.5 µg/ml, 25-100 µg/ml and 200 µg/ml over 24 hours, along with significant (P=0.001, P=0.0001, P<0.0001 and P=0.0016) differences observed at 12.5-25 µg/ml, 50-100 µg/ml and 200 µg/ml after 48 hours, and finally significant (P=0.0106, P=0.0095, P=0.0194) differences from 50-200 µg/ml after 72 hours of exposure.

3.2.3.4 S2x2-AuNP's and S2 extract

After being exposed to increasing concentrations of the S2 extract (A-F) and S2x2-AuNP's (G-L) over 24 hours, cell morphology was observed and recorded (Figure 3.80). When cells were treated with the extract, no change in typical cell morphology was observed between the control and 200 µg/ml (A-F). Conversely, cells were very marginally, but increasingly sparely spaced between the control and 200 µg/ml of the AuNP's (G-L), displaying some cell rounding and increasing signs consistent with cell stress between 50 µg/ml and 200 µg/ml (J-L).

After being exposed to increasing concentrations of the S2 extract (A-F) and S2x2-AuNP's (G-L) over 48 hours, cell morphology was observed and recorded (Figure 3.81). The extract yielded no observable cell growth or morphological changes between control and 100 µg/ml (A-E), while exhibiting slight cell rounding and sings of stress at 200 µg/ml (F). Contrariwise, cells appeared progressively sparely spaced between the control and 200 µg/ml of the AuNP's (G-L), exhibiting cell rounding and increasing signs of cell stress between 25 µg/ml and 200 µg/ml (I-L).

Post 72-hour exposure to S2 extract (A-F) and S2x2-AuNP's (G-L), cell morphology was observed and recorded (Figure 3.82). When treated with the extract, no observable change in cell number or morphology was found between the control and 100 µg/ml (A-E), while exhibiting signs indicative of cell stress at 200 µg/ml (F). When treated with the AuNP's, cells appeared notably more sparely spaced between control and 200 µg/ml of the AuNP's, displaying increasingly notable signs consistent with cell stress between 25 µg/ml and 200 µg/ml (I-L).

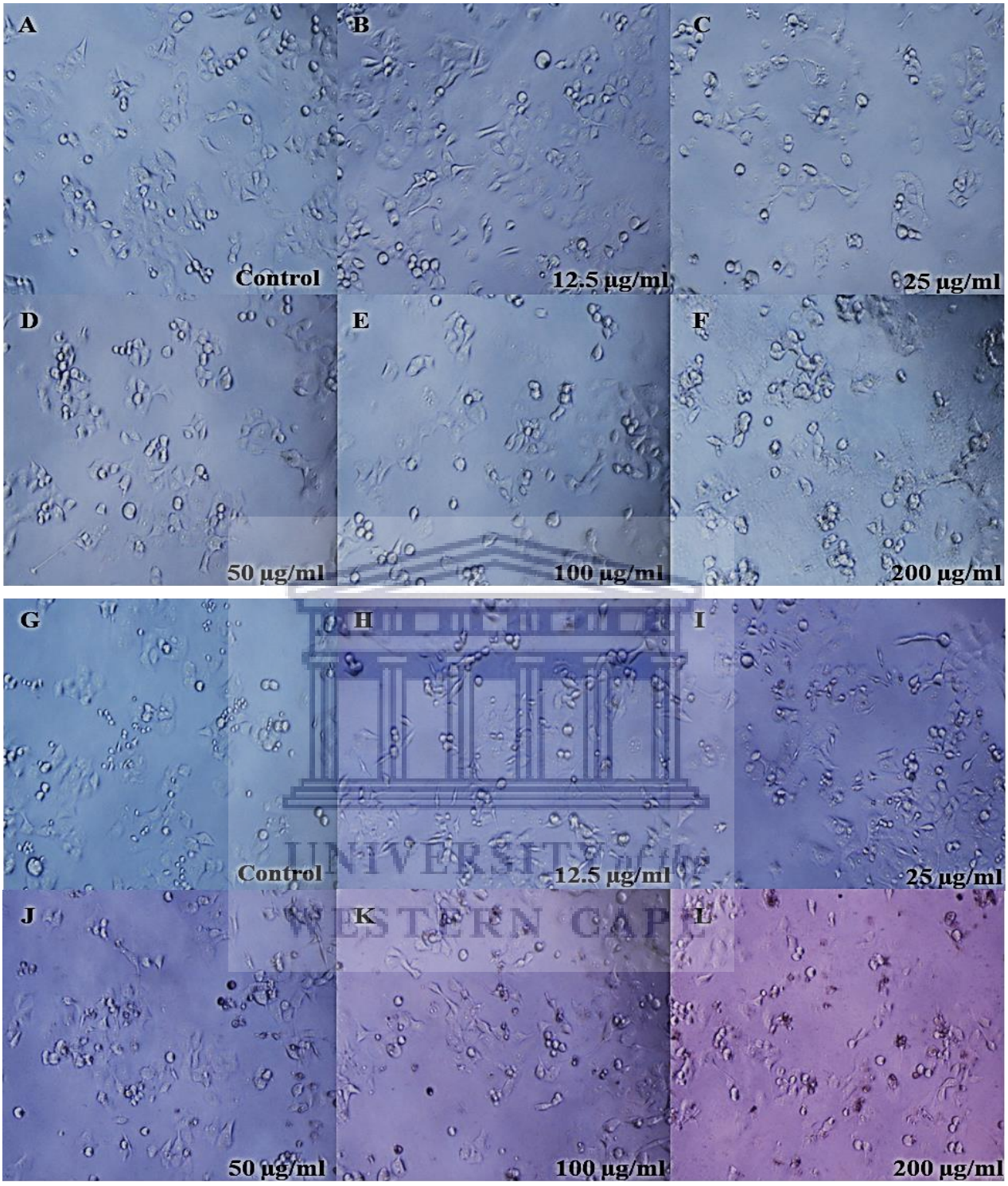

Figure 3.80: Panc1 Cell morphology after being exposed to increasing concentrations of S2 extract and S2x2-AuNP's over a 24-hour period. The extract (A-F) yielded no discernible change to cell morphology, while AuNP's exhibited slight decreases in cell number between the control and highest concentration (G-L), along with indications of cell rounding and stress at higher concentrations (J-L).

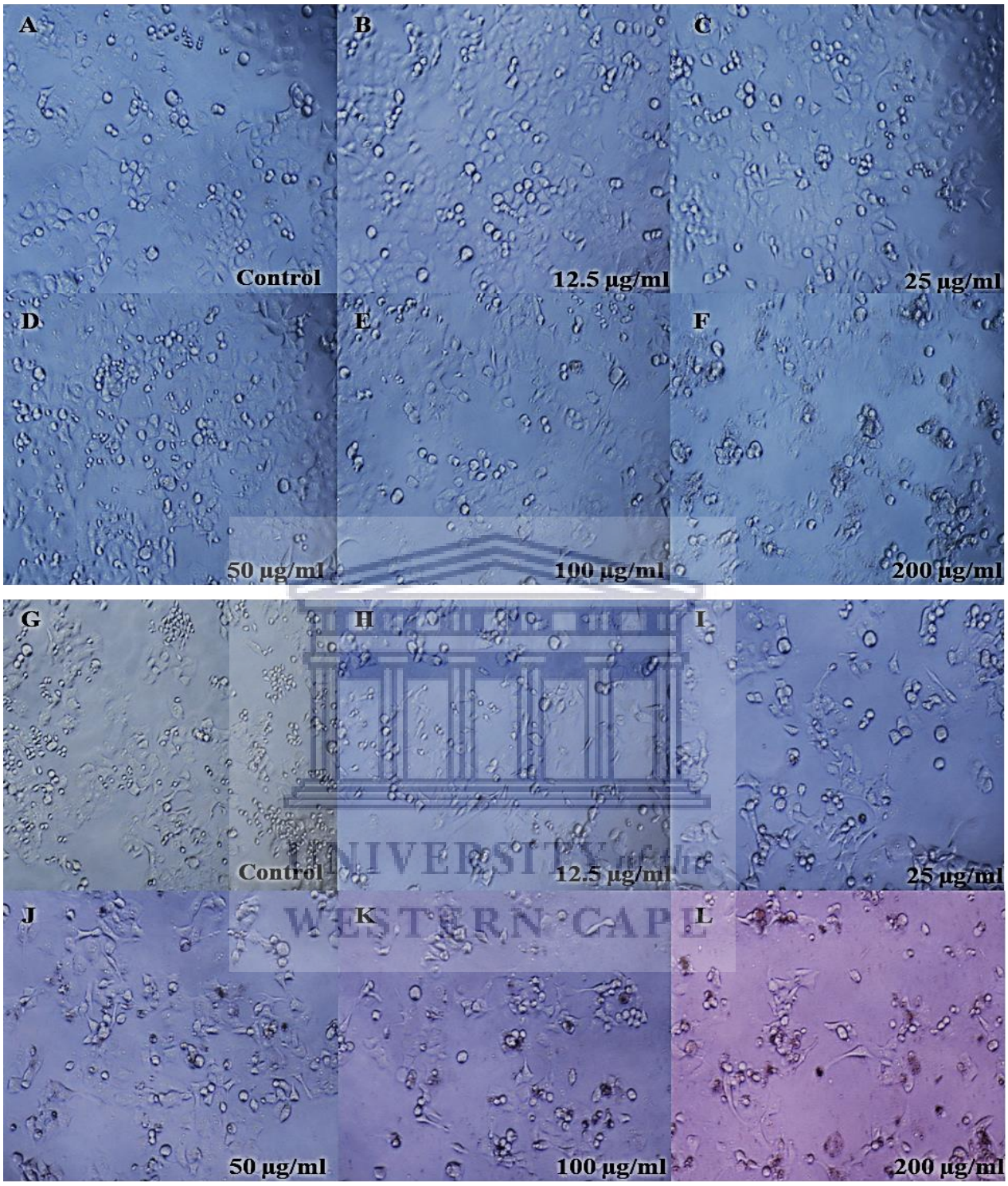

Figure 3.81: Panc1 cell morphology after being exposed to increasing concentrations of S2 extract and S2x2-AuNP's over a 48-hour period. The extract (A-F) exhibited no morphological changes between control and 100 µg/ml, while exhibiting signs of stress at the highest concentration (F). The AuNP's exhibited decreases in the overall observed cell number (G-L), along with signs indicative of cell rounding and cell stress at higher concentrations (I-L).

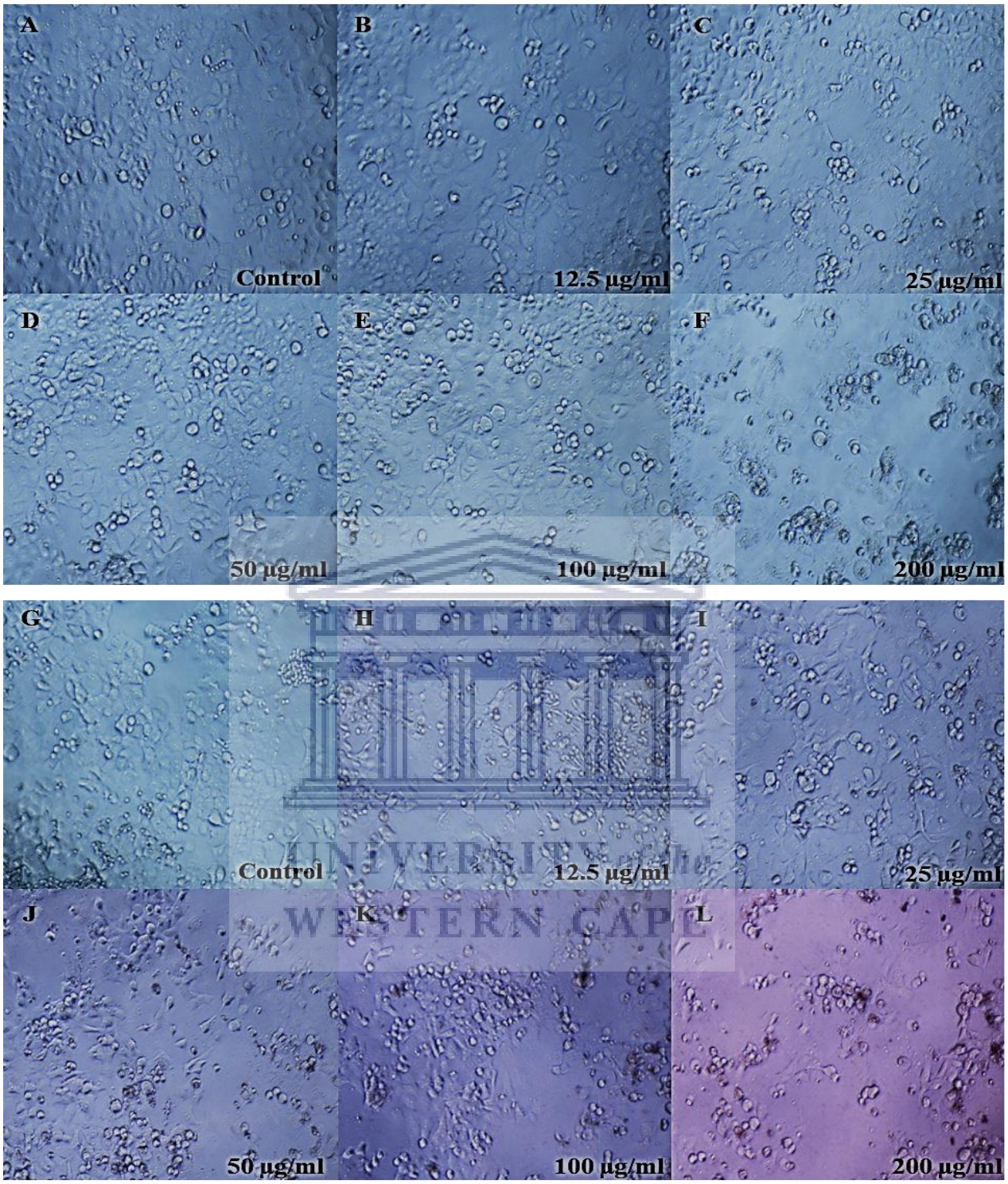

Figure 3.82: Panc1 cell morphology after being exposed to increasing concentrations of S2 extract and S2x2-AuNP's over a 72-hour period. The extract (A-F) exhibited no morphological changes at lower concentrations (A-E), with cell stress at the highest concentration (F). The AuNP's exhibited progressive decreases in observed cell number (G-L), with increasing signs of stress at higher concentrations (I-L).

The MTT assay revealed dose-dependent effects at 24, 48 and 72-hour exposure periods, respectively. Following 24-hours of treatment (Figure 3.83 A) with the extract, cell viability was slightly elevated at each concentration between the control and 200 µg/ml. The AuNP's exhibited increasing reductions in cell viability between the control and 200 µg/ml, differing significantly (P=0.013, P=0.0008, P=0.0001, P=0.0012) from the extract at 25 µg/ml, 50 µg/ml, 100 µg/ml and 200 µg/ml, respectively. For the extract, the repeated measures ANOVA revealed an insignificant positive trend from control-200 µg/ml, along with AuNP's yielding a significant (P=0.0001) negative trend from control-200 µg/ml. One-way ANOVA yielded a significant (P=0.004) trend from control-200 µg/ml following treatment with the AuNP's.

Following 48-hours of exposure (Figure 3.83 B), the extract yielded marginal increases in cell viability at 25 µg/ml and 100 µg/ml, followed by a slight decreases in cell viability at 12.5 µg/ml, 50 µg/ml and 200 µg/ml. Conversely, the AuNP's yielded steady, dose-dependent decreases in cell viability from control-200 µg/ml, differing significantly (P=0.0001, P<0.0001 and P=0.0004) from the extract at 12.5 µg/ml, 25-100 µg/ml and 200 µg/ml, respectively. The repeated measures ANOVA revealed a significant (P=0.0003) negative trend from control-200 µg/ml when exposed to the AuNP's, and one-way ANOVA revealing a significant (P<0.001) trend from control-200 µg/ml for both the AuNP's,

After 72-hours (Figure 3.83 C) the extract exhibited slight elevations in cell viability from control-100 µg/ml, followed by a sharp decrease from 100-200 µg/ml. The AuNP's yielded progressive, dose-dependent decreases in cell viability from control-200 µg/ml, differing significantly (P=0.0342, P=0.0192 and P=0.0185) from the extract at 12.5 µg/ml, 25 µg/ml and 50-100 µg/ml, respectively. The repeated measures ANOVA revealed a significant (P=0.0069) negative trend from control-200 µg/ml when treated with the AuNP's, along with one-way ANOVA similarly revealing a significant (P=0.01) trend from control-200 µg/ml for the AuNP's

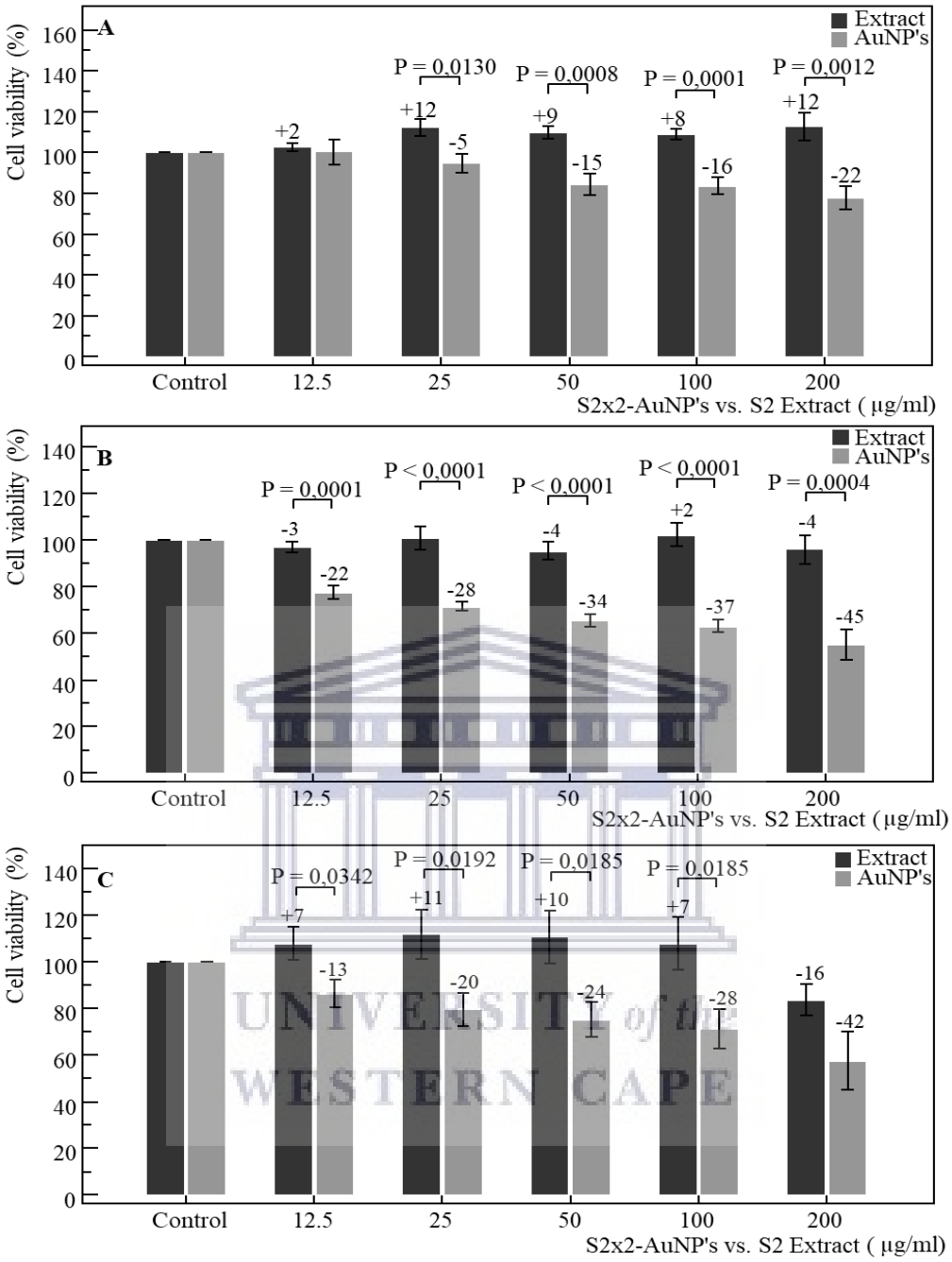

Figure 3.83: Panc1 cell viability as determined by the MTT assay over 24 (A), 48 (B) and 72 (C) hour exposure to the S2 extract and S2-AuNP's respectively. Significant (P=0.013, P=0.0008, P=0.0001, P=0.0012) differences were observed between the extract and AuNP's from 25-200 µg/ml over 24 hours, along with significant (P=0.0001, P<0.0001 and P=0.0004) differences observed at 12.5 µg/ml, 25-100 µg/ml and 200 µg/ml after 48 hours, and finally significant (P=0.0342, P=0.0192 and P=0.0185) differences at 12.5 µg/ml, 25 µg/ml and 50-100 µg/ml after 72 hours of exposure.

3.2.3.5 Ng-AuNP's pH 7 and naringenin

After being exposed to increasing concentrations of naringenin (A-F) and the Ng-AuNP's pH 7 (G-L) over 24 hours, cell morphology was observed and recorded (Figure 3.84). Cells were increasingly sparely spaced between the control and 200 µg/ml when treated with naringenin (A-F), exhibiting cell rounding and stress at higher concentrations (D-F). Similarly, cells were increasingly sparely spaced between the control and 200 µg/ml of the AuNP's, displaying cell rounding and increasing signs of cell stress between 50 µg/ml and 200 µg/ml (J-L).

After being exposed to increasing concentrations of naringenin (A-F) and Ng-AuNP's pH 7 (G-L) over 48 hours, cell morphology was observed and recorded (Figure 3.85). Naringenin yielded progressively fewer observable cells between the control and 200 µg/ml (A-F), exhibiting increasing cell rounding and sings of stress at higher concentrations (C-F). Similarly, cells appeared progressively sparely spaced between the control and 200 µg/ml of the AuNP's (G-L), exhibiting increasingly notable signs of cell stress between 25 µg/ml and 200 µg/ml (I-L).

Post 72-hour exposure to naringenin (A-F) and Ng-AuNP's pH 7 (G-L), cell morphology was observed and recorded (Figure 3.86). Increasingly fewer observable cells were found between the control and 200 µg/ml (A-F) of naringenin, along with increasingly evident cell rounding and signs of stress at higher concentrations (C-F). Similarly, cells appeared increasingly sparely spaced between the control and 200 µg/ml of the AuNP's (G-L), exhibiting notable signs of cell stress between 25 µg/ml and 100 µg/ml (I-K), and cell death at 200 µg/ml (L).

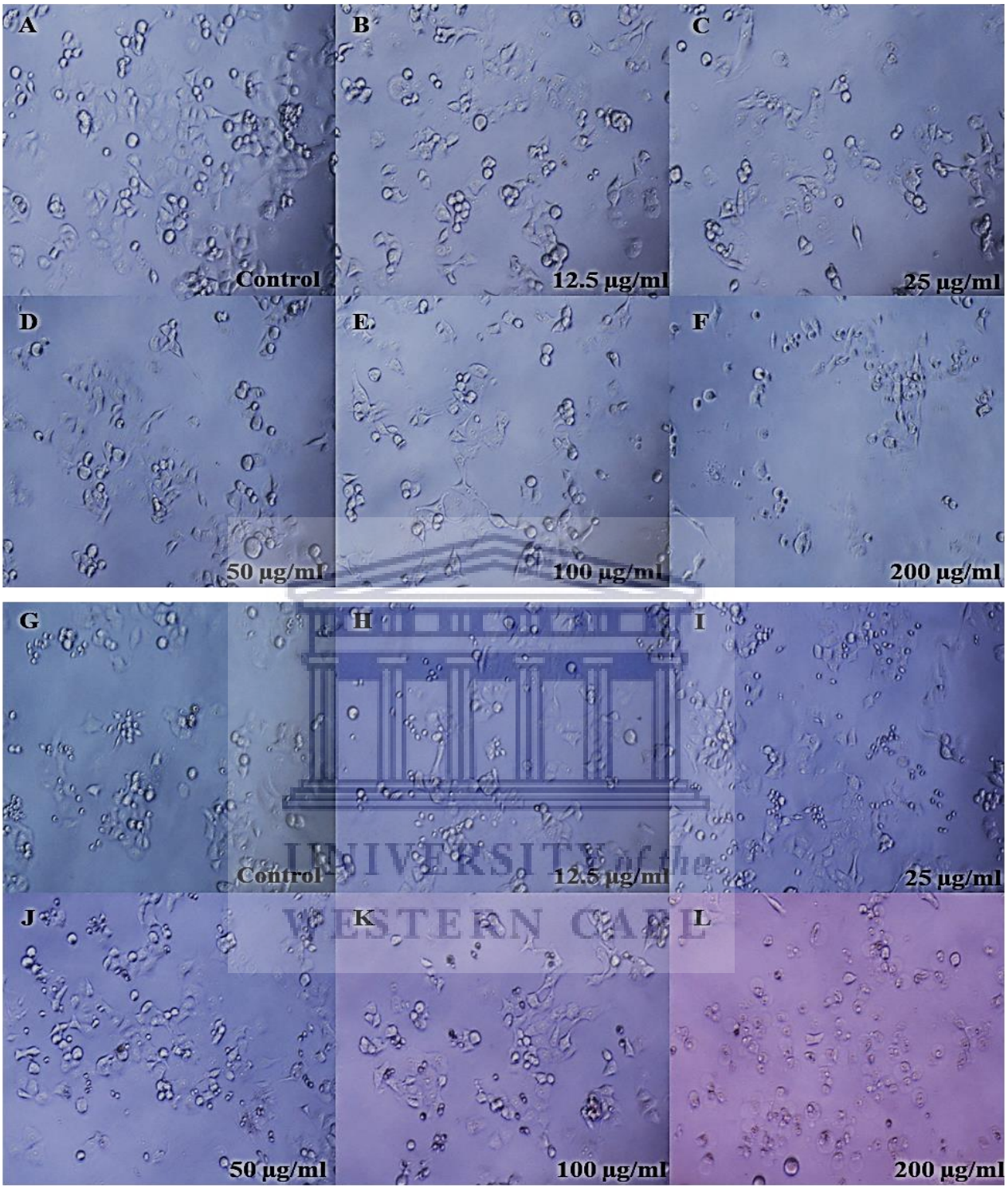

Figure 3.84: Panc1 Cell morphology after being exposed to increasing concentrations of naringenin and Ng-AuNP's pH 7 over a 24-hour period. Naringenin yielded a progressive decrease in cell number (A-F), along with the presence of stress at higher concentrations (D-F). The AuNP's exhibited decreases in cell number between the control and highest concentration (G-L), along with indications of cell rounding and stress at higher concentrations (J-L).

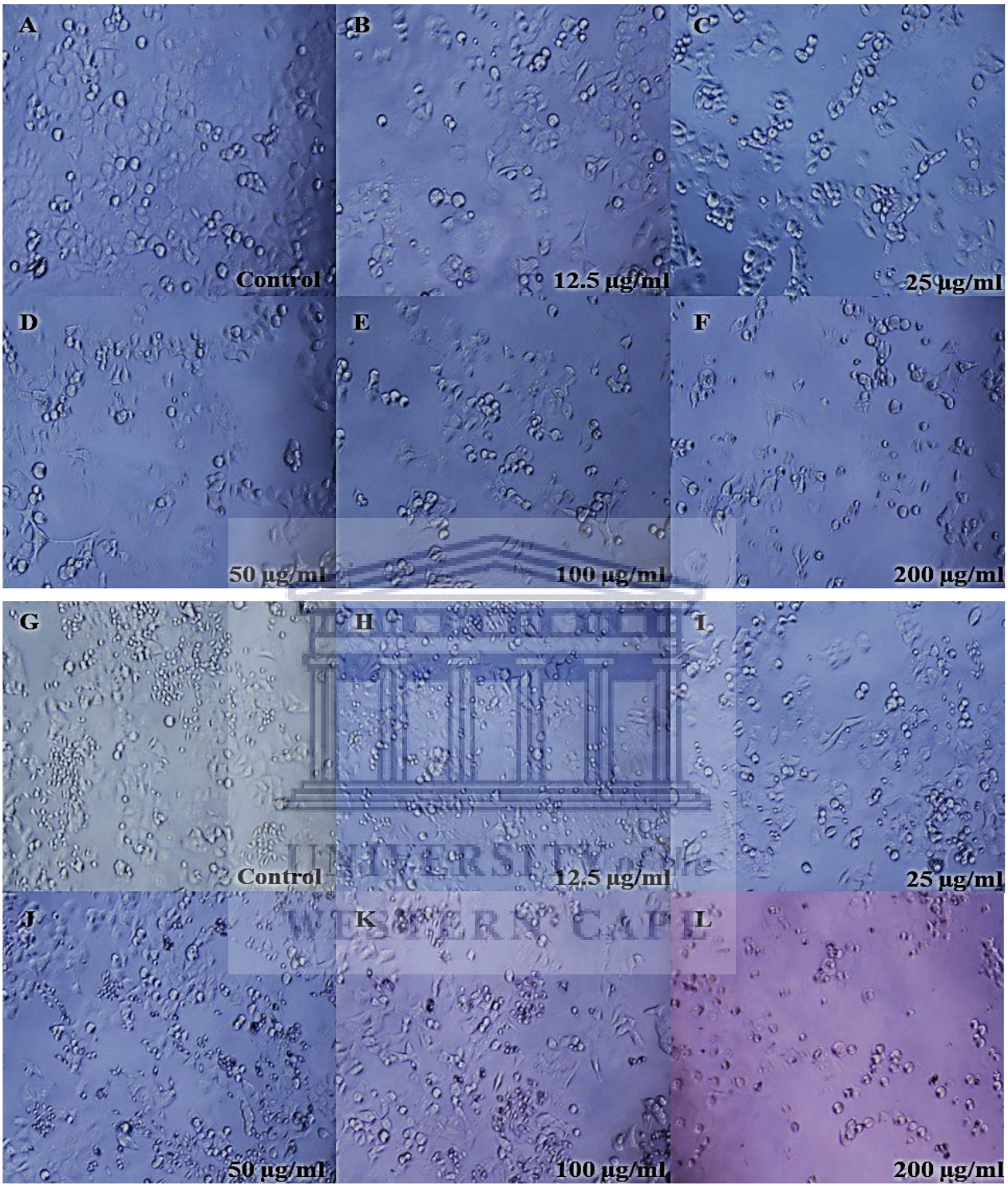

Figure 3.85: Panc1 cell morphology after being exposed to increasing concentrations of naringenin and Ng-AuNP's pH 7 over a 48-hour period. Naringenin exhibited fewer cells between control and 100 µg/ml (A-F), with increasing signs of stress at the highest concentration (F). The AuNP's exhibited decreases in the overall observed cell number (G-L), along with increasing signs consistent with cell rounding and cell stress at higher concentrations (I-L).

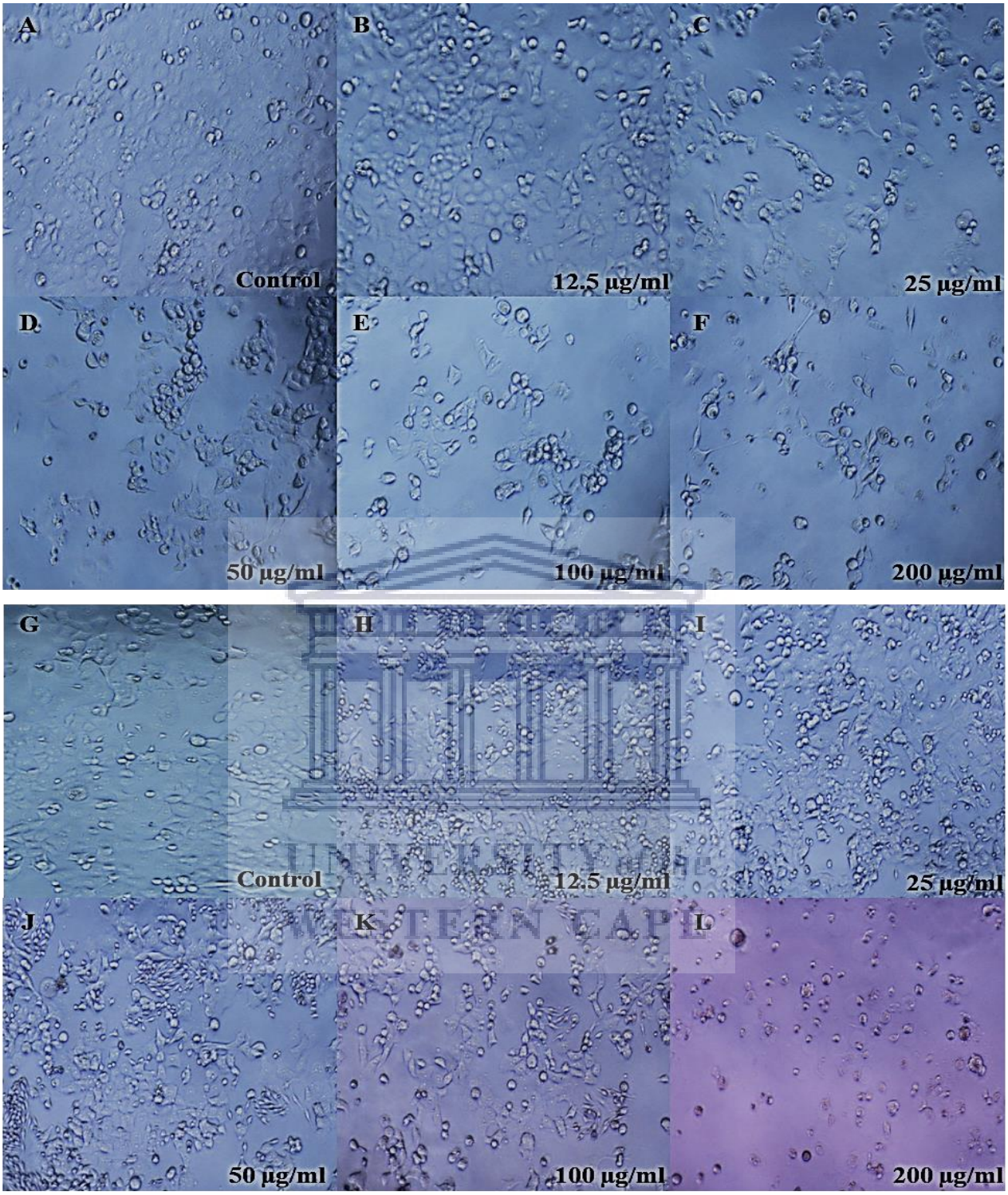

Figure 3.86: Panc1 cell morphology after being exposed to increasing concentrations of naringenin and Ng-AuNP's pH 7 over a 72-hour period. Naringenin exhibited fewer cells between control and 200 µg/ml (A-F), with cell stress at the highest concentration (F). The AuNP's exhibited overall decreases in cell number (G-L), with increasing cell stress (I-K) and death (L).

The MTT assay revealed dose-dependent effects at 24, 48 and 72-hour exposure periods, respectively. Following 24-hours of treatment (Figure 3.87 A), both naringenin and the AuNP's yielded marginal, but steady decreases in cell viability from the control-100 µg/ml, followed by a notably sharper drop in viability at 200 µg/ml, whereby the AuNP's yielded a significantly ($P<0.0001$) greater reduction in cell viability. For naringenin, the repeated measures ANOVA revealed a significant ($P=0.0001$) negative trend from control-200 µg/ml, along with AuNP's yielded a significant ($P<0.0001$) negative trend from control-200 µg/ml. One-way ANOVA yielded significant ($P<0.001$) trends from control-200 µg/ml following treatment with both naringenin and the AuNP's, respectively.

Following 48 hours of exposure (Figure 3.87 B), both naringenin and the AuNP's yielded dose-dependent decreases in cell viability from the control-200 µg/ml, with naringenin yielding a greater reduction at 100 µg/ml, and the AuNP's yielding a greater reduction at 200 µg/ml. Furthermore, significant ($P=0.0041$, $P=0.0001$) difference were observed between naringenin and the AuNP's at 100 µg/ml and 200 µg/ml, respectively. The repeated measures ANOVA revealed significant ($P<0.0001$) negative trends from control-200 µg/ml when exposed to naringenin and the AuNP's, respectively. One-way ANOVA revealed a significant ($P<0.001$) trend from control-200 µg/ml for both naringenin and the AuNP's, respectively.

After 72 hours (Figure 3.87 C), both, naringenin and the AuNP's yielded progressive, dose-dependent decreases in cell viability from the control-200 µg/ml, remaining fairly comparable in their effects toward cell viability at each concentration. Although no significant difference could be found, naringenin did exhibit a slightly greater reduction in cell viability between 25-100 µg/ml. The repeated measures ANOVA revealed significant ($P<0.0001$, $P=0.0001$) negative trends from control-200 µg/ml for naringenin and the AuNP's, respectively, along with one-way ANOVA revealing significant ($P<0.001$) trends from control-200 µg/ml for both naringenin and the AuNP's, respectively.

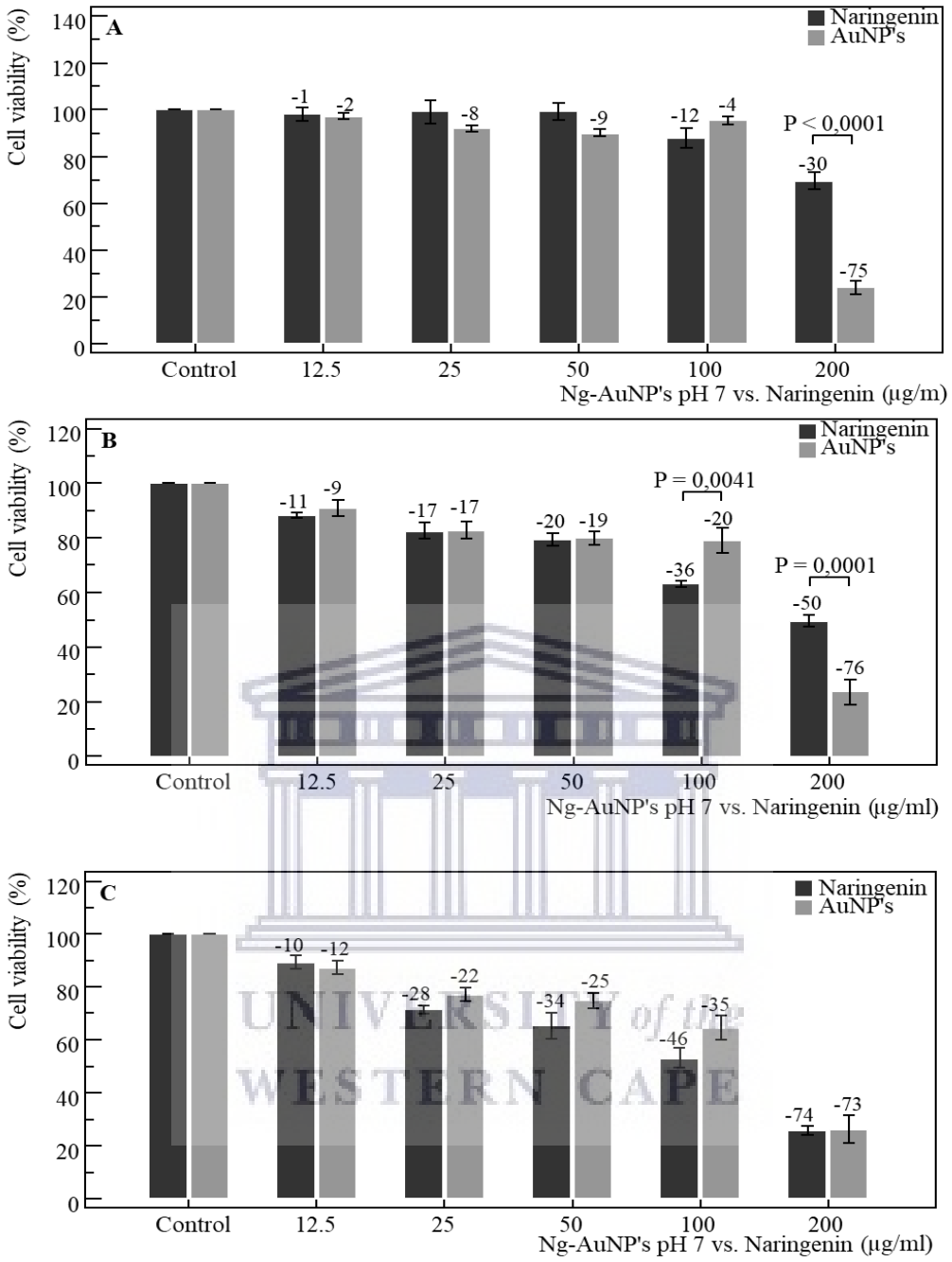

Figure 3.87: Panc1 cell viability as determined by the MTT assay over 24 (A), 48 (B) and 72 (C) hour exposure to naringenin and Ng-AuNP's pH 7 respectively. A significant (P<0.0001) difference was observed between naringenin and the AuNP's at 200 µg/ml over 24 hours, along with significant (P=0.0041, P=0.0001) differences from 100-200 µg/ml after 48 hours. Following 72-hours of exposure, naringenin yielded a slightly greater reduction in cell viability between 25-100 µg/ml. However, no statistically significant differences could be found between naringenin and the AuNP's at each of the concentrations used in the present study.

3.2.3.6 Ng-AuNP's pH 8 and naringenin

After being exposed to increasing concentrations of naringenin (A-F) and the Ng-AuNP's pH 8 (G-L) over 24 hours, cell morphology was observed and recorded (Figure 3.88). For naringenin, cells became increasingly sparely spaced between the control and 200 µg/ml (A-F), exhibiting cell rounding and stress at higher concentrations (D-F). Similarly, cells appeared increasingly sparely spaced between the control and 200 µg/ml of the AuNP's, appearing rounded and increasingly stressed between 25 µg/ml and 100 µg/ml (J-K), and cell death at 200 µg/ml (L).

After being exposed to increasing concentrations of naringenin (A-F) and Ng-AuNP's pH 8 (G-L) over 48 hours, cell morphology was observed and recorded (Figure 3.89). Naringenin yielded progressively fewer observable cells between the control and 200 µg/ml (A-F), exhibiting increasing cell rounding and sings of stress at higher concentrations (C-F). Similarly, cells appeared progressively sparely spaced between the control and 200 µg/ml of the AuNP's (G-L), exhibiting increasingly notable signs of cell stress between 25 µg/ml and 200 µg/ml (I-K) and sings consistent with cell death at the highest concentration (L).

Post 72 hour exposure to naringenin (A-F) and Ng-AuNP's pH 8 (G-L), cell morphology was observed and recorded (Figure 3.90). Increasingly fewer observable cells were found between the control and 200 µg/ml (A-F) of naringenin, along with increasingly evident cell rounding and signs of stress at higher concentrations (C-F). Similarly, cells appeared incrementally sparely spaced between the control and 200 µg/ml of the AuNP's (G-L), exhibiting increasingly notable signs of cell stress between 12.5 µg/ml and 100 µg/ml (H-K), and cell death at 200 µg/ml (L).

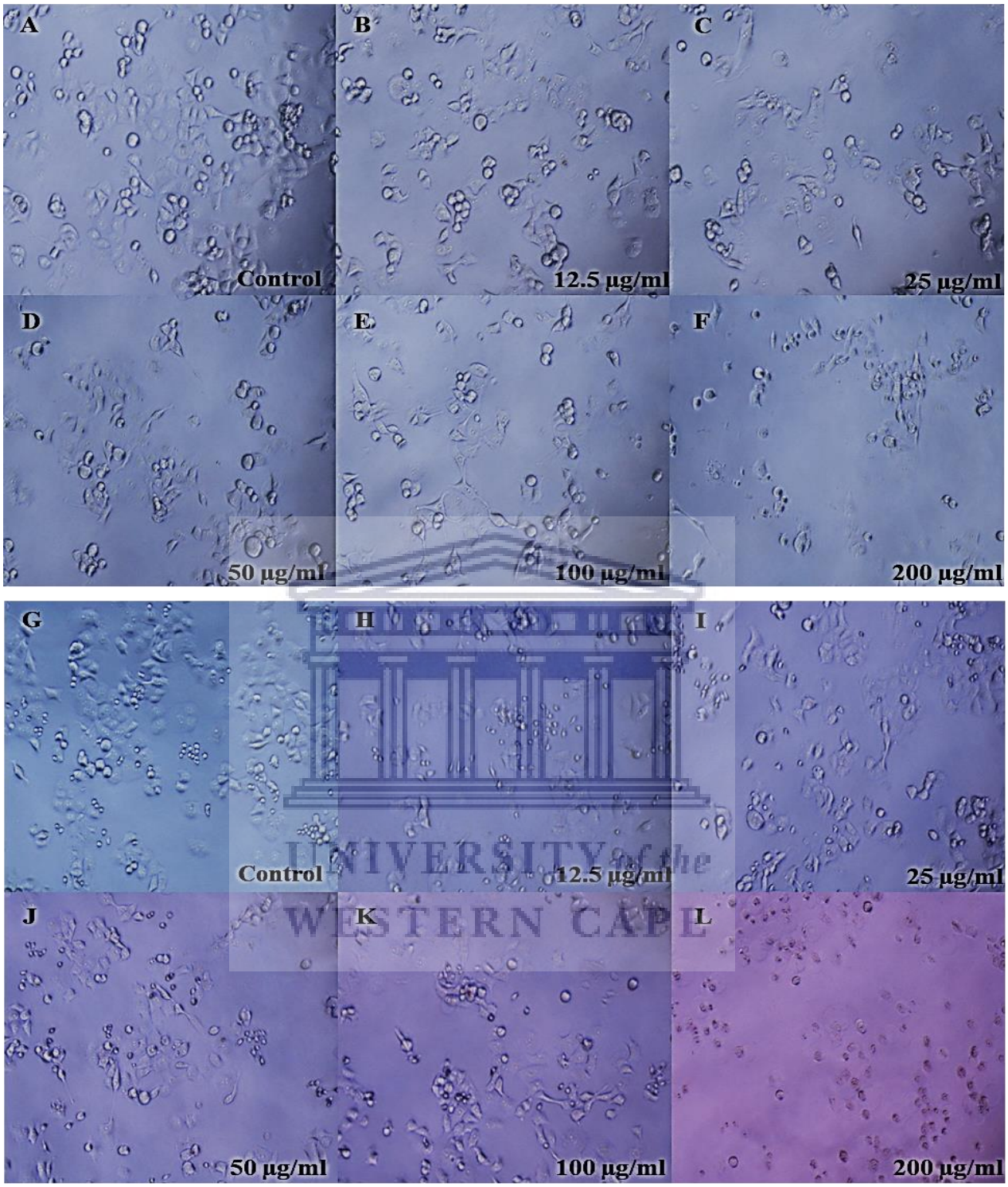

Figure 3.88: Panc1 Cell morphology after being exposed to increasing concentrations of naringenin and Ng-AuNP's pH 8 over a 24-hour period. Naringenin yielded a progressive decrease in cell number (A-F), along with the presence of stress at higher concentrations (D-F). The AuNP's exhibited decreases in cell number between the control and highest concentration (G-L), along with indications of cell rounding and stress at (J-k) and cell death (L) at higher concentrations.

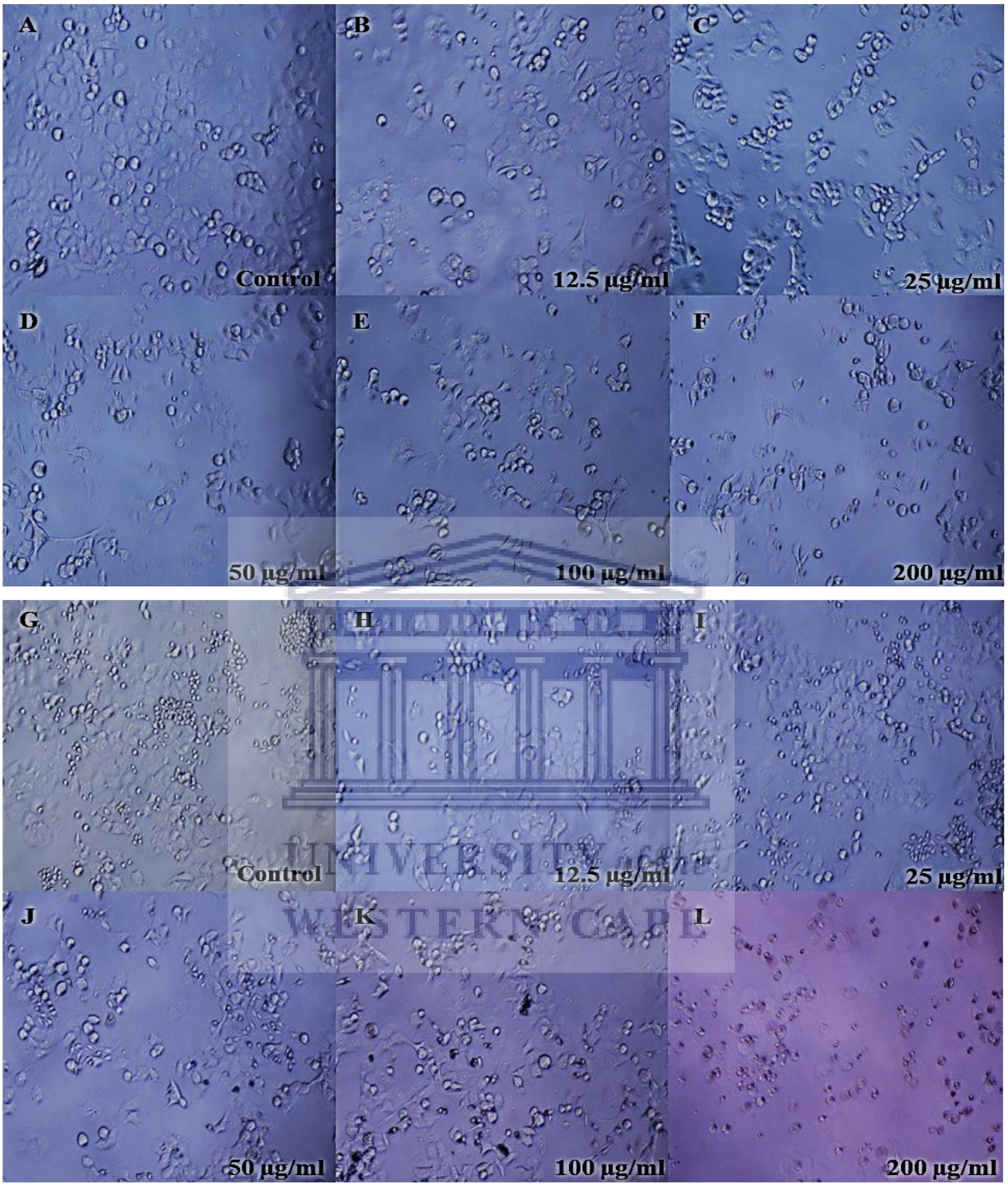

Figure 3.89: Panc1 cell morphology after being exposed to increasing concentrations of naringenin and Ng-AuNP's pH 7 over a 48-hour period. Naringenin exhibited fewer cells between control and 100 µg/ml (A-F), with increasing signs of stress at the highest concentration (F). The AuNP's exhibited decreases in the overall observed cell number (G-L), along with increasing cell stress (I-K) and death (L) at the higher concentrations.

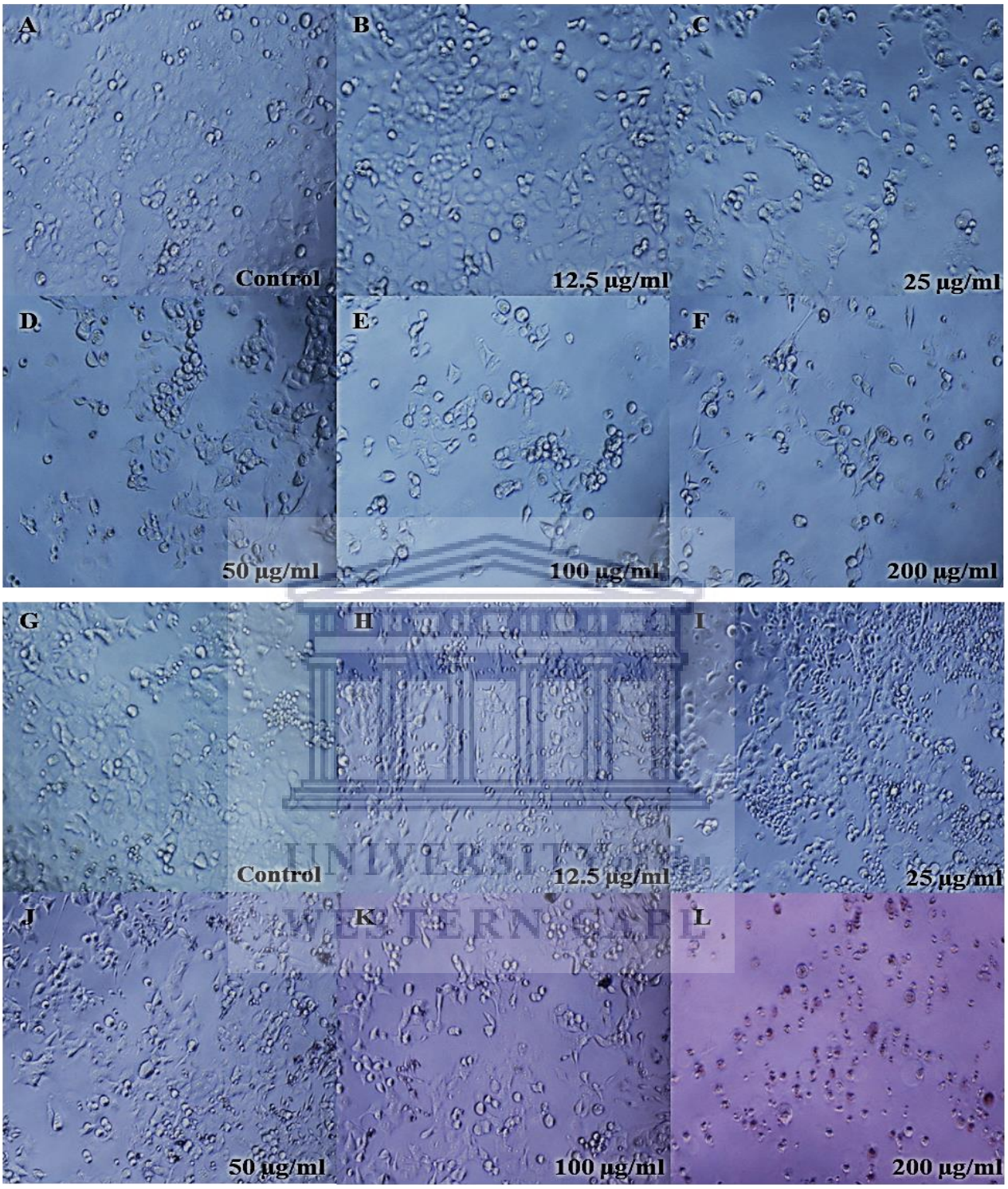

Figure 3.90: Panc1 cell morphology after being exposed to increasing concentrations of naringenin and Ng-AuNP's pH 7 over a 72-hour period. Naringenin exhibited fewer cells between control and 200 µg/ml (A-F), with cell stress at the highest concentration (F). The AuNP's exhibited progressive decreases in cell number (G-L), with increasing cell stress (H-K) and death at the highest concentration (L).

The MTT assay revealed dose-dependent effects at 24, 48 and 72-hour exposure periods, respectively. Following 24-hours of treatment (Figure 3.91 A), both naringenin and the AuNP's yielded consistent decreases in cell viability from the control-100 µg/ml, followed by a notably greater drop in viability at 200 µg/ml. The AuNP's yielded greater decreases in cell viability at each concentration, differing from naringenin significantly ($P=0.003$, $P<0.0001$) at 50 µg/ml and 200 µg/ml, respectively. The repeated measures ANOVA revealed a significant ($P=0.0001$) negative trend from control-200 µg/ml for naringenin, along with AuNP's yielding a significant ($P<0.0001$) negative trend from control-200 µg/ml. One-way ANOVA yielded significant ($P<0.001$) trends from control-200 µg/ml following treatment with both naringenin and the AuNP's, respectively.

Following 48-hours of exposure (Figure 3.91 B), both naringenin and the AuNP's yielded decreases in cell viability from the control-200 µg/ml, with the AuNP's yielding a markedly sharp drop in viability at 200 µg/ml. Greater decreases in cell viability were yielded by the AuNP's, differing significantly ($P=0.0332$, $P=0.0013$, $P=0.0004$, $P<0.0001$) from naringenin at 25 µg/ml, 50 µg/ml, 100 µg/ml and 200 µg/ml, respectively. The repeated measures ANOVA revealed significant ($P<0.0001$) negative trends from control-200 µg/ml when exposed to naringenin and the AuNP's, respectively. Similarly, one-way ANOVA revealed significant ($P<0.001$) trends from control-200 µg/ml for both naringenin and the AuNP's, respectively.

After 72-hours (Figure 3.91 C) both naringenin and the AuNP's yielded comparable decreases in cell viability from control-100 µg/ml. At 200 µg/ml, the AuNP's yielded a notably greater reduction in viability, differing significantly ($P=0.0004$) from naringenin. The repeated measures ANOVA revealed significant ($P<0.0001$) negative trends from control-200 µg/ml for naringenin and the AuNP's, respectively, along with one-way ANOVA revealing significant ($P<0.001$) trends from control-200 µg/ml for both naringenin and the AuNP's, respectively.

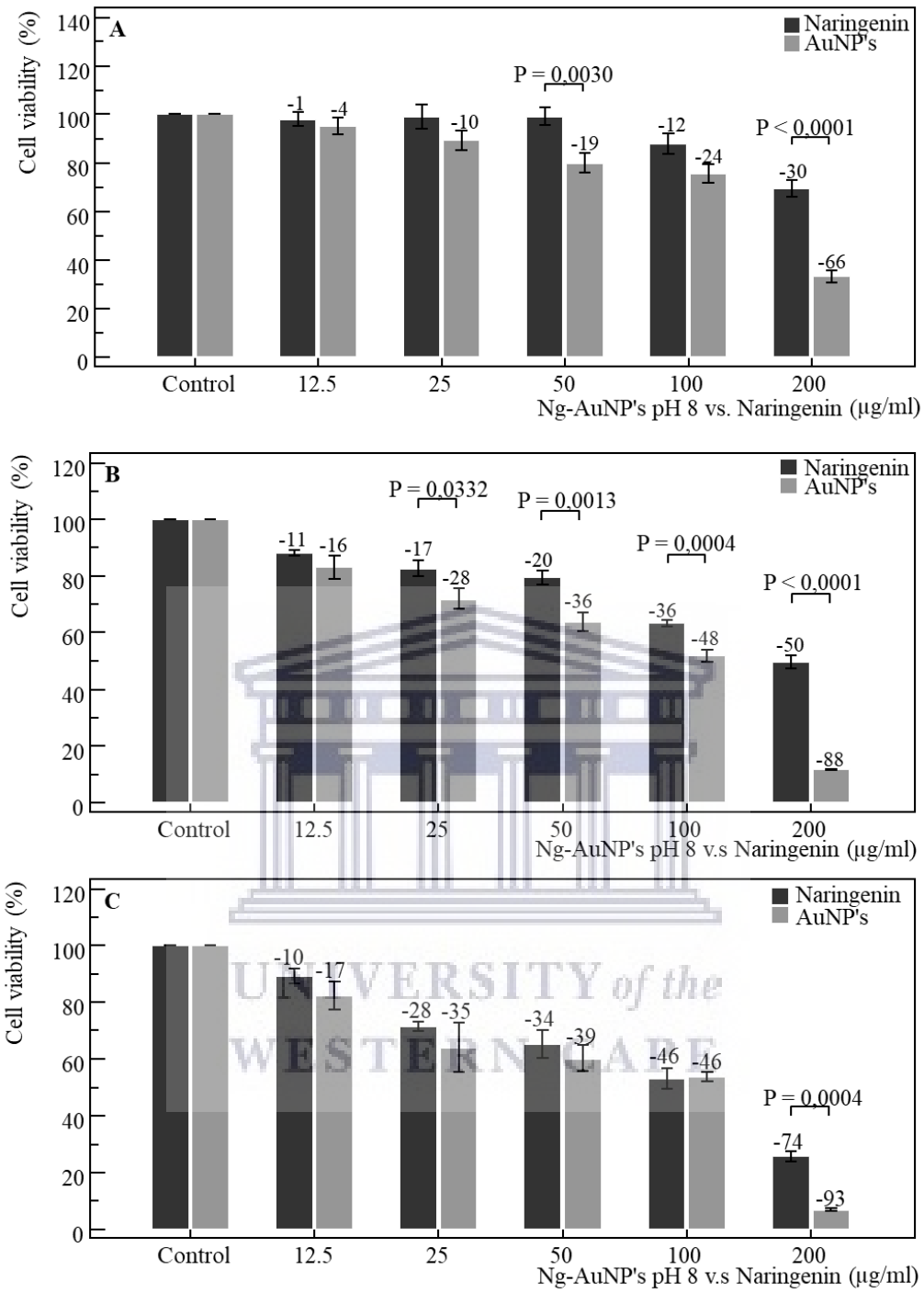

Figure 3.91: Panc1 cell viability as determined by the MTT assay over 24 (A), 48 (B) and 72 (C) hour exposure to naringenin and Ng-AuNP's pH 8 respectively. A significant (P<0.0001) difference was observed between naringenin and the AuNP's at 200 µg/ml over 24 hours, along with significant (P=0.0332, P=0.0013, P=0.0004, P<0.0001) differences observed at 25 µg/ml, 50 µg/ml, 100 µg/ml and 200 µg/ml, respectively, after 48 hours, and finally a significant (P=0.0004) difference was observed at 200 µg/ml following 72 hours of exposure.

3.2.4 HAEC cell viability

3.2.4.1 S1-AuNP's and extract

After being exposed to increasing concentrations of the S1 extract (A-F) and S1-AuNP's (G-L) over 24 hours, cell morphology was observed and recorded (Figure 3.92). Cells appeared increasingly sparely spaced between the control and 200 µg/ml of the extract (A-F), exhibiting progressive signs of stress between 25 µg/ml and 200 µg/ml (C-F). Similarly, cells were increasingly sparely spaced between the control and 200 µg/ml of the AuNP's (G-L), displaying cell rounding and increasing signs of cell stress at higher concentrations (J-L).

After being exposed to increasing concentrations of the S1 extract (A-F) and S1-AuNP's (G-L) over 48 hours, cell morphology was observed and recorded (Figure 3.93). Morphology remained unchanged up until 12.5 µg/ml of the extract, after which cells became progressively fewer between control and 200 µg/ml (A-F), exhibiting signs of cell stress (D-E) and cell death (F) at the higher concentrations. Likewise, cells appeared progressively sparely spaced between the control and 200 µg/ml of the AuNP's (G-L), appearing increasingly stressed between 25 µg/ml and 100 µg/ml (I-K), along with exhibiting signs of cell death at 200 µg/ml (L).

Post 72-hour exposure to S1 extract (A-F) and S1-AuNP's (G-L), cell morphology was observed and recorded (Figure 3.94). When treated with the extract, cell appeared progressively fewer and stressed between the control and 100 µg/ml (A-E), exhibiting signs indicative of cell death at 200 µg/ml (F). When treated with the AuNP's, cells appeared notably more sparely spaced between control and 200 µg/ml of the AuNP's, displaying increasingly notable signs of cell stress between 25 µg/ml and 100 µg/ml (I-K), along with cell death at 200 µg/ml (L).

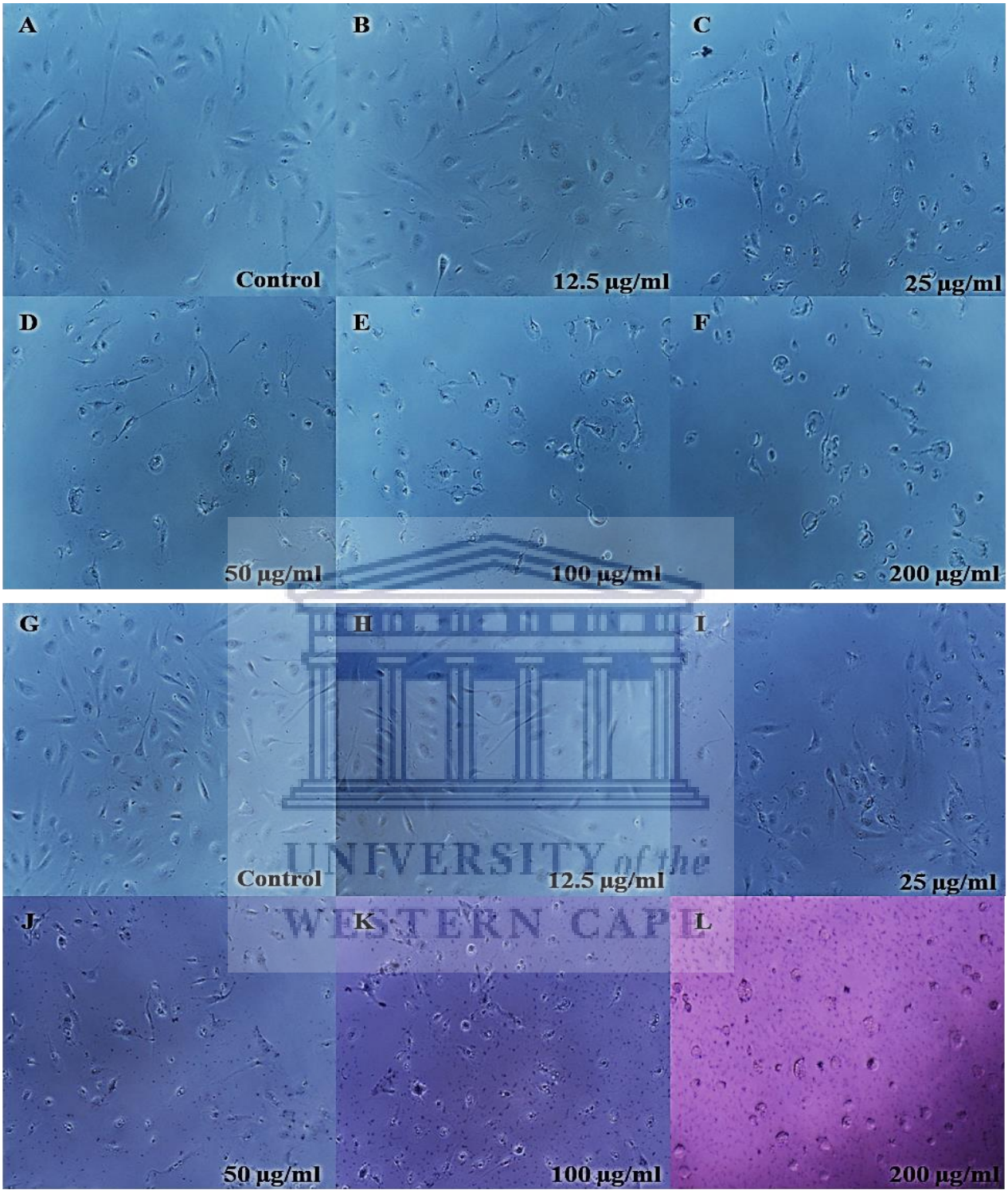

Figure 3.92: HAEC Cell morphology after being exposed to increasing concentrations of S1 extract and S1-AuNP's over a 24-hour period. The extract yielded signs of cell stress at higher concentrations (C-F). Similarly, the AuNP's exhibited indications of cell rounding and stress at higher concentrations (J-L).

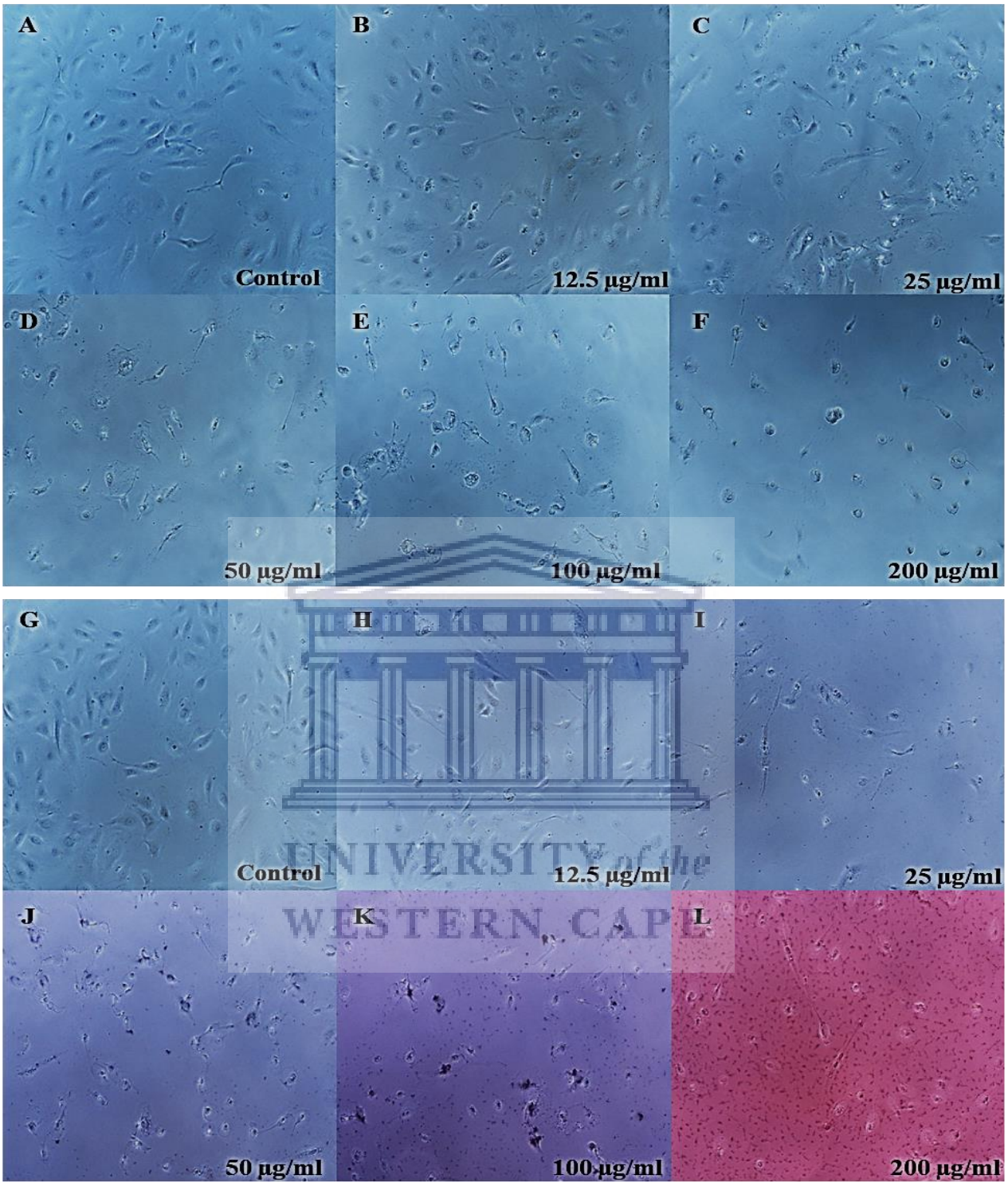

Figure 3.93: HAEC cell morphology after being exposed to increasing concentrations of S1 extract and S1-AuNP's over a 48-hour period. No morphological changes were observed between control and 12.5 µg/ml of the extract, with signs of stress (D-E) and death (F) at higher concentrations. The AuNP's exhibited decreases in the overall observed cell number (G-L), along with signs indicative of cell stress (I-K) and death (L) at higher concentrations.

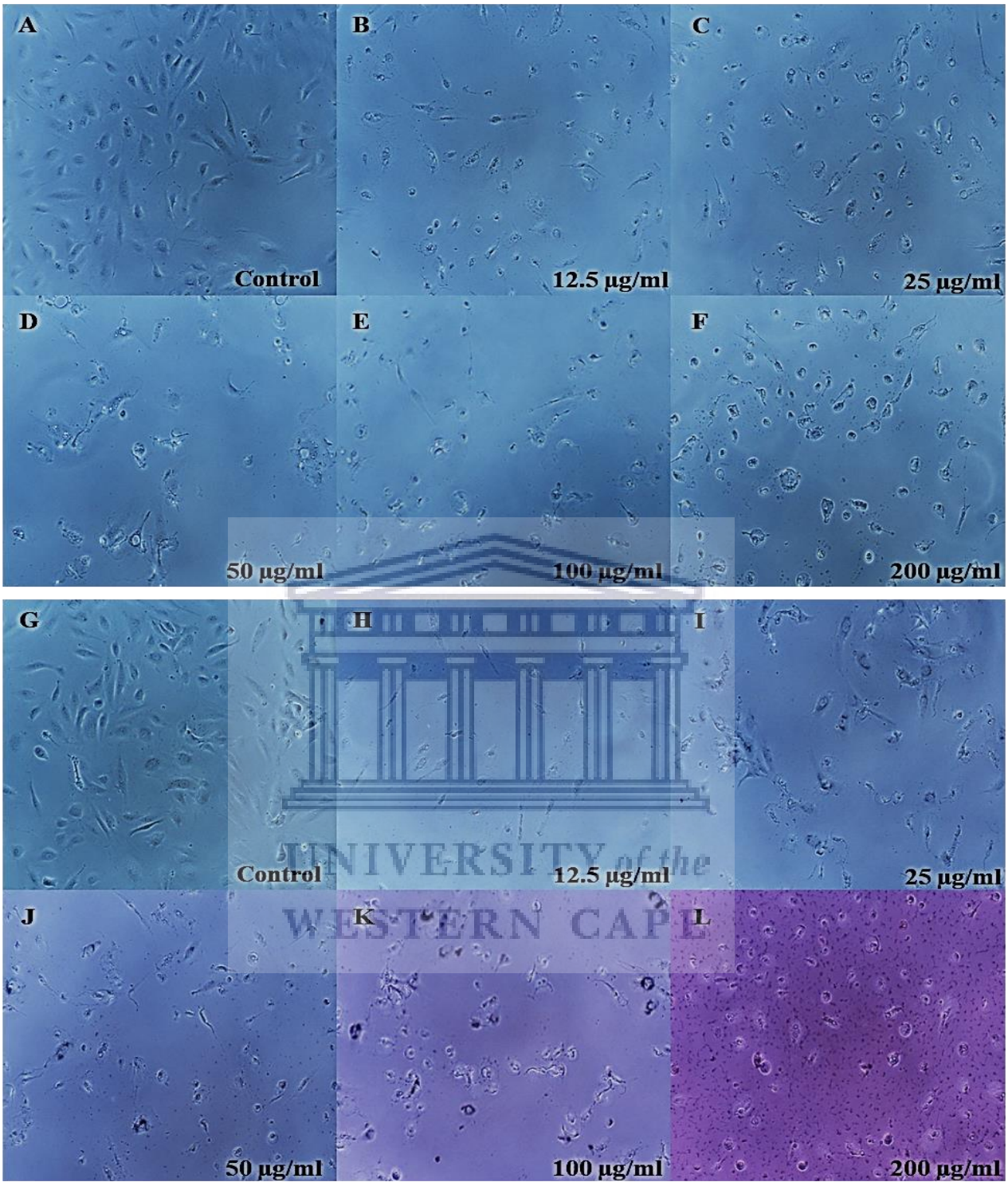

Figure 3.94: HAEC cell morphology after being exposed to increasing concentrations of S1 extract and S1-AuNP's over a 72-hour period. The progressively fewer, but stressed cells between the control and 100 µg/ml (A-E), along with cell death at the highest concentration (F). The AuNP's exhibited progressive decreases in observed cell number (G-L), with increasing signs of stress (I-K) and cell death (L) at the higher concentrations.

The MTT assay revealed dose-dependent effects at 24, 48 and 72-hour exposure periods, respectively. Following 24-hours of treatment (Figure 3.95 A) with the extract, cell viability was slightly elevated between the control and 25 µg/ml, after which a steady decrease in viability was observed from 25-200 µg/ml. The AuNP's exhibited progressive reductions in cell viability between the control and 200 µg/ml, differing significantly (P=0.0021, P=0.0067, P=0.0197) from the extract at 25 µg/ml, 50 µg/ml and 100 µg/ml, respectively. For the extract, the repeated measures ANOVA revealed a significant (P<0.0001) negative trend from control-200 µg/ml, along with AuNP's yielding a significant (P=0.0001) negative trend from control-200 µg/ml. One-way ANOVA yielded significant (P<0.001) trends from control-200 µg/ml following treatment with the extract and AuNP's, respectively.

Following 48-hours of exposure (Figure 3.95 B), both the extract and AuNP's yielded progressive decreases in cell viability from the control-200 µg/ml. The AuNP's yielded greater decreases in viability at each concentration, differing from the extract significantly (P=0.018, P=0.0004, P=0.0026, P=0.0001) at 12.5 µg/ml, 25 µg/ml, 50 µg/ml and 100 µg/ml. The repeated measures ANOVA revealed significant (P<0.0001) negative trends from control-200 µg/ml when exposed to the extract and AuNP's, respectively. Similarly, one-way ANOVA revealed significant (P<0.001) trends from control-200 µg/ml for both the extract and AuNP's,

After 72-hours (Figure 3.95 C) both the extract and AuNP's yielded progressive decreases in cell viability from the control-200 µg/ml, with AuNP's yielding greater decreases in viability from control-100 µg/ml, followed by the extract yielding slightly greater decreases at 200 µg/ml. Significant (P=0.0209, P=0.0013) differences between the extract and AuNP's were observed at 50 µg/ml and 100 µg/ml. The repeated measures ANOVA revealed significant (P<0.0001) negative trends from control-200 µg/ml when treated with the extract and AuNP's, respectively. Similarly, one-way ANOVA revealed significant (P<0.001) trends from control-200 µg/ml for both the extract and AuNP's, respectively.

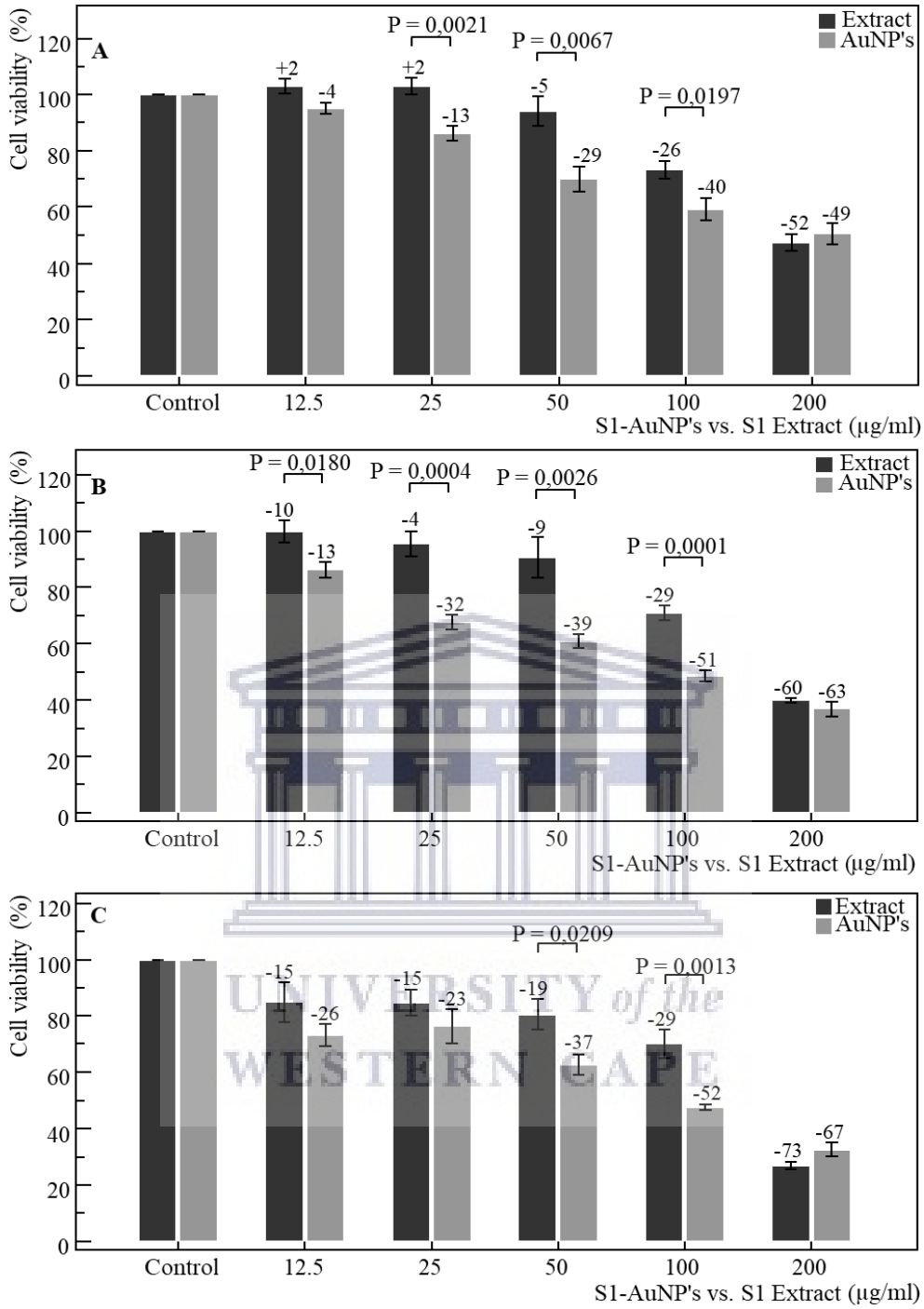

Figure 3.95: HAEC cell viability as determined by the MTT assay over 24 (A), 48 (B) and 72 (C) hour exposure to the S1 extract and S1-AuNP's respectively. Significant (P=0.0021, P=0.0067, P=0.0197) differences were observed between the extract and AuNP's at 25 µg/ml, 50 µg/ml and 100 µg/ml, over 24 hours, along with significant (P=0.018, P=0.0004, P=0.0026, P=0.0001) differences observed at 12.5 µg/ml, 25 µg/ml, 50 µg/ml and 100 µg/ml after 48 hours, and finally significant (P=0.0209, P=0.0013) differences from 50-100 µg/ml after 72 hours of exposure.

3.2.4.2 S1x2-AuNP's and extract

After being exposed to increasing concentrations of the S1 extract (A-F) and S1x2-AuNP's (G-L) over 24 hours, cell morphology was observed and recorded (Figure 3.96). Cells appeared increasingly sparely spaced between the control and 200 µg/ml of the extract (A-F), exhibiting progressive signs of stress between 25 µg/ml and 200 µg/ml (C-F). Similarly, cells were slightly, but increasingly sparely spaced between the control and 200 µg/ml of the AuNP's (G-L), displaying some cell rounding and signs of cell stress at higher concentrations (J-L).

After being exposed to increasing concentrations of the S1 extract (A-F) and S1x2-AuNP's (G-L) over 48 hours, cell morphology was observed and recorded (Figure 3.97). Morphology remained unchanged up until 12.5 µg/ml of the extract, after which cells became progressively fewer between control and 200 µg/ml (A-F), exhibiting signs of cell stress (D-E) and cell death (F) at the higher concentrations. Likewise, cells appeared progressively sparely spaced between the control and 200 µg/ml of the AuNP's (G-L), appearing stressed between 12.5 µg/ml and 200 µg/ml (I-L).

Post 72-hour exposure to S1 extract (A-F) and S1x2-AuNP's (G-L), cell morphology was observed and recorded (Figure 3.98). When treated with the extract, cell appeared progressively fewer and stressed between the control and 100 µg/ml (A-E), exhibiting signs indicative of cell death at 200 µg/ml (F). When treated with the AuNP's, cells appeared progressively more sparely spaced between control and 200 µg/ml of the AuNP's, displaying notable signs of cell stress between 12.5 µg/ml and 200 µg/ml (I-L).

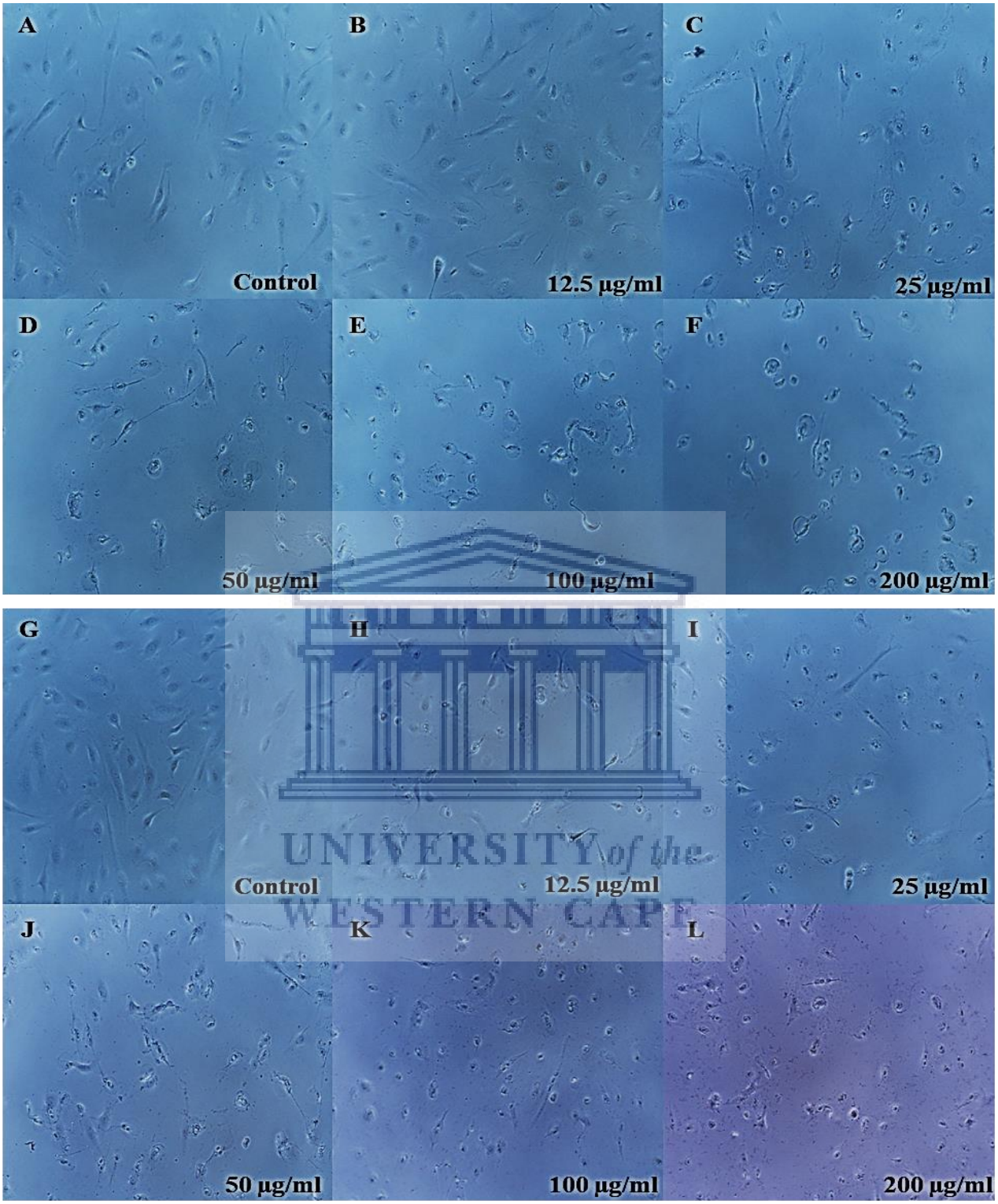

Figure 3.96: HAEC Cell morphology after being exposed to increasing concentrations of S1 extract and S1x2-AuNP's over a 24-hour period. The extract yielded signs of cell stress at higher concentrations (C-F). Similarly, the AuNP's exhibited indications of cell rounding and stress at higher concentrations (J-L).

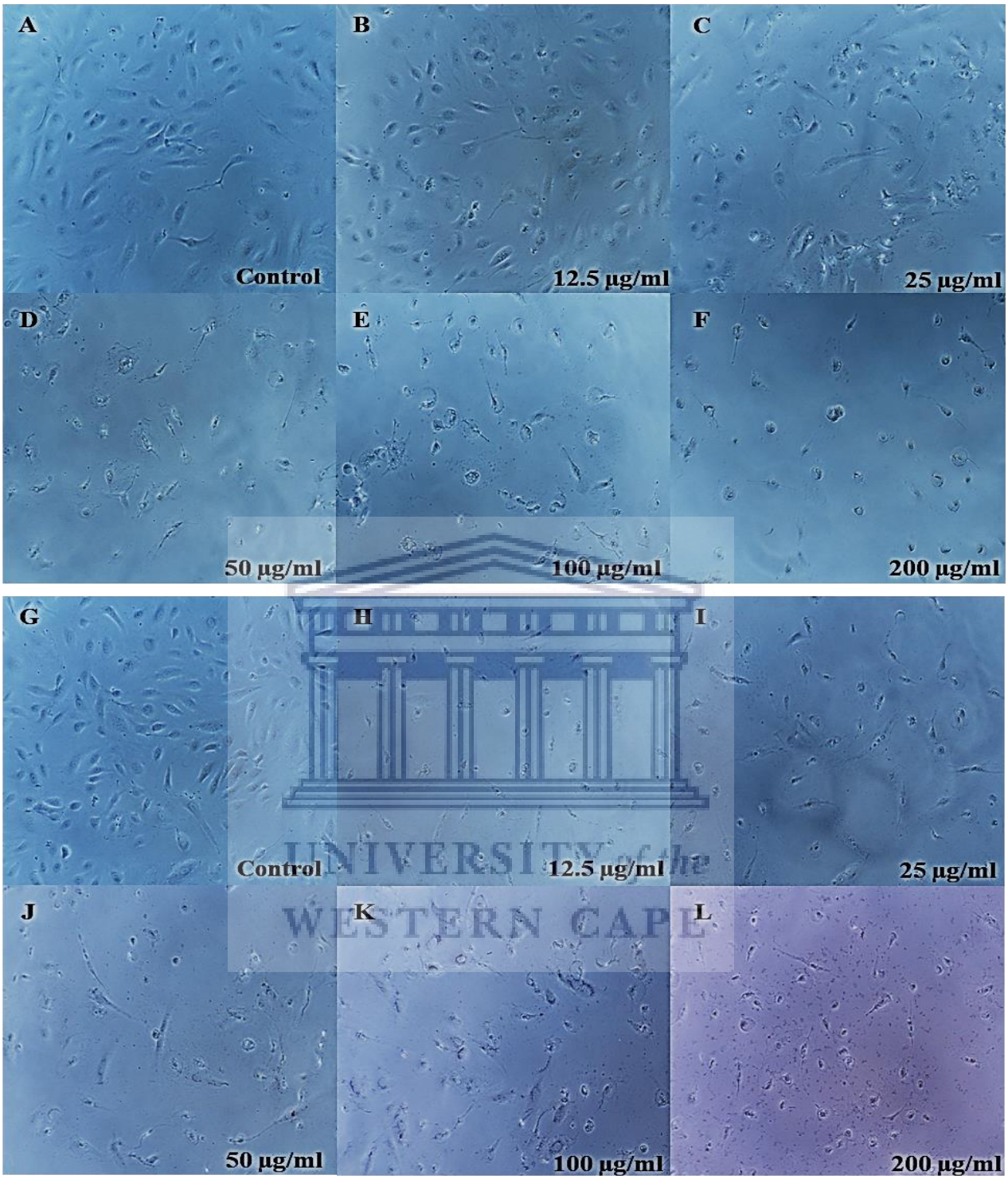

Figure 3.97: HAEC cell morphology after being exposed to increasing concentrations of S1 extract and S1x2-AuNP's over a 48-hour period. No morphological changes were observed between control and 12.5 µg/ml of the extract, with signs of stress (D-E) and death (F) at higher concentrations. The AuNP's exhibited decreases in the overall observed cell number (G-L), along with signs indicative of cell stress between 12.5 µg/ml and 200 µg/ml (I-L).

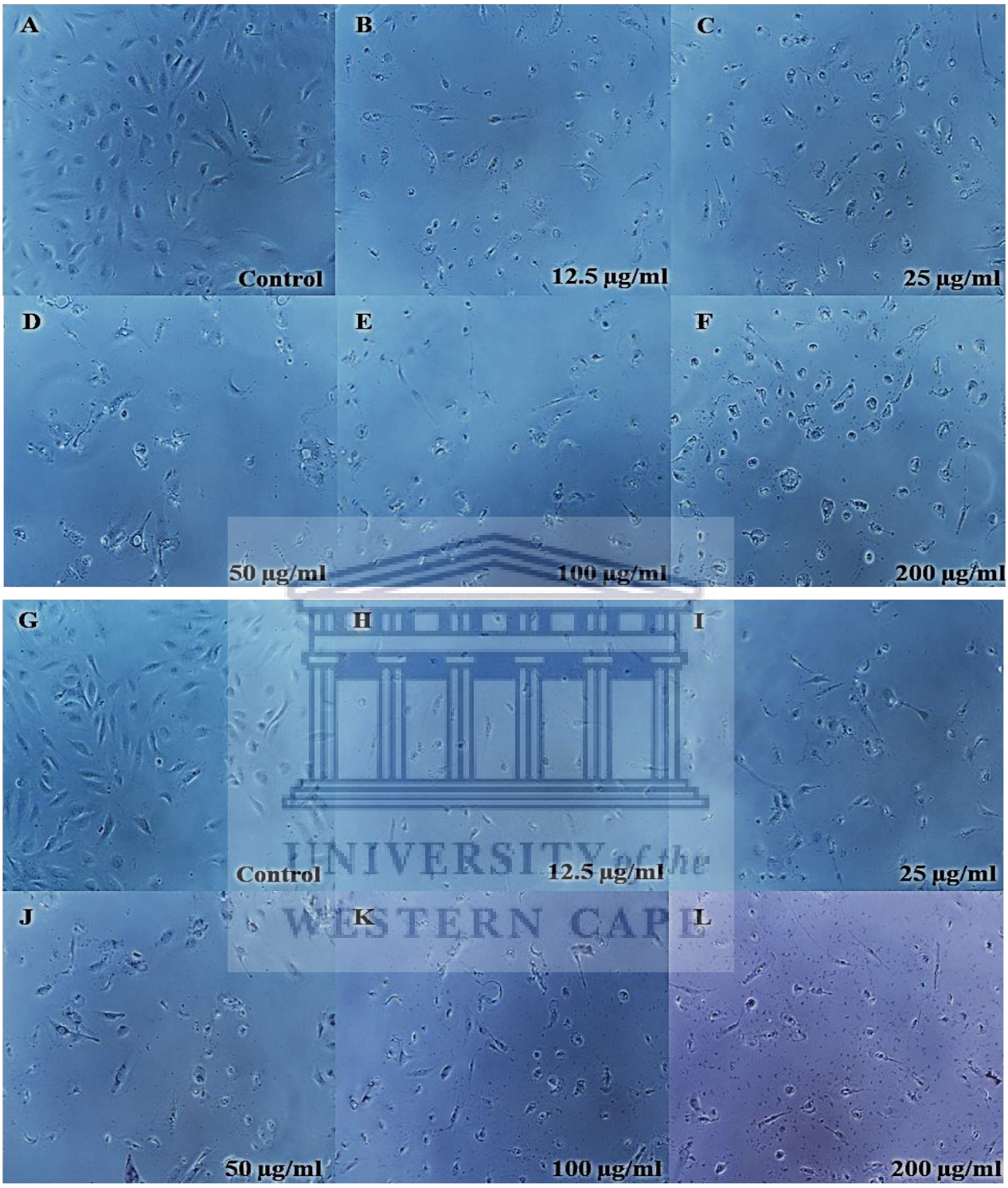

Figure 3.98: HAEC cell morphology after being exposed to increasing concentrations of S1 extract and S1x2-AuNP's over a 72-hour period. The progressively fewer, but stressed cells between the control and 100 µg/ml (A-E), along with cell death at the highest concentration (F). The AuNP's exhibited progressive decreases in observed cell number (G-L), with increasing signs of stress between 12.5 µg/ml and 200 µg/ml (I-L).

The MTT assay revealed dose-dependent effects at 24, 48 and 72-hour exposure periods, respectively. Following 24-hours of treatment with the extract (Figure 3.99 A), cell viability was slightly elevated between the control and 25 µg/ml, after which a steady decrease in viability was observed from 25-200 µg/ml. The AuNP's yielded progressive reductions in cell viability between the control and 200 µg/ml, differing significantly (P=0.0104, P=0.0082, P=0.0001) from the extract at 12.5 µg/ml, 25 µg/ml and 200 µg/ml, respectively. For the extract, the repeated measures ANOVA revealed a significant (P<0.0001) negative trend from control-200 µg/ml, along with AuNP's yielding a significant (P=0.0011) negative trend from control-200 µg/ml. One-way ANOVA yielded significant (P<0.001) trends from control-200 µg/ml following treatment with the extract and AuNP's, respectively.

Following 48-hours of exposure (Figure 3.99 B), both the extract and AuNP's yielded progressive decreases in cell viability from the control-200 µg/ml. The AuNP's yielded greater decreases in viability from 12.5-50 µg/ml, followed by the extract yielding greater decreases at 200 µg/ml. significant (P=0.0182, P=0.0119, P=0.0233) differences between the extract and AuNP's were observed at 12.5 µg/ml, 25 µg/ml and 200 µg/ml. The repeated measures ANOVA revealed significant (P<0.0001, P=0.0008) negative trends from control-200 µg/ml for the extract and AuNP's, respectively. Similarly, one-way ANOVA revealed significant (P<0.001) trends from control-200 µg/ml for both the extract and AuNP's,

After 72-hours (Figure 3.99 C) both the extract and AuNP's yielded progressive, but fairly comparable decreases in cell viability from the control-100 µg/ml. At 200 µg/ml, the extract yielded a greater decrease in viability, differing significantly (P=0.0041) from the extract. The repeated measures ANOVA revealed significant (P<0.0001, P=0.0007) negative trends from control-200 µg/ml when treated with the extract and AuNP's, respectively. Similarly, one-way ANOVA revealed significant (P<0.001) trends from control-200 µg/ml for both the extract and AuNP's, respectively.

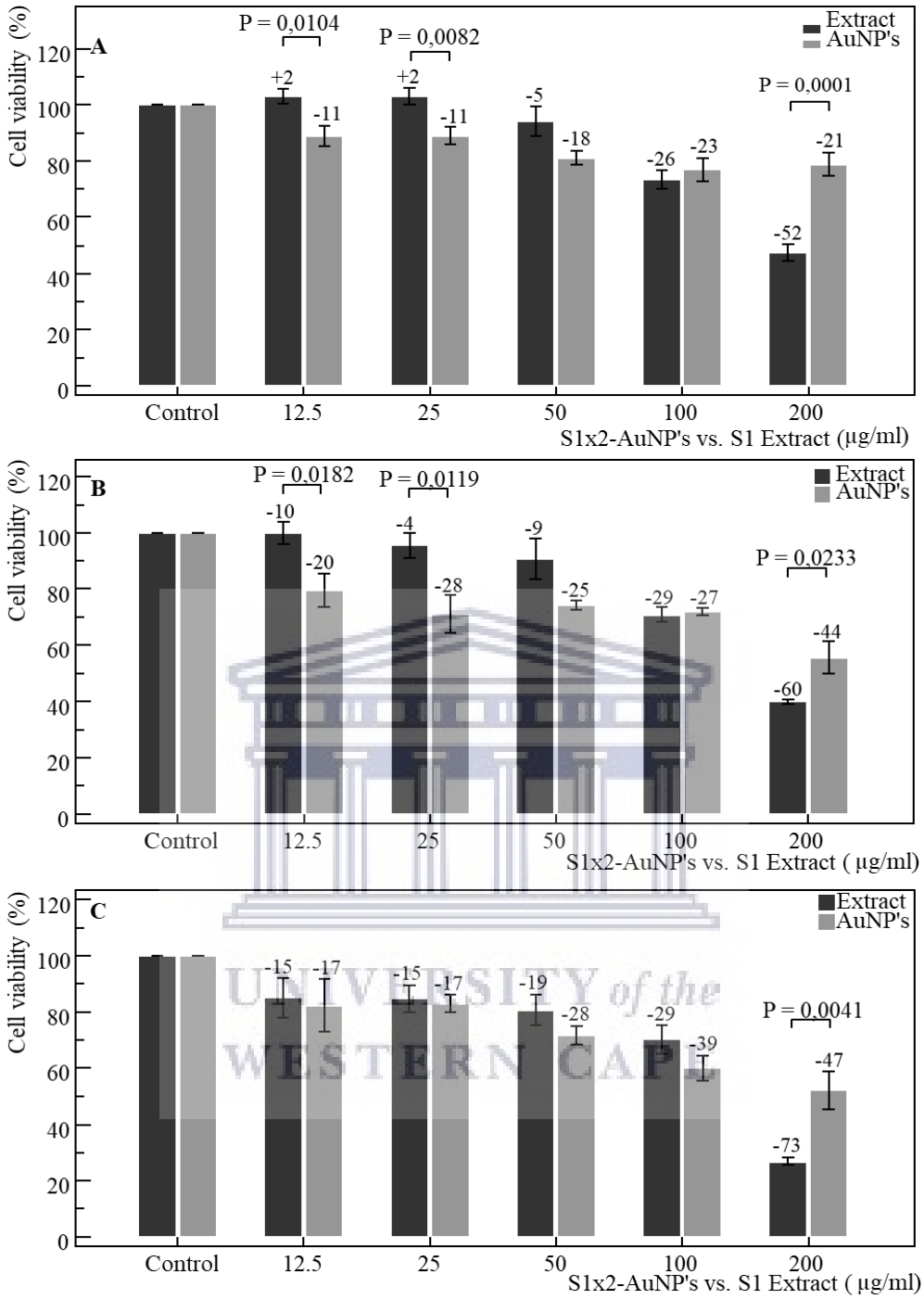

Figure 3.99: HAEC cell viability as determined by the MTT assay over 24 (A), 48 (B) and 72 (C) hour exposure to the S1 extract and S1x2-AuNP's respectively. Significant (P=0.0104, P=0.0082, P=0.0001) differences were observed between the extract and AuNP's at 12.5 µg/ml, 25 µg/ml and 200 µg/ml, over 24 hours, along with significant (P=0.0182, P=0.0119, P=0.0233) differences observed at 12.5 µg/ml, 25 µg/ml and 200 µg/ml, respectively, after 48 hours. Following 72 hours of exposure, a significant (P=0.0041) difference was only observed at 200 µg/ml.

3.2.4.3 S2-AuNP's and S2 extract

After being exposed to increasing concentrations of the S2 extract (A-F) and S2-AuNP's (G-L) over 24 hours, cell morphology was observed and recorded (Figure 3.100). Cells appeared progressively fewer and atypically rounded between the control and 200 µg/ml of the extract (A-F), exhibiting increasing signs of stress (C-E), and signs consistent with cell death at 200 µg/ml (F). Similarly, cells appeared increasingly sparely spaced and rounded between the control and 200 µg/ml of the AuNP's (G-L), displaying signs indicative of cell stress between 25 µg/ml and 200 µg/ml (I-L).

After being exposed to increasing concentrations of the S2 extract (A-F) and S2-AuNP's (G-L) over 48 hours, cell morphology was observed and recorded (Figure 3.101). Increasingly fewer cells were observed between control and 200 µg/ml the extract (A-F), along with evidence of cell stress between 12.5 µg/ml and 50 µg/ml (B-D), and signs indicative of cell death at higher concentrations (E-F). Likewise, cells appeared progressively sparely spaced between the control and 200 µg/ml of the AuNP's (G-L), appearing stressed between 12.5 µg/ml and 50 µg/ml (H-J), and exhibiting signs of death at higher concentrations (K-L).

Post 72-hour exposure to S2 extract (A-F) and S2-AuNP's (G-L), cell morphology was observed and recorded (Figure 3.102). Cells appeared increasingly fewer between the control and 200 µg/ml of the extract (A-F), exhibiting signs indicative of cell stress (B-D) and cell death at 200 µg/ml (F). When treated with the AuNP's, cells appeared notably more sparely spaced between control and 200 µg/ml of the AuNP's, displaying signs of cell stress between 12.5 µg/ml and 50 µg/ml (H-J), followed by cell death at higher concentrations (K-L).

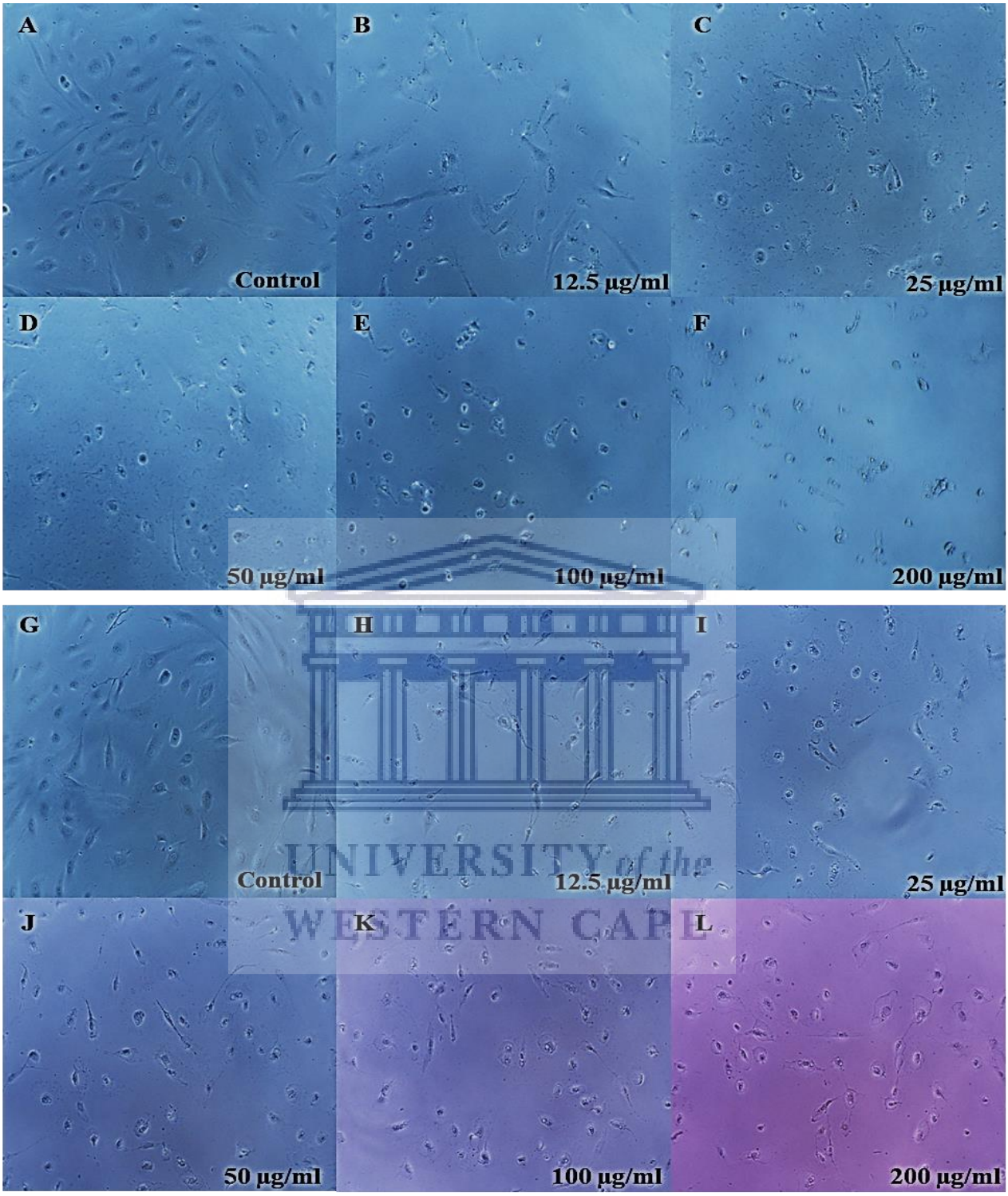

Figure 3.100: HAEC Cell morphology after being exposed to increasing concentrations of S2 extract and S2-AuNP's over a 24-hour period. The extract (C-F) yielded signs of cell stress (C-E) and signs of death (F) at higher concentrations. Similarly, the AuNP's (G-L) exhibited indications of cell rounding and stress at higher concentrations (I-L).

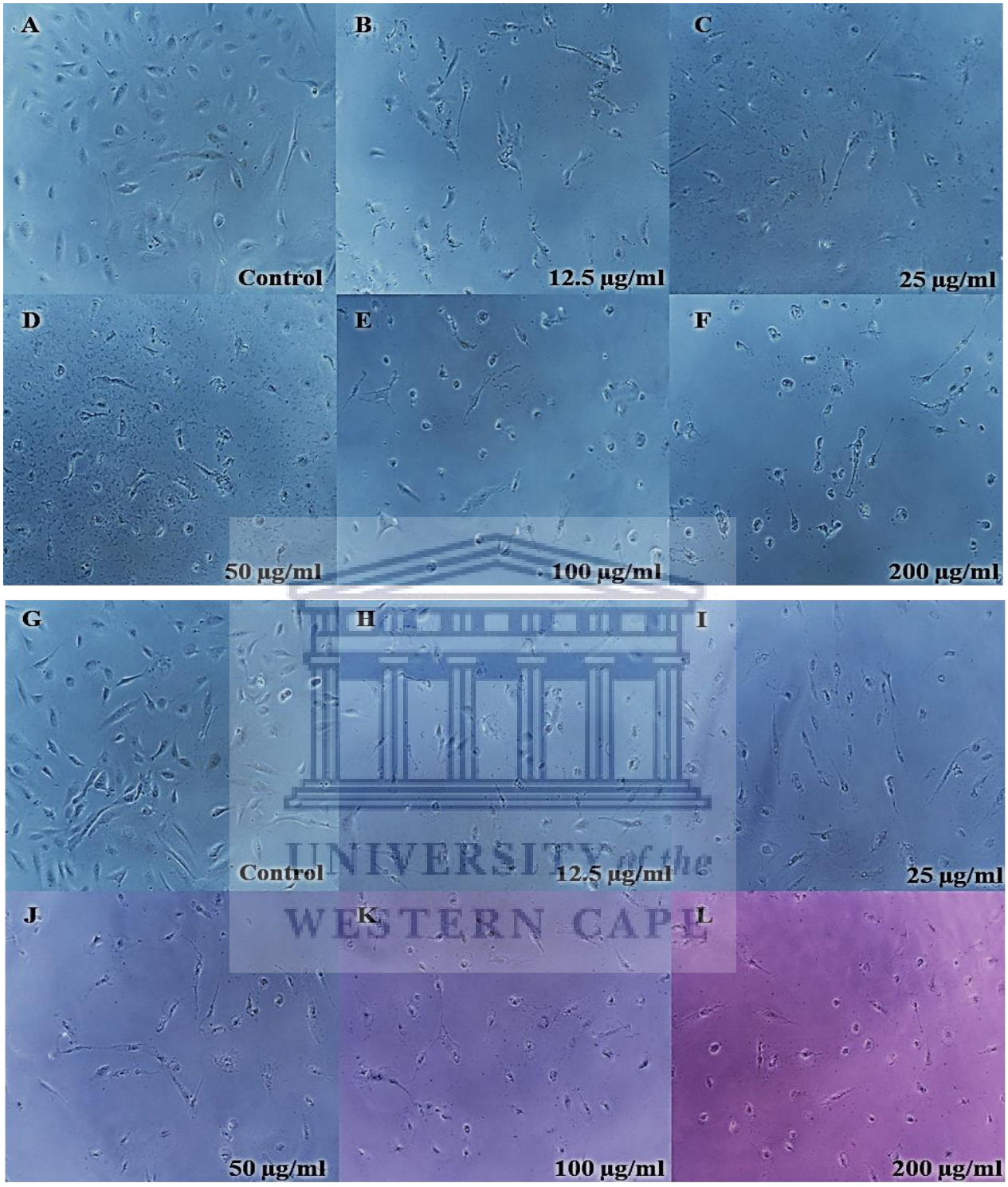

Figure 3.101: HAEC cell morphology after being exposed to increasing concentrations of S2 extract and S2-AuNP's over a 48-hour period. Increasingly fewer cells were evident between control and 12.5 µg/ml of the extract, with signs of stress (B-D) and death (E-F) at higher concentrations. The AuNP's exhibited decreases in the overall observed cell number (G-L), along with cell stress (H-J) and cell death (K-L) at higher concentrations.

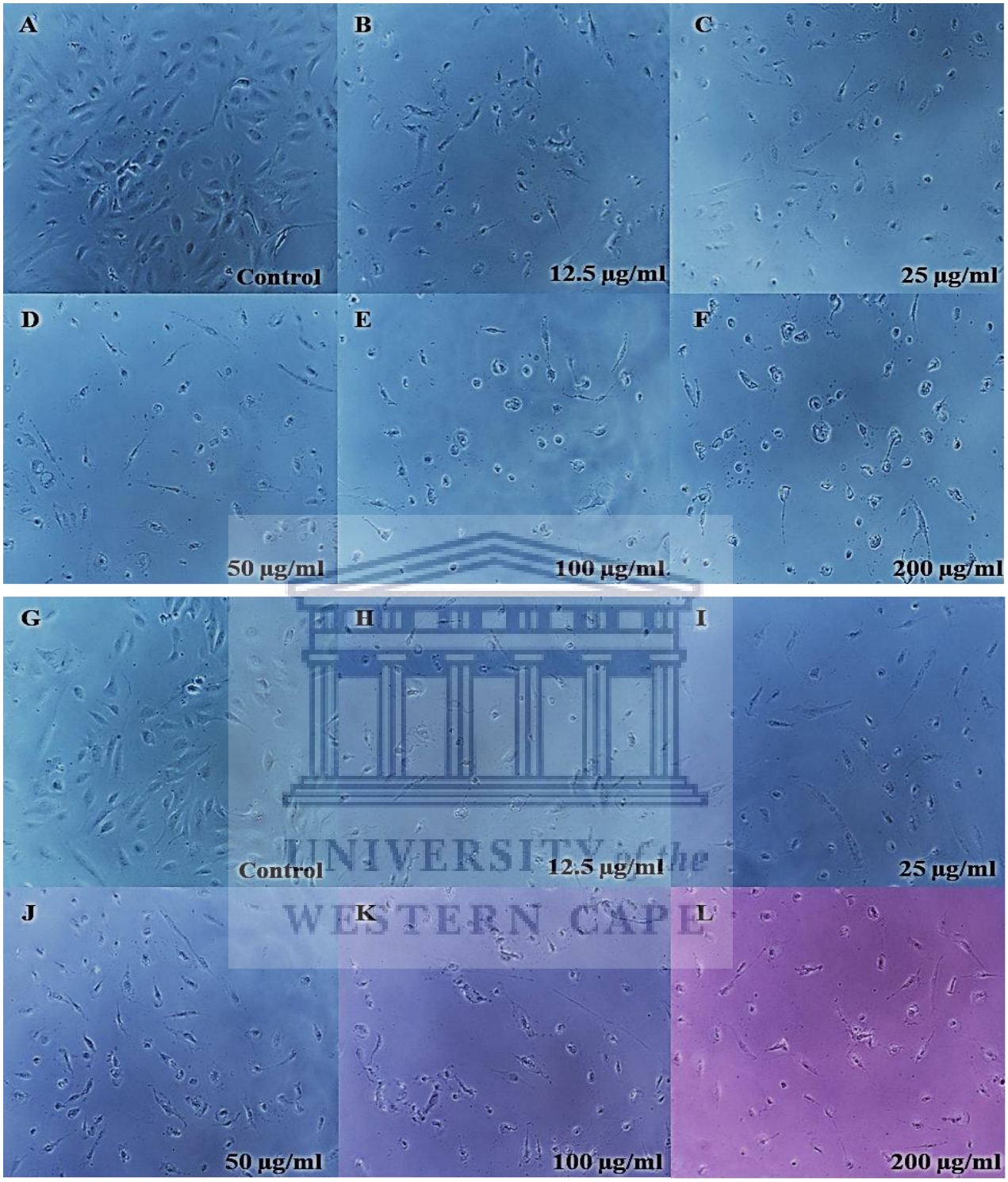

Figure 3.102: HAEC cell morphology after being exposed to increasing concentrations of S2 extract and S2-AuNP's over a 48-hour period. Progressively fewer cells were observed between the control and 12.5 µg/ml of the extract, with signs of stress (B-D) and death (E-F) at higher concentrations. Similarly, the AuNP's exhibited decreases in the observed cell number (G-L), along with signs of cell stress (H-J) and cell death at higher concentrations (K-L).

The MTT assay revealed dose-dependent effects at 24, 48 and 72-hour exposure periods, respectively. Following 24-hours of treatment (Figure 3.103 A), both the extract and AuNP's yielded dose-dependent decreases in cell viability from control-200 µg/ml, with more notable decreases in viability observed at 100-200 µg/ml. The extract yielded greater decreases in viability that differed from the AuNP's significantly (P=0.0091, P=0.0372) at 100 µg/ml and 200 µg/ml, respectively. The repeated measures ANOVA revealed significant (P<0.0001) negative trends from control-200 µg/ml for both the extract and AuNP's, respectively. Similarly, one-way ANOVA yielded significant (P<0.001) trends from control-200 µg/ml following treatment with the extract and AuNP's, respectively.

Following 48-hours of exposure (Figure 3.103 B), both the extract and AuNP's yielded progressive decreases in cell viability from the control-200 µg/ml, with notably sharp drops in cell viability between 100 µg/ml and 200 µg/ml. The extract yielded greater decreases in cell viability, differing significantly (P=0.0023, P=0.0061) from the AuNP's at 100 µg/ml and 200 µg/ml. The repeated measures ANOVA revealed significant (P<0.0001) negative trends from control-200 µg/ml for both the extract and AuNP's, respectively. Similarly, one-way ANOVA revealed significant (P<0.001) trends from control-200 µg/ml for both the extract and AuNP's,

After 72-hours (Figure 3.103 C) both the extract and AuNP's yielded progressive, fairly comparable decreases in cell viability from the control-50 µg/ml. Between 100 µg/ml and 200 µg/ml, the extract yielded greater decreases in viability, differing significantly (P=0.0002) from the AuNP's at 200 µg/ml. The repeated measures ANOVA revealed significant (P<0.0001) negative trends from control-200 µg/ml when treated with the extract and AuNP's, respectively. Similarly, one-way ANOVA revealed significant (P<0.001) trends from control-200 µg/ml for both the extract and AuNP's, respectively.

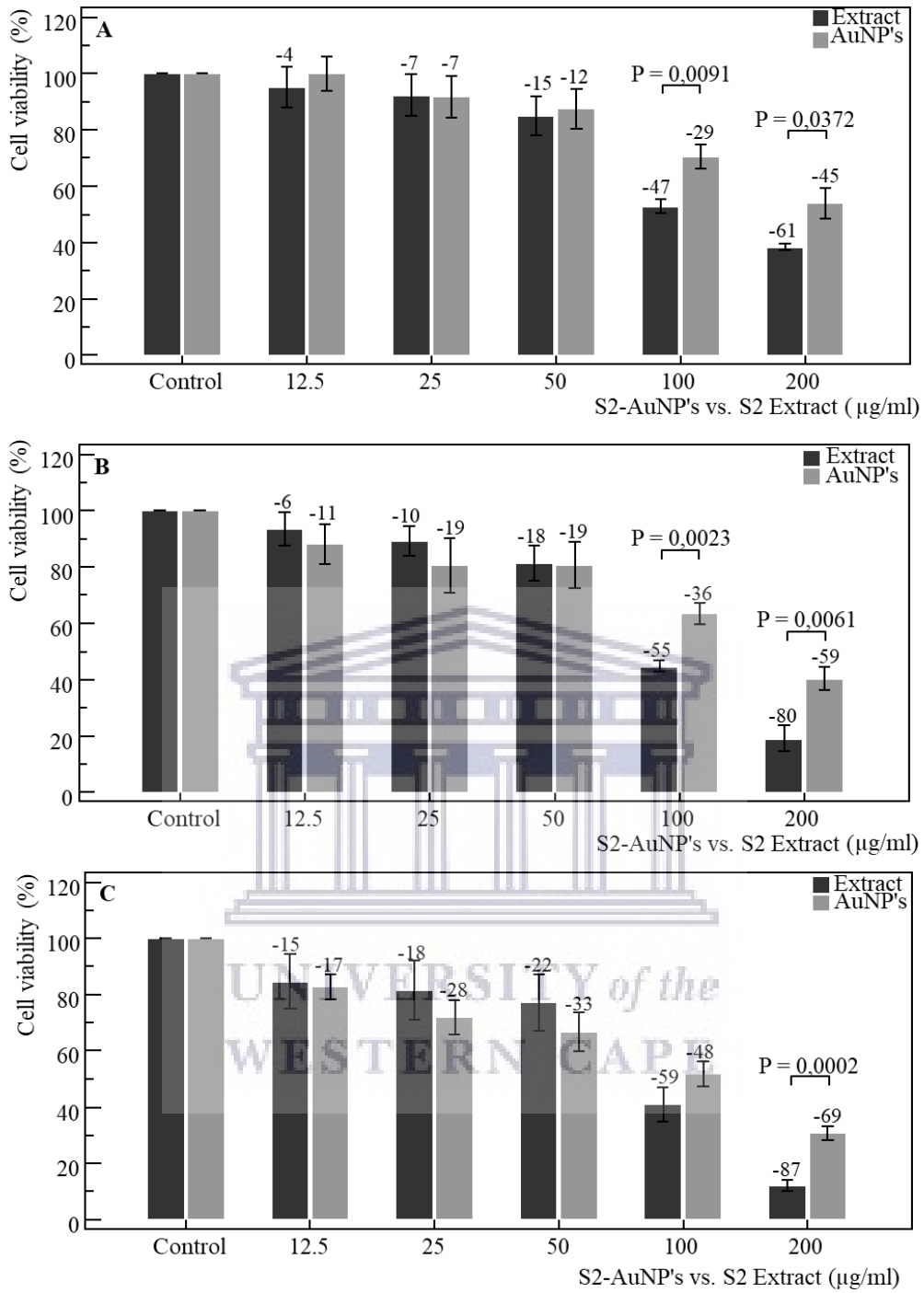

Figure 3.103: HAEC cell viability as determined by the MTT assay over 24 (A), 48 (B) and 72 (C) hour exposure to the S2 extract and S2-AuNP's respectively. Significant (P=0.0091, P=0.0372) differences were observed between the extract and AuNP's at 100 µg/ml and 200 µg/ml, over 24 hours, along with significant (P=0.0023, P=0.0061) differences observed at 100 µg/ml and 200 µg/ml, respectively, after 48 hours. Following 72 hours of exposure, a significant (P=0.0002) difference between the extract and AuNP's was only observed at 200 µg/ml.

3.2.4.4 S2x2-AuNP's and S2 extract

After being exposed to increasing concentrations of the S2 extract (A-F) and S2x2-AuNP's (G-L) over 24 hours, cell morphology was observed and recorded (Figure 3.104). Cells appeared progressively fewer and atypically rounded between the control and 200 µg/ml of the extract (A-F), exhibiting increasing signs of stress (C-E), and signs consistent with cell death at 200 µg/ml (F). Similarly, cells appeared increasingly sparely spaced and atypically rounded between the control and 200 µg/ml of the AuNP's (G-L), displaying signs indicative of cell stress between 12.5 µg/ml and 200 µg/ml (H-L).

After being exposed to increasing concentrations of the S2 extract (A-F) and S2x2-AuNP's (G-L) over 48 hours, cell morphology was observed and recorded (Figure 3.105). Increasingly fewer cells were observed between control and 200 µg/ml the extract (A-F), along with evidence of cell stress between 12.5 µg/ml and 50 µg/ml (B-D), and signs indicative of cell death at higher concentrations (E-F). Likewise, cells appeared progressively, and notably sparely spaced between the control and 200 µg/ml of the AuNP's (G-L), displaying signs indicative of cell stress between 12.5 µg/ml and 200 µg/ml (H-L).

Post 72-hour exposure to S2 extract (A-F) and S2-AuNP's (G-L), cell morphology was observed and recorded (Figure 3.106). Cells appeared increasingly fewer between the control and 200 µg/ml of the extract (A-F), exhibiting signs indicative of cell stress (B-D) and cell death at 200 µg/ml (F). When treated with the AuNP's, cells appeared notably more sparely spaced between control and 200 µg/ml of the AuNP's, and displayed signs of cell stress between 12.5 µg/ml and 50 µg/ml (H-J).

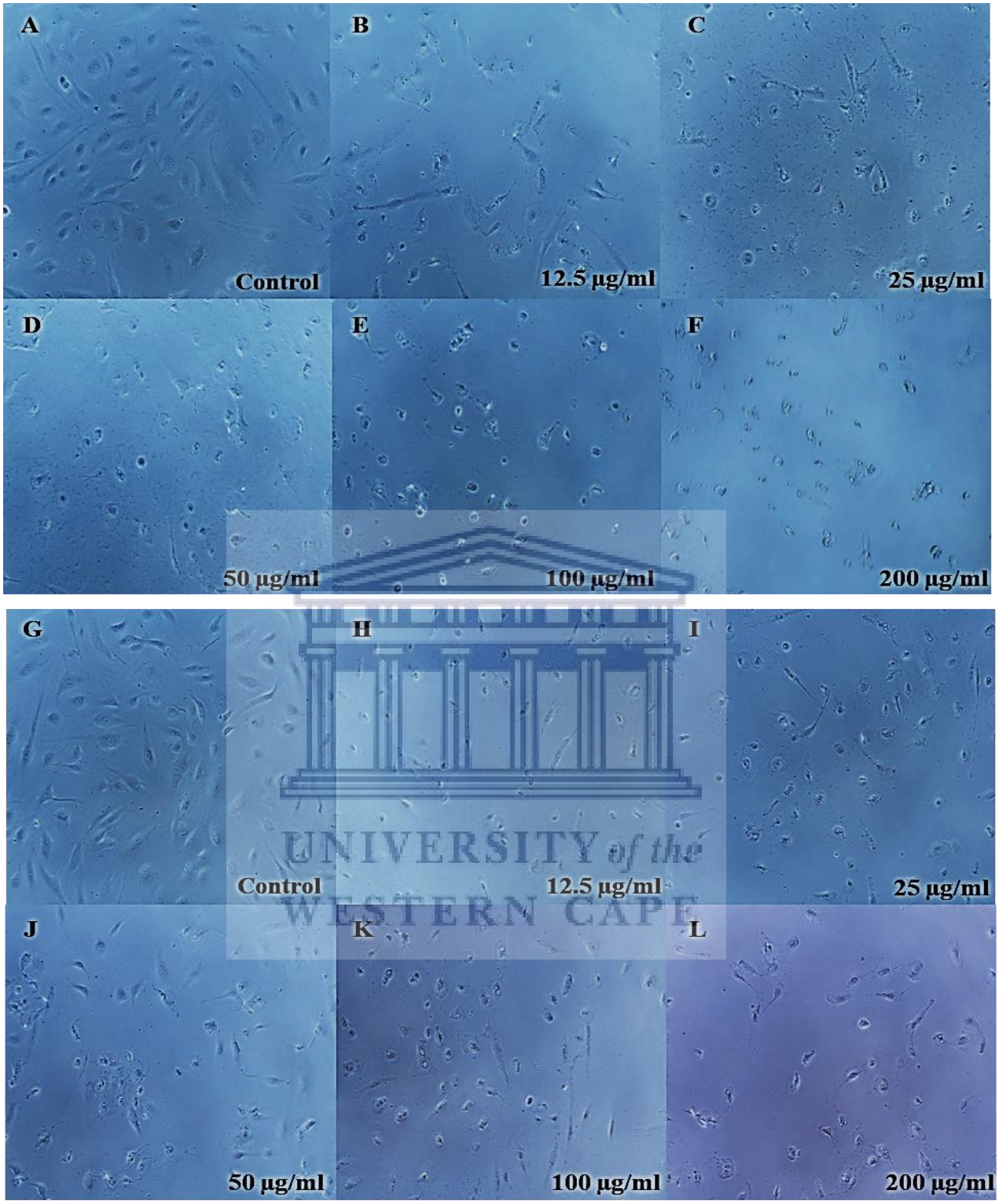

Figure 3.104: HAEC Cell morphology after being exposed to increasing concentrations of S2 extract and S2-AuNP's over a 24-hour period. The extract (C-F) yielded signs of cell stress (C-E) and signs of death (F) at higher concentrations. Similarly, the AuNP's (G-L) exhibited indications of cell rounding and stress at higher concentrations (H-L).

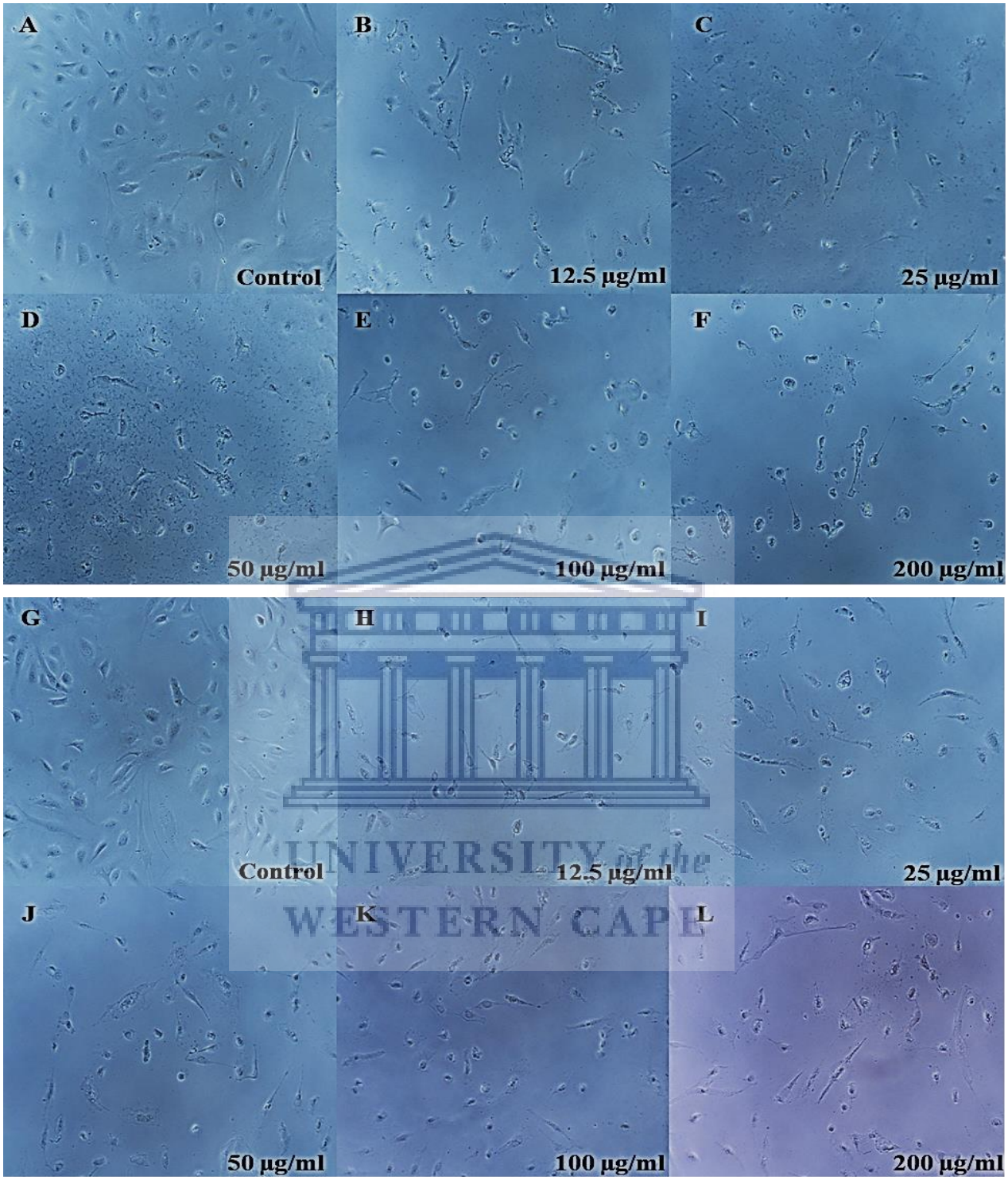

Figure 3.105: HAEC cell morphology after being exposed to increasing concentrations of S2 extract and S2-AuNP's over a 48-hour period. Increasingly fewer cells were evident between control and 12.5 µg/ml of the extract, with signs of stress (B-D) and death (E-F) at higher concentrations. The AuNP's exhibited notable decreases in the overall observed cell number (G-L), along with cell stress between 12.5 µg/ml and 200 µg/ml (H-J).

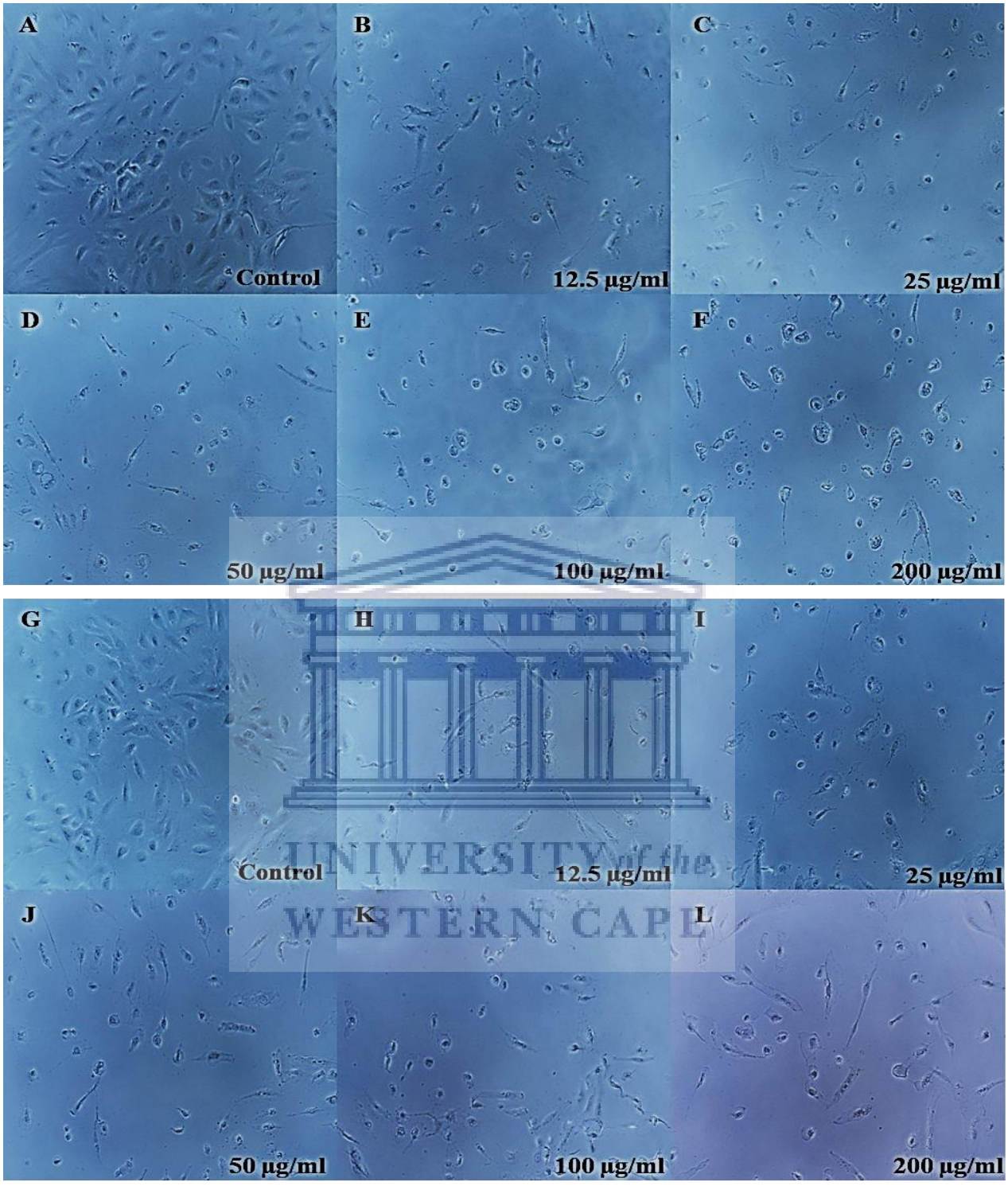

Figure 3.106: HAEC cell morphology after being exposed to increasing concentrations of S2 extract and S2-AuNP's over a 48-hour period. Progressively fewer cells were observed between the control and 12.5 µg/ml of the extract, with signs of stress (B-D) and death (E-F) at higher concentrations. Similarly, the AuNP's exhibited decreases in the observed cell number (G-L), along with signs of cell stress between 12.5 µg/ml and 200 µg/ml (H-J).

The MTT assay revealed dose-dependent effects at 24, 48 and 72-hour exposure periods, respectively. Following 24-hours of treatment (Figure 3.107 A), both the extract and AuNP's yielded decreases in cell viability from control-200 µg/ml, with the AuNP's yielding greater decreases from control-50 µg/ml, followed by the extract yielding greater decreases from 50-200 µg/ml. The extract differed from the AuNP's significantly (P=0.0004, P=0.0002) at 100 µg/l and 200 µg/ml, respectively. The repeated measures ANOVA revealed significant (P<0.0001, P=0.0231) negative trends from control-200 µg/ml for the extract and AuNP's, respectively. Similarly, one-way ANOVA yielded significant (P<0.001, P=0.003) trends from control-200 µg/ml following treatment with the extract and AuNP's, respectively.

Following 48-hours of exposure (Figure 3.107 B) both the extract and AuNP's yielded progressive decreases in cell viability from control-200 µg/ml, with the AuNP's yielding greater decreases from control-50 µg/ml, followed by the extract yielding greater decreases from 50-200 µg/ml. Significant (P=0.0003, P=0.0001) differences between the extract and the AuNP's were observed at 100 µg/ml and 200 µg/ml, respectively. The repeated measures ANOVA revealed significant (P<0.0001, P=0.0136) negative trends from control-200 µg/ml for the extract and AuNP's, respectively. Similarly, one-way ANOVA revealed significant (P<0.001, P=0.008) trends from control-200 µg/ml for the extract and AuNP's, respectively.

After 72-hours (Figure 3.107 C) both the extract and AuNP's yielded progressive decreases in cell viability from the control-200 µg/ml. The extract yielded greater decreases in viability at each concentration, differing significantly (P=0.0071, P=0.0031) from the AuNP's at 100 µg/ml and 200 µg/ml, respectively. The repeated measures ANOVA revealed significant (P<0.0001, P=0.0263) negative trends from control-200 µg/ml when treated with the extract and AuNP's, respectively. Similarly, one-way ANOVA revealed significant (P<0.001, P=0.064) trends from control-200 µg/ml for both the extract and AuNP's, respectively.

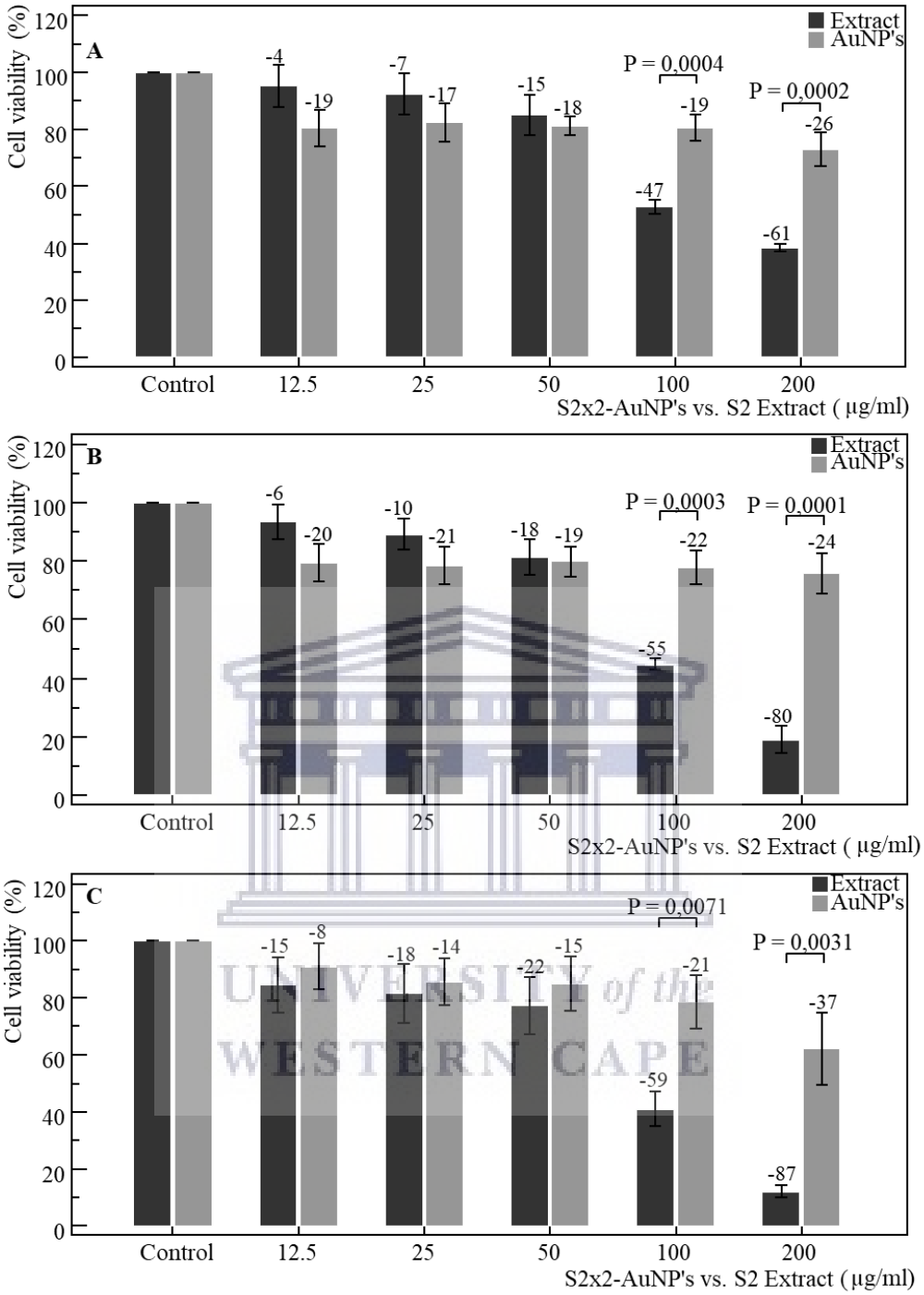

Figure 3.107: HAEC cell viability as determined by the MTT assay over 24 (A), 48 (B) and 72 (C) hour exposure to the S2 extract and S2x2-AuNP's respectively. Significant (P=0.0004, P=0.0002) differences were observed between the extract and AuNP's at 100 µg/ml and 200 µg/ml, over 24 hours, along with significant (P=0.0003, P=0.0001) differences observed at 100 µg/ml and 200 µg/ml, respectively, after 48 hours. Following 72 hours of exposure, a significant (P=0.0071, P=0.0031) differences were observed between the extract and AuNP's at 100 µg/ml and 200 µg/ml.

3.2.4.5 Ng-AuNP's pH 7 and naringenin

After being exposed to increasing concentrations of the naringenin (A-F) and Ng-AuNP's pH 7 (G-L) over 24 hours, cell morphology was observed and recorded (Figure 3.108). Cells appeared progressively fewer and atypically rounded between the control and 200 µg/ml of naringenin (A-F), exhibiting increasing signs of stress (B-D), and signs consistent with cell death between 100 µg/ml and 200 µg/ml (E-F). Similarly, cells appeared marginally sparely fewer between the control and 200 µg/ml of the AuNP's (G-L), displaying slight signs indicative of cell stress at the highest concentration (L).

After being exposed to increasing concentrations of the naringenin (A-F) and Ng-AuNP's pH 7 (G-L) over 48 hours, cell morphology was observed and recorded (Figure 3.109). Increasingly fewer cells were observed between control and 200 µg/ml of naringenin (A-F), with cell stress becoming increasingly evident between 12.5 µg/ml and 50 µg/ml (B-D), and signs indicative of cell death at higher concentrations (E-F). Likewise, cells appeared progressively, albeit marginally fewer between the control and 200 µg/ml of the AuNP's (G-L), displaying slight signs indicative of cell stress between 100µg/ml and 200 µg/ml (K-L).

Post 72-hour exposure to naringenin (A-F) and Ng-AuNP's pH 7 (G-L), cell morphology was observed and recorded (Figure 3.110). Cells appeared increasingly fewer between the control and 200 µg/ml of naringenin (A-F), exhibiting signs indicative of cell stress (B-C) and cell death between 50 µg/ml and 200 µg/ml (D-F). When treated with the AuNP's, cells appeared only slightly more sparely spaced between control and 200 µg/ml of the AuNP's, displaying slight signs of cell stress between 50 µg/ml and 100 µg/ml (J-K), followed by cell death at 200 µg/ml (L).

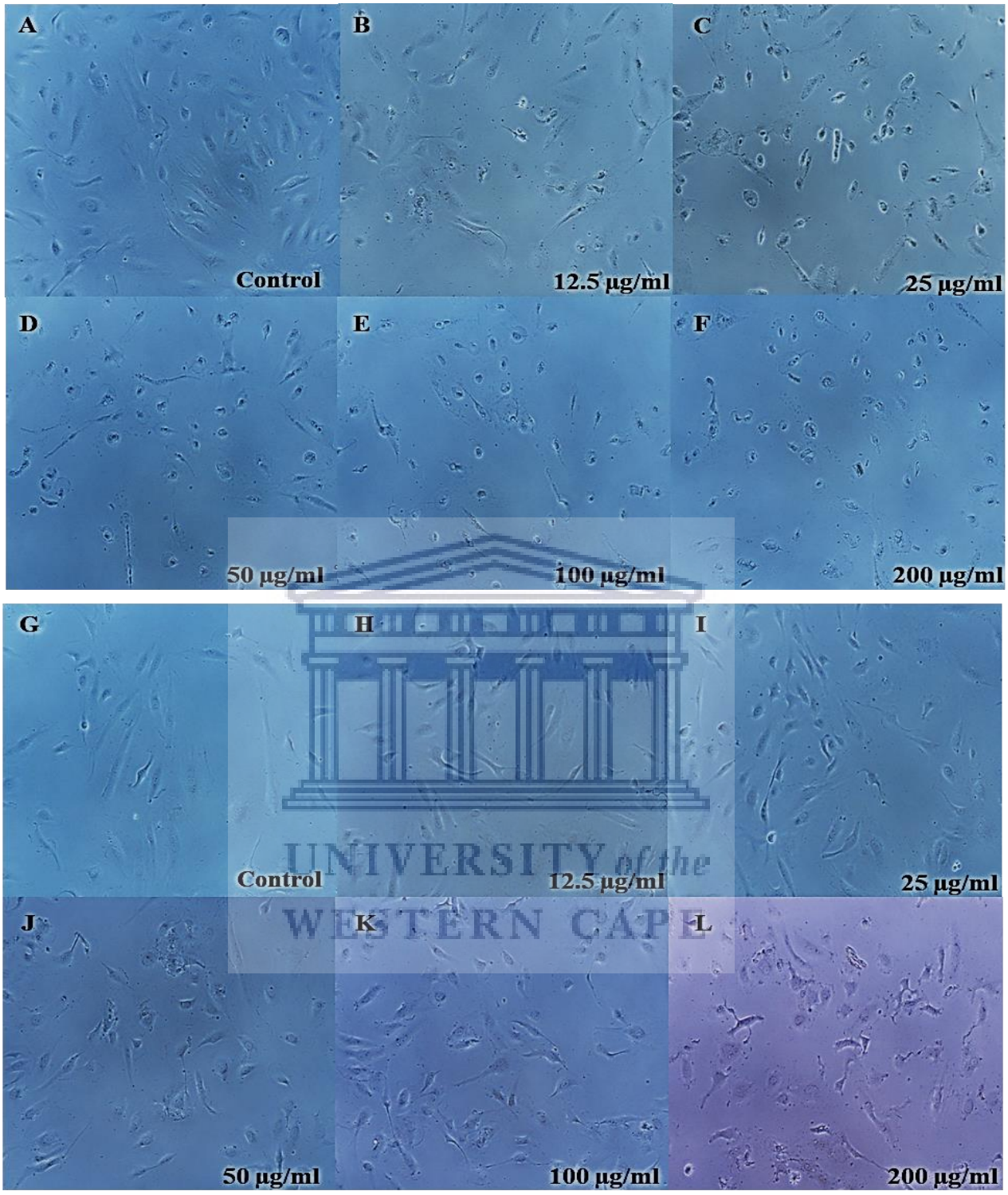

Figure 3.108: HAEC Cell morphology after being exposed to increasing concentrations of naringenin and Ng-AuNP's pH 7 over a 24-hour period. The extract (C-F) yielded signs of cell stress (B-D) and signs of death (E-F) at higher concentrations. Similarly, the AuNP's (G-L) exhibited fewer overall cells and slight indications stress at the highest concentrations (L).

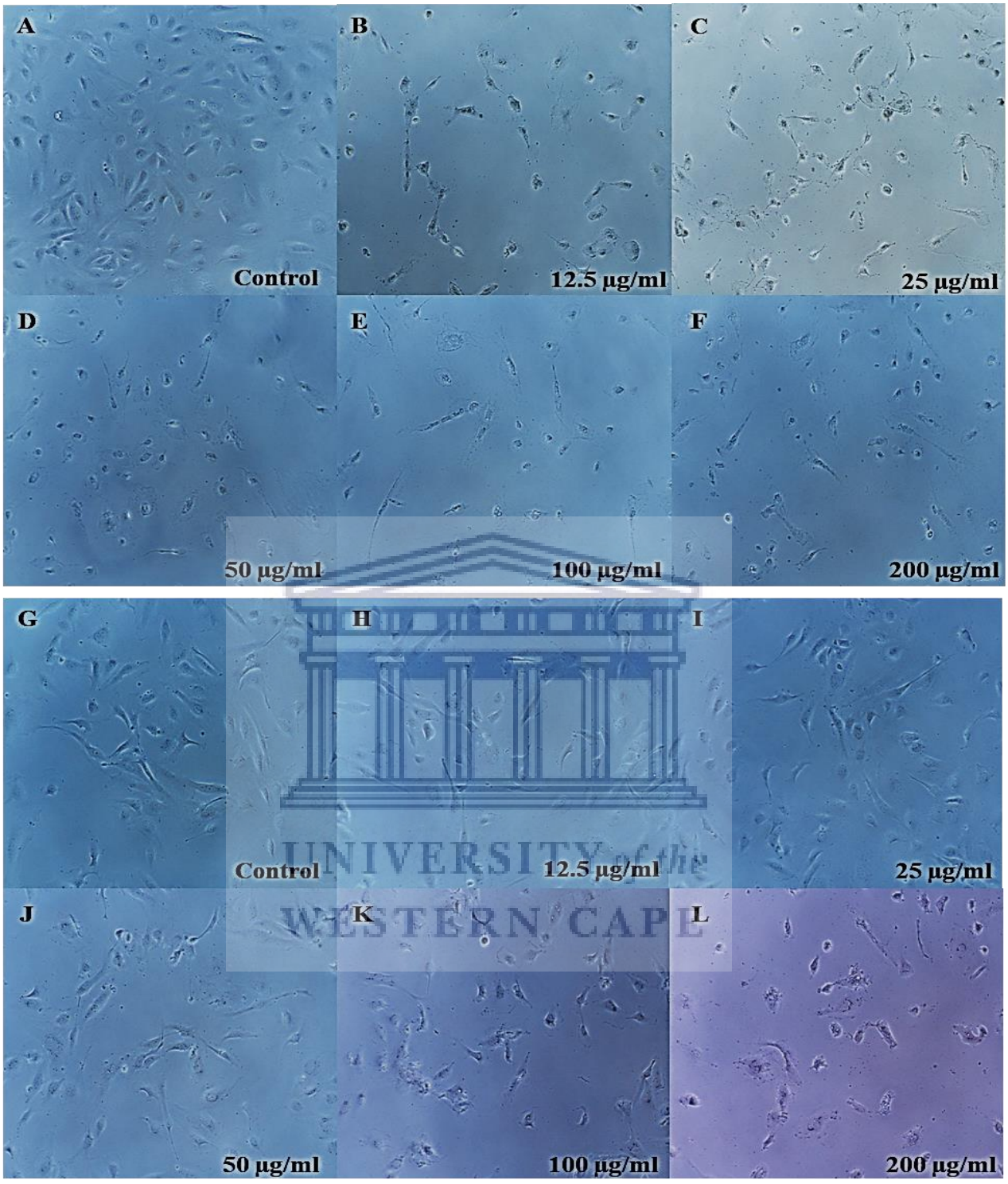

Figure 3.109: HAEC cell morphology after being exposed to increasing concentrations of naringenin and Ng-AuNP's pH 7 over a 48-hour period. Increasingly fewer cells were evident between control and 200 µg/ml of the extract, with signs of stress (B-D) and death (E-F) at higher concentrations. The AuNP's exhibited marginal decreases in the overall observed cell number (G-L), along with slight cell stress between 100 µg/ml and 200 µg/ml (K-L).

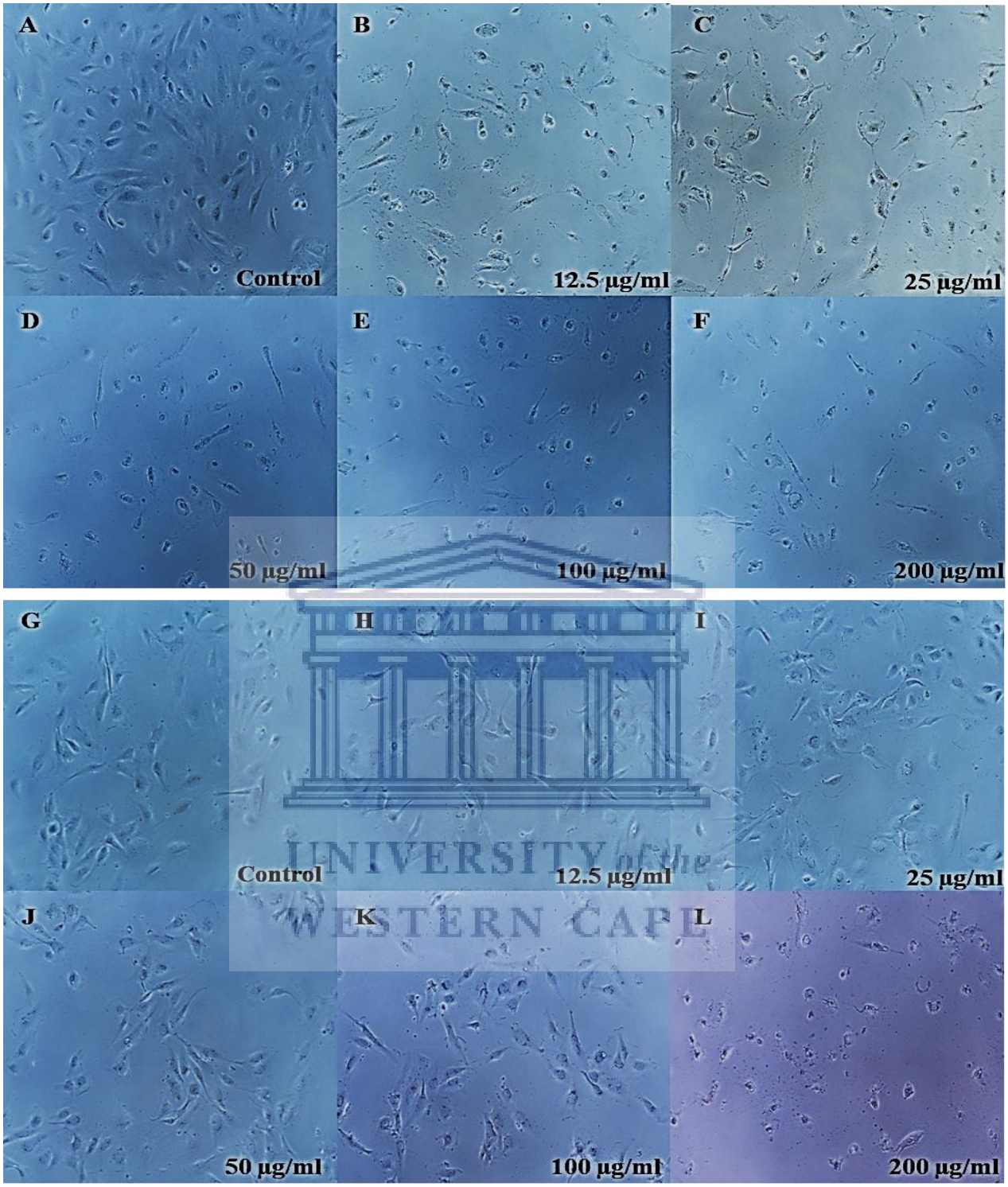

Figure 3.110: HAEC cell morphology after being exposed to increasing concentrations of naringenin and Ng-AuNP's pH 7 over a 72-hour period. Progressively fewer cells were observed between the control and 200 µg/ml of naringenin with signs of stress (B-C) and death (D-F) at higher concentrations. The AuNP's exhibited decreases in the observed cell number (G-L), with signs of cell stress between 50 µg/ml and 100 µg/ml (K-K), and cell death at 200 µg/ml (L).

The MTT assay revealed dose-dependent effects at 24, 48 and 72-hour exposure periods, respectively. Following 24-hours of treatment (Figure 3.111 A), both naringenin and AuNP's yielded consistent, dose-dependent decreases in cell viability from control-200 µg/ml. The extract yielded greater decreases at each concentration, differing from the AuNP's significantly (P=0.0137, P=0.0005 and P<0.0001) at 12.5 µg/l, 25 µg/l and 50-200 µg/ml, respectively. The repeated measures ANOVA revealed significant (P<0.0001) negative trends from control-200 µg/ml for both naringenin and AuNP's, respectively. Similarly, one-way ANOVA yielded significant (P<0.001) trends from control-200 µg/ml following treatment with naringenin and AuNP's, respectively.

Following 48-hours of exposure (Figure 3.111 B) both naringenin and AuNP's yielded progressive decreases in cell viability from control-200 µg/ml, with naringenin yielding greater decreases at each concentration. Significant (P<0.0001 and P=0.0024) differences between the extract and the AuNP's were observed at 25-100 µg/ml and 200 µg/ml, respectively. The repeated measures ANOVA revealed significant (P<0.0001) negative trends from control-200 µg/ml for both naringenin and AuNP's, respectively. Similarly, one-way ANOVA revealed significant (P<0.001) trends from control-200 µg/ml for both naringenin and AuNP's, respectively.

After 72-hours (Figure 3.111 C) both the extract and AuNP's yielded progressive, dose-dependent decreases in cell viability from the control-200 µg/ml. Naringenin yielded greater decreases in viability at each concentration, differing significantly (P=0.0014 and P<0.0001) from the AuNP's at 12.5 µg/ml and 25-200 µg/ml, respectively. The repeated measures ANOVA revealed significant (P<0.0001) negative trends from control-200 µg/ml for both naringenin and AuNP's, respectively. Similarly, one-way ANOVA revealed significant (P<0.001) trends from control-200 µg/ml for both naringenin and AuNP's, respectively.

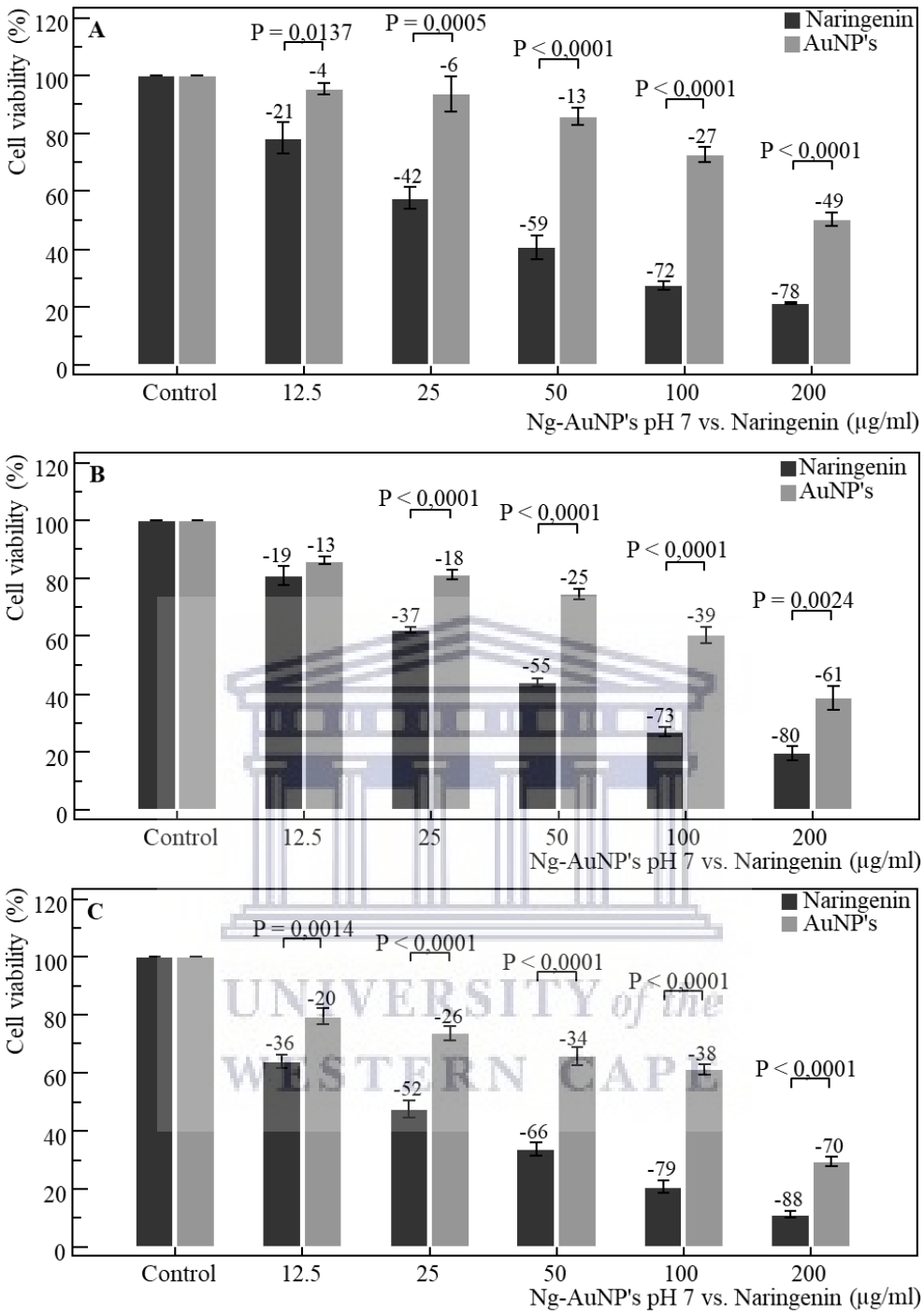

Figure 3.111: HAEC cell viability as determined by the MTT assay over 24 (A), 48 (B) and 72 (C) hour exposure to naringenin and Ng-AuNP's pH 7. Significant (P=0.0137, P=0.0005 and P<0.0001) differences were found from 12.5 -25 µg/ml and 50-200 µg/ml over 24 hours, along with significant (P<0.0001 and P=0.0024) differences observed at 25-100 µg/ml and 200 µg/ml after 48 hours. After 72 hours of exposure, a significant (P=0.0014 and P<0.0001) differences were observed between naringenin and AuNP's at 12.5 µg/ml and 25-200 µg/ml.

3.2.4.6 Ng-AuNP's pH 8 and naringenin

After being exposed to increasing concentrations of the naringenin (A-F) and Ng-AuNP's pH 8 (G-L) over 24 hours, cell morphology was observed and recorded (Figure 3.112). Cells appeared progressively fewer and atypically rounded between the control and 200 µg/ml of naringenin (A-F), exhibiting increasing signs of stress (B-D), and cell death between 100 µg/ml and 200 µg/ml (E-F). Similarly, cells appeared fewer between the control and 200 µg/ml of the AuNP's (G-L), displaying increasing rounding and signs of cell stress between 12.5 µg/ml and 200 µg/ml (H-J), along with cell death at higher concentrations (K-L).

After being exposed to increasing concentrations of the naringenin (A-F) and Ng-AuNP's pH 8 (G-L) over 48 hours, cell morphology was observed and recorded (Figure 3.113). Increasingly fewer cells were observed between control and 200 µg/ml of naringenin (A-F), with cell stress becoming increasingly evident between 12.5 µg/ml and 50 µg/ml (B-D), and signs indicative of cell death at higher concentrations (E-F). Likewise, cells appeared progressively and notably fewer between the control and 200 µg/ml of the AuNP's (G-L), displaying increasing signs of cell stress (H-J), followed by cell death at 100µg/ml and 200 µg/ml (K-L).

Post 72 hour exposure to naringenin (A-F) and Ng-AuNP's pH 7 (G-L), cell morphology was observed and recorded (Figure 3.114). Cells appeared increasingly fewer between the control and 200 µg/ml of naringenin (A-F), exhibiting signs indicative of cell stress (B-C) and cell death between 50 µg/ml and 200 µg/ml (D-F). When treated with the AuNP's, cells were notably fewer between control and 200 µg/ml of the AuNP's, appearing increasingly stressed between 12.5 µg/ml and 50 µg/ml (H-J), followed by signs of cell death between 100 µg/ml and 200 µg/ml (K-L)

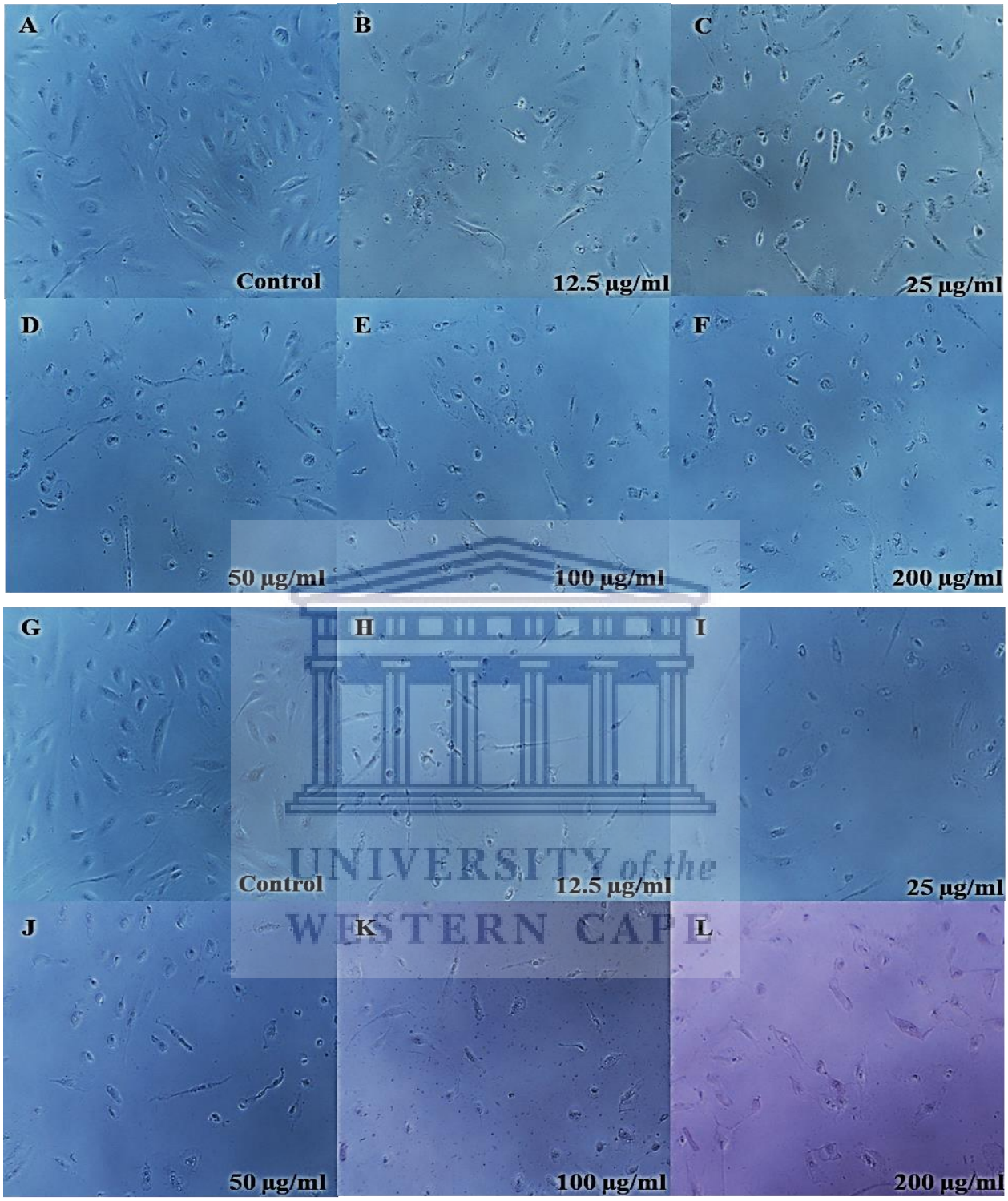

Figure 3.112: HAEC Cell morphology after being exposed to increasing concentrations of naringenin and Ng-AuNP's pH 8 over a 24-hour period. The extract (C-F) yielded signs of cell stress (B-D) and signs of death (E-F) at higher concentrations. The AuNP's (G-L) exhibited fewer overall cells and slight indications stress (H-J) followed by death at higher concentrations (K-L).

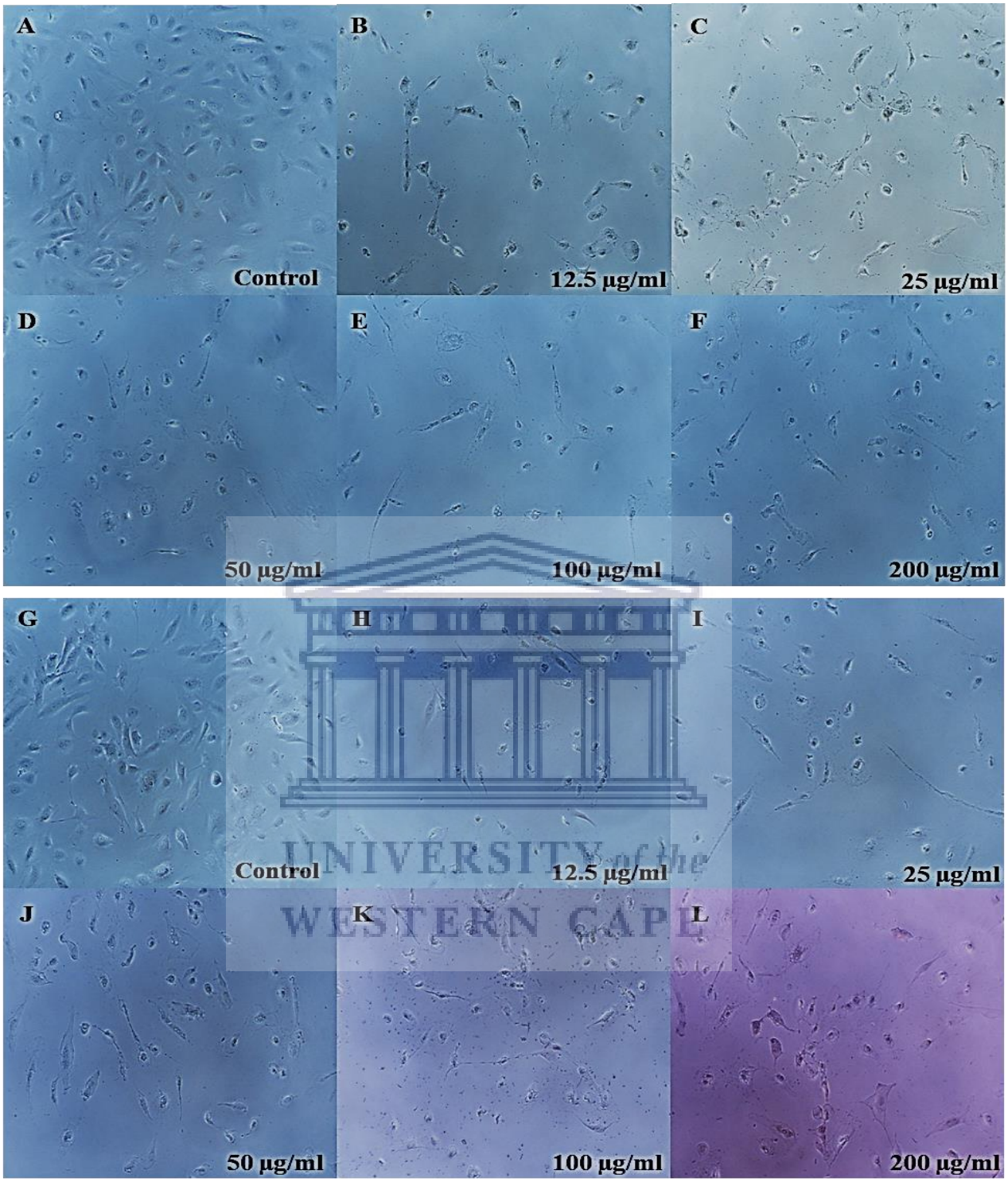

Figure 3.113: HAEC cell morphology after being exposed to increasing concentrations of naringenin and Ng-AuNP's pH 7 over a 48-hour period. Increasingly fewer cells were evident between control and 200 µg/ml of the extract, with signs of stress (B-D) and death (E-F) at higher concentrations. Similarly, the AuNP's (G-L) yielded fewer observable cells, along with increasing cell stress (H-J), followed by death at higher concentrations (K-L).

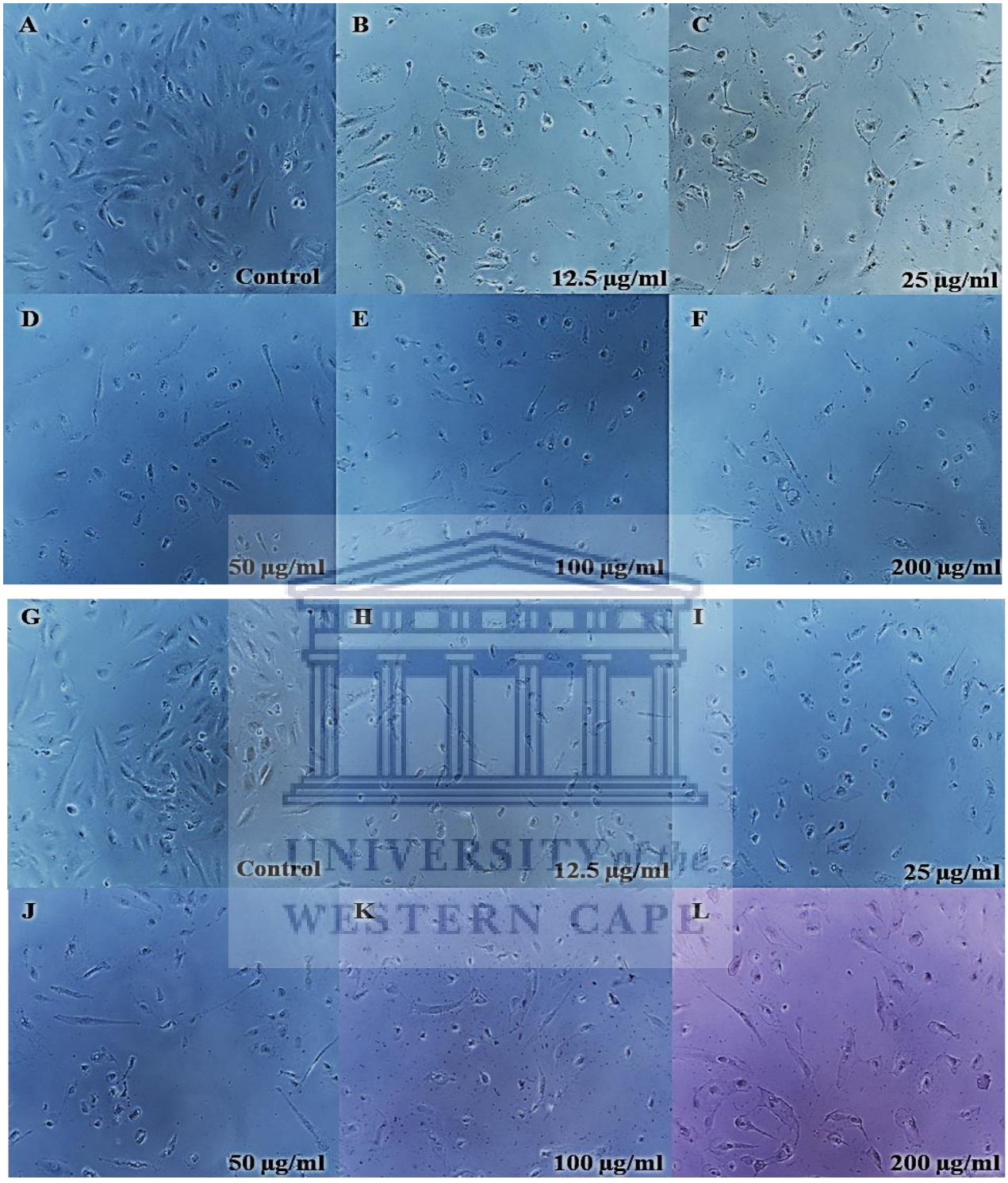

Figure 3.114: HAEC cell morphology after being exposed to increasing concentrations of naringenin and Ng-AuNP's pH 7 over a 72-hour period. Progressively fewer cells were observed between the control and 200 µg/ml of naringenin with signs of stress (B-C) and death (D-F) at higher concentrations. Similarly, the AuNP's (G-L) exhibited fewer observable cells, along with increasing cell stress (H-J), followed by death at higher concentrations (K-L).

The MTT assay revealed dose-dependent effects at 24, 48 and 72-hour exposure periods, respectively. Following 24-hours of treatment (Figure 3.115 A), both naringenin and AuNP's yielded consistent, dose-dependent decreases in cell viability from control-200 µg/ml. Naringenin yielded greater decreases at each concentration, differing from the AuNP's significantly (P=0.0419, P=0.0006) at 50 µg/ml and 100 µg/ml, respectively. The repeated measures ANOVA revealed significant (P<0.0001) negative trends from control-200 µg/ml for both naringenin and AuNP's, respectively. Similarly, one-way ANOVA yielded significant (P<0.001) trends from control-200 µg/ml following treatment with naringenin and AuNP's, respectively.

Following 48-hours of exposure (Figure 3.115 B) both the naringenin and AuNP's yielded progressive decreases in cell viability from control-200 µg/ml, with naringenin yielding greater decreases at each concentration. Significant (P=0.0192, P=0.0052, P<0.0001) differences between the naringenin and the AuNP's were observed at 25 µg/ml, 50 µg/ml and 100 µg/ml, respectively. The repeated measures ANOVA revealed significant (P<0.0001) negative trends from control-200 µg/ml for both naringenin and AuNP's, respectively. Similarly, one-way ANOVA revealed significant (P<0.001) trends from control-200 µg/ml for both naringenin and AuNP's, respectively.

After 72-hours (Figure 3.115 C) both naringenin and AuNP's yielded progressive, dose-dependent decreases in cell viability from the control-200 µg/ml. Naringenin yielded greater decreases in viability at each concentration, differing significantly (P=0.0092, P=0.0105, P=0.0073) from the AuNP's at 50 µg/ml, 100 µg/ml and 200 µg/ml, respectively. The repeated measures ANOVA revealed significant (P<0.0001) negative trends from control-200 µg/ml for both the naringenin and AuNP's, respectively. Similarly, one-way ANOVA revealed significant (P<0.001) trends from control-200 µg/ml for both the naringenin and AuNP's, respectively.

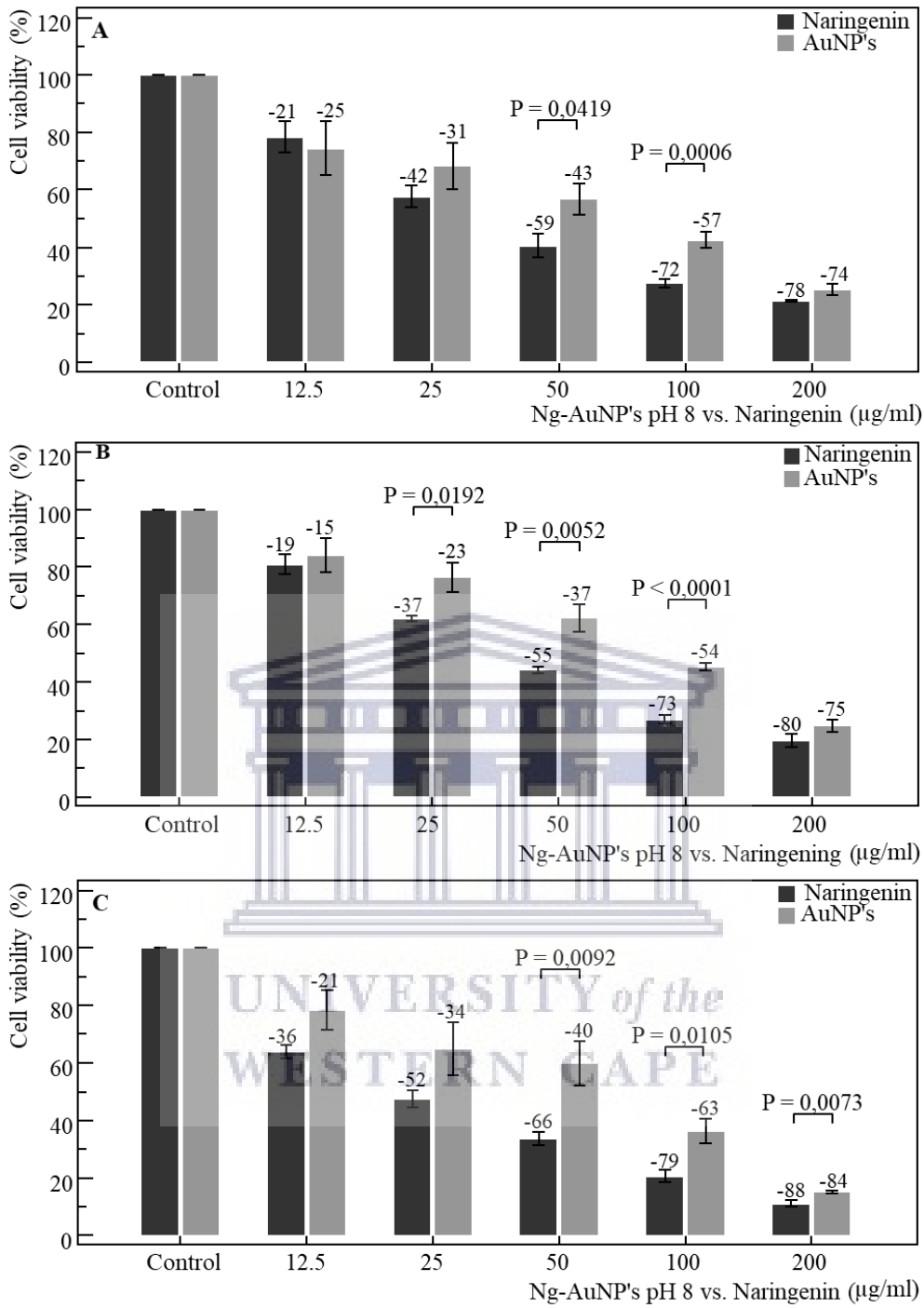

Figure 3.115: HAEC cell viability as determined by the MTT assay over 24 (A), 48 (B) and 72 (C) hour exposure to naringenin and Ng-AuNP's pH 8, respectively. Significant (P=0.0419, P=0.0006) differences were observed between naringenin and the AuNP's at 50 µg/ml and 100 µg/ml over 24 hours, along with significant (P=0.0192, P=0.0052, P<0.0001) differences from 25-100 µg/ml after 48 hours. Following 72 hours of exposure, significant (P=0.0092, P=0.0105, P=0.0073) differences were observed between naringenin and the AuNP's from 50-200 µg/ml, respectively.

3.3 AuNP-cell internalisation by Dark-field microscopy (Cytoviva)

3.3.1 PC-3 Cells

3.3.1.1 S1-AuNP's

Following treatment with 50 µg/ml (A-C) and 100 µg/ml (D-F) of the S1-AuNP's over 2 (A and D), 6 (B and E), and 24 (C and F) hours, respectively, cells were stained and observed for possible AuNP internalisation (Figure 3.116).

Following exposure to 50 µg/ml (A-C), AuNP's exhibited a clear affinity toward cells, displaying progressively increasing AuNP accumulation between the lowest and highest incubation periods (B-C) in a time-dependent manner. Specifically, 2 hours of treatment (A) yielded minimal AuNP-cell accumulation which exhibited particular affinity toward cell nuclei. Similarly, low levels of AuNP-cell accumulation was observed following 6 hours of treatment, displaying affinity toward both cell cytoplasm and nuclei (B). Finally, following 24 hours of treatment, notably higher levels of AuNP-cell accumulation was observed with indiscriminate affinity toward cytoplasm and nuclei (C).

Following exposure to 100 µg/ml (D-F), notably higher levels of overall AuNP-cell accumulation was observed, in comparison to 50 µg/ml, which progressively increased between the lowest and highest incubation periods in a time-dependent fashion (B-E). After 2 hours of treatment (A), small AuNP-cell accumulates were observed, displaying affinity toward cell cytoplasm and nuclei. Next, noticeably larger AuNP-cell accumulates were observed following 6 hours of treatment (B), exhibiting affinity toward both cytoplasm and nuclei. Finally, following 24 hours of treatment, the highest degree of AuNP-cell accumulation was observed, whereby large portions of cells were engulfed by AuNP aggregates (C).

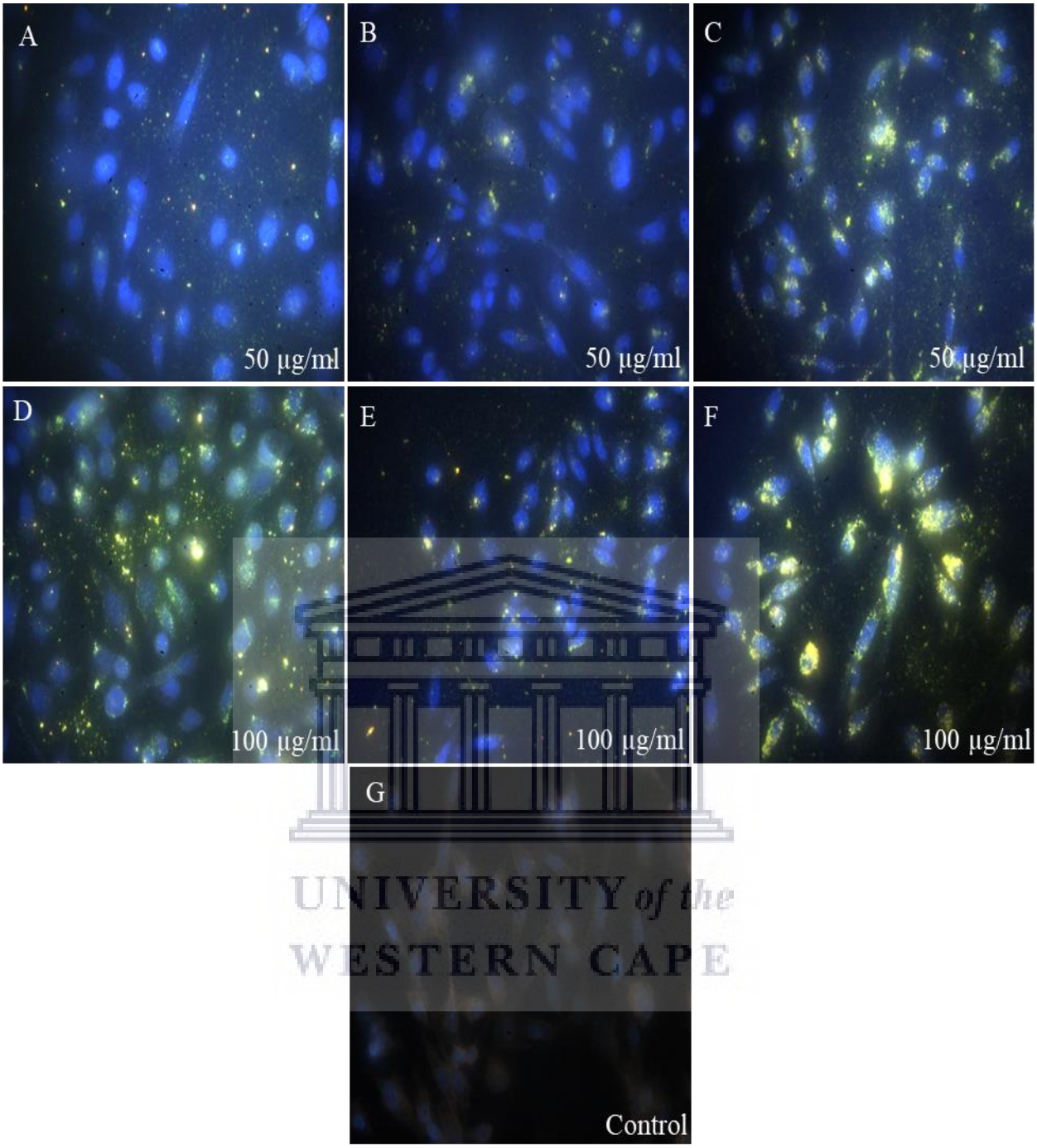

Figure 3.116: S1-AuNP PC-3 cell internalisation by dark-field microscopy (Cytoviva) following treatment with 50 µg/ml (A-C) and 100 µg/ml (D-F) over 2 (A and D), 6 (B and E), and 24 (C and F) hours, respectively.

3.3.1.2 S2-AuNP's

Following treatment with 50 µg/ml (A-C) and 100 µg/ml (D-F) of the S2-AuNP's over 2, 6 and 24 hours, respectively, cells were stained and observed for possible AuNP internalisation (Figure 3.117).

Following exposure to 50 µg/ml (A-C), AuNP's exhibited a distinct affinity toward cells, exhibiting increasing AuNP-cell accumulation between the lowest and highest incubation periods (B-C), in a time-dependent manner. After 2 hours of treatment (A), low levels of AuNP-cell accumulation was observed, with accumulates observed over both cytoplasm and nuclei. Next, 6 hours of treatment yielded noticeably higher levels of AuNP-cell accumulation, whereby affinity toward both cell cytoplasm and nuclei was observed (B). Finally, following 24 hours of treatment, notably higher levels of AuNP-cell accumulation was observed with affinity toward both cytoplasm and nuclei, covering large areas of individual cells (C).

Following exposure to 100 µg/ml (D-F), levels of overall AuNP-cell accumulation was not observed to exceed those seen at a dose of 50 µg/ml (A-C). Nevertheless, a progressive increase in AuNP-cell accumulation was observed between the lowest and highest incubation periods, in a time-dependent fashion (B-E). After 2 hours of treatment (A), small amounts of AuNP-cell accumulation was observed, particularly over both cytoplasm and nuclei. Following this, greater amounts of AuNP-cell accumulation was observed, following 6 hours of treatment (B), having affinity toward both cytoplasm and nuclei. Finally, after 24 hours of treatment, notably higher levels of AuNP-cell accumulation was observed, in relation to cytoplasm and nuclei, where large portions of cells were covered by AuNP aggregates (C).

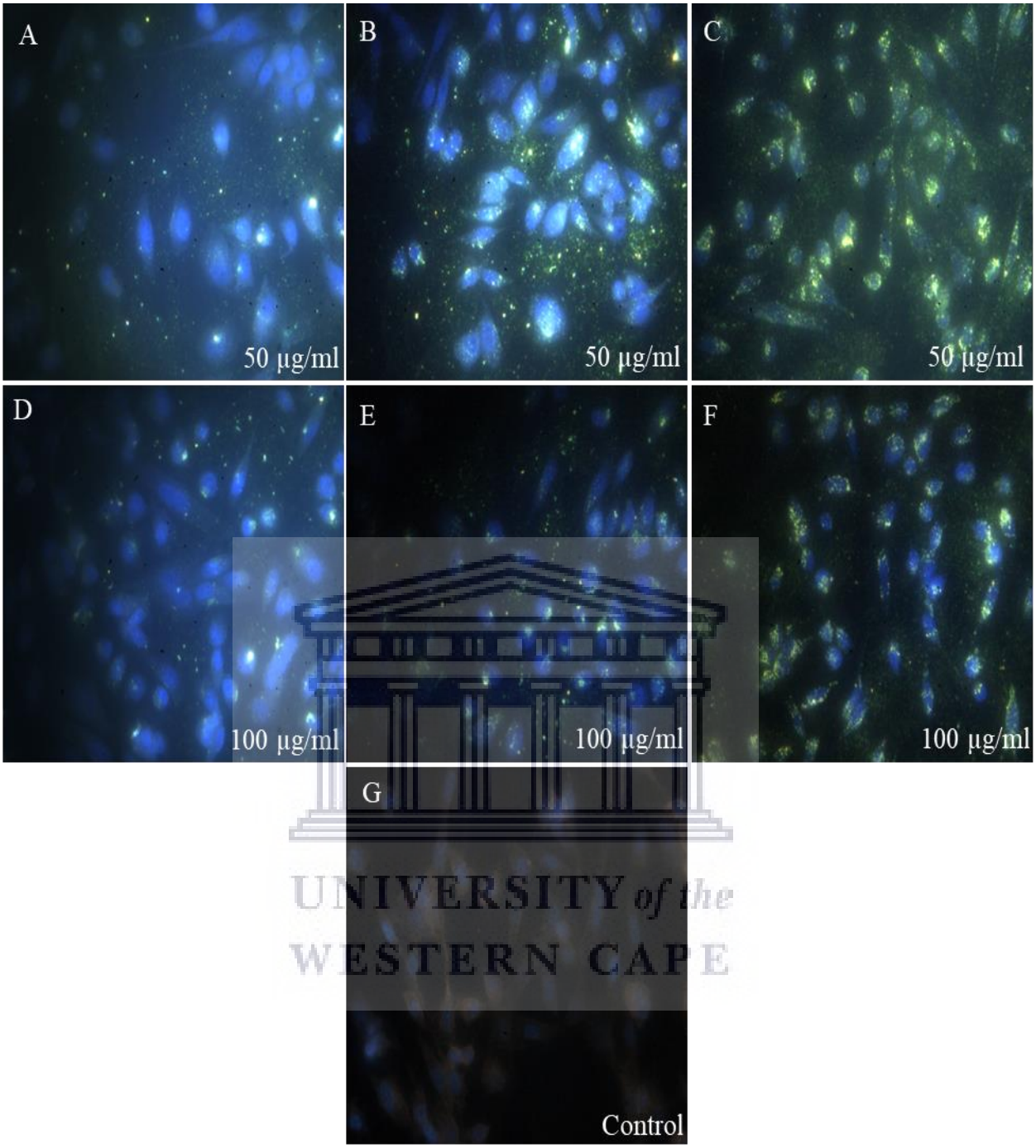

Figure 3.117: S2-AuNP PC-3 cell internalisation by dark-field microscopy (Cytoviva) following treatment with 50 µg/ml (A-C) and 100 µg/ml (D-F) over 2 (A and D), 6 (B and E), and 24 (C and F) hours, respectively.

3.3.1.3 Ng-AuNP's pH 8

Following treatment with 50 µg/ml (A-C) and 100 µg/ml (D-F) of the Ng-AuNP's pH 8 over 2, 6 and 24 hours, respectively, cells were stained and observed for possible AuNP internalisation (Figure 3.118).

Following exposure to 50 µg/ml (A-C), an affinity toward cells was exhibited by the AuNP's, yielding progressively increasing cell-accumulation between the lowest and highest incubation periods (B-C), in a time-dependent fashion. After 2 hours of treatment (A), very few AuNP-cell accumulation was observed, with the presence of a few extracellular AuNP aggregates. Following 6 hours of incubation, however, a notably greater level of AuNP-cell accumulation was observed, with particular affinity toward both cell cytoplasm and nuclei (B). Finally, following 24 hours of treatment, markedly higher levels of AuNP-cell accumulation was observed, with large AuNP aggregates covering cell surfaces (C).

Following exposure to 100 µg/ml (D-F), notably higher levels of overall AuNP-cell accumulation was observed, in comparison to 50 µg/ml, which similarly progressively increased between the lowest and highest incubation periods in a time-dependent fashion (B-E). After 2 hours of treatment (A), relatively higher AuNP-cell accumulation was noted, displaying affinity toward both the cell cytoplasm and nuclei. Hereafter, noticeably higher amounts of AuNP-cell accumulation was observed, following 6 hours of treatment (B), exhibiting affinity toward both cytoplasm and nuclei. Finally, following 24 hours of treatment, a notably higher level of AuNP-cell accumulation was observed, engulfing large portions of cells (C).

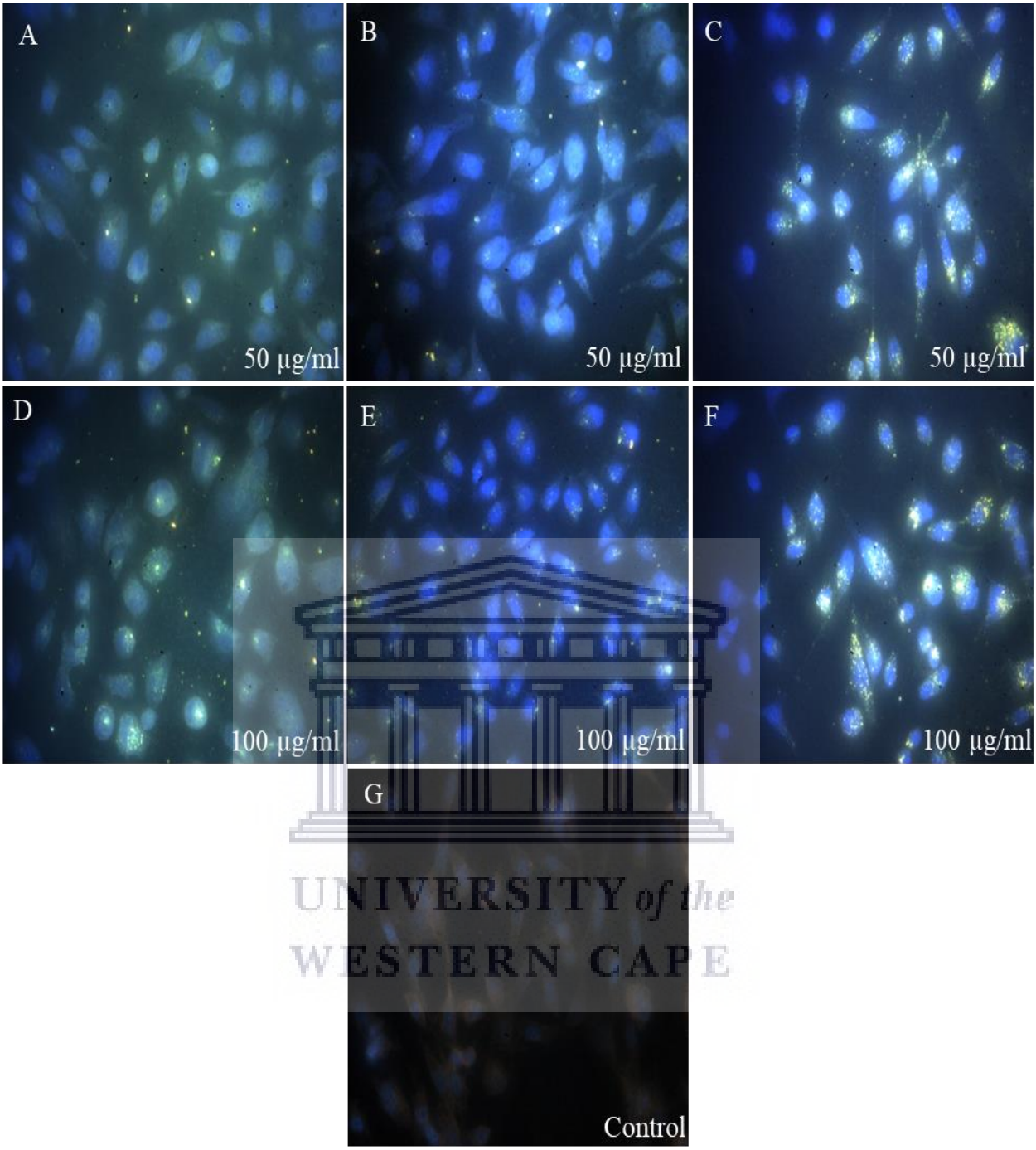

Figure 3.118: Ng-AuNP's pH 8 PC-3 cell internalisation by dark-field microscopy (Cytoviva) following treatment with 50 µg/ml (A-C) and 100 µg/ml (D-F) over 2 (A and D), 6 (B and E), and 24 (C and F) hours, respectively.

3.3.2 LNCaP Cells

3.3.2.1 S1-AuNP's

Following treatment with 50 µg/ml (A-C) and 100 µg/ml (D-F) of the S1-AuNP's over 2, 6 and 24 hours, respectively, cells were stained and observed for possible AuNP internalisation (Figure 3.119).

Following exposure to 50 µg/ml (A-C), progressively increasing AuNP-cell accumulation was observed between the lowest and highest incubation periods (B-C) in a time-dependent manner. After 2 hours of treatment (A) very low levels of overall AuNP-cell accumulation was observed, with only a few AuNP accumulates being present. Following this, marginally higher levels of AuNP-cell accumulation was observed following 6 hours of treatment (B). Finally, following 24 hours of treatment, notably higher levels of AuNP-cell accumulation was observed with clear affinity toward cell cytoplasm (C).

Following exposure to 100 µg/ml (D-F), notably higher levels of overall AuNP-cell accumulation was observed, in comparison to 50 µg/ml, which progressively increased between the lowest and highest incubation periods in a time-dependent fashion (B-E). After 2 hours of treatment (A), AuNP-cell accumulates with affinity toward cell cytoplasm was observed. Similarly, AuNP-cell accumulates were observed following 6 hours of treatment (B), exhibiting affinity toward both cytoplasm. Finally, following 24 hours of treatment, the highest degree of AuNP-cell accumulation was observed, whereby both large and small AuNP aggregates displayed affinity toward cell cytoplasm and nuclei (C).

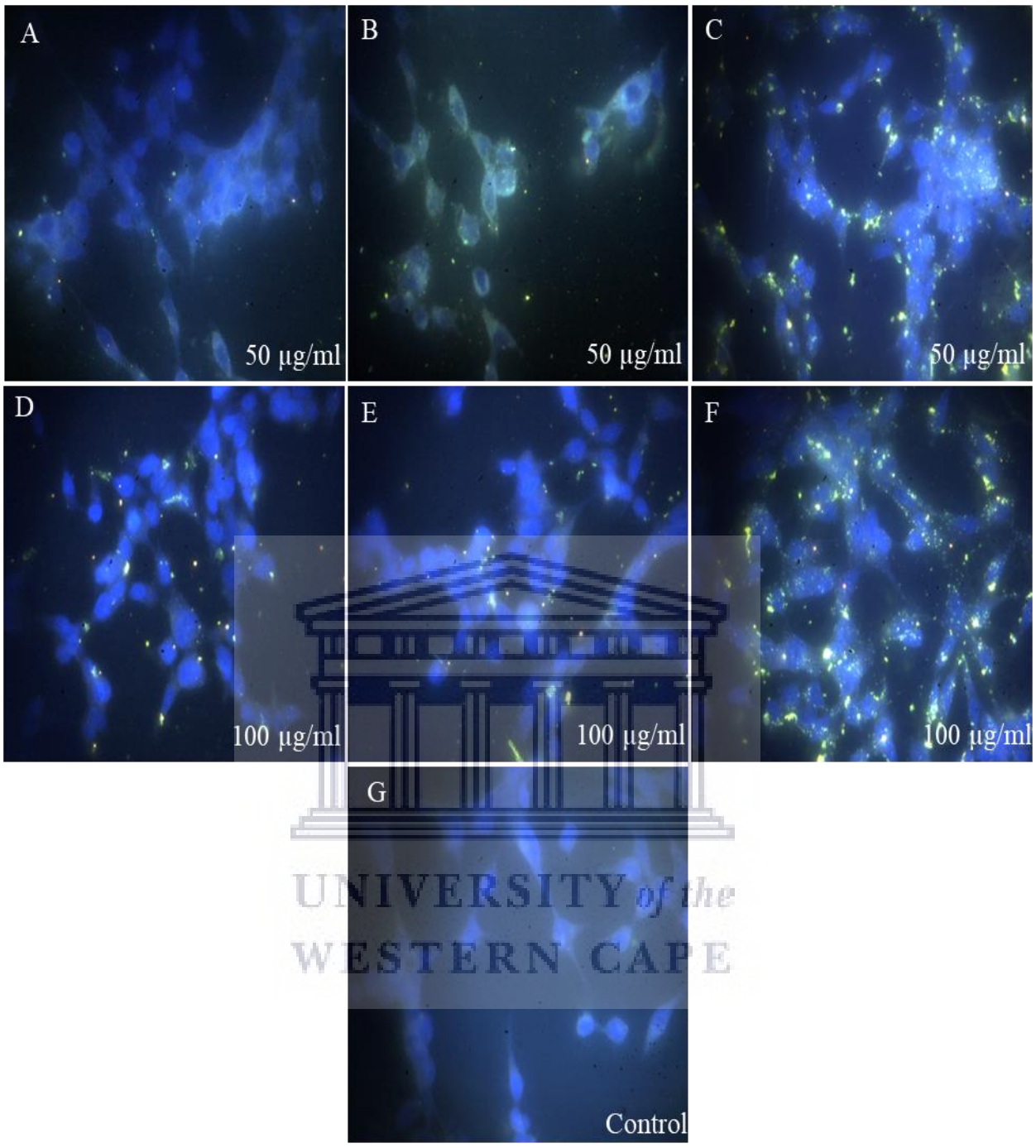

Figure 3.119: S1-AuNP LNCaP cell internalisation by dark-field microscopy (Cytoviva) following treatment with 50 µg/ml (A-C) and 100 µg/ml (D-F) over 2 (A and D), 6 (B and E), and 24 (C and F) hours, respectively.

3.3.2.2 S2-AuNP's

Following treatment with 50 µg/ml (A-C) and 100 µg/ml (D-F) of the S2-AuNP's over 2, 6 and 24 hours, respectively, cells were stained and observed for possible AuNP internalisation (Figure 3.120).

Following exposure to 50 µg/ml (A-C), AuNP's exhibited affinity toward cells, displaying increasing AuNP-cell accumulation between the 2-hour and 6-hour incubation periods (A-B), followed by no observable increase in AuNP-cell accumulation between 6-hour and 24-hour incubation periods (B-C). Specifically, 2 hours of treatment (A) yielded low levels of AuNP-cell accumulation which exhibited an apparent affinity towards cell cytoplasm. Conversely, higher levels of AuNP-cell accumulation was observed after 6 hours of treatment, whereby AuNP accumulates displayed affinity toward both cell cytoplasm and nuclei (B). Similarly, following 24 hours of treatment, AuNP-cell accumulation was observed with an affinity toward cytoplasm and nuclei (C).

Following exposure to 100 µg/ml (D-F), AuNP's exhibited affinity toward cells, displaying comparable AuNP-cell accumulation between the 2-hour and 24-hour incubation periods (D-F). After 2 hours of treatment (A), small AuNP-cell accumulates were observed, displaying affinity toward cell cytoplasm, along with some affinity toward nuclei. Next, marginally larger AuNP-cell accumulates were observed following 6 hours of treatment (B), exhibiting affinity toward both cytoplasm and nuclei. Following 24 hours of treatment, additional AuNP-cell accumulation was not observed with AuNP accumulates displaying an affinity toward cytoplasm and nuclei (C).

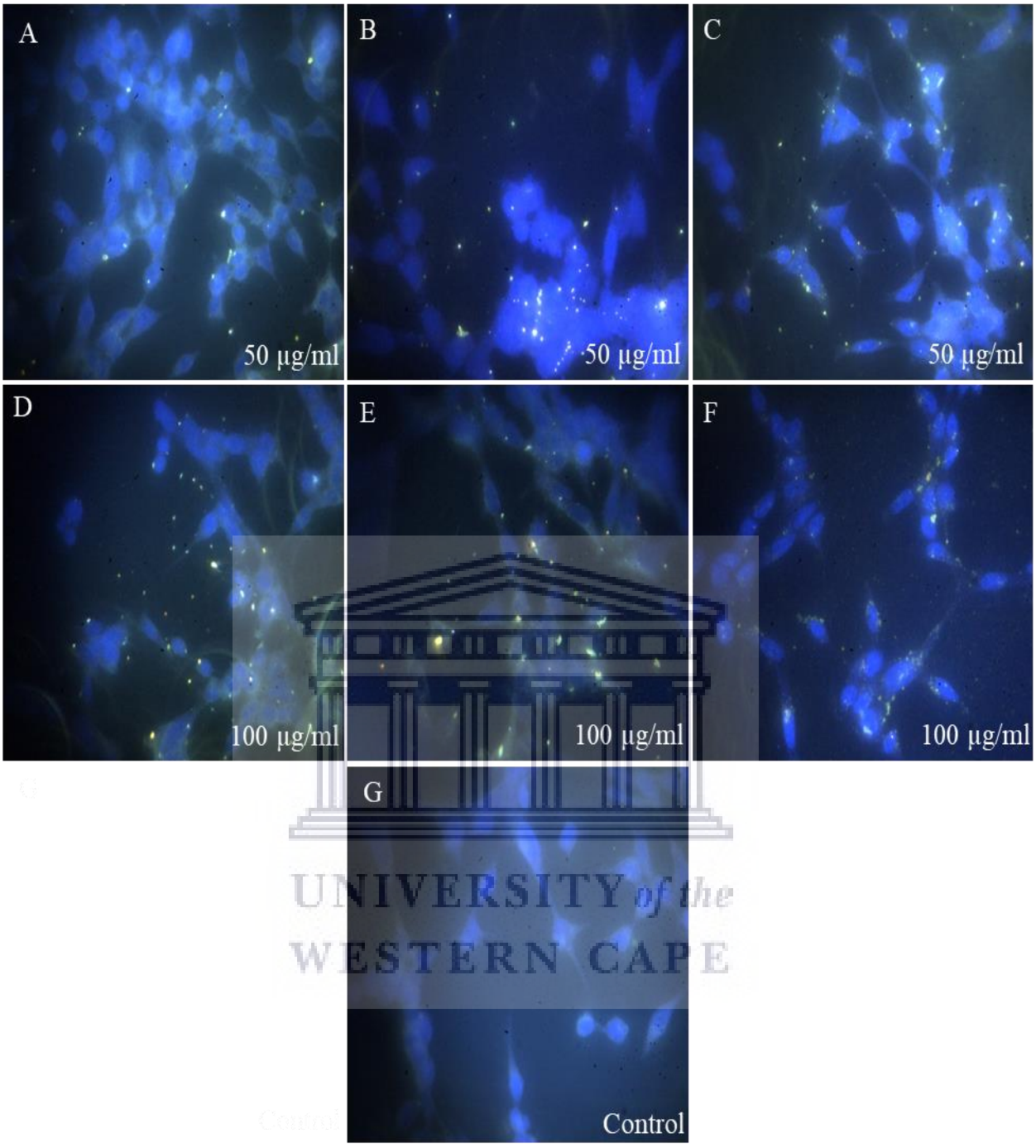

Figure 3.120: S2-AuNP LNCaP cell internalisation by dark-field microscopy (Cytoviva) following treatment with 50 µg/ml (A-C) and 100 µg/ml (D-F) over 2 (A and D), 6 (B and E), and 24 (C and F) hours, respectively.

3.3.2.3 Ng-AuNP's pH 8

Following treatment with 50 µg/ml (A-C) and 100 µg/ml (D-F) of the Ng-AuNP's over 2, 6 and 24 hours, respectively, cells were stained and observed for possible AuNP internalisation (Figure 3.121).

Following exposure to 50 µg/ml, affinity toward cells was observed, along with a progressively increasing AuNP-cell accumulation between the lowest and highest incubation periods (A-C). After 2 hours of treatment (A), notably low overall levels of AuNP-cell accumulation was observed, with very few AuNP accumulates seen covering cells. Similarly, low levels of AuNP-cell accumulation was observed following 6 hours of treatment, displaying affinity toward cell cytoplasm (B). Hereafter, following 24 hours of treatment, higher levels of AuNP-cell accumulation was observed, with an apparent affinity toward both cell cytoplasm and nuclei (C).

Following exposure to 100 µg/ml, affinity toward the cells was observed, along with a progressively increasing AuNP accumulation between the lowest and highest incubation periods (B-E). After 2 hours of treatment (A), low levels of AuNP-accumulation was observed, with very few AuNP aggregates being present. Conversely, notably higher levels of AuNP-cell accumulation was observed following 6 hours of incubation, displaying affinity toward both cell cytoplasm and cell nuclei (B). Finally, following 24 hours of treatment, the greatest deal of AuNP-cell accumulation was observed, whereby large portions of cells, including cytoplasm and nuclei, were covered by AuNP aggregates (C).

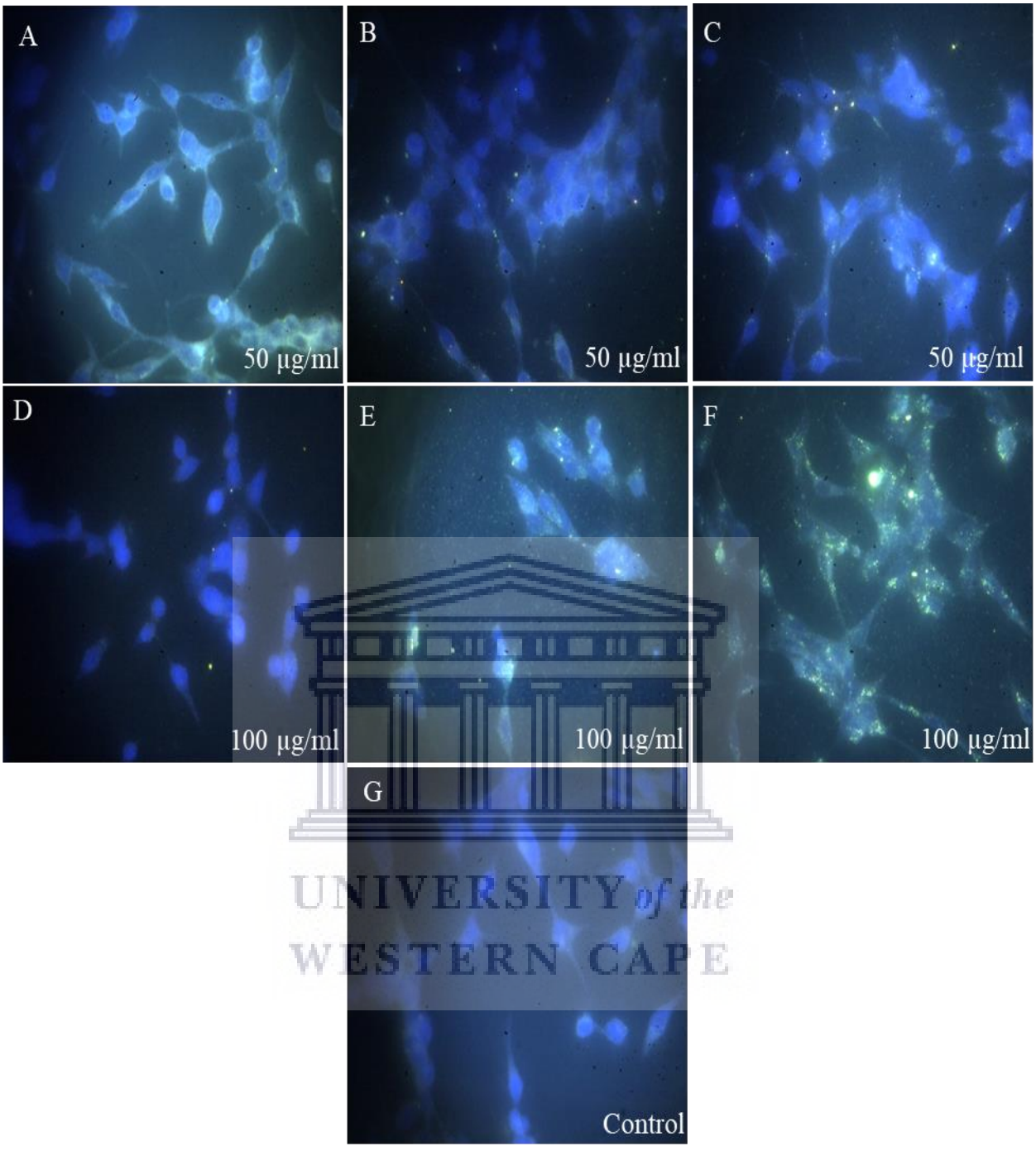

Figure 3.121: Ng-AuNP pH 8 LNCaP cell internalisation by dark-field microscopy (Cytoviva) following treatment with 50 µg/ml (A-C) and 100 µg/ml (D-F) over 2 (A and D), 6 (B and E), and 24 (C and F) hours, respectively.

3.4 PC-3 cell AuNP internalisation by transmission electron microscopy (TEM)

3.4.1 S1-AuNP's 50 µg/ml

Following treatment with 50 µg/ml of the S1-AuNP's over 6 (A) and 24 hours (B), cells were sectioned and observed for AuNP internalisation (Figure 3.122). AuNP's were observed to have been internalised by cells each time point, with low levels of internalisation observed after 6 hours of incubation (A), followed by a notably greater quantity of internalised AuNPs after 24 hours of incubation (B).

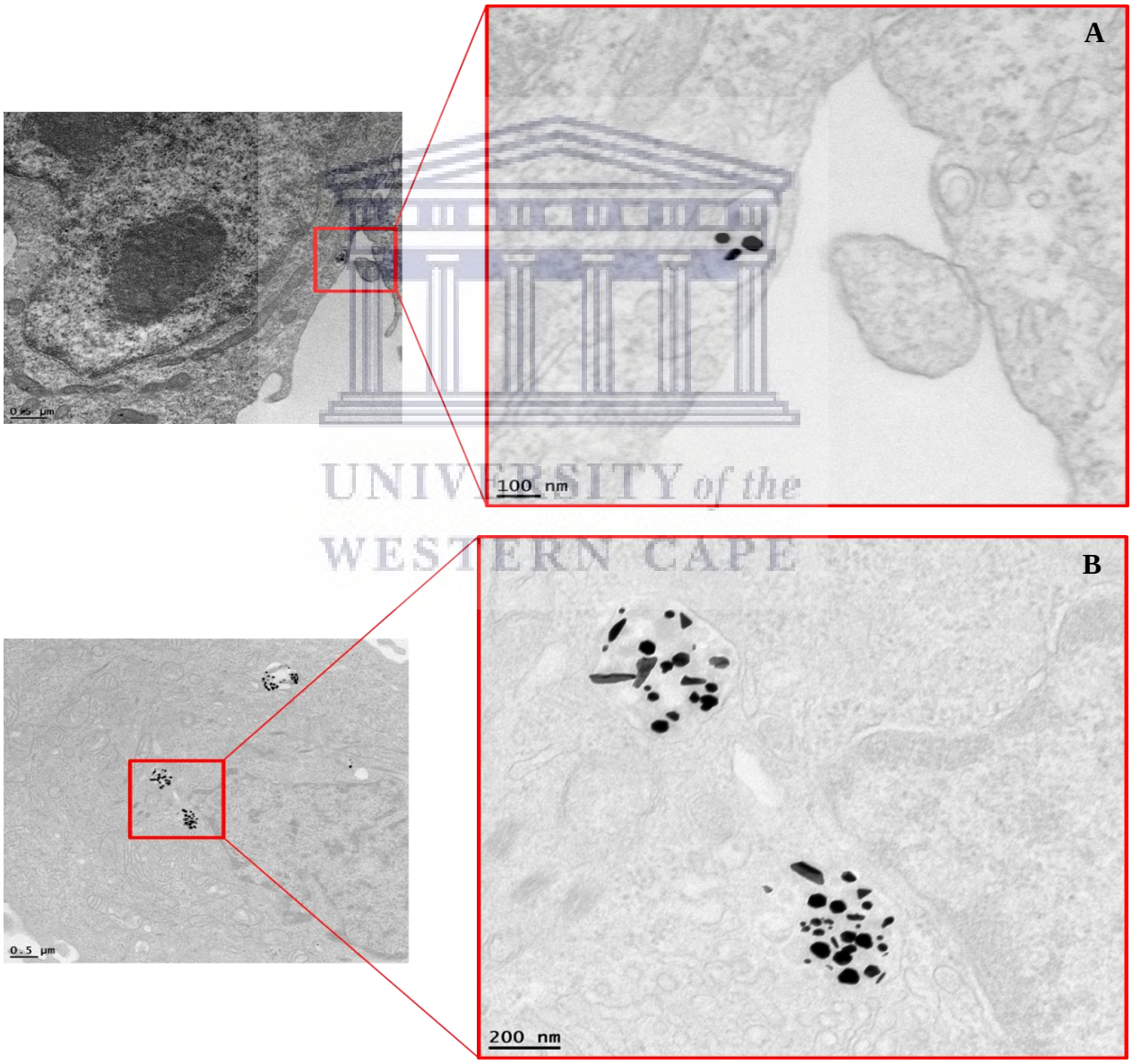

Figure 3.122: S1-AuNP cell internalisation by transmission electron microscopy following treatment with 50 µg/ml over 6 (A), and 24 (B) hours, respectively.

3.4.2 S1-AuNP's 100 µg/ml

Following treatment with 100 µg/ml of the S1-AuNP's over 6 (A) and 24 hours (B), cells were sectioned and observed for AuNP internalisation (Figure 3.123). High levels of AuNP's were found to be internalised by cells each time point used, with marginally lower levels of internalisation observed after 6 hours of incubation (A), followed by slightly higher levels of AuNP internalisation following 24 hours of incubation (B)

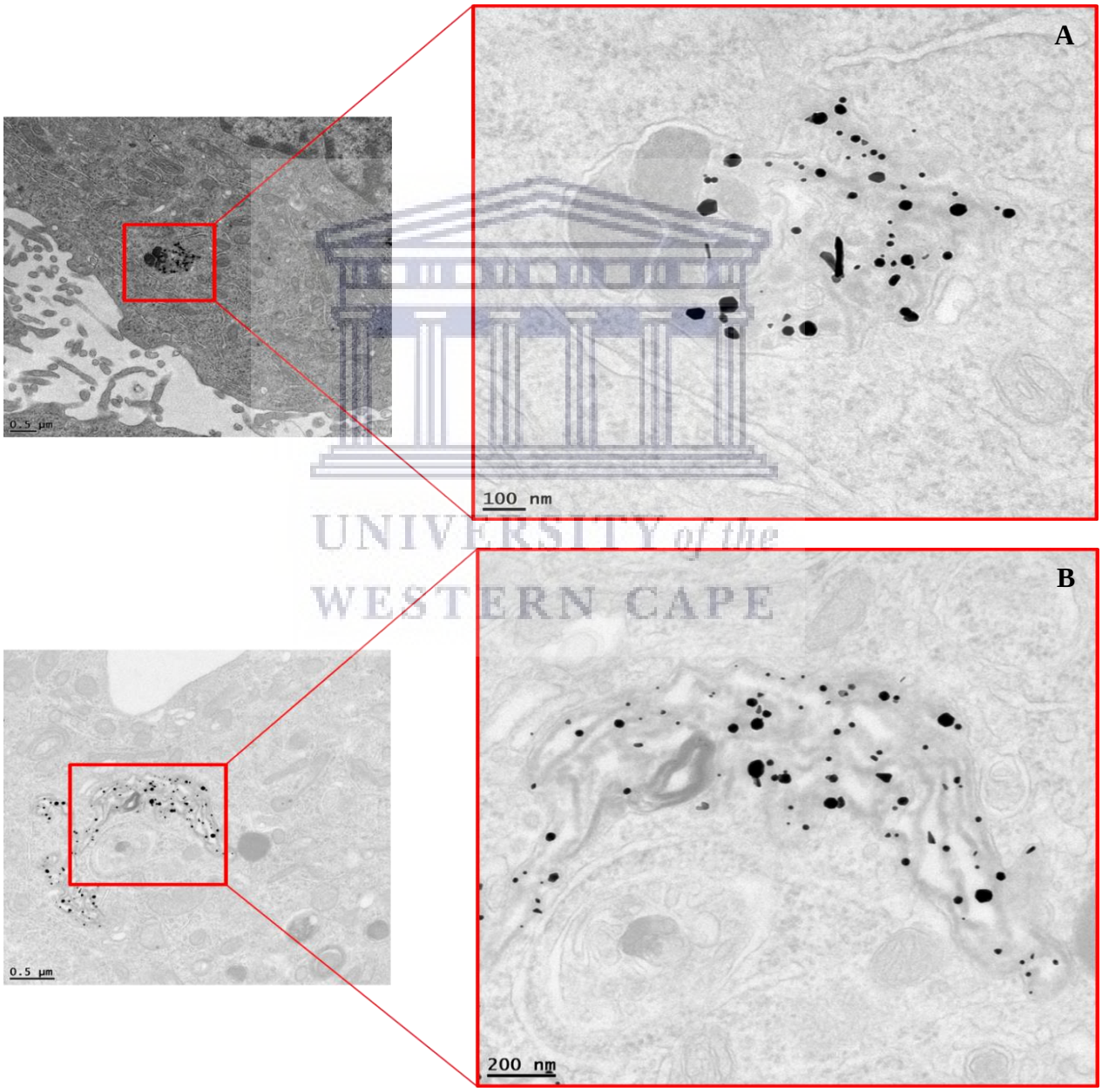

Figure 3.123: S1-AuNP cell internalisation by transmission electron microscopy following treatment with 100 µg/ml over 6 (A), and 24 (B) hours, respectively.

3.4.3 Ng-AuNP's pH 8 50 µg/ml

Following treatment with 50 µg/ml of the Ng-AuNP's pH 8 over 6 (A) and 24 hours (B), cells were sectioned and observed for AuNP internalisation (Figure 3.124). Comparable levels of AuNP's were found to be internalised by cells after 6 hours of incubation (A), and following 24 hours of incubation (B)

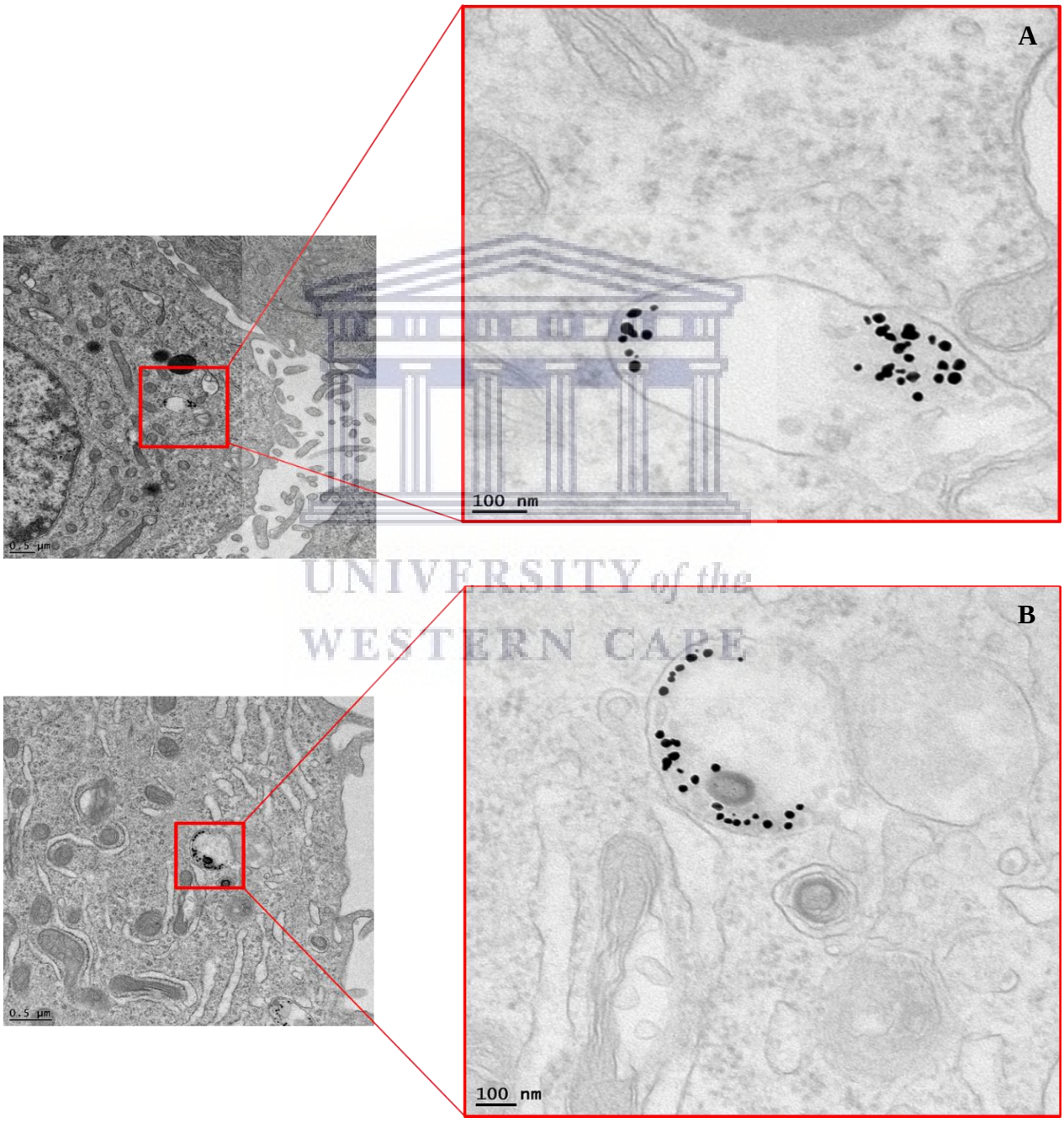

Figure 3.124: Ng-AuNP pH 8 cell internalisation by transmission electron microscopy following treatment with 50 µg/ml over 6 (A), and 24 (B) hours, respectively.

3.4.4 Ng-AuNP's pH 8 100 µg/ml

Following treatment with 100 µg/ml of the Ng-AuNP's pH 8 over 6 (A) and 24 hours (B), cells were sectioned and observed for AuNP internalisation (Figure 3.125). When cells were observed, very marginal differences in the amount of internalised AuNP's were found after 6 hours of incubation (A), and following 24 hours of incubation (B).

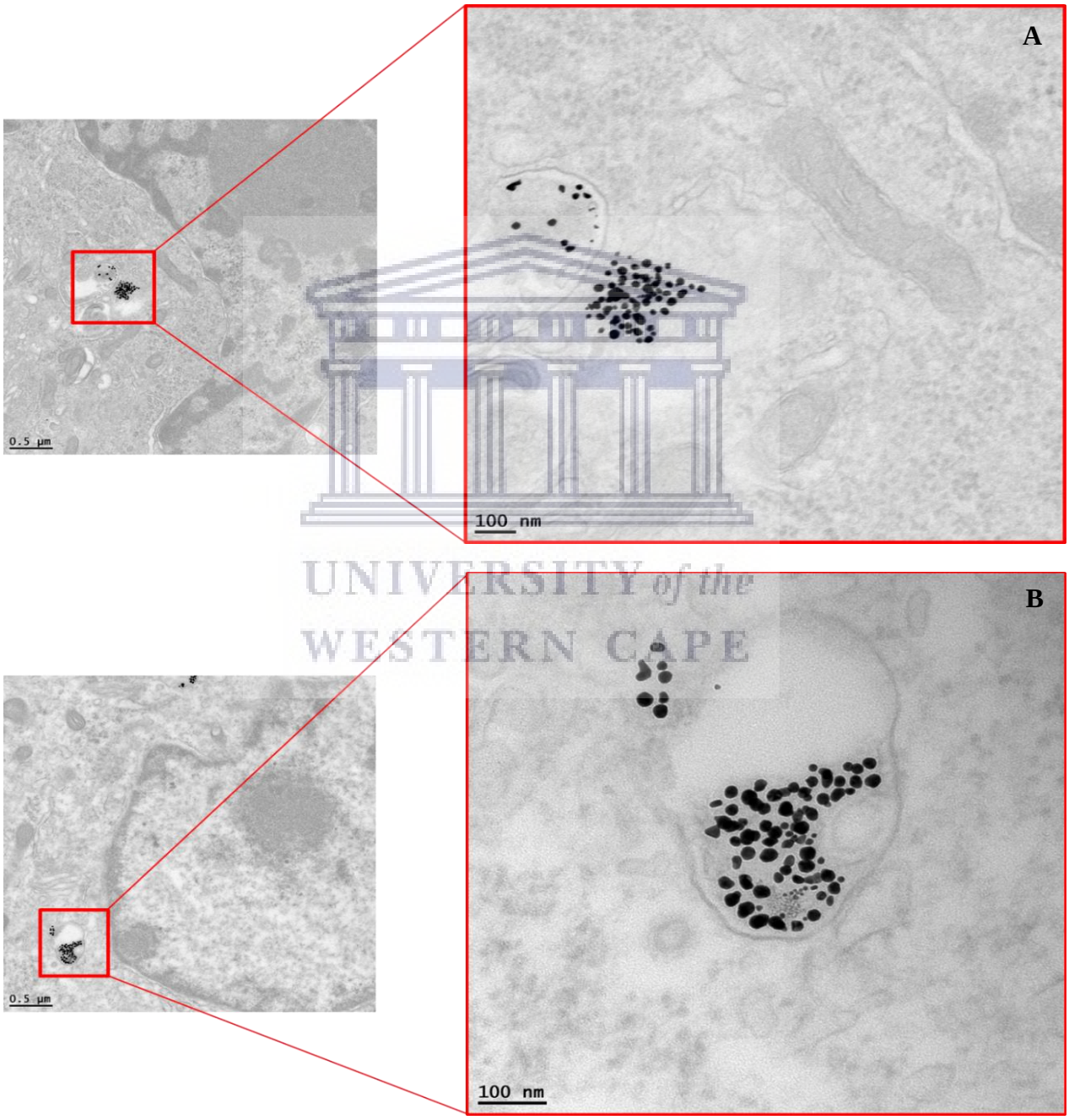

Figure 3.125: Ng-AuNP pH 8 cell internalisation by transmission electron microscopy following treatment with 100 µg/ml over 6 (A), and 24 (B) hours, respectively.

3.5 *In vivo* studies

3.5.1 Change in Tumour Volume

Following PC-3 cell inoculation and palpable tumour formation, SCID-mice were randomised and treated twice weekly with the S1 extract (0.5mg/kg), S1-AuNP's (0.5 and 1.5 mg/g), naringenin (0.5mg/kg) and Ng-AuNP's pH 8 (0.5 and 1.5 mg/kg), respectively. Tumours were measured prior to each treatment, and tumour volumes calculated (Table 3.5).

Mice in control groups yielded consistent, time-dependent increases in tumour volumes between the beginning and end of the study, reaching a mean size of 0.4603±0.2375 cm^3 by day 29. When compared to control groups, only mice treated with the S1-AuNPs (0.5 mg/kg) were found to yield similar increases in tumour volume between day 1 and day 29, exhibiting the second greatest tumour volume by the end of the study (Figure 3.126 A). Conversely, each of the remaining treatment groups yielded comparable inhibitory effects toward tumours, exhibited by considerably slowed growth between day 1 and day 15 of the study. Hereafter, consistent, albeit slowed, tumour growth was noted between day 15 and day 29 of the study, with the S1 extract (0.5 mg/kg) yielding the third greatest tumour volume by day 29 of the study. Mice treated with the Ng-AuNPs pH 8 (0.5 and 1.5 mg/kg), S1-AuNP's (1.5mg/kg) and naringenin (0.5 mg/kg) exhibited the lowest overall tumour volumes by the end of the study.

When the effects of the S1 extract and S1-AuNP's (0.5 and 1.5 mg/kg) were compared (Figure 3.126 B), tumour growth appeared slowed between day 1 and day 11 of the study, with no appreciable difference between each treatment group. Hereafter, the S1 extract (0.5mg/kg) exhibited a sharp, progressive increase in tumour volume between day 11 and day 29, reaching a mean size of 0.4246±0.2614 cm^3 by the end of the study. Conversely, the S1-AuNPs (0.5 and 1.5 mg/kg) only exhibited notable increases in tumour volume between day 22 and day 29, reaching mean sizes of 0.2123±0.1542 cm^3 and 0.0976±0.0582 cm^3, respectively, by the end of the study.

When analysed further, statistically relevant differences could be found between the control and treatment groups between day 11 and day 29 of the study (Figure 3.127 A). Specifically, control groups differed significantly (P=0.0275, P=0.0239, P=0.044) from the S1 extract, S1-AuNP's (0.5mg/kg) and S1-AuNP's (1.5mg/kg), respectively, at day 11 of the study, followed by a significant (P=0.044) difference between control and S1-AuNP's (1.5mg/kg) at day 15 of the study. Next, a significant (P=0.0242) difference was found between control and S1-AuNP's (1.5mg/kg) at day 18 of the study, along with significant (P=0.0275, P=0.0143) differences yielded by the S1 extract and S1-AuNP's (1.5mg/kg), respectively, at day 22 of the study. Finally, the S1 extract and S1-AuNP's (1.5mg/kg) yielded significant (P=0.0167, P=0.002) differences at day 25, followed by the S1-AuNP's (1.5mg/kg) yielding a significant (P=0.0027) difference at day 29 of the study.

When naringenin and Ng-AuNPs were compared, tumour growth appeared dramatically slowed between day 1 and day 15 of the study, without discernible differences between each treatment group (Figure 3.126 C). Hereafter, each treatment group demonstrated very slight, but progressive increases in tumour volume between day 15 and day 25, followed by sharp overall increases in tumour volume between day 25 and day 29 of the study. By the end of the study, mice treated with naringenin (0.5 mg/kg) had a mean tumour volume of 0.0802±0.0463 cm^3, followed by a mean tumour volume of 0.1207±0.0477 $cm^3$for those treated with Ng-AuNP pH 8 (0.5mg/kg), and finally a mean tumour volume of 0.1319±0.0756 cm^3 for mice treated with Ng-AuNP pH 8 (1.5 mg/kg).

When analysed further, statistically relevant differences could be found between the control and treatment groups, between day 11 and day 29 of the study (Figure 3.127 B). Specifically, control groups differed significantly (P=0.0076, P=0.0085, P=0.0111) from naringenin, Ng-AuNP's pH 8 (0.5mg/kg) and Ng-AuNP's pH 8 (1.5mg/kg), respectively, at day 11 of the study, followed by a significant (P=0.0240, P=0275, P=0.0365) difference between control naringemnin, Ng-AuNP's pH 8 (0.5mg/kg) and Ng-AuNP's pH 8 (1.5mg/kg) at day 15 of the study, respectively. Next, significant (P=0.0256, P=0.0363, P=0.016) differences were found between control and

naringenin, Ng-AuNP's pH 8 (0.5mg/kg), Ng-AuNP's pH 8 (1.5mg/kg) at day 18 of the study, respectively, along with significant (P=0.0138, P=0.0044, P=0.0027) differences yielded by naringenin, Ng-AuNP's pH 8 (0.5mg/kg) and Ng-AuNP's (1.5mg/kg), respectively, at day 22 of the study. Finally, naringenin, Ng-AuNP's pH 8 (0.5mg/kg) and Ng-AuNP's pH 8 (1.5mg/kg) yielded significant (P=0.0047, P=0.0044, P=0.0027) differences at day 25, followed by significant (P=0.0038, P=0.0038, P=0.006) difference, for naringenin, Ng-AuNP's pH 8 (0.5mg/kg) and Ng-AuNP's pH 8 (1.5mg/kg), at day 29 of the study.

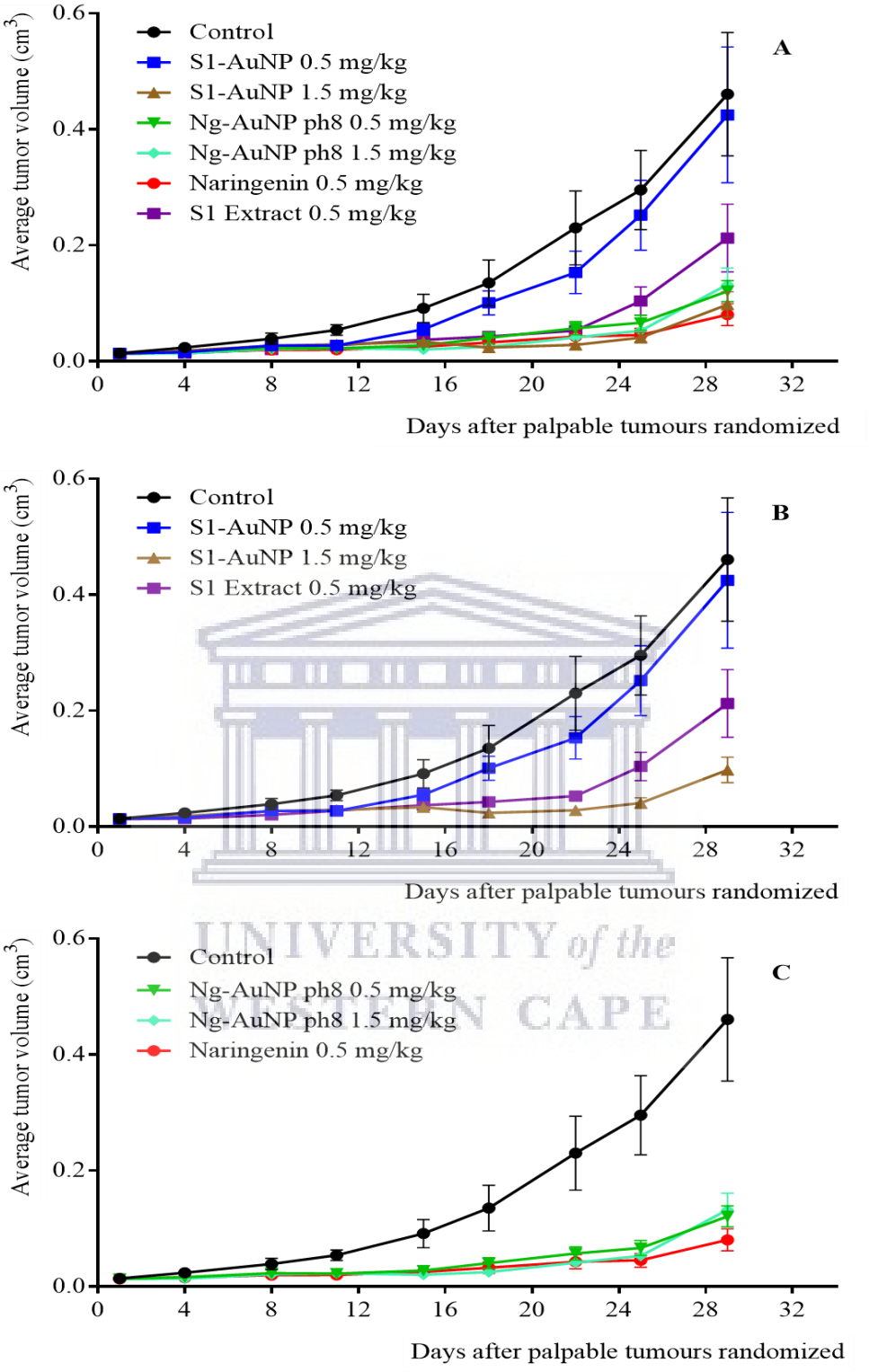

Figure 3.126: PC-3 tumour volumes in SCID-mice treated with gold nanoparticles and extracts over a 29-day period (A), comparing the effects of the S1-AuNPs (0.5 and 1.5 mg/kg) with the S1-extract (0.5 mg/kg) (B), and the Ng-AuNP's pH 8 (0.5 mg/kg and 1.5 mg/kg) with naringenin (0.5 mg/kg) (C).

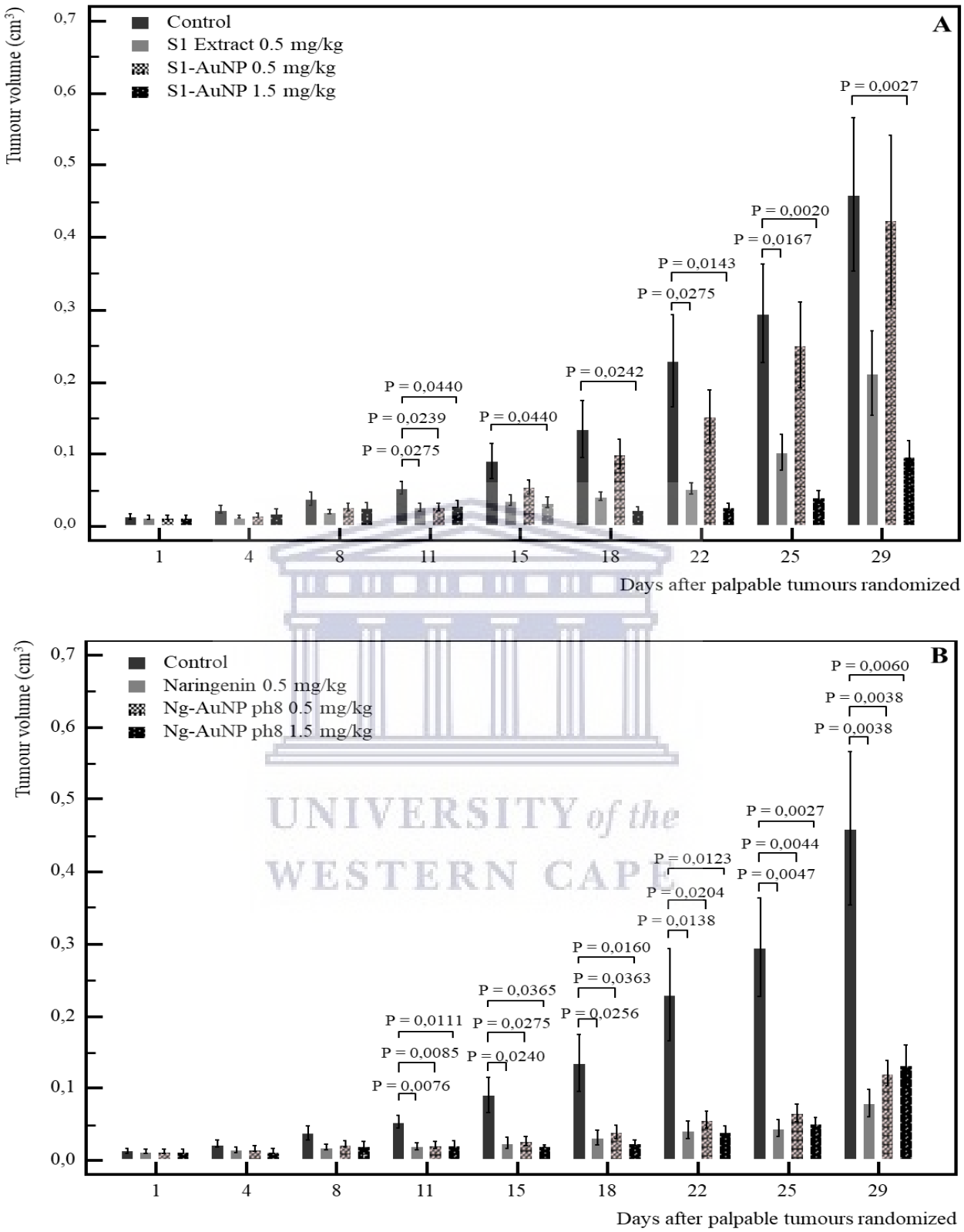

Figure 3.127: PC-3 tumour volumes in SCID-mice treated with the S1-AuNPs (0.5 and 1.5 mg/kg) and S1-extract (0.5 mg/kg) (A), along with the Ng-AuNP's pH 8 (0.5 mg/kg and 1.5 mg/kg) and naringenin (0.5 mg/kg) (B).

Table 3.5: Mean PC-3 tumour volumes in SCID-mice treated with the S1-AuNPs (0.5 and 1.5 mg/kg), S1-extract (0.5 mg/kg), Ng-AuNP's pH 8 (0.5 mg/kg and 1.5 mg/kg), and naringenin (0.5 mg/kg), over a 29-day treatment period.

Day of study	Control	S1 extract (0.5 mg/kg)	S1-AuNP (0.5 mg/kg)	S1-AuNP (1.5 mg/kg)	Naringenin (0.5mg/kg)	Ng-AuNP pH 8 (0.5 mg/kg)	Ng-AuNP pH 8 (1.5 mg/kg)
			Mean Tumour Volume ± SD (cm^3)				
1	0,013±0,008	0,012±0,007	0,013±0,007	0,013±0,007	0,012±0,007	0,013±0,006	0,012±0,007
4	0,023±0,013	0,013±0,006	0,015±0,008	0,018±0,015	0,015±0,009	0,016±0,009	0,013±0,009
8	0,038±0,025	0,02±0,009	0,027±0,012	0,026±0,018	0,019±0,011	0,022±0,012	0,021±0,014
11	0,053±0,024	0,027±0,005	0,027±0,012	0,028±0,021	0,02±0,014	0,022±0,011	0,022±0,013
15	0,091±0,064	0,036±0,006	0,054±0,025	0,033±0,019	0,025±0,019	0,027±0,017	0,02±0,003
18	0,13±0,103	0,042±0,006	0,101±0,054	0,023±0,01	0,032±0,025	0,04±0,024	0,024±0,01
22	0,230±0,168	0,052±0,008	0,153±0,088	0,028±0,01	0,042±0,032	0,056±0,029	0,04±0,019
25	0,295±0,167	0,104±0,0243	0,252±0,147	0,04±0,023	0,045±0,032	0,066±0,034	0,052±0,017
29	0,460±0,237	0,212±0,058	0,425±0,261	0,097±0,058	0,080±0,028	0,121±0,047	0,132±0,076

3.5.2 Change in bodyweight

Following PC-3 cell inoculation and palpable tumour formation, SCID-mice bodyweight was measured and recorded, prior to each treatment (Table 3.6).

Mice in control groups exhibited fairly stable bodyweights between the beginning and day 15, followed by progressively falling bodyweights hereafter, reaching a mean of 25.871±7.042 grams by the end of the study (Figure 3.128 A). When compared to each treatment group, only mice treated with the S1-AuNP's (0.5mg/kg) appeared to exhibit a similar downward trend in bodyweight. Conversely, mice treated with S1-AuNP's (1.5mg/kg), Ng-AuNP's (0.5 and 1.5 mg/kg) and S1 extract exhibited relatively stable bodyweights up to day 28 of the study, where after bodyweights began to decline. Mice treated with naringenin, however, exhibited the most stable bodyweight of all treatment groups, showing no sudden decline toward the end of the study.

The effects of the S1 extract and S1-AuNP's (0.5 and 1.5 mg/kg) were compared (Figure 3.128 B). Mice treated with the S1-AuNP's (0.5mg/kg) exhibited a starting bodyweight of 28.95±2.85 grams, which remained relatively stable up until day 25, followed by a sharp drop hereafter that yielded a mean bodyweight of 25.5±3.87 grams by the end of the study. Statistically, the S1-AuNP's (0.5mg/kg) yielded a significant (P=0.0075) difference in body weights between the beginning and end of the study. Similarly, mice treated with the S1 extract and S1-AuNP's (1.5mg/kg) exhibited starting bodyweights of 31.41±1.76 and 32.34±1.16 grams, respectively, which remained relatively stable up until day 25, after which marginal decreases in mean bodyweights was observed, reaching 30.05±3.96 and 32.18±2.89 grams, respectively, by the end of the study. When the naringenin and the Ng-AuNP's pH 8 (0.5 and 1.5 mg/kg) were compared (Figure 3.128 C), relatively stable body weights were observed throughout the study. Specifically, mice treated with the Ng-AuNP's pH 8 (0.5 and 1.5 mg/kg) exhibited starting bodyweights of 31.95±1.82 and 30.75±2.19 grams, respectively, which remained comparable until day 29, reaching means of 31.02±2.05 and 30.85±2.43 grams, respectively, by the end of the study.

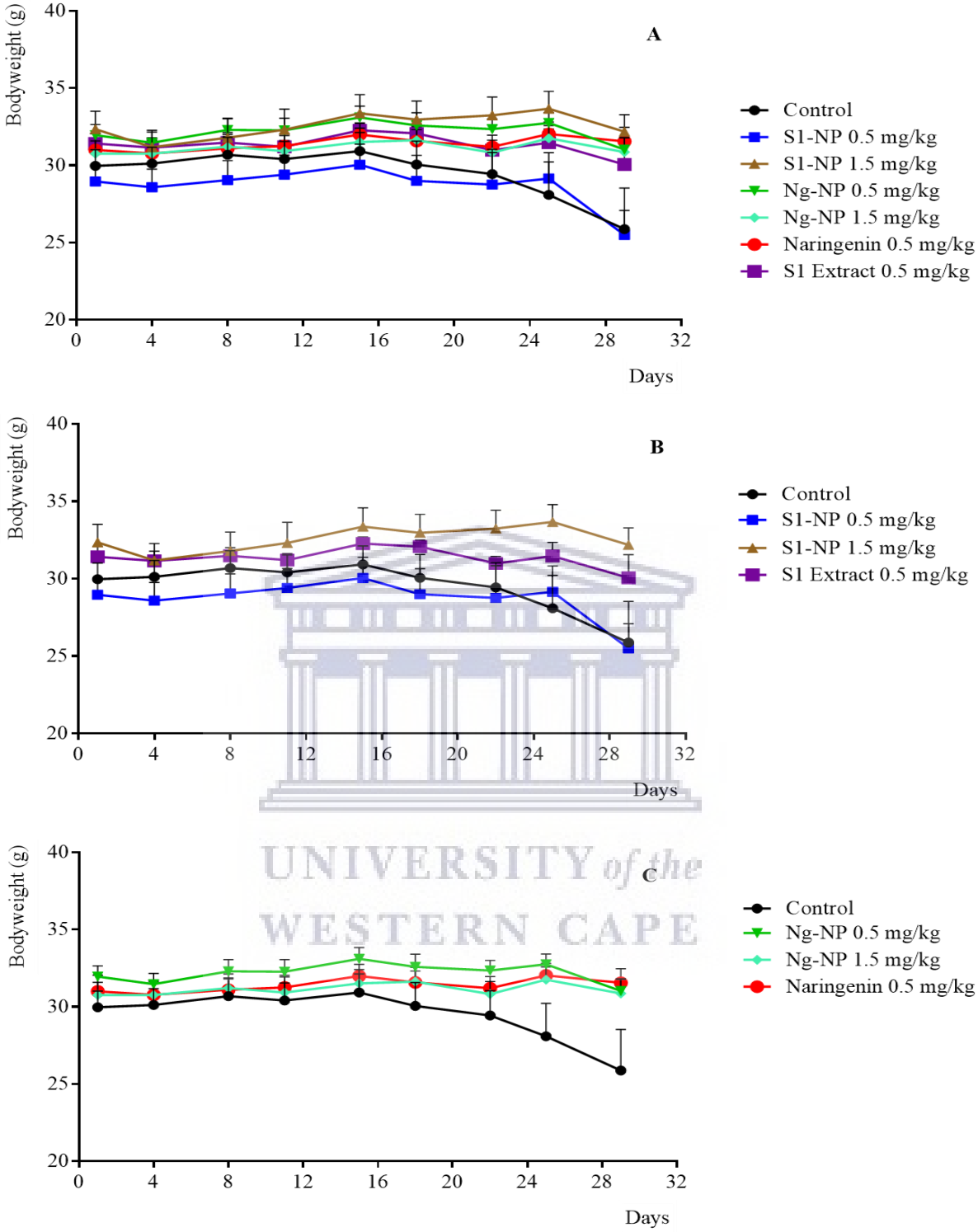

Figure 3.128: Bodyweight in SCID-mice treated with gold nanoparticles and extracts over a 29-day period (A), comparing the effects of the S1-AuNPs (0.5 and 1.5 mg/kg) with the S1-extract (0.5 mg/kg) (B), and the Ng-AuNP's pH 8 (0.5 mg/kg and 1.5 mg/kg) with naringenin (0.5 mg/kg) (C).

Table 3.6: Mean Bodyweight in SCID-mice treated with the S1-AuNPs (0.5 and 1.5 mg/kg), S1-extract (0.5 mg/kg), Ng-AuNP's pH 8 (0.5 mg/kg and 1.5 mg/kg), and naringenin (0.5 mg/kg), over a 29-day treatment period.

Day of study	Control	S1 extract (0.5 mg/kg)	S1-AuNP (0.5 mg/kg)	S1-AuNP (1.5 mg/kg)	Naringenin (0.5mg/kg)	Ng-AuNP pH 8 (0.5 mg/kg)	Ng-AuNP pH 8 (1.5 mg/kg)
			Mean Bodyweight ± SD (g)				
1	29,971±2,759	31,414±1,767	28,957±2,854	32,343±3,069	31±2,753	31,957±1,828	30,757±2,192
4	30,114±2,797	31,157±1,667	28,586±3,098	31,171±2,918	30,771±2,402	31,471±1,807	30,757±2,27
8	30,686±2,979	31,486±1,396	29,043±3,336	31,8±3,23	31,1±2,039	32,3±1,993	31,214±2,393
11	30,414±2,969	31,2±1,1075	29,400±3,353	32,314±3,516	31,257±2,054	32,271±2,056	30,929±2,655
15	30,929±3,153	32,271±1,128	30,043±3,547	33,371±3,203	32±1,985	33,1±1,93	31,514±2,363
18	30,057±4,003	32,071±1,139	29,±4,352	32,971±3,164	31,586±1,93	32,586±2,186	31,629±2,434
22	29,443±4,238	30,986±1,222	28,757±5,491	33,243±3,133	31,2±2,021	32,343±1,734	30.829±2,127
25	28,086±5,635	31,471±2,325	29,150±4,107	33,671±2,981	32,029±2,06	32,757±1,761	31,757±2,18
29	25,871±7,042	30,057±3,969	25,5±3,876	32,186±2,898	31,557±2,404	31,029±2,058	30,857±2,438

3.5.3 Blood analysis

To evaluate potential toxicity of the nanoparticles and extracts, blood parameters were analysed. Baseline readings from heathy, non-tumour bearing SCID mice were compared to tumour bearing groups treated with the various AuNP's and extracts, along with untreated tumour-bearing control groups (Figure 3.129).

When white blood cell (WBC) was analysed (Figure 3.129 A), the normal, healthy control group exhibited a mean WBC count of 0.9±0.24x10^3/µl, whereas untreated control groups displayed much higher WBC count, reaching a mean of 2.6±1.5x10^3/µl. Each treatment group yielded mean WBC counts elevated above baseline, with the S1-AuNP's (1.5mg/kg), yielding the least elevation, reaching a mean of 1.61±0.5 x10^3/µl. Mice treated with the S1-AuNP's (0.5 mg/kg), however, exhibited the second highest WBC count, reaching a mean of 2.26±0.77 x10^3/µl, along with the S1 extract yielded mean WBC counts of 1.91±0.63 x10^3/µl. The Ng-AuNP's groups (0.5 and 1.5 mg/kg) exhibited mean WBC counts of 2.05±0.55 x10^3/µl and 1.82±0.54 x10^3/µl, respectively, along with mice treated naringenin displaying a mean WBC count of 1.74±0.33 x10^3/µl. Upon analysis of red blood cells (RBC) (Figure 3.129 B), normal control group exhibited a mean count of 9.06±0.98 M/µl, whereas the untreated control groups exhibited a slightly elevated RBC count of 11.02±1.16 M/µl. Only mice treated with the S1-AuNPs (1.5 mg/kg) exhibited a RBC count comparable to baseline control, reaching a mean of and 9.35±0.71 M/µl. Mice treated with the S1-AuNP's (0.5), however, exhibited mean RBC counts of 10.86±0.82 M/µl, along with the S1 extracts yielding mean RBC count of 10.63±0.63 M/µl. Similarly, mice treated with the Ng-AuNP's (0.5 and 1.5 mg/kg) had elevated mean RBC counts of 10.22±0.3 M/µl and 10.23±0.4 M/µl, respectively, along with naringenin exhibiting a mean RBC count of 10.35±0.24 M/µl.

When platelets were analysed (Figure 3.129 C), baseline control groups exhibited mean counts of 737.85±313.25x10^3/µl, whereas untreated control groups had mean values of

1115.28±338.2 x10^3/µl. Mice treated with the S1-AuNP's (1.5mg/kg) and Ng-AuNP's (1.5 mg/kg) exhibited platelet counts comparable to baseline control, reaching means of 516.33±446.95 x10^3/µl and 731.66±259.99 x10^3/µl, respectively. Mice in each of the remaining groups displayed platelets counts elevated beyond baseline, with the S1-AuNP's (0.5 mg/kg) exhibiting mean values of 1321.4±231.78 x10^3/µl, the S1 extract yielding a mean count of 1024±339.27 x10^3/µl, Ng-AuNP's (0.5 mg/kg) displaying mean platelet counts of 1008.42±283.98 x10^3/µl, and finally naringenin yielding mean counts of 905.28±338.04 x10^3/µl. When lymphocytes were analysed (Figure 3.129 D), baseline controls had mean values of 0.32±0.13 x10^3/µl, along with tumorous controls exhibited a similar mean count of 0.36±0.18 x10^3/µl. In comparison, the S1-AuNP's (0.5 and 1.5 mg/kg) exhibited notably higher lymphocyte levels, reaching mean counts of 0.54±0.22 x10^3/µl and 0.61±0.31 x10^3/µl, respectively, along with the S1 extract yielding a mean value of 0.5±0.2 x10^3/µl. Furthermore, similarly elevated lymphocyte counts were observed for the Ng-AuNP's (0.5 and 1.5 mg/kg), exhibiting mean counts of 0.53±0.14 x10^3/µl and 0.5±0.16 x10^3/µl, along with naringenin yielding a mean lymphocyte count of 0.54±0.2 x10^3/µl.

When Neutrophils were analysed (Figure 3.129 E), mice in the baseline control group exhibited mean neutrophil counts of 0.43±0.11 x10^3/µl, whereas tumour-bearing controls exhibited notably lower counts, reaching a mean of 2.02±1.56 x10^3/µl. When compared, the S1-AuNP's (0.5 and 1.5 mg/kg) yielded notably lower neutrophil counts, reaching mean values of 1.52±0.58 x10^3/µl and 0.73±0.34 x10^3/µl, respectively, along with the S1 extracts exhibiting mean counts of 1.07±0.32 x10^3/µl. Similarly, noticeably lower neutrophil counts were exhibited by mice treated with the Ng-AuNP's (0.5 and 1.5 mg/kg), exhibiting means of 1.21±0.37 x10^3/µl and 1.07±0.39 x10^3/µl, along with naringenin exhibiting mean neutrophil counts of 0.92±0.2 x10^3/µl.

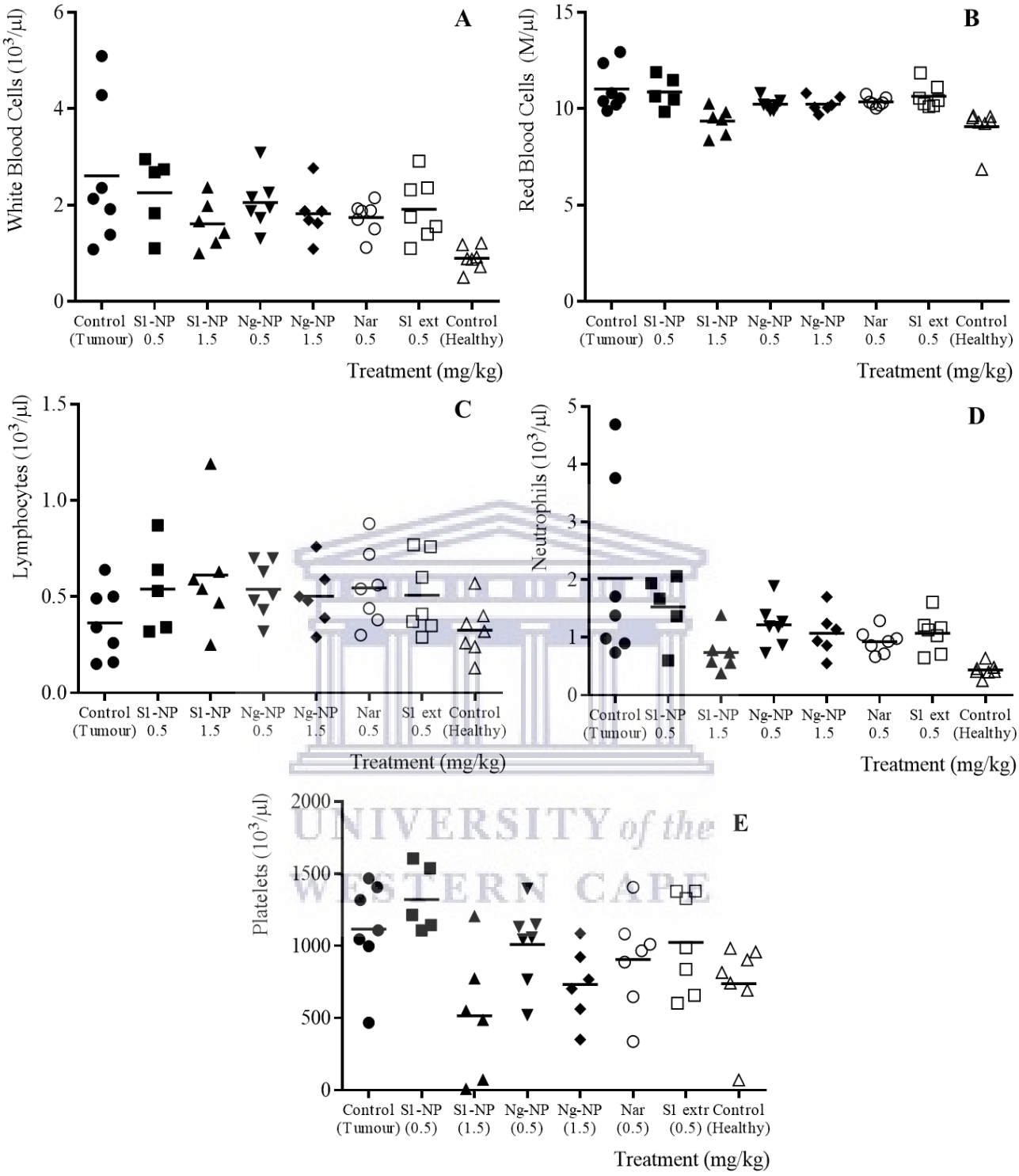

Figure 3.129: Blood analysis of SCID-mice following treatment with the with S1-AuNP's and Ng-AuNP's pH 8 (0.5 and 1.5 mg/kg), along with the S1-extracts and naringenin (0.5 mg/kg) over a 29-day period, showing the effect toward white blood cells (A), red blood cells (B), lymphocytes (C), neutrophils (D), and platelets (E).

3.5.4 Neutrophil-Lymphocyte ratio

To obtain an indication of tumour progression or regression, in response to the various treatments, the neutrophil to lymphocyte ratio (NLR) was calculated (Table 3.7) and used as a biomarker (Figure 3.130). Non-tumour bearing SCID-mice, which were not subjected to any form of treatment, were considered healthy, and subsequently used as baseline controls.

When analysed, mice in baseline control exhibited a mean calculated NRL of 1.45±0.35, whereas the tumour bearing control groups exhibited the greatest overall NRL, reaching a mean of 3.07±1.25.When compared, a similarly elevated NLR was observed for mice treated with the S1-AuNP's (0.5mg/kg), exhibiting a mean value of 2.97±1.13. Similarly, the Ng-AuNP's (0.5 and 1.5 mg/kg) exhibited elevated mean NRL values of 2.27±0.42 and 1.86±0.38, respectively, along with naringenin exhibited elevated mean NRL of 1.9±0.82. Furthermore, mice treated with the S1 extract similarly exhibited an elevated mean NRL value of 2.26±0.68. Conversely, mice treated with the S1-AuNPs (1.5 mg/kg) were found to have the lowest overall NRL, reaching a mean of 1.47±0.86.

When analysed further, a statistically significant (P=0.0339) difference was found between tumour bearing control mice and those treated with the S1-AuNPs (1.5mg/kg), along with a significant (P=0.0082) difference between the healthy control mice and the tumour bearing control.

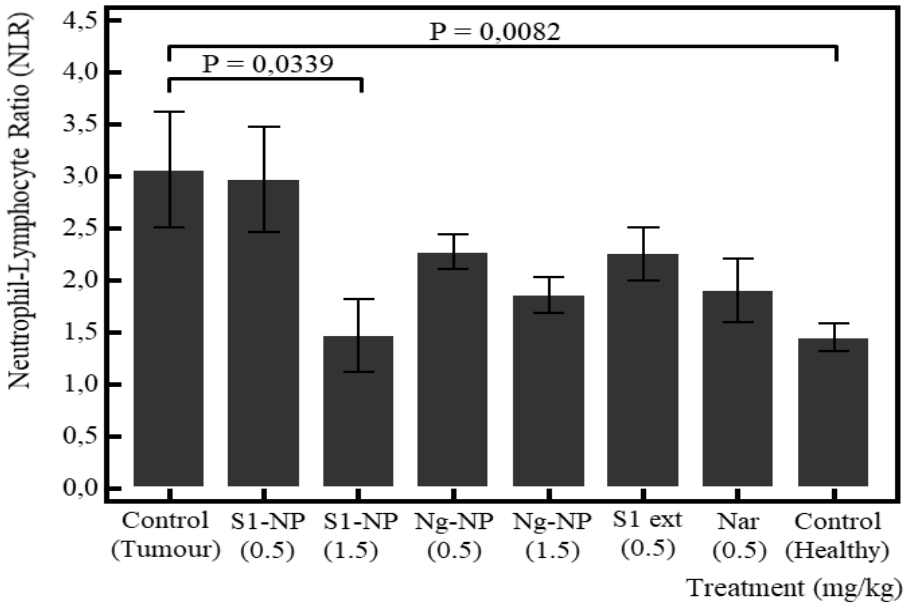

Figure 3.130: Neutrophil to lymphocyte ratio (NLR) of SCID-mice following treatment with the S1-AuNP's and Ng-AuNP's pH 8 (0.5 and 1.5 mg/kg), along with the S1-extracts and naringenin (0.5 mg/kg) over a 29-day period.

Table 3.7: Neutrophil-Lymphocyte ratio for SCID-mice following treatment with gold nanoparticles and extracts

Sample	NLR ± SD	Significant difference to Tumour-bearing control
Healthy control	1.45 ± 0.35	P=0,0082
Tumour bearing control	3.07 ± 1.25	
S1-AuNP's (0.5mg/kg)	2.97 ± 1.13	
S1-AuNP's (1.5mg/kg)	1.47 ± 0.86	P=0,0339
Ng-AuNP's (0.5mg/kg)	2.27 ± 0.42	
Ng-AuNP's (1.5mg/kg)	1.86 ± 0.38	
Naringenin (0.5mg/kg)	1.9 ± 0.82	
S1-extract (0.5mg/kg)	2.26 ± 0.68	

Chapter 4

Discussion

4.1 Gold nanoparticle synthesis and characterisation

4.1.1 Introduction:

Green synthesis principles were used to synthesise gold nanoparticles from two varying aqueous *T. capensis* rhizome extracts, namely the S1 and S2 extracts. Additionally, gold nanoparticles were also synthesised from the bioactive compound naringenin; a phytochemical previously found to be one of two major compounds within *T. capensis*. Subsequently, each gold nanoparticle formulation was characterised using a multi-method approach, utilizing analytical and imaging techniques to reveal their physiochemical properties.

4.1.2 Gold nanoparticle synthesis

The use of plant phytochemicals in the synthesis of gold nanoparticles has become an increasingly popular practice, due to the relative ease of synthesis, reduced cost and low environmental toxicity (Elia et al. 2014b; Shah et al. 2014; Ahmed and Ikram 2015; Lakshmanan et al. 2016; Parveen et al. 2016; Chahardoli et al. 2018). Furthermore, many of these plant-derived gold nanoparticles have been found to be particularly biocompatible, and to possess medicinal properties often owed to the presence of plant phytochemicals on the particle surface (Rao et al. 2016a; Chahardoli et al. 2018). Subsequently, various plants have been investigated for their ability to drive the chemical reduction of gold salt to gold nanoparticles, along with their potential medicinal usage, including *Moringa oleifera* (Chakraborty et al. 2013), *Morinda citrifolia L* (Suman et al. 2014), *Amomum villosum* (Soshnikova et al. 2018), *Mussaenda glabrata* (Francis et al. 2017), *Ziziphus zizyphus* (Aljabali et al. 2018), *Nigella arvensis* (Chahardoli et al. 2018), and *Citrus maxima* (Yuan et al. 2017) to name but a few.

It is commonly accepted that the ability of plant extracts to reduce gold salt to gold nanoparticles is dependent on the presence of easily oxidised phytochemicals (Oueslati et al. 2018). Additionally, these phytochemicals often have the ability to play dual roles during gold nanoparticle synthesis, acting as both reducing and capping agents (Choi et al. 2014; Santhoshkumar et al. 2017; Biao et al. 2018; Oueslati et al. 2018). The generally accepted mechanism for green nanoparticle synthesis is by a phytochemical-driven reduction of gold cations to gold atoms, which agglomerate to form nano-scale particles. Once formed, these particles are subsequently stabilised by available phytochemicals, ultimately yielding isotropic gold nanoparticles (Bindhu and Umadevi 2014; Arun et al. 2014; Aljabali et al. 2018)

A study conducted by Nune et al (2009) investigating the synthesis of gold nanoparticles from tea leaves outlined the role of tea phytochemicals in the synthesis process. Their study demonstrated that isolated catechins commonly found in tea leaves were capable of efficiently driving the chemical reduction of gold salt to the corresponding nanoparticles, simultaneously acting as reducing and capping agents during the synthesis procedure. These included catechin, epicatechin gallate, catechin gallate, epigallocatechin and epigallocatechin gallate (EGCG). In addition to catechins, they also demonstrated that tea theaflavins were capable of reducing the gold salt to gold nanoparticles (Nune et al. 2009b). Since then, the reduction of gold salt to gold nanoparticles by flavonoids, alkaloids, terpenoids, antioxidants and various other plant metabolites, from a range of plant extracts, has been investigated and well documented (Kuppusamy et al. 2016; Yadav and Ranade 2016; Mansoori 2017).

Considering that *T. capensis* rhizomes were previously shown to possess strong antioxidant capabilities (Henkel et al. 2012), and to be a source of catechin, epicatachin and a plethora of other phytochemicals, including afzelechin, epiafzelechin, typharin and typhaphthalide (Shode et al. 2002), it comes as no surprise that the aqueous rhizomes extracts used in the present study were capable of synthesising gold nanoparticles. Furthermore, based on the research conducted

by Shode et al. (2002) and Nune et al. (2009), it may be hypothesised that catechin and epicatechin were present in the extracts used in the current study and played a role in the synthesis of gold nanoparticles. Moreover, the presence and action of catechin and epicatechin may serve to explain the ability of the extracts to act as both reducing and stabilising agents. However, it must be mentioned that while both extracts were found to be capable of simultaneously reducing the gold salt and stabilising the nanoparticles, the addition of gum arabic, an agent often used to confer stability to nanoparticles, yielded a marked improvement in particle stability and was subsequently included in the standard synthesis procedure. Considering that catechin and epicatechin in isolation were previously shown to be capable of fully stabilising gold nanoparticles, it may be hypothesised that low levels of these compounds existed within the extracts used in the present study, yielding the necessity of further stabilisation.

It is essential to note that while the research conducted by Nune et al (2009) demonstrated individual phytochemicals present in tea leaves, such as catechin, were capable of synthesising gold nanoparticle in isolation, whole tea infusions were also shown to yield gold nanoparticles, which were distinctly different from those synthesised from individual phytochemicals. This indicates the possibility of synergistic action between two or more of the individual phytochemicals during the synthesis procedure. For this reason, the possibility of synergistic action in the current study cannot be excluded, whereby two or more phytochemicals present in the extracts acted synergistically in the synthesis and stabilisation of the respective gold nanoparticles, rather than being closely tied to the presence and quantity of individual phytochemicals. Thus, it is possible that catechin and epicatechin may have acted synergistically with one or more compounds commonly found within *T. capensis* rhizomes, namely afzelechin, epiafzelechin, typharin and typhaphthalide, in the reduction of gold salt to gold nanoparticles.. However, further investigation would be required to definitively identify

the exact phytochemicals, along with any potential synergistic action, responsible for the reduction of gold salt to the presently reported gold nanoparticles.

It is also essential to note that plant physiology and biochemistry is greatly influenced by changes in external factors such as precipitation, average temperature and sunshine duration, (Sultan et al. 2018). In the case of medicinal plants in particular, seasonal variations in bioactive compounds, and thereby the optimal season of harvest for maximal medicinal value, has been well documented for multiple plants, including *Withania somnifera*, *Rosmarinus officinalis, Salvia officinalis, Barleria dinteri* and *Zyyphus spina christi*, to name few (Soni et al. 2015; Gololo et al. 2016; Sultan et al. 2018). *T. capensis* is no exception to the effect of seasonality.

Ilfergane (2016) investigated various aspects of *T. capensis*, including the identification and seasonal variation of bioactive active compounds (Ilfergane 2016). Therein, it was reported that *T. capensis* extracts were more bioactive toward prostate cancer and testosterone production during the summer harvest, and subsequently two bioactive compounds were identified, namely quercetin and naringenin (Ilfergane 2016). Furthermore, it was also demonstrated via HPLC profiling that clear variation existed in the observed peaks, and thus phytochemicals present, between each season tested. However, while Ilfergane (2016) provided valuable insight into the seasonal biochemistry and bioactivity of *T. capensis*, the study did not specify the exact months during which rhizomes were collected within each season. Considering the impact of environmental factors on phytochemical production, the exact month of collection is essential, particularly when favourable bioactivity for therapeutic application is concerned. Thus, the present study utilised two separate harvests within the summer season, namely January, representing the start of summer, and March, representing the end of summer, to determine if potential differences in bioactive compounds existed. Interestingly, ICP-MS revealed varying concentrations of naringenin and quercetin within the summer season, whereby January harvests (S2 extract) exhibited more quercetin and less

naringenin, while the March harvests (S1 extract) exhibited more naringenin and less quercetin. While it is not possible to indicate which environmental factor specifically resulted in the compound difference, or how it may have impacted these compound levels, the observed variation outlines the necessity of tightly controlled standardisation of plant extracts, particularly when the desired bioactivity is attributed to the actions of one or more specific phytochemicals.

While it was beyond the scope of the present study to investigate variation in each phytochemical present, it stands to reason that based on the variation of naringenin and quercetin the levels of other previously identified phytochemicals, such as catechin and epicatechin, would also have varied within the summer season. Should this be true, it would serve to explain the two distinctly different gold nanoparticles yielded by the S1 and S2 extracts, namely the S1-AuNP's and S2-AuNP's.

Additionally, quercetin has also previously been shown to act as a strong reducing agent, yielding exceptionally stable gold nanoparticles with a high degree of biocompatibility (Levchenko et al. 2011; Das et al. 2013; Devendiran et al. 2016). It, therefore, stands to reason that quercetin may have acted as a reducing agent, and thereby influenced the synthesis reported in the present study. Should this be true, the varying quercetin concentrations observed between the S1 and S2 extract may partly serve to explain the distinctly different gold nanoparticles reported, namely the S1-AuNP's and S2-AuNP's. It must be mentioned that while this may be true for quercetin, no information regarding the use of naringenin in gold nanoparticle synthesis exists in the currently available literature. However, the present study demonstrated that naringenin is capable of driving the chemical reduction of gold salt to gold nanoparticles when pH is controlled, specifically between pH 7 and pH 8. It has previously been shown that adjustments made to the starting pH of the gold salt solution, with agents such as sodium hydroxide or hydrochloric acid, can directly influence the amount of $AuCl_4$ available

for reaction, ionic strength, resulting particle stability, and the overall activities of the reducing agent (Sirajuddin et al. 2010; Wuithschick et al. 2015). A study conducted by Sun et al. (2019), for example, demonstrated the absolute necessity of pH adjustment by using sodium hydroxide for the successful reduction of gold salt, using carboxymethyl chitosan as a reducing agent, to uniform gold nanoparticles.

Presently, when the pH of the $NaAuCl_4$ salt solution was adjusted with sodium hydroxide, a specific range of pH 7-pH 8 was found to be optimal for the synthesis of gold nanoparticles. While this pH range yielded successful reduction, it must be mentioned that the best outcomes were noted at pH 7 and pH 8, and subsequently the Ng-AuNP's pH 7 and pH 8 were selected for further analyses. Furthermore, considering that complete reduction of the gold salt was not observed outside of pH adjustment, it may be concluded that the addition of sodium hydroxide was essential to stimulate the reductive capabilities of naringenin.

Nevertheless, the present study reports for the first time the synthesis of gold nanoparticles using the bioflavonoid naringenin as both reducing and stabilising agent. Based on this, it may be hypothesised that the varying concentrations of both naringenin and quercetin between the S1 and S2 extracts may have varied the precise phytochemicals involved with gold salt reduction, ultimately leading to different phytochemicals adsorbing to the surface of ,the S1-AuNP's and S2-AuNP's during stabilisation. In order to identify the precise mechanism, however, further investigation will be required.

4.1.3 Characterisation of gold nanoparticles

Each of the nanoparticles synthesised in the present study were subjected to various characterisation techniques to evaluate their physiochemical properties. Specifically, the size,

shape, surface plasmon resonance, monodispersity, surface charge and stability in varying physiological media was analysed

4.1.3.1 Presence of gold nanoparticles

Each gold nanoparticle formulation reported in the present study yielded distinct colour reactions. For the nanoparticles synthesised from the S1 and S2 extracts, a colour shift from yellow-brown to a deep violet was observed within 1 hour of reacting, while those synthesised from naringenin gradually shifted from milky white to deep ruby over the course of 24 hours. It is widely accepted that an observable colour shift toward the red spectrum, such as red, ruby or violet, is indicative of the presence of gold nanoparticles. This is due to the interaction of visible light with metallic nanoparticles, during which surface electrons begin oscillating and subsequently resonate at a particular wavelength, hereby creating the unique optical property of metallic nanoparticles known as surface plasmon resonance (SPR) (Mody et al. 2010; Amendola et al. 2017; Elahi et al. 2018). Each formulation reported in the present study exhibited a colour shift toward the red-purple spectrum, thereby being highly indicative of the presence of gold nanoparticles (Vijayakumar et al. 2011; Xin Lee et al. 2016; Santhoshkumar et al. 2017). However, while the reported colour shifts were highly indicative of gold nanoparticles, it was not sufficient to confirm their presence. Thus, UV-vis spectroscopic analysis was conducted.

UV-vis spectroscopic analysis is a sensitive, cheap and rapid technique used to analyse nanoparticles, often employed to confirm nanoparticle formation, and to reveal valuable information regarding the size, shape and potential agglomeration (Amendola and Meneghetti 2009; Martínez et al. 2013; Tomaszewska et al. 2013). In the case of spherically shaped gold nanoparticles, it is widely considered characteristic to obtain an absorption maxima within the 500-600 nm range (Homberger and Simon 2010; Mody et al. 2010b; Elahi et al. 2018; San

Diego et al. 2018). When this is compared to the UV-vis spectroscopic results obtained in the present study, it is clear that each formulation yielded an absorption maximum well within the 500-600 nm range. Thus, the reduction of gold salt to gold nanoparticles was confirmed for each formulation reported, based on both observable colour change and obtaining characteristic absorption maxima's. However, while UV-vis spectroscopy is useful in revealing the presence of nanoparticles, and can be used to calculate size and concentration (Haiss et al. 2007; Martínez et al. 2013), additional techniques were essential to fully characterise the presently reported gold nanoparticles.

4.1.3.2 Size and size distribution

For each gold nanoparticle formulations, the size and distribution was analysed by various techniques, including dynamic light scattering (DLS), transmission electron microscopy (TEM) and size analysis using the graphic analyses software, ImageJ.

4.1.3.3 DLS measurements

Dynamic light scattering (DLS) is a widely accepted characterisation technique used to determine the size of various forms of nanoparticles (Clayton et al. 2016). Specifically, DLS is a measure of the time-dependent fluctuations of light scattered from particles undergoing Brownian motion (Clayton et al. 2016; Stetefeld et al. 2016). Additionally, DLS provides insight into the polydispersity index (PDI) of nanoparticles, which is an essential indication of nanoparticle distribution. In terms of mono-dispersity, a PDI lower than 0.5 is considered acceptable (Stetefeld et al. 2016). Thus, each nanoparticle reported by the present study was subjected to DLS analyses.

Presently, the S1-AuNP's were found to have an average hydrodynamic size of 88.36 d.nm, while the S2-AuNP's had and average size of 95.73 d.nm, along with the S1x2-AuNP's and

S2x2-AuNP's exhibited average sizes of 160.9 d.nm and 200.3 d.nm, respectively. Considering that the near-two fold increase in particle size occurred alongside doubling the amount of extract used in the S1x2-AuNP's and S2x2-AuNP's, it would indicate that the increased particle size was due to an increase in phytochemicals available during the reaction. It is important to note, however, that DLS measures the entire nanoparticle diameter, rather than individual parts such as the core or cap (Clayton et al. 2016; Stetefeld et al. 2016). Thus, based on DLS alone, it is not possible to state if the observed increase in size was due to increased size of the core, cap, or a combination of the two. Nevertheless, the extract-initiated gold nanoparticles each exhibited relatively low PDI values, indicating a more mono-dispersed nature. In comparison, the Ng-AuNP's at pH 7 and pH 8 were notably smaller, having an average size of 27.1 nm and 29.28 nm, respectively, exhibiting acceptable levels of mono-dispersity (table 3.1). These observations are in line with previous research demonstrating that gold nanoparticle synthesis, particular with regard to particle size, may be directly influenced by adjusting the starting pH (Kang et al. 2015; Mukha et al. 2016; Conde Rodriguez et al. 2017).

Previously, studies investigating the effect of pH on green synthesis have demonstrated than adjusting the starting pH, often towards alkalinity, favoured the synthesis of smaller, spherically shaped gold nanoparticles, while adjusting toward acidity yielded the opposite effect (Shah et al. 2012; Singh and Srivastava 2015; Teimuri-mofrad et al. 2017; Bogireddy et al. 2018; Qiu et al. 2018). Thus, adjusting the pH toward alkalinity in the present study may account for the smaller particle size achieved with the naringenin-initiated gold nanoparticles, in comparison to those initiated by the S1 and S2 extract. Nevertheless, it was observed that increased levels of alkalinity yielded a slight increase in particle size between the Ng-AuNP's pH 7 and Ng-AuNP's pH 8, rather than decreasing particle size. However, it is important to note that the observed increase was measured by DLS, which is a measure of both the metallic

core and substances adsorbed onto the particle surface, and thus the entire particle diameter (Tomaszewska et al. 2013), while the reported tendency toward smaller nanoparticle usually refers to the metallic core size only. Thus, the presently obtained results may still be in line with previous research when the metallic core size is considered, rather than hydrodynamic size. Hence, transmission electron microscopy (TEM) was conducted to further analyse the particle size and structure.

4.1.3.4 TEM imaging and size distribution analysis

In order to further analyse the presently reported gold nanoparticles, TEM images were taken using the Joel200. The images generated clearly show the presence of overall spherically shaped gold nanoparticles for both extract and naringenin initiated nanoparticles. However, when each of the currently reported nanoparticles were compared, clear differences emerged. Specifically, the S1-AuNP's were visually larger when imaged via TEM, with the majority of the observable particles being spherical in shape, along with the appearance of a few triangle and hexagonally shaped particles. However, when the extract concentration was increased in the S1x2-AuNPs, the particles were observably smaller and showed no deviation from a spherical shape. A similar observation was made for the S2-AuNP's and S2x2-AuNP's.

Previously, a study investigating gold nanoparticle synthesis using olive leaf extracts as a reducing agent revealed that the shape of the resulting particles were directly influenced by the extract concentration (Khalil et al. 2012). They demonstrated that low extract concentrations, and thereby low levels of reducing agent, yielded irregularly shaped gold nanoparticles with triangular and hexagonal shapes, while the step-wise increase in extract concentration, and thereby reducing agent, yielded a shift towards smaller, spherically shaped gold nanoparticles (Khalil et al. 2012).

Similar findings were reported in studies investigating nanoparticle synthesis from various plants, such as *Cinnamomum camphora* (Huang et al. 2007), *Volvariella volvacea* (Philip

2009), and *Corchorus olitorius* (Ismail et al. 2018), to name a few. Considering that the *T. capensis* extracts used in the present study acted in a similar manner, and that notable differences in size and shape were observed with an increased extract concentration, it would further suggest that one or more specific phytochemicals present within the extract was responsible for reduction of the gold salt to gold nanoparticles. Furthermore, the necessity of a higher extract concentration to accumulate a higher proportion of reducing agent suggests that the specific phytochemical, or phytochemicals, responsible existed in minute amounts.

Subsequent analysis of TEM images and particle size calculations demonstrated the S1-AuNP's dropped from an average size of 28.29 nm to an average of 13.05 nm in the S1x2-AuNP's, while the S2-AuNP's decreased from 18.99 nm to 13.02 nm in the S2x2-AuNP's. For the naringenin-initiated gold nanoparticles, analyses showed an average size of 15.71 nm for the pH 7 particles, and an average size of 12.53 nm for pH 8 particles. Interestingly, the observed reduction in calculated particle size between the extract-initiated particles, as result of doubling the extract concentration, and the naringenin-initiated particles, as a result of pH adjustment, occurred alongside the previously mention increased hydrodynamic size.

However, it is important to note that TEM imaging reveals the metallic core of the nanoparticle, whereas DLS measures the total nanoparticle diameter, including both the metallic core and all adsorbed substances, otherwise known as stabilisers (Tomaszewska et al. 2013). Considering that doubling the extract concentration yielded a near two-fold increase in total particle diameter, despite the reduction in core size, it would further suggest that the proportion of phytochemicals responsible for stabilisation vastly outnumbered those responsible for reduction. Furthermore, the increased hydrodynamic size, despite reduced core size, in the Ng-AuNP's pH 8 suggests that naringenin was able to more readily reduce the gold salt, and simultaneously stabilise the nanoparticles, more efficiently under pH 8 conditions.

4.1.3.5 Zeta potential

Zeta potential is scientific term describing the difference between the dispersion medium and the layer surrounding dispersed particles, expressed as the electro-kinetic potential of a colloidal system, and is considered an estimate of surface charge in nano-scale materials (Harmata and Guelcher 2016; Gumustas et al. 2017; Krstić et al. 2018). Zeta potential provides valuable information regarding the nature of nanoparticles, as it has previously been shown to directly influence nanoparticle stability and cellular uptake (Harmata and Guelcher 2016; Gumustas et al. 2017).

As a measure of nanoparticle stability, a zeta potential closer to the neutral spectrum confers an increased tendency toward particle aggregation, and thereby low stability, while nanoparticles with stronger zeta potentials typically tend to repel one another, thereby preventing aggregation and maintaining colloidal stability (Gumustas et al. 2017; Gupta and Trivedi 2018). Specifically, zeta potentials, which are strongly positive or negative, typically around +30 mV or -30 mV, confer greater repulsive forces, creating less tendency toward particle aggregation, thereby possessing a high degree of stability. Conversely, lower positive or negative zeta potentials, typically in the range of 5-15 mV, exhibit less repulsive forces, creating a tendency toward aggregation, thereby possessing low levels of stability (Fonte et al. 2012; Gumustas et al. 2017; Gupta and Trivedi 2018). Furthermore, zeta potential may be influenced by altering various factors, including ionic strength, pH, temperature, particle concentration and the concentration of stabilising agent (Lu and Gao 2010; Bhattacharjee 2016; Gumustas et al. 2017).

In previous studies, the concentration of extract used during green synthesis of gold nanoparticle has been shown to influence the zeta potential. In a study investigating gold nanoparticle synthesis using *Fagonia indica* extract, it was found that increasing the extract concentration influenced the measured zeta potential. Specifically, incremental increases in

extract concentration yielded step-wise increases in zeta potential (Ahmad et al. 2015b). Similar findings were reported for gold nanoparticles synthesised from *Artemisia capillaris* (Lim et al. 2016), whereby gradual increases in the extract concentration yielded increases in the measured zeta potential. However, it should also mentioned that the inverse has also been found, whereby increasing concentrations of *Garcinia mangostana*, for example, yielded decreases in the measured zeta potential in gold nanoparticles (Park et al. 2017b). Similarly, stepwise reduction in zeta potential were also observed for gold nanoparticles synthesised from increasing chitosan concentrations (Mohan et al. 2019).

These reports are in line with observations made in the present study. Specifically, zeta potential differences were observed for the extract-initiated gold nanoparticles. The S1-AuNP's exhibited a zeta potential of -27.1±0.2 mV, while doubling the extract concentration, in the S1x2-AuNP's, yielded a zeta potential of -26.2±0.78 mV, which is a negligible decrease at best. The S2-AuNP's, however, demonstrated a slightly greater decrease in zeta potential, dropping from 29.3±0.8 mV to 26.7±0.25 in the S2x2-AuNP's. While these reductions in zeta potential are not significant, they do indicate that increasing the extract concentration, and thereby the amount of phytochemicals potentially adsorbed onto the nanoparticle surface, holds no benefit toward particle stability from an electrostatic point of view. Furthermore, the zeta potential of nanoparticles, particularly in green synthesis, is generally attributed to phytochemicals stabilising the particle, and whether they are anionic or cationic in nature (Shabestarian et al. 2016; Abdel-Raouf et al. 2017; Somchaidee and Tedsree 2018).

The observed decrease in zeta potential may, thus suggest the adsorption of more cationic compounds to the particle surface, rather than predominantly anionic compounds, when the extract concentration was doubled. Moreover, considering that only the S2 extract, when doubled, yielded a more notable decrease in zeta potential, it may further support the notion that phytochemical differences, beyond just that of naringenin and quercetin, existed between

the S1 and S2 extract. Furthermore, the observed decreases in zeta potential were not limited to the extract-initiated gold nanoparticles, and were also observed for the naringenin-initiated nanoparticles where the zeta potential measured dropped from -41.2±0.17 mV, with the Ng-AuNP's pH 7, to a zeta potential of -33.3±1.31 mV in the ng-AuNP's pH 8. While the concentration of naringenin used for synthesis was not altered, the pH conditions were adjusted for each formulation.

These findings are in accordance with a host of research that clearly demonstrates that adjusting pH, above all other factors, has the greatest influence on the resulting zeta potential (Wang et al. 2014; Chang et al. 2015; Shabestarian et al. 2016; Abdel-Raouf et al. 2017; Contreras-Trigo et al. 2018; Somchaidee and Tedsree 2018; Luo et al. 2018). Often, a shift from an acidic pH towards an alkaline pH yields stronger negative charges, however, this shift in charge sometimes only occurs to a point, beyond which further increasing the pH yields weaker negative charges (Ostolska and Wiśniewska 2014; Romdhane et al. 2015; Luo et al. 2018).

Nevertheless, strongly negative zeta potentials were obtained for each gold nanoparticle formulation reported in the present, ranging from -26.2±0.78 mV to -41±3.17 mV, with the naringenin-initiated nanoparticles representing the highest zeta potentials. The presently obtained values are in accordance with the previously mentioned zeta potentials conferring strong repulsive forces, and thereby, nanoparticle stability (Fonte et al. 2012; Gumustas et al. 2017; Gupta and Trivedi 2018). Thus, each nanoparticle produced in the present study was found to conform to generally accepted stability standards.

4.1.4 Phenolic quantification

In order to gain insight into the surface chemistry of the gold nanoparticles, the total polyphenolic concentration was analysed by means of the widely used Folin-ciocalteu phenol (FC) method (Ahmad et al. 2015; Abdelhady et al. 2016; Madhanraj et al. 2017). This technique provides a good idication of the amount of phenolic compounds bound to the nnanoparticle surface.

When analysed, variations in the calculated total polyphenolic content was noted between each of the gold nanoparticle formulations. More specifically, the S1-AuNP's were found to have a total polyphenolic concentration of 447 µg/ml, while the S1x2-AuNP's exhibited and increased concentration of 694 µg/ml. Similarly, the S2-AuNP's had a total polyphenolic concentration of 487 µg/ml, while the S2x2-AuNP's exhibited an increase concentration of 728 µg/ml. In both cases, the extract-initiated gold nanoparticles displayed a near two-fold increase in the total polyphenols measured when the extract concentration used in the synthesis was doubled. These findings are in accordance with the previously suggested increased adsorption of phytochemicals upon doubling of the extract concentration during synthesis, observed as increased hydrodynamic size despite decreased metallic core size, along with alterations to zeta potential. The naringenin-initiated gold nanoparticles also exhibited slight differences in polyphenolic concentration, whereby the Ng-AuNP's pH 7 had a calculated polyphenolic concentration of 423 µg/ml, and the Ng-AuNP's pH 8 had a concentration of 288 µg/ml. Considering that pH has previously been shown to affect the binding of functional groups to nanoparticles (Zhu et al. 2014; Lazarus et al. 2014; Gargi et al. 2018), it may be suggested that the pH differences in the present study affected the action of naringenin during the synthesis procedure. Specifically, it is possible that the more neutral pH 7 may have allowed naringenin to have a lesser affinity towards reduction and a greater affinity toward stabilisation, which would account for the higher total polyphenol concentration along with the previously

mentioned larger metallic core. Conversely, at pH 8, naringenin may have had a greater affinity toward reduction, rather than stabilisation, accounting for the lowered polyphenol concentration and the previously mentioned smaller core size. However, without further analysis, these suggestions remain speculative.

Furthermore, it is important to note that while the FC assay represents a simple and robust method of determining total polyphenols (Ahmad et al. 2015; Abdelhady et al. 2016; Madhanraj et al. 2017), it is subject to limitations, particularly with some plant compounds, such as certain sugars, interfering with the reaction (Sánchez-Rangel et al. 2013). Thus, more sensitive and in depth techniques would provide a greatly improved understanding of the surface chemistry of the current reported nanoparticles. Nevertheless, the current findings provided valuable, albeit limited, insight.

4.1.5 Stability studies

Gold nanoparticles have become favourable agents for various biomedical applications, such as drug delivery, diagnostics and biological sensing (Babu et al. 2013; Das et al. 2014; Elahi et al. 2018). However, the introduction of gold nanoparticles into biological systems can cause alterations to their physiochemical properties, such as size, surface chemistry, surface charge and aggregation tendencies (Vijayakumar S 2014; Dhamecha et al. 2016; Li and Lane 2019). Thus, it is essential that gold nanoparticles intended for biomedical purposes maintain their physiochemical properties, and thereby stability under *in vitro* and *in vivo* conditions. For this reason, the ability of the current gold nanoparticle to maintain stability these conditions was investigated. To achieve this, nanoparticles were observed for agglomeration and shifts in absorption maxima when exposed to diluents and commonly used blood mimicking components, namely cysteine, histidine, bovine serum albumin (BSA), human serum albumin

(HSA), sodium chloride (NaCl), and phosphate buffered saline (PBS) at pH 7, over varying time periods (Nune et al. 2009b; Dhamecha et al. 2016; Jiménez Pérez et al. 2017).

Cysteine and histidine are both naturally occurring amino acids, which are present in blood. As cysteine is a thiol containing amino acid and has the capability of displacing nanoparticle coating materials, thus causing particle aggregation and thereby impairing stability (Satnami et al. 2015; Rani et al. 2016; Dhamecha et al. 2016). Histidine, on the other hand, is commonly associated with allergic immune response, and any interaction between nanoparticles and this amino acid opens the possibility of immunological complications under *in vivo* conditions (Dhamecha et al. 2016). Moreover, proteins have been found to readily interact with nanoparticles, often having affinity towards adsorption (Sotnikov et al. 2019). Considering that albumin is an abundantly occurring blood protein, and that both BSA and HSA, specifically, have previously been shown to interact with gold nanoparticles, testing for possible interaction was essential (Shi et al. 2012; Shao and Hall 2017). Furthermore, the ability of nanoparticles to maintain stability in diluents, and diluent components, used under *in vivo* conditions, such as PBS and sodium chloride, is essential and was therefore tested (Dhamecha et al. 2016).

Presently, the S1-AuNP's exhibited no notably shifts in absorption maxima, or peak widening in each of the media used for up to 48 hours of constant exposure. After 7 days, a slightly increased absorbance, without noticeable peak widening, was observed for groups exposed to BSA, possibly indicating minor protein interaction and possible formation of BSA-AuNP complexes (Shi et al. 2012; Sechi et al. 2014). Furthermore, a slightly decrease absorbance, without substantial peak widening was observed in groups exposed to PBS, following 7 days. Considering that PBS has previously been shown to aggregate gold nanoparticles (Moore et al. 2015), the observed increased absorbance may indicate PBS causing slow, but eventual particle aggregation. Overall, however, the S1-AuNP's exhibited excellent stability up to 7 days of constant exposure. Similarly, the S1x2-AuNP's exhibited excellent stability over each time

point used, showing no signs of peak widening or shifts in absorption maxima up to 7 days of constant exposure. Furthermore, the absorbance changes observed for the S1-AuNP's in BSA or PBS groups were not observed for the S1x2-AuNP's, following 7 days of constant exposure. Similar stability outcomes in each medium was observed for the S2-AuNP's and the S2x2-AuNP's up to 7 days of constant exposure. However, improved stability was not observed in the S2x2-AuNP's.

The improved stability, albeit minor, observed in the S1x2-AuNP's may further support the notion that increasing the extract concentration led to more phytochemicals being present on the particle surface, yielding an improved overall particle stability. However, considering that the S2x2-AuNP's did not display improved stability, despite the potential addition of more phytochemicals to its surface, may further support the notion that phytochemical differences, beyond that of naringenin and quercetin, existed between the S1 and S2 extracts. Furthermore, stability in physiological media has previously been attributed to the presence or absence of particular polyphenols, such as catechins and theaflavins (Nune et al. 2009b). This is in line with the current observations, as differences between the two extracts may have led to different phytochemicals being present on the respective nanoparticle surfaces, and thus varying stability outcomes.

Moreover, the naringenin-initiated gold nanoparticles yielded varying results. More specifically, the Ng-AuNP's pH 7 exhibited no notable shifts or peak widening over each time point, maintaining stability up to 7 days of constant exposure, while the Ng-AuNP's pH 8 demonstrated more noticeable peak widening and decreased absorbance in PBS and NaCl groups. Considering that PBS and NaCl have previously been shown to induce nanoparticle aggregation (Moore et al. 2015; Lee et al. 2015), it is possible that the Ng-AuNP's pH 8 began aggregating in the present study. However, it must be mentioned that while noticeable, changes to these peaks were not dramatic enough to indicate complete particle aggregation, and thereby

total loss of stability. Nevertheless, these differences in stability between these two gold nanoparticles may further support the previously mentioned notion that the pH difference affected the action of naringenin during the synthesis of these nanoparticles, possibly altering affinity toward particle stabilisation being higher in the pH 7 group, and lower in the pH 8 group. If true, the higher concentration of surface-bound naringenin in the pH 7 group may account for higher stability, while the inverse would be true for the pH 8 group.

Nonetheless, it must be noted that the loss of stability noted for the Ng-AuNP's pH 8 only occurred following 7 days of constant exposure to PBS and NaCl, while showing no signs of stability loss at each preceding time point. However, these findings indicated sufficient stability in each tested medium, and therefore suitability for *in vitro* and *in vivo* application, for each of the currently reported gold nanoparticles.

4.2. *In vitro* studies

4.2.1 LNCaP and PC-3 cell viability and gold nanoparticle uptake

4.2.1.1 Extracts, S1-AuNPs, S1x2-AuNP's, S2-AuNP's, and S2x2-AuNP's.

A previous study by Ilfergane (2016) investigated the effect of seasonally produced *T. capensis* rhizome extracts on prostate cancer (LNCaP) cells, benign prostatic hyperplasia PWR-1E cells, and testosterone production in TM3 Leydig cells. With regard to the prostate cancer cells, summer extracts were found to yield the greatest deal of bioactivity, subsequently leading to fractionation and eventual isolation of two bioactive compounds, namely quercetin and naringenin, to which the overall therapeutic effects of the plant were subsequently attributed.

However, while the study conducted by Ilfergane (2016) produced valuable insight into the effects of *T. capensis* extracts, the effects of seasonality towards the plants bioactivity, and the bioactive compounds responsible, the precise points of harvest within each season was not

clearly specified and therefore left to interpretation. Considering that plant to plant compound variations are common place (Sultan et al. 2018), along with geographical location and various external environmental factors altering overall compound production (Sultan et al. 2018), precision is necessary to limit variability, thereby maintaining biomedical validity. For this reason, the present study investigated compound variation, with particular regard to naringenin and quercetin, within the summer season, by producing extracts representing the beginning (S2 extract) and the end (S1 extract) of summer in South Africa.

Upon analysis, differences between S1 and S2 extracts were found, including their colour, odour, and the quantities of quercetin and naringenin. While both extracts were found to contain both bioactive compounds, their ratios differed between the two extracts, with the S2 extracts exhibiting higher concentrations of quercetin to naringenin, and the S1 extract the inverse. Subsequently, these extracts were tested with the prostate cancer LNCaP and PC-3 cells to determine whether the fluctuation ratio of bioactive compounds influenced the previously reported therapeutic effects.

Upon examination, the S1 and S2 extracts were found to yield comparable results in both the LNCaP and PC-3 cell lines. In LNCaP cells, each extract yielded dose- and time-dependent decreases in cell viability, with the S2 extract exhibiting slightly more toxicity at lower concentrations, followed by near identical effects at higher concentrations. Similarly, both the S1 and S2 extracts yielded near identical effects toward PC-3 cells, decreasing cell viability in a dose- and time-dependent manner. Thus, the varying quantities of quercetin and naringenin, were not found to hold any significant influence over their overall effects toward prostate cancer cells. Furthermore, this is in line with observations Ilfergane (2016) made regarding the action of quercetin and naringenin.

Ilfergane (2016) reported that *T. capensis* extracts exhibited cytotoxic effects toward LNCaP cells, along with inducing DNA fragmentation, and activating apoptosis. More importantly,

these effects were replicated using the newly identified bioactive compounds, quercetin and naringenin in isolation, subsequently leading to them being attributed with the bulk of the plants medicinal value toward prostate cancer. Interestingly, it was also shown that while each compound was effective in these regards in isolation, more favourable results were achieved by using them in combination, indicating potential synergistic action between the two compounds.

This synergistic effect observed by Ilfergane (2016) may serve to explain the comparable results yielded by the S1 and S2 extracts in the present study, despite their varying ratios of quercetin to naringenin, suggesting the medicinal value of *T. capensis* extracts toward prostate cancer may not be affected by the specific quantity of quercetin or naringenin, but simply their overall presence and synergistic effects.

Furthermore, it stands to reason that the present extracts acted in a similar way reported by Ilfergane (2016), inducing DNA fragmentation and apoptosis in LNCaP and PC-3 cells. Moreover, considering that both, naringenin and quercetin, have been shown more recently to induce apoptosis in LNCaP and PC-3 cells, it makes sense that a similar effect was achieved by the S1 and S2 extracts. Nevertheless, while this may be true for the extracts, varying results were obtained for the extract-initiated gold nanoparticles.

Presently, the S1-AuNPs were found to yield dose- and time-dependent decreases in LNCaP cell viability similar to the S1 extract, while the S1x2-AuNP's exhibited low overall levels of toxicity, that were significantly lower than the extract at higher concentrations. Furthermore, significantly less overall toxicity was exhibited over each time point when cells were treated with the S2-AuNP's and the S2x2-AuNP's, as compared to the S2 extract. Conversely, significantly more overall toxicity was observed when PC-3 cells were treated with the S1-AuNP's and S1x2-AuNP's, as compared to the S1 extract, over each time point. Similarly, the S2-AuNP's and S2x2-AuNP's were also found to exhibit significantly higher toxicity when

compared to the S2 extract in PC-3 cells. These observations suggest a degree of cell-specificity between the LNCaP and PC-3 cells that was exhibited by the presently reported gold nanoparticles, and may be due to their individual cell uptake rates.

A study conducted by Chavva et al. (2019) investigating cytotoxicity and cell uptake of gold nanoparticles synthesised using Epigallocatechin gallate (EGCG) as a reducing agent (EGCG-AuNP's), compared these nanoparticles to the action of free EGCG, along with citrate-derived gold nanoparticles (Cit-AuNP's), in A375SM melanoma cells, MDA-MB-231 breast cancer, MIA PaCa pancreatic cancer cells, and PC-3 prostate cancer cells. Their study reported that the EGCG-AuNP's exhibited more toxicity in each cancerous cell line, as compared to free EGCG, free citrate, and Cit-AuNP's. Furthermore, they demonstrated that EGCG-AuNP's were more readily taken up by cells than the cit-AuNP's. The improved uptake and cytotoxicity was attributed to the presence of EGCG on the metallic surface, making the nanoparticles more favourable to cellular uptake, thereby increasing intracellular nanoparticle and EGCG accumulation. Considering this, it is possible that the presently reported gold nanoparticles may have acted in a manner similar to those reported by Chavva et al. (2019).

Presently, possible cellular uptake was analysed by dark-field microscopy in LNCaP and PC-3 cells over various time points and nanoparticle concentrations. It was observed that both the S1-AuNP's and S2-AuNP's displayed affinity toward LNCaP and PC-3 cells, but notably higher AuNP-cell accumulation was noted for the PC-3 cells, indicating a higher probability of cell internalisation. Furthermore, subsequent analysis using TEM imaging confirmed dose- and time-depend entry of the S1-AuNP's and S2-AuNP's in PC-3 cells. Nevertheless, these observations suggest that the AuNP's had a greater affinity toward PC-3 cells, rather than LNCaP cells, thereby yielding a greater intracellular accumulation of both gold nanoparticles and phytochemicals.

Likewise, a previous study investigating the action of naringenin toward LNCaP and PC-3 cells demonstrated that naringenin was capable of yielding cytotoxicity and inducing apoptosis in both cell lines. However, the authors noted that naringenin acted in a cell-line specific fashion, having more favourable effects toward PC-3 cells, rather than LNCaP (Lim et al. 2017). It has also been demonstrated that quercetin can readily act as a reducing agent in gold nanoparticle synthesis (Levchenko et al. 2011; Das et al. 2013; Devendiran et al. 2016), while naringenin was found to only reduce gold salt under the correct conditions. With this in mind, it is, therefore, possible that quercetin present in the extracts was utilised for reduction during the synthesis, leading to naringenin and other available phytochemical adsorbing to the metallic surface during stabilisation, yielding particles more conducive to uptake in PC-3 cell based on naringenin-based cell selectivity, resulting in greater intracellular naringenin accumulation. This notion may be further supported by the decreased toxicity observed by the S1x2-AuNP's and S2x2-AuNP's in LNCaP and PC-3 cells, as compared to the S1-AuNP's and S2-AuNP's, as overall particle size and shape has been shown to heavily influence cellular uptake (Arnida et al. 2010; Sun et al. 2018). Therefore, it is possible that the size increase seen for the S1x2-AuNP's and S2x2-AuNP's impaired their ability to be internalised, leading to lower intracellular naringenin accumulation, and thereby lower overall toxicity.

In addition to intracellular naringenin accumulation, it is also possible that the increased presence of the gold nanoparticles themselves may have contributed to the observed toxicity, as metallic particles have previously been shown to interact with and, in cases, disrupt various cell components, including cell membranes, mitochondria and cell nuclei, yielding an array of adverse effects, namely; oxidative stress, DNA damage, mutagenesis, necrosis, stimulation of signalling pathways, lysosomal damage, and apoptosis (Alkilany and Murphy 2010; Rao et al. 2016b; Sun et al. 2018). Consequently, the perceived toxicity toward PC-3 cells may be as a

result of increases intracellular naringenin accumulation, the increased presence of intracellular gold nanoparticles, or a combination of both these factors.

4.2.1.2 Naringenin, Ng-AuNP's pH 7, and Ng-AuNP's pH 8

Naringenin, also known as 2,3-dihydro-5,7-dihydroxy-2-(4-hydroxyphenyl)-4H-1-benzopyran-4-one, is a plant derived flavonoid commonly found in many fruits, particularly citrus fruits, resulting from the hydrolysis of the glycone precursors naringin or narirutin (Park et al. 2017a; Salehi et al. 2019). Furthermore, a wide range of therapeutic effects have been attributed to the action of naringenin, including scavenging reactive oxygen species, exerting anti-inflammatory effects, having anti-atherogenic applications, anti-viral activities, anti-microbial activities, metabolic modulation, along with anti-carcinogenic effects (Park et al. 2017a; Salehi et al. 2019). Predominantly, naringenin has shown therapeutic effects in studies investigating breast cancer, melanoma, brain cancer, pancreatic cancer and prostate cancer (Ilfergane 2016; Lim et al. 2017; Park et al. 2017a; Salehi et al. 2019).

In work conducted by Ilfergane (2016), naringenin was shown to have inhibitory effects towards prostate cancer LNCaP cells, reducing cell viability in a dose dependent fashion. Furthermore, it was found that naringenin caused DNA fragmentation, along with the induction of apoptosis. Similar findings were reported in a study conducted by Lim et al. (2017) investigating the action of naringenin toward prostate cancer PC-3 and LNCaP cells. During their study, naringenin was found to affect LNCaP and PC-3 cells in a number of ways, influencing cell proliferation and migration, inducing reactive oxygen species production and apoptosis, and causing cells to lose mitochondrial membrane potential (Lim et al. 2017).

More specifically, they found that naringenin induced a loss of mitochondrial membrane potential, along with generation of reactive oxygen species and thereby induction of apoptosis

in PC-3 cells, while yielding no loss of mitochondrial membrane potential in LNCaP cells, but with the induction of reactive oxygen species. Furthermore, the authors noted that naringenin was capable of inducing apoptosis via regulation of PI3 and AKT, along with inhibition of ERK1/2, P38 and JNK signalling pathways (Lim et al. 2017). Moreover, they concluded that naringenin acted in a cell-line specific fashion. The observations made in the current study are in line with those reported by Ilfergane (2016) and Lim et al. (2017).

Presently, the Ng-AuNP's pH 7 and Ng-AuNP's pH 8 were compared to the therapeutic action of naringenin in LNCaP and PC-3 cells. Naringenin was found to reduce cell viability in both a dose and time dependent manner, yielding the highest reduction in cell viability and best observable cell death at the highest concentration. Conversely, the PC-3 cells were observably more sensitive to the action of naringenin, showing clear signs of cell death at higher concentrations over each time point tested, along with greater overall reduction in cell viability. Thus, naringenin can be said to act in a cell-line specific manner consistent with the observations made by Lim et al. (2017). Moreover, considering that Lim et al. (2017) reported the induction of apoptosis in both these cell lines, albeit by different mechanisms, it is possible that naringenin acted in a similar manner in the present study. Should this be true, it would suggest that naringenin presently yielded a decrease in cell viability, and produced signs consistent with cell death via the induction of apoptosis in the PC-3 and LNCaP cells. Furthermore, when the results obtained for the Ng-AuNP's are considered, it is possible that they may have acted in a similar manner.

Presently, the Ng-AuNP's appeared to have favourable effects towards prostate cancer cells, particularly in overcoming the resistance to naringenin exhibited by LNCaP cells. It was noted that Ng-AuNPs showed improved effects towards the LNCaP cells, particularly at lower concentrations, whereby the Ng-AuNP's pH 7 and Ng-AuNP's pH 8 both exhibited enhanced cell viability reduction, and the visual appearance of cell death at lower concentrations, over

24 and 48 hours incubation periods. However, these improved effects were not noted following 72 hours of incubation, particular at the highest concentration, whereby free naringenin slightly exceeded the capabilities of the nanoparticles. Conversely, the Ng-AuNP's were not found to hold any improved effects towards PC-3 cells. Particularly, the Ng-AuNP's pH 7 were found to be less effective at lower concentrations over each time point, while exhibiting comparable effects at the highest concentration. The Ng-AuNP's pH 8 however displayed very comparable effects to free naringenin at each concentration.

At first glance these findings may appear to offer no biologically significant benefit over free naringenin, but a closer look at the limitations inherent to the flavonoid reveals the true potential of the nanoparticles. While naringenin has been shown to enormous medicinal value, ranging from being anti-carcinogenic, an anti-inflammatory, to being radio-protective, its clinical usage is severely limited (Salehi et al. 2019). Specifically, the limitations arise due to poor water solubility, poor oral bioavailability and intestinal absorption, low stability, rapid metabolism and ineffective transport across biological membranes yielding low tumour site bioavailability (Goncalves et al. 2015; Sangpheak et al. 2015; Gera et al. 2017; Rajamani et al. 2018; Salehi et al. 2019).

To overcome these issues, various approaches have been investigated to improved bioavailability and absorption, such as complexing the flavonoid with β-cyclodextrin to improve uptake (Sangpheak et al. 2015), forming polymeric nano-suspensions of naringenin (Rajamani et al. 2018) and binding naringenin to gold nanoparticles synthesised via citrate reduction (Dalwadi et al. 2019). While these methods were found to improve delivery, they were complex in nature, labour intensive and expensive. Conversely, the present study produced gold nanoparticles directly from naringenin, using it as a reducing and stabilising agent. Furthermore, the presently reported Ng-AuNP's were significantly smaller in size in comparison to the naringenin-bound gold nanoparticles reported by Dalwadi et al. (2019),

along with stronger zeta potentials, and thereby stability. Moreover, the presently used Ng-AuNP's showed effects comparable to free naringenin towards LNCaP and PC-3 cells, which may be due to intracellular Ng-AuNP accumulation.

In the present study, the possibility of Ng-AuNP pH 8 cellular uptake was analysed by dark-field microscopy in LNCaP and PC-3 cells over various time points and nanoparticle concentrations. It was observed that both Ng-AuNP's pH 8 displayed affinity toward the both LNCaP and PC-3 cells. However, notably higher AuNP-cell accumulation was noted for the PC-3 cells. Furthermore, subsequent analysis using TEM imaging confirmed dose and time depend entry of the Ng-AuNP's in PC-3 cells. Moreover, the higher AuNP-cell accumulation observed with PC-3 cells occurred alongside the increased sensitivity to the Ng-AuNP's pH 8 displayed by these cells. Thus, it stands to reason that the greater sensitivity exhibited by PC-3 cells occurred as a result of greater intracellular gold nanoparticles accumulation, and thereby greater intracellular naringenin accumulation, as compared to the LNCaP cells. However, it must also be mentioned that the presence of intracellular gold nanoparticles, particularly in great quantities, can have adverse effects towards cells, such as DNA damage, necrosis, oxidative stress and apoptosis (Alkilany and Murphy 2010; Rao et al. 2016b; Sun et al. 2018). Thus, it remains a possibility that the observed effects occurred simply as a result of intracellular gold nanoparticle accumulation at levels sufficient to incite one or more adverse effects, such as DNA damage or oxidative stress, leading to cell death, rather than intracellular naringenin accumulation. Furthermore, it is also possible that a degree of synergism existed between the effects of intracellular gold nanoparticle, and intracellular naringenin accumulation, and thereby yielding the observations made for the LNCaP and PC-3 cells.

Nevertheless, the present findings may signify a simple, low cost method of overcoming the aforementioned clinical limitations associated with naringenin. This notion may be further supported by considering that the Ng-AuNPs exhibited effects comparable to free naringenin

towards LNCaP and PC-3 cells, indicating a likely similar mode of action. Should that be true, it may suggest that the presently reported Ng-AuNP's would exert effects similar to free naringenin, such as the ability to induce apoptosis, lower mitochondrial membrane potential and inhibit cell migration ,reported by Lim et al. (2017). This notion may be further supported by considering the effects of the Ng-AuNP's towards the pancreatic cancer Panc1 cell line.

4.2.2 Panc1 cell viability

Pancreatic cancer has been described as one of the most aggressive, and often metastatic cancers, being the third most common causes of cancer-related deaths (Park et al. 2017a; Zhu et al. 2018). Treatment options for pancreatic cancer range from immune therapy, endoscopic therapy, chemotherapy and radiotherapy, and surgery which still represents the only curative option to date (Zhu et al. 2018). However, despite surgical advances, patients often report a greatly diminished quality of life as the result of post-operative complications, such as pancreatic fistula, post-pancreatectomy haemorrhage, bile leakage and delayed gastric emptying (Zhu et al. 2018; Heerkens et al. 2018). Furthermore, long term survival following surgery is questionable, with a reported 90% of patients relapsing following surgery, in addition to an overall long term survival rate of 28-37% when surgery is combined with chemotherapy (Zhu et al. 2018; Takahashi et al. 2018). For these reasons, various medicinal plants have been investigated as a safe and effective alternative to more conventional means of treatment. Various plant extracts have previously exhibited promising effects toward pancreatic cancer, including *Achillea millefolium, Calendula officinalis, Melissa officinalis, Origanum majorana*, and *Geissospermum vellosii* to name a few (Dong et al. 2018; Mouhid et al. 2018). Furthermore, isolated plant flavonoids, such as quercetin and naringenin, have also been investigated.

Lee et al. (2013) showed that quercetin was capable of inducing cytotoxicity in Panc1 cells, disrupting mitochondria function, inducing reactive oxygen species production and inducing apoptosis. Similarly, a study conducted by Park et al. (2017) investigating naringenin as a potential therapeutic agent in the treatment of pancreatic cancer also demonstrated the induction of increased intracellular reactive oxygen species production, and apoptosis when cells were treated with the flavonoid. Thus, both quercetin and naringenin have clear benefits toward pancreatic cancer. However, these benefits were not seen when Panc1 cells were treated with the S1 and S2 extract, despite the presence of these flavonoids.

No toxicity toward Panc1 cells was observed when treated with the S1 extract over 24, 48 and 72 hour periods. The S2 extract, however, yielded modest toxicity at the highest extract concentration, accounting for a 4.07% and 16.32% reduction in cell viability over 48 and 72 hour periods, respectively. Thus, despite the presence of both quercetin and naringenin, these findings suggest the S1 extract exhibit no therapeutic benefits, while the S2 extract exhibited weak anti-cancer effects toward these cells. Furthermore, considering that the S2 extract was found to contain a higher ratio of quercetin to naringenin, and that the S2 extract exhibited weak anti-cancer effects, it may be hypothesised that these cells were more sensitive to the effects of quercetin.

Additionally, pancreatic cancer has previously been shown to exhibit a great deal of drug resistance, inherently having a high rate of drug efflux, aberrant gene expression mutations, dysregulation of apoptotic pathways, and exhibiting epithelial-mesenchymal transition (Zhou et al. 2008; Long et al. 2011; Grasso et al. 2017). Accordingly, it is possible that the levels of quercetin and naringenin present in the extract may have been too low to overcome the resistance mechanism exhibited by these cells, yielding little to no intracellular accumulation of the flavonoids, and thereby being unable to exert any meaningful therapeutic effect.

Moreover, the use of gold nanoparticles has been investigated to overcome these resistance mechanisms.

A recent example is the study conducted by Wang et al. (2019) investigated the synthesis of gold nanoparticles using *Panax notoginseng* extracts, and the potential therapeutic effects toward the pancreatic cancer Panc1 cells. Therein, Wang et al. (2019) showed that their ginseng-derived gold nanoparticles were capable of inducing cytotoxicity, intracellular reactive oxygen species production, and apoptosis in Panc1 cells. Finally, they concluded that their gold nanoparticles represented an easily produced, and environmentally friendly anti-cancer agent in the treatment of pancreatic cancer (Wang et al. 2019). The same may be said for the presently produced extract-derived gold nanoparticles.

While the extracts yielded only modest effects toward the Panc1 cells, both the S1-AuNP's and S1x2-AuNP's exhibited dose- and time-dependent decreases in Panc1 cell viability, accounting for a 58.49% and 36.63% reduction at the highest concentration, respectively, following 72 hours of incubation. Similarly, the S2-AuNP's and S2x2-AuNP's exhibited dose and time dependent reduction in cell viability, accounting for 38.16% and 42.59% at the highest concentration, respectively, following 72 hours of incubation. As previously mentioned, it is far more likely, due to their natures, that quercetin present in the extracts was used as a reducing agent for the gold nanoparticle synthesis, while naringenin was used for particle stabilisation (Levchenko et al. 2011; Das et al. 2013; Devendiran et al. 2016). Hence, it is possible that the notably greater therapeutic effects exerted by the gold nanoparticles was a function of cellular uptake, leading to greater intracellular naringenin accumulation, and therefore, significantly better therapeutic effects. Furthermore, this notion may be further supported by observations made by Lou et al. (2012), along with the present observations made for free naringenin, and the Ng-AuNP's.

Research conducted by Lou et al. (2012) shows that naringenin was capable of reducing cell viability in pancreatic cancer ASPC-1 and Panc-1 cell lines over 24, 48 and 72 hour incubation periods, along with supressing cell migration and invasion, and reversing resistance to the chemotherapeutic agent gemcitabine. More recently, Park et al. (2017) investigated the use of naringenin in the treatment of pancreatic cancer using the human pancreatic cancer SNU-213 cell line. They demonstrated that the flavonoid was capable of inducing apoptosis in pancreatic cancer cells by increasing levels of reactive oxygen species production, which in turn yielded up-regulation of apoptosis signal-regulation kinase 1 (ASK 1), along with the JNK, p38 and p53 proteins (Park et al. 2017a). Thus, evidence for the therapeutic benefits of naringenin in the treatment of pancreatic cancer exists, and results of the present study are in accordance with previous data.

Presently, naringenin was also found to reduce Panc1 cell viability, and produce visible signs of cell death, in a dose-depend fashion over 24, 48 and 72 hour incubation periods, which is consistent with the findings of Lou et al. (2012). More importantly, similar effects were exhibited by the Ng-AuNP's. The Ng-AuNP's pH 7 yielded dose-depend reduction in cell viability, differing significantly from free naringenin at the highest concentration over 24 and 48 hours. Following 72 hours of incubation however, the effects were comparable to free naringenin at each concentration. Similarly, the Ng-AuNP's pH 8 yielded significantly greater reductions in cell viability at the highest concentration at each time point. Based on these observations, the Ng-AuNP's may be said to have presented similar therapeutic benefits to free naringenin toward the Panc1 cells. Furthermore, the effects exhibited by the Ng-AuNPs' may also be said to be in line with those reported by Lou et al. (2012) and Park et al. (2017a), for free naringenin toward pancreatic cancer.

It is important to note that while the work by Lou et al. (2012) and Park et al. (2017a) demonstrated the potential usage of naringenin in the treatment of pancreatic cancer, they did

not account for the limitations associated with the flavonoid. For this reason, the present findings further suggest that the Ng-AuNP's may serve as a simply produced therapeutic agent for the treatment of pancreatic cancer, in addition to prostate cancer. Moreover, considering that free naringenin has previously shown benefits toward various other forms of cancer, such as breast cancer, melanoma and brain cancer (Lim et al. 2017; Salehi et al. 2019), it stands to reason that the Ng-AuNP's may have application as therapeutic agents in their treatment as well.

Additionally, the simple presence of intracellular gold nanoparticle may have also contributed to the increased toxicity, as their presence has been shown to disrupt mitochondria and cell nuclei, induce oxidative stress, DNA damage, mutagenesis, necrosis, stimulation of signalling pathways, lysosomal damage, and apoptosis (Alkilany and Murphy 2010; Rao et al. 2016b; Sun et al. 2018). Based on these findings, it is possible that the present observations for the extract and naringenin derived gold nanoparticles simply occurred as a consequence of intracellular particle accumulation, rather than phytochemical delivery.

4.2.3 HAEC cell viability

In recent years, alternative and traditional forms of medicine have become an increasingly popular choice among patients, often owed to the belief that they represent a more natural and therefore safe therapeutic option (Fatima and Nayeem 2016; Subramanian et al. 2018). However, while extensive investigation has proven validity to many claims made for medicinal plants, along with the identification of bioactive compounds, a growing body of research have outlined potential dangers associated with many commonly used medicinal plants. Examples include nephrotoxicity in the case of herbs such as *Tripterygium wilfordii* and *Averrhoa carambola*, hepatotoxicity for herbs such as *Cimicifuga racemosa*, *Celtis occidentalis* and *Scutellaria baicalensis*, neurotoxicity for *Papaver somniferum* and *Conium maculantum*, and

cardiotoxicity for herbs such as *Glycyrrhiza glabra*, *Ephedra distachya* and *Aconitum napellus*, to name a few (Fatima and Nayeem 2016; Mensah et al. 2019). It must be mentioned that while a great deal of the toxicity associated with commonly used medicinal plants stems from improper dosing, plant-drug interaction, treatment via unqualified practitioners or self-treatment, toxicity was also shown for plants used as the sole treatment (Fatima and Nayeem 2016; Mensah et al. 2019). Nevertheless, the potential for unwanted toxicity exists for commonly used medicinal plants, and therefore investigating the safety of these plants is essential.

T. capensis is a commonly used medicinal plant in South African traditional medicine, often used as a treatment for infertility, dysmenorrhea and to boost libido in men (Steenkamp 2003; Masoko et al. 2008; Abdillahi and Van Staden 2012; Henkel et al. 2012a). Furthermore, *T. capensis* extracts were previously shown to act as a powerful scavenger of reactive oxygen and nitrogen species under *in vitro* conditions (Henkel et al. 2012), along with more recent investigations demonstrating favourable effects of the extracts and isolated bioactive compounds towards prostate cancer LNCaP cells, and testosterone production in TM3 leydig cells (Ilfergane 2016). However, while these reports are favourable, information regarding potential systemic toxicity is limited, and therefore must be evaluated. For these reasons, the safety of the S1 and S2 extracts, naringenin, and subsequent nanoparticles were investigated in the human aortic endothelial HAEC cell line.

The S1 extract yielded low levels of toxicity toward HAEC cells at lower concentrations, accounting for a 29.69 % reduction in cell viability following exposure to 100 µg/ml over a 72-hour period. However, the highest concentration yielded more pronounced toxicity, yielding a 52.61 %, 60.17 % and 73.18 % reduction in cell viability over 24, 48 and 72-hour periods, respectively. Similarly, the S2 extract yielded comparably low levels of toxicity up until a concentration of 50 µg/ml. Hereafter, increasing levels of toxicity was noted following 72

hours of incubation at 100-200 µg/ml, accounting for a 59 % and 87.91 % respective reduction in cell viability. Furthermore, these findings may be explained by observations made by Daubney et al. (2015).

Previously, a study conducted by Daubney et al. (2015) investigating the action of quercetin toward H9c2 cardiomyocyte cells demonstrated that the flavonoid exerted a dual function, acting as both a cardio protective and cardio toxic agent. More specifically, these authors found that at low doses quercetin exerted a cardio protective effect, protecting cells from hydrogen peroxide induced damage, while high doses exerted a cardio toxic effect, reducing cell viability, increasing lactate dehydrogenase release and inducing apoptosis in a dose and time dependent manner (Daubney et al. 2015).

Considering that both the S1 and S2 extracts were shown to contain quercetin, it is possible that greater accumulation of quercetin occurred at high extract concentrations, beyond what would be considered protective for the HAEC cells, thereby exerting cardio toxic effects. This notion may be further supported by the action of the S2 extract, which was found to contain a higher proportion of quercetin to naringenin, yielding a slightly greater deal of toxicity in comparison to the S1 extract. Nevertheless, these findings suggest that the rhizome extracts are relatively safe toward cardiac cells at low doses, while higher doses may yield cardiotoxicity, particularly over prolonged periods of time. Furthermore, these effects appeared to be more pronounced when treated with the S1-AuNP's and S2-AuNP's.

The S1-AuNP's, exhibited relatively low overall toxicity at lower concentrations, but were found to exhibit a significantly greater reduction in cell viability when compared to lower concentrations of the S1 extract, while being near identical to the extract at the highest concentration. Similarly, the S2-AuNP's also exhibited greater reductions in cell viability at lower concentrations when compared to the S2 extract, while exhibiting significantly lower levels of toxicity at higher concentrations. Interestingly, the S1x2-AuNP's and S2x2-AuNP's

exhibited the least amount of toxicity toward HAEC cells, accounting for 47.91% and 37.82% reduction in cell viability, respectively, following 72 hours of exposure to the highest concentration.

Considering that quercetin was previously shown to readily reduce gold salt, it is far more likely that quercetin present in the extracts drove the reduction of gold salt, potentially in a synergistic manner with catechin and epicatechin, during the gold nanoparticle synthesis procedure and thus would no longer be present, and therefore unable to exert any effects (Levchenko et al. 2011; Das et al. 2013; Devendiran et al. 2016). Furthermore, it was also previously shown that the mere presence of intracellular gold nanoparticles, particularly when accumulated in high numbers, can have adverse effects towards cells, such as DNA damage, necrosis, oxidative stress and apoptosis (Alkilany and Murphy 2010; Rao et al. 2016b; Sun et al. 2018). Thus, it is more likely that the observed toxicity occurred as a result of intracellular gold nanoparticle accumulation at levels sufficient to incite one or more adverse effects, such as DNA damage or oxidative stress, leading to cell death.

This notion may be further supported by the decreased toxicity exerted by the S1x2-AuNP's and S2x2-AuNP's, as these nanoparticles were nearly double the size of the S1-AuNP's and S2-AuNP's, considering that overall particle size was previously been shown to directly influence cellular uptake (Arnida et al. 2010; Sun et al. 2018). Therefore, it is possible that fewer of the S1x2-AuNP's and S2x2-AuNPs were internalised by the HAEC cells, thereby limiting adverse effects such as DNA damage and oxidative stress, thus yielding lower overall toxicity. This may be further supported by the comparing the S1x2-AuNP's and S2x2-AuNP's, as the S2x2-AuNP's were larger in size and yielded slightly less overall toxicity as compared to the S1x2-AuNP's. However, while the observed toxicity is likely due to intracellular

nanoparticle accumulation, the action of naringenin that may adsorbed to the particle surface during stabilisation might have played a role.

Presently, naringenin was found to lower HAEC cell viability in a dose-dependent fashion over 24, 48 and 72-hour incubation periods, along with yielding observable signs of cell death. Conversely, the Ng-AuNP's were found to exhibit less overall toxicity toward HAEC cells, particularly at lower concentrations. More specifically, the Ng-AuNP's pH 7 yielded significantly less toxicity when compared to free naringenin at each concentration, over each time point. However, while less overall toxicity was observed, the highest concentration still accounted for a 70.5% reduction in cell viability following 72 hours of exposure. The Ng-AuNP's pH 8 also yielded less toxicity in comparison to naringenin at lower concentration, albeit less effectively than seen with the Ng-AuNP's pH 7. At the highest concentration, however, the Ng-AuNP's pH 8 exerted near identical effects to free naringenin, accounting for an 84.87% reduction in cell viability following 72 hours of incubation. These observations indicate that despite the promising results obtained for the prostate and pancreatic cancer cells, naringenin may pose potential risks toward non-cancerous cells. Furthermore, these observations directly contradict previously reported cardio-protective effects exerted by naringenin.

A study conducted by Testai et al. (2017) investigating cardiovascular disorders reported that naringenin administration conveyed cardio-protective effects toward ischemia/reperfusion injury in both young and aged rats. Similarly, a study conducted by Liu et al. (2016) investigating potential cardio-protective effects of naringenin toward cardio-renal syndrome reported the flavonoid attenuated cardiac remodelling and dysfunction, along with decreased lipid profiles, lowered cardiac inflammation, and reduced oxidative stress in rats. Furthermore, naringenin was reported by Da Pozzo et al. (2017) to exert anti-ageing effects towards the myocardial H9C2 cell line, reducing cell cycle arrest and modulating markers of aging induced

damage, such as reactive oxygen species levels and mitochondrial metabolic activity. However, it is important to note that while these studies show cardio-protective effects, these effects were reported for rat models, or under *in vitro* conditions using mouse-derived, immortalised cardiac cell lines. By comparison, the present study utilised primary cardiac cells derived from humans. With this in mind, it is possible that the differing effects may be due to differing cell sensitivity, and differing cell metabolism, along with potential species specificity. Additionally, the contradicting effects may also be as a result of differing dosages of naringenin being used. Another possibility is the antioxidant effects of naringenin.

Being a flavonoid, naringenin has previously been shown to act as a powerful antioxidant, exerting protective effects. However, previous research has also shown that antioxidants, when consumed in excess, can cause negative effects. This is due to disruption of the delicate balance between oxidation and reduction, often termed redox equilibrium, which is necessary for normal bodily function and optimal health (Lu et al. 2013; Balcerczyk et al. 2014; Pérez-Torres et al. 2017). Particularly, low levels of oxidants, such as reactive oxygen species (ROS) and reactive nitrogen species (RNS), are needed for cellular maturation, defence against pathogens, cellular signalling systems, cellular maturation and apoptosis. When levels of oxidants exceeds antioxidant capacity, however, the redox equilibrium will be disrupted, and oxidative stress will ensue. Oxidative stress has previously been shown to adversely affect a number of cell structures, including cell membranes, proteins, lipids, and DNA, along with favouring mutagenicity and apoptosis (Pérez-Torres et al. 2017; Pizzino et al. 2017). Furthermore, oxidative stress has also been linked to the occurrence of several diseases, including cardiovascular disease, kidney disease, rheumatoid arthritis, and cancer (Pizzino et al. 2017). Thus, antioxidant consumption is pivotal in preventing the deleterious effects associated with oxidative stress (Balcerczyk et al. 2014; Pérez-Torres et al. 2017). However, should antioxidants be consumed in excess, beyond what is necessary to maintain redox equilibrium,

adverse effects may still occur as the result of reductive stress. Reductive stress may result in a number of deleterious effects, including diminished cell growth, alterations in protein production, reduced mitochondrial function, double stranded DNA breaks, and apoptosis (Lu et al. 2013; Pérez-Torres et al. 2017).

Examples these adverse effects include the work by Lu et al. (2013) who demonstrated, using the flavonoid epigallocatechin gallate (ECGC), that excessive antioxidant supplementation could cause adverse effects in humans. Specifically, these authors showed that excessive amounts of ECGC resulted in reductive DNA damage, precisely double stranded breaks, in the non-cancerous human lung WI-38 and MRC-5 cell lines, along with non-cancerous human skin GM05757 cells (Lu et al. 2013). Similarly, van Doorn-Khosrovani et al. (2007) also demonstrated the occurrence of reductive DNA damage, particularly double stranded breaks, in primary human $CD34^+$ cells when high concentrations of the flavonoids quercetin and kaempferol were used. More recently, Pérez-Torres et al. (2017) highlighted several common polyphenols capable of inducing reductive stress at elevated doses. These included quercetin, catechins, resveratrol and coumaric acid, which they reported to yield mitochondrial and DNA damage, apoptosis, intracellular reactive oxygen species production and cytotoxicity (Pérez-Torres et al. 2017). Furthermore, they showed that these deleterious effects were reported in non-cancerous human endothelial cells (Pérez-Torres et al. 2017).

Based on these findings, it is possible that naringenin exerted similar effects in the present study, by unfavourably shifting the redox equilibrium toward reductive stress in HAEC cells, yielding reductive cell damage and cytotoxic effects. Should this be the case, it would serve to explain the effects observed with the S1-AuNP's and S2-AuNP's, as intracellular gold nanoparticle accumulation may have simultaneously increased intracellular naringenin accumulation and shifted the redox balance reductive stress, ultimately yielding cytotoxic effects. Additionally, this notion would serve to explain lower toxicity observed for the Ng-

AuNP's, as a particular quantity of the available naringenin would have been used in the reduction of the gold salt, leading to less being present on the nanoparticle surface, thereby lowering the ability to shift redox balance.

Nevertheless, while these notions remained purely speculative without further investigation, it does outline the potential for the extracts and bioactive compounds to have unfavourable effects toward cardiac cells, and therefore the necessity of establishing doses, which mitigate the associated risk. Furthermore, this would appear to be of particular importance with regard to unfavourably shifting redox equilibrium. Moreover, this also suggests that a degree of caution must be exercised regarding any method of improving naringenin bioavailability, including the presently reported gold nanoparticles, when intended for therapeutic application in humans.

4.3 *In vivo* studies

Preclinical prostate cancer mouse models provide an essential tool to improve our understanding of prostate cancer progression and development. These include xenograft mouse models, allograft mouse models, genetically engineered mouse models and knockout models. For the purpose of this study, the xenograft mouse model was used (Rea et al. 2016). This model is used to represents a "recipient" of human prostate cancer, often created through implantation of tumour tissue, cell lines or primary cells in a variety of mice, including, but not limited to, nude mice, severe combined immunodeficiency (SCID) mice and non-obese diabetic (NOD) SCID mice (Rea et al. 2016). Thus, this model was used in the present study to ascertain the effects of the S1 extract, naringenin and subsequent gold nanoparticles toward prostate cancer tumour xenografts.

4.3.1 Change in tumour volume

Following PC-3 cell inoculation and palpable tumour formation, SCID-mice were randomised into separate groups, namely those treated with the S1 extract (0.5mg/kg), S1-AuNP's (0.5 and 1.5 mg/g), naringenin (0.5mg/kg) and Ng-AuNP's pH 8 (0.5 and 1.5 mg/kg), along with the untreated control group. Treatments were administered twice weekly via intra peritoneal (IP) injection, over the course of 29 days and differing effects were noted for each group. Furthermore, each treatments used, namely the S1-AuNP's, S1 extract, Ng-AuNP's pH 8 and naringenin, was well tolerated by the mice, yielded no immediate toxicity, no obvious adverse effects toward overall health, or obvious behavioural changes over the course of the study. Body weights and general health of the mice are discussed further elsewhere.

When treated with the S1 extract, a considerable inhibitory effect toward tumour growth was observed by the end of the study, having a mean tumour volume of 0,212 ± 0,058 cm^3, which was notably, albeit not significantly, lower than the mean of 0,46 ± 0,237 cm^3 exhibited by control groups. These findings are of particular relevance considering the plants common use as an anti-cancer agent in traditional medicine, and are in accordance with the observations made toward the LNCaP prostate cancer cells made by Ilfergane (2016) as well as the present findings toward LNCaP and PC-3 cells. Furthermore, these findings are in accordance with those presented by Pratheeshkumar et al. (2012) and Yang et al. (2015), and may suggest that the previously identified bioactive compound, quercetin, may be responsible.

A study conducted by Pratheeshkumar et al. (2012) investigated the use of quercetin as an anti-cancer agent under both *in vitro* and *in vivo* conditions. They demonstrated that when BALB/cA nude mice, bearing PC-3 prostate cancer tumour xenografts, were treated with 20 mg/kg of quercetin, via daily IP injection, a significant level of tumour growth inhibition was noted. Furthermore, they attributed the tumour growth inhibition in quercetin treated groups to the suppression of the AKT, mTOR and P70S6K angiogenesis signalling pathways

(Pratheeshkumar et al. 2012). Similarly, a study conducted by Yang et al. (2015) investigating the effects of flavonoid quercetin, the anti-cancer agent 2-Methoxyestradiol (2-ME) and their combined effects towards both LNCaP and PC-3 prostate cancer tumour xenografts, in BALB/cA nude mice, demonstrated that quercetin yielded notable tumour growth inhibition when administered at a dosage of 75 mg/kg. However, these authors further demonstrated that quercetin, when combined with 2-ME, yielded more significant tumour growth inhibition and survival outcomes than either agent used in isolation, further highlighting the combinations ability to yield greater apoptosis and suppression of angiogenesis signalling pathways in both androgen-dependent and androgen independent forms of prostate cancer (Yang et al. 2015).

Based on the findings of Pratheeshkumar et al. (2012) and Yang et al. (2015), it is possible that the presently reported inhibitory effect toward prostate cancer tumours occurred due to the action of quercetin present in the S1 extract. Should this be true, it stands to reason that a similar mode of action reported by Pratheeshkumar et al. (2012) occurred in the present study, whereby quercetin present in the S1 extract exerted suppressive effects toward angiogenesis pathways. However, while the S1 extract was shown to contain quercetin, it was only present in the nano-gram range. Furthermore, considering that a relatively low dose of 0.5 mg/kg of the S1 extract was used, it may be said, with a degree of certainty, that the final amount of quercetin per dose was drastically lower than the 20 mg/kg or 75 mg/kg used in the studies conducted by Pratheeshkumar et al. (2012) and Yang et al. (2015). Additionally, while quercetin has been shown to be effective alone, Yang et al. (2015) clearly demonstrated its potential to act synergistically with other compounds, such as 2-ME. Thus, it is unlikely that quercetin present in the S1 extract acted alone, but rather in combination with the second bioactive compound, naringenin.

Lentini et al. (2007) investigated the effects of orally administered naringenin and hesperitin toward metastatic lung cancer in C57BL/6 mice and showed that both flavonoids exerted

favourable effects. With regard to naringenin specifically, the flavonoid was found to reduce the detectable amount of lung metastases by a reported 69%, while also improving survival rates by 50%.

Similarly, a study conducted by Qin et al. (2011) reported that administrating naringenin at a dose of 100 mg/kg, via the oral route, inhibited the detectable lung metastases in BALB/c mice inoculated with 4T1 breast cancer cells. It must be mentioned that while these authors demonstrated inhibition of metastases, they also reported that naringenin was not able to prevent cancer cell proliferation, concluding that the flavonoid was not directly toxic toward the breast cancer cells. However, it is also important to note that these studies used the oral route of administration, which is subject to first pass metabolism by the liver, and would have severely limited the action of naringenin, due to the previously mentioned poor oral bioavailability, poor intestinal absorption, rapid metabolism and low tumour site bioavailability inherent to the flavonoid (Goncalves et al. 2015; Sangpheak et al. 2015; Gera et al. 2017; Rajamani et al. 2018; Salehi et al. 2019). Nevertheless, these findings clearly demonstrate the potential of naringenin to act as an anti-cancer agent.

However, while these findings are promising, currently available literature dealing with prostate cancer and naringenin specifically is limited to *in vitro* conditions, rather than *in vivo*. Nonetheless, based on all previous reported, and presently observed, *in vitro* effects of naringenin toward PC-3 cells, the flavonoid contributed to the inhibitory effects toward the prostate cancer tumours exhibited by the S1 extract. Furthermore, considering that naringenin present in the S1 extract also only existed within the nano-gram range, and that the extract itself was used at low dosage, it is more likely that the observed tumour growth inhibition occurred as a result of a synergistic effect between low levels of quercetin and naringenin. Should this be true, it would be in line with the work conducted by Ilfergane (2016), which demonstrated an enhanced cytotoxicity toward prostate cancer cells when quercetin and naringenin were used

in combination, rather than in isolation. However, further investigation would be needed to evaluate these notions. Nevertheless, these findings remain promising, particularly when the relatively low extract dose is considered, and based on available literature represent the first account of *T. capensis* exerting inhibitory effects toward prostate cancer under *in vivo* conditions. Furthermore, it stands to reason that evaluating higher extract doses may lead to more favourable outcomes.

However, while the low dose of 0.5 mg/kg of the S1 extract exerted favourable effects, similar findings were not exerted by an equal concentration of the S1-AuNP's. Specifically, groups treated with 0.5 mg/kg of the S1-AuNP's yielded mean tumour volumes only slightly lower than control groups by the end of the study, suggesting extremely weak anti-cancer effects. These observations directly contradict those observed for an equal dose of the S1 extract, and may be due to specific compound availability.

As previously mentioned, a greater likelihood exists for quercetin present in the S1 extract to be used as a reducing agent during nanoparticle synthesis, and naringenin used for particle stabilisation, leading to gold nanoparticles mainly coated with naringenin and other available phytochemicals, while exhibiting little to no quercetin coating (Levchenko et al. 2011; Das et al. 2013; Devendiran et al. 2016). Thus, the potential synergistic action between quercetin and naringenin would not have existed in groups treated with the S1-AuNP's, as any intracellular accumulation of S1-AuNP's would only have yielded intracellular accumulation of naringenin. Furthermore, considering that naringenin was only found to exist within the nano-gram range within the S1 extracts, it stands to reason that intracellular accumulation at a dose of 0.5 mg/kg would not yield significant naringenin accumulation, thereby limiting the effects of the flavonoid. This notion may be further supported by the effects of the S1-AuNP's at a dose of 1.5 mg/kg.

More specifically, mice treated with the S1-AuNP's at a dose of 1.5 mg/kg exhibited far greater tumour growth inhibition, exhibiting mean tumour volume of 0.097 ± 0.058 cm^3 by the end of the study, while at a dose of 0.5 mg/kg and the S1-AuNP's and S1 extract yielded mean tumour volumes of 0.425 ± 0.058 and 0.212 ± 0.058, respectively. Furthermore, the tumour growth inhibition observed in the 1.5 mg/kg was statistically significant (Figure 3.127), when compared to the tumour bearing control. While these findings are favourable, and indicate a greater deal of tumour growth inhibition for the higher dose S1-AuNP's, it is important to note that a dose three times larger was required to elicit these effects. The necessity of a higher dose to elicit a more favourable response may further support the notion that low levels of naringenin were bound to the nanoparticles. A higher dose of gold nanoparticles may have increased the quantity of nanoparticles internalised within tumour cells, and thereby increased intracellular compound accumulation. Nevertheless, considering that the lower dose of the S1 extract exhibited tumour growth inhibition similar to the high dose S1-AuNPs, it makes sense that a higher dose of the extract may equal, or possibly surpass, the effects of the high dose S1-AuNP's. If true, the extract could be said to hold more benefit toward the treatment of prostate cancer, rather than extract-initiated gold nanoparticles. Furthermore, the same may be said for naringenin in isolation. This may be observed in groups treated with 0.5 mg/kg of naringenin exhibiting a substantial amount of tumour growth inhibition, which was found to yield significantly lower tumour volumes when compared to tumour-bearing control groups. Additionally, the growth inhibition was notably greater than what was observed for an equal dose of the S1-AuNPs and S1 extract.

Nevertheless, these findings are in line with those reported by Lentini et al. (2007) and Qin et al. (2011), demonstrating anti-cancer activities of naringenin toward lung cancer cells under *in vivo* conditions. Furthermore, these findings also suggest that previous accounts of the flavonoids anti-cancer effects toward prostate cancer cells under *in vitro* conditions is

maintained under *in vivo* conditions, and thereby opens the possibility of substantial clinical application. However, it is important to note that naringenin was presently administered via IP injection, a parenteral route of delivery, which is generally unaffected by first-pass metabolism. Therefore, the mode of administration currently used may have alleviated some of the previously mentioned limitations associated with the flavonoids, such as rapid metabolism and poor tumour site bioavailability (Goncalves et al. 2015; Sangpheak et al. 2015; Gera et al. 2017; Rajamani et al. 2018; Salehi et al. 2019). Thus, while favourable, these findings may not be fully representative of potential clinical applications. However, the naringenin-derived gold nanoparticles may mitigate this issue.

In the present study, when mice were treated with the Ng-AuNPs pH 8, both the 0.5 mg/kg and 1.5 mg/kg groups exhibited comparable mean tumour volumes of 0.212±0.047 cm^3 and 0.132±0.076 cm^3, respectively, by the end of the study. While these tumour volumes were slightly higher than the 0.08±0.028 cm^3 exhibited by the naringenin group, they were still found to yield statistically significant tumour growth inhibition when compared to tumour-bearing control. Thus, these findings suggest that the Ng-AuNP's were able to maintain the anti-cancer effects of free naringenin under *in vivo* conditions, albeit to a slightly diminished extent. Considering that nanoparticle-bound naringenin would be far less likely to be subject to the limitations inherent to the flavonoid, the Ng-AuNP's may allow for a greatly improved clinical applications. It must be mentioned, however, that while the Ng-AuNP's yielded comparable effects to free naringenin, increasing the dose of the nanoparticles from 0.5 mg/kg to 1.5 mg/kg did not lead to greater tumour growth inhibition. Consequently, although these nanoparticles may represent an effective, cheaply produced means of increasing the bioavailability of naringenin, it is unclear whether increasing the dose beyond what was presently used would confer improved tumour growth inhibition. Nevertheless, these findings suggest that the nanoparticles were able to closely mimic the effects of free naringenin, thereby potentially

improving the bioavailability of the flavonoid, opening new channels in the treatment of prostate cancer.

4.3.2 Change in bodyweight

Often, tumour xenograft mice models are used for preclinical evaluation of anti-cancer agents, during, which various aspects are considered indications of the treatment, or lack thereof, adversely affecting the animals, and thereby serve to indicate that animals are nearing endpoints. These aspects include physical appearance, measurable clinical signs, body condition scores, and bodyweight changes (Paster et al. 2009; Jung 2014; Dimitrova et al. 2017). Body condition scores and bodyweight was monitored as an indication of adverse effects, whereby a reduction in bodyweight of approximately 15-20 % of the starting weight was considered an indication of endpoint, and thus cause for euthanasia, in accordance with the outlines stipulated by Foltz and Ullman-Cullere (1999).

Mice in the tumour-bearing control groups were found to have mean bodyweights of 5.871±7.0424 grams by day 29 of the study, representing a near 20% reduction from the mean starting bodyweight of 29.971±2.7597 grams, and accordingly just cause for cessation of the study. By contrast, mice receiving 0.5 mg/kg of the S1 extract exhibited mean bodyweights of 30.057±3.9694 grams by the end of the study, which was an approximate 5% reduction from the starting weight of 31.414±1.7677 grams. While not statistically significant, mice treated with the S1 extract clearly demonstrated more favourable bodyweights, and thus better health outcomes, when compared to the control group. Furthermore, these improved health outcomes coincide with the previously discussed tumour growth inhibition observed for the S1 extract, suggesting an improved overall health outcome. However, an equal dose of the S1-AuP's did not yield these same improvements, yielding a mean bodyweight of 25.500±3.8766 grams by the end of the study, an approximate 12% reduction from the mean starting weight of

28.957±2.8542 grams. Yet, increasing the dose of the S1-AuNP's from 0.5mg/kg to 1.5 mg/kg yielded a drastic improvement, whereby mice exhibited mean end bodyweights of 32.186±2.898, which was nearly identical to the mean starting weight of 32.343±3.0691. Subsequently, this trend toward maintaining normal mean bodyweights up until the end of the study was further observed for groups treated with 0.5 mg/kg of naringenin, along with groups receiving 0.5mg/kg and 1.5mg/kg of Ng-AuNP's pH 8. Considering these favourable effects towards bodyweight coincides with the tumour growth inhibition reported for these groups, it may be assumed that the favourable outcomes occurred due to the actions of available phytochemicals, including the bioactive compounds quercetin and naringenin.

As previously discussed, the work conducted by Pratheeshkumar et al. (2012) and Yang et al. (2015) demonstrated that quercetin administration to BLAB/cA mice bearing tumour xenografts lead to favourable tumour growth inhibition, particularly when combined with the anti-cancer agent 2-ME, in the study conducted by Yang et al. (2015). However, despite the favourable outcomes, they noted that quercetin had little to no effect toward body weight in mice. Based on this, the bioactive compound, quercetin, may not be entirely responsible for the favourable bodyweight outcomes observed in mice treated with the S1 extract, particularly when the amount of quercetin present in the extract is considered. In this study, quercetin was found to be present within the S1 extract in the nano-gram range, while the studies conducted by Pratheeshkumar et al. (2012) and Yang et al. (2015) dosed mice with 20 mg/kg or 75 mg/kg of quercetin, respectively. However, considering the potential for synergism outlined by Yang et al. (2015), it is unlikely that quercetin present in the S1 extract acted alone, if at all, but rather more likely synergistically with the second bioactive compound, naringenin.

It is likely that both naringenin and quercetin within the S1 extract acted together to inhibit tumour growth, while also improving bodyweight outcomes, and thereby indicating improved health conditions. This may further explain the lack of tumour and deteriorating bodyweights

seen in groups treated with 0.5 mg/kg of the S1-AuNP's, as it is likely that quercetin was uses as reducing agent, while naringenin was adsorbed to the particle surface during stabilisation. Thus, the potential synergistic action between quercetin and naringenin would no longer be applicable, thereby yielding unfavourable results. Furthermore, this may further explain the necessity of the high dose of the S1-AuNP's to achieve favourable outcomes, as this dose would allow for a greater potential of intracellular naringenin accumulation, and thereby more favourable tumour growth inhibition and bodyweight improvements. Moreover, the present findings for naringenin are in line with reports made by Lentini et al. (2007) and Qin et al. (2011) demonstrating the potential for naringenin to improve survival outcomes in tumour bearing mice. Additionally, the present findings suggest that the Ng-AuNP's exhibit near identical effects toward bodyweight outcomes, further suggesting that they may represent a viable means of overcoming the limitations associated with the flavonoids, such as rapid metabolism and poor tumour site bioavailability, particularly when administered via the oral route (Goncalves et al. 2015; Sangpheak et al. 2015; Gera et al. 2017; Rajamani et al. 2018; Salehi et al. 2019).

However, a study conducted by Henning et al. (2012) investigating the effects of green tea polyphenols, such as catechins, epicatechin and epigallocatechin gallate (EGCG) toward prostate cancer tumour xenografts showed that tumour growth was notably reduced in mice receiving the tea polyphenols, in comparison to those receiving plain water. Considering that *T. capensis* rhizomes were previously shown to possess some of the same phytochemicals present in green tea, such as catechin and epicatechin, along with other polyphenols with strong antioxidant properties, such as afzelechin, epiafzelechin, typharin and typhaphthalide (Shode et al. 2002), it remains possible that these phytochemicals may have been present in the S1 extract and contributed to the favourable effects observed for both tumour growth and bodyweight outcomes, rather than being entirely due to the actions of quercetin and naringenin.

Furthermore, the likelihood of these polyphenols being adsorbed to the surface of the S1-AuNPs are high, and are likely to have contributed, in part, to the observations made for the S1-AuNP's. Nevertheless, the findings clearly demonstrate the potential for improved outcomes toward prostate cancer, particularly in the case of the S1 extract, naringenin and the Ng-AuNP's.

4.3.3 Blood analysis

While some of the reported treatments, namely the S1 extract at 0.5 mg/kg, S1-AuNP's at 1.5mg/kg, Ng-AuNP's pH 8 at 0.5 and 1.5 mg/kg, and naringenin at 0.5mg/kg, may have exhibited favourable effects towards the treatment of prostate cancer, it is essential to evaluate potential toxicity. This is particularly true in the case of gold nanoparticles, as they have previously been shown to readily by be taken up by peripheral blood cells, including red blood cells, leukocytes and platelets (He et al. 2018; Sembratowicz and Ognik 2019). In the case of red blood cells (RBCs), nanoparticles possess the potential to elicit various effects, ranging from haemolysis of erythrocytes, leading to haemolytic anaemia, to increasing RBC count by modulating haematopoiesis mechanism and stimulating erythropoietin secretion (Zhang et al. 2010; Ziaee Ghahnavieh et al. 2013; Sembratowicz and Ognik 2019). A slight reduction in the RBC count was observed in each of the presently reported treatment groups, apart from those treated with the S1-AuNP's at a dose of 0.5 mg/kg, which was near identical to the tumour bearing control (Figure 3.129). While a slight reduction was observed for the remaining treatment groups, no significant decreases were found when compared to both the tumour-bearing and healthy control groups. These observations suggest that the S1-AuNP's (1.5mg/kg),Ng-AuNP's pH 8 (0.5 and 1.5 mg/kg) ,S1 extract and naringenin may have exerted modest effects toward RBC's, showing very minor potential for modulation of haematopoiesis mechanisms, and virtually no potential for the occurrence of haemolysis, at least at the doses

presently used. Thus, based on these observations, it may be suggested that treatment S1-AuNP's (1.5mg/kg), Ng-AuNP's pH 8 (0.5 and 1.5 mg/kg), S1 extract and naringenin held little to no toxicity toward RBCs. When white blood cells were measures, however, more pronounced reductions in overall counts were observed

White blood cells (WBCs) constitute approximately 45% of whole blood and serves various essential bodily functions, including destruction of virus-infected cells, secretion of antibodies for phagocytosis detection, destruction of pathogens by phagocytosis, and directing the inflammatory response to insult and injury through cytokine secretion, to name a few (Yuksel et al. 2016; Wirth et al. 2018) Furthermore, a number of WBCs, such a neutrophils and lymphocytes, have been shown to participate in the inflammatory response to diseases such as type 2 diabetes, rheumatoid arthritis, and are found within tumour microenvironments (Yuksel et al. 2016; Feng et al. 2018). Based on this, WBC measurements have been considered reliable cellular biomarkers for systemic inflammation, and thus a valuable prognostic tool in inflammatory diseases (Yuksel et al. 2016; Feng et al. 2018)..

Systemic inflammation may be measured by a multitude of biochemical and haematological parameters (Yuksel et al. 2016). More specifically, these parameters include total white blood cell (WBC) counts, leukocyte counts, neutrophil counts, lymphocyte counts, and often a calculated ratio between these parameters (Paik et al. 2014; Yuksel et al. 2016; Ferro et al. 2019). For example, neutrophils generally mediate inflammation by various mechanism, such as release of arachidonic acid metabolites and platelet aggravation factors, and when elevated may indicate the potential of bacterial infection, but may also be an indication of cancer-related inflammation as a result of tissue destruction and cytokine release (Yuksel et al. 2016; Sembratowicz and Ognik 2019). Lymphocytes, on the other hand, are more associated with cortisol release in response to stressors, and thus provide valuable insight into the levels of systemic inflammation (Geiger et al. 2015; Yuksel et al. 2016). Furthermore, the ratio of

neutrophils to lymphocytes has also previously been shown to be a useful biomarker of systemic inflammation. With regard to cancer, systemic inflammation plays integral roles toward tumour development and progression, with immune cells often having dual function in both the development and progression of cancer. Immune cells may destroy cancerous cells, or they may promote their growth and invasiveness, and enhance their metastatic capabilities (Yuksel et al. 2016; Sembratowicz and Ognik 2019). Thus, markers of inflammation, such as white blood cells, can provide valuable insights into the nature of tumour progression.

When mice were treated with the S1 extract, naringenin and subsequent gold nanoparticles, total WBC counts were found to be lower than tumour bearing controls in each treatment group. However, only mice treated with the 1.5 mg/kg of the S1-AuNP's were found to exhibit WBC counts more consistent with the healthy, tumour-free control. Considering that total WBC count have previously been used as a marker for tumour-associated inflammation (Paik et al. 2014; Yuksel et al. 2016), and that treatment with the S1 extract, naringenin and subsequent gold nanoparticles yielded varying degrees of tumour growth inhibition, it may be assumed that the reduction in WBC counts observed in each group may indicate a lowered overall systemic inflammation as a result of tumour growth inhibition.

While lowered overall systemic inflammation and tumour growth inhibition is a favourable outcome toward prostate cancer, it must be mentioned that each treatment group also yielded a slight increase in the lymphocyte count above both tumour bearing and tumour free control groups. Elevated lymphocyte counts are generally associated with the cortisol-induced stress response (Geiger et al. 2015; Yuksel et al. 2016), and it may therefore be assumed that these elevated levels indicated a degree of systemic stress in response to treatment with the S1 extract, naringenin and gold nanoparticles. However, while elevated, the increased lymphocyte counts were not found to be statistically significant, and thus may not indicate cause for

concern, particularly when the overall tumour growth inhibition and improved bodyweight scores are considered.

Furthermore, each treatment group also yielded decreased neutrophil counts when compared to tumour bearing controls, with mice receiving 1.5 mg/kg of the S1-AuNP's exhibiting levels more consistent with healthy controls. Considering that elevated neutrophil counts are generally associated with cancer-related inflammation as a result of tissue destruction, tumour progression and angiogenesis (Yuksel et al. 2016; Sembratowicz and Ognik 2019), the reduction exhibited in each treatment group may further support the aforementioned notion that tumour growth was inhibited by the actions of S1 extract, naringenin and the subsequent gold nanoparticles. If true, treatments may thereby have led to lower cancer-related inflammation, and thus lowered neutrophil counts. This notion may be further supported by considering the neutrophil to lymphocyte ratios (NLR).

The NLR has previously been shown to be a string predictor of systemic inflammation, has been found to be a significant prognostic tool for multiple tumour types and stages. An elevated NLR has been associated with poor prognosis of gastric cancer, renal cancer, lung cancer, oesophageal cancer, and prostate cancer (Faria et al. 2016; Zhang et al. 2017; Li et al. 2018; Ferro et al. 2019). Thus, the ability of anti-cancer agents to lower the NLR may confer lowered systemic, cancer-related inflammation, and thereby better prognosis. The present study noted that each treatment group exhibited an NLR lower than the tumour bearing controls by the end of the study, where groups treated with 1.5 mg/kg of the S1-AuNP's exhibiting a significantly lowered NLR, when compared to the controls. Based on the lowered NLR, the currently reported treatments may represent a viable means of improving prognostic outcomes, by yielding lowered levels of cancer-associated systemic inflammation. Furthermore, these favourable effects coincide with the previously reported tumour growth inhibition, which may

further support the notion that the present treatments exerted favourable anti-cancer activities, Moreover, this notion may be further supported by the effects toward platelet counts.

Previously, platelets have been shown to play key roles in tumour formation, progression and angiogenesis. Platelets can be activated by tumour cells, resulting in the release of various biological molecules, such as vascular endothelial growth factor, leading to the modulation of tumour progression and metastases (Yuksel et al. 2016; Meikle et al. 2017; Elaskalani et al. 2017). Apart from those treated treatment groups with 0.5 mg/kg of the S1-AuNP's, each group yielded a decreased platelet counts at the end of the study. Those in the 0.5 mg/kg S1-AuNP group exhibited platelet levels elevated beyond rhea tumour-bearing controls. Based on the role of platelets outlined by (Meikle et al. 2017; Elaskalani et al. 2017), the present findings toward platelets may suggest that the S1 extract, naringenin, Ng-AuNP's and high dose S1-auNP's may have had an inhibitory effect toward platelet-modulation of tumour growth. However, it is also possible that the lowered platelet count is simply due to overall tumour growth inhibition, leading to lowered platelet activation, and overall lowered platelet count. Furthermore, it must be mentioned that the group receiving the 1.5 mg/kg S1-AuNP's exhibited platelet counts below healthy controls. While the reduction was not statistically significant, it is notable and may due to the anti-cancer actions of these nanoparticles, as chemotherapeutic agents have previously been show to lower overall platelet counts (Elaskalani et al. 2017). Nevertheless, the overall reduction in platelet counts coincides with the favourable effects observed total WBC count, lymphocytes and overall tumour growth, which may further suggest that each treatment acted to inhibit the growth of prostate cancer tumours.

4. Conclusion

It may be concluded that aqueous *T. capensis* rhizome extracts, along with the bioactive compounds quercetin and naringenin, are well suited to the synthesis of highly stable gold nanoparticles encapsulated with a plethora of phytochemicals, using green synthesis techniques. More importantly, this study reports for the first time the successful synthesis of highly stable gold nanoparticles using the bioactive compound naringenin in isolation, as both reducing and stabilising agent. Subsequently, these nanoparticles exhibited robust stability under *in vitro* conditions and clear signs of cell internalisation, observed using dark-field microscopy and TEM. When compared to the effects of the extracts, similar levels of toxicity were observed in the case of the LNCaP and PC-3 cells. However, these nanoparticles were found to yield improved toxicity toward Panc1 cells in both a dose- and time-dependent manner. Nevertheless, these findings indicated their potential use as treatment agents in multiple forms of cancer.

Despite these positive outcomes, however, the effects observed toward the non-cancerous HAEC cells demonstrated the potential for adverse effects when using the S1 and S2 extracts, naringenin, and the subsequent nanoparticles, suggesting that a degree of caution must be exercised, particular when intended for clinical use. Moreover, these observations highlighted the need for more extensive investigation into the overall safety of these agents.

Furthermore, the present study demonstrated for the first time the positive therapeutic effects of *T. capensis* extract toward prostate cancer under *in vivo* conditions, adding a degree of validity to its clinical usage suggested by Ilfergane (2016). However, these positive effects were not found to be improved, nor maintained, by nano-encapsulation of the extract. The Ng-AuNP's, however, were able to maintain the anti-cancer effects of free naringenin under *in vivo* conditions, having favourable outcomes toward tumour growth, body weight and blood parameters in tumour-bearing SCID-mice. While the Ng-AuNP's held no improvement over

free naringenin, the nanoparticle-bound naringenin would be far less likely to be subject to the limitations inherent to the flavonoid, such as rapid metabolism and poor bio-availability. Thus, based on the these findings it may be concluded that the Ng-AuNP's represent a potential means of greatly improving the clinical application of the flavonoid, thereby opening new channels in the treatment of prostate cancer. Furthermore, it may also be concluded that crude *T. capensis* extracts, particular those produced in the summer season, are well suited to the treatment of prostate cancer under clinical settings.

Chapter 5

References

Aaron L, Franco OE, Hayward SW (2016) Review of Prostate Anatomy and Embryology and the Etiology of Benign Prostatic Hyperplasia. Urol Clin North Am 43:279–88.

Abdel-Raouf N, Al-Enazi NM, Ibraheem IBM (2017) Green biosynthesis of gold nanoparticles using Galaxaura elongata and characterization of their antibacterial activity. Arab J Chem 10:S3029–S3039.

Abdelhady NM, Badr KA, Nevein Abdelhady CM (2016) Comparative study of phenolic content, antioxidant potentials and cytotoxic activity of the crude and green synthesized silver nanoparticles′ extracts of two Phlomis species growing in Egypt. J Pharmacogn Phytochem JPP 377:377–383.

Abdillahi HS, Van Staden J (2012) South African plants and male reproductive healthcare: Conception and contraception. J Ethnopharmacol 143:475–480.

Ahmad A, Husain A, Mujeeb M, Khan SA, Alhadrami HAA, Bhandari A (2015a) Quantification of total phenol, flavonoid content and pharmacognostical evaluation including HPTLC fingerprinting for the standardization of Piper nigrum Linn fruits. Asian Pac J Trop Biomed 5:101–107.

Ahmad A, Wei Y, Syed F, Imran M, Khan ZUH, Tahir K, Khan AU, Raza M, Khan Q, Yuan Q (2015b) Size dependent catalytic activities of green synthesized gold nanoparticles and electro-catalytic oxidation of catechol on gold nanoparticles modified electrode. RSC Adv 5:99364–99377.

Ahmed S, Ikram S (2015) Synthesis of Gold Nanoparticles using Plant Extract: An Overview. J Bacteriol 1:1–5.

Ali H, Ahmed M, Baig M, Ali M (2007) Realtionship of zinc concentrations in blood and seminal plasma with various semen parameters in infertile subjects. Pak J Med Sci 23:111–114.

Ali SA, Begum T, Reza F (2018) Hormonal Influences on Cognitive Function. Malaysian J Med Sci 25:31–41.

Aljabali A, Akkam Y, Al Zoubi M, Al-Batayneh K, Al-Trad B, Abo Alrob O, Alkilany A,

Benamara M, Evans D (2018) Synthesis of Gold Nanoparticles Using Leaf Extract of Ziziphus zizyphus and their Antimicrobial Activity. Nanomaterials 8:174.

Alkilany AM, Murphy CJ (2010) Toxicity and cellular uptake of gold nanoparticles: What we have learned so far? J Nanoparticle Res 12:2313–2333.

Amendola V, Meneghetti M (2009) Size Evaluation of Gold Nanoparticles by UV−vis Spectroscopy. J Phys Chem C 113:4277–4285.

Amendola V, Pilot R, Frasconi M, Maragò OM, Iatì MA (2017) Surface plasmon resonance in gold nanoparticles: a review. J Phys Condens Matter 29:1–48.

Andel T, Carvalheiro LG (2013) Why urban citizens in developing countries use traditional medicines: the case of suriname. Evidence-based Complement Altern Med 2013:687197.

Anothaisintawee T, Attia J, Nickel JC, Thammakraisorn S, Numthavaj P, McEvoy M, Thakkinstian A (2011) Management of chronic prostatitis/chronic pelvic pain syndrome: a systematic review and network meta-analysis. JAMA 305:78–86.

Arnida, Malugin A, Ghandehari H (2010) Cellular uptake and toxicity of gold nanoparticles in prostate cancer cells: A comparative study of rods and spheres. J Appl Toxicol 30:212–217.

Arun G, Eyini M, Gunasekaran P (2014) Green synthesis of silver nanoparticles using the mushroom fungus Schizophyllum commune and its biomedical applications. Biotechnol Bioprocess Eng 19:1083–1090.

Assi MA, Mohd Noor MH, Haron AW, Yusoff SM, Rajion M ali (2017) Male reproductive system. PJSRR 3:1–16.

Babu A, Templeton AK, Munshi A, Ramesh R (2013) Nanoparticle-Based Drug Delivery for Therapy of Lung Cancer: Progress and Challenges. J Nanomater 2013:1–11.

Bahrami B, Hojjat-Farsangi M, Mohammadi H, Anvari E, Ghalamfarsa G, Yousefi M, Jadidi-Niaragh F (2017) Nanoparticles and targeted drug delivery in cancer therapy. Immunol Lett 190:64–83.

Balcerczyk A, Gajewska A, Macierzyńska-Piotrowska E, Pawelczyk T, Bartosz G, Szemraj J (2014) Enhanced antioxidant capacity and anti-ageing biomarkers after diet micronutrient supplementation. Molecules 19:14794–808.

Banerjee PP, Banerjee S, Brown TR, Zirkin BR (2018) Androgen action in prostate function and disease. Am J Clin Exp Urol 6:62–77.

Barabadi H, Ovais M, Shinwari ZK, Saravanan M (2017) Anti-cancer green bionanomaterials: present status and future prospects. Green Chem Lett Rev 10:285–314.

Bardin CW, Grunsalus GL, Chen CY (1993) The cell biology of the Sertoli cell. In: Desjardins C, Ewing LL (eds) Cell and Molecular Biology of the Testis. Oxford University Press, pp 190–220.

Bassil N, Alkaade S, Morley JE (2009) The benefits and risks of testosterone replacement therapy: a review. Ther Clin Risk Manag 5:427–448.

Basu SC (2011) Male reproductive anatomy and physiology. In: Basu SC (ed) Male Reproductive Dysfunction. JP Medical Ltd, pp 15–27.

Begg AC, Stewart FA, Vens C (2011) Strategies to improve radiotherapy with targeted drugs. Nat Rev Cancer 11:239–253.

Bell MA, Campbell JD, Joice G, Sopko NA, Burnett AL (2018) Shifting the Paradigm of Testosterone Replacement Therapy in Prostate Cancer. World J Mens Health 36:103.

Bhasin S, Cunningham GR, Hayes FJ, Matsumoto AM, Snyder PJ, Swerdloff RS, Montori VM (2010) Testosterone therapy in men with androgen deficiency syndrome: An Endocrine Socienty practical guideline. J Clin Endocrinol Metab 95:2536–2559.

Bhatia S (2016) Natural polymer drug delivery systems: Nanoparticles, plants, and algae. In: Natural Polymer Drug Delivery Systems: Nanoparticles, Plants, and Algae. pp 1–225.

Bhattacharjee S (2016) DLS and zeta potential - What they are and what they are not? J Control Release 235:337–351.

Bhavsar A, Verma S (2014) Anatomic Imaging of the Prostate. Biomed Res Int 2014:1–9.

Biao L, Tan S, Meng Q, Gao J, Zhang X, Liu Z, Fu Y (2018) Green Synthesis, Characterization and Application of Proanthocyanidins-Functionalized Gold Nanoparticles. Nanomaterials 8:53.

Bindhu MR, Umadevi M (2014) Antibacterial activities of green synthesized gold nanoparticles. Mater Lett 120:122–125.

Bogireddy NKR, Pal U, Gomez LM, Agarwal V (2018) Size controlled green synthesis of gold nanoparticles using Coffea arabica seed extract and their catalytic performance in 4-nitrophenol reduction. RSC Adv 8:24819–24826.

Boss C, Fredeen K (2004) Concepts,Instrumentation and Techniques in Inductively Coupled

Plasma Optical Emission Spectroscopy. In: Emission Spectroscopy. pp 1–22

Bray F, Ferlay J, Soerjomataram I, Siegel RL, Torre LA, Jemal A (2018) Global cancer statistics 2018: GLOBOCAN estimates of incidence and mortality worldwide for 36 cancers in 185 countries. CA Cancer J Clin 68:394–424.

Briganti A, Capitanio U, Suardi N, Gallina A, Salonia A, Bianchi M, Tutolo M, Girolamo VD, Guazzoni G, Rigatti P, Montorsi F (2009) Benign Prostatic Hyperplasia and Its Aetiologies. Eur Urol 8:865–871.

Brust M, Walker M, Bethell D, Schiffrin DJ, Whyman R (1994) Synthesis of thiol-derivatised gold nanoparticles in a two-phase Liquid–Liquid system. J Chem Soc, Chem Commun 1:801–802.

Burden HP, Holmes CH, Persad R, Whittington K (2006) Prostasomes--their effects on human male reproduction and fertility. Hum Reprod Update 12:283–92.

C. Martínez J, A. Chequer N, L. González J, Cordova T (2013) Alternative Metodology for Gold Nanoparticles Diameter Characterization Using PCA Technique and UV-VIS Spectrophotometry. Nanosci Nanotechnol 2:184–189.

Carson C, Rittmaster R (2003) The Role of dihydrotestosterone in benign prostatic hyperplasia. Urology 61:2–7.

Chahardoli A, Karimi N, Sadeghi F, Fattahi A (2018) Green approach for synthesis of gold nanoparticles from Nigella arvensis leaf extract and evaluation of their antibacterial, antioxidant, cytotoxicity and catalytic activities. Artif Cells, Nano-medicine, Biotechnol 46:579–588.

Chakraborty A, Das D, Sinha M, Dey S, Bhattacharjee S (2013) Moringa oleifera Leaf Extract Mediated Green Synthesis of Stabilized Gold Nanoparticles. J Bionanoscience 7:415–419.

Chanda N, Shukla R, Zambre A, Mekapothula S, Kulkarni RR, Katti K, Bhattacharyya K, Fent GM, Casteel SW, Boote EJ, Viator JA, Upendran A, Kannan R, Katti K V. (2011) An Effective Strategy for the Synthesis of Biocompatible Gold Nanoparticles Using Cinnamon Phytochemicals for Phantom CT Imaging and Photoacoustic Detection of Cancerous Cells. Pharm Res 28:279–291.

Chang SH, Lin HTV, Wu GJ, Tsai GJ (2015) pH Effects on solubility, zeta potential, and correlation between antibacterial activity and molecular weight of chitosan. Carbohydr Polym 134:74–81.

Chavva S, Deshmukh S, Kanchanapally R, Tyagi N, Coym J, Singh A, Singh S (2019) Epigallocatechin Gallate-Gold Nanoparticles Exhibit Superior Antitumor Activity Compared to Conventional Gold Nanoparticles: Potential Synergistic Interactions. Nanomaterials 9:396.

Chen CY, Mruk DD (2012) The blood-testis barrier and its implications for male contraception. Pharmacol Rev 64:16–64.

Chinkwo KA (2005) Sutherlandia frutescens extracts can induce apoptosis in cultured carcinoma cells. J Ethnopharmacol 98:163–170.

Chithrani DB, Jelveh S, Jalali F, van Prooijen M, Allen C, Bristow RG, Hill RP, Jaffray DA (2010) Gold Nanoparticles as Radiation Sensitizers in Cancer Therapy. Radiat Res 173:719–728.

Chitindingu E, George G, Gow J (2014) A review of the integration of traditional, complementary and alternative medicine into the curriculum of South African medical schools. BMC Med Educ 14:40.

Choi Y, Choi M, Cha S, Kim YS, Cho S, Park Y (2014) Catechin-capped gold nanoparticles : green synthesis , characterization , and catalytic activity toward 4-nitrophenol reduction. Nanoscale Res Lett 9:1–8.

Choudhury A, Cuddihy A, Bristow R (2006) Radiation and New Molecular Agents Part I: Targeting ATM-ATR Checkpoints, DNA Repair, and the Proteasome. Semin Radiat Oncol 16:51–58.

Chuu CP, Kokontis JM, Hiipakka RA, Fukuchi J, Lin HP (2011) Androgens as therapy for androgen receptor-positive castration-resistant prostate cancer. J Biomed Sci 18:63–68.

Clayton KN, Salameh JW, Wereley ST, Kinzer-Ursem TL (2016) Physical characterization of nanoparticle size and surface modification using particle scattering diffusometry. Biomicrofluidics 10:054-107.

Conde J (2015) The Golden Age in Cancer Nanobiotechnology: Quo Vadis? Front Bioeng Biotechnol 3:142.

Conde Rodriguez GR, Gauthier GH, Ladeira LO, Sanabria Cala JA, Laverde Catano D (2017) Effect of pH and chloroauric acid concentration on the geometry of gold nanoparticles obtained by photochemical synthesis. J Phys Conf Ser 935:12–27.

Contreras-Trigo B, Díaz-García V, Guzmán-Gutierrez E, Sanhueza I, Coelho P, Godoy S,

Torres S, Oyarzún P (2018) Slight pH Fluctuations in the Gold Nanoparticle Synthesis Process Influence the Performance of the Citrate Reduction Method. Sensors 18:2246.

Corona G, Sforza A, Maggi M (2017) Testosterone Replacement Therapy: Long-Term Safety and Efficacy. World J Mens Health 35:65–76.

Costanzo M, Carton F, Malatesta M (2017) Microscopy techniques in nanomedical research. Microscopie 14:66–71.

Da Pozzo E, Costa B, Cavallini C, Testai L, Martelli A, Calderone V, Martini C (2017) The Citrus Flavanone Naringenin Protects Myocardial Cells against Age-Associated Damage. Oxid Med Cell Longev 2017:1–12.

Dalwadi P, Patani P, Singhavi I (2019) Preparation and Characterization of Naringenin Gold Nano Suspension for Breast Cancer. Int Res J Pharm 9:128–133.

Daraee H, Eatemadi A, Abbasi E, Aval SF, Kouhi M, Akbarzadeh A (2016) Application of gold nanoparticles in biomedical and drug delivery. Artif Cells, Nano-medicine Biotechnol 44:410–422.

Das DK, Chakraborty A, Bhattacharjee S, Dey S (2013) Biosynthesis of stabilised gold nanoparticle using an aglycone flavonoid, quercetin. J Exp Nanosci 8:649–655.

Das S, Bag BG, Basu R (2014) Abroma augusta Linn bark extract-mediated green synthesis of gold nanoparticles and its application in catalytic reduction. Appl Nanosci 5:867.

Daubney J, Bonner PL, Hargreaves AJ, Dickenson JM (2015) Cardioprotective and cardiotoxic effects of quercetin and two of its in vivo metabolites on differentiated H9c2 cardiomyocytes. Basic Clin Pharmacol Toxicol 116:96–109.

Davidiuk AJ, Broderick GA (2016) Adult-onset hypogonadism: evaluation and role of testosterone replacement therapy. Transl Androl Urol 5:824–833.

De la Guardia M (2014) The challenges of green nanotechnology. BioImpacts 4:1–2.

Della Greca M, Mangoni L, Molinaro A, Monaco P, Previtera L (1990) (20S)-4α methyl-24methylenecholest-7-en-3β-ol, an allelopathic sterol from Typha latifolia. Phytochemistry. Phytochemistry 29:1797–1798.

Deryabin DG, Efremova L V, Vasilchenko AS, Saidakova E V, Sizova EA, Troshin PA, Zhilenkov A V, Khakina EA, Khakina EE (2015) A zeta potential value determines the aggregate's size of penta-substituted [60]fullerene derivatives in aqueous suspension whereas

positive charge is required for toxicity against bacterial cells. J Nanobiotechnology 13:50.

Devendiran RM, Chinnaiyan S kumar, Yadav NK, Ramanathan G, Singaravelu S, Perumal PT, Sivagnanam UT (2016) Facile synthesis and evaluation of quercetin reduced and dextran sulphate stabilized gold nanoparticles decorated with folic acid for active targeting against breast cancer. RSC Adv 6:32560–32571.

Dhamecha D, Jalalpure S, Jadhav K, Sajjan D (2016) Green synthesis of gold nanoparticles using Pterocarpus marsupium : Characterization and biocompatibility studies. Part Sci Technol 34:156–164.

Dimitrova N, Zamudio JR, Jong RM, Soukup D, Resnick R, Sarma K, Ward AJ, Raj A, Lee J, Sharp PA, Jacks T (2017) Public Access NIH Public Access.

Dobrowolska P, Krajewska A, Gajda-Rączka M, Bartosewicz B, Nyga P, Jankiewicz B (2015) Application of Turkevich Method for Gold Nanoparticles Synthesis to Fabrication of SiO2@Au and TiO2@Au Core-Shell Nanostructures. Materials (Basel) 8:2849–2862.

Dong R, Chen P, Chen Q (2018) Extract of the Medicinal Plant Pao Pereira Inhibits Pancreatic Cancer Stem-Like Cell In Vitro and In Vivo. Integr Cancer Ther 17:1204–1215.

Dudek P, Kozakowski J, Zgliczyński W (2017) Late-onset hypogonadism. Prz menopauzalny = Menopause Rev 16:66–69.

Ebisch IMW, Thomas CMG, Wetzels AMM, Willemsen WNP, Sweep FCGJ, Steegers-Theunissen RPM (2008) Review of the role of the plasminogen activator system and vascular endothelial growth factor in subfertility. Fertil Steril 90:2340–2350.

Edwards PP, Thomas JM (2007) Gold in a metallic divided state - From Faraday to present-day nanoscience. Angew Chemie - Int Ed 46:5480–5486.

Ekor M (2014) The growing use of herbal medicines: issues relating to adverse reactions and challenges in monitoring safety. Front Pharmacol 4:177.

Elahi N, Kamali M, Baghersad MH (2018) Recent biomedical applications of gold nanoparticles: A review. Talanta 184:537–556.

Elaskalani O, Berndt M, Falasca M, Metharom P (2017) Targeting Platelets for the Treatment of Cancer. Cancers (Basel) 9:94.

Elbagory AM, Cupido CN, Meyer M, Hussein AA (2016) Large scale screening of southern African plant extracts for the green synthesis of gold nanoparticles using microtitre-plate

method. Molecules.

Elia P, Zach R, Hazan S, Kolusheva S, Porat Z, Zeiri Y (2014a) Green synthesis of gold nanoparticles using plant extracts as reducing agents. Int J Nano-medicine 9:4007–4021.

Elia P, Zach R, Hazan S, Kolusheva S, Porat Z, Zeiri Y (2014b) Green synthesis of gold nanoparticles using plant extracts as reducing agents. Int J Nano-medicine 9:4007–4021.

Elliott J, Kelly SE, Millar AC, Peterson J, Chen L, Johnston A, Kotb A, Skidmore B, Bai Z, Mamdani M, Wells GA (2017) Testosterone therapy in hypogonadal men: a systematic review and network meta-analysis. BMJ Open 7:152–184.

Faria SS, Fernandes PC, Silva MJB, Lima VC, Fontes W, Freitas R, Eterovic AK, Forget P (2016) The neutrophil-to-lymphocyte ratio: A narrative review. Ecancermedicalscience 10:1–12.

Farooq MU, Novosad V, Rozhkova EA, Wali H, Ali A, Fateh AA, Neogi PB, Neogi A, Wang Z (2018) Gold Nanoparticles-enabled Efficient Dual Delivery of Anticancer Therapeutics to HeLa Cells. Sci Rep 8:2907.

Fatima N, Nayeem N (2016) Toxic Effects as a Result of Herbal Medicine Intake. In: Toxicology - New Aspects to This Scientific Conundrum. InTech, p 13.

Feldman HA, Longcope C, Derby CA (2002) Age trends in the new level of serum testosterone and other hormones in middle-aged men: longitudinal results from the Massachusetts male aging study. J Clin Endocrinol Metab 87:589–598.

Feng L, Gu S, Wang P, Chen H, Chen Z, Meng Z, Liu L (2018) White Blood Cell and Granulocyte Counts Are Independent Predictive Factors for Prognosis of Advanced Pancreatic Caner. Gastroenterol Res Pract 2018:1–6.

Fennell CW, Lindsey KL, McGawb LJ, Sparg SG, Stafford GI, Elgorashi EE, Grace OM, Staden J (2004) Assessing African medicinal plants for efficacy and safety: pharmacological screening and toxicology. J Ethnopharmacol 94:205–217.

Ferro M, Musi G, Serino A, Cozzi G, Mistretta FA, Costa B, Bianchi R, Cordima G, Luzzago S, Di Trapani E, Tagliabue E, Vartolomei MD, Terracciano D, Cassatella MC, Salvatici M, Conti A, Sandri MT, Cioffi A, Turetti M, Catellani M, Bottero D, Matei DV, Mirone V, de Cobelli O (2019) Neutrophil, Platelets, and Eosinophil to Lymphocyte Ratios Predict Gleason Score Upgrading in Low-Risk Prostate Cancer Patients. Urol Int 102:43–50.

Foltz CJ, Ullman-Cullere M (1999) Guidelines for Assessing the Health and Condition of Mice. Lab Anim (NY) 28:28–31.

Fonte P, Andrade F, Araújo F, Andrade C, Neves J das, Sarmento B (2012) Chitosan-Coated Solid Lipid Nanoparticles for Insulin Delivery. In: Methods in Enzymology. pp 295–314.

Francis S, Joseph S, Koshy EP, Mathew B (2017) Green synthesis and characterization of gold and silver nanoparticles using Mussaenda glabrata leaf extract and their environmental applications to dye degradation. Environ Sci Pollut Res 24:17347–17357.

Gadogbe M, Ansar SM, He G, Collier WE, Rodriguez J, Liu D, Chu IW, Zhang D (2013) Determination of colloidal gold nanoparticle surface areas, concentrations, and sizes through quantitative ligand adsorption. Anal Bioanal Chem 405:413–422.

Galardo MN, Regueira M, Riera MF, Pellizzari EH, Cigorraga SB, Meroni SB (2014) Lactate regulates rat male germ cell function through reactive oxygen species. PLoS One 9:88024.

Ganesh Kumar C, Poornachandra Y, Chandrasekhar C (2015) Green synthesis of bacterial mediated anti-proliferative gold nanoparticles: inducing mitotic arrest (G2/M phase) and apoptosis (intrinsic pathway). Nanoscale 7:18738–18750.

Gao L, Yang L, Qian S, Tang Z, Qin F, Wei Q, Han P, Yuan J (2016) Cryosurgery would be An Effective Option for Clinically Localized Prostate Cancer: A Meta-analysis and Systematic Review. Sci Rep 6:27490.

Gargi D, Dipankar H, Atanu M (2018) Synthesis of Gold Colloid using Zingiber officinale: Catalytic Study. Nano Mat Chem Bio Dev 1:10–14.

Gay HA, Michalski JM (2018) Radiation Therapy for Prostate Cancer. Mo Med 115:146–150.

Ge R, Chen G, Hardy MP (2008) The Role of the Leydig Cell in Spermatogenic Function. Adv Exp Med Biol 636:255–269.

Geiger AM, Pitts KP, Feldkamp J, Kirschbaum C, Wolf JM (2015) Cortisol-dependent stress effects on cell distribution in healthy individuals and individuals suffering from chronic adrenal insufficiency. Brain Behav Immun 50:241–248.

Geng F, Song K, Xing JZ, Yuan C, Yan S, Yang Q, Chen J, Kong B (2011) Thio-glucose bound gold nanoparticles enhance radio-cytotoxic targeting of ovarian cancer. Nanotechnology 22:285101.

Gera S, Talluri S, Rangaraj N, Sampathi S (2017) Formulation and Evaluation of Naringenin

Nanosuspensions for Bioavailability Enhancement. AAPS PharmSciTech 18:3151–3162.

Gololo SS, Shai LJ, Agyei NM, Mogale MA (2016) Effect of seasonal changes on the quantity of phytochemicals in the leaves of three medicinal plants from Limpopo province, South Africa. J Pharmacogn Phyther 8:168–172.

Goncalves VSS, Rodriguez-Rojo S, De Paz E, Mato C, Martin T, Cocero MJ (2015) Production of water soluble quercetin formulations by pressurized ethyl acetate-in-water emulsion technique using natural origin surfactants. Food Hydrocoll 51:295–304.

Gott B (2008) Indigenous Use of Plants in South-Aastern Australia. Telopea 12:215–226.

Gradiz R, Silva HC, Carvalho L, Botelho MF, Mota-Pinto A (2016) MIA PaCa-2 and PANC-1 - pancreas ductal adenocarcinoma cell lines with neuroendocrine differentiation and somatostatin receptors. Sci Rep 6:21648.

Graefe EU, Wittig J, Mueller S, Riethling AK, Uehleke B, Drewelow B, Pforte H, Jacobasch G, Derendorf H, Veit M (2001) Pharmacokinetics and bioavailability of quercetin glycosides in humans. J Clin Pharmacol 41:492–499.

Grasso C, Jansen G, Giovannetti E (2017) Drug resistance in pancreatic cancer: Impact of altered energy metabolism. Crit Rev Oncol Hematol 114:139–152.

Grayhack JT, McVary KT, Kozlowski JM (2002) Carcinoma of the prostate. In: Gillenwater JY (ed) Adult and pediatric urology. Lippincott Williams & Wilkins, pp 1411–1414.

Griswold MD (1988) Protein secretions of Sertoli cells. Int Rev CYtol 110:133–156.

Gumustas M, Sengel-Turk CT, Gumustas A, Ozkan SA, Uslu B (2017) Effect of Polymer-Based Nanoparticles on the Assay of Antimicrobial Drug Delivery Systems. In: Multifunctional Systems for Combined Delivery, Biosensing and Diagnostics. Elsevier, pp 67–108.

Gupta V, Trivedi P (2018) In vitro and in vivo characterization of pharmaceutical topical nanocarriers containing anticancer drugs for skin cancer treatment. In: Lipid Nanocarriers for Drug Targeting. Elsevier, pp 563–627.

Haiss W, Thanh NTK, Aveyard J, Fernig DG (2007) Determination of Size and Concentration of Gold Nanoparticles from UV−Vis Spectra. Anal Chem 79:4215–4221.

Hammerich KH, Ayala GE, Wheeler TM (2008) Anatomy of the prostate gland and surgical pathology of the prostate. In: Hricak H, Scardino PT (eds) Prostate cancer. Cambridge

University Press, pp 2–10.

Hanafi MMM, Afzan A, Yaakob H, Aziz R, Sarmidi MR, Wolfender J-L, Prieto JM (2017) In Vitro Pro-apoptotic and Anti-migratory Effects of Ficus deltoidea L. Plant Extracts on the Human Prostate Cancer Cell Lines PC-3. Front Pharmacol 8:895.

Harmata AJ, Guelcher SA (2016) Effects of surface modification on polymeric biocomposites for orthopedic applications. In: Nanocomposites for Musculoskeletal Tissue Regeneration. Elsevier, pp 67–91.

Hasan S (2015) A Review on Nanoparticles : Their Synthesis and Types A Review on Nanoparticles : Their Synthesis and Types. Res J Recent Sci 4:7–10.

He Z, Li C, Zhang X, Zhong R, Wang H, Liu J, Du L (2018) The effects of gold nanoparticles on the human blood functions. Artif Cells, Nano-medicine, Biotechnol 46:720–726.

Heerkens HD, van Berkel L, Tseng DSJ, Monninkhof EM, van Santvoort HC, Hagendoorn J, Borel Rinkes IHM, Lips IM, Intven M, Molenaar IQ (2018) Long-term health-related quality of life after pancreatic resection for malignancy in patients with and without severe postoperative complications. HPB 20:188–195.

Hegarty J, Beirne P V, Walsh E, Comber H, Fitzgerald T, Wallace Kazer M (2010) Radical prostatectomy versus watchful waiting for prostate cancer. Cochrane database Syst Rev 10:6590.

Henkel R, Fransman W, Hipler UC, Wiegand C, Schreiber G, Menkveld R, Weitz F, Fisher D (2012a) Typha capensis (Rohrb.)N.E.Br. (bulrush) extract scavenges free radicals, inhibits collagenase activity and affects human sperm motility and mitochondrial membrane potential in vitro: A pilot study. Andrologia 44:287–294.

Henkel R, Fransman W, Hipler UC, Wiegand C, Schreiber G, Menkveld R, Weitz F, Fisher D (2012b) Typha capensis (Rohrb.)N.E.Br. (bulrush) extract scavenges free radicals, inhibits collagenase activity and affects human sperm motility and mitochondrial membrane potential in vitro: a pilot study. Andrologia 44:287–294.

Henning SM, Wang P, Said J, Magyar C, Castor B, Doan N, Tosity C, Moro A, Gao K, Li L, Heber D (2012) Polyphenols in brewed green tea inhibit prostate tumor xenograft growth by localizing to the tumor and decreasing oxidative stress and angiogenesis. J Nutr Biochem 23:1537–1542.

Hohl A, Marques MO, Coral MH, Walz R (2009) Evaluation of late-onset hypogonadism

(andropause) treatment using three different formulations of injectable testosterone. Arq Bras Endocrinol Metab 53:989–995.

Homberger M, Simon U (2010) On the application potential of gold nanoparticles in nanoelectronics and biomedicine. Philos Trans R Soc A Math Phys Eng Sci 368:1405–1453.

Horoszewicz JS, Leong SS, Chu TM, Wajman ZL, Friedman M, Papsidero L, Kim U, Chai LS, Kakati S, Arya SK, Sandberg AA (1980) The LNCaP cell line--a new model for studies on human prostatic carcinoma. Prog Clin Biol Res 37:115–132.

Horoszewicz JS, Leong SS, Kawinski E, Karr JP, H R, Chu TM (1983) LNCaP model of human prostatic carcinoma. Cancer Res 43:809–1818.

Hsiao Y-H, Kuo S-J, Tsai H-D, Chou M-C, Yeh G-P (2016) Clinical Application of High-intensity Focused Ultrasound in Cancer Therapy. J Cancer 7:225–231.

Huang J, Li Q, Sun D, Lu Y, Su Y, Yang X, Wang H, Wang Y, Shao W, He N, Hong J, Chen C (2007) Biosynthesis of silver and gold nanoparticles by novel sundried Cinnamomum camphora leaf. Nanotechnology 18:104–109.

Huggins C, Stevens RE, Hodges C V (1941) The effects of castration on advanced carcinoma of the prostate gland. Arch Surg 43:209–223.

Ilfergane A (2016) Investigations on the effects of Typha capensis on male reproductive functions. University of the Western Cape.

Ismail EH, Saqer AMA, Assirey E, Naqvi A, Okasha RM (2018) Successful green synthesis of gold nanoparticles using a corchorus olitorius extract and their antiproliferative effect in cancer cells. Int J Mol Sci 19:1–14.

Jemal A, Bray F, Center M, Ferlay J, Ward E, Forman D (2011) Global cancer statistics. J Clin Cancer 61:69–90.

Jiménez Pérez ZE, Mathiyalagan R, Markus J, Kim Y-J, Kang HM, Abbai R, Seo KH, Wang D, Soshnikova V, Yang DC (2017) Ginseng-berry-mediated gold and silver nanoparticle synthesis and evaluation of their in vitro antioxidant, antimicrobial, and cytotoxicity effects on human dermal fibroblast and murine melanoma skin cell lines. Int J Nano-medicine Volume 12:709–723.

Jin JK, Dayyani F, Gallick GE (2011) Steps in prostate cancer progression that lead to bone metastasis. Int J Cancer 128:2545–2561.

Jiwrajka M, Yaxley W, Ranasinghe S, Perera M, Roberts MJ, Yaxley J (2018) Drugs for benign prostatic hypertrophy. Aust Prescr 41:150–153.

Johnson L, Thompson DL, Varner DD (2008) Role of Sertoli cell number and function on regulation of spermatogenesis. Anim Reprod Sci 105:23–51.

Jokerst J V, Lobovkina T, Zare RN, Gambhir SS (2011) Nanoparticle PEGylation for imaging and therapy. Nano-medicine 6:715–728.

Jung J (2014) Human tumor xenograft models for preclinical assessment of anticancer drug development. Toxicol Res 30:1–5.

Kaighn ME, Narayan KS, Ohnuki Y, Lechner JF, Jones LW (1979) Establishment and characterization of a human prostatic carcinoma cell line (PC-3). Invest Urol 17:16–23.

Kang A, Park DK, Hyun SH, Kim YH, Yun WS (2015) PH-dependent size distribution of gold nanoparticles investigated by in situ pH-monitoring throughout the synthetic reaction. Chem Phys Lett 639:230–233.

Kannan R, Rahing V, Cutler C, Pandrapragada R, Katti KK, Kattumuri V, Robertson JD, Casteel SJ, Jurisson S, Smith C, Boote E, Katti K V. (2006) Nanocompatible chemistry toward fabrication of target-specific gold nanoparticles. J Am Chem Soc 128:11342–11343.

Kaşıkcı M, Bağdatlıoğlu N (2016) Bioavailability of Quercetin. Curr Res Nutr Food Sci J 4:146–151.

Kastan MB, Bartek J (2004) Cell-cycle checkpoints and cancer. Nature 432:316–323.

Katerere DR, Eloff JN (2005) Antibacterial and antioxidant activity of Sutherlandia frutescens (Fabaceae), a reputed Anti-HIV/AIDS phytomedicine. Phyther Res 19:779–781.

Katti K, Chanda N, Shukla R, Zambre A, Suibramanian T, Kulkarni RR, Kannan R, Katti K V (2009) Green Nanotechnology from Cumin Phytochemicals: Generation of Biocompatible Gold Nanoparticles. Int J Green Nanotechnol Biomed 1:B39–B52.

Kavanagh JN, Redmond KM, Schettino G, Prise KM (2013) DNA Double Strand Break Repair: A Radiation Perspective. Antioxid Redox Signal 18:2458–2472.

Kelleher SL, McCormick NH, Velasquez V, Lopez V (2011) Zinc in specialized secretory tissues: roles in the pacreas, prostate, and mammary gland. Adv Nutr 2:101–111.

Kessler AT, Purich DL (2019) Biochemistry, Histidine. In: StatPearls. p 1.

Khalil MMH, Ismail EH, El-Magdoub F (2012) Biosynthesis of Au nanoparticles using olive leaf extract. 1st Nano Updates. Arab J Chem 5:431–437.

Khan FU, Ihsan AU, Khan HU, Jana R, Wazir J, Khongorzul P, Waqar M, Zhou X (2017) Comprehensive overview of prostatitis. Biomed Pharmacother 94:1064–1076.

Khoobchandani M, Katti K, Maxwell A, Fay W, Katti K (2016) Laminin Receptor-Avid Nanotherapeutic EGCg-AuNPs as a Potential Alternative Therapeutic Approach to Prevent Restenosis. Int J Mol Sci 17:316.

Kimling J, Maier M, Okenve B, Kotaidis V, Ballot H, Plech A (2006) Turkevich Method for Gold Nanoparticle Synthesis Revisited. J Phys Chem B 110:15700–15707.

Klempner SJ, Bubley G (2012) Complementary and Alternative Medicines in Prostate Cancer: From Bench to Bedside? Oncologist 17:830–837.

Kong F-Y, Zhang J-W, Li R-F, Wang Z-X, Wang W-J, Wang W (2017) Unique Roles of Gold Nanoparticles in Drug Delivery, Targeting and Imaging Applications. Molecules 22:64–83.

Koukourakis G, Kelekis N, Armonis V, Kouloulias V (2009) Brachytherapy for prostate cancer: a systematic review. Adv Urol 2009:327945.

Krishna VD, Wu K, Su D, Cheeran MCJ, Wang J-P, Perez A (2018) Nanotechnology: Review of concepts and potential application of sensing platforms in food safety. Food Microbiol 1–8.

Krstić M, Medarević Đ, Đuriš J, Ibrić S (2018) Self-nanoemulsifying drug delivery systems (SNEDDS) and self-microemulsifying drug delivery systems (SMEDDS) as lipid nanocarriers for improving dissolution rate and bioavailability of poorly soluble drugs. In: Lipid Nanocarriers for Drug Targeting. Elsevier, pp 473–508.

Kuppusamy P, Yusoff MM, Maniam GP, Govindan N (2016) Biosynthesis of metallic nanoparticles using plant derivatives and their new avenues in pharmacological applications – An updated report. Saudi Pharm J 24:473–484.

Lakshmanan A, Umamaheswari C, Nagarajan NS (2016) A Facile Phyto-Mediated Synthesis of Gold Nanoparticles using Aqueous Extract of Momordica cochinchinensis Rhizome and Their Biological Activities. 2:76–80.

Lazarus GG, Revaprasadu N, López-Viota J, Singh M (2014) The electrokinetic characterization of gold nanoparticles, functionalized with cationic functional groups, and its' interaction with DNA. Colloids Surfaces B Biointerfaces 121:425–431.

Lee C-F, You P-Y, Lin Y-C, Hsu T-L, Cheng P-Y, Wu Y-X, Tseng C-S, Chen S-W, Chang H-P, Lin Y-W (2015) Exploring the Stability of Gold Nanoparticles by Experimenting with Adsorption Interactions of Nanomaterials in an Undergraduate Lab. J Chem Educ 92:1066–1070.

Lee J, Chatterjee DK, Lee MH, Krishnan S (2014) Gold nanoparticles in breast cancer treatment: Promise and potential pitfalls. Cancer Lett 347:46–53.

Lee JH, Lee HB, Jung GO, Oh JT, Park DE, Chae KM (2013) Effect of quercetin on apoptosis of PANC-1 cells. J Korean Surg Soc 85:249–260.

Lee SH, Shen MM (2015) Cell types of origin for prostate cancer. Curr Opin Cell Biol 37:35–41.

Lentini A, Forni C, Provenzano B, Beninati S (2007) Enhancement of transglutaminase activity and polyamine depletion in B16-F10 melanoma cells by flavonoids naringenin and hesperitin correlate to reduction of the in vivo metastatic potential. Amino Acids 32:95–100.

Levchenko LA, Golovanova SA, Lariontseva N V., Sadkov AP, Voilov DN, Shul'Ga YM, Nikitenko NG, Shestakov AF (2011) Synthesis and study of gold nanoparticles stabilized by bioflavonoids. Russ Chem Bull 60:426–433.

Li B, Lane LA (2019) Probing the biological obstacles of nano-medicine with gold nanoparticles. Wiley Interdiscip Rev Nano-medicine Nanobiotechnology 11:1–27.

Li X, Dai D, Chen B, Tang H, Xie X, Wei W (2018) The value of neutrophil-to-lymphocyte ratio for response and prognostic effect of neoadjuvant chemotherapy in solid tumors: A systematic review and meta-analysis. J Cancer 9:861–871.

Lieber M, Mazzetta J, Nelson-Rees W, Kaplan M, Todaro G (1975) Establishment of a continuous tumor-cell line (panc-1) from a human carcinoma of the exocrine pancreas. Int J cancer 15:741–747.

Lim K Bin (2017) Epidemiology of clinical benign prostatic hyperplasia. Asian J Urol 4:148–151.

Lim SH, Ahn E-Y, Park Y (2016) Green Synthesis and Catalytic Activity of Gold Nanoparticles Synthesized by Artemisia capillaris Water Extract. Nanoscale Res Lett 11:474.

Lim W, Park S, Bazer FW, Song G (2017) Naringenin-Induced Apoptotic Cell Death in Prostate Cancer Cells Is Mediated via the PI3K/AKT and MAPK Signaling Pathways. J Cell

Biochem 118:1118–1131.

Liu Y, An W, Gao A (2016) Protective effects of naringenin in cardiorenal syndrome. J Surg Res 203:416–423.

Long J, Zhang Y, Yu X, Yang J, Le Brun D, Chen C, Yao Q, Li M (2011) Microplate Nutrient Analysis: NH 4+ , NO 3- , PO 43+. Solutions 15:817–828.

Lou C, Zhang F, Yang M, Zhao J, Zeng W, Fang X, Zhang Y, Zhang C, Liang W (2012) Naringenin Decreases Invasiveness and Metastasis by Inhibiting TGF-β-Induced Epithelial to Mesenchymal Transition in Pancreatic Cancer Cells. PLoS One 7:1–9.

Lu GW, Gao P (2010) Emulsions and Microemulsions for Topical and Transdermal Drug Delivery. In: Handbook of Non-Invasive Drug Delivery Systems. Elsevier, pp 59–94.

Lu LY, Ou N, Lu Q-B (2013) Antioxidant induces DNA damage, cell death and mutagenicity in human lung and skin normal cells. Sci Rep 3:3169.

Luo S, Nie X, Yang M, Fu Y, Zeng P, Wan Q (2018) Sorption of Differently Charged Gold Nanoparticles on Synthetic Pyrite. Minerals 8:428.

Macaluso MP (2007) Chronic Prostatitis Syndrome: A Common, but Poorly Understood Condition. Part I. Eur Assoc Urol 5:1–15.

Mackey MA, El-Sayed MA (2014) Chemosensitization of Cancer Cells via Gold Nanoparticle-Induced Cell Cycle Regulation. Photochem Photobiol 90:306–312.

Madhanraj R, Eyini M, Balaji P (2017) Antioxidant Assay of Gold and Silver Nanoparticles from Edible Basidiomycetes Mushroom Fungi. Free Radicals Antioxidants 7:137–142.

Mansoori GA (2017) An Introduction to Nanoscience and Nanotechnology. In: Nanoscience and Plant–Soil Systems. pp 3–20.

Mansoori GA, Soelaiman TAF (2005) Nanotechnology – An Introduction for the Standards Community. J ASTM Int 2:1–21.

Marciscano AE, Hardee ME, Sanfilippo N (2012) Management of high-risk localized prostate cancer. Adv Urol 2012:641689.

Marloth R (1915) The flora of South Africa: with synopical tables of the genera of the higher plants, 4th edn. Darter bros. & Co.

Martínez-Piñeiro L (2007) Prostatic fascial anatomy and positive surgical margins in

laparoscopic radical prostatectomy. Eur Urol 51:598–600.

Marzorati C, Monzani D, Mazzocco K, Pavan F, Cozzi G, De Cobelli O, Monturano M, Pravettoni G (2019) Predicting trajectories of recovery in prostate cancer patients undergone Robot-Assisted Radical Prostatectomy (RARP). PLoS One 14:e0214682.

Masoko P, Mokgotho MP, Mbazima VG, Mampuru LJ (2008) Biological activity of Typha capensis (Typhaceae) from Limpopo Province (South Africa). Afri J Biotechnol 20:3743–8.

McQuaid HN, Muir MF, Taggart LE, McMahon SJ, Coulter JA, Hyland WB, Jain S, Butterworth KT, Schettino G, Prise KM, Hirst DG, Botchway SW, Currell FJ (2016) Imaging and radiation effects of gold nanoparticles in tumour cells. Sci Rep 6:19442.

Mearini L, Porena M (2010) Transrectal high-intensity focused ultrasound for the treatment of prostate cancer: Past, present, and future. Indian J Urol 26:4–11.

Mehrbod P, Abdalla MA, Njoya EM, Ahmed AS, Fotouhi F, Farahmand B, Gado DA, Tabatabaian M, Fasanmi OG, Eloff JN, McGaw LJ, Fasina FO (2018) South African medicinal plant extracts active against influenza A virus. BMC Complement Altern Med 18:112.

Meikle CKS, Kelly CA, Garg P, Wuescher LM, Ali RA, Worth RG (2017) Cancer and Thrombosis: The Platelet Perspective. Front Cell Dev Biol 4:147–157.

Mendes R, Carreira B, Baptista P V., Fernandes AR (2016) Non-small cell lung cancer biomarkers and targeted therapy - two faces of the same coin fostered by nanotechnology. Expert Rev Precis Med Drug Dev 1:155–168.

Mendes R, Fernandes A, Baptista P (2017) Gold Nanoparticle Approach to the Selective Delivery of Gene Silencing in Cancer—The Case for Combined Delivery? Genes (Basel) 8:94.

Menon JU, Jadeja P, Tambe P, Vu K, Yuan B, Nguyen KT (2013) Nanomaterials for Photo-Based Diagnostic and Therapeutic Applications. Theranostics 3:152–166.

Mensah M, Komlaga G, Forkuo A, Firempong C, Anning A, Dickson R (2019) Toxicity and Safety Implications of Herbal Medicines Used in Africa. In: Herbal Medicine. IntechOpen,

Mikami Y, Dhakshinamoorthy A, Alvaro M, García H (2013) Catalytic activity of unsupported gold nanoparticles. Catal Sci Technol 3:58–69.

Mody V, Siwale R, Singh A, Mody H (2010a) Introduction to metallic nanoparticles. J Pharm Bioallied Sci 2:282–289.

Mody V V, Siwale R, Singh A, Mody HR (2010b) Introduction to metallic nanoparticles. J

Pharm Bioallied Sci 2:282–289.

Mohan CO, Gunasekaran S, Ravishankar CN (2019) Chitosan-capped gold nanoparticles for indicating temperature abuse in frozen stored products. npj Sci Food 3:2.

Mohanty SK, Singh R (2017) Overview of the Male Reproductive System. In: Male Infertility: Understanding, Causes and Treatment. Springer Singapore, Singapore, pp 3–12.

Mongra U, Kerrigan AJ, Thronby J, Monga TN (1999) Prospective Study of Fatigue in Localized Prostate Cancer Patients Undergoing Radiotherapy. Radiat Oncol Investig 7:178–185.

Moore TL, Rodriguez-Lorenzo L, Hirsch V, Balog S, Urban D, Jud C, Rothen-Rutishauser B, Lattuada M, Petri-Fink A (2015) Nanoparticle colloidal stability in cell culture media and impact on cellular interactions. Chem Soc Rev 44:6287–6305.

Morgentaler A (2009) Testosterone therapy in men with prostate cancer: Scientific and ethical considerations. J Urol 181:972–979.

Morgentaler A (2006) Testosterone therapy for men at risk for or with history of prostate cancer. Curr Treat Options Oncol 7:363–369.

Morgentaler A, Lipshultz LI, Bennett R, Sweeney M, Avila D, Khera M (2011) Testosterone therapy in men with untreated prostate cancer. J Urol 185:1256–1251.

Mouhid L, Gómez de Cedrón M, Vargas T, García-Carrascosa E, Herranz N, García-Risco M, Reglero G, Fornari T, Ramírez de Molina A (2018) Identification of antitumoral agents against human pancreatic cancer cells from Asteraceae and Lamiaceae plant extracts. BMC Complement Altern Med 18:1–11.

Moyer HR, Delman KA (2008) The role of hyperthermia in optimizing tumor response to regional therapy. Int J Hyperth 24:251–261.

Mukha I, Vityuk N, Severynovska O, Eremenko A, Smirnova N (2016) The pH-Dependent Stucture and Properties of Au and Ag Nanoparticles Produced by Tryptophan Reduction. Nanoscale Res Lett 11:1–7.

Nelles JL, Hu W-Y, Prins GS (2011) Estrogen action and prostate cancer. Expert Rev Endocrinol Metab 6:437–451.

Nelson WG, De Marzo AM, Isaacs WB (2003) Prostate Cancer. N Engl J Med 349:366–381.

Noruzi M (2015) Biosynthesis of gold nanoparticles using plant extracts. Bioprocess Biosyst

Eng 38:1–14.

Nune SK, Chanda N, Shukla R, Katti K, Kulkarni RR, Thilakavathy S, Mekapothula S, Kannan R, Katti K V. (2009a) Green nanotechnology from tea: phytochemicals in tea as building blocks for production of biocompatible gold nanoparticles. J Mater Chem 19:2912–2929.

Nune SK, Chanda N, Shukla R, Katti K, Kulkarni RR, Thilakavathy S, Mekapothula S, Kannan R, Katti K V. (2009b) Green nanotechnology from tea: phytochemicals in tea as building blocks for production of biocompatible gold nanoparticles. J Mater Chem 19:2912–2920.

O'Donnell L, McLachlan RI (2012) The role of testosterone in spermatogenesis. In: Nieschlag E, Behre HM, Nieschlag S (eds) Testosterone. Cambridge University Press, Cambridge, pp 123–153.

Ostolska I, Wiśniewska M (2014) Application of the zeta potential measurements to explanation of colloidal Cr2O3 stability mechanism in the presence of the ionic polyamino acids. Colloid Polym Sci 292:2453–2464.

Oueslati MH, Tahar L Ben, Harrath AH (2018) Catalytic, antioxidant and anticancer activities of gold nanoparticles synthesized by kaempferol glucoside from Lotus leguminosae. Arab J Chem 2018:003.

Paik KY, Lee IK, Lee YS, Sung NY, Kwon TS (2014) Clinical Implications of Systemic Inflammatory Response Markers as Independent Prognostic Factors in Colorectal Cancer Patients. Cancer Res Treat 46:65–73.

Pal SK, Shukla Y (2003) Herbal Medicine : Current Status and the Future. Asian Pacific J Cancer Prev 4:281–288.

Park HJ, Choi YJ, Lee JH, Nam MJ (2017a) Naringenin causes ASK1-induced apoptosis via reactive oxygen species in human pancreatic cancer cells. Food Chem Toxicol 99:1–8.

Park JS, Ahn E-Y, Park Y (2017b) Asymmetric dumbbell-shaped silver nanoparticles and spherical gold nanoparticles green-synthesized by mangosteen (Garcinia mangostana) pericarp waste extracts. Int J Nano-medicine Volume 12:6895–6908.

Parveen K, Banse V, Ledwani L (2016) Green synthesis of nanoparticles: Their advantages and disadvantages. AIP Conf Proc.

Parveen S, Misra R, Sahoo SK (2012) Nanoparticles: a boon to drug delivery, therapeutics, diagnostics and imaging. Nano-medicine 8:147–66.

Paster E V, Villines KA, Hickman DL (2009) Endpoints for mouse abdominal tumor models: refinement of current criteria. Comp Med 59:234–41.

Pawlik TM, Keyomarsi K (2004) Role of cell cycle in mediating sensitivity to radiotherapy. Int J Radiat Oncol 59:928–942.

Pedrosa P, Vinhas R, Fernandes A, Baptista P (2015) Gold Nanotheranostics: Proof-of-Concept or Clinical Tool? Nanomaterials 5:1853–1879.

Peisch SF, Van Blarigan EL, Chan JM, Stampfer MJ, Kenfield SA (2017) Prostate cancer progression and mortality: a review of diet and lifestyle factors. World J Urol 35:867–874.

Peng J, Liang X (2019) Progress in research on gold nanoparticles in cancer management. Medicine (Baltimore) 98:e15311.

Pérez-Torres I, Guarner-Lans V, Rubio-Ruiz ME (2017) Reductive stress in inflammation-associated diseases and the pro-oxidant effect of antioxidant agents. Int J Mol Sci 18:1–26.

Philip D (2009) Biosynthesis of Au, Ag and Au-Ag nanoparticles using edible mushroom extract. Spectrochim Acta - Part A Mol Biomol Spectrosc 73:374–381.

Pizzino G, Irrera N, Cucinotta M, Pallio G, Mannino F, Arcoraci V, Squadrito F, Altavilla D, Bitto A (2017) Oxidative Stress: Harms and Benefits for Human Health. Oxid Med Cell Longev 2017:1–13.

Pratheeshkumar P, Budhraja A, Son Y-O, Wang X, Zhang Z, Ding S, Wang L, Hitron A, Lee J-C, Xu M, Chen G, Luo J, Shi X (2012) Quercetin inhibits angiogenesis mediated human prostate tumor growth by targeting VEGFR- 2 regulated AKT/mTOR/P70S6K signaling pathways. PLoS One 7:47516.

Prezioso D, Naber KG, Lobel B, Weidner W, Algaba F, Denis LJ, Griffiths K (2006) Review paper: Changing concepts on prostatitis. Arch Med Sci 2:71–84.

Qin L, Jin L, Lu L, Lu X, Zhang C, Zhang F, Liang W (2011) Naringenin reduces lung metastasis in a breast cancer resection model. Protein Cell 2:507–516.

Qiu W-Y, Wang K, Wang Y-Y, Ding Z-C, Wu L-X, Cai W-D, Yan J-K (2018) pH dependent green synthesis of gold nanoparticles by completely C6-carboxylated curdlan under high temperature and various pH conditions. Int J Biol Macromol 106:498–506.

Rajamani S, Radhakrishnan A, Sengodan T, Thangavelu S (2018) Augmented anticancer activity of naringenin-loaded TPGS polymeric nanosuspension for drug resistive MCF-7

human breast cancer cells. Drug Dev Ind Pharm 44:1752–1761.

Ramezani N, Ehsanfar Z, Shamsa F, Amin G, Shahverdi HR, Monsef Esfahani HR, Shamsaie A, Bazaz RD, Shahverdi AR (2008) Screening of medicinal plant methanol extracts for the synthesis of gold nanoparticles by their reducing potential. Zeitschrift fur Naturforsch - Sect B J Chem Sci 63:903–908.

Rani M, Moudgil L, Singh B, Kaushal A, Mittal A, Saini GSS, Tripathi SK, Singh G, Kaura A (2016) Understanding the mechanism of replacement of citrate from the surface of gold nanoparticles by amino acids: a theoretical and experimental investigation and their biological application. RSC Adv 6:17373–17383.

Rao PV, Nallappan D, Madhavi K, Rahman S, Jun Wei L, Gan SH (2016a) Phytochemicals and Biogenic Metallic Nanoparticles as Anticancer Agents. Oxid Med Cell Longev 2016:1–15.

Rao PV, Nallappan D, Madhavi K, Rahman S, Jun Wei L, Gan SH (2016b) Phytochemicals and Biogenic Metallic Nanoparticles as Anticancer Agents. Oxid Med Cell Longev 2016:1–15.

Rea D, Del Vecchio V, Palma G, Barbieri A, Falco M, Luciano A, De Biase D, Perdonà S, Facchini G, Arra C (2016) Mouse Models in Prostate Cancer Translational Research: From Xenograft to PDX. Biomed Res Int 2016:9750795.

Regulla D, Schmid E, Friedland W, Panzer W, Heinzmand U, Harder D (2002) Enhanced Values of the RBE and H Ratio for Cytogenetic Effects Induced by Secondary Electrons from an X-Irradiated Gold Surface. Radiat Res 158:505–515.

Roehm NW, Rodgers GH, Hatfield SM, Glasebrook AL (1991) An improved colorimetric assay for cell proliferation and viability utilizing the tetrazolium salt XTT. J Immunol Methods 142:257–65.

Romdhane A, Aurousseau M, Guillet A, Mauret E (2015) Effect of pH and ionic strength on the electrical charge and particle size distribution of starch nanocrystal suspensions. Starch/Staerke 67:319–327.

Rosa S, Connolly C, Schettino G, Butterworth KT, Prise KM (2017) Biological mechanisms of gold nanoparticle radiosensitization. Cancer Nanotechnol 8:2.

Rosenberg MT, Albala F, Miner MM, Froehner M (2010) Biology and natural history of prostate cancer and the role of chemoprevention. Int J Clin Pract 64:1746–1753.

Saeb ATM, Alshammari AS, Al-Brahim H, Al-Rubeaan KA (2014) Production of silver nanoparticles with strong and stable antimicrobial activity against highly pathogenic and multidrug resistant bacteria. Sci World J 2014:1–9.

Saeed MEM, Meyer M, Hussein A, Efferth T (2016) Cytotoxicity of South-African medicinal plants towards sensitive and multidrug-resistant cancer cells. J Ethnopharmacol 186:209–223.

Sajanlal PR, Pradeep T (2012) Gold Nanoparticles. In: John Wiley & Sons Inc (ed) Kirk-Othmer Encyclopedia of Chemical Technology. John Wiley & Sons, Inc., Hoboken, NJ, USA, pp 4–6.

Salehi B, Fokou PVT, Sharifi-Rad M, Zucca P, Pezzani R, Martins N, Sharifi-Rad J (2019) The therapeutic potential of naringenin: A review of clinical trials. Pharmaceuticals 12:1–18.

San Diego KDG, Alindayu JIA, Baculi RQ (2018) Biosynthesis of gold nanoparticles by bacteria from hyperalkaline spring and evaluation of their inhibitory activity against pyocyanin production. J Microbiol Biotechnol Food Sci 8:781–787.

Sánchez-Rangel JC, Benavides J, Heredia JB, Cisneros-Zevallos L, Jacobo-Velázquez DA (2013) The Folin–Ciocalteu assay revisited: improvement of its specificity for total phenolic content determination. Anal Methods 5:59–90.

Sangpheak W, Kicuntod J, Schuster R, Rungrotmongkol T, Wolschann P, Kungwan N, Viernstein H, Mueller M, Pongsawasdi P (2015) Physical properties and biological activities of hesperetin and naringenin in complex with methylated p-cyclodextrin. Beilstein J Org Chem 11:2763–2773.

Santhoshkumar J, Rajeshkumar S, Venkat Kumar S (2017) Phyto-assisted synthesis, characterization and applications of gold nanoparticles – A review. Biochem Biophys Reports 11:46–57.

Satnami ML, Chandraker K, Vaishanav SK, Nagwanshi R (2015) Interaction of thiolated amino acids and peptide onto the gold nanoparticle surface: Radical scavenging activity. Indian J Chem 54:1206–1214.

Schenk JM, Kristal AR, Neuhouser ML, Tangen CM, White E, Lin DW, Kratz M, Thompson IM (2009) Biomarkers of Systemic Inflammation and Risk of Incident, Symptomatic Benign Prostatic Hyperplasia: Results From the Prostate Cancer Prevention Trial. Am J Epidemiol 171:571–582.

Schmidt B, Ribnicky D, Poulev A (2008) A natural history of botanical therapeutics. J Metab

57:1–12.

Schulman AA, Polascik TJ (2017) Most of patients with localized prostate cancer will be treated in the future? | Opinion: No. Int braz j urol 43:584–587.

Sechi M, Sanna V, Pala N, Manconi P, Mariani A, Dedola S, Rassu M, Crosio C, Iaccarino C, Dessi G (2014) Single-step green synthesis and characterization of gold-conjugated polyphenol nanoparticles with antioxidant and biological activities. Int J Nano-medicine 9:4935–4951.

Sembratowicz I, Ognik K (2019) Redox status, hematological as well liver and kidney function indicators in blood of chickens receiving gold nanoparticles. Ann Anim Sci 19:453–468.

Shabestarian H, Homayouni-Tabrizi M, Soltani M, Namvar F, Azizi S, Mohamad R, Shabestarian H (2016) Green Synthesis of Gold Nanoparticles Using Sumac Aqueous Extract and Their Antioxidant Activity. Mater Res 20:264–270.

Shah M, Badwaik V, Kherde Y, Waghwani HK, Modi T, Aguilar Z, Rodgers H, Hamilton W, Marutharaj T, Webb C, Lawrenz M, Dakshinamurthy R (2014) Gold nanoparticles: various methods of synthesis and antibacterial applications. Front Biosci 19:1320–1344.

Shah R, Oza G, Pandey S, Sharon M (2012) Biogenic Fabrication of Gold Nanoparticles using Halomonas salina. J Microbiol Biotechnol Res Sch Res Libr J Microbiol Biotech Res 2:485–492.

Shaheen H, Qaseem MF, Amjad MS, Bruschi P (2017) Exploration of ethno-medicinal knowledge among rural communities of Pearl Valley; Rawalakot, District Poonch Azad Jammu and Kashmir. PLoS One 12:e0183956.

Shao Q, Hall CK (2017) Allosteric effects of gold nanoparticles on human serum albumin. Nanoscale 9:380–390.

Shapley N, Mello C (2011) Nanoparticles and Their Applications in Cell and. Anal Chem 6:9–26.

Sharma V, Park K, Srinivasarao M (2009) Colloidal dispersion of gold nanorods: Historical background, optical properties, seed-mediated synthesis, shape separation and self-assembly. Mater Sci Eng R Reports 65:1–38.

Shi X, Li D, Xie J, Wang S, Wu Z, Chen H (2012) Spectroscopic investigation of the interactions between gold nanoparticles and bovine serum albumin. Chinese Sci Bull 57:1109–

1115.

Shode FO, Mahomed AS, Rogers CB (2002) Typhaphthalide and typharin, two phenolic compounds from Typha capensis. Phytochemistry 61:955–957.

Shukla R, Nune SK, Chanda N, Katti K, Mekapothula S, Kulkarni RR, Welshons W V., Kannan R, Katti K V. (2008) Soybeans as a phytochemical reservoir for the production and stabilization of biocompatible gold nanoparticles. Small 4:1425–1436.

Shulman M, Cohen M, Soto-Gutierrez A, Yagi H, Wang H, Goldwasser J, Lee-Parsons CW, Benny-Ratsaby O, Yarmush ML, Nahmias Y (2011) Enhancement of naringenin bioavailability by complexation with hydroxypropoyl-β-cyclodextrin. PLoS One.

Simoneau AR (2006) Treatment- and Disease Related Complications of Prostate Cancer. Rev Urol 2:56–67.

Simpson MG (2010) Plant Systematics, 2nd edn. Academic Press.

Singh AK, Srivastava ON (2015) One-Step Green Synthesis of Gold Nanoparticles Using Black Cardamom and Effect of pH on Its Synthesis. Nanoscale Res Lett 10:353.

Singh P, Pandit S, Mokkapati VRSS, Garg A, Ravikumar V, Mijakovic I (2018) Gold nanoparticles in diagnostics and therapeutics for human cancer. Int J Mol Sci. 7:1979.

Sirajuddin, Mechler A, Torriero AAJ, Nafady A, Lee C-Y, Bond AM, O'Mullane AP, Bhargava SK (2010) The formation of gold nanoparticles using hydroquinone as a reducing agent through a localized pH change upon addition of NaOH to a solution of HAuCl4. Colloids Surfaces A Physicochem Eng Asp 370:35–41.

Snyder PJ (2009) Yen & Jaffe's Reproductive Endocrinology (sixth Edition). In: Strauss JF, Barbeiri RL (eds). Saunders, pp 357–363.

Somchaidee P, Tedsree K (2018) Green synthesis of high dispersion and narrow size distribution of zero-valent iron nanoparticles using guava leaf (Psidium guajava L) extract. Adv Nat Sci Nanosci Nanotechnol 9:35–60.

Soni U, Brar S, Gauttam VK (2015) Effect of Seasonal Variation on Secondary Metabolites of Medicinal Plants. Int J Pharm Sci Res 6:3654–3662.

Soshnikova V, Kim YJ, Singh P, Huo Y, Markus J, Ahn S, Castro-Aceituno V, Kang J, Chokkalingam M, Mathiyalagan R, Yang DC (2018) Cardamom fruits as a green resource for facile synthesis of gold and silver nanoparticles and their biological applications. Artif Cells,

Nano-medicine, Biotechnol 46:108–117.

Sotnikov D V., Berlina AN, Ivanov VS, Zherdev A V., Dzantiev BB (2019) Adsorption of proteins on gold nanoparticles: One or more layers? Colloids Surfaces B Biointerfaces 173:557–563.

Stangelberger A, Waldert M, Djavan B (2008) Prostate Cancer in Elderly Men. Rev Urol 10:111–119.

Steenkamp V (2003) Traditional herbal remedies used by South African women for gynaecological complaints. J Ethnopharmacol 86:97–108.

Steers WD (2011) Physiology and pharmacology of the prostate. In: Steers WD (ed) Practical urology: essential principles and practice. ScholarlyEditions, pp 239–241

Stetefeld J, McKenna SA, Patel TR (2016) Dynamic light scattering: a practical guide and applications in biomedical sciences. Biophys Rev 8:409–427.

Subramanian K, Sankaramourthy D, Gunasekaran M (2018) Toxicity Studies Related to Medicinal Plants. In: Natural Products and Drug Discovery. Elsevier, pp 491–505

Sulman JD, Drew BT, Drummond C, Hayasaka E, Sytsma KJ (2013) Systematics, biogeography, and character evolution of sparganium (Typhaceae): Diversification of a widespread, aquatic lineage. Am J Bot 100:2023–2039.

Sultan R, Majid N, Nissar S, Rather A (2018) Seasonal variation of Phytochemicals. Int J Pharm 8:987–990.

Suman TY, Radhika Rajasree SR, Ramkumar R, Rajthilak C, Perumal P (2014) The Green synthesis of gold nanoparticles using an aqueous root extract of Morinda citrifolia L. Spectrochim Acta Part A Mol Biomol Spectrosc 118:11–16.

Sumbayev V, Yasinska I, Gibbs B (2012) Biomedical Applications of Gold Nanoparticles. Recent Adv Circuits, Commun Signal Process Biomed 1:10–25.

Sun H, Jia J, Jiang C, Zhai S (2018) Gold Nanoparticle-Induced Cell Death and Potential Applications in Nano-medicine. Int J Mol Sci 19:754.

Sun L, Pu S, Li J, Cai J, Zhou B, Ren G, Ma Q, Zhong L (2019) Size controllable one step synthesis of gold nanoparticles using carboxymethyl chitosan. Int J Biol Macromol 122:770–783.

Taher A (2005) Proportion and acceptance of andropause symptoms among elderly men. Acta

Med Indones 37:82–86.

Takahashi C, Shridhar R, Huston J, Meredith K (2018) Correlation of tumor size and survival in pancreatic cancer. J Gastrointest Oncol 9:910–921.

Teimuri-mofrad R, Hadi R, Tahmasebi B, Farhoudian S, Mehravar M, Nasiri R (2017) Green synthesis of gold nanoparticles using plant extract: Mini-review. Nanochemistry Res 2:8–19.

Teo MY, Rathkopf DE, Kantoff P (2019) Treatment of Advanced Prostate Cancer. Annu Rev Med 70:479–499.

Testai L, Pozzo E Da, Piano I, Pistelli L, Gargini C, Breschi MC, Braca A, Martini C, Martelli A, Calderone V (2017) The citrus flavanone naringenin produces cardioprotective effects in hearts from 1 year old rat, through activation of mitoBK channels. Front Pharmacol 8:1–11.

Thakur A, Chun YS, October N, Yang HO, Maharaj V (2019) Potential of South African medicinal plants targeting the reduction of Aβ42 protein as a treatment of Alzheimer's disease. J Ethnopharmacol 231:363–373.

Thipe VC, Amiri KP, Bloebaum P, Raphael AK, Khoobchandani M, Katti KK, Jurisson SS, Katti K V. (2019) Development of resveratrol-conjugated gold nanoparticles: interrelationship of increased resveratrol corona on anti-tumor efficacy against breast, pancreatic and prostate cancers. Int J Nano-medicine Volume 14:4413–4428.

Thompson DT (2008) Michael Faraday's recognition of Ruby Gold: The birth of modern nanotechnology. Gold Bull 40:267–269.

Thorsen RS, Pouliot M (2016) Traditional medicine for the rich and knowledgeable: challenging assumptions about treatment-seeking behaviour in rural and peri-urban Nepal. Health Policy Plan 31:314–324.

Tomaszewska E, Soliwoda K, Kadziola K, Tkacz-Szczesna B, Celichowski G, Cichomski M, Szmaja W, Grobelny J (2013) Detection Limits of DLS and UV-Vis Spectroscopy in Characterization of Polydisperse Nanoparticles Colloids. J Nanomater 2013:1–10.

Torres-Roca JF (2006) The Role of External-Beam Radiation Therapy in the Treatment of Clinically Localized Prostate Cancer. Cancer Control 13:188–193.

Tsametis CP, Isidori AM (2018) Testosterone replacement therapy: For whom, when and how? Metabolism 86:69–78.

Turkevich J, Stevenson PC, Hillier J (1951) A study of the nucleation and growth processes in

the synthesis of colloidal gold. Discuss Faraday Soc 11:55.

Ullah MI, Riche DM, Koch CA (2014) Transdermal testosterone replacement therapy in men. Drug Des Devel Ther 8:101–112.

van Doorn-Khosrovani SB van W, Janssen J, Maas LM, Godschalk RWL, Nijhuis JG, van Schooten FJ (2007) Dietary flavonoids induce MLL translocations in primary human CD34+ cells. Carcinogenesis 28:1703–1709.

van Meerloo J, Kaspers GJL, Cloos J (2011) Cell sensitivity assays: the MTT assay. Methods Mol Biol 731:237–45.

Vasanwala FF, Wong MYC, Ho HSS, Foo KT (2017) Benign prostatic hyperplasia and male lower urinary symptoms: A guide for family physicians. Asian J Urol 4:181–184.

Vijayakumar R, Devi V, Adavallan K, Saranya D (2011) Green synthesis and characterization of gold nanoparticles using extract of anti-tumor potent Crocus sativus. Phys E Low-Dimensional Syst Nanostructures 44:665–671.

Vijayakumar S (2014) In vitro stability studies on gold nanoparticles with different stabilizing agents. Int J Curr Sci 11:84–93.

Vines JB, Yoon J-H, Ryu N-E, Lim D-J, Park H (2019) Gold Nanoparticles for Photothermal Cancer Therapy. Front Chem 7:1–16.

Vlotman N (2003) A study of Typha capensis (Rohrb) N.E.Br. It'd biodiversity, role as a potential anti-infective candidate and its effect on metabolism and health. University of the Western Cape

Wahjoepramono E, Prita A, Vilia A, Taddei K, Satvinder S, Fuller S, Foster J, Carruthers M, Verdile G, Sohrabi H, Martins R (2016) The Effects of Testosterone Supplementation on Cognitive Functioning in Older Men. CNS Neurol Disord - Drug Targets 15:337–343.

Walker WH, Cheng J (2005) FSH and testosterone signaling in Sertoli cells. Reproduction 130:15–28.

Wallace TJ, Torre T, Grob M, Yu J, Avital I, Brücher BLDM, Stojadinovic A, Man YG (2014) Current Approaches, Challenges and Future Directions for Monitoring Treatment Response in Prostate Cancer. J Cancer 5:3–24.

Walters K a, Simanainen U, Handelsman DJ (2010) Molecular insights into androgen actions in male and female reproductive function from androgen receptor knockout models. Hum

Reprod Update 16:543–58.

Wang A, Ng HP, Xu Y, Li Y, Zheng Y, Yu J, Han F, Peng F, Fu L (2014) Gold Nanoparticles: Synthesis, Stability Test, and Application for the Rice Growth. J Nanomater 2014:1–6.

Wang F, Wang Y-C, Dou S, Xiong M-H, Sun T-M, Wang J (2011) Doxorubicin-Tethered Responsive Gold Nanoparticles Facilitate Intracellular Drug Delivery for Overcoming Multidrug Resistance in Cancer Cells. ACS Nano 5:3679–3692.

Wang L, Xu J, Yan Y, Liu H, Li F (2019) Synthesis of gold nanoparticles from leaf Panax notoginseng and its anticancer activity in pancreatic cancer PANC-1 cell lines. Artif cells, nano-medicine, Biotechnol 47:1216–1223.

Weinbauer GF, Luetjens, C M, Simoni M, Nieschlag E (2010) Physiology of testicular function. Andrology 24:765–774.

White k. Y, Rodemich L, Nyalwidhe JO, Comunale MA, Clements MA, Lance RS, Schellhammer PF, Mehta AS, Semmes OJ, Drake RR (2009) Glycomic characterization of prostate-specific antigen and prostatic acid phosphatase in prostate cancer and benign disease seminal plasma fluids. J Proteome Res 8:620–630.

WHO (2005a) WHO Traditional Medicine Strategy 2002–2005.

WHO WHO (2005b) National Policy on Traditional Medicine and Regulation of Herbal Medicine. Geneva

Wilt TJ, Shamliyan T, Taylor B, MacDonald R, Tacklind J, Rutks I, Koeneman K, Cho C-S, L. K (2008) Comparative Effectiveness of Therapies for Clinically Localized Prostate Cancer. Comparative Effectiveness Review No. 13. Rockville

Wirth MD, Sevoyan M, Hofseth L, Shivappa N, Hurley TG, Hébert JR (2018) The Dietary Inflammatory Index is associated with elevated white blood cell counts in the National Health and Nutrition Examination Survey. Brain Behav Immun 69:296–303.

Wong IY, Bhatia SN, Toner M (2013) Nanotechnology: Emerging tools for biology and medicine. Genes Dev 27:2397–2408.

Wu FCW, Tajar A, Beynon JM (2010) Identification of late-onset hypogonadism in middle-aged and elderly men. N Engl J Med 363:123–135.

Wuithschick M, Birnbaum A, Witte S, Sztucki M, Vainio U, Pinna N, Rademann K, Emmerling F, Kraehnert R, Polte J (2015) Turkevich in New Robes: Key Questions Answered

for the Most Common Gold Nanoparticle Synthesis. ACS Nano 9:7052–7071.

Xia S, Xu X, Teng J, Xu C, Tang X (2002) Characteristic pattern of human prostatic growth with age. Asian J Androl 4:269–271.

Xin Lee K, Shameli K, Miyake M, Kuwano N, Bt Ahmad Khairudin NB, Bt Mohamad SE, Yew YP (2016) Green Synthesis of Gold Nanoparticles Using Aqueous Extract of Garcinia mangostana Fruit Peels. J Nanomater 2016:1–7.

Xu X, Ho W, Zhang X, Bertrand N, Farokhzad O (2015) Cancer nano-medicine: from targeted delivery to combination therapy. Trends Mol Med 21:223–32.

Yadav A, Ranade S (2016) Properties and bioactivity of flavonoids and sugar induced gold nanoparticles. Indian J Biotechnol 15:531–537.

Yakubu MT, Afolayan AJ (2008) Effect of aqueous extract of Bulbine natalensis (Baker) stem on the sexual behaviour of male rats. Int J Androl 32:629–636.

Yang F, Song L, Wang H, Wang J, Xu Z, Xing N (2015) Combination of Quercetin and 2-Methoxyestradiol enhances inhibition of human prostate cancer LNCaP and PC-3 cells xenograft tumor growth. PLoS One 10:1–15.

Yeo ELL, Cheah JU-J, Neo DJH, Goh WI, Kanchanawong P, Soo KC, Thong PSP, Kah JCY (2017) Exploiting the protein corona around gold nanorods for low-dose combined photothermal and photodynamic therapy. J Mater Chem B 5:254–268.

Yin S-Y, Wei W-C, Jian F-Y, Yang N-S (2013) Therapeutic applications of herbal medicines for cancer patients. Evid Based Complement Alternat Med 2013:302426.

Yu L (2012) Estimate the Population Density of Gold Nanoparticles in Suspensions from Experimental Data. Biochem Physiol Open Access 1:111–112.

Yuan C-G, Huo C, Gui B, Cao W-P (2017) Green synthesis of gold nanoparticles using Citrus maxima peel extract and their catalytic/antibacterial activities. IET Nanobiotechnology 11:523–530.

Yuan H, Ma Q, Ye L, Piao G (2016) The Traditional Medicine and Modern Medicine from Natural Products. Molecules 21:559.

Yuksel OH, Verit A, Sahin A, Urkmez A, Uruc F (2016) White blood cell counts and neutrophil to lymphocyte ratio in the diagnosis of testicular cancer: A simple secondary serum tumor marker. Int Braz J Urol 42:53–59.

Zhang J, Zhang H-Y, Li J, Shao X-Y, Zhang C-X (2017) The elevated NLR, PLR and PLT may predict the prognosis of patients with colorectal cancer: a systematic review and meta-analysis. Oncotarget 8:68837–68846.

Zhang XD, Wu HY, Wu D, Wang YY, Chang JH, Zhai Z Bin, Meng AM, Liu PX, Zhang LA, Fan FY (2010) Toxicologic effects of gold nanoparticles in vivo by different administration routes. Int J Nano-medicine 5:771–781.

Zhou B, Tu T, Kong F, Wen J, Xu X (2018) Revised phylogeny and historical biogeography of the cosmopolitan aquatic plant genus Typha (Typhaceae). Sci Rep 8:1–7.

Zhou J, Wang CY, Liu T, Wu B, Zhou F, Xiong JX, Wu HS, Tao J, Zhao G, Yang M, Gou SM (2008) Persistence of side population cells with high drug efflux capacity in pancreatic cancer. World J Gastroenterol 14:925–930.

Zhu H, Li T, Du Y, Li M (2018) Pancreatic cancer: Challenges and opportunities. BMC Med 16:18–20.

Zhu J, Li W, Zhu M, Zhang W, Niu W, Liu G (2014) Influence of the pH value of a colloidal gold solution on the absorption spectra of an LSPR-assisted sensor. AIP Adv 4:31–38.

Ziaee Ghahnavieh M, Ajdary M, Ghahnavieh MZ, Naghsh N (2013) Effects of intraperitoneal injection of gold nanoparticles in male mice Intraperitoneal injection of gold nanoparticles in mice. Nanomed J 1:121–127.